Quantifying the climate and air quality impacts of non-CO_2 species from the combustion of standard and alternative fuels in aviation

Zarashpe Zarir Kapadia

Submitted in accordance with the requirements for the degree of Doctor of Philosophy as part of the Integrated PhD with MSc in Low Carbon Technologies

November 2015

Doctoral Training Centre in Low Carbon Technologies,
Energy Research Institute, School of Chemical and Process Engineering,
University of Leeds
and
School of Earth and Environment, University of Leeds
and
School of Civil Engineering

Declaration of authorship

The candidate confirms that the work submitted is his own, except where work which has formed part of jointly-authored publications has been included. The contribution of the candidate and the other authors to this work has been explicitly indicated below. The candidate confirms that appropriate credit has been given within the thesis where reference has been made to the work of others.

Work from Chapters 4, 5 and 6 of this thesis appears in publication as follows: Kapadia, Z. Z., Spracklen, D. V., Arnold, S. R., Borman, D. J., Mann, G. W., Pringle, K. J., Monks, S. A., Reddington, C. L., Benduhn, F., Rap, A., Scott, C. E., Butt, E. W., and Yoshioka, M.: Impacts of aviation fuel sulfur content on climate and human health, *Atmos. Chem. Phys. Discuss.*, **15**, 18921-18961, doi:10.5194/acpd-15-18921-2015, 2015

The candidate, Zarashpe Zarir Kapadia, was responsible for the development of aviation emissions inventories, simulations, data interpretation, interpretation of work within the publication. The candidate wrote the manuscript with guidance from the co-authors.

The contributions of the other authors was as follows: A. Rap and C. E. Scott performed calculations of ozone radiative, aerosol direct radiative and aerosol cloud albedo effects. E. W. Butt developed the mortality impacts code, and aviation emissions were integrated in to GLOMAP-mode with the assistance of K. J. Pringle, S. A. Monks and D. V. Spracklen. G. W. Mann, K. J. Pringle and C. L. Reddington helped set up the nitrate-extended version of the TOMCAT-GLOMAP-mode coupled model.

Acknowledgements

Firstly I would like to thank my supervisors: Dominick Spracklen, Steve Arnold, Duncan Borman and Paul Williams. For without their invaluable support, advice, guidance, time and feedback over the past years this work and thesis would not have been possible, and for the opportunities and enthusiasm they have provided over the years. I would also like to thank Piers Forster for the support, guidance and opportunities he has provided me with.

I would like to thank Kirsty Pringle, Graham Mann, Catherine Scott, Carly Reddington and Sarah Monks for all their assistance and time helping me get set-up on TOMCAT-GLOMAP-mode, the nitrate-extended version of this model, and simulation processing codes. The Aerosol Modellers and BAG (Biosphere Atmosphere Group) research groups for their feedback, and Richard Rigby for his invaluable IT support.

I would like to thank the management committee of the Doctoral Training Centre in Low Carbon Technologies (DTC in LCT) for providing me with this opportunity. Paul Williams, James McKay, David Haynes, Eleanor Barham, Rachael Brown and Emily Bryan-Kinns for all their help, support, and for providing the DTC with an encouraging environment.

Being part of the DTC in LCT I have also been privileged to meet some amazing people working on a range of interesting projects feeding in to the topic of low carbon technologies, while making some very good friends along the way. You are all too numerous to mention, but I'll give it try... Jayne Windeatt, Gemma Brady, Ramzi Cherad, David Wyatt and Philippa Usher from my cohort, we have certainly been on a journey together – you guys have been amazing! Karaoke?... Tom Lynch, Shemaiah Weekes, (Aunty) Philippa Hardy, Sam Pickard, Hannah James and Gillian Harrison for all your pearls of wisdom and World Food nights.

Catherine Scott for being a great friend and fake sister, Jayne Windeatt there's no better way to sum you up than "you all round star!" – Thank you two for your invaluable friendship and advice. Sam Pickard for the care packages, advice and food discussions, and Edward Butt. Emma Tetstall the toughest running partner ever. Annabel Lea, Andrew Logue and Dwit Mehta who have provided much needed breaks away from work. Thom Best a great flatmate and friend, Andrew Dixon, David "Davey-J" Jacques, quiz and food guru Joanne Robinson, Berlin and fitness guru Paula McNamee for our coffee breaks and fun chats, James Gooding, Clare Linton and the otter aficionado Holly "Alfredo" Edwards for all your support and advice, and to the rest of you all – thank you. Thank you all for making this memorable and enjoyable time; one that I will never forget.

I also would like to mention some of my friends away from university; Bijan Talei Faz for all the advice and entertainment, Dahlia Revah, Matthew Cave, Sam Grove and Daniel Ivatt for all the encouragement, and helping me make the decision to back to University. Almost finally I would like to thank some people, who in my eyes, are stars of the pre-higher education process: John Pickering who helped me overcome my barriers with maths and helped me realise my abilities; and Stephen Persaud who always had faith in my skills and always pushed me to see to realise them, despite my resistance to Chemistry.

Finally I would like to thank my mum, dad and brothers who have been there for me throughout this journey. Especially my parents for their endless support through all my endeavours, the much needed sanity checks, and for leading by example – thank you. Oh, I expect you two have pretended to have read this!

Abstract

Aviation has the capacity to drive changes in atmospheric composition, and therefore climate and air quality, increasing human mortality through increases in cases in cardiopulmonary disease. Non-CO_2 aviation emissions are estimated to have a considerable effect on the climate, and with rapid growth in the aviation sector their associated impacts could increase. There is much uncertainty surrounding the climatic impact of aviation-induced ozone and aerosols, in part due to broad range of emissions species emitted, which are not always reported in aviation emissions inventories.

This thesis assesses the impact of aviation on atmospheric trace gas and aerosol concentrations, climate, air quality and human health effects for year 2000 civil aviation. These impacts are estimated through: (i) the development of an extended aviation emissions inventory, inclusive of speciated hydrocarbons; (ii) assessing the atmospheric and climatic impact from aviation based on an extend aviation emissions inventory, a comparison of these impacts with a reduced emissions aviation emissions inventory, along with a sensitivity study for emissions species included; (iii) assessing the impact of aviation on human health effects when variations in fuel sulfur content (FSC) are applied along with resulting impacts on radiative effects, and; (iv) the atmospheric, climatic, air quality and human health impacts of the use of alternative fuels in aviation.

An aviation emissions inventory was developed to represent aviation-borne non-CO_2 emissions: nitrogen oxides, carbon oxide, speciated hydrocarbons, sulfur dioxide, black carbon and organic carbon emissions while taking in to account the geometric mean diameter of carbonaceous particles released. Aviation non-CO_2 emissions are assessed to result in a radiative effect of –13.29 mW m^{-2} [assessed from the ozone (O3DRE) and aerosol (aDRE) direct radiative effects, and aerosol cloud albedo effect (aCAE)], primarily driven by a cooling aCAE. In comparison an emissions inventory which only considers aviation nitrogen dioxide and black carbon emissions results in a radiative effect of –8.19 mW m^{-2} primarily driven by reductions in the cooling aCAE assessed.

It is found that air pollution from aviation reaches ground level, as such modifying surface $PM_{2.5}$ (particulate matter within the 2.5 μm size range) which results in increased human exposure. Standard aviation is estimated to result in 3597 mortalities a^{-1}. Variations in FSC from 0–6000 ppm aviation's human health effects range from 2950–9057 mortalities a^{-1}. These variations in FSC result in an aviation non-CO_2 radiative effect ranging from –6.08 mW m^{-2} to –75.48 mW m^{-2}. It is found that variations in aviation FSC elicit a near-linear relationship

between aviation-induced mortality and non-CO_2 radiative effect. Additional investigations in the vertical release of aviation-borne sulfur dioxide emissions show that it possible to reduce aviation-induced mortality and increase aviation-induced cooling by adjusting the FSC of fuel used at different altitudes.

An investigation of the use of Fischer-Tropsch (FT) and fatty acid methyl ester (FAME) fuels (FT50, FT100, FAME20 and FAME40 fuel blends) within aviation found that aviation-induced nitrogen dioxide and ozone concentrations were reduced in tandem with associated ozone radiative effects. Additionally due relative reductions between sulfur dioxide and carbonaceous aerosol emissions FT fuel blends were estimated to produce negative aDREs, while FAME fuel blends gave a positive aDRE. In all cases FT and FAME fuel blends decreased the aCAE induced cooling effect from aviation.

FT50 is the only fuel blend currently specified for use in today's civil aviation fleet. This fuel blend is simulated to reduce aviation's non-CO_2 emissions cooling radiative effect to –10.89 mW m^{-2} and reduce aviation-induced mortality by 460 mortalities a^{-1}. Through the sustainable development of FT fuels from bio-sourced feedstocks this fuel blend has the potential to reduce aviation's climatic impact and human health effects (when reductions in aviation's net CO_2 emissions are considered in tandem).

Contents

List of Figures

List of Tables

1 Introduction

Aviation is known to affect gas- and aerosol-phase atmospheric composition (Lee et al., 2010; Holmes et al., 2011; Hoor et al., 2009; Myhre et al., 2011), air quality and human health (Barrett et al., 2010; Barrett et al., 2012; Yim et al., 2015; Woody et al., 2011), along with perturbing the climate (Penner et al., 1999; Sausen et al., 2005; Lee et al., 2009; Lee et al., 2010). Aviation is a fast growing transport sector (Boeing, 2008; Gudmundsson and Anger, 2012), which is projected to experience a near doubling of the global civil aviation fleet in 2026 in relation to 2006 (Kreutz et al., 2008).

By developing a new aviation emissions inventory, and using it in a size-resolved atmospheric chemistry aerosol microphysics model (the nitrate-extended version of the TOMCAT-GLOMAP-mode coupled model), this thesis aims to investigate the impact of aviation non-CO_2 emissions on gas- and aerosol-phase species in the atmosphere, air quality, human health and resulting climate impacts. This is done through investigating aviation-induced perturbations to gas- and aerosol-phase species in the troposphere, surface-level air quality, and the resulting impacts on human health and climate.

The four main investigations conducted in this thesis look at the:

1. Development of an extended aviation emissions inventory, which considers the speciation of aviation emitted hydrocarbons;
2. The impact of year 2000 aviation non-CO_2 emissions on atmospheric composition, and ozone and aerosol direct radiative and aerosol cloud albedo effect;
3. Impacts of variations in aviation fuel sulfur content on human health and climate, and;
4. Development of alternative fuel scenarios to investigate the atmospheric and climate impacts of proposed alternative aviation fuels.

1.1 Anthropogenic climate change

Anthropogenic climate change refers to perturbations in the Earth's radiation budget due to the influence of the human emitted greenhouse gases (GHGs) and aerosols. GHGs are also emitted naturally in to the atmosphere. Without these naturally occurring GHGs, the Earth's average temperature would be –18 °C as opposed to +15 °C (Berger, 2012; Jacobson, 2002), and the Earth would not be able to sustain human life.

Since the industrial revolution (circa 1850) anthropogenic activity has caused global atmospheric CO_2 (carbon dioxide) concentrations to rise from 280 ppm (IPCC, 2007b) to 397.64 ppm (monthly mean concentrations for September 2015) (NOAA, August 2015). This is associated with the release of 375 [345–405] PgC between the period of 1750–2011 from fossil fuel combustion and cement production (estimated from energy and fuel use statistics) (Stocker et al., 2014). Additionally since 1765–2005 land-use change has resulted in the net release of 4.3 $Mg(CO_2)eq\ ha^{-1}\ yr^{-1}$ (Kim and Kirschbaum, 2015).

In addition to anthropogenic CO_2 emissions, anthropogenic activity has affected global concentrations of non-CO_2 greenhouse gases. Concentrations of N_2O (nitrous oxide) have increased by a factor of 1.2 since pre-industrial times, while CH_4 (methane) concentrations have increased by a factor of 2.5 over the same period (1750–2011) (Stocker et al., 2014). These changes in atmospheric composition have resulted in a rise in global mean land and ocean surface temperatures of 0.85 °C over the period of 1880–2012 (IPCC, 2013b). The IPCC's AR5 estimates that the total anthropogenic radiative forcing (RF) in 2011 relative to 1750 as 2.29 [1.13–3.33] $W\ m^{-2}$ (Figure 1.1) (IPCC, 2013b).

Figure 1.1: Radiative forcing estimates in 2011 relative to 1750 and aggregated uncertainties for the main drivers of climate change (IPCC, 2014a).

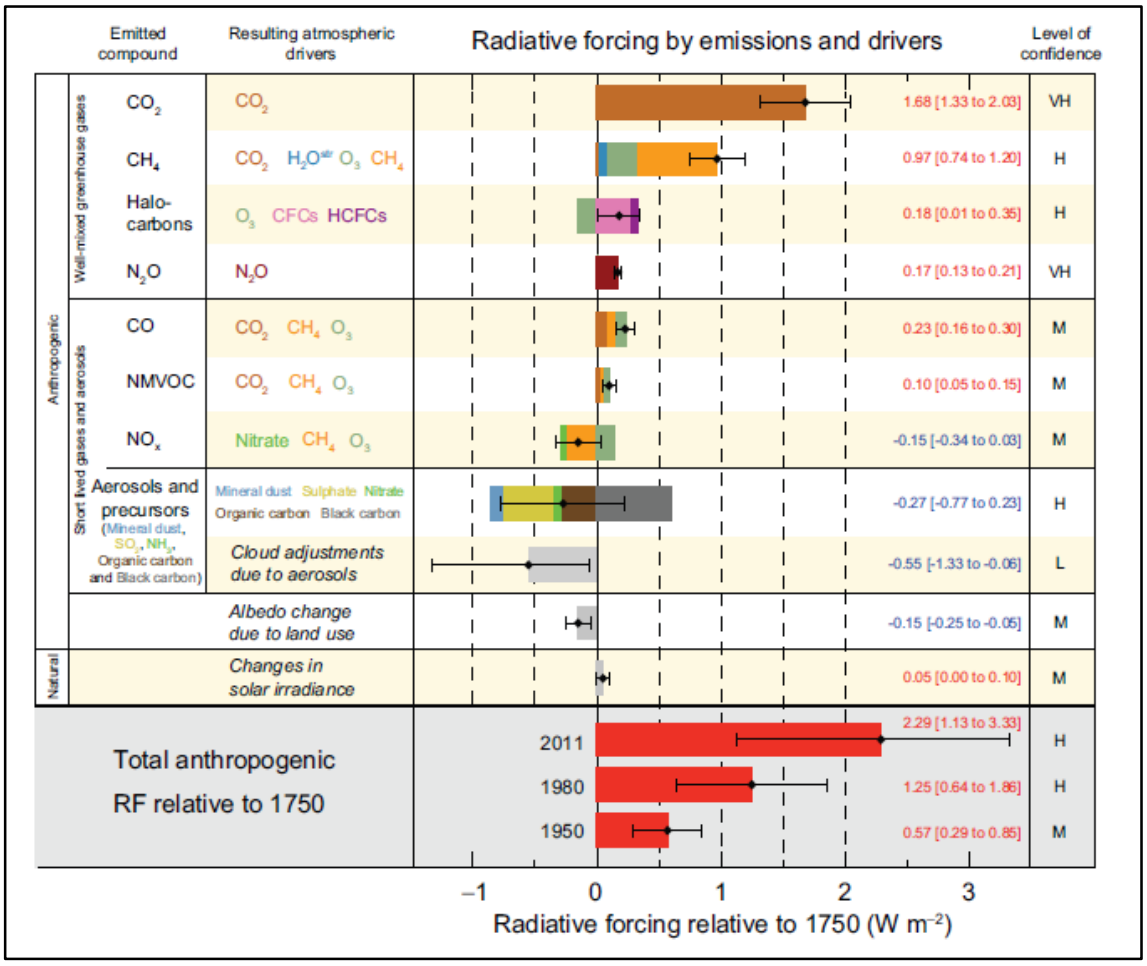

Radiative forcing (RF) is defined as the change in net downward flux of both shortwave (ultra violet) and longwave (infrared) radiation (incoming minus outgoing) at the tropopause (in W m^{-2}), after allowing for stratospheric temperatures to readjust to radiative equilibrium, while holding other state variables fixed at unperturbed values, e.g. tropospheric temperatures, water vapour and cloud cover (Ramaswamy et al., 2007; Forster et al., 2007; Stocker et al., 2014). Through assessment of the radiative forcing a positive value indicated a net warming influence, while a negative value indicates a cooling influence.

1.1.1 Drivers of anthropogenic climate change

Figure 1.1 and Figure 1.2 present anthropogenic drivers of climate change, split in to the following groups: well mixed GHGs; short lived gases; aerosols and precursors; and others (Stocker et al., 2014).

Figure 1.2: Radiative forcing (RF) of climate change during the Industrial era shown by emitted components from 1750 to 2011 – taken from Stocker et al. (2014).

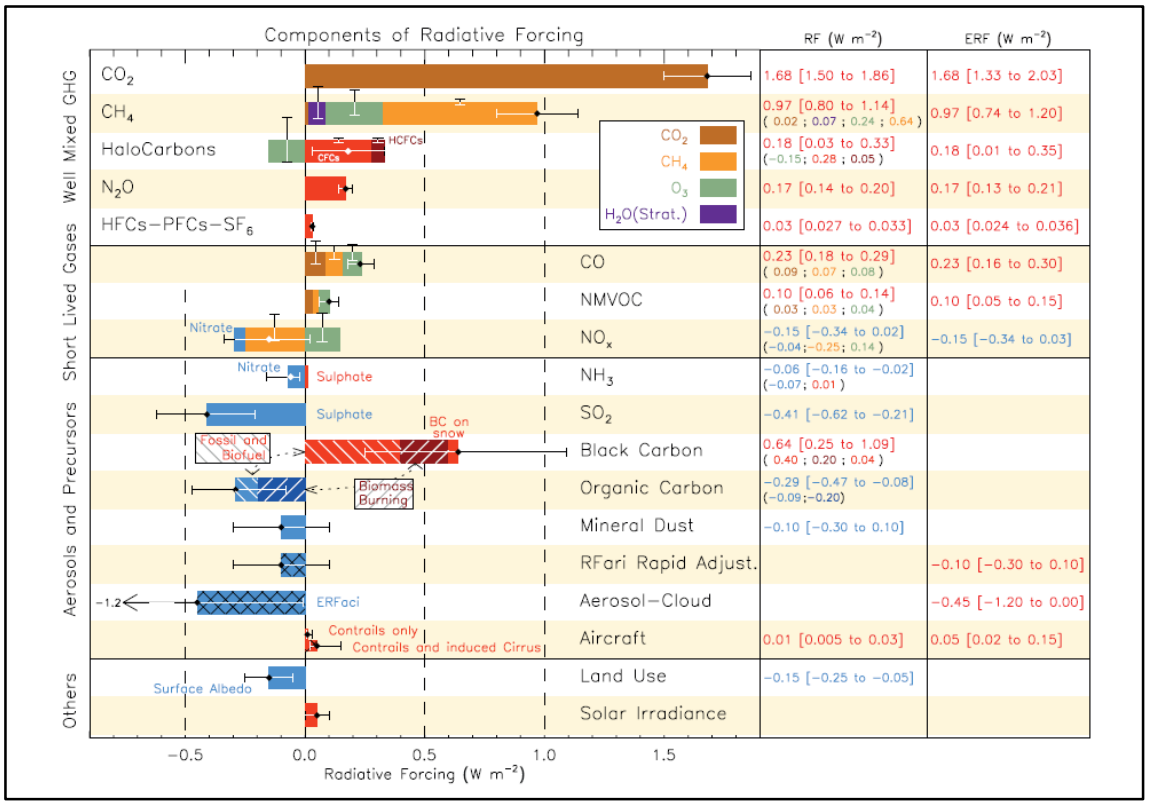

In relation to the pre-industrial era (2011–1750) well-mixed GHGs (CO_2, CH_4, halocarbons, N_2O and HFCs (hydrofluorocarbons) and PFCs (perfluorocarbons)), return a combined RF of 3.03 [2.497 to 3.563] W m^{-2}. Short lived gases (CO (carbon monoxide), NMHCs (non-methyl volatile hydrocarbons) and NO_X (nitrogen oxides)) return a RF of 0.18 [–0.1 to 0.45] W m^{-2}. Aerosols and their precursors give a net RF of –0.21 [–1.295 to +0.91] W m^{-2}, while land use changes result in a cooling effect of –0.15 [–0.25 to –0.05] W m^{-2} (Stocker et al., 2014).

From Figure 1.1 the different emitted anthropogenic components can be identified, along with their resulting atmospheric drivers, e.g. the emission of NO_X result in changes in concentrations of nitrates (NO_3^-), CH_4 and ozone (O_3). These emitted components have the capacity to perturb the RF at the top-of-the-atmosphere (TOA). Importantly Figure 1.1 shows that human activities have both warming and cooling influences (IPCC, 2014a). Additionally, Figure 1.1 highlights the uncertainty in estimated RF for each anthropogenic emitted compound due to current levels of scientific understanding (IPCC, 2014a).

When considering future projected decreases in global anthropogenic SO_2 emissions between 2000 and 2100, in tandem with projected increases in global ammonia (NH_3) emissions (Bellouin et al., 2011; Lamarque et al., 2011) nitrate aerosols have the potential to become the more dominant forcing component in the future. Hauglustaine et al. (2014) estimated that by 2050 the global sulfate burden could be reduced by between 14.3–35.7% accompanied by an increase in the global nitrate burden between 11.1–33.3%, while estimating that in 2100 the global sulfate burden could reduce by between 40.5–47.6% accompanied by an increases in the global nitrate burden of up to 38.9%. Taking this in to account consideration of the atmospheric, climate and air quality impacts of anthropogenic-induced nitrates will be of importance. As such future atmospheric and climate assessments would be well placed when they are capable of considering the formation of nitrate aerosols (as such this thesis will be using the nitrate-extended version of the TOMCAT-GLOMAP-mode coupled model).

Fossil fuels have powered an explosive rise and growth of industrial civilisations since the 1850s (Mathews, 2010) emitting greenhouse gases (GHGs), such as CO_2, CH_4 and N_2O which have been increasing as industrial and human growth continues (Bala et al., 2013). This rise in atmospheric CO_2 concentrations since the industrial revolution is heavily influenced by anthropogenic emissions of CO_2 from fossil fuel combustion and cement production (IPCC, 2014b). The U.S. Energy Information Administration (EIA) estimated World energy consumption could increase by 49% in 2035 in relation to 2007 levels of consumption. Resulting in CO_2 emissions levels reaching 33.8 $GtCO_2$ by 2020 and 42.4 $GtCO_2$ by 2035 (U.S. Energy Information Administration, 2010), compared to current (2009) emission levels of 31.2 $GtCO_2$ (The Royal Society, September 2009).

Since the pre-industrial era (1750) a O_3 RF of 0.35 W m^{-2} has been estimated for 2011 (Stocker et al., 2014), while present day radiative effect (RE) tropospheric O_3 estimates stand at 1.17 W m^{-2} (Rap et al., 2015), i.e. the radiative effect from ozone due to present day atmosphere (Rap et al., 2013). As per Rap et al. (2015) the tropospheric O_3 RE is defined as the as the radiative flux imbalance between the incoming SW solar radiation and the outgoing LW infrared

radiation resulting from the presence of all (natural and anthropogenic) tropospheric ozone. The RE differs from the RF metric. The RF is essentially the change in RE over time, calculated between the PI and PD (Rap et al., 2015).

Since the pre-industrial era O_3 concentrations in the Northern Hemisphere (NH) have more than doubled to 35–40 ppbv, with peak values exceeding WHO (World Health Organization) guideline values of 50 ppbv (Royal Society, 2008) (Figure 1.3). Figure 1.3 shows that over the NH anthropogenic emissions have increased background O_3 concentrations by around 40–55%, with some regions (South-east China, East India, South-east and the Western coast of the United States) seeing anthropogenic contributions to increases in background O_3 of between 55–65% (Royal Society, 2008).

Figure 1.3: Multi-model mean surface global surface ozone concentrations: for pre-industrial times (top-right), present-day (top-left), difference between present-day and pre-industrial (bottom-left) and percentage increase attributable to anthropogenic sources (bottom-right) **(Royal Society, 2008).**

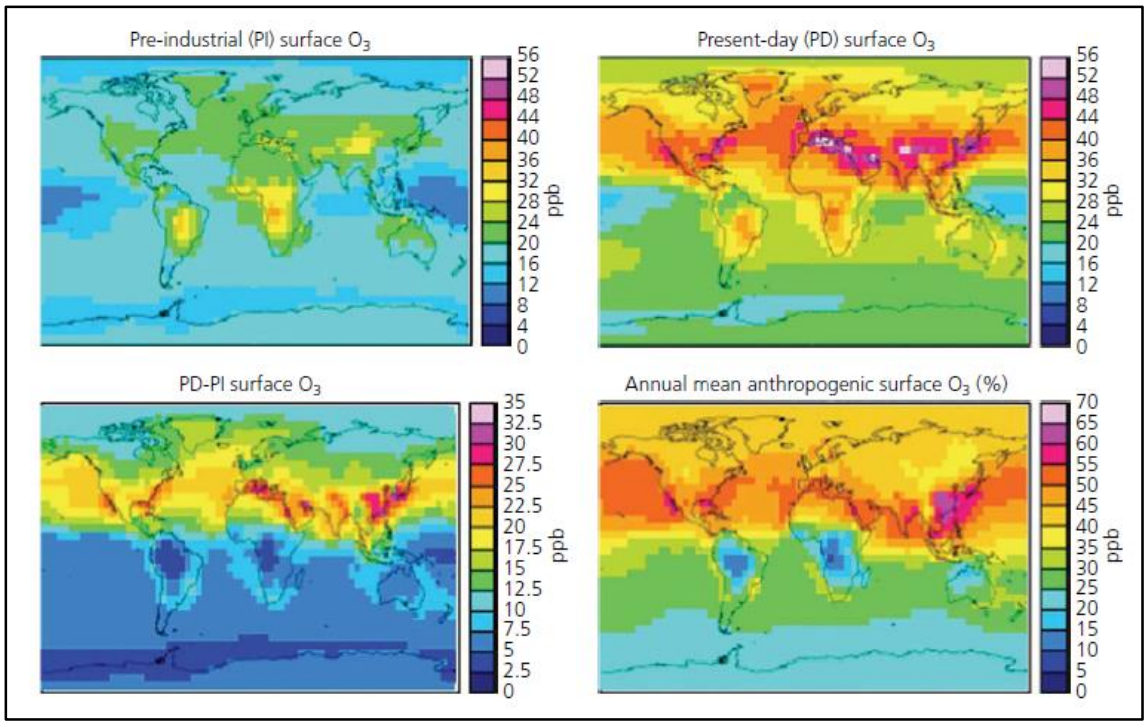

1.1.2 Observed changes and the projected consequences of anthropogenic climate change

Anthropogenic influenced changes in the RF result in climatic impacts. Over the period of 1880–2012 the combined land and ocean surface temperature has warmed by 0.85 [0.65–1.06] °C (IPCC, 2014a). The Fifth Assessment Report (AR5) produced by Working Group 1

(WG1) of the Integrated Panel on Climate Change (IPCC) stated in its Summary for Policymakers that "*It is extremely likely that human influence has been the dominant cause of the observed warming since the mid-20th century.*" Where their term extremely likely denotes a confidence level of 95–100% (IPCC, 2013b). A view reflected by 97.1% of the scientific literature investigating the impact of anthropogenic activity, where the consensus is that the rise in global average temperatures witnessed is of an anthropogenic nature, i.e. human influenced (Cook et al., 2013).

Increases in global mean surface temperatures (Rhein et al., 2013) driven by increases in anthropogenic emissions, rises in the global average sea level of ~200 mm due to melting of Northern Hemisphere ice-caps, sea-ice, glaciers and thermal expansion of sea water have been seen (IPCC, 2013b; Houghton, 2009). Additionally over the Northern Hemisphere decreases in snow cover of ~2 million km^2 has been estimated, occurring mainly at the Poles and Greenland (IPCC, 2007b), with the potential to result in the melting of permafrost and an associated release of methane (P. Lemke et al., 2007). Since the 1950s Arctic sea ice has been diminishing (Vinnikov et al., 1999), reaching a minima in coverage of $10.5x10^6$ km^2 in 2011 (Vaughan et al., 2013); indicating a reduction in 2.38 [± 0.05] $x10^6$ km^2 of coverage below the 1979–2000 minima (Jacobson et al., 2012). Reductions in sea ice and snow cover can result in the aforementioned release of methane from permafrost, and a reduction in surface albedo (Jacobson et al., 2012; Burroughs, 2007), which feeds back in to the system further enhancing temperatures and further increasing ice loss and perpetuating the cycle, i.e. a positive feedback loop (Burroughs, 2007).

Rogner and Zhou (2007) reported that over a 30 year period global GHG emissions had been increasing at a rate of 1.6 ppm yr^{-1} and that without adaptations to current policies and the implementation of binding agreements this rate is set to increase; increases that have since been seen. Alexander et al. (2013) have since reported that there has been a 7.5% increase in the radiative forcing from GHGs from 2005 to 2011, with CO_2 attributable for 80% of this increase. In light of this, it is acknowledged that mitigating global atmospheric GHG concentrations to within 450–550 ppm by 2050 gives the global community a 50% chance of limiting mean global temperature changes to 2 ˚C by 2100 (if the 450 ppm target is met) (Jowit and Wintour, 2008; Stern, 2006; CENEX, Undated; G.A. Meehl et al., 2007).

With current increases in global emissions and the high levels of uncertainty in the climate sensitivity (Figure 1.4) the actual climatic impacts of a doubling in atmospheric CO_2 concentrations could be far greater (Meehl et al., 2007).

Figure 1.4: PDF distributions of mean temperature responses to a doubling of CO_2 (constrained by the transient evolution of the atmospheric temperature, radiative forcing and ocean heat uptake) (Meehl et al., 2007).

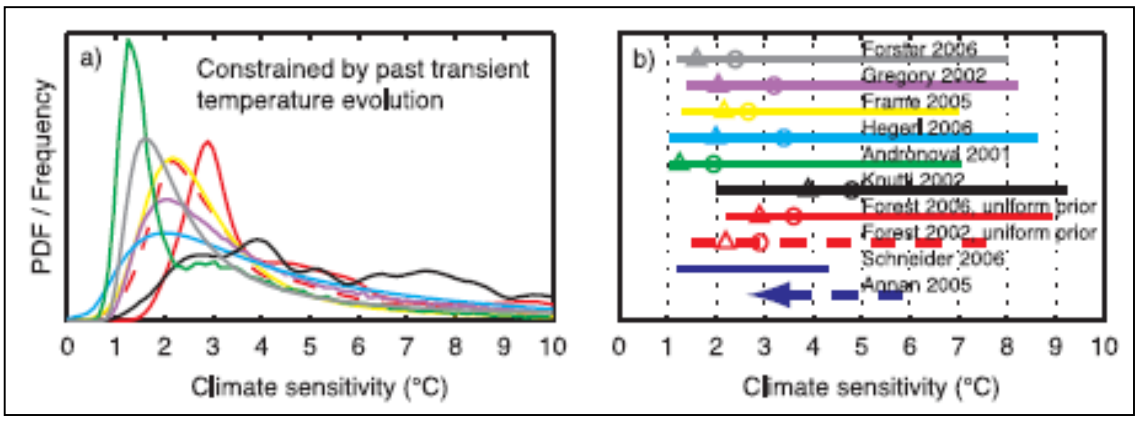

The climate impacts on vegetation and crop development through changes to the agricultural calendar have already been observed (Challinor, 2011; IPCC, 2007a), furthermore global mean temperature, sea level and snow cover will affect human life, increasing flood risks (Hall et al., 2003), extreme weather events, the distribution of impacts, large-scale singular events (IPCC, 2014a), and in extreme conditions changes to the Thermohaline Circulation (Houghton, 2009).

With current trends and increases in global greenhouse (GHG) emissions (Bala et al., 2013; NOAA, August 2015) there is a risk the global mean temperatures could rise to a level not seen for the last 45 million years (Mayewski et al., 2009), i.e. mean global temperatures could rise by over 4 °C and up to 4.8 °C, dependant on the Representative Concentration Pathway (RCP) the global community follows (Mayewski et al., 2009; Arblaster et al., 2013). RCPs (representative concentration pathways) are scenarios that consider time series emissions and concentrations of the full suite of GHGs, aerosols, chemically active gases, along with land use/cover. These have been used by the IPCC and associated CMIP5 (5^{th} Coupled Model Intercomparison Project) models to investigate the climatic impacts up until 2100 via RCP2.6, RCP4.5, RCP6.0 and RCP8.5; where the change in radiative forcing by 2100 is given in the RCP scenario suffix (IPCC, 2013a).

Current range of projections show in the near-term future according to RCP4.5 the projected global mean surface temperature rises in 2020, 2030 and 2050 could be between ~0.25 to ~0.9 °C, 0.5 to ~1.25 °C, and between 0.8 to ~1.9 °C respectively; within the 5–95% confidence range (Adedoyin et al., 2013). By 2100 the likely result will be that the global mean temperature will witness a rise in temperature ranging between 0.3–4.8 °C, as demonstrated by Figure 1.5 (Arblaster et al., 2013).

Figure 1.5: Time series of global annual mean surface air temperature anomalies (relative to 1986–2005) from CMIP5 (Arblaster et al., 2013).

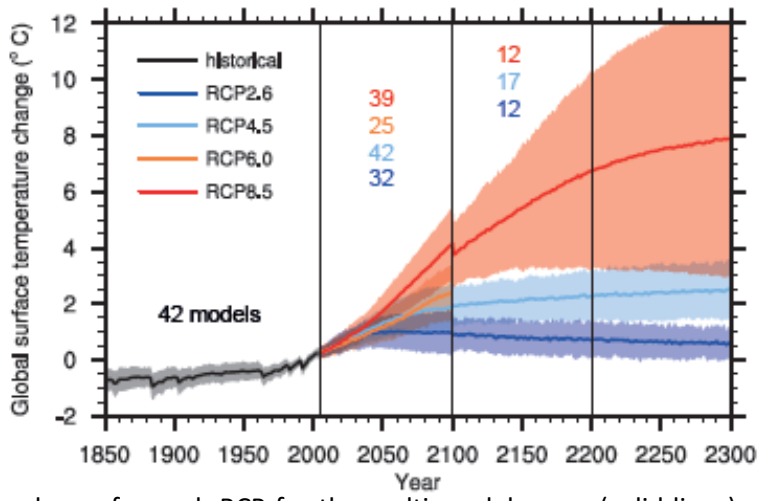

Projections are shown for each RCP for the multi model mean (solid lines) and the 5–95% range (±1.64 standard deviation) across the distribution of individual models (shading).

The CMIP5 models have projected increases in sea surface temperature ranging between 1 °C for RCP2.6 to >3 °C for RCP8.5 for the 2081–2100 time period, in relation to the 1986–2005 time period. For the same time period a reduction in sea-ice extent is projected of between 8% for RCP2.6 to 34% for RCP8.5 for February, with this range in September increasing to 43% for RCP2.6 to 94% for RCP8.5 (Arblaster et al., 2013). Which in turn (along with other climate feedback responses) could result in a rise in global mean sea level for the 2081–2100 time period (in relation to the 1986–2005 time period) between 0.26–0.82 m (IPCC, 2013b).

1.1.3 Political discussions relating to anthropogenic climate change

Without changes to the rates at which anthropogenic emissions are released, land use change, adequate policies put in to place to force industry to act, projected patterns of growth, their associated release of CO_2 emissions could be very high (IPCC, 2013b; Arblaster et al., 2013). Under this case anthropogenic climate change is likely to get far worse by the end of the century (Figure 1.5) (Meehl et al., 2007; Arblaster et al., 2013). In order to achieve these changes the link between energy consumption and economic growth needs clarifying, as this will determine future policies and whether they will have impacts on economic growth (Mahadevan and Asafu-Adjaye, 2007).

Many nations still have voluntary targets with the need for more nations to adopt legally binding reduction targets, like here in the UK and in the EU (Department of Energy and Climate Change, 2008; Department of Trade and Industry, May 2007; Commission of the European Communitites, 2009), the need for change is far greater than realised. More countries need to

adopt clear goals and emissions reduction targets. This change needs to occur in not just in one sector, but across the board.

Stern (2015) discusses that one of the main obstacles that exists is the limited understanding of the feasibility and potential of a low-carbon path. Where with wise investment and the commitment to foster innovation a transition to a low-carbon economy can be achieved. One which combines economic growth with climate and environmental responsibility can be achieved. The movement to a low-carbon economy will not only allow for global reductions in CO_2 emissions, but also for the reduction in the global non-CO_2 emissions; particularly in the case where combustion processes are involved.

At the eagerly awaited COP21 to be held in Paris, France this year (2015) it is hoped that a universal climate agreement can be achieved, and brought in to force in 2020. Leading up to COP21, at the G7 summit meeting held in Krün, Germany G7 leading industrial nations have agreed to cut GHG emissions by phasing out fossil fuel use through decarbonising the global economy by the end of the century (Connolly, 2015). Additionally six major energy companies have written to the United Nations asking for help setting up a carbon pricing scheme (Johnson, 2015); which could be construed as an indicator that energy companies will act, but only with policy intervention.

The aviation sector acknowledges that change is required, i.e. reductions in emissions and improvements in technologies, due to projected increases in aviation growth and aviation-induced O_3 increases resulting from aviation-NO_X (Penner et al., 1999). The aviation industry believes that emission reductions can be realised through: the use of alternative fuels; improvements in operations and managements; and through changes in technologies and aircraft design which could implemented in the long-term future (Penner et al., 1999; Department for Transport, July 2009; ACARE, 2011; European Commission, January 2001; Committee on Climate Change, December 2009; Sustainable Aviation, 2011).

In 2007 IATA (International Air Transport Association) laid out an environmental vision to mitigate GHG emissions from aviation via a four-pillar strategy consisting of: improved technologies; effective operations; efficient infrastructure and; positive economic measures (IATA, August 2009). In January 2012 aviation was included within the EU ETS (European Union Emissions Trading Scheme), limited to all flights from, to and within the EEA (European Economic Area) (European Commission, 2015).

1.2 Growth in the transport sector

In 2000 the transport sector was responsible for 16.09% of the world's GHG emissions, which according to the World Bank's Development Indicators equated to 4.57 $GtCO_2$, (Figure 1.6) (The Shift Project Data Portal, Undated).

Over the 20th century, cumulative emissions from the transport sector were 184.24 $GtCO_2$, with road transport [114.49 $GtCO_2$; 55.1%] dominating over maritime [31.94 $GtCO_2$; 15.4%], rail [20.91 $GtCO_2$; 10.1%] and aviation [16.89 $GtCO_2$; 8.1%]. Historically, shipping dominated until the growth of road transport, circa 1910. In the 1930s aviation started to contribute to emission from the transport sectors, with large rates of growth seen after the 1960s (Uherek et al., 2010; Fuglestvedt et al., 2008).

Figure 1.6: Sectoral breakdown of global greenhouse gas emissions in 2000 (The Shift Project Data Portal, Undated).

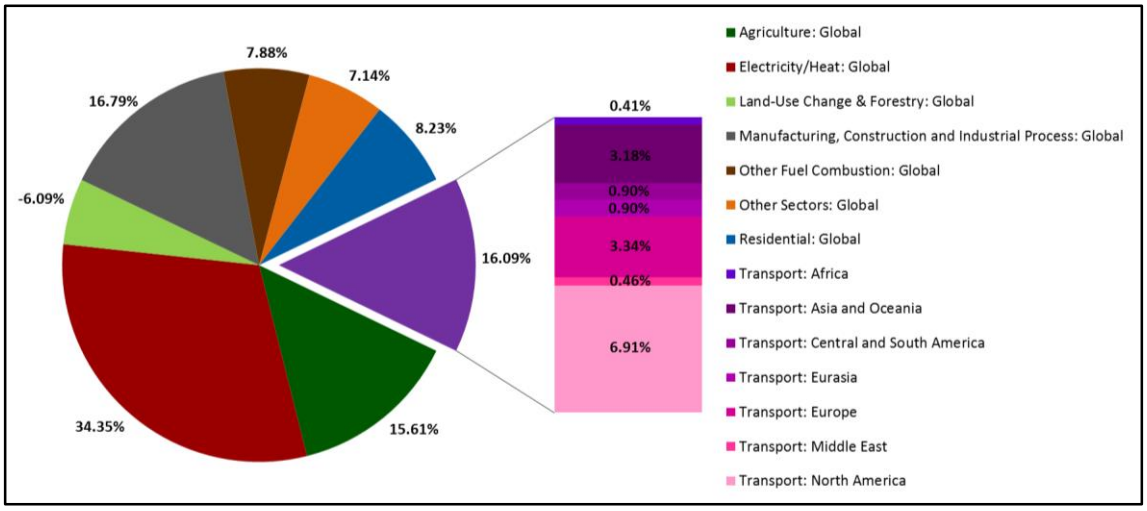

Between 1990 and 2006 the European Environmental Agency report an increase in GHG emissions from transportation of ~26%; with transportation being estimated to contribute 23.8% of all GHG emissions within the EU-27 member states (European Commission, 2009c).

Since 1973 the global transport sector has increased from being accountable for 23% of world's total final energy consumption to 27% in 2011. In 2011 transport's contribution to total final energy consumption (i.e. total end energy consumption from all sectors) was broken down as: 62% of final oil consumption; 5% of total biofuels, 2% of natural gas consumption and; 2% of electricity consumption (IEA, 2014).

The transport sector is set to continue to grow. By 2050 it is estimated that there will be an estimated 3–4 fold increase in global mobility (passenger-kilometres travelled) in relation to a year 2000 baseline, resulting from an increase in global population of 6 billion in 2000 to 9

billion by 2050, coupled to social drivers such as increases in GDP, economic growth and increases in tourism (Penner et al., 1999; Sausen, 2002; ITF, 2011). But associated CO_2 emissions are estimated to rise to a lesser extent (by a factor of 2.5–3) due to continuing improvements in fuel economy (ITF, 2011).

1.3 Growth in aviation

Despite aviation being a relatively young form of transport (compared with rail, shipping and road transport), the aviation industry has undergone rapid growth and this growth is seen as critical component of the global economic infrastructure (Penner et al., 1999; Clarke, 2003). Aviation (as per 2014 figures) contributes 3.2% of the World's GDP (Gross Domestic Product). Global GDP is forecast to rise by 3.2% over the next 20 years, projected to drive passenger traffic growth by 5.0% a^{-1} (Boeing).

Aviation is the fastest growing fossil fuel based sector (Unger, 2011). Since the 1960s until the mid-1990s it had grown at nearly 9% yr^{-1} equating to 2.4 times the average GDP over the same period (Penner et al., 1999). The International Civil Aviation Organization (ICAO) and industrial sources suggesting that RPK will grow over the next 20 years at a rate of 4.5-6% yr^{-1}, causing passenger traffic to double every 15 years (Lee et al., 2009). Under this rate of growth a near doubling of civil aviation could result in a growth in the civil aviation fleet from ~20,500 (in 2006) to 40,500 (in 2026) (Kreutz et al., 2008; Gudmundsson and Anger, 2012), along with a 3.5 fold increase by 2050 (Gudmundsson and Anger, 2012).

Owen et al. (2010) investigated projected increases in aviation-borne CO_2 and NO_X emissions using the emissions derived from the QUANTIFY Integrated Project, which considers a range of IPCC SRES (special report on emission scenarios) scenarios. It is projected that aviation-borne CO_2 emissions will increase by a factor of 1.59 by 2020, a factor ranging between 1.51–3.57 by 2050, and a factor ranging between 1.06–7.48 by 2100. Aviation borne NO_X emissions are projected to increase by a factor of 1.38 by 2020, a factor ranging between 0.90–2.59 by 2050, and factor ranging between 0.62–5.41 by 2100.

Aviation growth driven by economic and social factors in the absence of policy intervention and industry action growth in civil aviation has the potential to grow unabated (Penner et al., 1999), along with the potential to further contribute to global warming and climate change. Bodies such as ACARE (Advisory Council for Aeronautics Research in Europe), the EC (European Commission) and the Committee on Climate Change (CCC) investigate how the aviation sector can progress in this changing environment. ACARE, the EC and the CCC have all investigated

growth in aviation, its economic and societal contributions along with how technological and operational changes, and innovation (European Commission, January 2001; ACARE, June 2010; ACARE, 2011; Committee on Climate Change, December 2009) can help aviation reach industry goals of reducing aviation CO_2 emissions to 50%; as discussed by ATAG (Air Transport Action Group) (ATAG, 2011).

1.4 Aviation emissions

Aviation emissions have the capacity to alter the composition of the atmosphere, varying concentrations of gas- and aerosol-phase species, resulting in perturbations to the Earth's radiative balance (Lee et al., 2010; Myhre et al., 2011). The extent of this change is driven by the array of species emitted by the sector (Lee et al., 2009; Owen et al., 2010; Eyers et al., 2004; Kim et al., 2007; Wilkerson et al., 2010; DuBois and Paynter, 2006; Wayson et al., 2009; Knighton et al., 2007; Yelvington et al., 2007; Anderson et al., 2006) and the altitudinal distribution of these emission species (Olsen et al., 2013b), in comparison to other forms of transport (Quantify Integrated Project, 2005-2012).

Aviation is responsible for the release of both CO_2 and non-CO_2 emissions. Non-CO_2 emission chemical species released by aviation include NO_X, H_2O, CO, HCs (hydrocarbons), SO_2 (sulfur dioxide), BC (black carbon) and OC (organic carbon). This thesis concentrates on the changes these aviation-borne non-CO_2 emission species induce in the troposphere, health effects due to perturbation in air quality and resulting climatic impacts.

Theoretically the complete combustion of kerosene (with a theoretical chemical composition of C_nH_m + S (Lee et al., 2009)), results in the release of CO_2, H_2O, N_2, O_2, and SO_2, but in reality complete combustion does not occur leading to more actual products of combustion: CO_2, H_2O, N_2, O_2, NO_X, CO, HCs, BC, OC and SO_2 (Lee et al., 2009; Bond et al., 2004) (described in greater detail Section 2.2 and illustrated in Figure 2.6). The NASA EXCAVATE (EXperiment to Characterize Aircraft Volatile Aerosol and Trace-species Emissions) experiment identified that aviation is responsible for the emission of 33 hydrocarbon species (Anderson et al., 2006). The historical emissions dataset for the CMIP5 model simulations used by the IPCC 5th Assessment Report typically only included NO_X and BC aviation emissions (Lamarque et al., 2009). Recently there have been efforts to include aviation emissions of HCs, CO and SO_2 in aviation emission inventories (Wilkerson et al., 2010; Eyers et al., 2004). The development of aviation emission inventories to include a greater array of gas- and aerosol-phase perturbing species is fundamental to gaining a better understanding of aviation-induced perturbations in the UTLS

(upper troposphere and lower stratosphere) which cannot simply be calculated from aviation-borne involving NO_X emissions alone (Pitari et al., 2002).

Akin to land-based transportation aviation emissions vary on a horizontal plane, but in addition on a vertical plane too; entering the atmosphere at a variety of altitudes. This vertical distribution allows emissions to enter the UTLS, where O_3 production efficiency (OPE) may be enhanced, as a result of lower background NO_X and NMHCs concentrations at these altitudes (Olsen et al., 2013b; Hoor et al., 2009; Koffi et al., 2010; Meilinger et al., 2001; Quantify Integrated Project, 2005-2012; Lamarque et al., 2010b; Snijders and Melkers, 2011). Additionally when aerosol species enter at the troposphere at higher altitudes, aerosol lifetimes can be increased as previously evaluated when considering explosive volcanic SO_2 emissions and associated sulfate formation in the free troposphere (Schmidt et al., 2012). This increase in aerosol lifetime is primarily due to the altitude of release of the majority of aviation emissions (i.e. in to the free troposphere), whereas anthropogenic emissions are generally entrained in the planetary boundary layer where species experience reduced lifetimes (Graf et al., 1998; Stevenson et al., 2003).

1.5 Impacts of the aviation sector on climate, air quality and human health

Many previous studies have focused on the climatic impacts of aviation (Penner et al., 1999; Lee et al., 2009; Lee et al., 2010; Sausen, 2002), but aviation is also known to affect air quality, and as a result human health (Barrett et al., 2010; Barrett et al., 2012; Yim et al., 2015).

1.5.1 Aviation's impact on climate

The total radiative forcing (RF) contribution from aviation (excluding aviation induced-cirrus) has been assessed at 55 [23–87] mW m^{-2} (90% likelihood range) (Lee et al., 2009) (i.e. providing a net warming effect), equating to 2.40% [1.00–3.80%] of total anthropogenic radiative forcing (Lee et al., 2009; Myhre et al., 2013). When aviation-induced cirrus clouds are included, aviation is estimated to provide 78 [28–139] mW m^{-2} (90% likelihood range) (Lee et al., 2009). Indicating aviation's contribution to total global anthropogenic forcing could be as high as 3.41% [1.22–6.07%] (Lee et al., 2009; Myhre et al., 2013).

Breaking this down (Lee et al., 2009) assess that CO_2, NO_X via the production of O_3 and CH_4 destruction, BC and aviation-induced cirrus cloudiness provide warming effects of 28.0 mW m^{-2}, 13.8 mW m^{-2}, 3.4 mW m^{-2} and 33.0 mW m^{-2} respectively, with sulphate aerosols providing a cooling effect of 4.8 mW m^{-2} (Lee et al., 2009). As comprehensive as Lee et al. (2009)'s

assessment is, assessing aviation's climatic impact is a complex task. Lee et al. (2009) does not investigate the cooling effect of nitrate aerosols via the aerosol direct effect or aerosol first indirect effect, nor include the effect of aviation-borne speciated hydrocarbons; which are precursors for O_3 formation.

With a projected doubling in civil aviation by 2026 relative to 2006 (Kreutz et al., 2008) (as discussed in Section 1.3), aviation is one of the fastest growing transport sectors. In tandem with the upper troposphere's greater levels of sensitivity towards O_3 production and aerosol lifetime, aviation has the potential to increase its percentage contribution of total anthropogenic forcing.

Industry targets set by ACARE aim to reduce aviation CO_2 and NO_X emissions, along with perceived sound, i.e. noise pollution (Sustainable Aviation, Undated-a; ACARE, 2011). These targets specifically aim to reduce CO_2 and NO_X, but will ideally return additional reductions in CO_2, HCs, SO_2, BC and OC. These additional reductions will be achieved through reductions in fuelburn and improvements in efficiency.

Along with improvements in combustion, the use of alternative fuels in the aviation sector is being investigated. The use of FT (Fischer-Tropsch) and FAMEs (fatty acid methyl esters) have the potential to reduce aviation NO_X, CO, BC and OC emissions, while primarily increasing emissions of speciated HCs (depending on fuel and fuel blend) (Lobo et al., 2011; Timko et al., 2011). This is due to both changes in species specific emissions indices (EI_x) and fuelburn adjustment factors applied in order to maintain the same energy content as currently required. Emissions indexes (EI_x) represent the amount of specie of interest (x) emitted per kg of aviation fuel combusted.

Additionally the use of FT and FAMEs fuel blends have the potential to reduce the number of BC and OC particles emitted In the case of FAMEs fuel blends the geometric mean diameter of the emitted BCOC can potentially increase. Changes like this can potentially affect the associated aerosol direct radiative and aerosol cloud albedo effects. The aerosol direct and aerosol cloud albedo effects from aviation are also related to the sulfur content of the resulting fuel blend. Alternative fuel blends have a fuel sulfur content (FSC) related to the fraction of kerosene in the fuel blend. Reductions in the amount of kerosene (Jet A/Jet A-1) in the fuel blend will reduce sulfates formed from aviation emissions, and therefore the cooling aerosol cloud albedo effect imparted by aviation. This reduction in FSC will also result in the warming effect induced by the aerosol direct radiative effect.

Reductions in emissions resulting from the use of alternative fuels in aviation will be dependent on the type of fuel used, due to their varying life-cycle GHG emissions. Where full life-cycle emissions consider emissions from the complete fuel cycle; recovery and transportation of feedstock, production, processing, transportation and distribution to combustion (Stratton et al., June 2010).

Stratton et al. (June 2010) assessed numerous alternative fuels, and found a range of lifecycle CO_2e (carbon dioxide equivalent) emissions ranging from –2.0 $gCO_2e\ MJ^{-1}$ to 698.0 $gCO_2e\ MJ^{-1}$, compared to lifecycle emissions of Jet A/Jet A-1 at 80.7 $gCO_2e\ MJ^{-1}$ (in 2013) (Winchester et al., 2013). Through use of the CO_2e metric the impact of different GHGs in terms of the amount of CO_2 that would result in the same amount of warming can be evaluated. Largest lifecycle emissions arise from fuels that require large land-use changes, such as Palm oil to HRJ (Hydroprocessed Renewable Jet) fuel (Stratton et al., June 2010).

Due to the increased costs associated with alternative fuels, with a cost of \$2.69 gal^{-1} for HEFA (hydroprocessed esters and fatty acid) fuels compared to \$0.35 gal^{-1} for Jet A/Jet A-1 in 2013, it is projected that the increased costs of operation will drive airline efficiency improvements. Along with subsides being provided to renewable fuel producers from airlines (Winchester et al., 2013).

1.5.2 Air quality and human health

In addition to climatic impacts, studies have shown that aviation can impact ground level air quality resulting in adverse human health impacts (Barrett et al., 2010; Woody et al., 2011; Barrett et al., 2012; Jacobson et al., 2013; Morita et al., 2014; Yim et al., 2015), due to aviation-induced O_3 (Seinfeld and Pandis, 2006; Penner et al., 1999; Lee et al., 2009; Lee et al., 2010) and particulate matter (PM) (Fowler et al., 1997; Jenkin and Clemitshaw, 2000; Wayne, 2000; Arrowsmith and Hedley, 1975; Committee on the Environment and Natural Resources, June 2000; Lee et al., 2009; Lee et al., 2010; Penner et al., 1999).

Aviation-induced increases in surface-layer $PM_{2.5}$ (particulate matter within a diameter of 2.5 µm) concentrations have been assessed as being responsible for increases in premature mortality from cardiopulmonary disease and cases of lung cancer (Barrett et al., 2010; Barrett et al., 2012; Yim et al., 2015). Additionally aviation-induced increases in surface-layer O_3 concentrations have been assessed for increases in premature mortality due to perturbations in ambient air quality (Yim et al., 2015).

Increases in ambient concentrations of aerosol species can cause adverse human health effects, with smaller size particulate matter ($PM_{2.5}$) penetrating deeper in to the respiratory system (Ostro, 2004; Löndahl et al., 2006; Kim et al., 2015). Epidemiological studies show that this can result in a range of PM induced health effects such as Increased hospital admissions from cardiopulmonary and respiratory disease, exacerbation in cases of asthma, increases in respiratory symptoms and other health outcomes such as missed work days (Ostro, 2004).

Human exposure to increased levels of O_3 is associated with increases hospital admissions and mortality (World Health Organisation, 2003), due to the exacerbation of respiratory ailments, increases in cases of cardiopulmonary disease and by inducing a variety of pulmonary effects (Brunekreef and Holgate, 2002; Bergamaschi et al., 2001).

Barrett et al. (2010) and Barrett et al. (2012) estimate that ground level increases in $PM_{2.5}$ from global aviation are responsible for ~10,000 mortalities a^{-1}. Yim et al. (2015) go on further to consider the impact aviation-induced $PM_{2.5}$ and O_3 on surface-layer ambient concentrations, assessing that global aviation is responsible for ~16,000 mortalities a^{-1} [90% CI: 8,300–24,000].

Strategies such the use of ultra-low sulfur jet (ULSJ) fuel have been suggested with a FSC of 15 ppm (Barrett et al., 2012) as opposed to a usual global average of 600 ppm (Wilkerson et al., 2010). The implementation of a ULSJ fuel strategy has been estimated to be capable of reducing aviation-induced premature mortalities by ~2,300 mortalities a^{-1} (Barrett et al., 2012). Additionally reductions in aviation fuel sulfur content will have effects on aviation-induced cooling through a reduction in the aerosol cloud albedo effect (aCAE), thus providing policy makers with difficult decision and potentially require them to make a trade-off between the health benefits and climate effects (Fiore et al., 2012).

1.6 How the aviation sector aims to reduce its emissions

The majority of climate policy focuses on reductions in CO_2 emissions (Department of Trade and Industry, May 2007; European Commission, 2011; Department of Energy and Climate Change, 2008). In addition to CO_2 emissions, non-CO_2 emissions have been shown to impact climate (Fiore et al., 2012; Lee et al., 2009; Stocker et al., 2014), air quality and human health (Fiore et al., 2012; Yim et al., 2015; Barrett et al., 2012; Woody et al., 2011). In order to deal with the air quality and health impacts of non-CO_2 emissions ambient air quality standards have already been put in place for NO_X (U.S. Environmental Protection Agency, 2014a; European Commission, 2009a), SO_2 (U.S. Environmental Protection Agency, 2014d; European Commission, 2009a), the secondary pollutant O_3 (U.S. Environmental Protection Agency,

2014b; U.S. Environmental Protection Agency, 2008), and $PM_{2.5}$ (U.S. Environmental Protection Agency, 2014c; European Commission, 2009a).

In light of projected rates of growth in global aviation (RPK) and the associated release of aviation borne emissions the aviation industry aims to reduce not only CO_2 emissions, but NO_X emissions in addition to perceived noise pollution; relative to year 2000 aircraft. These targets are set out by ACARE for 2020 and 2050 (presented in Table 1.1) (Sustainable Aviation, Undated-a; ACARE, 2011).

Table 1.1: Advisory Council for Aeronautics Research in Europe's (ACARE) carbon dioxide, nitrogen oxides and perceived reduction targets for 2020 and 2050, in relation in year 2000 (Sustainable Aviation, Undated-a; ACARE, 2011).

Pollutant	Year	
	2020	2050
CO_2	50%	75%
NO_X	80%	90%
Perceived noise	50%	65%

The industry aims to reduce aviation CO_2 emissions via the following five key mechanisms: Improvements in technology; improvements in operations; improvements in infrastructure; the use of economic measures (e.g. emissions trading schemes) and; the use of additional technologies and biofuels (Figure 1.7) (ATAG, 2011).

The use of biofuels has the potential to reduce net CO_2 emissions from the aviation industry, but has the risk of increasing the effects of some non-CO_2 emission species (Committee on Climate Change, December 2009). Section 7.3.1 shows that the use of alternative fuels has the potential to increase the release of some hydrocarbon species (Timko et al., 2011) as well increasing the geometric mean diameter (D_g) (Lobo et al., 2011).

To reduce the impact of aviation NO_X emissions improvements in engine design are being investigated (Committee on Climate Change, December 2009) in order to meet ACARE's targets (Table 1.1) (Sustainable Aviation, Undated-a; ACARE, 2011). Reductions in aviation CO_2 or NO_X emissions, may lead to an increase in other aviation-borne emission species (Committee on Climate Change, December 2009; Sustainable Aviation, September 2010); illustrating the complex relationship between CO_2 and NO_X formation during the combustion process. A simplified form of the Zeldovich mechanism (mechanism of the formation of thermal NO formation due to the production of reactive nitrogen from molecular nitrogen)

illustrates that reductions in reaction time and combustion temperature results in a reduction of thermal NO_X formed; where thermal NO_X denotes NO_X formed as a function of temperature (De Nevers, 2000). Whereas with the Brayton cycle (which describes the combustion process within a jet engine), to increase combustion efficiency the exit temperature from the combustor needs to be as high as possible (Eastop and McConkey, 1993); which would in turn increase NO_X emissions.

Figure 1.7: Aviation industry commitments to reduce emissions in line with 2050 targets (ATAG, 2011).

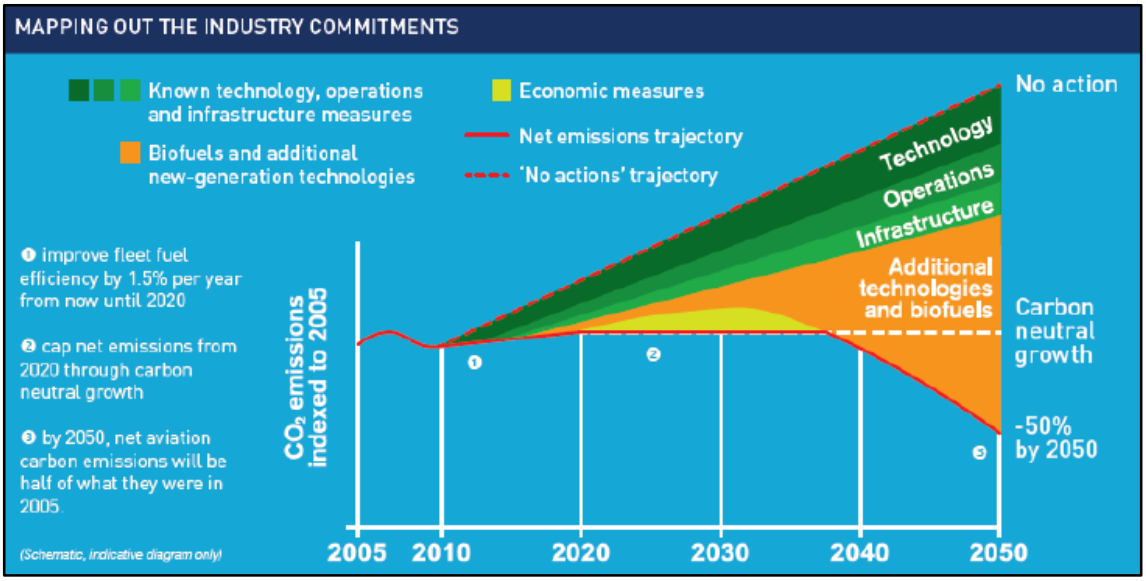

Technological improvements are seen to have the biggest prospect in aviation emissions reductions, through the development of revolutionary aircraft design and new engine advance, and the development of sustainable alternative jet fuels. Blended Wing Bodied (BWB) craft have been in development for the last 25 years and revolutionary designs like this, which are projected to increase aerodynamic efficiency by 30%, will be required to reduce fuel consumption, air and noise pollution from aviation by 2030 (Ordoukhanian and Madni, 2014; Nasir et al., 2014; Leifsson et al., 2013; Koster et al., 2012).

The development and use of sustainable alternative jet fuels are projected to play a key role in the reduction of aviation CO_2 emissions; offering a reduction in CO_2 emissions of 15–24% by 2050 based on a penetration of 25–40% in the global aviation fuel market (Sustainable Aviation, July 2013). Currently coal to liquid (CTL), gas to liquid (GTL), biomass to liquid (BTL) and hydrogenated oil derived alternative fuels are suitable for aviation at a blend of 50:50 (ASTM International, 2012a), with other fuels requiring technological adaptations (fatty acid methyl esters - FAMEs) and others requiring significant technological changes (such as hydrogen, methane and ethanol/methanol based fuels) (Sustainable Aviation, Undated-b). Technological improvements, and operational and management improvements have the

potential to reduce fuelburn and associated emissions of CO_2 (and non-CO_2 emissions) from aviation (Table 1.2) (ATAG, 2011; ATAG, 2014; Eurocontrol, March 2009; ATAG, May 2013; Edwards et al., 2015).

Table 1.2: Projected reductions in aviation carbon dioxide (CO_2) emissions from improvements in operational and management systems.

Aviation emissions reduction measure	Reduction in annual CO_2 emissions ($GtCO_2\ a^{-1}$)	Reference
Continuous decent approach (CDA)	0.5 (Europe)	ATAG (2014)
Air traffic management (ATM)	28 (Global)	Eurocontrol (March 2009) ATAG (May 2013)
Cost Index (CI) optimisation	7 (Global)	Edwards et al. (2015)

From tests conducted in Copenhagen, Denmark the implementation of a continuous descent approach (CDA) has the potential reduce European aviation CO_2 emissions by 0.5 $GtCO_2\ a^{-1}$ (ATAG, 2014; Eurocontrol, March 2009). The move from air traffic control (ATC) to air traffic management (ATM) paradigm has the potential to reduce global CO_2 emissions by 28 $GtCO_2\ a^{-1}$; returned through a projected reduction in fuel consumption of 9 Gt(fuel) a^{-1} due to reducing annual flight by $5x10^6$ hours a^{-1} (ATAG, May 2013). To achieve these savings cross-border arrangements along with the adoption of more efficient ATM operations driven by effective regulatory practices will be needed (ATAG, May 2013). Optimising operational tools such as the cost index (CI) could further reduce global aviation emission by 7 $GtCO_2\ a^{-1}$ (Edwards et al., 2015). Combining these three mechanisms annual CO_2 reductions from management and operational adjustments have the potential to reduce aviation's CO_2 emissions by 35.5 GtCO2 a^{-1} (ATAG, 2014; Eurocontrol, March 2009; ATAG, May 2013; Edwards et al., 2015).

Additionally changes in infrastructure have the potential to reduce delays, which can reduce operational costs, increase runway and airport capacity and provide the infrastructure to deal with new and larger aircraft. Additionally the use of next generation of air traffic management (ATM) systems will allow for fuel optimisation which reductions in departure delays (Dray, 2014; Forsyth, 2007; ATAG, 2014).

Economic measures have been identified as a key requirement for achieving carbon neutral growth from 2020 (ATAG, 2011; ATAG, 2014). There are two issues currently underlying the implementation such measures, that primarily these need to be global and secondarily if non-

CO_2 emissions and their effects are to be included the metrics utilised adequately represent them and the timeframe of their effects; as previously proposed metrics such as the Radiative Forcing Index (RFI) have been shown to exaggerate the climate impact of aviation emissions (Forster et al., 2006).

Despite adaptation of the aforementioned methodologies and mechanisms to reduce aviation emissions (Figure 1.7), reductions in ticket prices could arise due to reductions in operating costs and improvements in efficiency, resulting in a "rebound effect". Reduced ticket fares could result in an increase in flight demand, off-setting some of the emissions reductions the mechanisms outlined in Figure 1.7 could achieve (Evans and Schäfer, 2013; Evans, 2014).

1.7 Aims and objectives

Through use of the size-resolved atmospheric chemistry aerosol microphysics model, nitrate-extended version of the TOMCAT-GLOMAP-mode coupled model (GMV4-nitrate), this thesis aims to quantify the impact of aviation non-CO_2 emissions on atmospheric composition, climate, air quality and human health via the following key investigations:

- The baseline impact of an extended aviation emissions inventory (CMIP5-extened) on atmospheric composition (gas- and aerosol-phase species) and climate through the radiative effect (RE) metric. How these quantified impacts using CMIP5-extended compare to the impacts simulated using CMIP5 recommended historical aviation emissions for year 2000. Along with sensitivity studies to highlight the importance of including additional aviation-borne emissions species.
- An investigation on the impact variations in aviation fuel sulfur content (FSC) have on atmospheric composition, climate, air quality and human health. This study is influenced by strategies that have been proposed to reduce the human health impacts of aviation emissions, while investigating the climate impacts that occur alongside such strategies.
- Finally an investigation of the impacts the use of Fischer-Tropsch (FT) and Fatty Acid Methyl Ester (FAME) fuels within global civil aviation can have on atmospheric composition, climate, air quality and human health.

Aviation emissions within each study are provided through the CMIP-extended aviation emissions inventory developed in this thesis. CMIP5-extended uses the CMIP5 recommended historical aviation emissions inventory (Lamarque et al., 2009) to provide aviation NO_X and BC mass emissions, and through deriving aviation fuelburn calculates aviation CO, speciated HCs, SO_2 and OC emissions, as well as particle number.

2 Background and literature review

This section has two main objectives: introduce and discuss the background required to understand key aspects within this project, and to review key and recent literature in the field relating this thesis.

Section 2.1 discusses how gas- and aerosol-phase emission species, emitted directly or formed in the atmosphere, interact in the atmosphere and ultimately affect the Earth's climate.

Section 2.2 outlines the idealised products of combustion from aviation in comparison to its actual products of combustion, in order to allow this Chapter to home in on the interactions and processes aviation-borne emissions undergo.

Section 2.3 discusses the interactions of gas- and aerosol-phase emissions from aviation, secondary pollutants and other species that are formed, and how these interact with each other in the atmosphere.

Section 2.4 discusses aviation-induced perturbations in gas- and aerosol-phase species, associated aviation non-CO_2 emissions induced radiative effects (ozone direct radiative, aerosol direct radiative and cloud albedo effects), before summarising the radiative forcing impact of aviation using high impact key literature.

Section 2.5 investigates the history of, and specifications on aviation fuel (standard kerosene) currently in use in today's commercial civil aviation sector.

Section 2.6 discusses the impact of $PM_{2.5}$ and ozone on human health and vegetation, paying attention to how $PM_{2.5}$ can penetrate in to the human respiratory system and associated impacts.

A summary of this Chapter is provided in Section 2.7, before identifying the research aims and objectives of this thesis in Section 2.8.

2.1 Chemistry-climate interactions

This section provides an understanding on how gas-phase and aerosol-phase emission species, either directly emitted or formed in the atmosphere (i.e. emitted indirectly) by aviation, affect the climate; thus aiming to put in to context the science behind this work and how these species interact with incoming and outgoing radiation.

2.1.1 Climate interactions of gas-phase species

The Earth emits radiation in the infrared (IR), while radiation received from the Sun ranges from the ultraviolet (UV), visible to IR. Gas-phase species present in the atmosphere, from either natural or anthropogenic sources, interact with either incoming (shortwave) or outgoing IR radiation (Burroughs, 2007); thus introducing how aviation-borne primary or secondary gas-phase species can interact with the atmosphere and the Earth's mean energy balance (Alexander et al., 2013).

Figure 2.1: Earth's emissions spectrum in the infrared between wavelengths of 6.67 – 25 µm (wavenumber 1500 – 400 cm^{-1}) – taken from Houghton (2009).

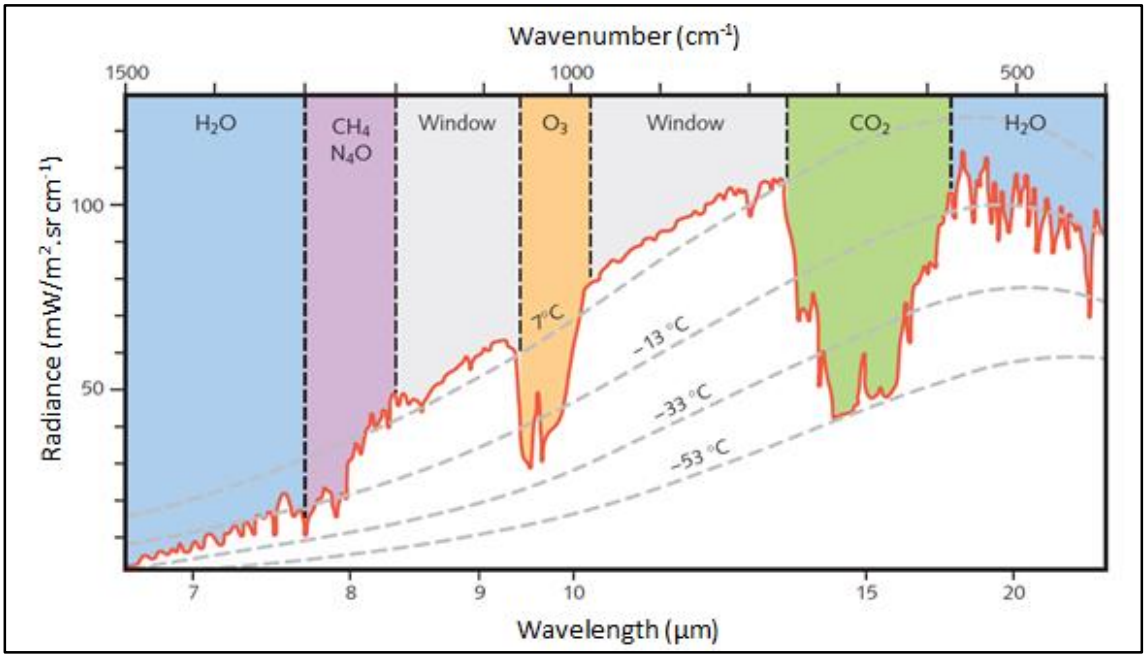

These radiatively active trace gases each have their own absorption and emissions properties which are dependent on their molecular structure, thus giving rise to their own and specific molecular spectrums which are made up of features referred to as spectral lines which form spectral bands, which occur at wavelengths specific to the different chemical specie of interest, e.g. referring to Figure 2.1 for carbon dioxide (CO_2) this is centred at ~15 µm (Burroughs, 2007).

It is the presence of Earth's atmospheric constituents and their spectral characteristics that give rise to the conditions that we have on Earth; which in turn has allowed life to develop (Berger, 2012).

Through the use of the Stefan-Boltzmann law (Equation 2.1) (Eastop and McConkey, 1993; Jacobson, 2002), which evaluates the rate of energy emitted by a non-black body ($\dot{E}$ in W m^{-2}) that the Earth's atmosphere has a substantial impact on the temperature on Earth. $\dot{E}$ is a function of the Earth's emissivity, i.e. measure of emission efficiency (ε), the Stefan-Boltzmann constant (σ in W m^{-2} K^{-4}) and temperature resulting in the derivation of the rate of energy emitted by a non-black body ($\dot{E}$ in W m^{-2}). Emissivity is related to the combined surface and atmospheric albedo (α) (Equation 2.2). Rearranging (Equation 2.1) and (Equation 2.2) and using $\dot{E}=S/4$ (where S represents incoming solar insolation of 1360 W m^{-2} (Alexander et al., 2013)) it can be demonstrated that without an atmosphere earth's temperature would be would be 255 K (–18 °C) (Burroughs, 2007; Berger, 2012) in comparison to the average surface temperature of Earth (T_s) of 288 K (+15 °C) (Jacobson, 2002; Berger, 2012).

$$\dot{E}=\varepsilon\sigma T^4$$

Equation 2.1

$$\varepsilon=(1-\alpha)$$

Equation 2.2

Thus it is seen that Earth's natural greenhouse gas effect has helped provide conditions suitable to life. In tandem this demonstrates how changes in concentrations in gas-phase species within Earth's atmosphere can affect the climate.

With changes in concentrations of these gas-phase species, due to natural sources and anthropogenic activities, there is the potential for rises in global mean temperatures; as observed since the pre-industrial era. For example increases in CO_2 emissions and the further build-up of atmospheric CO_2 concentrations which could cause the CO_2 absorption band to become more opaque (i.e. absorb more IR radiation) and effectively broaden, causing increases in the global climate (Burroughs, 2007). Specific to this work and the transport sector the same could occur with ozone (O_3) due to the release of NO_X (nitrogen oxides) emissions and their subsequent production of O_3; thus increasing global O_3 concentrations. Since the industrial revolution (circa ~1750) O_3 has been assessed to impart a radiative forcing of 0.35 W m^{-2} (Stocker et al., 2014). Radiative forcing is metric that represents the change in the net,

downward minus upward, radiative flux at the tropopause or top-of-atmosphere (TOA) due to a change in an external driver of climate change over a period of time, usually expressed in W m^{-2} (IPCC, 2013a).

2.1.2 Climate interaction of aerosol-phase species

This section discusses the interactions of aerosols that may be formed or emitted directly in to the atmosphere and their resultant interactions on the climate. Since the industrial era (circa 1750) nitrates, sulfates, black carbon (BC), organic aerosols (OC) have been assessed to return a net cooling radiative forcing of –0.11 W m^{-2} (Stocker et al., 2014), while all natural and anthropogenic aerosols have been assessed to have a radiative effect of –0.27 W m^{-2} (IPCC, 2013b).

Figure 2.2: Factors influencing the formation of aerosol particles and their growth processes, and how these can result in the formation of cloud condensation nuclei (CCN) – adapted from Verheggen (2009) using information from Boucher et al. (2013) and Spracklen et al. (2005a).

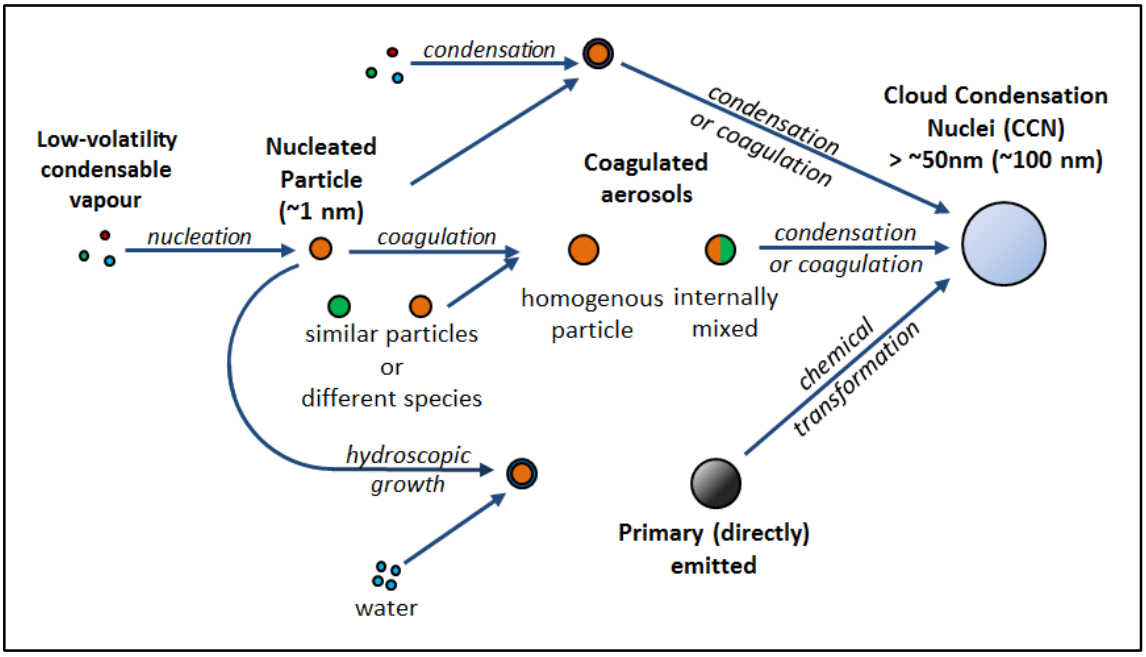

Particles can be either primary (e.g. carbonaceous from combustion, sea-salt from bubble bursting in the ocean, uplift of mineral dust) or secondary (e.g. nucleation of sulfuric acid and water). Nucleation occurs when new particles are formed when low-volatility vapours nucleate in to stable molecular clusters, (i.e. nucleation), which can rapidly grow to produce nanometre-sized aerosol particles under set conditions (Figure 2.2). Sulfuric acid (H_2SO_4) is the main driver for nucleation, but this nucleation rate is affected by ammonia, amines in addition to low-volatility organic vapours (Boucher et al., 2013; Mann et al., 2010). Aerosol particles can be of either natural origin, e.g. dust and sea spray, or from both anthropogenic and natural origins,

e.g. in the case of sulfate, BC and OC which originate from combustion, volcanic activity and wildfires (Boucher et al., 2013; Stettler et al., 2013; Spracklen et al., 2008a; Graf et al., 1997). This results in varying physical and chemical properties dependant on size, chemical composition and shape (Boucher et al., 2013).

Whether aerosols scatter or absorb light energy is dependent on their properties and environmental conditions. Aerosol species which absorb light are black carbon, while aerosol species which scatter light are sulfates, nitrates, organic carbon, mineral dust and sea spray (Boucher et al., 2013). Scattering aerosols have a cooling effect through their ability to increase the reflectivity of the local regions, with this resulting in a regionally and vertically extended cooling through atmospheric circulation and mixing processes – Figure 2.3(a,b) respectively (Boucher et al., 2013).

Figure 2.3: Aerosol-radiation interactions – adapted from Boucher et al. (2013).

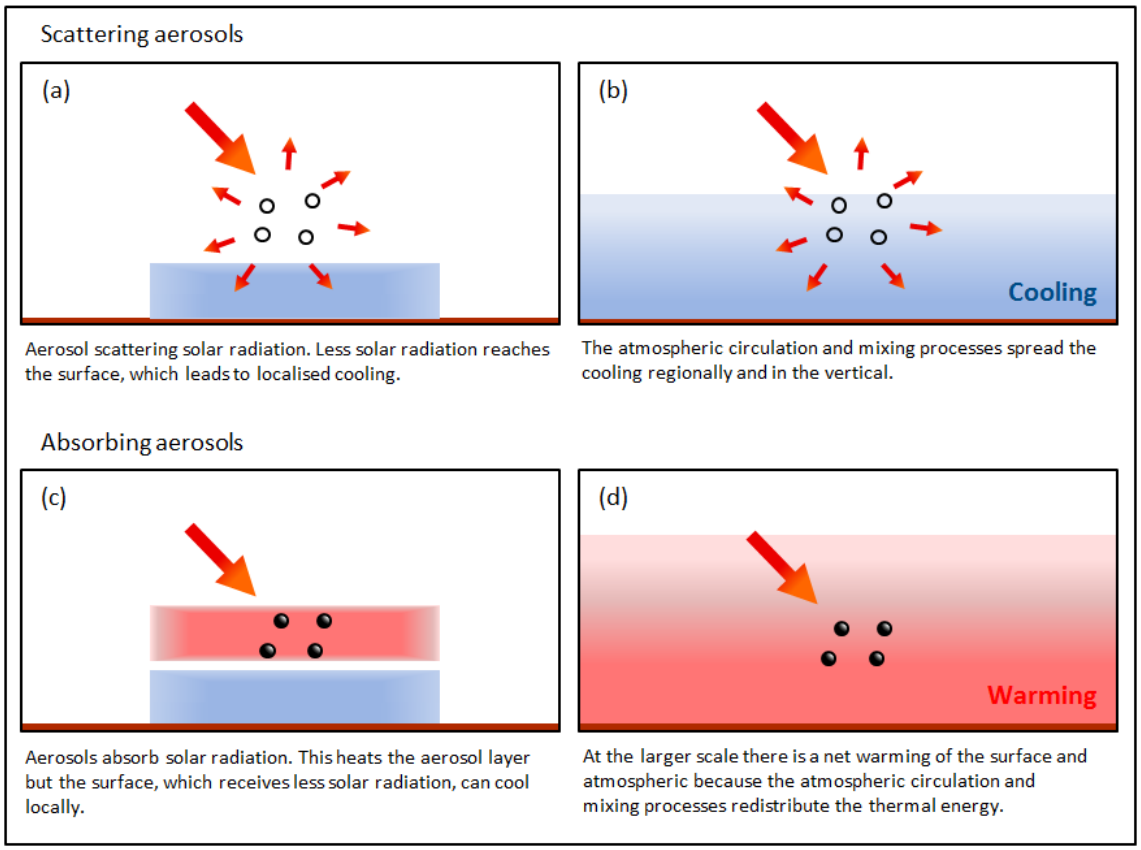

Absorbing aerosols absorb incoming solar radiation (shortwave) initially heating up the aerosol layer, with the region below this layer initially cooling locally as this initially receives less solar radiation. On a larger scale the thermal energy absorbed by this aerosol layer is redistributed via atmospheric circulation and mixing processes resulting in a net warming effect (Figure 2.3(c,d)) (Boucher et al., 2013). Absorbing aerosols like BC have been demonstrated to provide a considerable direct climate forcing of +0.71 W m^{-2} (with an uncertainty range of +0.08 to

+1.27 W m^{-2}) in relation to a pre-industrial climate (Bond et al., 2013), equating their direct impact at 42.3% of the radiative forcing imposed by CO_2 since the pre-industrial era (IPCC, 2013b; Bond et al., 2013).

In addition the direct effect on radiation, aerosols can interact with clouds, i.e. aerosol-cloud interactions; that aerosols, from natural or of anthropogenic origin, can act as CCN (Figure 2.4(a)) in addition to ice nucleation sites. When more aerosols are introduced in to the system one of the resultant effects is the formation of a larger concentration of smaller droplets (Pincus and Baker, 1994; Boucher et al., 2013), leading to 'cloud brightening,' i.e. have an increased scattering effect on incoming radiation (Figure 2.4 (b)) (Boucher et al., 2013).

Figure 2.4: Aerosol-cloud interactions – adapted from Boucher et al. (2013).

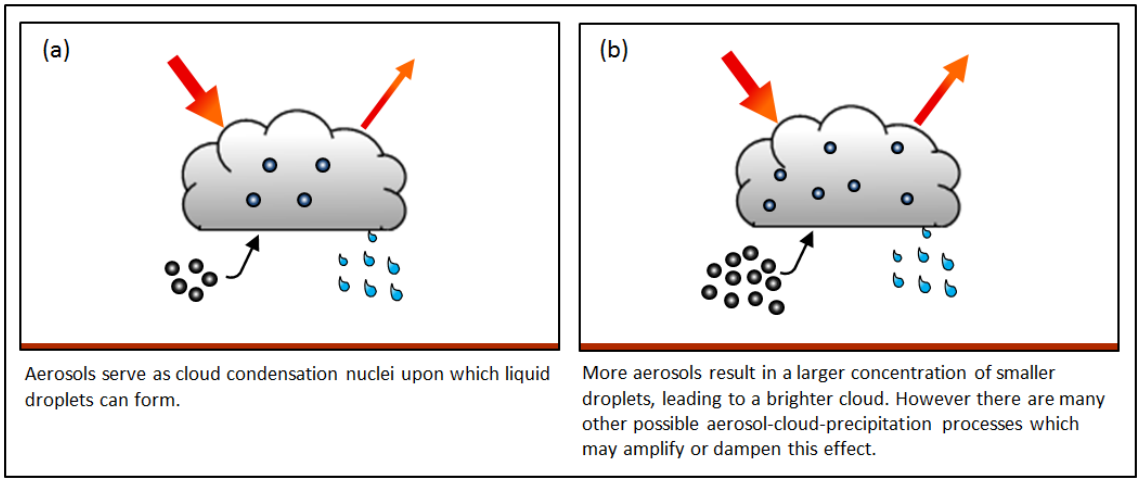

Figure 2.5 demonstrates that in addition to the aerosol-radiation interactions (ari) and aerosol-cloud interactions (aci) there are cloud adjustments associated with each type of interaction, returning effective radiative forcings for ari and aci, i.e. ERFari and ERFaci. Within each of these classes of interactions there are instantaneous forcing and rapid adjustment components: ERFari consist of the RFari from the direct effect of aerosols and rapid adjustments (semi-direct effect), while ERFaci consist of the RFaci from the cloud albedo effect and lifetime effects (Boucher et al., 2013).

If absorbing aerosols such as BC are introduced in to the atmosphere, not only can they induce a warming of the atmosphere (Figure 2.3(c,d)), but the rapid adjustment associated with their introduction can induce the semi-direct effects (Figure 2.5) where the absorbing aerosols cause heating within the clouds resulting in cloud burn-off (Boucher et al., 2013; Forster et al., 2007).

The effect of BC on clouds is dependent on several factors, such as the altitude of the BC aerosols in relation to clouds, and cloud type. If BC are within the cloud layer, cloud cover is

decreased due to heating induced cloud burn-off, inducing the original "semi-direct effect" (Koch and Del Genio, 2010; Forster et al., 2007; Bauer and Menon, 2012). If BC are present below the cloud layer convection and cloud cover may be increased, and if the BC are above the cloud layer the cloud layer may be stabilised and there may be an enhancement in stratocumulus cloud cover, and possible reduction in cumulus clouds (Koch and Del Genio, 2010). Thus absorbing aerosols such as BC can alone induce semi-direct effects.

Figure 2.5: Schematic for new terminology used in the IPCC's Assessment Report 5 (AR5) for aerosol-radiation and aerosol-cloud interactions and how they relate to terminology used in AR4 – adapted from Boucher et al. (2013).

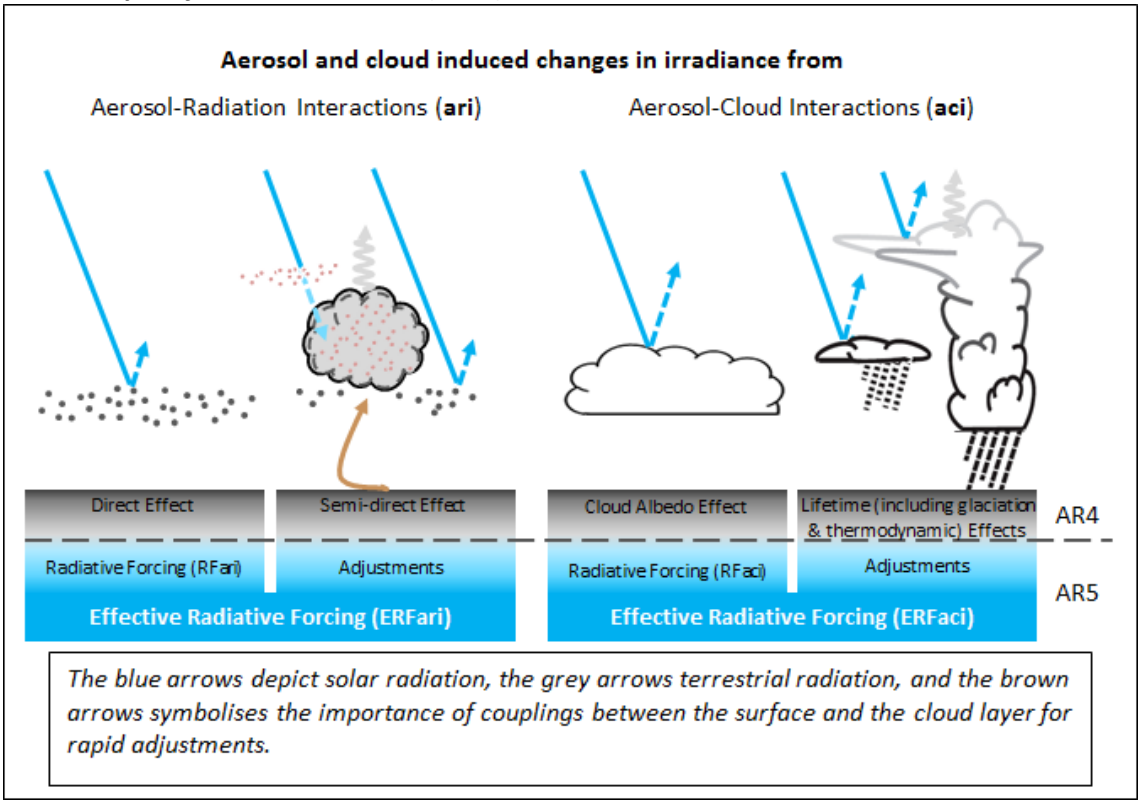

Akin to other aerosol matter BC contributes to the CCN concentrations, in turn impacting cloud cover and lifetime, along with acting as ice nuclei perturbing ice or mixed-phase clouds. Water droplets in the atmosphere do not freeze instantaneously at 0°C (Hoose and Möhler, 2012), ice nuclei (IN) are particles that allow for the formation of ice crystals (Boucher et al., 2013), as otherwise pure cloud droplets would remain in a liquid state until cooled to the homogeneous freezing threshold at around 237 K (Atkinson et al., 2013). Untreated BC particles show activity as deposition/sorption ice nuclei, while BC particles with a monolayer coverage of sulfuric acid showed homogeneous freezing characteristics and BC particles with multilayer coverage froze more readily (DeMott et al., 1999).

Absorbing aerosols like BC can alter the atmospheres temperature gradient, which can perturb atmospheric mixing and cloud distributions. In convergent regions absorbing aerosols enhance

deep convection and low level convergence, through the drawing up of moisture from ocean to land regions, increasing cloud cover (Bauer and Menon, 2012; Koch and Del Genio, 2010). Over land BC has the ability to reduce surface evaporation and in effect moisture available for cloud formation (Koch and Del Genio, 2010).

The rapid adjustments considered in relation to aerosol-cloud interactions are related to cloud lifetime effects (Figure 2.5), which pertains to the formation of smaller water droplets and resulting impacts on rain rates (Pincus and Baker, 1994; Boucher et al., 2013).

Ultimately understanding how aerosols affect the properties and lifetime of clouds is of importance as they (clouds) provide: both solid and liquid precipitation (providing a significant source of freshwater), remove trace chemicals from the atmosphere of pollutants through wet deposition, impact on global weather systems, and affect the radiation balance on a regional scale thus effecting local and global climate systems (Lamb and Verlinde, 2011).

Further compounding the importance of anthropogenic emissions on the perturbations of global aerosol burdens it has been assessed that between 20–40% of aerosol optical depth and between ~25 to ~33 % of CCN are of anthropogenic origin (Boucher et al., 2013).

Aerosols emitted directly from aviation emissions or as a result of reactions with other emitted species or atmospheric constituents are of great importance due to their release in to a sensitive region of the atmosphere (Snijders and Melkers, 2011; Unger, 2011), and their resultant direct and indirect effects due to varying interactions and radiative mechanisms (Figure 2.5) (Forster et al., 2007; Boucher et al., 2013). Aerosol indirect effects are the most uncertain aspects of investigating the impact of climate change, and are considered to likely contribute a negative radiative effect (Unger et al., 2009b). In addition, due to the low level of scientific understanding regarding aerosols originating from aviation sources (Lee et al., 2009; Lee et al., 2010), further research is required to assess the impact that these have and to project the impacts they may have based on not only increases in aviation use, civil aviation's impact on human health, but also with regards to potential changes to aviation fuels used.

When the lifetime of aerosols is also considered, which ranges from days to weeks (Unger, 2011; Boucher et al., 2013), their associated direct and indirect impacts could be sizable in light of a growing aviation sector.

A negative radiative forcing is provided by scattering aerosols, while partially absorbing aerosols may either result in a positive or negative radiative forcing (Figure 2.3 and Figure 2.4) (Boucher et al., 2013). Thus where shortwave radiative scattering aerosols are formed (e.g.

sulfates) regional cooling effects are potentially witnessed due to aerosol-radiation interactions. Additionally cloud albedo effects occur through instantaneous aerosol-cloud interactions (Boucher et al., 2013), through which aviation has the potential to reduce the amount of radiation being absorbed by darker surfaces (e.g. ocean masses); which have a lower surface albedo in comparison to cloud cover induced (brighter and more reflective) (Forster et al., 2007).

Aviation emitted aerosol mass concentrations are lower compared to surface anthropogenic sources, along with belonging to a smaller size fraction (i.e. smaller dry diameter) (Penner et al., 1999). This is due to the mix of hydrocarbons (HCs) and aromatics present in kerosene (Jet A-1/Jet A fuel) (ASTM International, 2010; Blakey et al., 2011).

The direct radiative forcing from aviation-borne BC and sulfate aerosols is small compared to other aviation borne emissions, but are accompanied by higher relative uncertainties in their resulting associated radiative forcings (Lee et al., 2010). But due to their interactions in the atmosphere and influences on cloud formation and lifetime and contributing to the formation of linear contrails, their role in altering cloud properties and resultant radiative forcing their interactions and effects need attention (Penner et al., 1999).

Changes in atmospheric loading of BC and sulfates, due to changes in the fuels combusted and/or more stringent regulations and standards imposed, could lead to a strong greenhouse gas warming. It has been suggested that decreases in sulfate aerosol in tandem with increases in BC concentrations have contributed to the recently seen acceleration in Arctic warming; due to a combined reduction in sulfate induced cooling and increase in BC induced warming (Arneth et al., 2009).

2.2 Aviation emission species

Before discussing how aviation borne emission species perturb atmospheric concentrations of trace species, e.g. O_3 (Section 2.3) and the resulting climatic impacts of these species (Section 2.4), this section pays attention to species emitted directly by aviation while touching upon secondary pollutants created as a result (Figure 2.6).

Figure 2.6 highlights the main aviation emissions released along with their associated emissions indexes (EI), (i.e. grams of pollutant released per kilogram of kerosene combusted) along with the products and effects typical of these emission species (Lee et al., 2009; Lee et al., 2010).

From Figure 2.6 it is seen that from the complete combustion of aviation fuel the products of complete combustion should be: CO_2; water vapour (H_2O_V); nitrogen (N_2); oxygen (O_2); and sulfur dioxide (SO_2) (Lee et al., 2009). But in reality incomplete combustion occurs, directly emitting (primary) species/pollutants are: CO_2; H_2O_V; N_2; O_2; NO_X; carbon monoxide (CO); HCs; sulfur oxides (SO_X); soot otherwise known as BC (Lee et al., 2009; Lee et al., 2010); and OC (Bond et al., 2004).

CO_2 emissions, the most abundant of aviation's emissions (Figure 2.6), are released directly and do not undergo any chemical transformations (Lee et al., 2010). CO emissions, the fourth most abundant emissions specie, are oxidised in the atmosphere to produce CO_2 though interactions with OH (Fowler et al., 1997; Jenkin and Clemitshaw, 2000), with their atmospheric interactions attributed to 60–75% of global OH radical loss (Kiselev and Karol, 2000). In addition this loss mechanism, OH can feed in to an O_3 production cycle (Fowler et al., 1997; Jenkin and Clemitshaw, 2000).

Figure 2.6: Aviation emissions, associated emissions indices and perturbations to atmospheric components – adapted from Lee et al. (2009).

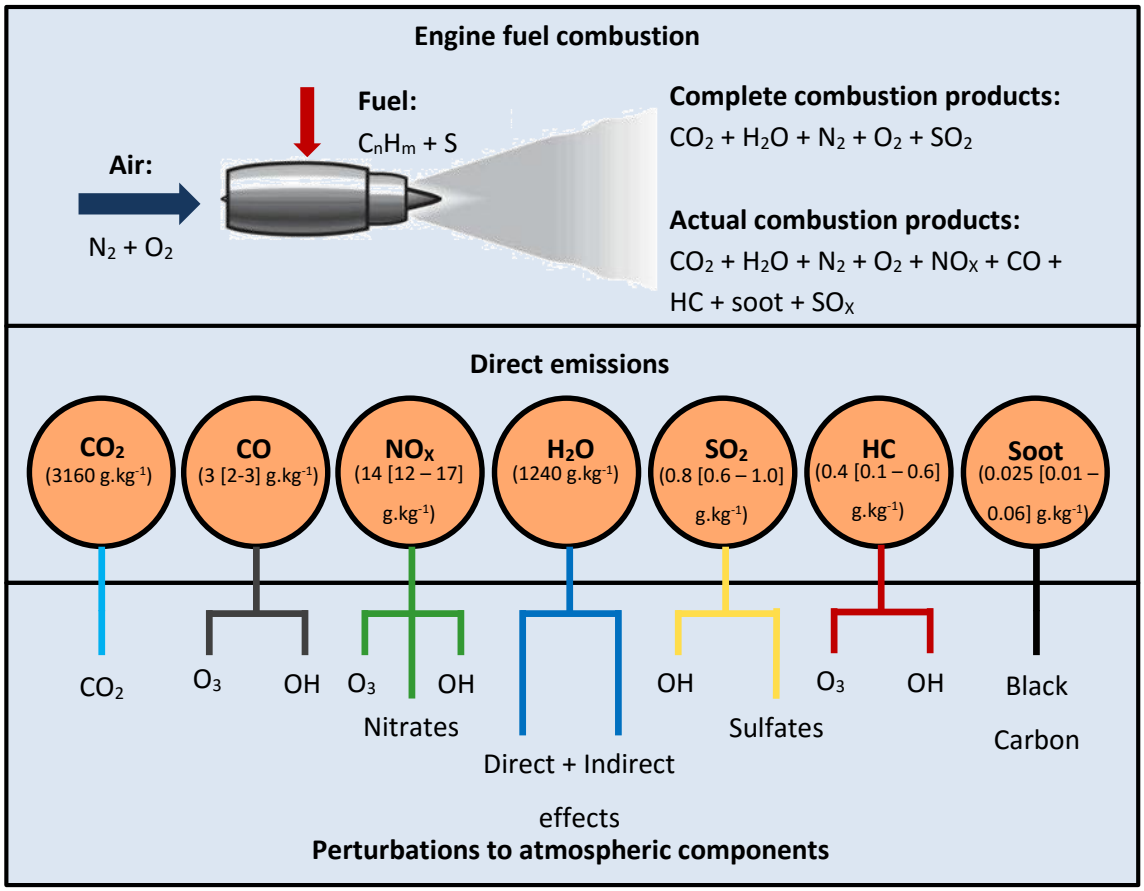

NO_X, the third most abundant aviation emissions species, forms O_3 via photochemical reactions (Section 2.3.1.2) (Lee et al., 2009; Holmes et al., 2011; Myhre et al., 2011; Fowler et

al., 1997; Jenkin and Clemitshaw, 2000), the production of OH radicals (Myhre et al., 2011; Fowler et al., 1997; Jenkin and Clemitshaw, 2000) which can aid in the reduction of atmospheric methane (CH_4) concentrations (Holmes et al., 2011; Myhre et al., 2011; Unger et al., 2006a). NO_X emissions also form nitrate aerosols via the formation of nitric acid (HNO_3) (Unger, 2011; Unger et al., 2009a).

H_2O_V emissions, the second most abundant of aviation's emissions, can have direct and indirect effects on the Earth's radiative balance. From Figure 2.1 it is observed that H_2O_V directly impacts by absorbing IR radiation between the wavelengths of 6.7–7.7 μm and 17–25 μm (Houghton, 2009). Indirect effects are the formation of linear contrails, which depending on atmospheric conditions can persist and form aviation induced cirrus clouds otherwise known as aviation-induced cloudiness (AIC) (Rap et al., 2010; Lee et al., 2009).

SO_2 emissions (the fifth most abundantly emitted specie from aviation) go on to form sulfates. This can be either via aqueous phase oxidation with H_2O_2 or O_3 or oxidation of SO_2 with the OH radical, thus reducing the concentration of OH radicals (Lee et al., 2010).

Emissions of HCs have the potential to increase aviation induced O_3 productions and thus atmospheric concentrations, and decrease OH radical concentrations (Kentarchos and Roelofs, 2002; Lee et al., 2010).

BC and OC are formed from the incomplete combustion of jet fuel and emitted directly (Kim et al., 2012), with the potential to have direct and indirect effects on climate.

2.3 Atmospheric interactions of aviation non-CO_2 emitted species

This section discusses the atmospheric interactions of aviation borne non-CO_2 emissions species (introduced in Section 2.2) such as NO_X, CO, HCs, SO_2, BC, organic carbon (OC) and H_2O_V which perturb the oxidative state of the atmosphere (Myhre et al., 2011). This section aims to highlight the species and interactions which are of particular importance to this thesis.

Non-CO_2 emissions give rise to tropospheric O_3, perturbing hydroxyl concentrations (OH), reducing atmospheric methane (CH_4), contrail formation and the formation of a variety of aerosol particulate matter such as sulfates (SO_4^{2-}), nitrates (NO_3^-), BC, OC and secondary organic aerosol (SOA); while also being adverse to human health (Unger, 2012; Fiore et al., 2012; Twomey, 1977; Myhre et al., 2011; Holmes et al., 2011; Hoor et al., 2009).

Non-CO_2 aviation emissions contribute towards 2–14% of anthropogenic climate forcing, with around a threefold uncertainty (Holmes et al., 2011; Preston et al., 2012; Unger, 2011; Lee et al., 2010) (Figure 2.6). This demonstrates the importance of including non-CO_2 emissions when assessing the climatic impact of aviation emissions, as their combined effects rival those from CO_2. Importantly it has to be considered that the uncertainty for Short-Lived Climate Forcers (SLCFs) is substantially larger than those for Long-Lived Greenhouse Gases (LLGHGs) (Lee et al., 2009; Lee et al., 2010).

Aviation primary and secondary emissions species and their impacts operate on a wide range of timescales: less than a second for OH (Hodnebrog et al., 2011); minutes to hours (linear-contrails and contrail cirrus) (Frömming et al., 2011; Unger, 2011); days to weeks (H_2O_V) (Mahashabde et al., 2011; Penner et al., 1999); days to months (O_3 and aerosols) (Poberaj et al., 2010; Unger, 2011); months (CO) (Poberaj et al., 2010); decades (CH4) (Unger, 2011); and decades to centuries (CO_2) (Gettelman and Chen, 2013; Unger, 2011).

Due to the relative impact of non-CO_2 species compared to CO_2 over short timeframes, these emissions need to be considered as they have the potential to outweigh benefits from typical emissions reductions policies currently in use (Unger, 2010). Conversely in order to consider non-CO_2 emissions accurately in reduction policies a suitable metric needs to be decided upon if these emissions are to be included in any emissions trading scheme (Forster et al., 2006).

In addition to the atmospheric lifetime of non-CO_2 emissions other factors make aviation emissions of further interest, such as their latitudinal and altitudinal. It has been demonstrated that at lower latitudes aviation borne non-CO_2 emissions have stronger responses to O_3 production and CH_4 lifetime (Köhler et al., 2013; Stevenson and Derwent, 2009; Pitari et al., 2002). In addition to these latitudinal responses, responses are influenced by background NO_X emissions at the emissions site, with less polluted sites being more responsive to the introduction of aviation NO_X emissions (Stevenson and Derwent, 2009).

Aviation borne emissions are unique as they are emitted directly in to the upper troposphere and lower stratosphere at cruise altitudes (8–12 km) (Lee et al., 2010; Snijders and Melkers, 2011; Beyersdorf et al., 2013; Righi et al., 2013; Köhler et al., 2013), where they can potentially have a greater impact on atmospheric composition due to the higher sensitivity of the atmosphere at these altitudes. This in turn can exacerbate increases in aviation-induced perturbation to the radiative balance of the Earth System (Snijders and Melkers, 2011; Unger, 2011; Stevenson and Derwent, 2009; Köhler et al., 2008), while contributing to air quality issues on the surface (Beyersdorf et al., 2013; Righi et al., 2013).

The relationship between the altitudinal release of aviation non-CO_2 emissions and responses has been investigated, demonstrating a reduction in climatic impacts and responses when aviation emissions are collapsed to ground level, i.e. introducing column integrated aviation emissions at the lowest model level (Unger, 2011; Frömming et al., 2012). This a response which can be attributed to the cleaner background conditions in higher altitude regions known to increase enhancement efficiencies of O_3 and OH (Hodnebrog et al., 2011).

In addition, it has been shown that O_3 and aerosol precursor emissions have larger climatic impacts when emitted in more photochemically active regions (such as at lower latitudes) (Unger, 2012).

The vertical mixing aviation emissions undergo and their resulting distribution will be dependent on their lifetime and altitude of release (Unger, 2012; Lee et al., 2013). Vertical mixing can affect concentrations of chemical species present in these regions, which for example can drive promote the destruction of O_3 in the lower stratosphere via the activation of halogen species or drive O_3 formation in the upper troposphere via the oxidation of non-methane HCs and CO (catalysed by NO_X and peroxyl radicals) (Meilinger et al., 2001; Jacob, 2000). In addition, tropospheric O_3 chemistry is of great interest as it is the primary source of the atmospheric oxidant OH (Jacob, 2000).

From here the chemical interactions aviation-borne emissions (as highlighted in Figure 2.6) are discussed in turn, aiming to highlight the species formed, how these can interact, and the impacts these could have on atmospheric concentrations.

2.3.1 Nitrogen oxides (NO_X)

Aviation borne NO_X are of importance when assessing the climatic impacts of aviation emissions, as these emissions induce the main perturbations to the chemical composition in the upper troposphere lower troposphere (UTLS) often in to some of the cleanest regions of the atmosphere (Stevenson et al., 2004; Pitari et al., 2002). These perturbations occur via three main pathways: the perturbation of O_3 via catalytic cycles involving HCs and hydrogen oxides radicals (HO_X); increases in the oxidative capacity of the atmosphere through increases in hydroxyl (OH) concentrations; and reductions in atmospheric methane (CH_4) lifetime (Holmes et al., 2011; Myhre et al., 2011; Lee et al., 2009; Lee et al., 2010; Hoor et al., 2009; Pitari et al., 2002; Wild et al., 2001; Köhler, 2010). In addition to these three main pathways reductions in atmospheric concentrations of CH_4 result in reductions long-lived O_3 burden (Stevenson and Derwent, 2009).

The impact of NO_X emissions on O_3 production has shown to be seasonally and regionally variable (Stevenson et al., 2004), with Autumnal aviation NO_X emissions providing greater O_3 responses to Springtime emissions and responses over the Pacific being greater (Gilmore et al., 2013). When emitted in the lower troposphere NO_X has a short residence time with mixing ratios marginally increasing due to surface emissions (Fiore et al., 2012; Frömming et al., 2012), whereas at higher altitudes aviation influenced NO_X mixing ratios increase disparately (Frömming et al., 2012). This is of importance as future aviation growth is likely to be heterogeneous, returning nonlinear responses (Köhler et al., 2013).

Aviation NO_X emissions perturb background NO_X (Gottschaldt et al., 2013), and with the long lifetime of NO_X reservoir species, has the capacity to be transported over significant distances and influence the oxidising capacity of the troposphere globally (Köhler et al., 2008).

Projected levels of growth in aviation emissions (Section 1.3) will be of significant interest as it has been shown that NO_Y deposition (where NO_Y = NO + NO_2 + other minor inorganic components and organic nitrogens) is currently larger than combined surface and upper air sources (inclusive of lightening) by approximately 1 Tg(N) yr^{-1} (~1.2 times the level of year 2000 aviation NO_X emissions) (Lamarque et al., 2013a; Quantify Integrated Project, 2005-2012); highlighting that stratospheric nitric acid (HNO_3) is a considerable source of tropospheric NO_Y. By 2050 aviation borne NO_X emissions could range between 0.79–3.33 Tg(N) yr^{-1} (Quantify Integrated Project, 2005-2012). With other factors remaining constant they could negate the gap between the tropospheric sink and source of NO_Y.

In addition to the gas-phase interactions of aviation borne NO_X emissions these emissions are of further interest as they generate nitrate aerosols (Stevenson and Derwent, 2009) and indirectly enable a more effective conversion of SO_2 to H_2SO_4 due to increases in OH concentrations subsequent formation of sulfates (Pitari et al., 2002), which can provide a negative climate forcing effect (Fiore et al., 2012).

The formation mechanism for ammonium nitrate ($NH_4.HNO_3$) is in competition with the formation mechanism for ammonium sulfate ($(NH_4)_2.SO_4$), with the formation of $(NH_3)_2.SO_4$ taking precedence in regions with lower ammonia (NH_3) concentrations (Bauer et al., 2007). Lamarque et al. (2011) looked at total global anthropogenic emissions under different RCPs (Representative Concentration Pathways) from 2000 to 2100 project that NH_3 emissions will increase by factors of 1.09–1.68 by 2100. Whereas for the same period, under all RCPs, total global anthropogenic emissions of SO_2 are projected to decrease by a factor of between 4.19 to 8.33. In tandem to this Lamarque et al., (2013) has shown that total (wet and dry) NH_X (NH_3

+ NH_4) deposition is projected to increase in all RCP scenarios to 2100 (Lamarque et al., 2013a). With future aviation emissions increasing along with greater global emissions of NH_3, decreases in SO_2 and flux of NH_X aviation derived ammonium nitrate has the potential to become a more dominant forcing component in future aviation climate assessments.

The rest of this section will delve in to detail the effects of aviation borne NO_X emissions on NO_X, O_3, the OH radical, formation of nitric acid (HNO_3) and nitrates (NO_3^-).

2.3.1.1 Nitrogen oxides (NO_X): formation and interactions

In the troposphere NO_X is an important specie and a major source of photochemically produced O_3, strongly influenced by Reaction 2.1 (Søvde et al., 2011).

$$HO_2 + NO \rightarrow NO_2 + OH$$

Reaction 2.1

Reaction 2.1 is one of many processes that enable the efficient recycling of NO_X compounds, before it is eventually converted to less photochemically active species like HNO_3. This is demonstrated by Reaction 2.2 where both the concentration of NO_2 is reduced along with the availability of the OH radical (De Nevers, 2000; Fowler et al., 1997; Jenkin and Clemitshaw, 2000). In addition, Reaction 2.1 is also dependent on altitude, latitude and season (Søvde et al., 2011); factors which greatly affect aviation NO_X emissions (DuBois and Paynter, 2006).

$$OH + NO_2 \ (+M) \rightarrow HNO_3 \ (+M)$$

Reaction 2.2

2.3.1.2 Ozone (O_3): formation and interactions

Ozone when present in the stratosphere is important to human life as it provides a barrier against short-wave radiation (Penner et al., 1999), but when present in the troposphere O_3 is a chemical specie that not only provides a positive radiative forcing (Lee et al., 2009; Forster et al., 2007), but a pollutant which is harmful to human life and vegetation (World Health Organisation, 2005; Unger and Pan, 2012; Unger et al., 2009b).

Aviation is a unique sub-sector of transportation as the majority of its emissions are released in to the upper troposphere/lower stratosphere (UTLS) where the atmosphere is more sensitive to changes in composition, resulting in a greater efficiency in O_3 formation mechanisms, which

in turn produces the effective increase of aviation's net radiative forcing (Penner et al., 1999; Hoor et al., 2009; Koffi et al., 2010).

As commercial aircraft travel through both the troposphere and the stratosphere (Lee et al., 2009; Vedantham and Oppenheimer, 1998) it will contribute to the formation of tropospheric O_3 through their NO_X emissions, as well as CO and un-burnt emissions of HCs, and the destruction of stratospheric O_3 (Holmes et al., 2011; Hoor et al., 2009; Myhre et al., 2011).

Due to global flight patterns it has been observed that aviation borne NO_X emissions have a greater impact on O_3 formation in the Northern Hemisphere compared to over the Southern hemisphere (Koffi et al., 2010; Johnson et al., 1992). Also it is observed that the atmosphere is most sensitive to O_3 formation in the UT (upper troposphere) at an altitude of ~12km (Hodnebrog et al., 2011) via the O_3 formation precursor NO_X; illustrating that atmosphere is ~30 times more sensitive to high altitude NO_X emissions in comparison to surface emissions (Hauglustaine et al., 1994; Johnson et al., 1992). In the stratosphere aviation NO_X emissions has a reducing effect on O_3 (Johnson et al., 1992). Recent studies investigating the present day and future impact of aviation NO_X emission on O_3 formation found that aviation is on average 4–5 times more efficient at perturbing the global O_3 burden, compared to road transport borne surface emissions (Hauglustaine and Koffi, 2012). This is as each NO_X molecule released in this region of the atmosphere a can be recycled more often to produce O_3, before it is removed via precipitation scavenging or dry deposition as part of nitric acid (NHO_3) (Hoor et al., 2009).

In addition, aviation-induced O_3 is found to result in elevated surface concentrations of O_3 due to vertical mixing aviation primary emissions and secondary pollutants witness (Whitt et al., 2011).

Tropospheric O_3 is not formed as a direct result of the combustion processes, with photolysis of NO_2 being the only known way of producing O_3 in the troposphere (Wayne, 2000; De Nevers, 2000).

The fundamental mechanism for the formation of tropospheric O_3 is via the photochemical reaction of NO_2, as in (Reaction 2.3) and (Reaction 2.4) (De Nevers, 2000; Wayne, 2000; Seinfeld and Pandis, 2006; Fowler et al., 1997). The rate of reaction (Reaction 2.3) is dependent on the zenith solar angle and thus varies globally (Saunders et al., 2003), with the photolysis of NO_2 occurring at wavelengths < 424 nm (Seinfeld and Pandis, 2006).

$NO_2 + hv \rightarrow O^{\cdot} + NO$

Reaction 2.3

$O^{\cdot} + O_2 (+M) \rightarrow O_3 (+M)$

Reaction 2.4

Where, hv = a photon of light,

M = represents any other molecule.

The product O_3 can then go on to react with NO to regenerate NO_2: the main loss mechanism for O_3 in polluted areas (Reaction 2.5) (Seinfeld and Pandis, 2006; De Nevers, 2000; Wayne, 2000).

$O_3 + NO \rightarrow NO_2 + O_2$

Reaction 2.5

The formation of ozone is a fast reaction occurring during the day when the photolysis rate of Reaction 2.3 is high. O_3 formation is part of the greater encompassing daytime tropospheric inter-conversions of oxidised nitrogen compounds interactions. The rate of destruction of NO (Reaction 2.5) is slow in comparison, but is not dependent on hv (sunlight) so it can continue throughout the night.

When assessing NO_X's ability to form O_3, the O_3 production efficiency $P(O_3)$, also referred to as OPE, needs to be considered (Figure 2.7). This has been found to be at a maximum in the upper troposphere when maximum NO_X levels are around 1 ppbv. But conversely, in the lower stratosphere where is chlorine activation is high enough, O_3 depletion will occur irrelevant of concentrations of NO_X emitted in to the region (Hoor et al., 2009; Meilinger et al., 2001). After this level, the O_3–NO_X regime will result in a reduction in amount of O_3 produced due to the associated reduction in O_3 production efficiency, as seen in Figure 2.7.

The OPE (ozone production efficiency) can be equated by considering the rate of production of O_3 (P_{O_3}) in relation to the rate of loss of NO_X (L_{NO_x}) as depicted in Equation 2.3, which relates to the main mechanism for the reduction of NO_X in the atmosphere Reaction 2.2 and formation of O_3 via Reaction 2.3 and Reaction 2.4, and due to the influence of hydroperoxy (HO_2) radical (Seinfeld and Pandis, 2006; Fowler et al., 1997).

$$OPE = \frac{P_{O_3}}{L_{NO_x}}$$

Equation 2.3

From Figure 2.7 it is observed that $P(O_3)$ reaches a maximum at $[NO_X] \approx 1$ ppbv. Hoor et al., (2009) state that for NO_X levels of 0.1–0.3 ppb, which is typical for regions influenced by aviation emissions, changes in O_3 are more sensitive to small decreases in NO_X than the total removal of aviation NO_X (Hoor et al., 2009).

It has been shown that in the upper troposphere O_3 production efficiency is at a maximum when NO_X levels are at around 1 ppbv (Hoor et al., 2009) and that at an altitude of 100 hPa (~15.8km) 1.48 mols of O_3 is created for every mole of N in NO_X emitted by aviation, compared to the surface emissions of road transport and shipping which have associated production rates for O_3 0.34 and 0.41 per mole of N in NO_X, respectively (Hauglustaine and Koffi, 2012).

Figure 2.7: Net ozone production rates $P(O_3)$ – adapted from Meilinger et al. (2001).

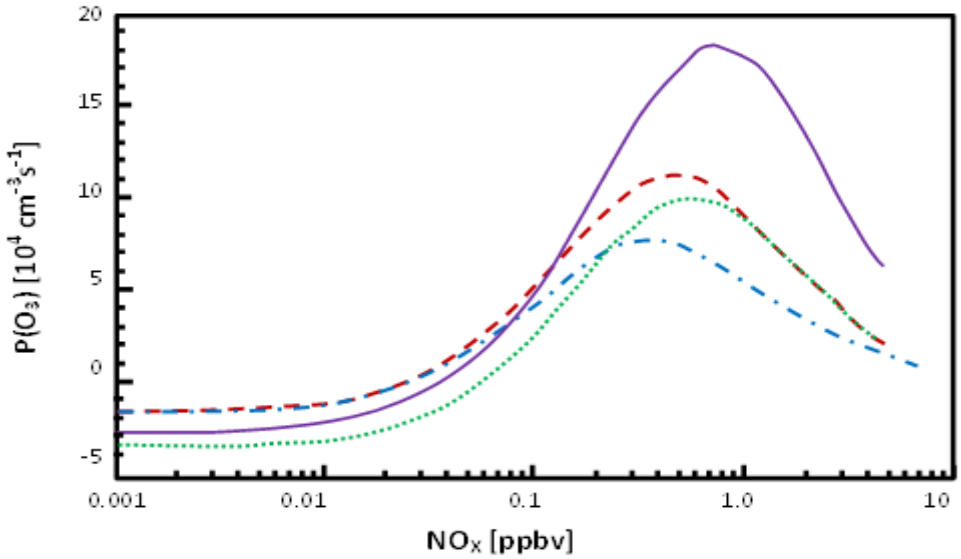

Dashed-dotted curve – Net $P(O_3)$ as calculated by Grooß et al.(1998). Dashed curve – and with the present model using updated kinetic reaction rates as a function of initial NO_X mixing ratio in 2-hr simulations for 220 K and 200 hPa. Dotted curve – addition of gas phase halogen chemistry assuming 80 pptv Cl_y and 5.5 pptv Br_y. Solid curve – addition of NMHC chemistry assuming 150 pptv acetone, 500 pptv ethane and 100 pptv PAN.

Due to the relationship between the $P(O_3)$ and background NO_X emissions (Meilinger et al., 2001), aviation NO_X emissions demonstrate that they are more than 2.5 times more efficient at producing O_3 than other transport sector's emissions (Hoor et al., 2009).

In addition to the NO_X formation mechanism for O_3 mentioned above which is part of a null-cycle, it is also produced by the non-linear photochemical oxidation of CO, non-methane volatile organic compounds (NMVOCs) in the presence of NO_X (Unger et al., 2006a; Unger et al., 2006b; Unger et al., 2008), along via the oxidation HCs and CO catalysed by HO_X (hydrogen oxides) (Jacob, 2000). This does not summarise the full O_3 formation mechanisms in the troposphere as O_3 can be formed by HCHO (formaldehyde) in the troposphere and destroyed by halogen species which are prevalent in the stratosphere (Wayne, 2000). These mechanisms and how they contribute to O_3 production when influenced by aviation borne emissions will be discussed in Section 2.3.2 and Section 2.3.3.

O_3 formation is not just related to background NO_X concentrations and the $P(O_3)$ (Figure 2.7) (Meilinger et al., 2001), and the photolysis of NO_2 (De Nevers, 2000; Seinfeld and Pandis, 2006; Fowler et al., 1997; Wayne, 2000), but also on the background concentrations of VOCs (volatile organic compounds) (Figure 2.8).

Figure 2.8: Calculated maximum afternoon O_3 concentrations as a function of the morning NO and VOC concentrations for the same air mass (N.B. most US cities have a VOC/NO_X ratios of between 8–15) – taken from De Nevers (2000).

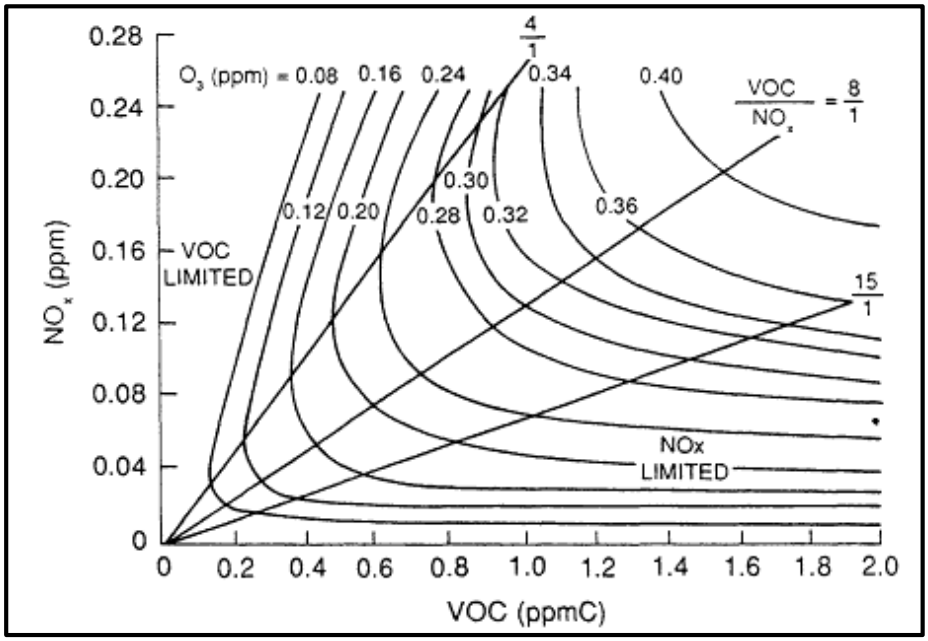

In the upper troposphere NO_X emissions participate in reactions that generate O_3 either through reactions outlined in Reaction 2.3 to Reaction 2.5 in this section, or through: the formation of H radicals (Reaction 2.21 in Section 2.3.2); the formation of RO_2 aiding NO_2 formation (Reaction 2.23 to Reaction 2.25 in Section 2.3.3); or HO_2 production from formaldehyde and other aldehydes (Reaction 2.26 to Reaction 2.28 in Section 2.3.3) (Fowler et al., 1997; Jenkin and Clemitshaw, 2000).

In general NO_X levels are sufficiently low in much of the troposphere, thus increases of anthropogenic NO_X raise average tropospheric O_3 concentrations which induces a positive (warming) forcing influence (Unger, 2011; Skowron et al., 2013; Fiore et al., 2012). This increase in O_3 and the higher regions of the atmosphere's sensitivity to NO_X induced O_3 production can be explained by the ratios of atmospheric constituents (Figure 2.8), O_3 production efficiency (Figure 2.7) and the build-up of O_3 in these regions can in part be explained by the increase O_3 lifetime with altitude (Wang et al., 1998). In addition NO_X increases atmospheric concentration of the OH radical (Section 2.3.1.3) (Unger, 2011).

As highlighted in Figure 2.7 the relative impact and of aviation borne NO_X emissions on O_3 formations is influenced by background NO_X concentrations, which may originate from either surface or lightening sources. Which when considered in tandem with abundances of VOCs (Figure 2.8), solar irradiance which affects the rate of photolysis of NO_2, and hydrogen oxides (HO_X) further illustrate the complexity of chemistry in this region (Köhler et al., 2013; De Nevers, 2000; Meilinger et al., 2001; Saunders et al., 2003).

In addition to background NO_X concentrations and how they can affect the $P(O_3)$ (Figure 2.7) other factors that affect the formation of O_3 influenced by NO_X emissions are the ratio of $OH:HO_2$ (Holmes et al., 2011) and how HO_2 (hydroperoxyl) and RO_2 (organic peroxyl) radicals affect NO and the conversion of NO back to NO_2 via Reaction 2.5 (Fowler et al., 1997; Jenkin and Clemitshaw, 2000).

HO_2 and RO_2 impact NO concentrations provide two additional pathways for the production of NO_2 from NO that doesn't involve O_3 as seen below in Reaction 2.1 and Reaction 2.6.

$$HO_2 + NO \rightarrow OH + NO_2$$

Reaction 2.1

$$RO_2 + NO \rightarrow RO + NO_2$$

Reaction 2.6

Reaction 2.1 and Reaction 2.6 provide pathways for the conversion of NO to NO_2 that doesn't involve the consumption of O_3, therefore creating another mechanism to produce NO_2 (in addition to Reaction 2.5), which can then be photolysed to create additional NO and O (Reaction 2.3), whose products can go on to create O_3 via (Reaction 2.4) (Fowler et al., 1997; Jenkin and Clemitshaw, 2000).

At lower flight levels the relative decrease in NO_X results in a lower rates of conversion of HO_2 to OH, along with decreases in O_3 production due to lower NO_X concentrations (Frömming et al., 2012).

Kiselev and Karol., (2000) used a homogeneous NO_X aircraft source to investigate perturbations in NO_X resultant from aviation NO_X emissions over the North Atlantic flight corridor. They found a positive correlation between emissions and perturbations, observing a maxima in perturbations between altitudes of 4–12 km (Kiselev and Karol, 2000).

As mentioned previously aviation NO_X emissions are 3.4 more efficient at producing O_3 than road emissions (Hauglustaine and Koffi, 2012). This is due to the lower background NO_X emissions in the regions that aviation operate, i.e. the upper troposphere/lower stratosphere.

2.3.1.3 Hydroxyl radical (OH): formation and interactions

Aviation NO emissions can contribute to OH formation through direct or indirect mechanisms. Directly aviation NO emissions participate in Reaction 2.1 which is a major source of OH in the troposphere through the recycling of HO_2. This reaction also produces NO_2, thus contributing to the formation of tropospheric O_3 (Søvde et al., 2011; Fowler et al., 1997; Jenkin and Clemitshaw, 2000).

$$HO_2 + NO \rightarrow OH + NO_2$$

Reaction 2.1

Indirect mechanisms can include the production of OH through the photo-dissociation of HONO. HONO is formed via the reaction of OH with NO (Reaction 2.7) acts as a temporary reservoir for NO_X, as it can be readily photolysed back in to its constituent parts: OH and NO (Reaction 2.8) (Jenkin and Clemitshaw, 2000; Fowler et al., 1997).

$$OH + NO\ (+M) \rightarrow HONO\ (+M)$$

Reaction 2.7

$$HONO + hv \rightarrow OH + NO$$

Reaction 2.8

The lifetime for NO prior to the formation of HONO ranges between 5 hours ([OH] = 0.04 ppt) to 2 days ([OH] = 0.4 ppt) dependant on OH concentration. Due to the interdependence

between the formation of HONO (Reaction 2.7) and the photolysis of HONO (Reaction 2.8), HONO does not accumulate significantly during the day (Jenkin and Clemitshaw, 2000; Fowler et al., 1997). Other indirect OH formation mechanisms are associated with the night-time NO_X cycle. These mechanisms involve the reaction of hydroperoxyl (HO_2) with either nitrates (Reaction 2.9) or O_3 (Reaction 2.10) (Jenkin and Clemitshaw, 2000; Fowler et al., 1997).

$$HO_2 + NO_3 \rightarrow OH + NO_2 + O_2$$

Reaction 2.9

$$HO_2 + O_3 \rightarrow OH + 2O_2$$

Reaction 2.10

2.3.1.4 Higher oxides of nitrogen: formation and interactions

In addition to NO_X chemistry described above the formation of higher oxides of nitrogen (NO_3 and N_2O_5), oxyacids (HNO_3, HO_2NO_2 and HONO), organic peroxyl nitrates (RO_2NO_2), organic nitrates ($RONO_2$) and nitrate aerosols provide (all grouped within the NO_Y classification) additional mechanisms for the consumption of NO_X, with most of these species being formed during the day (Jenkin and Clemitshaw, 2000; Fowler et al., 1997).

Oxyacids such as nitric acid (HNO_3), peroxynitric acid (HO_2NO_2) and nitrous acids (HONO) are formed from the reaction of NO_X with HO_X radicals (OH and HO_2); as in seen reactions Reaction 2.2, Reaction 2.11 and Reaction 2.7.

$$OH + NO_2 (+M) \rightarrow HNO_3 (+M)$$

Reaction 2.2

$$HO_2 + NO_2 (+M) \leftrightarrow HO_2NO_2 (+M)$$

Reaction 2.11

The formation mechanism for HNO_3 Reaction 2.2 is of particular importance as it is the main daytime removal mechanism for NO_X (Jenkin and Clemitshaw, 2000; Fowler et al., 1997; Wayne, 2000). The rate at which NO_2 can effect go on to form O_3 via Reaction 2.2 is dependent on the concentration of OH radicals, so if OH concentrations are reduced O_3 formation is

reduced. Additionally O_3 formation can be reduced through the formation of HNO_3 removed from the atmosphere; via dry or wet deposition from the atmosphere, adsorbed on to the surface of existing solid particles, or reactions involving HNO_3 which resulting in the formation of tropospheric aerosols (Jenkin and Clemitshaw, 2000; Fowler et al., 1997).

The formation mechanism for HO_2NO_2 Reaction 2.11 estimates the lifetime of NO_2 in the region of ~2hrs in respect to this reaction (when $[HO_2]$ = 10 ppt), but the resultant product only has a lifetime of about 30 seconds; dependant on atmospheric pressure and at a temperature of 288 K, thus NO_2 is readily regenerated (Jenkin and Clemitshaw, 2000; Fowler et al., 1997).

As discussed in Section 2.3.1.3 HONO can be formed via Reaction 2.7 (Fowler et al., 1997; Jenkin and Clemitshaw, 2000).

$$OH + NO\ (+M) \rightarrow HONO\ (+M)$$

Reaction 2.7

HONO demonstrates its importance in the NO_X cycle through its ability to act as a temporary reservoir for NO_X, allowing for the transportation of HONO and the resulting NO production through the photolysis of HONO (Reaction 2.8) (Fowler et al., 1997; Jenkin and Clemitshaw, 2000).

$$HONO + hv \rightarrow OH + NO$$

Reaction 2.8

In addition to the formation HNO_3 (Reaction 2.2), HO_2NO_2 (Reaction 2.11), HONO (Reaction 2.7) the formation of organic peroxyl nitrates can occur from the reaction of NO_2 with organic peroxy radicals (RO_2), as per (Reaction 2.12) (Fowler et al., 1997; Jenkin and Clemitshaw, 2000):

$$RO_2 + NO_2\ (+M) \leftrightarrow RO_2NO_2\ (+M)$$

Reaction 2.12

The lifetime of the resultant RO_2NO_2 product is dependent on the on the structure of the organic “R” group and the thermal decomposition rate, with simple alkyl peroxyl nitrates, such as where $R=CH_3$, having a lifetime of 12 seconds and more complex whereas more complex R

species with carbonyl groups (C=O) having lifetimes of about 1 hour – as per data from Lightfoot et al. (1992) (Fowler et al., 1997; Jenkin and Clemitshaw, 2000). Dependant on the R-functional groups and the resultant lifetime of the resultant organic peroxy nitrate formed this can provide a mechanism for the consumption of NO_X in to reservoir that is degraded in to NO_X over a prolonged period of time (Fowler et al., 1997; Jenkin and Clemitshaw, 2000).

Peroxyl acetyl nitrate (PAN), one such peroxyl nitrate, is of importance as it produced from the formation of $CH_3C(O)O_2$, which is produced via the degradation of a large range of organic compounds (with ≥ C_2) – Reaction 2.13 (Fowler et al., 1997; Jenkin and Clemitshaw, 2000).

$$CH_3C(O)O_2 + NO_2\ (+M) \leftrightarrow CH_3C(O)OONO_2\ (+M)$$

Reaction 2.13

The formation of PAN is of importance to aviation as the rate of thermal decomposition of PAN decrease as a function of altitude (Fowler et al., 1997; Jenkin and Clemitshaw, 2000) thus inferring that PAN formed as a result of aviation emissions have the potential to have transboundary impacts. Another consideration relating to the formation of aviation induced PAN is that as temperatures lower the equilibrium is shifted to the right-hand side of Reaction 2.13 (Wayne, 2000); with the atmospheric temperature profile (when considered between the Earth's surface and the lower stratosphere) reaching a minimum in the UTLS (De Nevers, 2000).

In addition PAN has been long recognised as a component of photochemical smog (Wayne, 2000) (in addition to O_3 (De Nevers, 2000; Jacobson, 2002)). Photochemical smog has been shown to impair the human respiratory system (Jacobson, 2002; De Nevers, 2000; Watkins et al., 2013; Cuijpers et al., 1994), impair visibility primarily due to $PM_{2.5}$ and accompanying pollutants while impacting regional ecosystems through photochemical oxidant damage due to the high levels of O_3 present in photochemical smog (Molina and Molina, 2004).

The formation of PAN, vertical transport and rapid decrease in temperature (under appropriate meteorological conditions), enable PAN and other peroxyl acyl nitrates to increase in stability allowing them to degrade and release NO_X over a greater timescale through photodissociation or reactions with OH radicals (Fowler et al., 1997; Jenkin and Clemitshaw, 2000).

Reaction 2.6 illustrates the production of NO_2 which can feedback in to the O_3 production cycle via the associated photolysis of NO and mechanism represented by reactions Reaction 2.3 and

Reaction 2.4), but the reaction between RO_2 and NO can also yield the formation of organic nitrates; as per Reaction 2.14.

$$RO_2 + NO\ (+M) \rightarrow RONO_2\ (+M)$$

Reaction 2.14

The rate of formation of organic nitrates is minor in comparison to Reaction 2.6, but the rate of reaction via this channel Reaction 2.14 increases with an increase in the RO_2 radical size. The product alkyl nitrate products from Reaction 2.14 are shown to be insoluble in water and do not transfer to the particulate phase, with their degradation occurring through reactions with OH or via photodissociation. The lifetime of $RONO_2$ decreases with as the size of the carbon skeleton $>C_5$, due to the rapid removal by OH (Fowler et al., 1997; Jenkin and Clemitshaw, 2000).

The production of organic peroxyl nitrates Reaction 2.12 such as PAN, and alkyl nitrates Reaction 2.14 can undergo long range transport which provides a sizeable source of background NO_X concentrations in the troposphere (Singh et al., 1992).

In addition to the daytime interactions of NO_X and NO_Y compounds, there is a night-time chemistry scheme which provides significant chemical processes which contribute to the chemical influences on O_3, NO_X and NO_Y (Fowler et al., 1997; Jenkin and Clemitshaw, 2000; De Nevers, 2000; Wayne, 2000; Seinfeld and Pandis, 2006). These night-time processes lead to the removal of O_3 (Fowler et al., 1997; Jenkin and Clemitshaw, 2000), but produce a series of secondary pollutants such as H_2O_2, along with oxidising NO_X leading to the production of additional secondary pollutants during the day, e.g. the regeneration of NO_2 from the photolysis of NO_3. (Fowler et al., 1997; Jenkin and Clemitshaw, 2000).

2.3.1.5 Nitrates (NO_3^-): formation and interactions

The nitrate radical has been shown to be important in both stratospheric and tropospheric chemistry, playing a part in chemical transformations (Wayne, 2000). NO_2 is converted in to NO_3 through reaction with O_3 during the diurnal cycle, occurring over a timescale of 12 hours (when boundary layer $[O_3]$ = 30 ppb); as per Reaction 2.15 (Fowler et al., 1997; Jenkin and Clemitshaw, 2000).

$$NO_2 + O_3 \rightarrow NO_3 + O_2$$

Reaction 2.15

During the day NO_3 is rapidly photolysed resulting in the regeneration of NO_2 and the subsequent regeneration of O_3 – Reaction 2.16 and Reaction 2.4 respectively. In addition NO_3 has the ability to regenerate NO_2 via reaction with NO (Reaction 2.17) (Fowler et al., 1997; Jenkin and Clemitshaw, 2000).

$$NO_3 + hv \rightarrow NO_2 + O^{\cdot}$$

Reaction 2.16

$$O^{\cdot} + O_2\ (+M) \rightarrow O_3\ (+M)$$

Reaction 2.4

$$NO_3 + NO \rightarrow 2NO_2$$

Reaction 2.17

NO_3 can be produced by the dissociation of N_2O_5 (dinitrogen pentoxide), through the reverse reaction of Reaction 2.18, but at night the principle reaction of NO_3 is towards the formation of N_2O_5 (Wayne, 2000; Jenkin and Clemitshaw, 2000; Fowler et al., 1997).

$$NO_3 + NO_2\ (+M) \leftrightarrow N_2O_5\ (+M)$$

Reaction 2.18

If concentrations of O_3 are high enough NO is rapidly converted to NO_2, and the slowly converted in to NO_3 by Reaction 2.15. At night concentrations of NO are not significant, so the principle reaction that occurs tends to the production of N_2O_5 Reaction 2.18 (Jenkin and Clemitshaw, 2000; Fowler et al., 1997). N_2O_5 plays an important role in the atmosphere through the formation of nitric acid (HNO_3) contributing to atmospheric acidification (Wayne, 2000; Jenkin and Clemitshaw, 2000; Fowler et al., 1997) and the formation of ammonium nitrate ($NH_4.NO_3$).

$$N_2O_5 + H_2O \rightarrow 2HNO_3$$

Reaction 2.19

In the laboratory it has been demonstrated that the gas-phase Reaction 2.19 occurs extremely slowly. While in the troposphere this reaction largely occurs in cloud water and on the surface of particulates (Fowler et al., 1997; Jenkin and Clemitshaw, 2000; Dentener and Crutzen, 1993), with Dentener and Crutzen (1993) finding that over summer Reaction 2.19 returns

higher decreases in NO_X concentration in winter than in summer. The formation of the ammonium nitrate ($NH_4.NO_3$) aerosol (Reaction 2.20) depends on the thermodynamic state of its precursor and environmental conditions. This reaction mechanism prefers conditions with high ammonia and nitric acid, and low sulfate concentration conditions. This is as the nitrate aerosol formation mechanism is coupled to that for (ammonium) sulfate, due to their competition for available ammonia (Bauer et al., 2007; Unger, 2011).

$$NH_3(g) + HNO_3(g) \leftrightarrow NH_4.NO_3(s)$$

Reaction 2.20

2.3.2 Carbon monoxide (CO)

In areas prone to pollution from anthropogenic combustion sources CO has the potential to contribute to O_3 formation. This occurs through the oxidation of CO by the OH radical (Reaction 2.21), which then goes on generate HO_2 (Reaction 2.22) (Fowler et al., 1997; Jenkin and Clemitshaw, 2000).

$$CO + OH \rightarrow H + CO_2$$

Reaction 2.21

$$H + O_2\ (+M) \rightarrow HO_2\ (+M)$$

Reaction 2.22

The product HO_2 goes on to react with NO from aviation (or other sources) to recycle and recreate the hydroxyl radical and oxidise NO in to NO_2 (Reaction 2.1) (Fowler et al., 1997; Jenkin and Clemitshaw, 2000).

$$HO_2 + NO \rightarrow NO_2 + OH$$

Reaction 2.1

In the presence of sunlight it is possible for the NO_2 product to be photolysed in to NO (Reaction 2.3), with the product oxygen radical going on to form O_3 (Reaction 2.4) (Fowler et al., 1997; Jenkin and Clemitshaw, 2000).

$NO_2 + hv \rightarrow O^{\cdot} + NO$

Reaction 2.3

$O^{\cdot} + O_2\ (+M) \rightarrow O_3\ (+M)$

Reaction 2.4

$O_3 + NO \rightarrow NO_2 + O_2$

Reaction 2.5

It is then possible for the product O_3 to be dissociated back in to O_2 and NO_2 (Reaction 2.5) (Fowler et al., 1997; Jenkin and Clemitshaw, 2000). Reaction 2.3 to Reaction 2.5 typically form a null cycle, i.e. where there is no net chemistry, but with the introduction of CO in to the system ultimately perturbing NO_2 concentrations, aviation-borne CO has the potential to perturb tropospheric O_3 (assessed in Section 5.4.3.1).

2.3.3 Hydrocarbons (HCs)

Here the formation of O_3 from non-methyl hydrocarbons (NMHCs) species in the atmosphere a discussed.

Initially this section starts with the conversion of alkanes to a peroxyl radical. OH reacts with alkanes (RH) to produce hydrogen or an organic fragment (R) through Reaction 2.23 (Fowler et al., 1997; Jenkin and Clemitshaw, 2000).

$RH + OH \rightarrow H_2O + R$

Reaction 2.23

Oxygen then reacts with hydrogen or the product organic fragment to form a peroxy radical (Reaction 2.24) (Fowler et al., 1997; Jenkin and Clemitshaw, 2000).

$R + O_2\ (+ M) \rightarrow RO_2\ (+ M)$

Reaction 2.24

This then leads to the key O_3 formation steps; the conversion of NO to NO_2, which then allows Reaction 2.3, Reaction 2.4 and Reaction 2.5 from Section 2.3.1.2 to occur (Fowler et al., 1997; Jenkin and Clemitshaw, 2000).

$RO_2 + NO \rightarrow NO_2 + RO$

Reaction 2.25

Hydrogen ions or the organic fragments, akin to those produced by Reaction 2.23, can also be produced through the photolysis of molecules which contain the carbonyl bond (C=O), such as formaldehyde (HCHO) and other aldehydes (RCHO) (Reaction 2.26 and Reaction 2.27) (Fowler et al., 1997; Jenkin and Clemitshaw, 2000).

$HCHO + hv \rightarrow H + HCO$

Reaction 2.26

$RCHO + hv \rightarrow R + HCO$

Reaction 2.27

After the formation of these hydrogen ions or organic fragments and carbonyl bond containing molecules (such as HCHO or RCHO) (Reaction 2.26 and Reaction 2.27), the hydrogen or organic fragments can continue along the pathway highlighted by Reaction 2.24; while the carbonyl bond containing molecules (HCO) can react to form hydroperoxyl (HO_2) – Reaction 2.28 (Fowler et al., 1997; Jenkin and Clemitshaw, 2000).

$HCO + O_2 \rightarrow HO_2 + CO$

Reaction 2.28

The products of Reaction 2.28 can either go through the mechanisms highlighted in Section 2.3.2 in the case of the CO product, or Reaction 2.1 in the case of the HO_2 production highlighted in Section 2.3.1.1 (Fowler et al., 1997; Jenkin and Clemitshaw, 2000).

2.3.4 Water vapour (H_2O_V)

H_2O_V is present within aircraft exhaust emissions in known amounts, due to the stoichiometry of near-complete combustion specifying an emissions index for water vapour ($EI_{H_2O_V}$) of 1240 g kg^{-1} (Penner et al., 1999; Lee et al., 2010).

Aviation emitted water vapour primarily interacts in the atmosphere in one of two ways (Lee et al., 2009; Penner et al., 1999):

- Through direct interactions with incoming solar radiation, or,

- Via the formation of contrails.

H_2O_V interacts directly with outgoing infrared radiation. From Figure 2.1 it can be seen that H_2O_V absorbs IR between wavelengths of 6.67–7.69 μm and ~17.54–25 μm (Houghton, 2009), resulting in a warming effect (Lee et al., 2009) (Figure 2.16). Additionally H_2O_V is a carrier of latent heat, thus has the capacity to retain heat within the atmosphere (Jacobson, 2005).

Contrails are produced from aviation-borne H_2O_V emissions in regions witness to liquid water saturation conditions, a result of heat and H_2O_V mixing between the warm and moist exhaust and the cool ambient air (Rap et al., 2010; Penner et al., 1999). When formed in dry unsaturated air contrails are usually short-lived (Rap et al., 2010).

When ambient conditions allow relative humidity to exceed ice saturation aviation-induced contrails can persist and develop in to extended cirrus cloud layers; due to the formation of ice particles (Penner et al., 1999; Rap et al., 2010; Forster et al., 2007).

Soot particles emitted by aviation are mostly hydrophobic due to the strong oxidation processes they will have undergone. Through being coated in H_2SO_4, soot particles have the potential to become suitable condensation nuclei (Schumann, 2005). At these conditions the condensation of H_2O_V forming liquid droplets can freeze on these emitted particles, forming ice particles, thus providing sites for the formation of persistent cirrus-contrails (Schumann et al., 2002).

The formation of ice nuclei and resulting ice clouds are not considered within this research project as TOMCAT-GLOMAP-mode is unable to consider their formation.

2.3.5 Sulfur dioxide (SO_2)

Aviation-borne SO_2 emissions play two important roles in the atmosphere. Firstly the formation of H_2SO_4 which is important for the nucleation of new particles (Fowler et al., 1997; Jenkin and Clemitshaw, 2000; Mann et al., 2010) and for its ability to allow insoluble aerosol modes to transition in to the soluble mode via the process of ageing (Mann et al., 2010), thus affecting the cloud condensation nuclei and the resulting cloud formation. Secondly SO_2 is fundamental to the formation of sulfate aerosols via the formation of H_2SO_4 (Fowler et al., 1997; Jenkin and Clemitshaw, 2000).

Stockwell and Calvert (1983) showed that the formation mechanism for H_2SO_4 from SO_2 undergoes the following process (Reaction 2.29, Reaction 2.30 and Reaction 2.31) (Stockwell and Calvert, 1983; Fowler et al., 1997; Jenkin and Clemitshaw, 2000):

$$OH + SO_2 (+M) \rightarrow HOSO_2 (+M)$$

Reaction 2.29

$$HOSO_2 + O_2 \rightarrow SO_3 + HO_2$$

Reaction 2.30

$$SO_3 + H_2O (+M) \rightarrow H_2SO_4 (+M)$$

Reaction 2.31

Additionally the aqueous-phase oxidation of SO_2 can also lead to the formation of H_2SO_4, as described below (Reaction 2.32) (Jacobson, 1997):

$$SO_{2(aq)} + O_3(aq) + H_2O (aq) \rightarrow SO_4^{2+} + 2H^+$$

Reaction 2.32

As discussed in Section 2.3.1.5 the formation of ammonium sulfates ($(NH_4)_2.SO_4$) and nitrates ($NH_4.HNO_3$) are in competition with each other, with the formation of $(NH_4)_2.SO_4$ taking precedent over the formation of $NH_4.HNO_3$ in low ammonia concentration conditions (Bauer et al., 2007).

Henceforth, in the atmosphere and in the presence of ammonia H_2SO_4 reacts rapidly to form ammonium sulfate (Reaction 2.33 and Reaction 2.34) (Committee on the Environment and Natural Resources, June 2000; Arrowsmith and Hedley, 1975).

$$NH_3 + H_2SO_4 \rightarrow NH_4.HSO_4$$

Reaction 2.33

$$NH_3.HSO_4 + NH_3 \rightarrow (NH_4)_2.SO_4$$

Reaction 2.34

2.3.6 Soot particles (black and organic carbon)

Carbonaceous aerosol species (BC and OC) formed from the incomplete combustion of fossil fuels, alternative fuel and biomass burning (Kim et al., 2012; Jacobson, 2005; Penner et al., 1999). BC is strongly light absorbing (Penner et al., 1999; Kim et al., 2012), while OC is an efficient scatter of light (Kim et al., 2012; Jacobson, 2005), and have the ability to increase the absorption efficiency of soot (Jacobson, 2005). The combustion of Jet A/Jet A-1 fuel results in greater emissions of BC in relation to OC (Jacobson, 2005; Bond et al., 2004). These species are of interest not only for their direct effect on the climate where they absorb solar radiation warming the atmosphere, but also due to the adverse effects on human health (Kim et al., 2012; Forster et al., 2007; Unger, 2011; Unger et al., 2010).

When absorbing particles, such as soot, are coated in relatively non-absorbing materials such as H_2SO_4 or OC the absorption efficiency of soot increases (Jacobson, 2005). Increases in absorption efficiency occur in two ways: when the particles are larger than the wavelength of light more light is incident on the particle either due to the size of the BC core or near-transparent coating which refract more lens to the BC core, or; when the particles are smaller than the wavelength of light there is enhanced diffraction at the edge of the aerosol particle, thus exposing the core to more light waves in comparison to a BC particle without a H_2SO_4 or OC coating (Jacobson, 2005). BC species impose large levels of uncertainty when it comes to quantifying the climatic impacts of aerosols (Kim et al., 2012; Forster et al., 2007; Lee et al., 2009; Lee et al., 2010). It has been suggested, based on global model simulations conducted, that the direct effect from BC may be larger than the total negative forcing imposed by all other anthropogenic aerosol species (Kim et al., 2012).

BC and OC particles are hydrophobic. As BC and OC particles age other chemicals coat or condense upon them, and if this condensable matter is soluble BC and OC particles can then potentially act as CCN (Jacobson, 2005). Through this conversion to more effective CCN BC and OC have the potential to perturb low-level cloud and aid in the formation of persistent cirrus-contrails through acting as ice nuclei (Wayne, 2000).

Soot particles can be partitioned in to two size ranges: the smaller particles (10–30 nm) which are larger than the volatile aerosol particles within a young plume and can rapidly immerse in to the background aerosol forming larger aerosol particles, and the larger particles (50–100 nm) which are observable at cruising levels (Penner et al., 1999).

Recently it was suggested that BC originating from fossil fuel and biofuel combustion is the second largest contributor to global warming, after CO_2 (Kim et al., 2012; Bauer and Menon, 2012). The implications of this are that by reducing global anthropogenic BC emissions the warming impact could be reduced. It has been suggested that by removing all BC emissions from fossil fuel and biomass burning a reduction in net warming of 20% could be realised within 5 years (Kim et al., 2012).

2.4 Assessing the impacts of aviation primary and secondary emitted species

Currently aviation is responsible for ~3% of all anthropogenic CO_2 emissions, but when all non-CO_2 emissions are considered its contribution is an estimated 2–14% of anthropogenic climate forcing (Lee et al., 2009; Lee et al., 2010; Unger, 2011). This section will pay particular attention to the atmospheric perturbations and climatic effects of aviation non-CO_2 emissions.

Section 2.4.1 investigates the impacts of aviation CO_2 emissions, Section 2.4.2 discusses the atmospheric impacts aviation non-CO_2 emissions, with Section 2.4.3 reviewing the climate effects of aviation non-CO_2 emissions highlighting the range of uncertainties in estimates.

2.4.1 Carbon dioxide (CO_2) emissions and associated effects

Road transport is responsible for 74% of transportation borne CO_2, whereas aviation is responsible for 12% of CO_2 of this figure (ATAG, 2012). CO_2 is the most predominant aviation emissions species (Figure 2.6) with an emissions index (EI) of 3160 $gCO_2\ kg^{-1}$ of kerosene burnt (Lee et al., 2010), contributing 50.9% of aviation's radiative forcing (when not considering aviation induced cirrus – Figure 2.16) (Lee et al., 2009). Aviation borne CO_2 emissions are projected to increase by a factor of ~3.5 by 2050 (Gudmundsson and Anger, 2012), further highlighting the impact CO_2 emissions could have.

CO_2 is the most abundant of the anthropogenic greenhouse gases emitted by aviation, receiving the majority of attention to date resulting in a high LOSU (Penner et al., 1999; S. Solomon et al., 2007; Lee et al., 2010); illustrated by the narrower distribution in aviation CO_2's RF estimates (Lee et al., 2009). The impact of CO_2 emissions on climate differs greatly from non-CO_2 emissions. In the short-term CO_2 has a smaller radiative forcing (RF), but as these emissions remain in the atmosphere for longer periods of time compared to non-CO_2 emissions (i.e. decades to centuries as opposed to days to months) their associated CO_2 RF increases with time (Forster et al., 2006; Unger, 2011; Wuebbles et al., 2007; ICAO, 2007).

20–30% of the CO_2 emitted in to the atmosphere remains there for timescales longer than 1000 years, 10% being removed from the atmosphere on a short timescale of 1–2 years, and with a large proportion of this CO_2 taken-up by the oceans over the period of centuries (Olivié et al., 2012).

Due to CO_2's longer lifetime it accumulates in the atmosphere over time and becomes dispersed globally, resulting in a global effect as opposed to regional effects from secondary pollutants (e.g. O_3) resultant of shorter lived emission species, such as NO_X (Lee et al., 2010; Olivié et al., 2012). Thus resulting in CO_2's impacts being independent to their location of and time of emission (Williams and Noland, 2006). Due to the long lifetime of these emissions the resultant impact on the atmosphere is irrelevant of the altitude at which there were emitted (ICAO, 2007) as it becomes well mixed in the troposphere and stratosphere (Olivié et al., 2012).

2.4.2 Non-CO_2 emissions and their associated impacts

Here aviation-induced gas-phase (Section 2.4.2.1) and aerosol-phase (Section 2.4.2.2) perturbations are discussed, with the aim of putting in to context the impact the presence and distribution of aviation non-CO_2 emissions have in the atmosphere.

2.4.2.1 Aviation-induced gas-phase perturbations

2.4.2.1.1 Ozone (O_3)

The impact of aviation borne NO_X on tropospheric O_3 formation started to receive attention in the early 1970s (Hidalgo and Crutzen, 1977). Since then research programmes in the US and Europe have investigated the effects of aircraft borne NO_X on tropospheric chemistry (Skowron et al., 2013), with a major milestone being Penner et al. (1999)'s special report on 'Aviation and the Global Atmosphere' summarising the results from various 3D chemical transport models (CTMs) which highlighted that while aviation borne NO_X emissions resulted in increases in tropospheric O_3, there are also a reductions in ambient CH_4 concentrations (Penner et al., 1999; Skowron et al., 2013).

O_3 is not emitted directly, but an important secondary pollutant formed via complex nonlinear chemical production and loss mechanisms, which are time and space dependant (Unger, 2012). O_3 formation mechanisms were discussed in detail in Section 2.3.1.2.

Penner et al. (1999) stated that the net effect of subsonic aircraft NO_X emissions results in an increase in total column O_3 with the largest increase in O_3 concentration being calculated near the tropopause. Civil aviation is responsible for increasing O_3 levels by 3–6% along the North Atlantic flight corridor, with a maximum of 5% in the northern tropopause region in the year 2000, along with seasonal variations showing a peak in summer and a trough in winter (Hoor et al., 2009; Gilmore et al., 2013).

Current literature shows that aviation-induced O_3 returns a peak increase in concentrations of between 5–8.8 ppbv (Khodayari et al., 2014b; Köhler et al., 2008), while providing a range in relative change of O_3 concentrations of 2–10% (Grooß et al., 1998; Koffi et al., 2010; Olsen et al., 2013a; Unger, 2011). Concentration changes due to aviation-induced O_3 are localised about the cruise region of flight (~8–12 km) (Khodayari et al., 2014b; Köhler et al., 2008; Lee et al., 2010), with percentage changes in O_3 occurring in the same region, while extending down to the surface (Koffi et al., 2010; Unger, 2011; Kentarchos and Roelofs, 2002; Søvde et al., 2014; Grooß et al., 1998). This broader distribution of O_3, in both the vertical and horizontal planes, are due to the higher O_3 lifetime in troposphere (Kentarchos and Roelofs, 2002).

In line with zonal concentration and percentage increases in aviation-induced O_3 horizontal spatial plots of aviation-induced O_3 at 250 hPa show that the majority of O_3 created by aviation occurs in the Northern Hemisphere (in between ~30°N to ~60°N), with seasonal trends highlighting peaks in O_3 production over the summer months and a trough in O_3 production over the winter period (Kentarchos and Roelofs, 2002; Hodnebrog et al., 2011).

It is estimated that future (2050) zonal mean aviation induced O_3 could reach concentrations of up to 5 ppbv at northern mid- and high-latitudes during summer, contributing 4.2% of total anthropogenic induced O_3 (Hodnebrog et al., 2011).

Aviation borne NO_X emissions peak in the UTLS in line with aviation fuelburn (Figure 4.1 in Section 4.3.1), perturbing the chemically and radiatively active species (Gottschaldt et al., 2013) discussed in Section 2.3.1.2.

The release of aviation-borne emissions in to these regions is of importance, as the placement of anthropogenic emissions in to chemically sensitive regions has the potential to strongly affect assessments and the total anthropogenic radiative impact; while introducing a previously unidentified uncertainty in modelled anthropogenic climate impacts (Skowron et al., 2013). These uncertainties which relate to aviation emissions inventories were highlighted

by Skowron et al. (2013) when investigating the impact of a range of emissions inventories on aviation-induced NO_X and O_3 perturbations.

The reduced impact of lower altitude flights on perturbations to global O_3 burdens is explained by the faster removal rates of aviation NO_X emissions, whereas at higher altitudes O_3 precursor emissions have higher residence times (Frömming et al., 2012).

Unger (2011) estimate that the greenhouse gas O_3 formation efficiency is 20-60% greater for aviation in comparison to surface-based transportation emissions, as the lifetime of tropospheric O_3 is larger than the vertical mixing. While Hodnebrog et al. (2011) assess that aviation emissions have ~4 times higher O_3 enhancement efficiency in relation to shipping, with the maximum impact being located in the UTLS, with the atmosphere demonstrating that it more sensitive to perturbations in aviation borne NO_X emissions.

Aviation borne NO_X emissions, compared to other land-based transport sources, demonstrate their importance due to their effects on O_3 (due to enhanced $P(O_3)$) and resultant effects on global warming potential (GWP) and global temperature change potential (GTP) (Gilmore et al., 2013; Fuglestvedt et al., 2010).

In addition to the enhanced creation of O_3 with increases in altitude, once the altitude considered is increased above the region of zero net effect (i.e. where O_3 production is equivalent to O_3 destruction), aviation NO_X emissions start to enhance the catalytic destruction of O_3. This cycle operates more efficiently in the stratosphere as NO_X is sequestered in to reservoir species (such as HNO_3) by peroxy radicals and NO_2 photolysis rates become less important at these elevated altitudes (Gottschaldt et al., 2013).

Latitudinal variations in aviation borne NO_X emissions interact with atmospheric O_3 chemistry in three ways: firstly when released at latitudes >40N or >40S NO_X is predominantly released above the tropopause, with emissions released at latitudes <40N and <40S being released below the tropopause; secondly emissions released in the lower latitudinal bands are exhibited to greater levels of solar irradiance resulting in the faster photochemical production of O_3; while finally due to the relatively low background NO_X concentrations (Köhler et al., 2013). NO_X emissions from lower latitudinal bands demonstrate greater levels of O_3 perturbations and associated aviation induced climate forcings as a result (Skowron et al., 2013; Köhler et al., 2013).

Recently Gilmore et al. (2013), Köhler et al. (2013) and Stevenson and Derwent (2009) all demonstrated that aviation emissions released in the lower latitudes produce greater amounts

of O_3 resulting in higher levels of radiative forcing imparted by short-term O_3, lower levels of radiative forcing imparted due to the destruction of atmospheric CH_4 resulting in a larger net O_3 radiative forcings about the lower latitude regions. While in addition demonstrating that in regions with lower background NO_X concentrations (such as in the Pacific) greater responses are observed. Indicating a relationship between the O_3 production 'centre of sensitivity' and lower background NO_X concentrations and the solar zenith angle (Gilmore et al., 2013; Saunders et al., 2003).

Dispersion of aviation-induced O_3 has been shown to be prevalent. Meridional transport of O_3 is pronounced in perturbations at lower latitudes. Westerlies have been shown to transport emissions from over the United States and China, resulting in the formation of O_3 over the North Atlantic and the central Pacific, respectively. The transportation of NO_X from India results in the formation of O_3 in the north-eastern Indian Ocean. Additionally variations in the geographical location of NO_X emission released has shown variations in convective transport of the resulting O_3 formed (Köhler et al., 2013).

Aviation-induced O_3 perturbations show general trends when investigating both the zonal distribution and the horizontal distributions (a cruise level), i.e. showing peaks in increases in O_3 over the Northern Hemisphere, between the NH mid-latitudes (~30°N to ~50°N) and between the cruise region of flight (between 8–12 km) (Koffi et al., 2010; Unger, 2011; Stevenson et al., 2004; Søvde et al., 2014; Grooß et al., 1998; Khodayari et al., 2014b; Kentarchos and Roelofs, 2002).

Looking at work by Kentarchos and Roelofs (2002) and Hodnebrog et al. (2011) O_3 concentrations in January are simulated to peak at around 1.5–2.4 ppbv, while over July the peak concentrations in O_3 are simulated between 3.0 to ~4.0 ppbv – again peaking in the Northern Hemisphere mid-latitudes.

When considering the vertical profile of perturbations in aviation-induced O_3 there is agreement within existing literature showing that O_3 concentrations peak between ~230–300 hPa (~8–12 km) (Hodnebrog et al., 2011; Köhler et al., 2008; Skowron et al., 2013; Khodayari et al., 2014b; Olsen et al., 2013a) (Figure 2.9(a)), showing correlation between the release of aviation NO_X emissions at cruise and the atmosphere's greater ability to form O_3 due to greater O_3 production efficiencies (OPE) (Skowron et al., 2013; Köhler et al., 2008; Stevenson and Derwent, 2009; Snijders and Melkers, 2011).

Ultimately aviation-induced concentration changes and their associated distributions result in a change in the global O_3 burden. Aviation-induced changes in the global O_3 burden have been shown to range between 2.3–9.1 Tg(O_3), with a mean increase of 5.41 Tg(O_3) and standard deviation of 2.89 Tg(O_3) (Wild et al., 2001; Gauss et al., 2006; Olsen et al., 2013a; Khodayari et al., 2014b). This range in aviation-induced O_3 burdens can be attributed to the altitude use to define tropospheric height, emissions inventories used, the year of simulation and models used to assess the impact of aviation-borne NO_X on O_3.

Figure 2.9: Globally and annually averaged vertical distribution of aircraft perturbation of (a) O_3, (b) NO_X, (c) OH and (d) HO_2 concentrations for a series of normalised aircraft inventories: all aircraft inventories have been normalised to REACT4C – taken from Skowron et al. (2013).

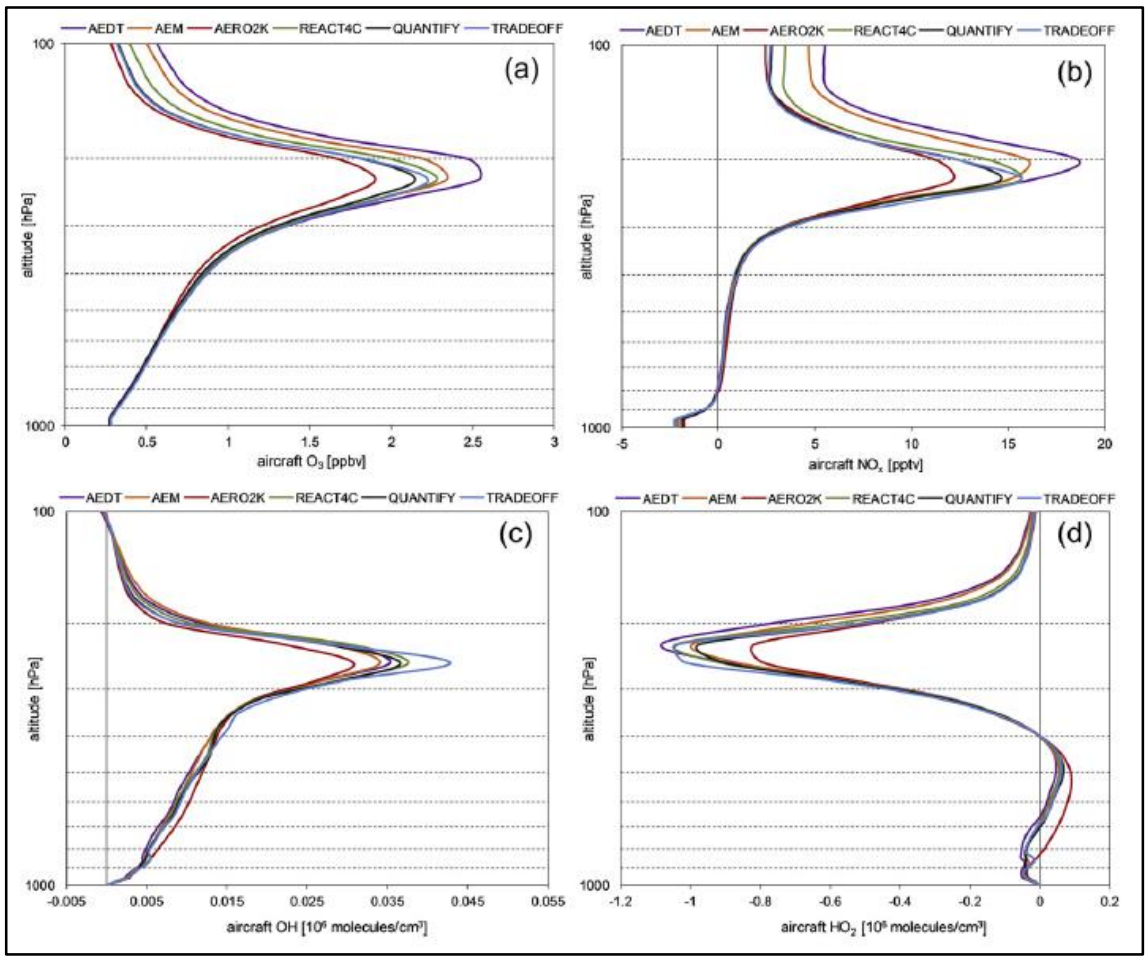

2.4.2.1.2 Nitrogen oxides (NO_X)

Literature show that aviation-induced NO_X perturbations occur in line with aviation-borne emissions; highlighting that the majority of aviation-induced increases in atmospheric NO_X

concentrations occur in the Northern Hemisphere mid-latitudes (Lee et al., 2010; Kentarchos and Roelofs, 2002; Stevenson et al., 2004).

Figure 2.9(b) further highlight the vertical profile of aviation-induced NO_X perturbations, illustrating that these perturbations occur between the cruise altitude of flight (~8–12 km; ~170–300 hPa) (Olsen et al., 2013a; Skowron et al., 2013).

This correlation between aviation-borne emission species and NO_X perturbations can be explained by the mechanisms which consume and destroy NO_X (discussed in Section 2.3.1).

In addition to the changes in NO_X induced by aviation-borne emissions discussed above, Fromming et al., (2012) found that increasing the altitude aviation emissions are released at (by +2000 ft) raises the altitude at which peak NO_X responses occur, to above the tropopause. And that lowering the altitude of the release of aviation NO_X emissions (by –6000 ft) lowered the altitudes at which peak aviation-induced NO_X responses occurred, to around 250 hPa (Frömming et al., 2012).

As seen with trans-boundary effects of aviation emitted NO_X on O_3 formation, changes in NO_X in one region may not be as effective as reducing NO_X (and associated impacts) in another (Gilmore et al., 2013).

2.4.2.1.3 Hydroxyl radical (OH) and hydroperoxyl (HO_2)

The hydroxyl radical (OH) is an important species required in the production of tropospheric O_3 due to NMHCs and CO in the presence of aviation borne NO_X emissions (Myhre et al., 2011). In the atmosphere the OH radical is the main oxidant, and perturbations in its concentration have knock on effects on the self-cleaning capacity of the atmosphere (Patra et al., 2014) (in terms of air pollution). Quantifying its impact in the atmosphere is difficult, as it has a lifetime of less than a second due to the reactivity of this oxidising species (Hodnebrog et al., 2011).

Aviation NO_X primarily leads to the production of O_3 and the hydroxyl radical (OH), especially in the regions where the majority of aviation emissions are released (Figure 2.9(c)) (Gottschaldt et al., 2013; Hoor et al., 2009). Additionally OH radicals are produced through the recycling of HO_2 (Søvde et al., 2011). The production of OH radicals contribute to the reduction in atmospheric methane concentrations, which provides a negative radiative forcing feedback (Gottschaldt et al., 2013; Søvde et al., 2011).

As with aviation-induced NO_X fields, aviation-induced OH occurs predominantly in the Northern Hemisphere mid-latitudes, at the cruise levels of flight (Figure 2.9(c)).

In general aircraft NO_X increases OH concentrations and reduces hydroperoxyl radical (HO_2) concentrations. These increases in OH are observed throughout the troposphere (Figure 2.9(c)), while the decreases in HO_2 are mainly observed over the cruise regions of flight (Figure 2.9(d)) (Skowron et al., 2013).

2.4.2.1.4 Peroxyacyl nitrates (PAN)

As seen in Section 2.3.1.4 non-methyl NMHCs react to form peroxyacetyl nitrates (PAN). PAN can act as a reservoir for NO_X, with the capacity to be transported over long distances, allowing for the formation of O_3 some distance from emission sources, i.e. participating in the trans-boundary formation of O_3 (Lee et al., 2010).

The inclusion of NMHCs, like acetone, and PAN chemistry is important when modelling the impacts of aviation emissions on O_3 formation in the upper troposphere (Brühl et al., 2000; Lee et al., 2010), contributing to aviation-induced reductions in NO_X atmospheric concentrations (Brühl et al., 2000; Kentarchos and Roelofs, 2002), but conversely aviation has been previously identified as an insignificant source of NHMCs (Lee et al., 2010).

PAN's ability to act as a reservoir specie for aviation-borne NO_X emissions enable aviation-borne emissions to have greater O_3 forming abilities (Hoor et al., 2009). PAN being temperature dependant, and at the low temperatures involved, acts as a reservoir for aviation-borne NO_X emissions (Kentarchos and Roelofs, 2002).

Aviation-induced PAN concentrations have been shown to increase slightly in the upper troposphere, by 3–7% (Kentarchos and Roelofs, 2002), with the NMHC oxidation leading to PAN formation reduces NO_X concentrations in the upper troposphere/tropopause by 5–15 % (Kentarchos and Roelofs, 2002).

2.4.2.2 Aviation-induced aerosol-phase perturbations

2.4.2.2.1 Sulfates (SO_4^{2-})

Limiting factors for the formation of sulfates is the availability of OH and H_2O_2 in the troposphere, and as O_3 is a source gas for OH creation a link between the relation in formation of these secondary pollutants from aviation is observed (Unger et al., 2006a; Unger et al.,

2008). Aviation-induced sulfates have been shown to predominately form in the Northern Hemisphere (Figure 2.10) (Righi et al., 2013; Barrett et al., 2012; Unger, 2011). With peaks in sulfate concentrations of ~10 ng m^{-3} occuring in the northern mid-latitude (~30°N) and peaks correlating with aviation cruise height (~250 hPa) of ~5–10 ng m^{-3} (Righi et al., 2013).

Literature shows agreement with percentage increases in aviation-induced sulfates, with relative changes peaking about cruise height (~250 hPa) and in the northern high-latitudes (~60°N–90°N), and associated relative changes ranging between ~5–15% (Righi et al., 2013; Unger, 2011).

Studies investigating the impacts of both aviation-induced sulfates and nitrates, highlighting the interdependencies between sulfate and nitrate formation, their precursor emissions and atmospheric species which need to be considered (Righi et al., 2013; Unger, 2011; Unger et al., 2013; Fiore et al., 2012; Unger et al., 2010). Unger (2011) reported that aviation-induced ammonium sulfate form partially at the expense of ammonium nitrate in the high northern altitudes and latitudes. The sulfate/nitrate formation mechanism competes for available ammonia in the atmosphere, as these aerosols are closely linked to O_3 photochemistry as they are formed from the SO_2, NH_3 and NO_X precursors, and the availability of atmospheric oxidants, OH and H_2O_2 (Unger, 2011; Unger et al., 2010).

Figure 2.10: Sulfate multi-year average (1996–2005) zonal means: (a) absolute and (b) percentage differences from Righi et al. (2013), and (c) percentage difference from Unger (2011).

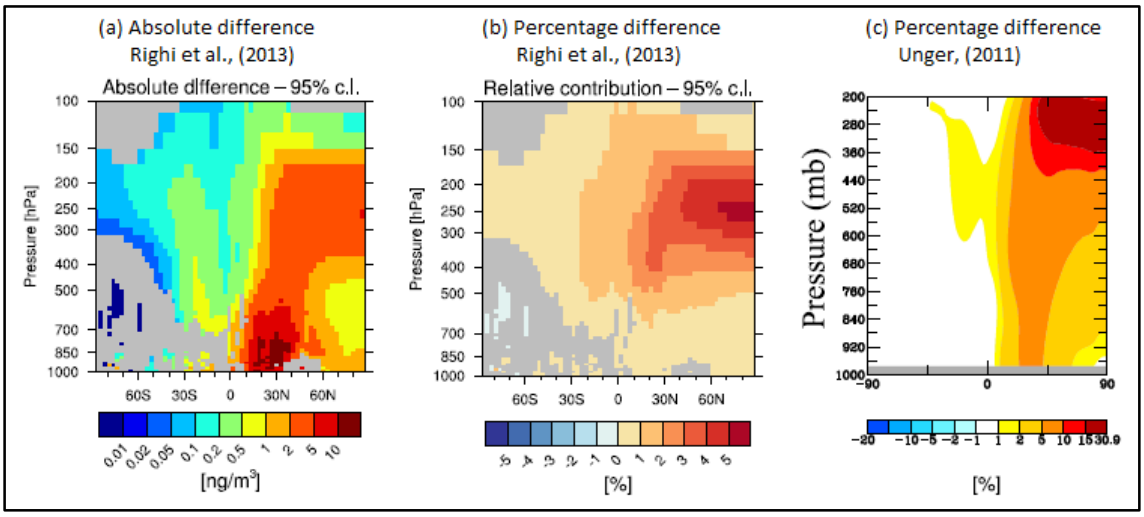

From literature investigating the impact of aviation-borne emissions on sulfate formation, it is observed that the distribution of aviation-induced sulfates in the Northern Hemisphere formed coincides with the region where the majority of aviation emissions are released (Unger, 2011; Unger et al., 2013; Olivié et al., 2012; Righi et al., 2013; Barrett et al., 2012).

In addition to the formation of aviation-induced sulfates from the release of aviation-borne SO_2 emissions, sulfates can also be induced from increases in aviation-induced OH from aviation-borne NO_X, a process which yields OH as well; with the resultant OH being able to participate in the oxidation of SO_2 from other anthropogenic or natural sources to form sulfate (Barrett et al., 2010) (Section 2.3.5).

2.4.2.2.2 Nitrate (NO_3^-)

Ammonium nitrate forms when the sulfate aerosol is fully neutralised or when there is excess ammonia in the atmosphere (Forster et al., 2007), with decreases in sulfate precursors benefiting the formation of ammonium nitrate (Bellouin et al., 2011). This is due to the coupling between sulfates and nitrates and their competition for ammonia available in the atmosphere (Unger, 2011).

Referring to Figure 2.11(a) over the northern mid-latitude there is a mean decrease in nitrate concentrations of ~1 ng m^{-3}, equating to a 20% relative decrease in atmospheric nitrate over this region (Righi et al., 2013). Breaking down perturbations in aviation-induced nitrates Figure 2.11(a) goes on to show that zonal mean concentrations increase by up to ~10 ng m^{-3} 20°–70°N, with the increases in zonal mean nitrate concentrations in the northern mid-latitudes of between 1–2 ng m^{-3} below cruise altitude. Above cruise altitude decreases in zonal mean nitrate concentrations of between ~–5 to –2 ng m^{-3} between ~30°N–90°N (Righi et al., 2013).

Figure 2.11: Nitrate multi-year average (1996–2005) zonal means: (a) absolute and (b) percentage differences from Righi et al. (2013), and (c) percentage difference from Unger (2011).

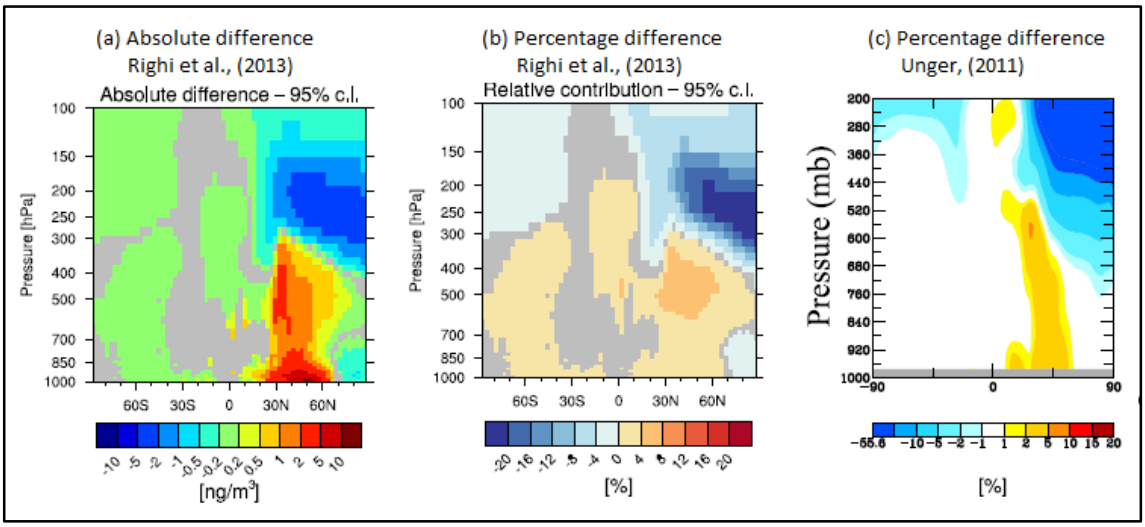

Figure 2.11(b) and Figure 2.11(c) show the relative changes in aviation-induced nitrates from Righi et al. (2013) and Unger (2011). These figures show relative increases in nitrate aerosols

below cruise phase of flight ranging between 0–5%, and decreases at cruise altitude and above.

Barrett et al. (2012) found aviation increased surface-layer nitrate concentrations by up to ~50 ng m^{-3} over South Canada and by up to ~130 ng m^{-3} over eastern China and central Europe.

As seen in the recent decrease in anthropogenic SO_2 emissions, nitrates becomes a more important aerosol specie, and may continue to be so in the future (Bellouin et al., 2011; Bauer et al., 2007). Bauer et al. (2007) through investigating reduced future SO_2 emissions simulates reductions in sulfate and increases in nitrates. This is as relatively smaller sulfate concentrations leads to favourable reactions of ammonia with nitric acid to form ammonium nitrate; instead of reacting with sulfates. And with projected increases in future nitrate precursor emissions and a decline in the formation of ammonium sulfate formed, the importance of nitrates in the future climate is further emphasised (Bauer et al., 2007). Unger (2011) demonstrated the interplay between the formation of ammonium sulfates and ammonium nitrates, when investigating the use of desulfurised jet fuel.

Through simulating a desulfurised aviation fuel case increases in aviation-induced nitrates of between 2–10% are estimated the NH mid-latitude up to an altitude of 200 mb (corresponding with cruise-level) with decreases of between –10 to –20% in the NH high-latitude above 500 mb. In comparison to standard jet fuel (Jet A/Jet A-1), increases in aviation-induced nitrates of between 2–10% are estimated in the NH mid-latitude up a latitude of ~480 mb, with decreases in aviation-induced nitrates of up to –55.6% in the NH high-latitude above ~440 mb (Figure 2.11(c)) (Unger, 2011).

2.4.2.2.3 Black carbon (BC)

Figure 2.12(a) and Figure 2.12(c) show that aviation-induced perturbations in BC concentrations dominate over the Northern Hemisphere in line with the release of aviation emissions (Lamarque et al., 2009), with high altitude peaks in absolute and relative BC concentrations about altitudes relating to aviation's cruise altitude (Righi et al., 2013; Wei et al., 2001). Wei et al. (2001) using NASA aviation emissions for 1992 find a peak difference in BC concentrations of ~1.5 ng m^{-3} between 10–12 km (267–200 hPa) for 1992 (Figure 2.12(c)). Righi et al. (2013) estimate peaks at the surface (~30°N) of between 0.2–0.5 ng m^{-3}, and at altitudes relating to a cruise altitude (~250 hPa) of between 0.1–0.2 ng m^{-3} in the Northern Hemisphere mid-latitudes. When considering the relative differences in BC induced by aviation emissions

these are again seen to dominate in the Northern Hemisphere peaking at 4–5% between 250–300 hPa.

Barrett et al. (2012) investigated aviation-induced surface-layer BC concentrations. From their work they find that the main regions which return increases in BC concentrations of up to ~0.5 ng m^{-3} over central Europe and the eastern US seaboard, increases of up to ~0.4 ng m^{-3} over the western US seaboard, and increases of up to ~0.2 ng m^{-3} over eastern China in line with total column integrated aviation BC emissions (Lamarque et al., 2009). These peaks in surface layer BC concentrations correlate with aviation fuelburn emissions (Lamarque et al., 2010b; Lamarque et al., 2009).

Figure 2.12: Black carbon multi-year average (1996–2005) zonal means: (a) absolute and (b) percentage differences from Righi et al. (2013), and (c) absolute difference for 2001 from Wei et al. (2001).

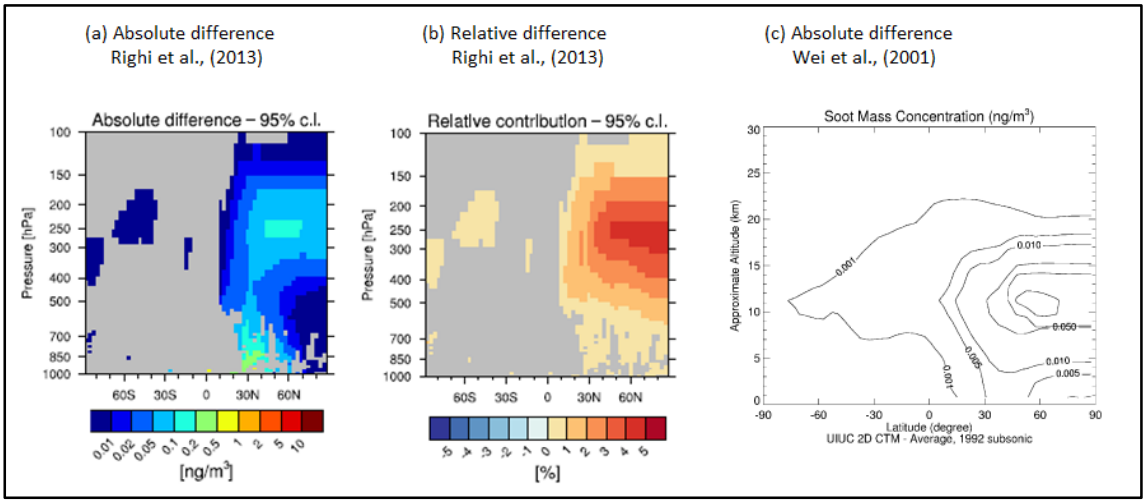

Aviation emitted BC is estimated to represent ~0.01% of total anthropogenic BC emissions from fossil fuel sources (Balkanski et al., 2010). The size of BC particles produced by aviation is much smaller than that from other emitters of BC (Balkanski et al., 2010). This is of importance as even though the total mass emitted by aviation may be small in comparison to other BC emitters the total number of particles actually emitted by aviation could represent more than 30% of the total particle numbers over a large part of the Northern Hemisphere free troposphere (Balkanski et al., 2010).

2.4.2.2.4 Organic carbon (OC)

Akin to BC aerosols OC is formed from the incomplete complete combustion (Kim et al., 2012), but unlike BC scatter light efficiently (Jacobson, 2005).

When these initially hydrophobic particles age and or other chemicals such as H_2SO_4 condense upon them they have the potential to act as cloud condensation nuclei (CCN) (Jacobson, 2005).

Surface layer OC perturbations follow a similar distribution in surface-layer aviation-induced BC found by Barrett et al. (2012), explained through the relationship of BC and OC emissions to aviation fuelburn (Eyers et al., 2004). Barrett et al. (2012) demonstrated that peak surface-layer aviation-induced OC perturbations occur in western Europe with peaks in concentrations of ~5 ng m^{-3}.

Aviation-induced OC perturbations are an aspect of aviation-emissions induced changes that have not received much attention to date (Olivié et al., 2012; Righi et al., 2013; Lee et al., 2010). This can be attributed to aviation-borne emissions species currently including in aviation emissions inventories used (Balkanski et al., 2010; Barrett et al., 2012; Unger, 2011; Olsen et al., 2013a; Eyers et al., 2004).

2.4.3 Summary of aviation-induced radiative effects

Here aviation-induced radiative effect (RE) estimates, as assessed by previous work, are presented. Assessments for CO_2 radiative forcing estimates are presented in Section 2.4.3.1, assessments for the net O_3 radiative effect (O3RE) are presented in Section 2.4.3.2, the aerosol direct radiative effect (aDRE) in Section 2.4.3.3, the aerosol cloud albedo effect (aCAE) in Section 2.4.3.4 and finally assessments of the net aviation radiative effect are discussed in Section 2.4.3.5.

2.4.3.1 Aviation carbon dioxide (CO_2) radiative effect

Recent studies by Olivié et al. (2012) and Fuglestvedt et al. (2008) suggest that RF from the CO_2 component of aviation emissions equate to around 21 mW m^{-2}, whereas Forster et al. (2006) return an RF value for CO_2 of ~25 mW m^{-2}. These aforementioned estimations lie within the estimate [28 mW m^{-2}] and errors bars presented by Lee et al. (2009), the IPCC's Fourth Assessment Report (AR4) [25.3 mW m^{-2}], and Sausen et al. (2005)'s and Penner et al. (1999)'s estimates from their 1999 report on Aviation and the Global Atmosphere [18–25.3 mW m^{-2}].

2.4.3.2 Aviation ozone (O_3) direct radiative effect

Since preindustrial times, changes in atmospheric O_3 concentration have resulted in a radiative forcing (RF) of +0.35 W m^{-2}, with Myhre et al. (2011) quantifying that the total transportation sector (road, shipping and aviation) contributing a third of this value. Lee et al. (2009) then

assessed that aviation NO_X induced O_3 production induces a RF of +26.3 mW m^{-2} (based on 2005 values) implying that aviation is responsible for 22.5% of the net anthropogenic induced RF caused by O_3 production by anthropogenic sources of NO_X (Rap et al., 2015). In addition aviation induced O_3 has a lifetime in the region of days to weeks (Unger, 2011), resulting in a response biased to the Northern Hemisphere, as well as regions which see the introduction of NO_X aviation emissions.

Figure 2.13 represents the range of estimates for aviation short-term O_3 (ST-O_3) radiative effect (RE), long-term (LT-O_3) RE, ozone-methane (O_3-CH_4) RE and net O_3 RE collated from literature (Unger et al., 2013; Khodayari et al., 2014a; Köhler et al., 2008; Myhre et al., 2011; Holmes et al., 2011; Hoor et al., 2009; Lee et al., 2009; Sausen et al., 2005; Frömming et al., 2012; Skowron et al., 2013; Unger, 2011) – represented in terms of mW m^{-2} $Tg(N)^{-1}$ to account for differences in NO_X emissions used in each study.

Figure 2.13: Range in net ozone radiative (Net RE) estimates, short-term ozone (ST-O_3) RE, long-term ozone (LT-O_3) RE, and the ozone-methane (O_3-CH_4) RE estimates from existing literature.

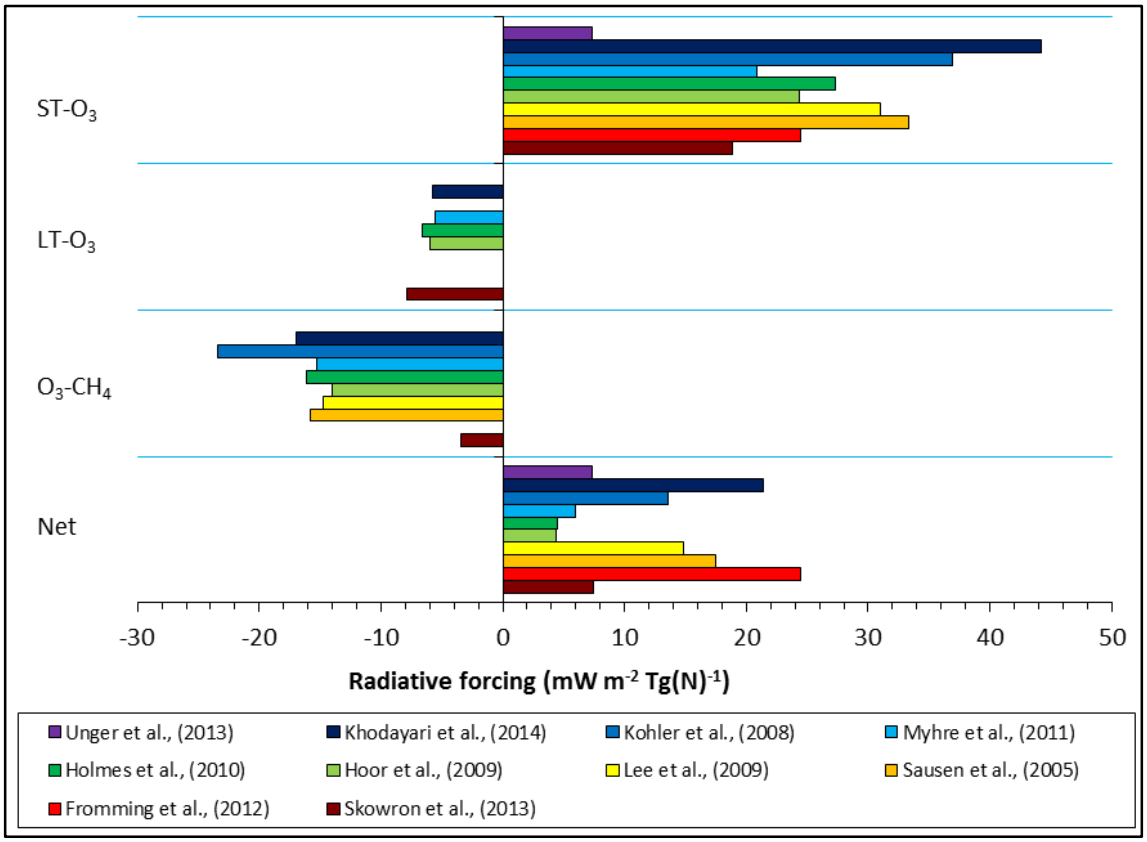

From previous work the aviation-induced ST-O_3 RE is estimated to range between 7.39–44.2 mW m^{-2} $Tg(N)^{-1}$, with a mean value of 25.10 mW m^{-2} $Tg(N)^{-1}$ and standard deviation (σ) of 11.39 mW m^{-2} $Tg(N)^{-1}$ – (Figure 2.13). The aviation LT-O_3 RE has been estimated to range between –

5.6 to –7.9 mW m^{-2} $Tg(N)^{-1}$, with a mean value of –6.37 mW m^{-2} $Tg(N)^{-1}$ and σ=0.93 mW m^{-2} $Tg(N)^{-1}$ (Holmes et al., 2011; Hoor et al., 2009; Khodayari et al., 2014a; Myhre et al., 2011; Skowron et al., 2013). With the O_3-CH_4 RE being estimated to range between –3.48 to –23.40 mW m^{-2} $Tg(N)^{-1}$, with a mean value of –14.98 mW m^{-2} $Tg(N)^{-1}$ and σ=5.48 mW m^{-2} $Tg(N)^{-1}$.

This in effect returns a range of estimates for the net O3RE of 4.5–21.4 mW m^{-2} $Tg(N)^{-1}$, a mean value of 11.71 mW m^{-2} $Tg(N)^{-1}$ and σ=7.06 mW m^{-2} $Tg(N)^{-1}$ when all studies referred to in Figure 2.13 are considered. But a range of 4.5–21.4 mW m^{-2} $Tg(N)^{-1}$, with a mean value of 8.73 mW m^{-2} $Tg(N)^{-1}$ and standard deviation of 10.09 mW m^{-2} $Tg(N)^{-1}$ when studies which consider all three components (ST-O_3 RE, LT-O_3 RE and O_3-CH_4 RE) are considered alone (Holmes et al., 2011; Hoor et al., 2009; Khodayari et al., 2014a; Myhre et al., 2011; Skowron et al., 2013).

2.4.3.3 Aviation aerosol direct radiative effect

The aviation aerosol direct radiative effect (aDRE) has been assessed as highly uncertain, ranging from –28 to +20 mW m^{-2} (Righi et al., 2013); as demonstrated by the range of estimates provided for BC, OC, sulfates (SO_4^{2-}) and nitrates (NO_3^-) (Figure 2.14).

Figure 2.14: Range in black carbon, organic carbon, sulfates and nitrates radiative effect estimates from existing literature.

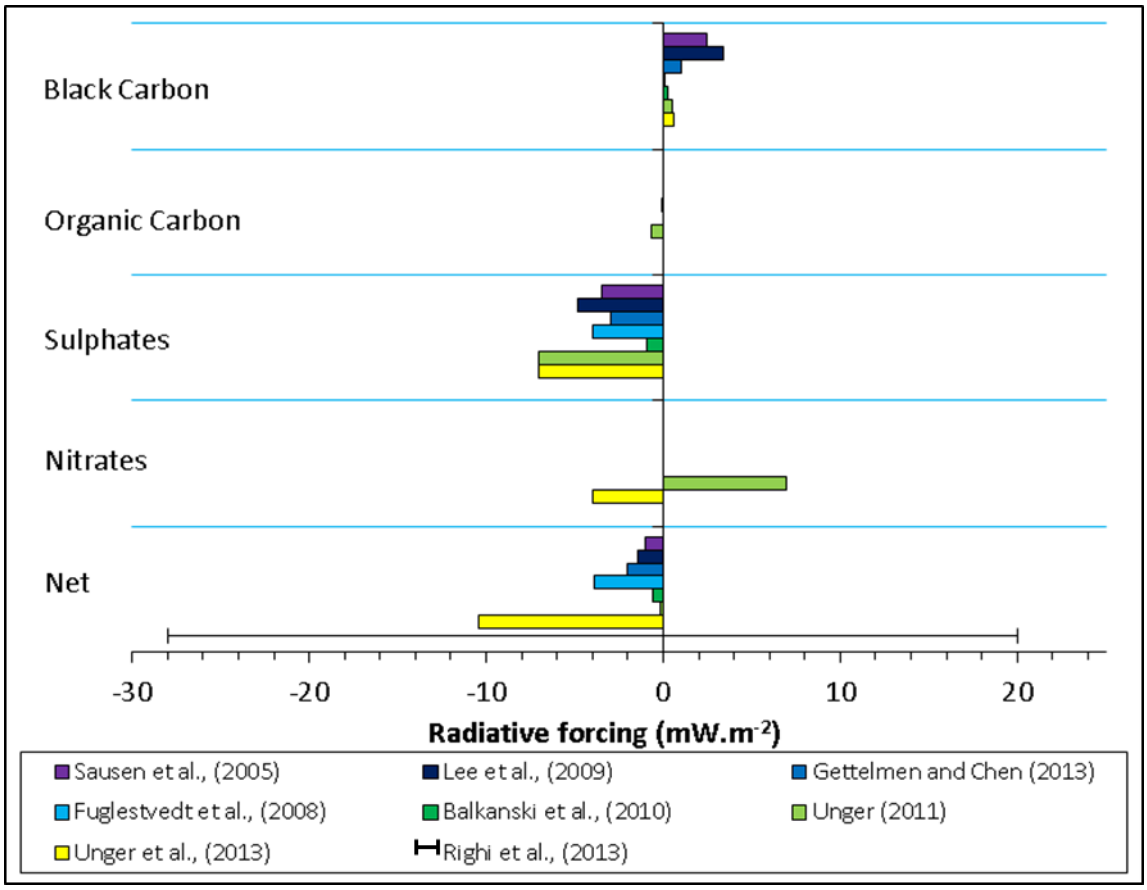

The BC aDRE is shown to range between 0.1–3.4 mW m^{-2}, with a mean value of 1.2 mW m^{-2} and σ=1.25 mW m^{-2} (Sausen et al., 2005; Lee et al., 2009; Gettelman and Chen, 2013; Fuglestvedt et al., 2008; Balkanski et al., 2010; Unger, 2011; Unger et al., 2013). Additionally uncertainties in BC aDRE estimates will be due to whether these RE estimates consider aviation-borne BC particles as externally mixed or internally mixed with sulfates; as with the latter case the BC aDRE have been shown to be greater by a factor of three (Balkanski et al., 2010). An external mixture is when all aerosol components are considered to be separated from all other components giving rise to chemically pure chemical aerosol modes, whereas internal mixtures are considered as a homogeneous material reflecting the chemical and physical average of all contributing aerosol components. In reality the real mixed state is expected to lie somewhere in between these two extremes (Lesins et al., 2002).

The aviation-induced OC aDRE returns a range of –0.67 to –0.01 mW m^{-2}, with a mean value of –0.34 mW m^{-2} and σ=0.47 mW m^{-2} (Fuglestvedt et al., 2008; Unger, 2011), demonstrating that despite the small range of values the aviation-induced OC aDRE is suggested to provide a cooling effect on the climate.

Aviation-induced sulfates return an aDRE ranging between –7 to –0.9 mW m^{-2}, mean value of –4.31 mW m^{-2} and standard deviation of 2.19 mW m^{-2} (Sausen et al., 2005; Lee et al., 2009; Gettelman and Chen, 2013; Fuglestvedt et al., 2008; Balkanski et al., 2010; Unger, 2011; Unger et al., 2013); illustrating the definitive cooling effect of aviation-induced sulfates on the aDRE.

The aDRE of aviation-induced nitrates is only reported by two studies thus far; Unger (2011) and Unger et al. (2013). The most recent of these studies identifies that aviation is capable of providing –4 mW m^{-2} of cooling (Unger et al., 2013), while the older of the two studies had previously assessed that the aDRE of aviation-induced nitrates was +7 mW m^{-2} (Unger, 2011). This is as in their 2013 paper stated that their revised estimate for aviation-induced aDRE nitrates was due to a revision in aviation-induced decrease in nitrates in the UTLS (upper troposphere/lower stratosphere) (Unger et al., 2013).

Considering these four aviation-induced aerosol components alone the net aDRE ranges between –10.4 to –0.17 mW m^{-2}, with a mean value of –2.78 mW m^{-2} and standard deviation of 3.57 mW m^{-2} (Sausen et al., 2005; Lee et al., 2009; Gettelman and Chen, 2013; Fuglestvedt et al., 2008; Balkanski et al., 2010; Unger, 2011; Unger et al., 2013), inclusive of the values returned by Unger (2011). When the aDRE for nitrates for Unger (2011) are changed to the values reported by Unger et al. (2013), this range changes to –11.17 to –0.6 mW m^{-2}, with a mean value of –4.36 mW m^{-2} and standard deviation of 4.52 mW m^{-2}.

2.4.3.4 Aviation aerosol cloud albedo effect

Not many studies report the aviation-induced aerosol cloud albedo effect (aCAE). Righi et al. (2013) and Gettelman and Chen (2013) both report the aCAE from aviation (Figure 2.15).

Figure 2.15: Range in aviation-induced aerosol cloud albedo effect (aCAE) estimates from existing literature (Righi et al., 2013; Gettelman and Chen, 2013).

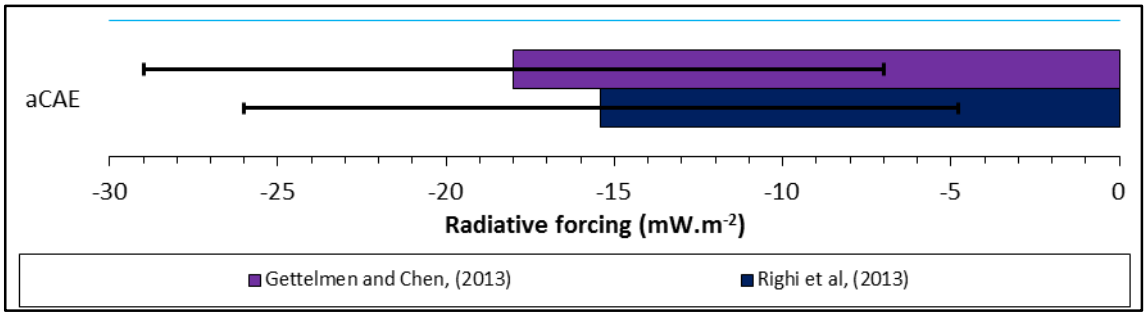

Righi et al. (2013) report an aCAE of –15.4 ± 10.6 mW m^{-2} while Gettelman and Chen (2013) report an aCAE of –18 ± 11 mW m^{-2}. Despite the small range of values to allow for such a comparison this gives rise to a mean aCAE of –16.7 ± 10.9 mW m^{-2}, with a standard deviation of 1.84 mW m^{-2} (Righi et al., 2013; Gettelman and Chen, 2013).

These values are based on the sum of shortwave and longwave radiative forcing calculations for the top-of-the-atmosphere (TOA) for all-sky conditions (Righi et al., 2013; Gettelman and Chen, 2013).

2.4.3.5 Assessments of net aviation radiative effect

There is much uncertainty around the climate impacts of non-CO_2 aviation emissions as seen in Section 2.4.3.2, Section 2.4.3.3 and Section 2.4.3.4, and by the differing levels of scientific understanding (LOSU) for different aviation radiative forcing components (Figure 2.16) (Lee et al., 2010). Figure 2.16 highlights how future work stands to address gaps in knowledge relating to the climatic effects of aviation aerosol emissions and O_3 production, and levels of uncertainty associated with these aviation forcing components.

To summarise the net radiative forcing from aviation is assessed as +55 mW m^{-2} excluding aviation induced cirrus, and +78 mW m^{-2} including the effect of aviation induced cirrus. O_3 production is responsible for +26.3 mW m^{-2} of warming, sulfates for (–)4.8 mW m^{-2} of cooling, while soot is assessed as providing +3.4 mW m^{-2} of warming (Lee et al., 2010).

Figure 2.16: Aviation radiative forcing components in 2005 – taken from Lee et al. (2010).

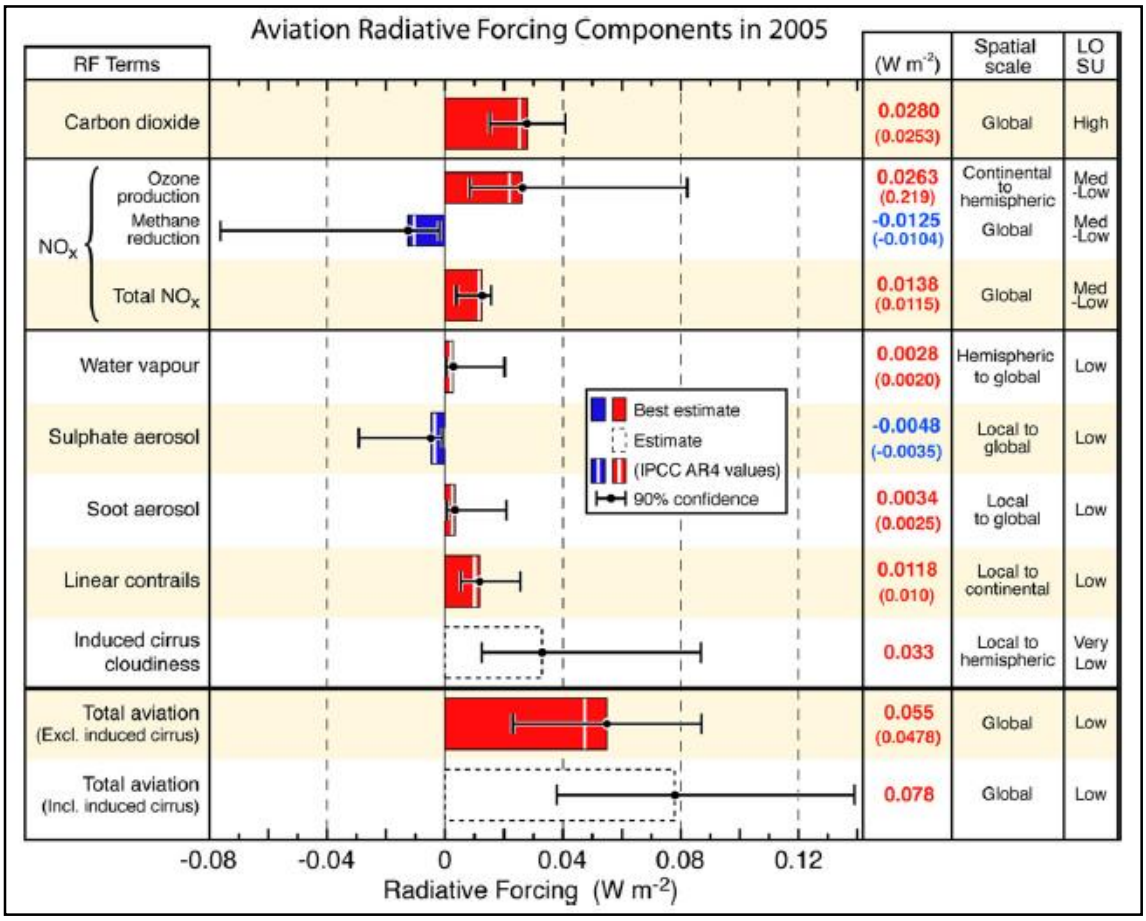

2.5 Aviation fuels

Currently modern commercial aircraft use fuels known as 'Jet A' or 'Jet A-1,' which are petroleum-derived (Airlines for America, 2011). Here a brief history (Section 2.5.1) and the specifications for Jet A/A-1 fuel (Section 2.5.2) are discussed for context.

2.5.1 History of Jet A/A-1 fuels

The first generation of turbojet engines utilised 'illuminating kerosene' otherwise known as lamp oil (Maurice et al., 2001; Blakey et al., 2011), as it was readily available and in current use in piston engine aircraft (Bernabei et al., 2000; Maurice et al., 2001).

The first true jet fuels in use were aviation gasoline (avgas), with the characteristics of successive jet fuels evolving from that of avgas. Due to identified issues with the high volatility of avgas causing 'vapour lock' at high altitudes the properties of avgas required modification in order to operate satisfactorily in jet aircraft (Maurice et al., 2001). Vapour lock and excessive

evaporation of aviation fuel was prevented through limiting vapour pressure, achieved through the introduction of additives in to the fuel mix such as aromatics, naphthaenes, isoparrafins, tetraethyl lead and other anti-detonants (McCulloch, 1946).

The development of aviation fuel was led by the US military, with the development of JP-1 (Jet Propellant 1) in 1944. Subsequently JP-2 was developed (1945), followed by JP-3 (1947) and JP-4 (1951). JP-5 was subsequently derived amid safety concerns and usage practices by the US Navy. JP-6 which followed in the 1950–60s due to specifications on the design temperature limit for commercial and military jet aircraft (Maurice et al., 2001).

In the 1960s, in line with expansion of commercial aviation, a kerosene based fuel designated Jet A (Jet A-1 in Europe) by the American Society for Testing and Materials (ASTM) became the standard fuel (Maurice et al., 2001).

2.5.2 Specification for aviation fuels

2.5.2.1 American Society for Testing and Materials (ASTM) D1655-11b: Specification for Aviation Turbine Fuels

ASTM specification D1655-11b prescribes specifications on the properties of aviation turbine fuels (jet A and Jet A-1) applicable at the point of sale (i.e. point of delivery) produced from refined HCs sourced from crude oil, natural gas liquid condensates, heavy oil, shale oil and oil sands (ASTM International, 2012b). These properties have been stipulated in order to ensure that the aviation fuels when in use or transportation are safe and fit for purpose (Airlines for America, 2011; ICAO, 2010).

Additionally ASTM 1655-11b provides stipulations on additives that can be used in conjunction with fuel produced to this specification. Ultimately these specifications along with engine and aircraft certifying authority will stipulate which fuels can be utilised (ASTM International, 2011c; ASTM International, 2012b) as per their 'Airline Fuelling Manual' (or equivalent document) (Airlines for America, 2011).

Not only does ASTM specification D1655-11b stipulate what types of fuels are covered and from which fuel stocks they are to be derived from, this specification puts in to place constraints on the type and amount of additives that can be used in conjunction with Jet A and Jet A-1 fuel in order to ensure the safe and economical operation of the aircraft (ASTM International, 2010; ASTM International, 2012b). Despite the specification put in to place by ATSM D1655-11b, the use of additives and fuels in any engines or associated aircraft

equipment is ultimately governed by certifying authorities, such as the FAA (Airlines for America, 2011; ASTM International, 2012b).

In order to ensure safety of the aircraft during operation, storage and transportation there are specifications in place regarding thermal stability of the fuel, on the aromatic composition, fuel freezing point, content of elastomer degrading species of the fuels as these have undesirable effects on the combustion properties of the fuel (ASTM International, 2012b). An elastomer is a natural or synthetic polymeric material which may experience large and reversible elastic deformations (Callister Jr, 1997). In addition to these there are stipulations on the minimum amount of additives required to ensure fuel lubricity, the total acid content of the fuel which could degrade equipment, the flash point to ensure safe handling and storage, controlling of microbial contamination which can corrode and deteriorate equipment and the use of surfactants which can allow water and solid particles to dissipate and settle out of the fuel at a slower and undesired rate (ASTM International, 2012b).

2.5.2.2 UK Defence Standard 91-91: Issue 7, Amendment 1

Initially developed as standard D.Eng RD 2494 by the UK's Ministry of Defence for military jet fuel, this standard was later adopted as the standard for UK civil aviation jet fuel. This standard was later renamed as the UK Defence Standard 91-91 (DEF STAN 91-91) in 1994 (Li, 2011; Ministry of Defence, 2011). DEF STAN 91-91 is currently the agreed standard for the UK Civil Aviation Authority (Ministry of Defence, 2011).

This specification has been derived to act as an overall performance specification for jet fuel; this is due to the variety of sources from which jet fuels can be produced. Jet fuels as per DEF STAN 91-91 are predominately defined as fuels derived from conventional sources inclusive of crude oil, natural gas liquid condensate, heavy oil, shale oil and oil sands. Other jet fuels derived from nonconventional sources, i.e. non-petroleum sources, such as fully synthetic and semi-synthetic jet fuel blends are included, as per stipulation in Annex A and Annex D of standard DEF STAN 91-91 (Ministry of Defence, 2011).

Similar to the ASTM International standards only permitted additives (such as lubricity improver, fuel system icing inhibitors and leak detection additives) approved by the Ministry of Defence's Aviation Fuels Committee are allowed (Ministry of Defence, 2011).

Standard DEF STAN 91-91 considers the mandatory target set by the European Commission to ensure that greenhouse gas emissions from transportation are reduced by at least 6% from the

use of biofuels by 2020, with the main target being a reduction of 10% (European Commission, 2009b; Ministry of Defence, 2011). This resulted in the mandatory introduction of trace amounts of Fatty Acid Methyl Esters (FAMEs) being introduced in to the fuel mix (Ministry of Defence, 2011).

2.6 Health related effects of aviation emissions

Studies have shown that aviation emissions contribute to increases in surface-level $PM_{2.5}$ concentrations (Lee et al., 2009; Balkanski et al., 2010; Barrett et al., 2010; Woody et al., 2011; Barrett et al., 2012; Levy et al., 2012; Jacobson et al., 2013; Yim et al., 2015), with increases in surface $PM_{2.5}$ concentrations being greatest near airports (Barrett et al., 2010; Woody et al., 2011; Yim et al., 2015), and global maxima in $PM_{2.5}$ concentrations ranging between 150–400 ng m^{-3} (Barrett et al., 2010; Barrett et al., 2012; Yim et al., 2015). In addition to increases in surface-level $PM_{2.5}$ concentrations, aviation has been shown to increase global mean surface-layer ozone concentrations by 0.6 ppbv (Yim et al., 2015). These increases in surface $PM_{2.5}$ and O_3 concentrations can have adverse effects on human health (Barrett et al., 2010; Barrett et al., 2012; Ostro, 2004; Ostro and Rothschild, 1989; World Health Organisation, 2000).

Primary and secondary gas-phase pollutants from aviation, NO_X and O_3 respectively, can affect the human respiratory system exacerbating respiratory ailments (World Health Organisation, 2000; World Health Organisation, 2005; De Nevers, 2000). Aerosol-phase aviation-borne emissions contribute to increases in atmospheric concentrations of pollutants such as sulfates, nitrates, BC and OC (Lee et al., 2009; Balkanski et al., 2010; Unger et al., 2013; Woody et al., 2011; Hendricks et al., 2004; Righi et al., 2013; Gettelman and Chen, 2013; Barrett et al., 2010; Barrett et al., 2012), which perturb surface $PM_{2.5}$ concentrations (Barrett et al., 2010; Barrett et al., 2012; Woody et al., 2011).

Fine mode particles (Dp < 2.5 µm, i.e. $PM_{2.5}$) have the ability to penetrate the human respiratory system (Righi et al., 2013). Due to increases in $PM_{2.5}$ concentrations since 1860 it is estimated that in year 2000 increases in levels of $PM_{2.5}$ are responsible for 1.5 million mortalities from cardiopulmonary disease and 95,000 mortalities from lung cancer, while over the same period O_3 exposure has caused 0.37 million respiratory related mortalities (Fang et al., 2013). With the vertically distributed nature of aviation emissions this places additional concern on the trans-boundary nature of aviation borne emissions (Unger, 2012).

2.6.1 Effects of gas-phase species affect human health and vegetation

Exposure to increased levels of pollutants such as O_3 has been associated with increased levels of hospital admissions and levels of mortality, particularly affecting the health of vulnerable members of the populous (World Health Organisation, 2003). This can be through the exacerbation of respiratory ailments such as asthma and increasing levels of cardiovascular disease, or by inducing a variety of variety of pulmonary effects, including decrement of lung function, increased airways responsiveness, and inflammatory reaction (Brunekreef and Holgate, 2002; Bergamaschi et al., 2001).

NO_X exposure increases susceptibility to respiratory infections, with exposure to O_3 reducing lung function and increasing susceptibility to infections (De Nevers, 2000; Kampa and Castanas, 2008). Bergamaschi et al., (2001) conducted a study on the effect of ambient O_3 levels between 32–103 ppb on 24 individuals performing 2 hour cycles and demonstrated on average there was a 3% decline in FEV_1 (forced expiratory volume in 1 s) (Lomas et al., 2008). The effects of exposure to O_3 and the concentration of the dosage the subjects are exposed to is further highlighted by De Nevers (2000) when discussing the work of Coffin et al., (1969) where the susceptibility of mice to the *Streptococus C* bacteria was investigated, demonstrating that as the level of O_3 mice were exposed to increased, their susceptibility to the bacterium in question increased (De Nevers, 2000; Coffin et al., 1969).

Currently the World Health Organisation's guidelines for O_3 exposure stands at 100 $\mu g.m^{-3}$ for an 8-hour mean, a reduction from 2003's level of 120 $\mu g.m^{-3}$ (World Health Organisation, 2003; World Health Organisation, 2005).

2.6.2 Effects of aerosol-phase species on human health

Fine $PM_{2.5}$ (a mixture of liquid and solid matter) has the potential to enter the respiratory system. Löndahl et al., (2006) highlights that particulates ranging between 1–5 µm can be deposited in the respiratory bronchioles and the alveoli where gas exchange occurs (Löndahl et al., 2006). Typically as the size of particles decreases, the more adverse the health effects these particles can have. With decreases in particle size PM is hypothesised to increase in acidity, along with their ability to penetrate into the lower airways (Kim et al., 2015).

Epidemiological studies have identified a multitude of PM induced adverse health effects, such as: mortality, lung cancer, hospitalisation, the exacerbation of asthma, hindrance to the

respiratory system, acute and chronic bronchitis and absences from work and school (Ostro, 2004).

Mortality related to short-term PM exposure examines daily changes in air pollution. This acute study on the effects of PM on mortality considers daily counts of mortality, or cause-specific hospitalisation.

In order to estimate Environmental Burden of Disease (EBD) from the health impacts due to short-term PM_{10} exposure Ostro (2004) put forward investigating the following two health outcomes: All-cause mortality and short-term from exposure to PM_{10} for all age ranges; and respiratory mortality from short-term exposure to PM_{10} for where age <5 (Ostro, 2004).

Meta-analysis of the relationship between percentage increases in mortality from short-term exposure to PM_{10} over various geographical regions, an average increase daily mortality of 0.8% per 10 $\mu g.m^{-3}$ (95% CI = 0.5 –1.6) increase in PM_{10} concentrations was found. Additionally it was also identified that where investigations were conducted outside Western industrialised nations, this value increased greatly due to high relative increases in PM_{10} concentrations. From this meta-analysis it was recommended to cap the range of the linearity of this relationship, as it risks overestimating mortality increase estimates in cities where PM_{10} concentrations are greater than 125 $\mu g.m^{-3}$ (Ostro, 2004).

Using data from the Pope et al. (1995) study a log-linear concentration-responses function (CRF) was developed to assess mortality from long-term exposure to $PM_{2.5}$ due to cases of cardiopulmonary disease and lung-cancer (Ostro, 2004). The CRF for these health outcomes is discussed further and derived in Section 6.3.2 when the impact of aviation-induced increases in $PM_{2.5}$ concentrations with variation in fuel sulfur content (FSC) is investigated.

Current literature estimate that aviation is annually responsible for 10,000 mortalities, with strategies to reduce aviation-induced mortalities (e.g. the use of ultra-low sulfur jet fuel with a fuel sulfur content of 15 ppm) estimated to reduce aviation-induced mortalities by 2,300 (Barrett et al., 2012).

2.7 Summary of background and literature review

Currently aviation is responsible for 2–14 % of all anthropogenic forcing when all aviation non-CO_2 emissions are accounted for (Lee et al., 2010).

Current scientific knowledge identifies that there is a medium-low level of scientific uncertainty (LOSU) surrounding estimates of aviation-induced ozone production, and low LOSUs for estimates relating to the direct climatic impact of sulfates and soot aerosols from aviation (Section 2.4.3.5). Current estimates of aviation-induced indirect effects (i.e. aerosol cloud albedo effects (aCAE)) are seen to have large uncertainties: Righi et al. (2013) assessed the aCAE to be –15.4 mW m^{-2} ± 69%, while Gettelman and Chen (2013) report an uncertainty of ± 61% associated with their estimate of –18 mW m^{-2}.

There are only a few studies that current investigate the human health impacts of aviation (Barrett et al., 2010; Barrett et al., 2012; Yim et al., 2015), and a fewer which also consider the impacts of air quality improvement strategies on the aviation-induced climate effects in addition to human health (Barrett et al., 2012). Due to rapid expansion of the aviation sector (discussed in Section 1.3) (Lee et al., 2009; Kreutz et al., 2008; Gudmundsson and Anger, 2012) its associated impact on human health now and in to the future has the potential to pose a significant impact.

Due to the projected rapid expansion of the aviation sector and its associated CO_2 impacts the sector aims to integrate alternative fuels in to the fuel mix currently in use, with the aims to reduce sectoral emissions (Section 1.6) (ATAG, 2011). The use of alternative fuels have the potential to reduce particulate formation due to reductions in fuel sulfur content and aromatics present in the fuel (ASTM International, 2011c; ASTM International, 2012b), but there is currently no literature investigating the ozone and aerosol direct radiative effects, aerosol cloud albedo effect along with the impacts of alternative fuel use on human health.

2.8 Research aims and questions

Taking in to account the levels in uncertainties present in assessments of the radiative effects of aviation-induced ozone and aerosols (Figure 2.16), along with projected decreases in global sulfate and increases nitrate burdens and the potential for nitrate forcing to become a more dominant forcing component, this thesis aims to help reduce these gaps in knowledge. This thesis aims to help reduce these gaps in knowledge through the use of a size-resolved coupled tropospheric chemistry-aerosol microphysics model (the nitrate-extended version of the TOMCAT-GLOMAP-mode coupled model described and evaluated in Chapter 3) this thesis aims to estimate the impacts of sulfate, nitrates, BC and OC aerosols and their associated climatic effects, while assessing aviation ozone and sulfate formation in tandem with nitrate aerosol formation mechanisms.

When considering the complex chemical interactions and emission species considered within current aviation emissions inventories, there is a drive to try and represent and replicate aviation emission species as accurately as possible, i.e. through the inclusion of speciated HCs. Using an expanded aviation emissions inventory created using CMIP5 (5th Coupled Model Intercomparison Project) recommended historical aviation emissions for year 2000 as a base (Chapter 4), this thesis aims to do the same. CMIP5 recommended historical aviation emissions currently only consider aviation-borne NO_X and BC emissions (Lamarque et al., 2009). Through using CMIP5 recommended historical emissions as a base for development and comparison, CMIP5-extended allows for atmospheric and climate impacts potentially not evaluated in ACCMIP (Atmospheric Chemistry and Climate Model Intercomparison Project) studies to be evaluated; thus evaluating the need for CMIP5 emissions to consider a wider and more comprehensive range of emissions species. Using the capabilities of the nitrate-extended version of the TOMCAT-GLOMAP-mode coupled model this thesis allows aviation to be represented to the best of the capabilities of the model available, while investigating the atmospheric and climatic impacts of an extended aviation emissions inventory.

Taking aviation's impact on human health and fuel sulfur content (FSC) reduction strategies in to account this thesis investigates the relationship between variations in FSC, aviation-induced surface-layer aerosols within the $PM_{2.5}$ size category, aviation-induced mortality from increases in cases of cardiopulmonary disease and lung cancer, resulting impacts on cloud condensation nuclei (CCN), and; climate (Chapter 6).

Finally, as the industry is considering the use of alternative fuels (Section 1.6), in order to reduce emissions from civil aviation, this thesis investigates the use of Fischer-Tropsch (FT) and Fatty Acid Methyl Esters (FAME) in aviation on the atmosphere, climate, air quality and human health impacts (Chapter 7). Here four alternative fuel scenarios are developed in order to investigate the atmospheric, climatic, air quality impacts as well as impacts on human health from the use of the four FT and FAME fuel blends.

The objectives of this thesis are:

- Development of a bespoke aviation emissions inventory for year 2000 inclusive of speciated HCs.
    - Development of a monthly resolved aviation emissions inventory for year 2000 based on CMIP5 (5th Coupled Model Intercomparison Project) recommended historical aviation emission.
    - Emissions inventory developed to include NO_X, CO, speciated HCs, SO_2, BC and OC.

- Investigate the atmospheric and climatic impact of historical (year 2000) aviation-borne emissions; aiming to reduce uncertainties and expand on estimates obtained using a coupled chemistry-aerosol microphysics model.
    - Investigate aviation-induced gas-phase (O_3, NO_X, OH, HO_X and SO_2) and aerosol-phase (sulfate, nitrates, BC, OH, ammonium) perturbations.
    - Investigate aviation-induced perturbations on cloud condensation nuclei (CCN).
    - Assess the radiative effect of aviation; paying attention to the O_3 direct radiative (O3DRE), aerosol direct radiative (aDRE), and aerosol cloud albedo effects (aCAE).
    - Sensitivity analysis of aviation-borne CO, HCs and SO_2 emissions in order to investigate their relative impacts.
- Investigate the changes in atmospheric concentrations and air quality, human health impacts, and impacts on climate influenced by variations aviation fuel sulfur content (FSC). In addition to perturbations in ground-level $PM_{2.5}$ and mortality, perturbations in low-cloud level CCN and radiative effect will be investigated.
    - Currently there is little work which considers and assesses premature mortalities due to aviation-induced perturbations in surface layer $PM_{2.5}$.
        - Current literature considers aviation-induced $PM_{2.5}$ from sulfate, nitrate and ammonium aerosols within the size category of <2.5 µm. This thesis will consider the contribution to the $PM_{2.5}$ size category of a wider range of aerosol species contributing to that size range (sulfates, BC, OC, sodium from sea-salt, dust, nitrates, ammonium and chloride from sea-salt), and their resulting impact on aviation-induced premature mortality.
    - This investigation will vary aviation FSC; in relation to the standard FSC of 600 ppm.
        - Initially FSC will be varied between 0–6000 ppm while, maintaining the distribution of current aviation-borne emissions.
        - Aviation emissions will be collapsed to ground-level while maintaining relative emitted abundances.
        - Finally, two scenarios will vary FSC above the cruise phase of flight, while implementing ULSJ fuel below cruise.
- Development of alternative fuel scenarios for year 2000.
    - Referring to specification for the use of alternative fuels in commercial aviation alternative fuel scenarios will be developed based on the use of:
        - Fischer-Tropsch fuel blends.
        - Fatty acid methyl esters (FAMEs) fuel blends.

- As per the aviation-emissions inventory derived the following species will be included: NO_X, CO, speciated HCs, SO_2, BC and OC.

- Investigate the atmospheric, climatic, air quality, and human health impacts of aviation alternative fuel scenarios.
  - Using the alternative fuel scenarios derived above and present day (2000) emissions and meteorology the impact of the use of alternative fuel blends on gas- and aerosol-phase perturbations and resulting climatic impacts will be investigated.

3 Model description and evaluation

3.1 Overview

In order to investigate the atmospheric, climatic, air quality and human health impacts of aviation-borne emissions, the nitrate-extended version of the TOMCAT-GLOMAP-mode coupled global model (GMV4-nitrate) is used. In this chapter the model is described (Section 3.2), and then evaluated (Section 3.3) to investigate how model simulated ozone and aerosol profiles compare to ozonesonde and aircraft observations.

Section 3.2 provides a discussion of the TOMCAT chemical transport model, the gas-phase and microphysical processes within the GLOMAP-mode aerosol model, meteorological drivers, the inorganic dissolution module of the nitrate-extension version and nitrate-extended version specific tracers. Finally, the theory behind calculation of the cloud condensation nuclei (CCN) concentrations and radiative effects (RE) are described.

In Section 3.3 GMV4-nitrate's gas-phase chemistry is evaluated against observational ozone profiles collated by Tilmes et al. (2012), and the model's aerosol-phase chemistry is evaluated against aerosol mass concentration profiles for sulfates, nitrates, ammonium and organic aerosol profiles from aircraft field campaigns collated by Heald et al. (2011).

3.2 Description of the nitrate-extended version of TOMCAT-GLOMAP-mode coupled model

A number of different versions of TOMCAT-GLOMAP are available. The GLOMAP-mode model with prescribed 3D oxidants (offline-oxidants) is described in Mann et al., (2010). The coupled TOMCAT-GLOMAP-mode global model has the same GLOMAP-mode aerosol scheme but with coupled tropospheric chemistry simulated online. This model version is described in Breider et al. (2010). In this thesis, the nitrate extended version of the TOMCAT-GLOMAP-mode coupled chemistry-aerosol model (GMV4-nitrate) is used. This version extends the coupled chemistry-aerosol version of TOMCAT-GLOMAP to include a NH_3 tracer and the formation of nitrate aerosols, the semi-volatile behaviour of nitrate aerosols and its portioning between the gas- and aerosol-phase (Benduhn et al., 2016).

This chapter presents the nitrate-extended version of the TOMCAT-GLOMAP-mode model. In this thesis, specific aspects of the model necessary for simulating nitrate aerosol (the dissolution module, additional chemical tracers and hybrid numerical solver) are introduced, which is discussed in detail by Benduhn et al. (2016).

3.2.1 TOMCAT chemical transport model

TOMCAT (Toulouse Off-line Model of Chemistry and Transport) is a global off-line 3-D Eulerian chemical transport model (CTM) (Arnold et al., 2005; Chipperfield, 2006), which considers a tropospheric gas-phase chemistry scheme (inclusive of O_X-NO_Y-HO_X), treating the degradation of C_1-C_3 non-methane hydrocarbons (NMHCs) and isoprene, together with a sulfur chemistry scheme (Breider et al., 2010; Mann et al., 2010; Spracklen et al., 2005a). Convection, wet and dry deposition, lightning and tropospheric gas-phase chemistry is simulated along with large-scale atmospheric transport driven by winds specified by European Centre for Medium-Range Weather Forecasts (ECMWF) analyses at 6-hourly intervals, together with boundary layer mixing (Chipperfield, 2006). Simulations are run at a horizontal resolution of 2.8° x 2.8° with 31 hybrid sigma-pressure (σ-p) levels (i.e. terrain tracking at the surface) extending from the surface to 10 hPa.

Investigations conducted in this thesis are for year 2000. Simulations are initiated on the 1st of September 1999 for 16 months: with the first four months used to allow the chemistry to stabilise, i.e. spin-up period, and the following 12 months used for analysis of year 2000.

3.2.1.1 Gas-phase processes

Here the gas-phase chemistry within GMV4-nitrate and, sulfur and trace gas emissions are discussed. Benduhn et al. (2016) provides an in-depth description of the dissolution solver used to accurately characterise the size-resolved partitioning of ammonia (NH_3) and nitric acid (HNO_3) in to ammonium (NH_4) and nitrate (NO_3) soluble mode components (in Section 3.2.4).

3.2.1.1.1 Gas-phase-chemistry

The gas-phase chemistry within this coupled version of TOMCAT-GLOMAP-mode is akin to that described in Breider et al. (2010). The coupled version of this model considers bimolecular, termolecular, thermal decomposition, heterogeneous and photolysis reactions.

Specific to the nitrate-extended version of the TOMCAT-GLOMAP-mode coupled model NH_3 emissions are considered, allowing for the simulation of transfer of gas-phase HNO_3, HCl and NH_3 into the aqueous-phase, ultimately allowing the model to simulate the formation of ammonium nitrate ($NH_4.NO_3$) and ammonium sulfate ($(NH_4)_2.SO_4$) (Benduhn et al., 2016).

3.2.1.1.2 Sulfur and trace gas emissions

GLOMAP-mode includes monthly sea-water concentrations of DMS from marine phytoplankton (Kettle and Andreae, 2000), SO_2 from both continuous (Andres and Kasgnoc, 1998) and explosive volcanoes (Halmer et al., 2002), and wildfire burning SO_2 emissions as per GFED v1 (Global Fire Emissions Database) for year 2000 (Dentener et al., 2006; Van Der Werf et al., 2003). Anthropogenic SO_2 emissions (including industrial, power-plant, road-transport, off-road-transport and shipping sectors) and are representative of the year 2000 (Cofala et al., 2005). In line with the standard version of GLOMAP-mode monthly terpene and isoprene emissions from Guenther et al. (1995) are used. NH_3 emissions come from the EDGAR inventory (Bouwman et al., 1997). NO_X emissions are considered from anthropogenic (Lamarque et al., 2010b), natural (Lamarque et al., 2005) and biomass burning (van der Werf et al., 2010) sources. The standard version of GMV4-nitrate includes year 2000 aviation NO_X emissions, as per CMIP5's recommended historical aviation emissions (Lamarque et al., 2009).

3.2.1.2 Meteorological conditions

Meteorology (wind, temperature and humidity) and large scale transport is specified from interpolation of 6-hourly reanalysis (ERA-40) fields (Mann et al., 2010; Scott, 2013; Breider et al., 2010). Cloud fraction and cloud top pressure fields are taken from the International

Satellite Cloud Climatology Project (ISCCP-D2) archive for the year 2000 (Rossow and Schiffer, 1999). The Prather (1986) advection scheme is used for tracer transport, the Tiedtke (1989) convection scheme, and the Holtslag and Boville (1993) scheme for boundary layer turbulence.

3.2.2 GLOMAP

Developed at the University of Leeds, GLOMAP (Spracklen, 2005; Spracklen et al., 2005a; Spracklen et al., 2005b; Pringle, 2006) is an aerosol extension of the TOMCAT CTM (Arnold et al., 2005; Chipperfield, 2006) (Figure 3.1). GLOMAP is a two-moment aerosol microphysics scheme, considering both aerosol mass and number. GLOMAP was originally developed to consider size sections (or bins) to capture particle dry diameters (D_g) from 0.001–25 µm; typically split across 20 bins (Spracklen et al., 2005a).

Figure 3.1: TOMCAT-GLOMAP-mode coupled model interactions and mechanisms used to model aerosol behaviour.

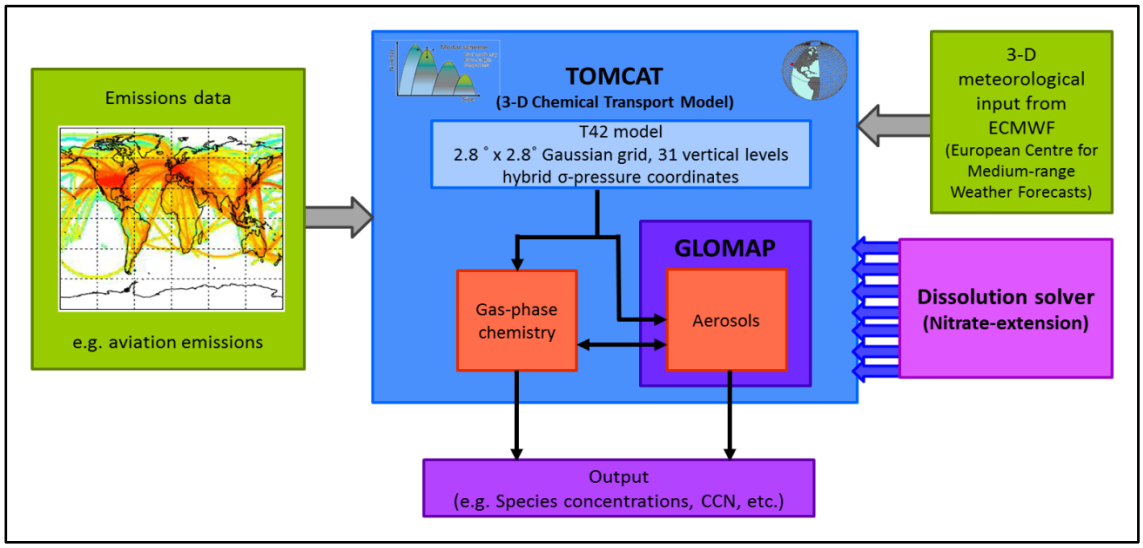

GLOMAP-mode uses a two-moment pseudo-modal aerosol dynamic approach, i.e. where the process rates for each mode are based on a particle size given by a single diameter rather than by integrating over the mode size range, while considering a log-normal size distribution of aerosols particles, while representing particles as an external mixture of 7 size modes (4 soluble and 3 insoluble) (Mann et al., 2010). This thesis uses the nitrate-extended version of the GLOMAP-mode coupled model (Benduhn et al., 2016), which as well as tracking size-resolved sulfate, black carbon (BC), organic carbon (OC), sea-salt and dust components, also includes a dissolution solver to accurately characterise the size-resolved partitioning of NH_3 and HNO_3 in to NH_4 and NO_3 components in each soluble mode.

Aerosol components are assumed to be internally mixed within each mode. GLOMAP-mode includes representations of nucleation, particle growth via coagulation, condensation and

cloud processing, wet and dry deposition, and in- and below-cloud scavenging (Mann et al., 2010).

3.2.3 GLOMAP-mode description

Here an in-depth description of GLOMAP-mode is provided, discussing modal distribution, gas-, aqueous- and aerosol-phase microphysical processes.

3.2.3.1 Modal version and size distribution

There is a need for aerosol schemes with aerosol microphysics with dynamically varying particle size, but at a lower computational cost than sectional schemes, which is where modal schemes come in (Mann et al., 2010). Sectional aerosol schemes partition the aerosol size distribution being investigated in to at least 20 size sections; a methodology which is computationally expensive (Spracklen et al., 2005a).

Figure 3.2: Representation of the log-normal aerosol number-size distribution represented within GLOMAP-mode. Components represented are sulfate (SU), black carbon (BC), organic carbon (OC), sea-salt sodium (SS), dust (DU), nitrate (NO_3), ammonium (NH_4) and sea-salt chloride (Cl).

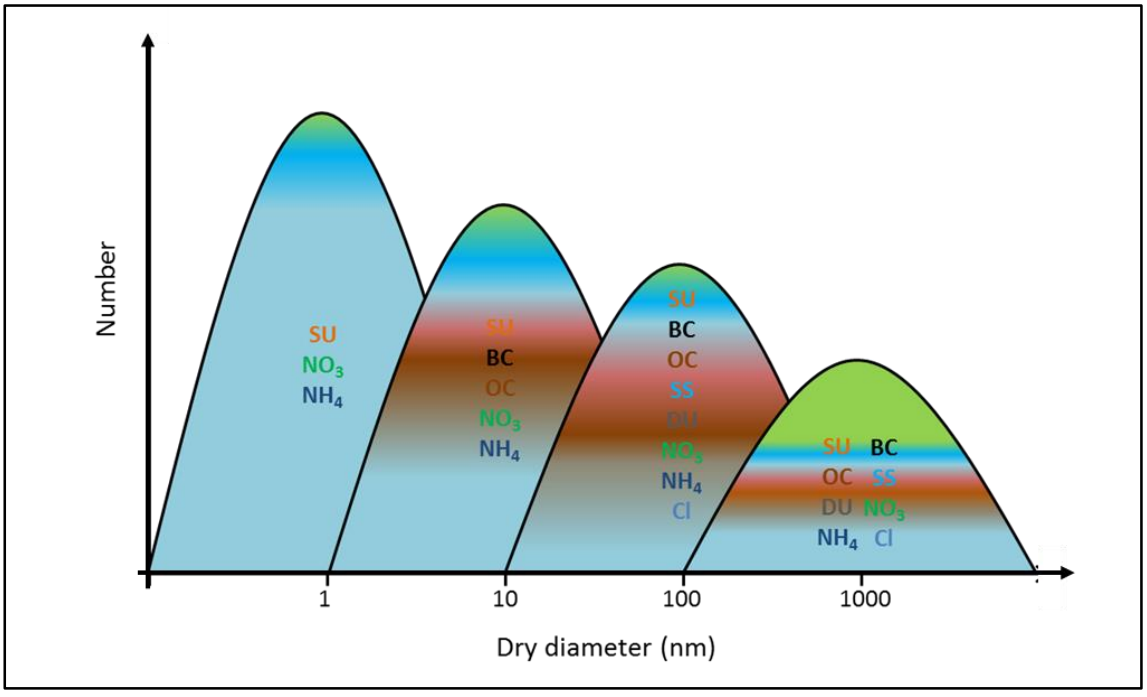

Modal schemes are designed to allow for longer integrations with greater computational efficiency and have been shown to compare well with their sectional counterparts and

observations (Scott, 2013; Mann et al., 2010; Mann et al., 2012). The modal distribution about the 4 size distributions (modes) is illustrated in Figure 3.2.

GMV4-nitrate considers eight aerosol components: sulfate (SO_4^{2-}), black carbon (BC), organic carbon (OC), sea-salt sodium (Na^+), dust (DU), nitrate (NO_3^-), ammonium (NH_4^+) and sea-salt chloride (Cl^-). These aerosol components are split between 7 size modes: 4 soluble and 3 insoluble (Mann et al., 2010) (Table 3.1).

Table 3.1: Aerosol configuration for the nitrate-extended version of the TOMCAT-GLOMAP-mode coupled model. Modal size ranges specified by geometric mean diameter (D_g) using specified standard deviations (σ_g) – adapted from Mann et al. (2010).

Index	Mode name	Size range	Mode composition	Soluble	σ_g
1	Nucleation soluble	D_g <10 nm	SO_4^{2+}, NO_3^-, NH_4^+	Yes	1.59
2	Aitken Soluble	10 nm < D_g <100 nm	SO_4^{2+}, BC, OC, NO_3^-, NH_4^+	Yes	1.59
3	Accumulation soluble	100 nm < D_g <1000 nm	SO_4^{2+}, BC, OC, Na^+, DU, NO_3^-, NH_4^+, Cl	Yes	1.59
4	Coarse soluble	D_g > 1000 nm	SO_4^{2+}, BC, OC, Na^+, DU, NO_3^-, NH_4^+, Cl^-	Yes	2.0
5	Aitken insoluble	10 nm < D_g <100 nm	BC, OC	No	1.59
6	Accumulation insoluble	100 nm < D_g <1000 nm	DU	No	1.59
7	Coarse insoluble	D_g > 1000 nm	DU	No	2.0

In order to determine which size mode aerosol particles will enter (as described in Table 3.1), the geometric mean diameter (GMD), otherwise denoted by D_g, for each aerosol component is calculated. The GMD ($D_{g,i}$) for each size mode (i) is determined through use of Equation 3.1 (Scott, 2013).

$$D_{g,i} = \sqrt[3]{\frac{6 \cdot V_{dry_i}}{\pi \cdot \exp\left(4.5 \left(\log\left(\sigma_{g,i}\right)\right)^2\right)}}$$

Equation 3.1

Where $D_{g,i}$ = geometric mean diameter (nm) for mode i

V_{dry_i} = total dry volume over all components j in that mode

$\sigma_{g,i}$ = geometric standard deviation for mode i

Where V_{dry_i} is calculated from Equation 3.2 (Scott, 2013).

$$V_{dry_i} = \sum_j \left(\frac{m_{i,j} M_j}{N_A \rho_j} \right)$$

Equation 3.2

Where $m_{i,j}$ = number of molecules of particle of each component j and size modes i

M_j = molar mass of each component j

N_A = Avogadro's constant

ρ_j = density of component j

The molar mass of each aerosol component (M_j) along with the density of each component (ρ_j) is presented in Table 3.2.

Table 3.2: Physical characteristics of aerosol components considered by the nitrate-extended version of the TOMCAT-GLOMAP-mode coupled model used in this thesis.

Aerosol component	Component abbreviation	Molar mass (M_j) (g mol^{-1})	Density (ρ_j) (kg m^{-3})
Sulfate	SU	96.06	1769
Black carbon	BC	12	1500
Organic carbon	OC	16.8	1500
Sea-salt (Sodium)	SS	22.99	2196
Dust	DU	100	2650
Nitrate	NO_3	62	1550
Ammonium	NH_4	18.04	1000
Sea salt (Chloride)	Cl	35.45	1460

As the model simulates the different aerosol processes considered, the fraction of each mode's geometric dry diameter ($D_{g,i}$) which propagates beyond the size ranges presented in Table 3.1, is transferred to the next largest mode (Mann et al., 2010).

3.2.3.2 Aqueous chemistry

Where low-level clouds are determined to be present as per monthly-mean International Satellite Cloud Climatology Project D-Series dataset (ISCCP-D2) (Rossow and Schiffer, 1999), the dissolution of SO_2 and H_2O_2 into cloud droplets is calculated along with the heterogeneous conversion of S(IV) (sulfuric acid) to S(VI) (sulfates) using a Henry's law approach (Mann et al., 2010). These associated dissociations occur over milliseconds or less, over which period $SO_2.H_2O$, HSO_3^- or SO_3^- are consumed and the corresponding aqueous-phase equilibrium is re-established instantaneously (Seinfeld and Pandis, 2006).

Low-level clouds are of particular interest here, as they are liquid clouds. At higher altitudes, ice clouds arise. At these higher altitudes the same processes cannot be applied, as ice nucleation arises. Ice nucleation occurs via immersion freezing, condensation freezing, contact freezing and deposition nucleation; with the understanding of these processes being very uncertain (Boucher et al., 2013). As such the resulting climatic impacts are less well understood than aerosol cloud interactions.

Through capping the availability of SO_2 and H_2O_2, the production (in molecules cm^{-3} s^{-1}) of S(VI) is determined by Equation 3.3 (Mann et al., 2010):

$$\Delta S_{cloud} = F\left(\frac{d[S(IV)]}{dt}\right) \cdot L \cdot N_A \cdot \frac{1}{\rho_w}$$

Equation 3.3

Where F = cloud fraction

L = cloud liquid water content (0.0002 kg m^{-3}) – for stratocumulus

ρ_w = density of water

3.2.3.3 Primary aerosol emissions

Annual mean emissions of BC and OC aerosol from fossil fuel and biofuel combustion are from Bond et al. (2004). Monthly wildfire emissions are taken from the GFED v1 (Global Fire Emissions Database) (Van Der Werf et al., 2003).

AEROCOM (Aerosol Comparisons between Observations and Models) recommended geometric mean diameters (D_g) with standard deviations described by (Stier et al., 2005) (σ_g) are used. Primary fossil fuel aerosols are considered to have a geometric mean diameter ($D_{g_{ff}}$) of 60 nm, and standard deviation ($\sigma_{g_{ff}}$) of 1.59. And primary biomass/biofuel aerosols are

considered to have a geometric mean diameter ($D_{g_{bf}}$) of 150 nm, and standard deviation ($\sigma_{g_{bf}}$) of 1.59 (Mann et al., 2010).

Following AEROCOM, 2.5% of all gas-phase SO_2 emissions are assumed to be emitted directly as sulfate particles, in order to represent sub-grid scale particle formation (Dentener et al., 2006; Stier et al., 2005). 50% of all sub-grid sulfate is emitted in to the accumulation mode, with D_g = 150 nm and σ_g = 1.59. For shipping, power plants and industrial sources (ind) 50% is emitted with $D_{g_{S(VI)\_ind}}$ = 1.5 µm and $\sigma_{g_{S(VI)\_ind}}$ = 2.00 in to the coarse mode. While for transport, domestic, wildfire and volcanic sources (other) the remaining 50% is emitted with a $D_{g_{S(VI)\_other}}$ = 60 nm and $\sigma_{g_{S(VI)\_other}}$ = 1.59, and in to the Aitken soluble mode (Scott, 2013).

GLOMAP-mode allows for size-resolved emissions of mineral dust to be included either via two alternative wind-speed-driven emissions parameterizations (Pringle, 2006; Manktelow et al., 2009) or prescribed daily-varying emissions fluxes provided for AEROCOM (Dentener et al., 2006). GMV4-nitrate uses AEROCOM prescribed dust emissions fluxes.

3.2.3.4 Microphysical processes

This section will discuss primary aerosol emission sources and aerosol processes pertaining to the formation, growth and the removal of atmospheric aerosols.

3.2.3.4.1 Nucleation of new sulfate aerosols

The formation of new nanometre-sized particles has been widely observed at numerous global sites (Kulmala et al., 2004; Kulmala et al., 2007); from the boundary layer (Clarke et al., 1998) to the free troposphere (Clarke et al., 1999). The majority of aerosol processes driving new aerosol formation occur at particle diameters of 3 nm or less, while observations are only able to cover larger particles (Kulmala et al., 2007).

Binary homogeneous nucleation (BHN) within GLOMAP-mode is parameterised using the classical nucleation theory. Critical nucleated particles within GLOMAP-mode contain usually less than 100 molecules of H_2SO_4 (Kulmala et al., 1998), and due to their size (<3 nm) (Kulmala et al., 2007) they are inserted in to the nucleation mode within GLOMAP-mode (Mann et al., 2010; Scott, 2013).

3.2.3.4.2 Condensation

GLOMAP-mode includes the condensation of gas-phase H_2SO_4 and low-volatility secondary organic material (SEC-ORG) on to all aerosol modes. The sulfate and particulate organic matter (POM) component masses are updated in the next timestep as per the mass of H_2SO_4 and SEC-ORG condensing on each mode (Mann et al., 2010). Within GLOMAP-mode particles grow due to condensation to a new particle diameter ($\overline{D}$), with the mass of H_2SO_4 and SEC-ORG condensate being stored and passed on to the ageing routine (Mann et al., 2010).

3.2.3.4.3 Ageing

Ageing is a process, through which the condensation of soluble gas-phase species or coagulation occurs with smaller particles, whereby previously water-insoluble particles can become partly soluble (Mann et al., 2010; Scott, 2013). Particles are transferred to the corresponding hydrophilic mode once adequate soluble material has been accumulated, assumed to be 10 monolayers in GLOMAP-mode in order to make the particle soluble; a process known as physical ageing (Mann et al., 2010; Scott, 2013).

In GLOMAP-mode the flux of soluble material to the insoluble modes is passed on to the corresponding soluble mode. This ensures that the ageing process only changes the number concentration of the insoluble modes, leaving their composition and size unperturbed (Mann et al., 2010).

3.2.3.4.4 Hygroscopic growth

Using parameters for calculating molalities of binary electrolytes as a function of relative humidity from Jacobson (2005) water uptake by each component within each aerosol mode is calculated using the Zdanovskii-Stokes-Robinson (ZSR) method (Zdanovskii, 1948; Stokes and Robinson, 1966; Mann et al., 2010). This method assumes spherical particles.

Any organic material present in the insoluble modes is assumed to be primary emitted material and non-hygroscopic. In the soluble modes organic material is considered as either primary or secondary organic material that has been aged. Moderate hygroscopicity is assigned to organic material in the soluble modes consistent with a water uptake per mole at 65% of sulfate assuming a molar mass of 0.15 kg mol^{-1} for the aged organic molecule (Mann et al., 2010).

3.2.3.4.5 Coagulation

GLOMAP-mode includes representations for both intra-modal and inter-modal coagulation, i.e. the collision of particles of the same and different modes respectively. Particles within soluble modes can coagulate with particles within the large soluble and insoluble modes. While insoluble mode particles can only coagulate with larger insoluble mode particles (Mann et al., 2010; Scott, 2013). Within the nucleation mode the source of nucleated particles is also included (Mann et al., 2010).

3.2.3.4.6 Aerosol dry deposition

Dry deposition is the removal of particles and gases from the atmosphere in the absence of precipitation. GLOMAP-mode represents dry deposition using the same approach as in Spracklen et al. (2005a), using the same methodology as Zhang et al. (2001) and Slinn (1982).

3.2.3.4.7 Aerosol scavenging

Aerosol removal via nucleation scavenging from both large-scale and convective scale precipitation is calculated using rain-rates diagnosed from ECMWF analysis fields (Mann et al., 2010). Akin to Spracklen et al., (2005) large-scale rain removes particles at a constant rate equivalent to 99.9% conversion of cloud water to rain over a 6 hour period (Spracklen et al., 2005a). Tiedtke (1989) is used to calculate the conversion rate for convective precipitations; assuming a rainfall fraction of 30%.

Nucleation scavenging only occurs where precipitation is formed in that model level; evaluated by comparing calculated rain-rates to those in the level above. In GLOMAP-mode, nucleation scavenging removes only soluble particles with a dry radius greater then r_{scav}, which here is taken as 103 nm (Mann et al., 2010; Scott, 2013).

Impact scavenging represents the removal of aerosols by falling raindrops, simulated in GLOMAP-mode in a way analogous to the method used in GLOMAP-bin; described in Pringle (2006) (Mann et al., 2010). Raindrop particle collection efficiencies are determined from a look-up table using the Marshall-Palmer raindrop size distribution modified by Sekhon and Srivastava (1971) and geometric mean diameter (D_g) for each mode (Mann et al., 2010). Following GLOMAP-bin, an empirical relationship from Easter and Hales (1983) is used to calculate raindrop terminal velocity.

3.2.3.4.8 Mode-merging

To prevent modes from continuing to grow indefinitely due the processes of coagulation and condensation, and grow outside their specified size ranges, a mode-merging approach is applied (Mann et al., 2010). The mode-merging routine used checks whether the geometric mean diameter (D_g) is outside the range given in Table 3.1. If this is the case, then the fractions of the mode number and mass concentrations outside the given ranges are transferred to the next largest mode as described Mann et al. (2010).

3.2.3.4.9 Cloud processing

The growth of aerosol particles through the uptake and chemical reaction of gases while the growing particle exists as a water droplet in non-precipitating clouds is known as cloud processing (Mann et al., 2010).

GLOMAP-mode simulates the activation of soluble particles to cloud droplets, and their subsequent growth (Mann et al., 2012; Mann et al., 2010). Following Spracklen et al. (2005a) the smallest particles that can be activated to cloud droplets are determined to have an activation dry radius (r_{act}) of 37.5 nm, corresponding to a cloud supersaturation of 0.2% which is typical of marine stratocumulus clouds (Mann et al., 2010). This defines the Aitken and accumulation modes frequently seen in size distribution observations within the marine boundary layer (Hoppel et al., 1994; Mann et al., 2010).

In GLOMAP-mode, cloud processing is treated as a two stage process. Firstly, the fractions of particle mass and number in the soluble Aitken mode from larger particles are calculated, and are transferred to the soluble accumulation mode. Secondly sulfate mass produced by the oxidation of SO_2 is portioned between the soluble accumulation and coarse modes. Through treating cloud processing in this way, particles at the larger end of the Aitken size range can be activated and cloud-processed, with the minimum between the soluble Aitken and accumulation modes created (Mann et al., 2010).

3.2.4 Nitrate-extended GLOMAP-mode coupled model specific differences

The nitrate-extended version of the GLOMAP-mode coupled model (GMV4-nitrate) is based on the GLOMAP-mode aerosol microphysics model described above and by Mann et al. (2010). The nitrate-extended model includes an additional inorganic dissolution solver to accurately characterise the size-resolved partitioning of NH_3 and HNO_3 into NH_4 and NO_3 components in

each soluble mode (Benduhn et al., 2016). Section 3.2.4.1 discusses the inorganic dissolution module, while Section 3.2.4.2 discusses the additional tracers used in GMV4-nitrate.

3.2.4.1 The inorganic dissolution module

The dissolution of semi-volatile inorganic gases into the aerosol-liquid-phase has an important influence on the composition of atmospheric aerosols, as the composition of inorganic atmospheric aerosol particles is subject to exchange with the gas-phase. Variations in particle size and hygroscopicity influenced by dissolution affect aerosol-radiation (ari) and aerosol-cloud (aci) interactions (described in Section 2.1.2), which in turn influence atmospheric circulation and the water cycle (Benduhn et al., 2016).

Dissolution is the combination of condensation and particle dissociation to and from the aerosol phase. Sulfuric acid (H_2SO_4) condenses irreversibly under tropospheric conditions, whereas semi-volatile species (such as H_2O, HNO_3, HCl and NH_3) may re-evaporate from the aerosol phase as a function of temperature and chemical composition of the atmosphere. Ammonium hydroxide (NH_4OH) is formed from the combination of NH_3 with H_2O in the aerosol liquid phase, which along with HNO_3 and hydrochloric acid (HCl) dissociate in the aerosol liquid phase, with water acting as a solvent (Benduhn et al., 2016).

The dissolution module within GMV4-nitrate accounts for only the gas- and aqueous-phase equilibria for the dissolution and dissociation of the following solutes (Reaction 3.1 to Reaction 3.9) (Mann, 2015; Zhang et al., 2000):

- Nitric acid ($HNO_{3(g)}$)

  $HNO_{3(g)} = H^+_{(aq)} + NO_3^-{}_{(aq)}$

  Reaction 3.1

- Hydrochloric acid ($HCl_{(g)}$)

  $HCl_{(g)} = H^+_{(aq)} + Cl^-_{(aq)}$

  Reaction 3.2

- Sulfuric acid ($HSO_4^-{}_{(aq)}$)

  $HSO_4^-{}_{(aq)} = H^+_{(aq)} + SO_4^{2-}{}_{(aq)}$

  Reaction 3.3

- Ammonium sulfate ($(NH_4)_2.SO_{4(s)}$)

  $(NH_4)_2.SO_{4(s)} = 2NH_4^+{}_{(aq)} + SO_4^{2-}{}_{(aq)}$

  Reaction 3.4

- Ammonium nitrate ($NH_4.NO_{3(s)}$)]

$$NH_4.NO_{3(s)} = NH_{3(g)} + HNO_{3(g)}$$

Reaction 3.5

- Ammonium chloride ($NH_4Cl_{(s)}$)

$$NH_4Cl_{(s)} = NH_{3(g)} + HCl_{(g)}$$

Reaction 3.6

- Sodium sulfate ($Na_2SO_{4(s)}$)

$$Na_2SO_{4(s)} = 2Na^+_{(aq)} + SO_4{}^{2-}_{(aq)}$$

Reaction 3.7

- Sodium nitrate ($NaNO_{3(s)}$)

$$NaNO_{3(s)} = Na^+_{(aq)} + NO_3{}^-_{(aq)}$$

Reaction 3.8

- Sodium chloride ($NaCl_{(s)}$)

$$NaCl_{(s)} = Na^+_{(aq)} + Cl^-_{(aq)}$$

Reaction 3.9

As such GMV4-nitrate doesn't include the liquid-solid phase equilibria, thus doesn't allow the formation of relevant salts at low relative humidity (Reaction 3.4 to Reaction 3.9). This means that the formation of the solid-phase salts is not calculated, but the concentrations of the associated ions are considered. In doing so the complexity of modelling the hysteresis effect, alongside deliquescence and effervescence is avoided (Mann, 2015).

Deliquescence, the hysteresis effect and effervescence are all related to particle growth due to hygroscopicity and relative humidity. The deliquescence point is a point at which aerosol particle experiences a sudden size increase due to the effect of relative humidity on aerosol growth. Aerosol growth with relative humidity occurs due to the transfer of water molecules from the gas- to solid-phase. The rate of growth due to relative humidity is neither linear nor a function of relative humidity, resulting in a sudden size increase, i.e. deliquescence point (Boucher, 2015).

The hysteresis effect describes the variations in aerosol particle size with relative humidity, which differs for increasing and decreasing relative humidities. When decreases in relative humidity occur crystallisation does not occur at the deliquescence point, but occurs when relative humidity reaches the efflorescence or crystallisation humidity, i.e. a critical value which promotes crystallisation (Boucher, 2015).

A dissolution module is a thermodynamic model required for the treatment of gas/aerosol partitioning of semi-volatile inorganic aerosols. Complications in modelling semi-volatile aerosol compound concentrations arise due to the relationship between saturation vapour pressure, aerosol composition and temperature of the atmosphere, and aerosol size distribution (Myhre et al., 2006; Benduhn et al., 2016). The dissolution of semi-volatile gases into the aerosol phase can have opposing effects on aerosol particle size. Dissolution of NH_3 within H_2SO_4 particles results in a decrease in water content and associated particle size, due to decreases in hygroscopicity. Chemical interactions between a dissolving acid and base (such as NH_3 and HNO_3), may result in an increase in particle size due to additional dissolved mass (Benduhn et al., 2016).

Here a hybrid-solver, which partitions between simulating dissolution as a dynamical or equilibrium process is applied to allow the GLOMAP-mode aerosol model to a tackle the issues surrounding numerical stability and computational expense in order to allow the simulation of semi-volatile inorganic gases in to the aerosol liquid phase.

Due to numerical instability, dissolution is usually treated as an equilibrium process. The treatment of dissolution as an equilibrium process reduces the computational expense related to treating complex differential equations relating to dissolution of inorganic aerosols and associated numerical stiffness, which requires small time steps in order compensate for large variations present until the solution curve straightens out as the system approaches stability. For example previous approaches have adopted iterative Gibbs free energy minimisation or the iterative bisection methods (Benduhn et al., 2016; Bassett and Seinfeld, 1983).

The hybrid-solver used in GMV4-nitrate treats some size increments (modal distributions) to be in equilibrium, while others are treated dynamically. The hybrid-solver developed by Benduhn et al., (In Prep) uses new formalisations and decision criteria such as time and size dependant (modal) choices between the equilibrium and transition approach, to combine computational efficiency with an accurate representation of the dynamical properties of the processes of dissolution (Benduhn et al., 2016).

Through the development and implementation of two frameworks for both transient and equilibrium formulations for dissolution the hybrid-solver treats dissolution as a choice-wise dynamic or static process (Benduhn et al., 2016). Benduhn et al., (In Prep) have shown that the hybrid-solver achieves numerical accuracy with modest computational expense through evaluation in box model experiments under a range of atmospheric conditions. This hybrid-solver has been evaluated to be in good agreement with observed surface concentrations of

NO_3 and NH_4 (in Europe, the U.S. and East Asia), capture the partitioning of HNO_3 and NH_3 into Aitken mode sized particle; with modest computation expense (Benduhn et al., 2016).

3.2.4.2 Gas- and aerosol-phase tracers within the nitrate-extended version of the TOMCAT-GLOMAP-mode coupled model

GMV4-nitrate has a total of 285 tracers, consisting of: 35 advected aerosol tracers; 77 gas-phase species; 164 budget terms, and; 4 water content and 5 cloud field tracers. The gas-phase advected tracers in GMV4-nitrate follow the same setup as version of GLOMAP-mode described in Mann et al. (2010), but with the addition of a NH_3 tracer.

3.2.5 Model output processing theory

3.2.5.1 Cloud condensation nuclei (CCN) concentration calculations

Water vapour cannot homogeneously nucleate under atmospheric conditions, as this process requires supersaturation levels of several hundred percent (Jacobson, 2005; Seinfeld and Pandis, 2006), but can readily heterogeneously nucleate on an existing surface, with the most prevalent atmospheric nucleation sites being on aerosol surfaces. Heterogeneous nucleation does not occur easily, with the aerosol particles on which this can occur forming liquid water being referred to as cloud condensation nuclei (CCN) (Jacobson, 2005).

In line with previous GLOMAP-mode studies (e.g. Scott et al. (2014); and Spracklen et al. (2008b)) CCN concentrations are calculated from GLOMAP-mode simulations using the "κ-Köhler" approach from Petters and Kreidenweis (2007), an extension to Köhler theory. Köhler theory uses aerosol physiochemical properties (i.e. solute mass, molecular weight, bulk density, dissociable ions and activity coefficient) to predict CCN activity (Petters and Kreidenweis, 2007).

3.2.5.2 Radiative effect calculations

Aerosol direct radiative (aDRE), aerosol cloud albedo (aCAE) and tropospheric ozone direct radiative (O3DRE) effects are calculated using the off-line Edwards and Slingo (1996) radiative transfer model.

The radiative transfer model considers 6 bands in the shortwave (SW) and 9 bands in the longwave (LW), adopting a delta-Eddington 2 stream scattering solver at all wavelengths, thus allowing the net radiative effects (REs) at the top of the atmosphere (TOA) to be determined.

TOA aerosols aDRE and aCAE are calculated using the methodology described in Rap et al. (2013) and Spracklen et al. (2011a), with the method for O3DRE as in Richards et al. (2013).

To determine the aCAE, cloud droplet number concentrations (CDNCs) are calculated using monthly mean aerosol size distributions simulated by GLOMAP combined with parameterisations from Nenes and Seinfeld (2003), updated by Fountoukis and Nenes (2005) and Barahona et al. (2010). CDNC are calculated using a prescribed updraft velocity of 0.15 m s^{-1} over ocean and 0.3 m s^{-1} over land, consistent with those commonly observed for low-level stratus and stratocumulus clouds (Guibert et al., 2003; Peng et al., 2005; Pringle et al., 2012). Changes in CDNC are then used to perturb the effective radii of cloud droplets in low- and mid-level clouds (up to 600 hPa).

Monthly mean climatology is based on ECMWF reanalysis data, with cloud fields from the ISCCP-D2 archive (Rossow and Schiffer, 1999) for the year 2000.

3.2.6 Inclusion of aviation-borne emissions

Aviation emissions, whether considering CMIP5 recommended historical aviation emissions of the extended aviation emissions inventory derived in Chapter 4 (CMIP5-extended), are read in to the model with a resolution of 1° longitude x 1° latitude x 610 m altitude. As discussed earlier in Section 3.2.1 TOMCAT-GLOMAP-mode mode has a resolution of 2.8° longitude x 2.8° latitude with 31 hybrid sigma-pressure (σ-p) levels (i.e. terrain tracking at the surface) extending from the surface to 10 hPa. As such in order to read aviation emissions in to the correct horizontal grids and vertical levels, these emissions are re-gridded as per Figure 3.3.

About the equator TOMCAT-GLOMAP-mode's resolution of 2.8° x 2.8° equates to 280 km x ~280 km, while the resolution of the aviation emissions read in of 1° x 1° equates to 100 km x 100 km, thus the emissions need to re-gridded in the horizontal plane to maintain the correct global distribution of aviation emissions – due to the differences in horizontal distribution seen in Figure 3.3(a). The redistribution of aviation-borne emissions in the horizontal plane partitions emissions in to the TOMCAT-GLOMAP-mode grid, while ensuring that where an emission bearing grid which falls between two model grids is partitioned accordingly due to level in which it overlaps in to the next, as seen from Figure 3.3(a).

Again, in the vertical plane the same methodology is utilised, but this time taking consideration of model height as denoted by the sigma-pressure levels specific to that point in the horizontal

plane Figure 3.3(b), as model heights for each horizontal cell are not necessarily the same, due to the terrain tracking nature near surface level of a hybrid sigma-pressure level system.

Figure 3.3: Illustration of horizontal and vertical re-gridding of aviation emissions in to TOMCAT-GLOMAP-mode.

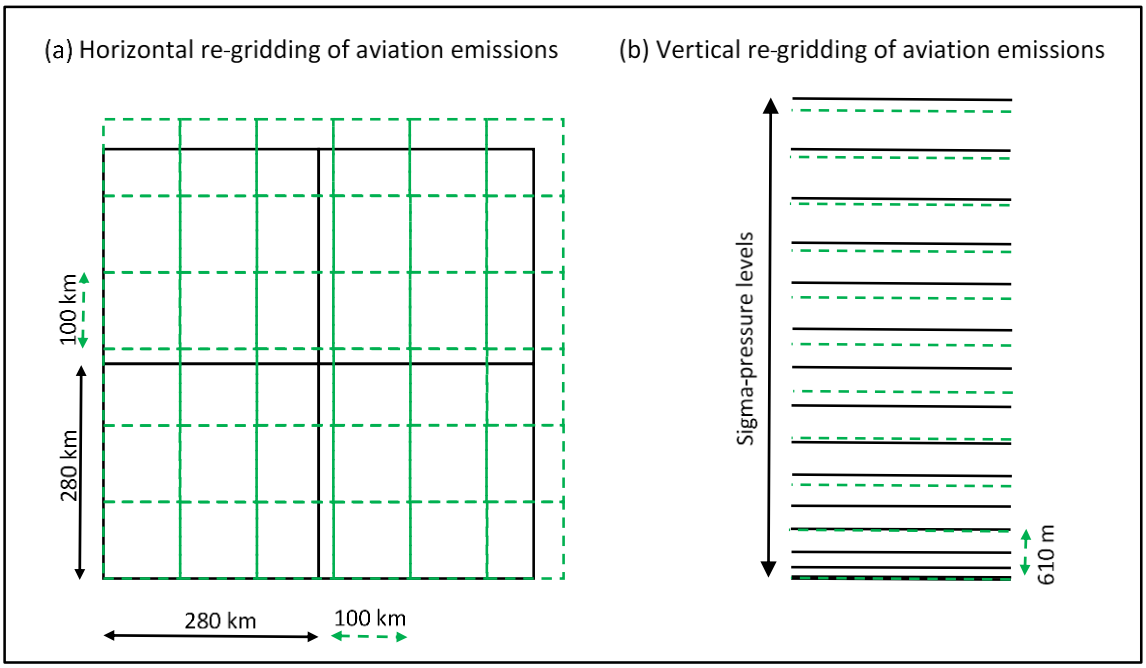

3.3 Model evaluation

Previous versions of GLOMAP-mode have been previously well evaluated. Mann et al., (2010), evaluated simulated DMS (dimethyl sulfide), SO_2 and terpene at the lowest model layer, monthly resolved DMS and SO_2 at Cape Grim, along with sulfate, BC, OC, sea-salt and dust regional surface fields with observational data (Mann et al., 2010). Spracklen et al. (2011b) evaluated SOA (secondary organic aerosols) and OC model simulated profiles with observational profiles summarising that through increasing best estimates in biogenic SOA emissions, biases between the model and observations could be reduced. Mann et al. (2012) evaluated that GLOMAP-mode produced similar responses to those from GLOMAP-bin, with the standard GLOMAP-mode setup showing good agreement with observed surface size distributions in MBL (Marine Boundary Layer) particles over the North Atlantic, and that BC profiles are in fair agreement with aircraft observations and generally with the 25^{th}–75^{th} percentile range from AEROCOM studies. This study also showed good agreement with aircraft profiles of observed concentrations of ultrafine condensation (UCN, D_p>3 nm) over the Pacific.

This section evaluates the nitrate-extended version of the TOMCAT-GLOMAP-mode coupled model (GMV4-nitrate) in two phases. Firstly simulated gas-phase concentrations are evaluated against observations from ozonesonde data from Tilmes et al. (2012), then secondly simulated aerosol-phase concentrations are evaluated against observations from aircraft field campaigns from Heald et al. (2011). Here, the standard version of GMV4-nitrate evaluated in this section considers CMIP5 recommended aviation emissions (NO_X and BC). In Section 5.5, the model is re-evaluated using the CMIP5-extended aviation emissions inventory developed in Section 4.

3.3.1 Gas-phase species model evaluation

In this section, the model is evaluated against observed ozone profiles from Tilmes et al. (2012). Model evaluation of the gas-phase chemistry within GMV4-nitrate focuses on ozone fields as this is the main gas-phase chemical specie perturbed by aviation emissions; when absolute concentrations are considered.

Figure 3.4: Ozonesonde launch locations. Key denotes different regions, with stations not included in selected regions are presented in grey – taken from **Tilmes et al. (2012).**

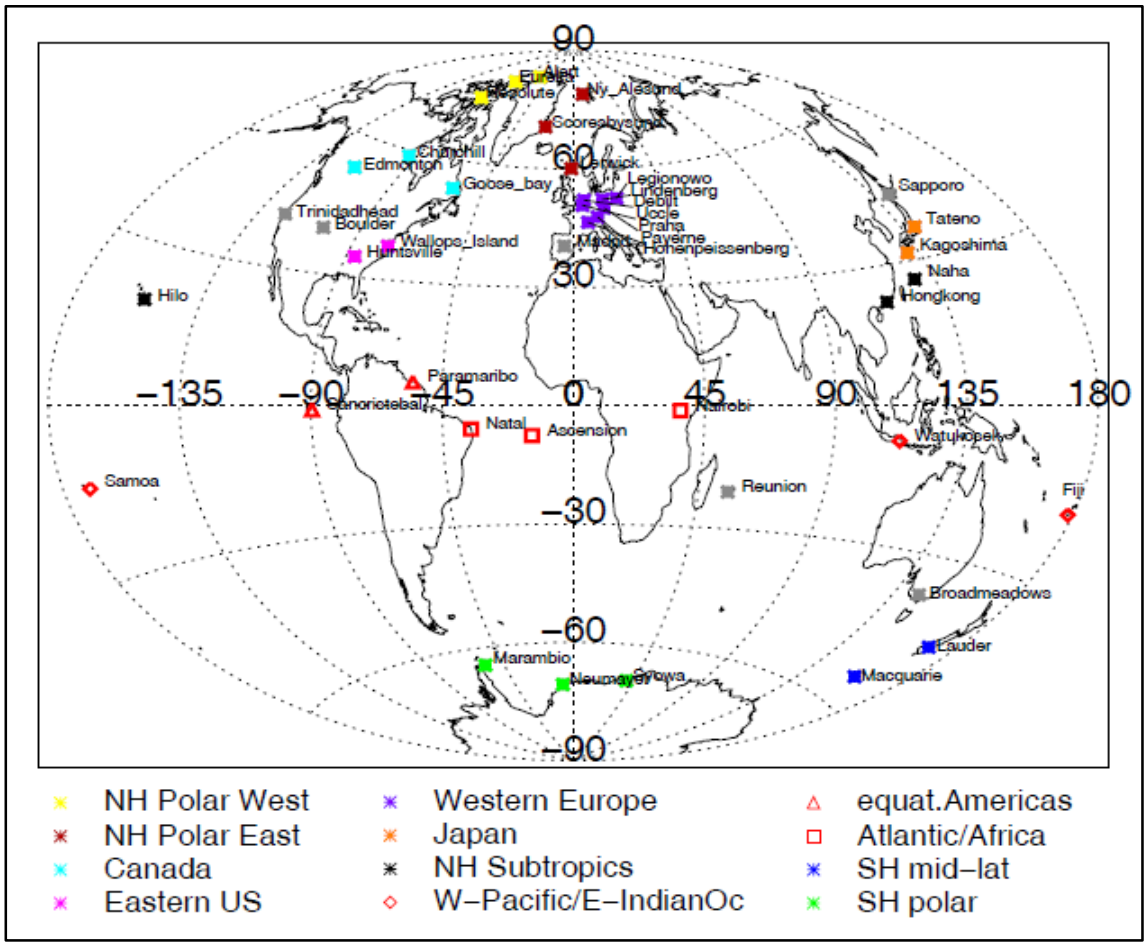

Model simulations are for the year 2000. Observations are from ozonesonde profiles collated between 1987–2011 from 41 different sites, distributed about both the Northern and

Southern Hemisphere. Ozonesonde launch locations are presented in Figure 3.4, where launch locations are split up in to different regions, e.g. Western Europe, Eastern US, etc. The names of specific launch locations for ozonesonde profile retrievals presented in Table 3.3 (Tilmes et al., 2012). Figure 3.5 presents GMV4-nitrate seasonal mean profiles in comparison to observational data from Tilmes et al. (2012) resolved in to the regions identified presented in Figure 3.4. The seasons are defined as: JFM (January, February and March); AMJ (April, May and June); JAS (July, August and September); and OND (October, November and December). In general GMV4-nitrate is able to skilfully replicate ozonesonde acquired ozone concentrations profiles, with regional variations in skill seen when comparing seasonal regionally resolved plots (Figure 3.5), and annual mean profiles resolved by regions (Figure 3.6).

Table 3.3: Ozonesonde launch stations and locations for profiles taken from 1987–2011 (Tilmes et al., 2012).

Station	Location	Station	Location
Alert	82°N, –62°E	Madrid	40°N, –4°E
Ascension	–7°N, –14°E	Marambio	–64°N, –56°E
Boulder	40°N, –105°E	Naha	26°N, 127°E
Broadmeadows	–37°N, 144°E	Nairobi	–1°N, 36°E
Churchill	58°N, –94°E	Natal	–5°N, –35°E
Debilt	52°N, 5°E	Neumayer	–70°N, –8°E
Edmonton	58°N, –14°E	Payerne	46°N, 6°E
Eureka	80°N, –86°E	Praha	50°N, 14°E
Fiji	–18°N, 178°E	Resolute	74°N, –94°E
Goose bay	53°N, –60°E	Reunion	–22°N, 55°E
Hilo	19°N, –155°E	Samoa	–14°N, –170°E
Hohenpeissenberg	47°N, 11°E	Sancristobal	–1°N, –89°E
Hong Kong	22°N, 114°E	Sapporo	43°N, 141°E
Huntsville	34°N, –86°E	Scoresbysund	70°N, –22°E
Kagoshima	31°N, 130°E	Syowa	–69°N, 39°E
Lauder	–45°N, 169°E	Tateno	36°N, 140°E
Legionowo	52°N, 20°E	Trinidad Head	41°N, –124°E
Lerwick	60°N, –1°E	Uccle	50°N, 4°E
Lindenberg	52°N, 14°E	Wallops Island	37°N, –75°E
Macquarie	–54°N, 158°E	Watukosek	–7°N, 112°E

Figure 3.5 shows that for regions in the Northern and Southern Hemisphere (NH and SH) high- and mid-latitudinal regions the model general overestimates ozone profiles in comparison to the ozonesonde acquired profiles, above an altitude of ~400 hPa in or approaching the NH and SH high-latitudinal bands (NH Polar West, NH Polar East, Canada, SH mid-latitude and SH Polar regions), i.e. overestimating ozone as the model crosses in to the tropopause and in to stratosphere. Along with overestimating ozone above an altitude of ~600 hPa in the NH and SH mid-latitude bands (Eastern US, Western Europe and Japan regions).

Figure 3.5: Seasonal comparison of nitrate-extended version TOMCAT-GLOMAP-mode coupled model simulated ozone profiles with ozonesonde observations from Tilmes et al. (2012) resolved in to regions presented in Figure 3.4. Black lines represent JFM (January, February and March), blue lines for AMJ (April, March and June), green lines for JAS (July, August and September), and red for OND (October, November and December). Solid lines present observations, while dashed represent model profiles.

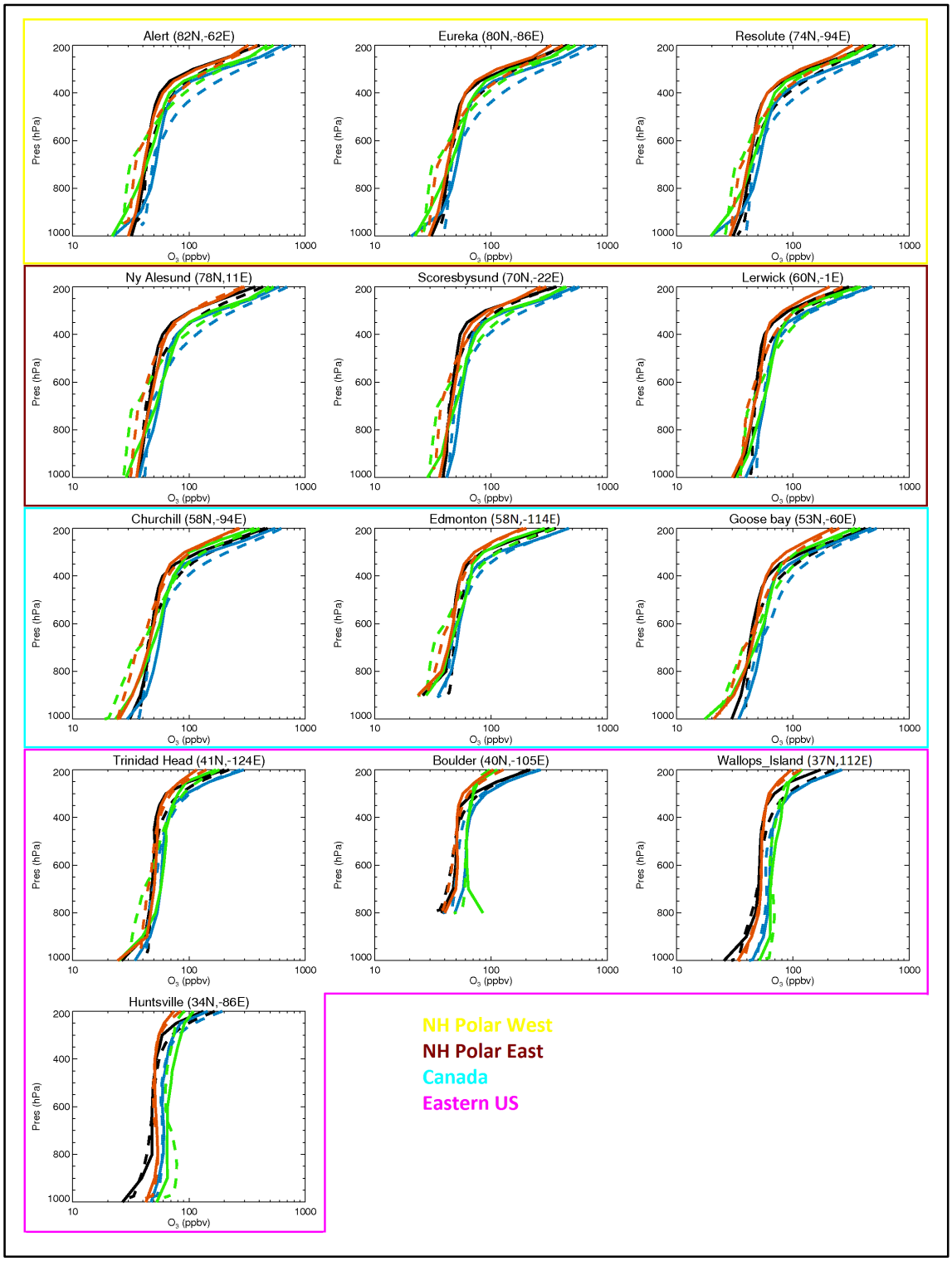

Figure 3.5 (continued): Seasonal comparison of nitrate-extended version TOMCAT-GLOMAP-mode coupled model simulated ozone profiles with ozonesonde observations from Tilmes et al. (2012) resolved in to regions presented in Figure 3.4. Black lines represent JFM, blue lines for AMJ, green lines for JAS, and red for OND. Solid lines present observations, while dashed represent model profiles.

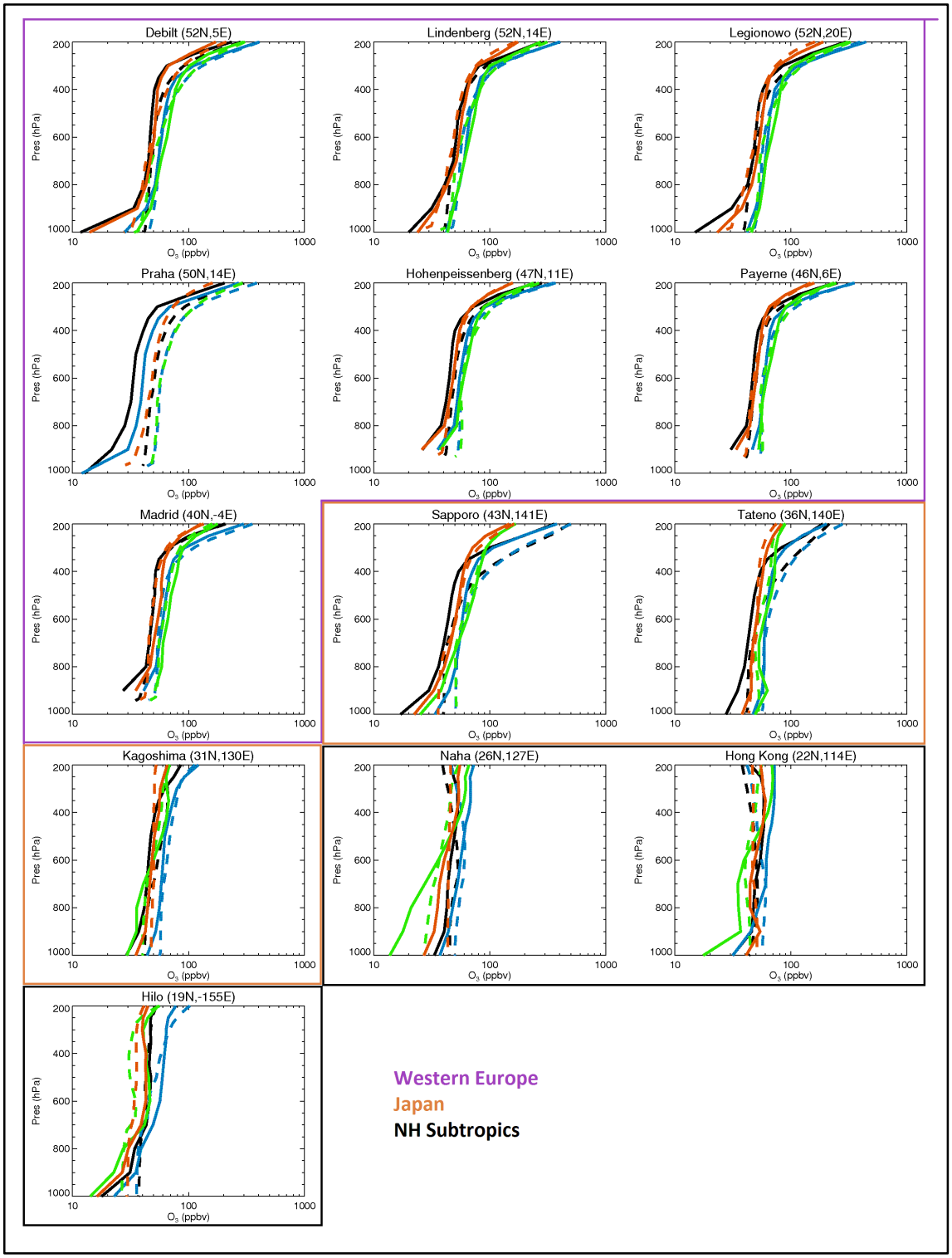

Figure 3.5 (continued): Seasonal comparison of nitrate-extended version TOMCAT-GLOMAP-mode coupled model simulated ozone profiles with ozonesonde observations from Tilmes et al. (2012) resolved in to regions presented in Figure 3.4. Black lines represent JFM, blue lines for AMJ, green lines for JAS, and red for OND. Solid lines present observations, while dashed represent model profiles.

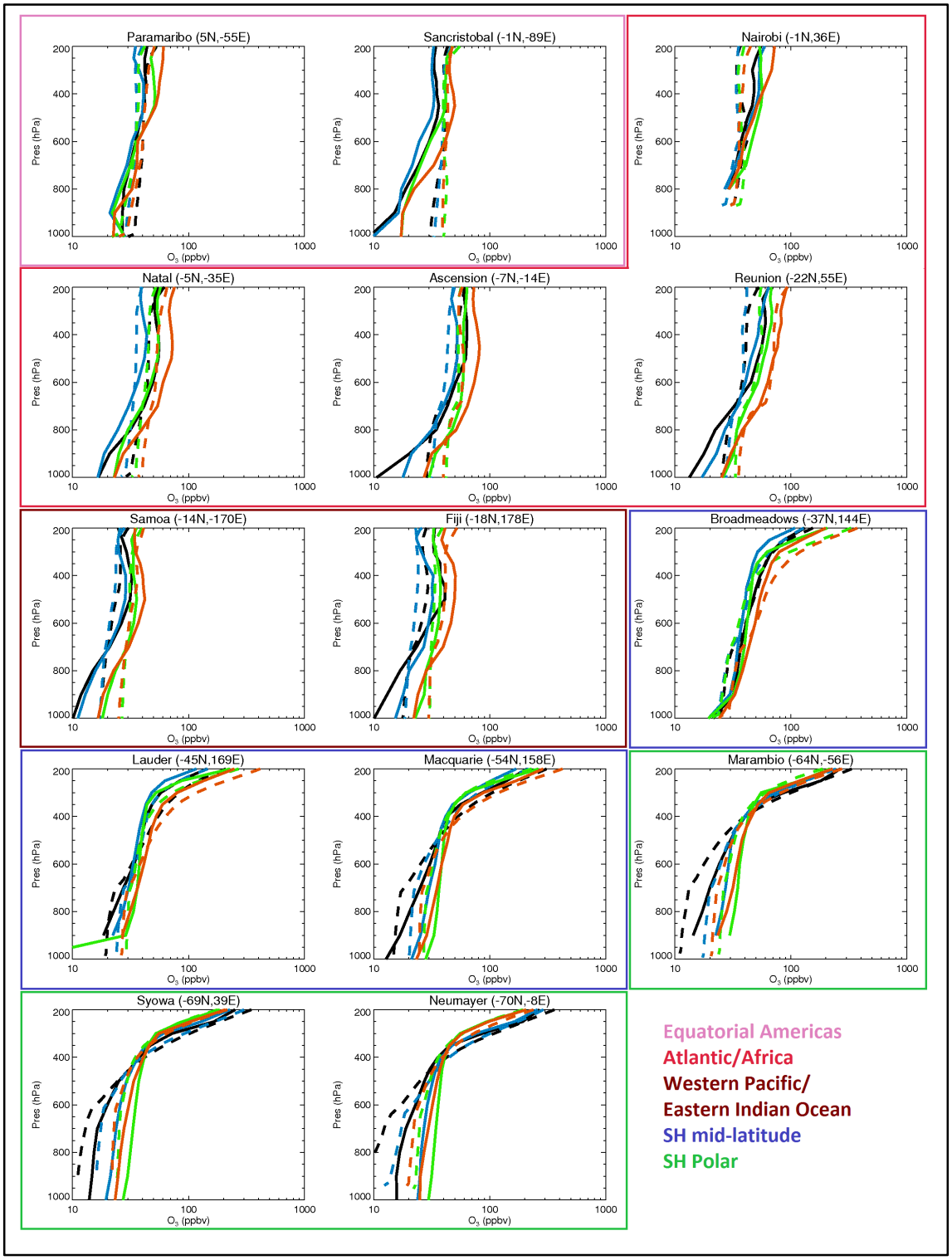

Differences between model simulated ozone profiles and observation profiles compiled by Tilmes et al. (2012) at high- and mid-latitudes are due to how TOMCAT represents stratospheric chemistry; using simple tracers to model stratospheric chemistry, forced by ECMWF meteorology, while extending to 10 hPa (Chipperfield, 2006; Arnold et al., 2005).

In line with how TOMCAT represents stratospheric chemistry, GMV4-nitrate demonstrates the greatest amount of skill in replicating ozonesonde profiles below the tropopause, with the greatest level of model skill returned in the NH mid-latitudes (Figure 3.5).

Paying attention to the seasonal model and ozonesonde acquired ozone profiles (Figure 3.5) seasonal trends are seen. Over ozonesonde launch sites in the NH between 90°N–60°N and 30°N–0°N greater tropospheric ozone concentration profiles are simulated and observed over the AMJ and JFM seasons, with greatest concentrations simulated and observed over the JAS and AMJ seasons between 60°N–30°N latitude. Over the SH between 0°S–30°S greatest tropospheric ozone concentration profiles are simulated and observed over the OND and JAS seasons, while between 30°S–90°S greatest concentrations are returned over the JAS and OND season. The trends seen here can be explained by the axial tilt of the Earth, the Earth's orbit around the Sun and the resulting levels of solar insolation received by the NH and SH over the NH and SH summers.

Over the NH summer months (AMJ/JAS) greater levels of solar insolation are received from the sun, due to the axial tilt of the Earth and its relative position to the Sun, resulting in increased rates of photodissociation of NO_2 which increases ozone production (Reaction 2.3–Reaction 2.4); hence the higher concentration ozone profiles seen over AMJ/JAS. Over the SH summer months (NH winter months), greater levels of solar insolation are received by the SH resulting in the higher tropospheric ozone concentrations over the OND and JAS seasons. It would be expected that the highest ozone concentrations

Over the NH there is a fairly even split between observations acquired over each season. While over the SH the majority of observations were acquired over the Autumn months, with the least acquired over the Winter months. Though despite this split in acquired ozonesonde observations simulated ozone profile concentrations match observational profiles from Tilmes et al. (2012).

Figure 3.5 and Figure 3.6 (which follows) shows that regions within 90°N–50°N and 50°S–90°S (NH Polar West, NH Polar East, Canada, SH mid-latitude and SH Polar) show that the model generally underestimates ozone concentrations in the lower troposphere. Additionally

between the 50°S–90°S latitudinal band (SH mid-latitude and SH Polar regions) the model is seen to underestimate near surface layer ozone. Figure 3.6 also shows how the ozonesonde launch locations affect ozone profiles and the model's ability to replicate changes in ozone concentrations indicative of ozone concentration changes above the tropopause.

Figure 3.6: Comparison of annual mean ozone profile simulated using the nitrate-extended version TOMCAT-GLOMAP-mode coupled model simulated ozone profiles with ozonesonde observations from Tilmes et al. (2012) resolved in to regions presented in Figure 3.4.

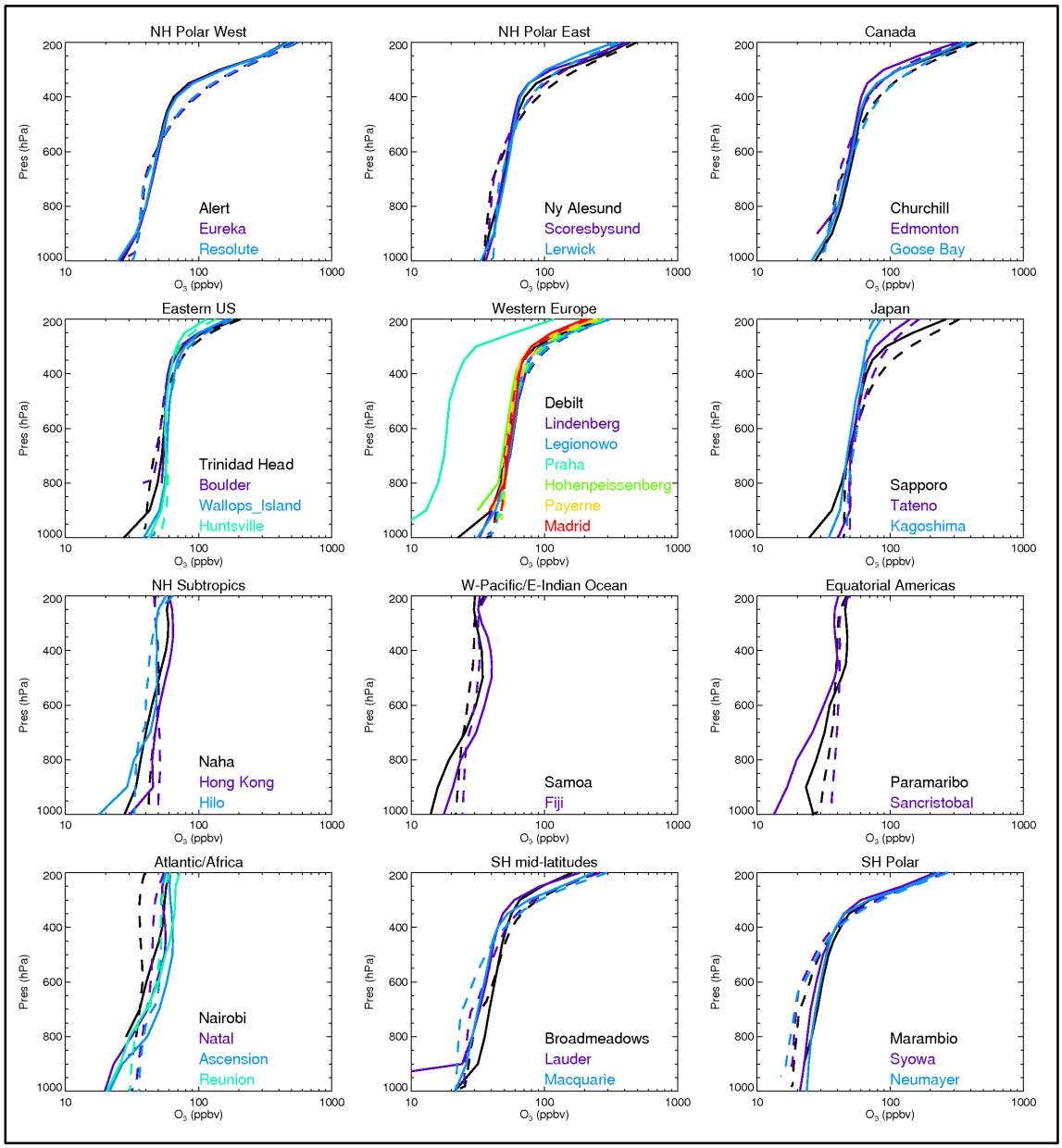

When considering individual ozonesonde launch sites and resolved in to the launch regions (Figure 3.4) GMV4-nitrate demonstrates skill in replicating ozonesonde profiles below the tropopause. The greatest level of model skill is seen in the NH mid-latitude.

In depth analysis was conducted through the production of model-observation scatter plots while investigating the normalised mean bias (bias) and Pearson regression (R). Since the model only contains detailed chemical processes for the simulation of tropospheric atmospheric composition, comparisons are only made for ozone in the troposphere. This is defined by assuming a chemical tropopause of 150 ppbv ozone, and not considering ozone concentrations exceeding this threshold value. Similar chemical tropopause approaches have been used extensively in evaluation of the tropospheric ozone distribution (e.g. Young et al. (2013); Stevenson et al. (2013); Rap et al. (2015)). This results in the omission of a greater number of observational data points at latitudinal regions where the tropopause is lower, i.e. towards the high-latitudes in both hemispheres.

The Pearson regression and normalised mean bias are calculated using Equation 3.4 and Equation 3.5 respectively.

$$R=\frac{n(\sum xy)-(\sum x)(\sum y)}{\sqrt{[n\sum x^2-(\sum x)^2][n\sum y^2-(\sum y)^2]}}$$

Equation 3.4

Where n = number of data points considered relating to vertical location
x = observational data from aircraft field campaigns
y = GMV4-nitrate simulation values

$$NMB=\left[\sum(x_n-y_n)/\sum x_n\right]\times 100\%$$

Equation 3.5

Figure 3.7 shows the seasonally resolved correlation between model simulations and ozonesonde profiles, regression and bias for each site. The seasons are defined as such: JFM (January, February and March); AMJ (April, May and June); JAS (July, August and September); and OND (October, November and December).

17 of the ozonesonde launch sites demonstrate positive biases throughout the year, with 14 of those sites being located in the NH (Alert, Churchill, Debilt, Edmonton, Eureka, Goose Bay, Hohenpeissenberg, Lerwick, Payerne, Praha, Resolute, Sapporo, Scoresbysund and Uccle), and 3 of these sites being located in the SH (Lauder, Samoa and Sancristobal). Out of the 41 launch sites four demonstrate negative model biases over all seasons: Ascension, Hong Kong, Naha and Nairobi (Figure 3.7).

Overall seasonal model-observation comparisons (Figure 3.7) show that GMV4-nitrate overestimates ozonesonde profiles across most locations and seasons, but demonstrates a good correlation with the ozonesonde profiles investigated. Across the 41 sites with all but one site providing four seasonal profiles (162 profiles in total), 111 of the profiles show positive biases, while 51 profiles show negative biases. Based on evaluation against seasonal profiles it is assessed that the model only slightly overestimates over all the profiles considered with a mean bias of +4.36%, and a model mean bias of 3.88% when observations at Praha are excluded.

When considering annual mean profiles (not presented here), the site with the lowest positive model bias Paramaribo [bias = +0.97%; R = 0.918] in the Equatorial Americas region, while the site with the lowest negative bias is Hilo [bias = –1.03%; R = 0.963] in the NH Subtropics. The site with the greatest positive bias is Praha [bias = +221.07%; R = 0.980] in the Western European region, while the site with greatest negative bias is Nairobi [bias = –15.42%; R = 0.835] in the Atlantic/Africa region. When taking all sites in to consideration an annual mean bias of +6.98% is calculated with a regression of 0.883, which is reduced to +5.31% with a regression of 0.914 when Parah is excluded. It is also seen that the site with lowest regression is Hong Kong where R = 0.786 [bias = –14.32%], whereas the sites with the highest regression value is Huntsville [R = 0.996; bias = +5.00%] and Neumayer [R = 0.994; bias = –6.04%].

When considering annual mean profiles, over the NH 23 sites return positive biases with 4 sites return negative biases, while over the SH 7 sites return positive biases with 7 sites returning negative biases. This gives an indication that over the NH GMV4-nitrate has a tendency to overestimate ozone profiles with a mean bias of 9.42%, and an annual NH model mean bias of +7.02% when observation over Praha (and its associated large model biases) are excluded.

When considering seasonal model-observation profile comparisons over the regions defined by Tilmes et al., (2012) 75% of these regions returning mainly positive biases (NH Polar West, NH Polar East, Canada, Eastern US, Western Europe, Japan, Western Pacific/Eastern Indian Ocean, Equatorial Americas and SH mid-latitude regions), with 25% of these regions returning negative biases (NH Subtropics, Atlantic/Africa and SH Polar regions).

Figure 3.7: Seasonally resolved model-observation comparison for all 41 ozonesonde launch sites compiled by Tilmes et al. (2012). Black lines represent JFM, blue lines for AMJ, green lines for JAS, and red for OND.

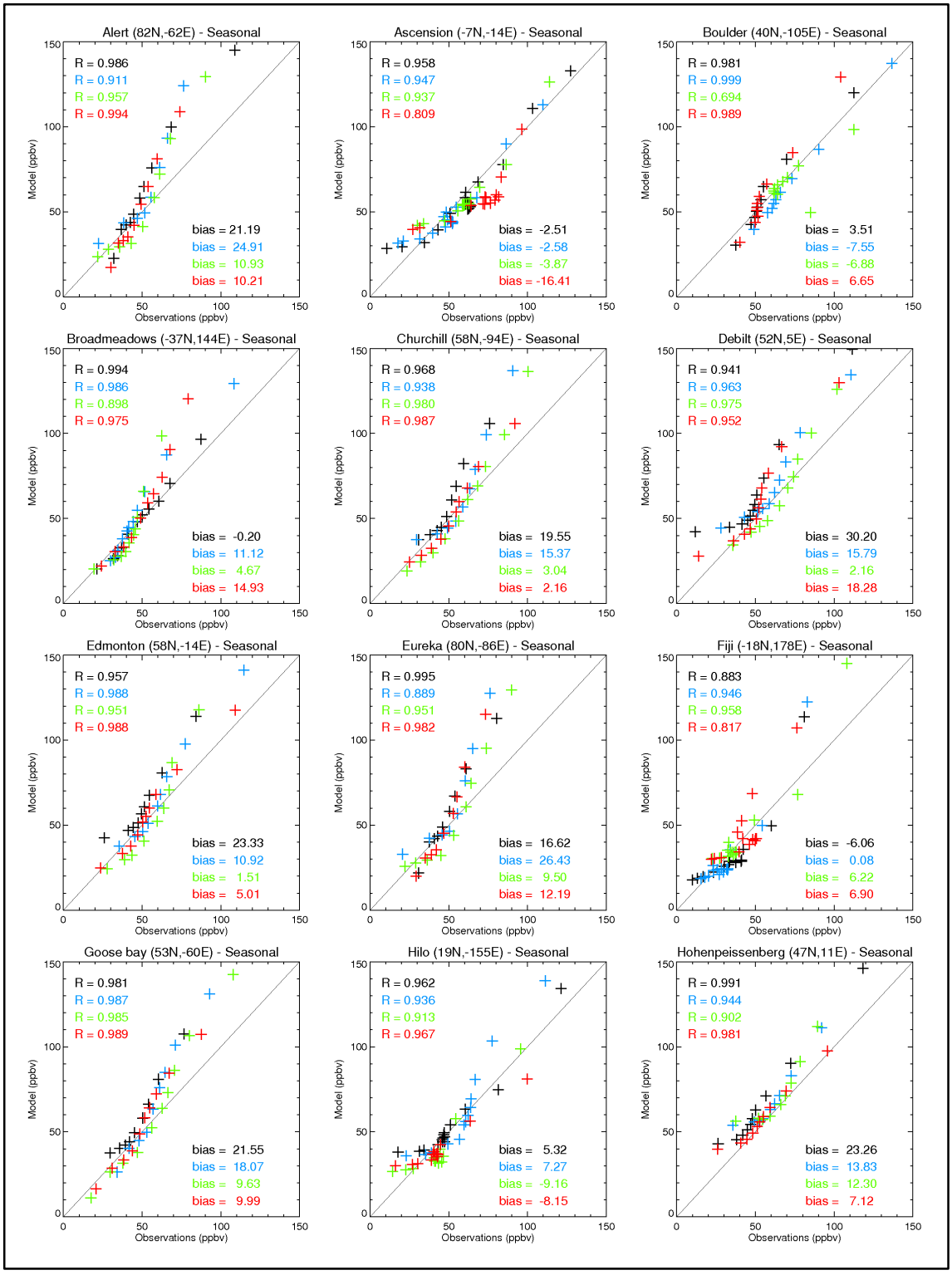

Figure 3.7 (continued): Seasonally resolved model-observation comparison for all 41 ozonesonde launch sites compiled by Tilmes et al. (2012). Black lines represent JFM, blue lines for AMJ, green lines for JAS, and red for OND.

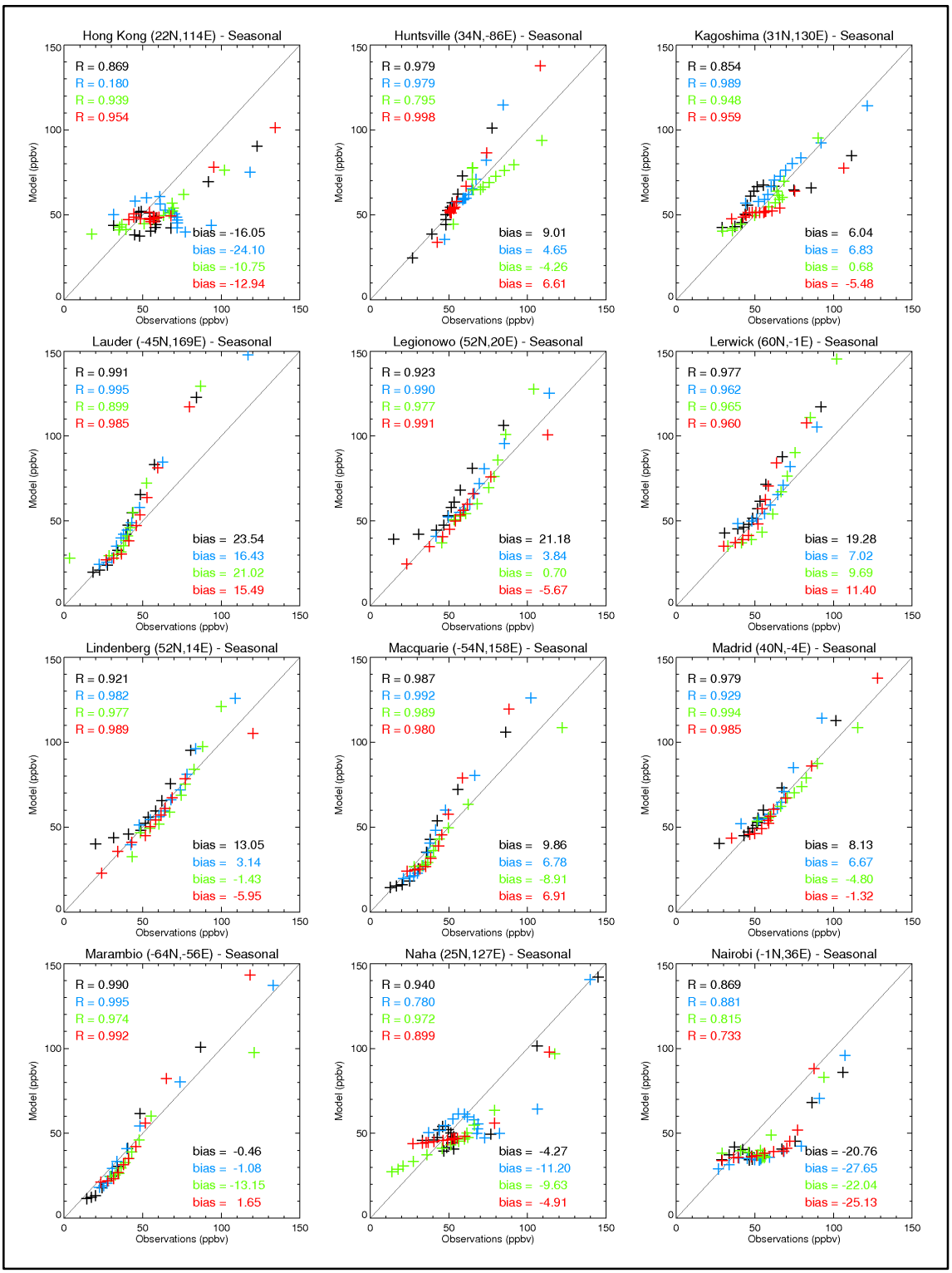

Figure 3.7 (continued): Seasonally resolved model-observation comparison for all 41 ozonesonde launch sites compiled by Tilmes et al. (2012). Black lines represent JFM, blue lines for AMJ, green lines for JAS, and red for OND.

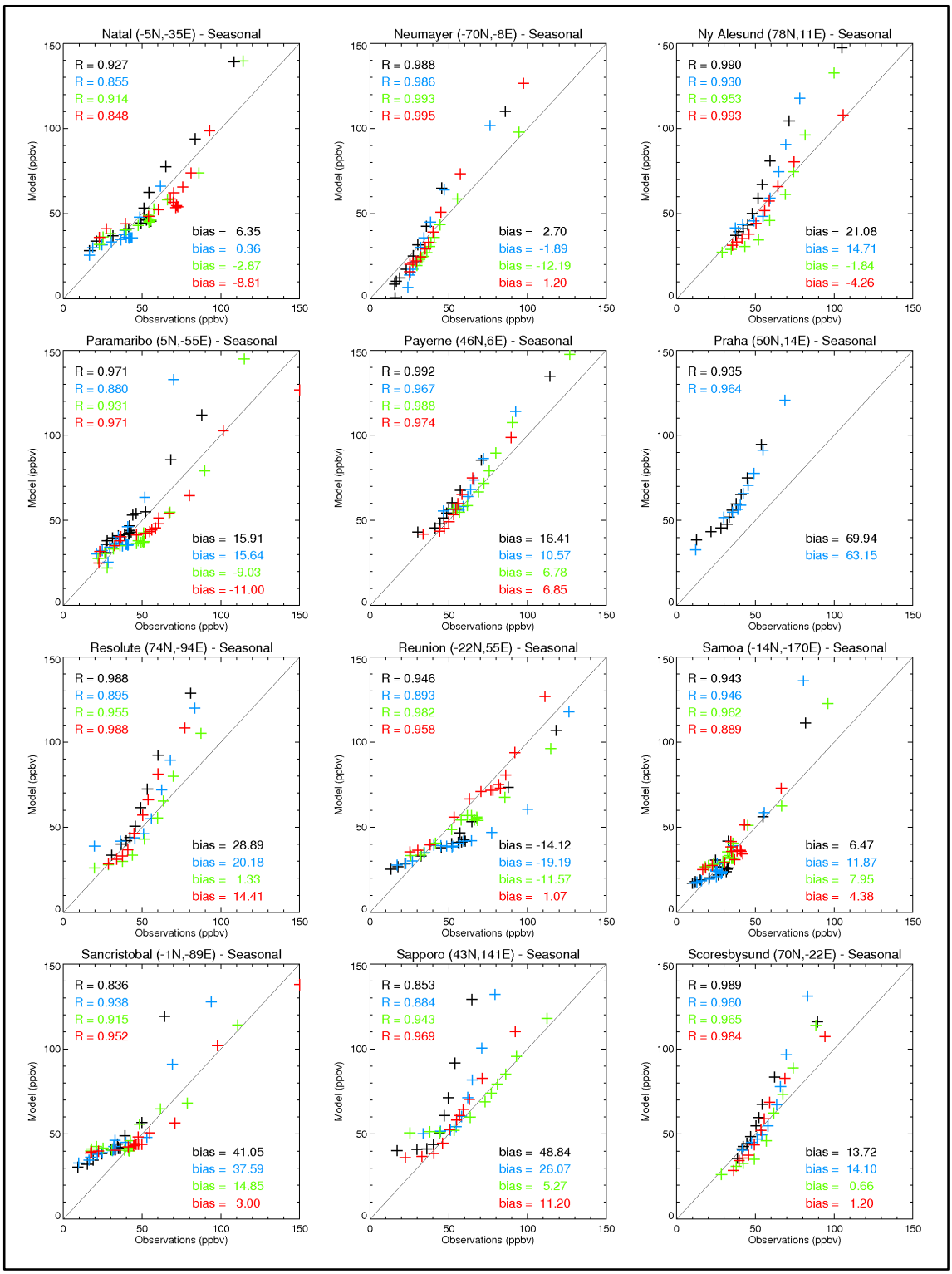

Figure 3.7 (continued): Seasonally resolved model-observation comparison for all 41 ozonesonde launch sites compiled by Tilmes et al. (2012). Black lines represent JFM, blue lines for AMJ, green lines for JAS, and red for OND.

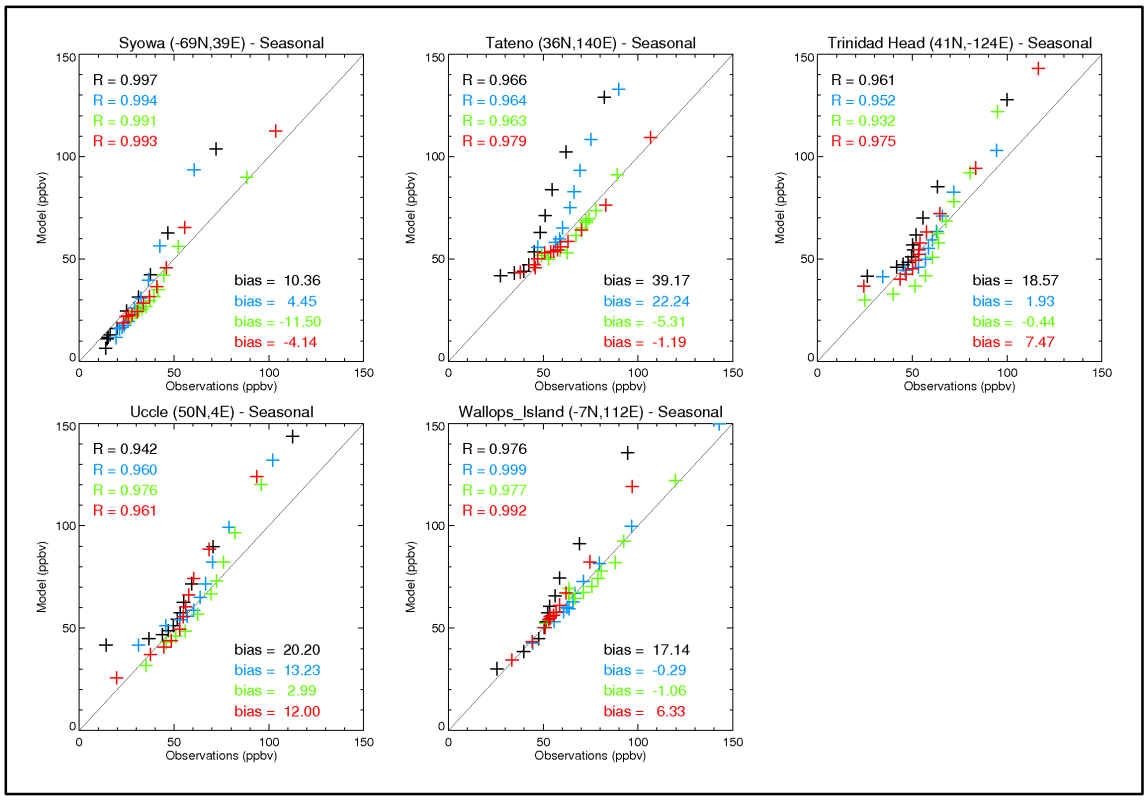

Table 3.4: Ozonesonde release sites from Tilmes et al. (2012) resolved in to latitudinal bands.

Latitudinal bands	Ozonesonde launch sites
90°N–60°N	Alert, Eureka, Resolute, Ny Alesund, Scoresbysund, Lerwick
60°N–30°N	Churchill, Edmonton, Goosebay, Trinidad Head, Boulder, Wallops Island, Huntsville, Legionowo, Lindenberg, Debilt, Uccle, Praha, Payerne, Hohenpeissenberg, Madrid, Sapporo, Tateno, Kagoshima
30°N–30°S	Hilo, Sancristobal, Paramaribo, natal, Ascension, Nairobi, Samoa, Watukosek, Fiji, Reunion
30°S–60°S	Broadmeadows, Lauder, Macquire
60°S–90°S	Marambio, Neumayer, Syowa

When considering seasonal profiles across each site, GMV4-nitrate is seen to slightly overestimate ozone profiles in comparison to ozonesonde acquired observations (66.87%), while when annual mean model-observation profiles are considered greater levels of overestimations are seen (73.17%). In order to gain a clearer picture of how the model performs Table 3.4 presents ozonesonde launch sites resolved in to latitudinal bands (90°N–60°N; 60°N–30°N; 30°N–30°S; 30°S–60°S; 60°N–90°). Through resolving model-observation comparisons in this way the performance of the model can be further investigated (Figure 3.8).

Figure 3.8: Seasonally resolved model-observation comparison for all 41 ozonesonde launch sites compiled by Tilmes et al. (2012), grouped in to latitudinal bands (90°N–60°N; 60°N–30°N; 30°N–30°S; 30°S–60°S; and 60°S–90°S). Black lines represent JFM, blue lines for AMJ, green lines for JAS, and red for OND. Data from Praha is excluded.

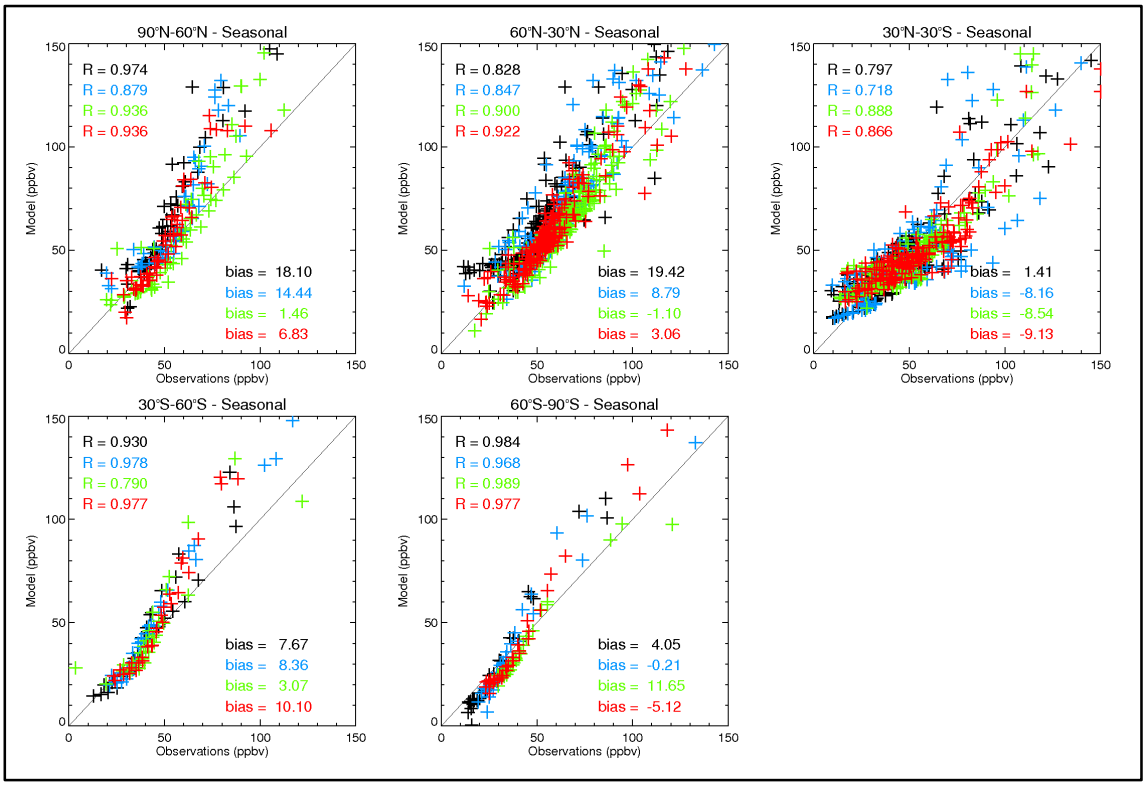

Figure 3.8 allows the latitudinal band at which GMV4-nitrate performs best to be identified. Some regional differences can arise due to discrepancies between anthropogenic and natural emissions inventories fed in to GMV4-nitrate, in comparison to real-world emissions which are difficult to accurately capture in emissions inventories. Additionally differences between model simulations and observations can be driven by meteorological drivers, such as deep convection. Thompson et al. (1997) discuss the impact of deep convection on atmospheric pollutants and ozone formation. The work by Thompson et al. (1997) highlights that ~10% of tropical convective events result in the advection of pollutants out of the free troposphere and beyond the tropopause, resulting in a 3–4 fold increase in upper troposphere ozone downwind; as such differences between how real-world deep convection occurs and this effect is simulated within models can explain regional variations in a model's ability to simulate ozone. An effect that could explain the greater levels of model underestimations seen in 30°N–30°S (as indicated by the negative NMB), and the model overestimations returned over the mid-latitudinal regions (60°N–30°N and 30°S–60°S) (as indicated by the positive NMBs).

Over the 90°N–60°N latitude band, seasonal biases range from 1.46–18.10% (Figure 3.8), indicating that throughout the year GMV4-nitrate overestimates ozone observations. The

annual mean bias over this region is +10.59% indicating that overall for year 2000 the model overestimates over this latitudinal band (Figure 3.9).

Figure 3.9: Annual mean model-observation comparisons for all 41 ozonesonde launch sites compiled by Tilmes et al. (2012), grouped in to latitudinal bands (90°N–60°N; 60°N–30°N; 30°N–30°S; 30°S–60°S; and 60°S–90°S). Purple cross-hairs denote ozonesonde data from the Praha launch site. For the 60°N–30°N latitude band biases and regression in purple includes data from Praha.

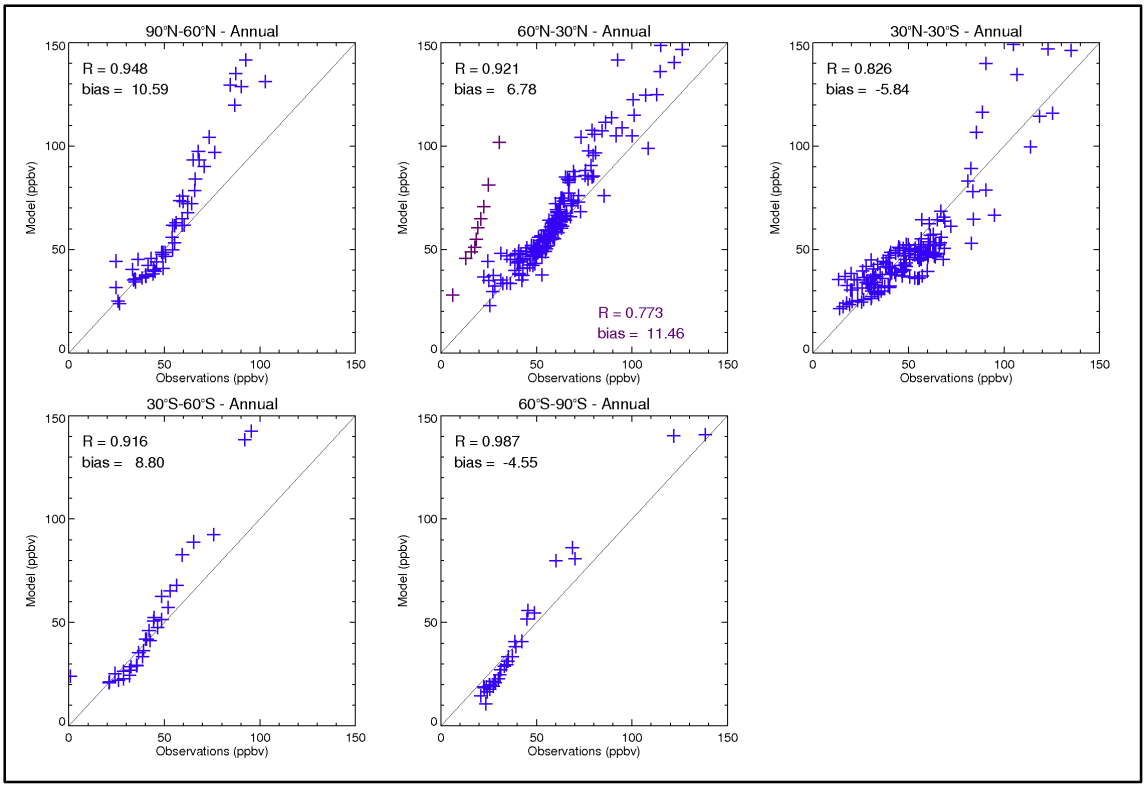

Over the 60°N–30°N latitude band, when omitting simulated ozone against observations over Praha due to the high biases returned, seasonal biases range between –1.10% to +19.42% (Figure 3.8). Combining this with seasonal regressions >0.828, this region shows high levels of correlation between model simulations and observational data. The annual mean bias for this latitudinal band is +11.46% [R = 0.773] (Figure 3.9) inclusive of Praha, and excluding Praha a model bias of +6.78% [R = 0.921] is returned.

Seasonal biases over the equatorial region (30°N–30°S) range from –9.13% to +1.41% (Figure 3.8), in comparison to the annual mean bias of –5.84% (Figure 3.9), indicating that the model underestimates ozone profiles over this region throughout the year. Underestimations in this region (the equatorial tropics) could be a result of the way deep convection is simulated within the model, and variations advection within this region over period of 1987–2011 when observational ozone profiles were acquired.

Seasonal biases over the 30°S–60°S latitudinal band, range from +3.07–10.10% (Figure 3.8), with an annual mean bias of +8.80% (Figure 3.9). The seasonal regressions of >0.790 are calculated, while an annual R value of 0.916 is obtained. Model over estimations in this mid-latitudinal region could be attributed to how GMV4-nitrate simulated deep convention; as mentioned above when discussing model performance over the 60°N–30°N latitude band. Over the 60°S–90°S latitudinal band seasonal biases range between –5.12% to +11.65% (Figure 3.8), with an annual mean bias of –4.55% (Figure 3.9). Despite the broad range in biases over this region, high levels of regression are seen over this region: >0.968.

From Figure 3.8 and Figure 3.9 it is seen that over the 90°N–60°N, 60°N–30°N and 30°S–60°S bands GMV4-nitrate overestimates ozone profiles (as indicated by positive biases returned), while underestimating over the 30°N–30°S and 60°S–90°S bands. When Praha model-observation comparisons are omitted, annual model-observation comparisons show that over the 60°N–30°N region the lowest positive biases are returned with an annual correlation of >0.9; indicating good model skill over this region.

Figure 3.10 not only shows annual mean model-observations within the troposphere, but model-observation comparisons in to five latitude bands (90°N–60°N; 60°N–30°N; 30°N–30°S; 30°S–60°S; and 60°S–90°S) and three different altitude ranges (100<hPa<400; 400<hPa<700; and 700<hPa<1000). As with Figure 3.7, Figure 3.8 and Figure 3.9 ozone concentrations are limited to 120 ppbv to limit the inclusion of stratospheric ozone.

Figure 3.10 investigates how the model performs in the upper troposphere (UT) [100<hPa<400 altitudinal band], lower troposphere (LT) [400<hPa<700 altitudinal band] and within the surface layer [700<hPa<1000 altitudinal band]. In the UT the model is seen to perform best within the equatorial region (30°N–30°S band) with a low negative bias of –11.36% [R = 0.819], i.e. this latitudinal band returns a bias closest to zero. When excluding Praha observations, the NH mid-latitudinal region (60°N–30°N band) is estimated to be the next best performing region [bias = +13.31%; R = 0.780], followed by the SH high-latitude (60°S–90°S) [bias = +20.77%; R = 0.958]. In the LT the model is seen to perform best in the SH and NH mid-latitudes with biases of +3.78% [R = 0.935] and +4.29% [R = 0.814], respectively. While over the surface layer lowest biases are seen over the NH and SH mid-latitudes, with biases of +3.62% [R = 0.720] and –4.89 [R = 0.591] respectively.

Figure 3.10: Annual mean model-observation comparison for all 41 ozonesonde launch sites compiled by Tilmes et al. (2012), grouped in to latitudinal bands (90°N–60°N; 60°N–30°N; 30°N–30°S; 30°S–60°S; 60°S–90°S) and altitudinal bands (100<hPa<400; 400<hPa<700; and 700<hPa<1000). Purple cross-hairs denote ozonesonde data from the Praha launch site. For the 60°N–30°N latitude band biases and regression in purple includes data from Praha.

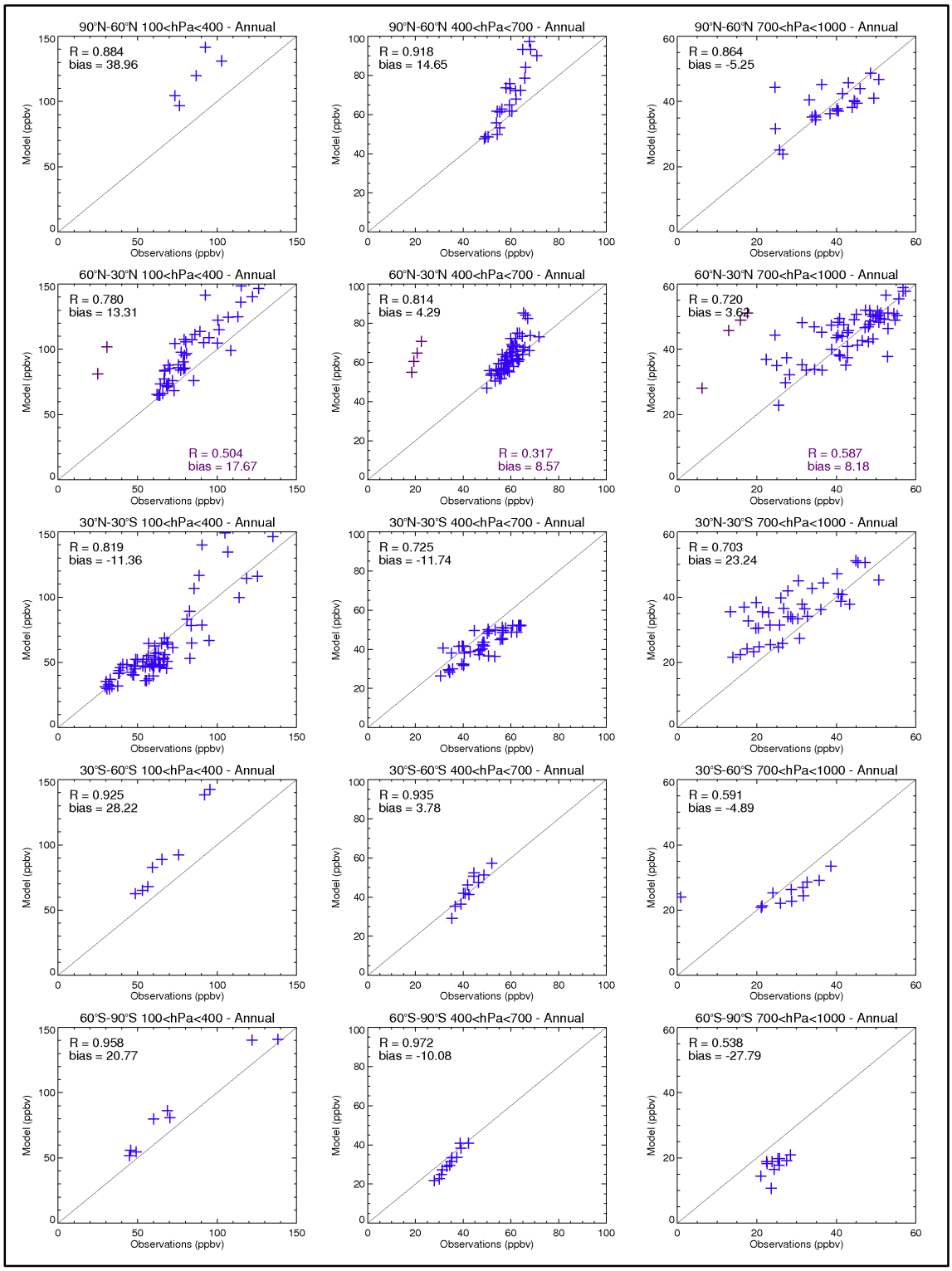

When focussing on each latitudinal band independently (and while omitting observations from Praha), a relationship between model skill and latitude can be identified (Figure 3.10). In the NH Polar region the model is seen to perform best in the surface layer [bias = –5.25%; R = 0.864], while over the NH mid-latitude region is again seen to best perform over the surface layer [bias = +3.62%; R = 0.720]. Over the Equatorial region the model is seen to best perform in the UT [bias = –10.36%; R = 0.819]. While over the SH mid-latitudinal and Polar regions the model is seen to show greatest correlation to observations over the LT: for the mid-latitudinal region [bias = +3.78%; R = 0.935] and for the Polar region [bias = –10.08%; R = 0.972].

In addition to model biases being a result of the model's ability to simulate processes such as deep convection (which drives ozone transport from the equatorial region to the mid-latitudinal regions), perceived model biases could also be a result of seasonal variations in the acquisition of ozonesonde data. 23.8% of ozonesonde observations were acquired between 1980–1994, while 76.2% of observations were acquired between 1995–2011. Globally there is a fairly even split between the seasonal acquisition of observational profiles over each time period, but when each site is considered in turn the seasonal split between the acquisition of ranges between: 12.4–39.8% between 1980–2011; 11.1–55.4% between 1980–1994, and; 11.1–37.0% between 1995–2011. This uneven distribution in seasonal acquisitions of ozonesonde profile data, could not only impact seasonal model-observation comparisons, but annual model-observation comparisons. Despite these variations, which could impact model evaluation, this dataset gives us a very good indication of how GMV4-nitrate simulates ozone profiles compare to real-world observational data.

Overall Figure 3.10 shows that the model best performs between 60°N–60°S and within the LT and surface layer, while in tandem illustrating the complexity of accurately simulating tropospheric ozone concentrations across the complete global domain.

3.3.2 Aerosol-phase species model evaluation

Here the nitrate-extended version of the TOMCAT-GLOMAP-mode coupled model (GMV4-nitrate) is used to simulate aerosol concentrations for the year 2000. Here, the standard version of GMV4-nitrate evaluated in this section considers CMIP5 recommended aviation emissions (NO_X and BC).

Sulfate (SO_4^{2-}), nitrate (NO_3^-), ammonium (NH_3^+) and organic carbon (OC) observations collated from 17 aircraft campaigns conducted between 2001–2009 by Heald et al. (2011) are used to evaluate GMV4-nitrate's simulated sulfate, nitrate, ammonium and organic aerosol profiles.

The flights tracks for the 17 aircraft field campaigns are presented in Figure 3.11, with the details of each campaign (campaign name, aircraft used, location, date and regional class of the campaign) presented in Table 3.5.

Figure 3.11: Flight tracks aircraft field campaigns used to evaluate the nitrate-extended version of TOMCAT-GLOMAP-mode coupled model – taken from Heald et al. (2011).

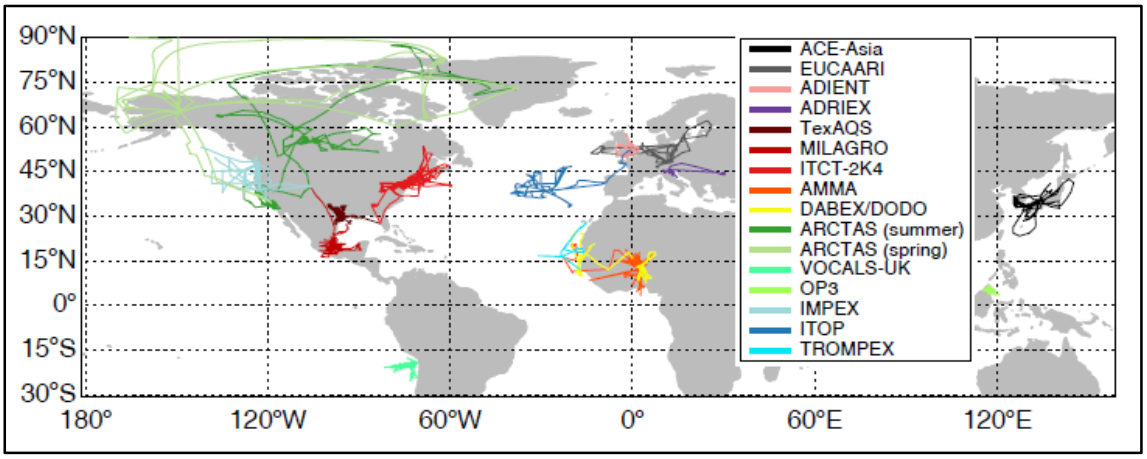

Out of the 17 aircraft field campaigns used for this evaluation step (Figure 3.11 and Table 3.5), 16 were located in the NH, with the majority of these campaigns being carried out in the Northern mid-latitudes. Five of these campaigns were conducted over polluted regions (ACE-Asia, ADRIEX, TexAQS, ADIENT and EUCAARI), five over regions influenced by fire (DABEX, DODO, AMMA, ARCTAS spring and ARCTAS summer), four remote regions (ITOP, OP3, VOCALS-UK and TROMPEX), one subject to pollution and fire (MILAGRO), and finally one remote region with aged particles (IMPEX) (Heald et al., 2011).

15 of the campaigns use the Aerodyne Aerosol Mass Spectrometer (AMS), one uses Fourier Transform Infrared Spectroscopy (FTIR) filter measurements and another uses Particle-Into-Liquid Sampler (PILS) measurements of water soluble organic carbon (WSOC). The Aerodyne AMS instrumentation focuses aerosols into a narrow beam via an aerodynamic lens inlet, transporting them in to a vacuum where the particle size can be determined (Jayne et al., 2000; Canagaratna et al., 2007). The Mattson Research Series 100 FTIR Spectrometer with DTGS (deuterated triglycine sulfate) detector was used to analyse filter samples with the filter paper analysed before sampling to ensure accuracy of aerosol detection (Maria et al., 2002). For PILS measurements of WSOC, ambient particles are directed in a liquid stream under supersaturated condition, allowed to grow, collected by an inertial impactor, finally deionized water used to create a liquid sample which is quantified (Sullivan et al., 2006).

Table 3.5: Aircraft campaigns collated used to obtain sulfate, nitrate, ammonium and organic carbon observational data – adapted from Heald et al. (2011).

Campaign	Aircraft	Location	Date	Regional Class
ACE-Asia	C-130	NW Pacific, near Japan	30/03 – 04/05/01	Pollution (mid-latitude)
ITCT-2K4	NOAA P3	E North America	05/07 – 15/08/04	Pollution/Fire (mid-latitude)
ITOP	BAE-146	Azores	12/07 – 03/08/04	Remote (mid-latitude)
ADRIEX	BAE-146	N Italy; Adriatic & Black Sea	27/08 – 06/09/04	Pollution (mid-latitude)
DABEX	BAE-146	W Africa	13/01 – 01/02/06	Fire (tropics)
DODO	BAE-146	W Africa	03/02 – 16/02/06	Fire (tropics)
MILAGRO	C130	Mexico city	04/03 – 31/03/06	Pollution/Fire (sub-tropics)
IMPEX	C130	W North America & E Pacific	17/04 – 15/05/06	Remote + aged (mid-latitude)
AMMA	BAE-146	W Africa	20/07 – 25/08/06	Fire (tropics)
TexAQS	NOAA P3	Texas	11/09 – 13/10/06	Pollution (mid-latitudes)
ADIENT	BAE-146	EU/Atlantic	18/12/07 - 25/09/08	Pollution (mid-latitudes)
EUCAARI	BAE-146	N EU	06/05 – 22/05/08	Pollution (mid-latitudes)
ARCTAS	DC-8	Arctic/N EU	01/04/ - 20/04/08 18/06 – 13/07/08	Fire (high-latitudes)
OP3	BAE-146	Borneo	10/07 – 20/07/08	Remote (tropical)
VOCALS-UK	BAE-146	Eastern S Pacific	27/10 – 13/11/08	Remote (tropical)
TROMPEX	BAE-146	Cape Verde	08/09 – 10/09/09	Remote (tropical)

As most of the observations are acquired using the Aerodyne AMS detector measuring particles within the PM_1 (Dp < 1 µm) size category (Canagaratna et al., 2007), GMV4-nitrate simulated aerosol concentrations within this size category (PM_1) will be used for comparison against observational aircraft field campaign data collated by Heald et al. (2011). This is as the AMS equipment is referred to as a PM_1 instrument, reflecting its transmissions efficiency; ~50% for PM_1 (Canagaratna et al., 2007).

Aerosol concentrations obtained are presented as mass concentrations at standard temperature and pressure (STP: 298 K, 1 atm), i.e. reported in μg sm^{-3} (Heald et al., 2011). Equation 3.6 is used to convert aerosol component concentrations from the model, at ambient monthly mean conditions within the model, to aerosol component concentrations at STP. This calculation is applied throughout the global domain and across each month: where the subscripts i, j, k and m represent the longitude, latitude, pressure levels and months respectively.

$$[\text{Aerosol}_X]_{STP_{i,j,k,m}} = [\text{Aerosol}_X]_{model_{i,j,k,m}} \cdot \frac{\rho_{air_{STP}}}{\rho_{air_{model_{i,j,k,m}}}} \cdot \frac{T_{model_{i,j,k,m}}}{T_{STP}}$$

Equation 3.6

Where $[\text{Aerosol}_X]_{STP}$ = Concentration of aerosol component X at STP

$[\text{Aerosol}_X]_{model}$ = Concentration of aerosol component X from model

$\rho_{air_{STP}}$ = Density of air at STP

$\rho_{air_{model}}$ = Density of air from model

T_{model} = Temperature from model

T_{STP} = Temperature at STP (273 K)

The following subsections present comparisons of GMV4-nitrate vertical profiles (excluding aviation emissions) in comparison to aircraft field campaign profiles, along with scatter plots which highlight the Pearson regressions (R) and normalised mean bias (NMB) between model simulations and observational data calculated using Equation 3.4 and Equation 3.5 in Section 3.3.1.

Due to issues with TROMPEX observational data, this section will not be able to evaluate GMV4-nitrate simulated sulfate, nitrate, ammonium and organic aerosol profiles over the TROMPEX aircraft field campaign region.

3.3.2.1 Evaluation against sulfate observations

Sulfate model-observation comparison profiles (Figure 3.12) show that GMV4-nitrate simulated profiles are in fair agreement with aircraft field campaign data, but with regional discrepancies. 10 of the model simulations lie within the standard deviations of the aircraft field campaign observations (ACE-Asia, EUCAARI, ADIENT, ADRIEX, MILAGRO, ITCT-2K4, ARCTAS summer, VOCALS-UK, OP3 and IMPEX). Model simulations over the ACE-Asia and

VOCALS-UK campaign tracks return the greatest correlation with observations (Heald et al., 2011). The greatest disparity between model simulations and field campaign data is seen over the TexAQS, ARCTAS spring, DABEX/DODO and ITOP field campaign sites.

Figure 3.12: Annual mean model simulated sulfate profiles compared against mean aircraft field campaign data collated by Heald et al. (2011): GMV4-nitrate vertical profiles in dashed orange; mean, median and standard deviation of aircraft field campaigns in black solid, dashed and solid horizontal lines respectively.

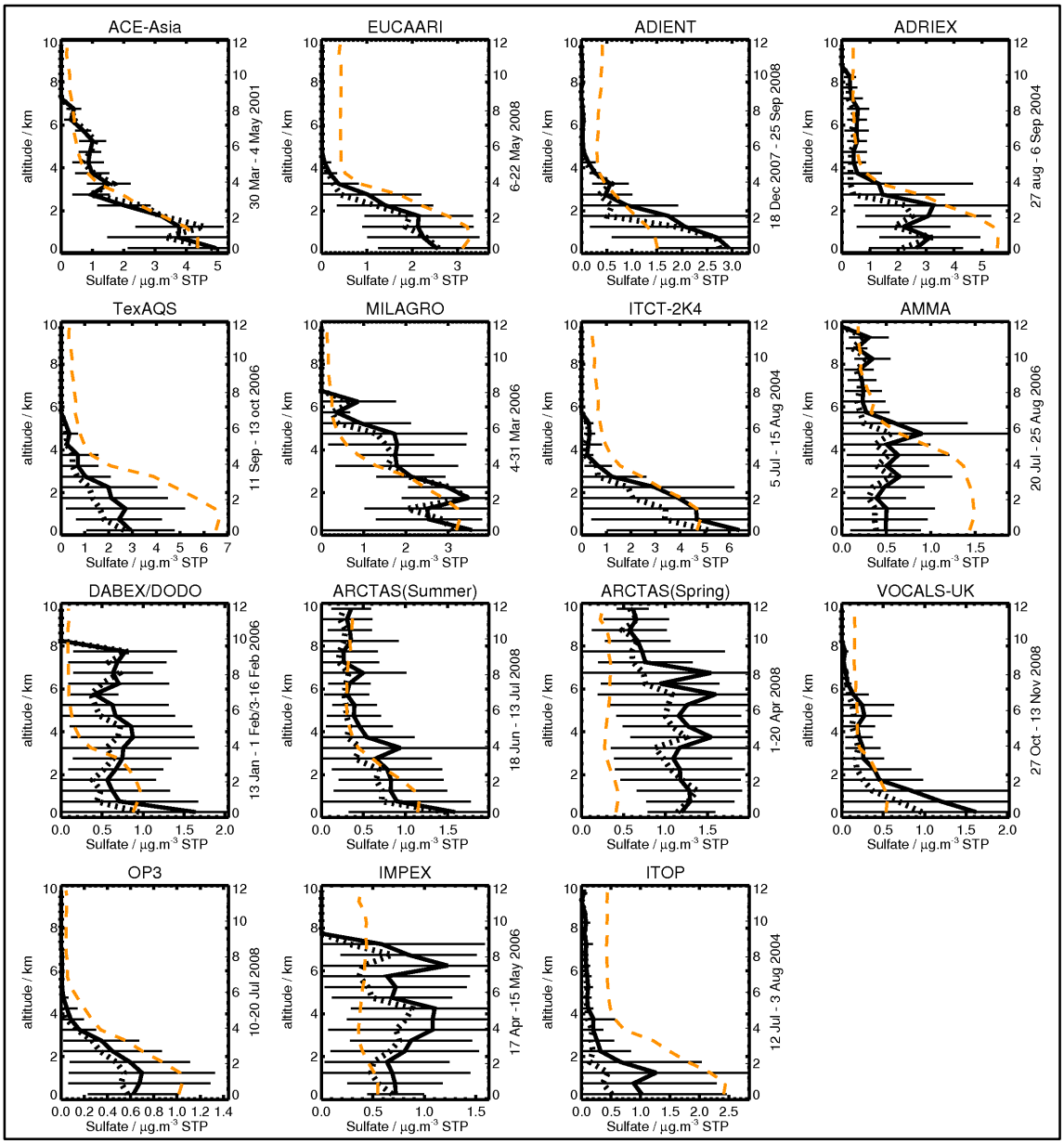

Differences in model-observation profiles can potentially be attributed to reductions in emission fields fed in to the model for the years observational data are acquired for, and due to the local conditions individual campaigns were investigating, e.g. fires (Heald et al., 2011), as well due to any differences in averaging periods between measurements and model simulations.

European SO_2 emission reductions were influenced by the Gothenburg Protocol (United Nations Economic Commission for Europe, 1999), which in relation to year 2000 emissions has seen a reduction in 2004 emissions of 18.15% across the 33 nations of the European Environment Agency (EEA33) and 17.94% over the 28 member states of the European Union (EU28) (European Environment Agency, January 2014c). While in 2008 over the EEA33 member states a 33.28% reduction in SO_X was observed in relation to 2000, and reduction in SO_X of 43.78% over the EU28 member states (European Environment Agency, January 2014c).

Model overestimations over the ACE-Asia, TexAQS, ITOP and MILAGRO field campaign routes, routes primarily affected by pollution, could be attributed by reductions in local emissions since year 2000 – though for ACE-Asia it is unlikely to be the case, as this campaign occurred in 2001. Model overestimations seen over the South climate region which includes the TexAQS campaign (as defined by the U.S. Environmental Protection Agency), could be due to a 14.15% reduction in SO_2 between 2000 and 2006 (U.S. Environmental Protection Agency, 2014e).

Model sulfate overestimations over Central America can be partially due to the model not capturing the enhanced photochemically reactive nature of the atmosphere over Mexico (Shirley et al., 2006) in addition to the biomass burning being investigated by this campaign (Heald et al., 2011). Due to both reductions in SO_2 emissions of ~1 $Gg(SO_2).a^{-1}$ (2010–2005), and globally relatively higher NH_3 emissions (from housing, storage, grazing and agriculture) (Beusen et al., 2008) the production of ammonium sulfate will be favoured over the formation of ammonium nitrate (Bauer et al., 2007) – explaining model underestimations of nitrate profiles over the MILAGRO field campaign site (Figure 3.17).

GMV4-nitrate simulations are in fair agreement to GEOS-Chem simulations from Heald et al., (2011). Greatest agreement between GMV4-nitrate and GEOS-Chem is seen over the ADIENT, ITCT-2K4 and DABEX/DODO campaign regions. While greatest differences are seen over the ACE-Asia, MILAGRO, VOCALS-UK, IMPEX and ITOP campaign regions. In general GMV4-nitrate and GEOS-Chem skilfully trace sulfate profiles over each site (Heald et al., 2011).

To further analyse the correlation between GMV4-nitrate model simulations and aircraft field campaign data model-observation scatter plots were created (Figure 3.13). The model overestimates observed sulfate concentrations over 9 of the 15 field campaigns, as indicated by the positive biases returned. Where the model underestimates observed sulfate profiles correlation between model and observations is also poor, indicating poorer model skill. Where the model is seen to greatly underestimate observations (Figure 3.12) a negative regression (R) value is returned (Figure 3.13), identifying regions where the model shows lower model skill.

Analyses of sulfate model-observation comparisons for all field campaigns indicate that biases range between –71.72% to +190.26%, with the model returning a global model bias of 8.90%.

Figure 3.13: Comparison of annual mean model simulated sulfate profile concentrations against mean aircraft field campaign profile concentrations for the aircraft field campaigns collated by Heald et al. (2011). Pearson regression (R) and normalised mean biases (bias) are presented to highlight disparity between model and observational data.

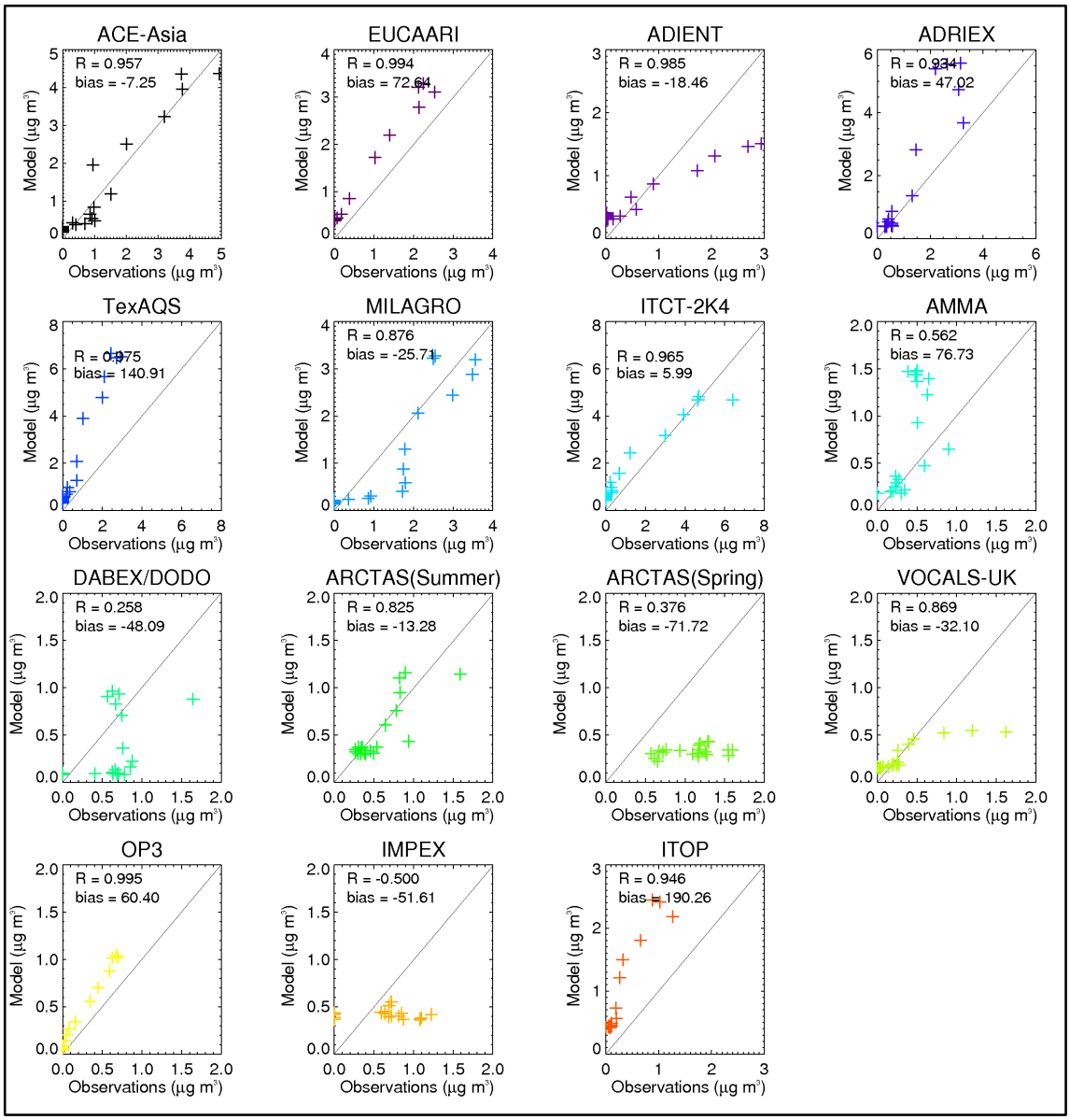

Figure 3.14 shows model-observation comparison at the continental scale: Europe, North America, South America, West Africa and Asia. Figure 3.14 shows that positive biases are returned over Europe [bias = +53.74%; R = 0.853], West Africa [bias = +2.40%; R = 0.075] and Asia [bias = +1.41%; R = 0.969], while negative biases are returned over North America [bias = – 6.22%; R = 0.737] and South America [bias = –32.10%; R = 0.869].

Mann et al. (2010) evaluated surface sulfate concentrations over Europe with EMEP (European Monitoring and Evaluation Programme) observations and concentrations over North America with the IMPROVE (Interagency Monitoring of Protected Visual Environments) observations. Mann et al. (2010) evaluated that the TOMCAT-GLOMAP-mode version 6 (uncoupled model) had a bias of +0.05% over Europe and a bias of +0.12% over North America. In comparison to Mann et al. (2010) GMV4-nitrate using data from Heald et al. (2011) returns a bias of +28.21% over Europe (EUCAARI, ADIENT, ADRIEX and ITOP) and bias of –6.21% over North America (Tex-AQS, MILAGRO, ITCT-2K4, ARCTAS summer, ARCTAS spring and IMPEX) for lowest level observations at 250 m.

Figure 3.14: Comparison of regionally partitioned annual mean model simulated sulfate profile concentrations against aircraft field campaign profile concentrations for the aircraft field campaigns collated by Heald et al. (2011): for Europe, North America, South America, West Africa and Asia. Pearson regression (R) and normalised mean biases (bias) are presented to highlight disparity between model and observational data.

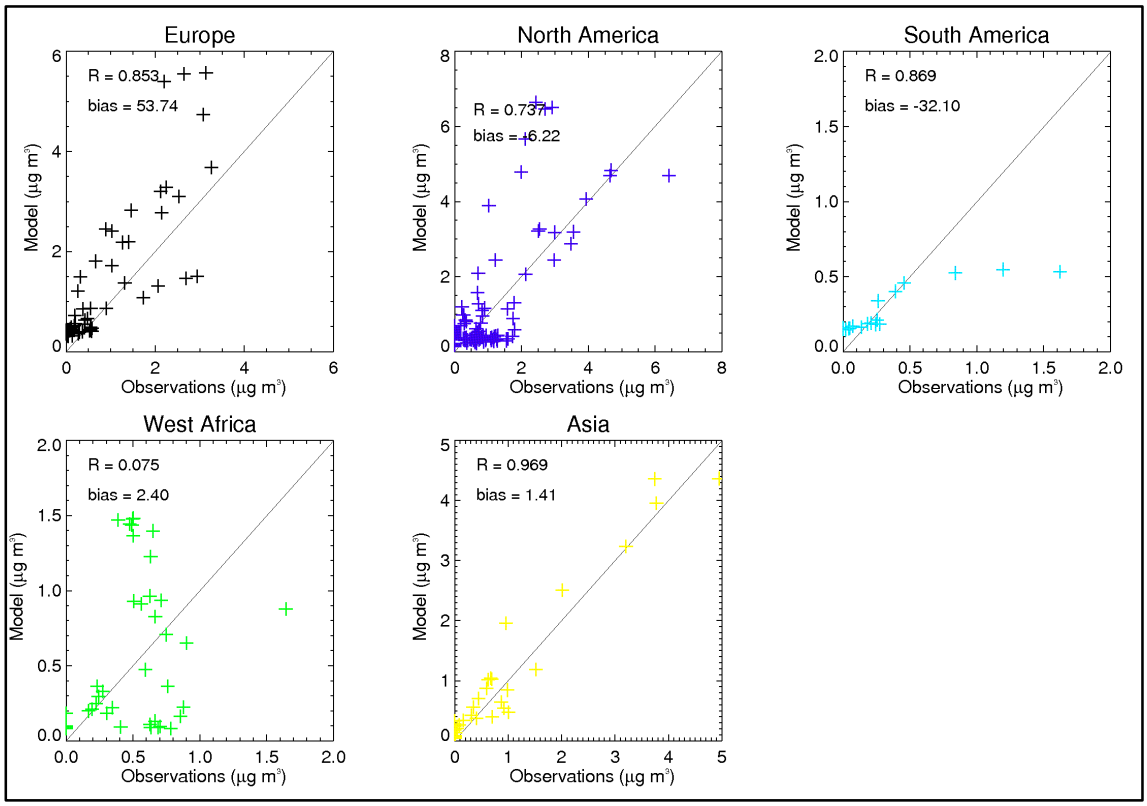

Figure 3.15 presents the differences between GMV4-nitrate model simulations and aircraft field campaigns for each aircraft field campaign (Table 3.5), along with the mean of all campaign site difference profiles.

From the mean difference profile presented in Figure 3.15 it is seen that globally GMV4-nitrate overestimates sulfate concentrations across the 15 field campaigns analysed here, while

presenting slight underestimation in sulfate concentrations between ~3.5 to ~8.0 km. Greatest overestimations are seen below 3 km, indicating that the disparity between model simulations and aircraft field campaign observations collated by Heald et al., (2011) could be a result of anthropogenic emissions used to drive GMV4-nitrate simulations.

Figure 3.15: Difference between annual mean model simulated sulfate profiles and aircraft field campaign observations collated by Heald et al. (2011) over field campaigns.

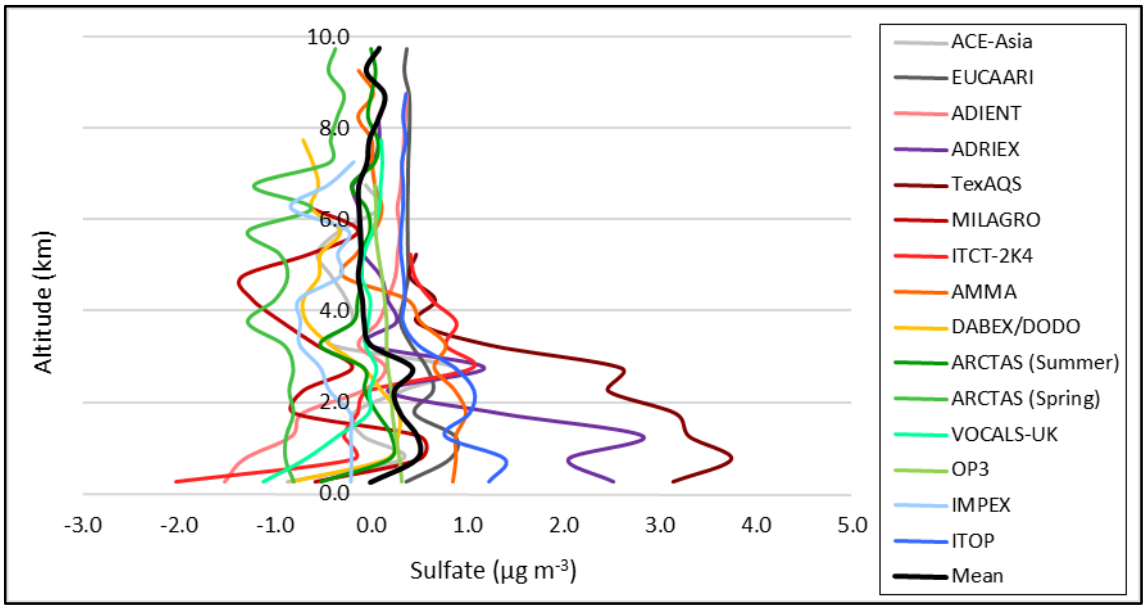

In addition to changes in global and regional SO_2 emissions, differences between model simulated and observational profiles will be partially due to the different times of the year, and periods of time each of the aircraft field campaigns were conducted. Over each field campaign path annual mean model simulated concentrations were used (for profile comparisons and model-observation comparisons), while each field campaign was conducted over different time frames times of the year (as shown in Figure 3.16).

From Figure 3.16 it is seen that some field campaigns were conducted over the period of only a month (such as EUCAARI, MILAGRO, ARCTAS spring and OP3), while the majority were conducted over 2–3 months (such as ACE-Asia, ADRIEX, TexAQS, ITCT-2K4, AMMA, DABEX/DODO, ARCTAS summer, VOCALS-UK, IMPEX and ITOP), with one being conducted over a period of 10 moths (ADIENT). As such differences between model and observations can be partially due to differences in time periods and time of year that observational were acquired over.

Figure 3.16: Illustration of time periods each of the aircraft field campaign conducted by Heald et al. (2011) was conducted.

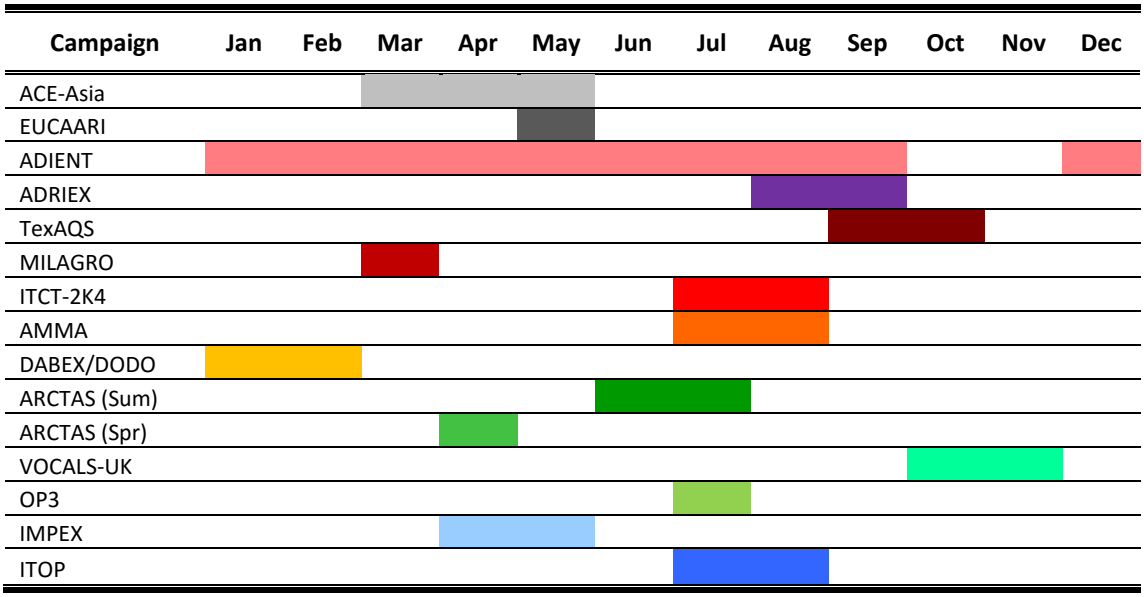

As such if reductions in regional global emissions were contributing factors, it would be expected that the model simulations would be able to most skilfully replication observations over the ADIENT campaign flight path, and show the greatest differences when compared to the ARCTAS spring field campaign which was conducted for a month, and investigated biomass burning events. In the case of model-observation comparisons with the Arctas summer field campaign the model is seen to greatly underestimate sulfate concentrations, demonstrating the effects of differences in periods and regional class of field campaign as classified by Heald et al. (2011) (fire in this case).

3.3.2.2 Evaluation against nitrate observations

Figure 3.17 presents a comparison of GMV4-nitrate simulated nitrate profiles with aircraft field campaign profiles. This comparison shows that seven of the campaign profiles are in reasonable agreement, with simulated profiles lying within the standard deviation of aircraft field campaign observations (ACE-Asia, EUCAARI, ADIENT, ADRIEX, ARCTAS spring, IMPEX and ITOP) (Heald et al., 2011). The greatest correlation between model profiles and observations are seen over the ADIENT and ADRIEX field campaigns, while the largest disparities between profiles and values are seen over the MILAGRO, ITCT-2K4, AMMA, ARCTAS summer, ARCTAS spring and OP3 campaigns (Heald et al., 2011).

Figure 3.17: Annual mean model simulated nitrate profiles compared against mean aircraft field campaign data collated by Heald et al. (2011): GMV4-nitrate vertical profiles in dashed green; mean, median and standard deviation of aircraft field campaigns in black solid, dashed and solid horizontal lines respectively.

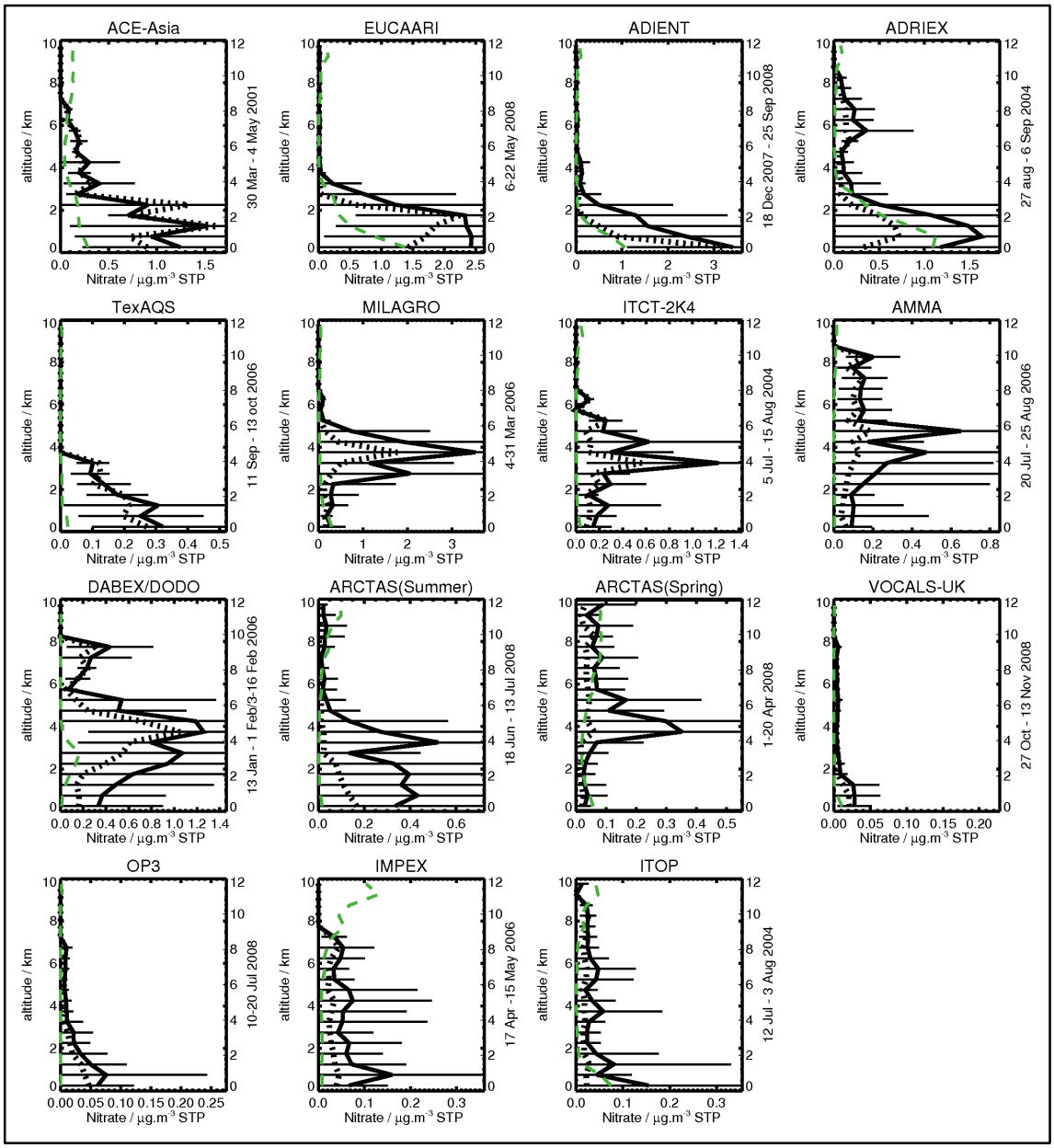

Over Europe (ADIENT, ADRIEX and EUCAARI) GMV4-nitrate is able to replicate field campaign nitrate profiles, within the mean and median produced by field campaign data, and within the standard deviation of this observational field campaign data (Heald et al., 2011). Differences in simulated profiles over Europe could be explained by reductions in SO_2, NH_3 and NO_X emissions seen between 1990 and 2011. Over this period of time there have been reductions in SO_2, NH_3 and NO_X (European Environment Agency, January 2014c; European Environment Agency, January 2014b; European Environment Agency, January 2014a). As relative reductions in SO_2 [ΔSO_{2_2004} = –18.15%; ΔSO_{2_2008} = –33.28%] have been far greater than those in NO_X

[ΔNO_{X_2004} = –6.07%; ΔNO_{X_2008} = –17.47%] and NH_3 [ΔNH_{3_2004} = –3.75%; ΔNH_{3_2008} = –6.96%] it would be expected that these relative reductions would adversely affect sulfate formation and allow for the formation of additional nitrates; due to the relationship between the formation mechanisms between ammonium sulfates and ammonium nitrates (Bauer et al., 2007).

Figure 3.18: Comparison of annual mean model simulated nitrate profile concentrations against mean aircraft field campaign profile concentrations for the aircraft field campaigns collated by Heald et al. (2011). Pearson regression (R) and normalised mean biases (bias) are presented to highlight disparity between model and observational data.

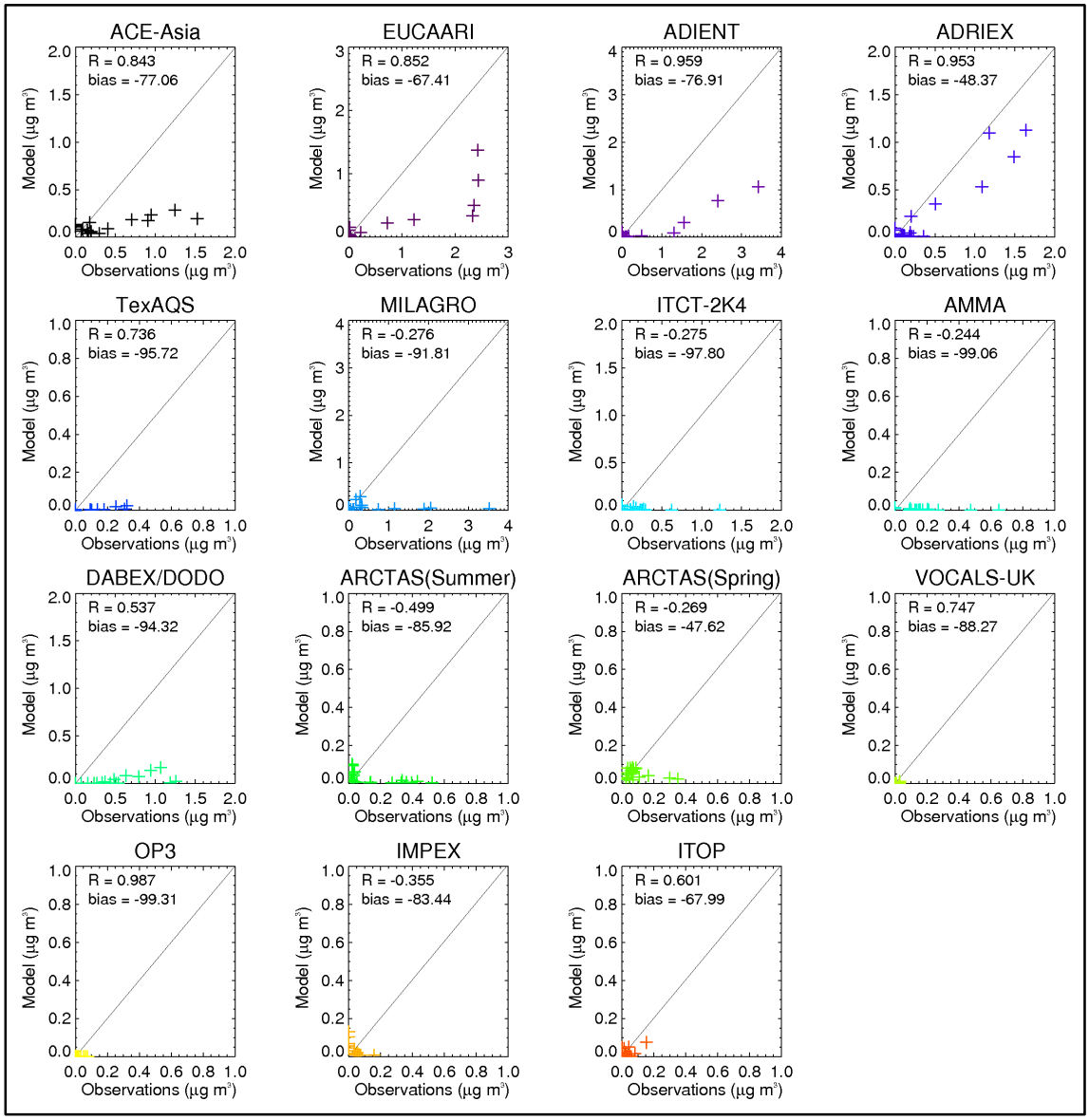

The model underestimates observed nitrate from the ARCTAS summer campaign (June–July 2008). This underestimation could be attributed to the small reductions in NH_3 emissions [–0.33%] seen over Canada in 2008 relative to 2000, in tandem with much larger reductions in SO_2 [–24.40%] and NO_X [–16.15%] (Environment Canada, 2014); thus again favouring the formation mechanism for ammonium nitrate (discussed in Section 2.3.1.5) (Bellouin et al.,

2011; Clarke et al., 1998; Fiore et al., 2012; Forster et al., 2007; Righi et al., 2013; Unger, 2011; Unger et al., 2010). Despite model underestimations of nitrate observations, as represented by negative biases over each field campaign (Figure 3.18), the model is able to replicate the shape of over 50% of field campaign profiles (Figure 3.17) as indicated by the positive R values.

Figure 3.19: Comparison of regionally partitioned annual mean model simulated nitrate profile concentrations against aircraft field campaign profile concentrations for the aircraft field campaigns collated by Heald et al. (2011): for Europe, North America, South America, West Africa and Asia. Pearson regression (R) and normalised mean biases (bias) are presented to highlight disparity between model and observational data.

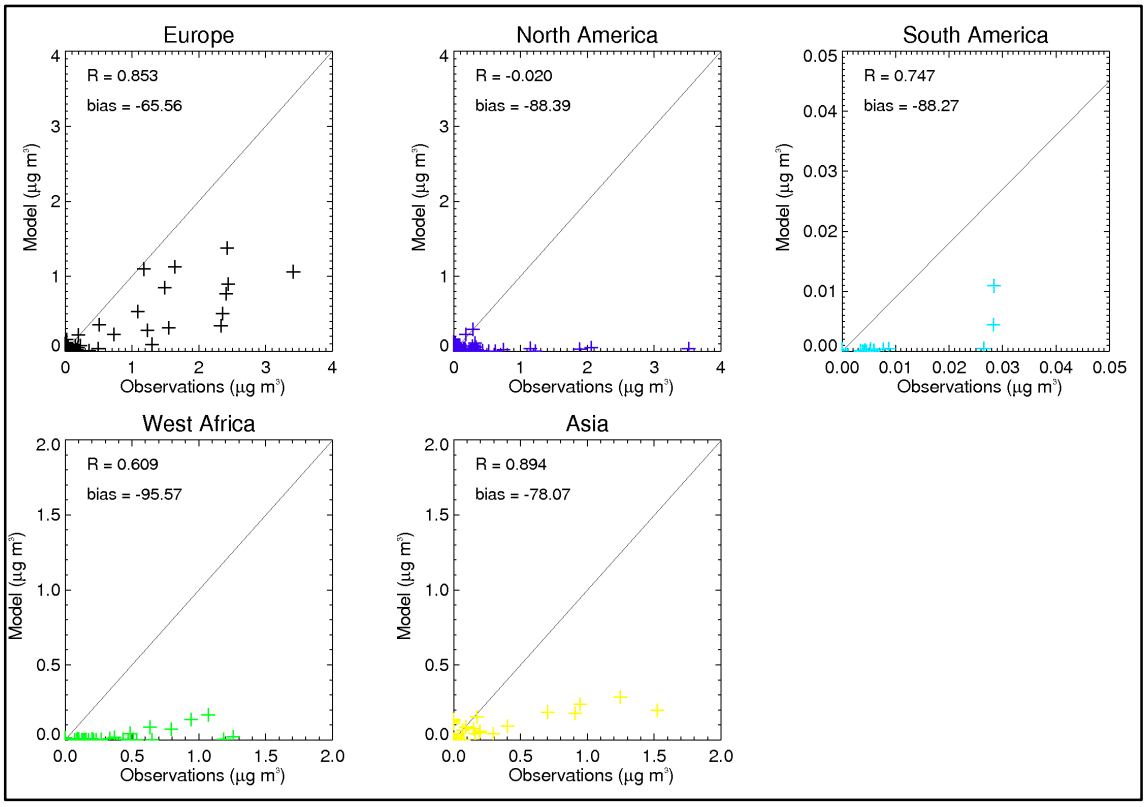

Analyses of nitrate model-observation comparisons for all field campaigns indicate that biases range between –99.31% to –47.62%, with the model returning a global model bias of –93.89%. When field campaign sites are grouped in to regions, the regional trends and characteristics of model simulations are seen. Figure 3.19 shows that negative biases are seen across each continental region investigated: Europe [bias = –65.56%; R = 0.854], North America [bias = –88.34%; R = 0.020], South America [bias = –88.27%; R = 0.747], West Africa [bias = –95.57%; R = 0.609] and Asia [bias = –78.07%; R = 0.894].

In relation to the aircraft field campaigns the mean model is compared to (Table 3.5), the model underestimates observed nitrate concentrations below ~8.75 km, and over estimates nitrate concentrations above ~8.75 km (Figure 3.20).

Figure 3.20: Difference between annual mean model simulated nitrate profiles and aircraft field campaign observations collated by Heald et al. (2011) over field campaigns.

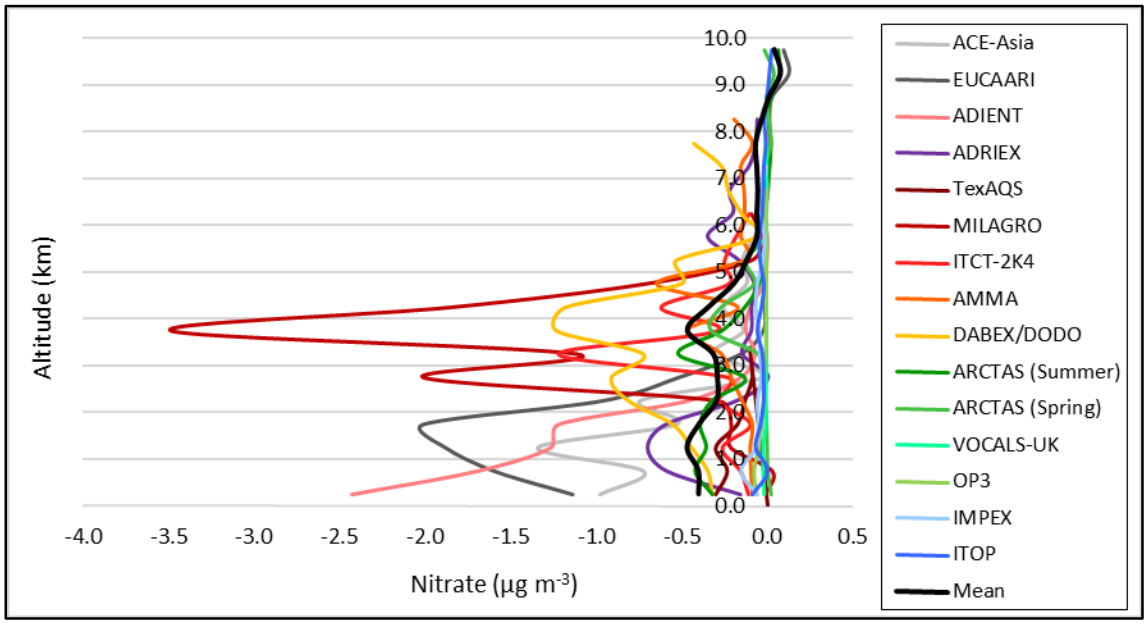

As with sulfate aerosol model-observation comparisons, the length of aircraft campaigns Figure 3.16 can partially contribute to the differences in nitrate profile comparisons (Figure 3.17) and model-observation scatter plots (Figure 3.18). These differences could contribute to explaining the large negative biases seen over the MILAGRO, ARCTAS spring and OP3 field campaign paths. Though despite this large negative model biases are seen over the ADIENT field campaign path, but as previously discussed this is partly due to the large reductions in SO_2, NH3 and NOX seen over Europe between 2000 and 2008 (European Environment Agency, January 2014c; European Environment Agency, January 2014b; European Environment Agency, January 2014a).

3.3.2.3 Evaluation against ammonium observations

GMV4-nitrate simulated ammonium profiles are found to be in agreement with observational ammonium profiles (Figure 3.21), i.e. demonstrating that model simulated vertical profiles replicate the profile shapes returned by aircraft field campaigns collated by Heald et al. (2011). 12 of the model simulation vertical profiles lie within the standard deviations of observational profiles (ACE-Asia, EUCAARI, ADIENT, ADRIEX, TexAQS, ITCT-2K4, AMMA, ARCTAS summer, ARCTAS spring, VOCALS-UK, OP3 and ITOP).

European (EUCAARI, ADIENT, ADRIEX and ITOP), Asian (ACE-Asia and OP3) and South American (OP3) model simulated profiles are seen to replicate field campaign profile concentrations and trends (Figure 3.21), with the model profiles skilfully replicating observational profile mean

and median values, especially over 2 km (Heald et al., 2011). Model overestimations over the ADRIEX and ITOP campaigns could be attributed to reductions in European emissions of SO_2 [–43.59%] and NO_X [–20.55%] despite reductions in European NH_3 emissions [–6.25%] (European Environment Agency, February 2015).

Figure 3.21: Annual mean model simulated ammonium profiles compared against mean aircraft field campaign data collated by Heald et al. (2011): GMV4-nitrate vertical profiles in dashed blue; mean, median and standard deviation of aircraft field campaigns in black solid, dashed and solid horizontal lines respectively.

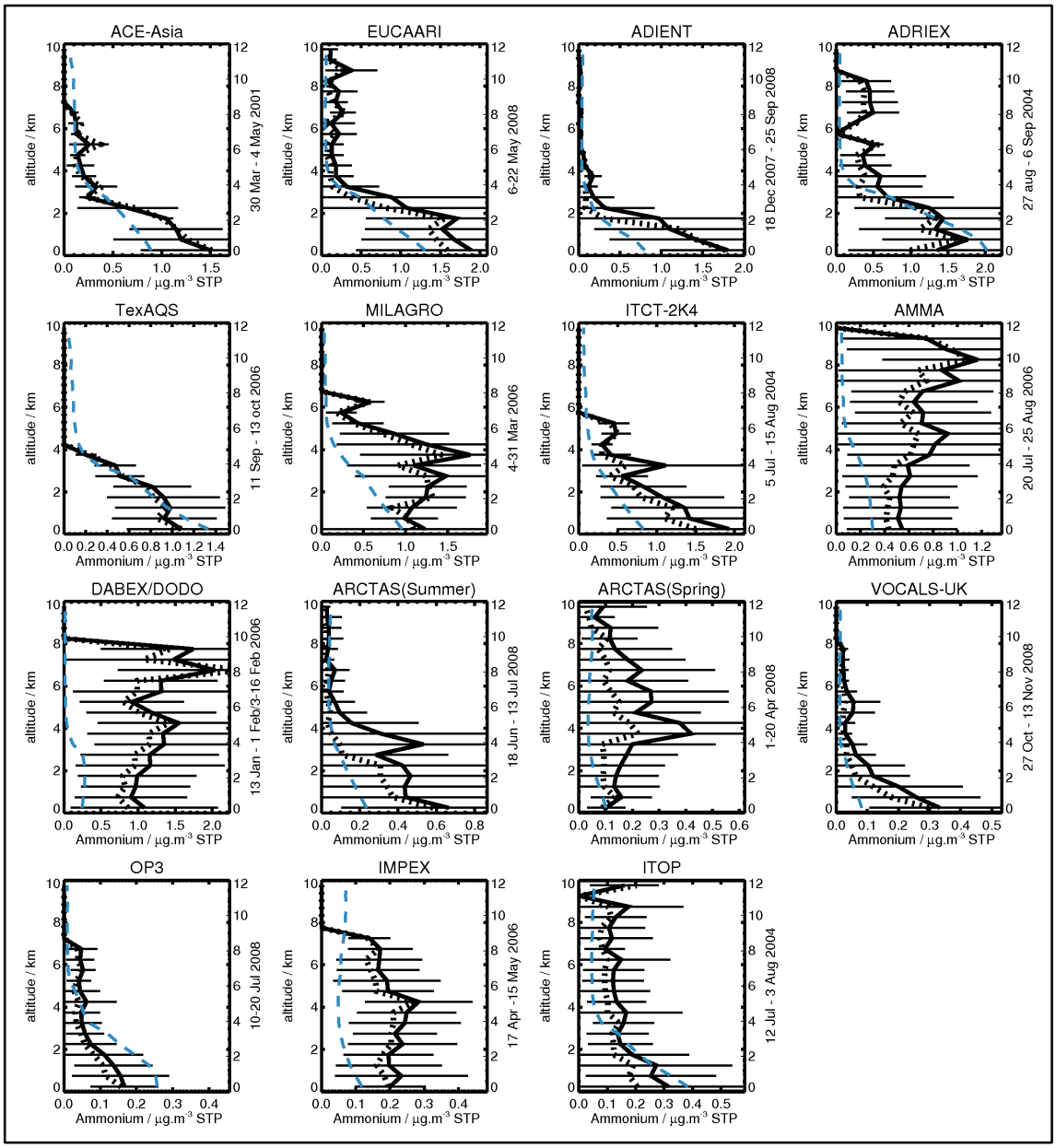

The ECCAD-GEIA (Emissions of atmospheric Compounds & Compilation of Ancillary Data – Global Emissions InitiAtive) ACCMIP inventories have examined global NH_3 emissions between 2000 and 2009 (Lamarque et al., 2010b; Lamarque et al., 2010a). Over Europe NH_3 emissions

have seen reductions over the 2004–2000 [–1.15x10^{7} kg(NH_3) m^{-2}] and 2008–2000 [–1.4x10^{7} kg(NH_3) m^{-2}] periods, which helps explain the differences between ammonium model-observation comparison profiles (Lamarque et al., 2010a).

Figure 3.22: Comparison of annual mean model simulated ammonium profile concentrations against mean aircraft field campaign profile concentrations for the aircraft field campaigns collated by Heald et al. (2011). Pearson regression (R) and normalised mean biases (bias) are presented to highlight disparity between model and observational data.

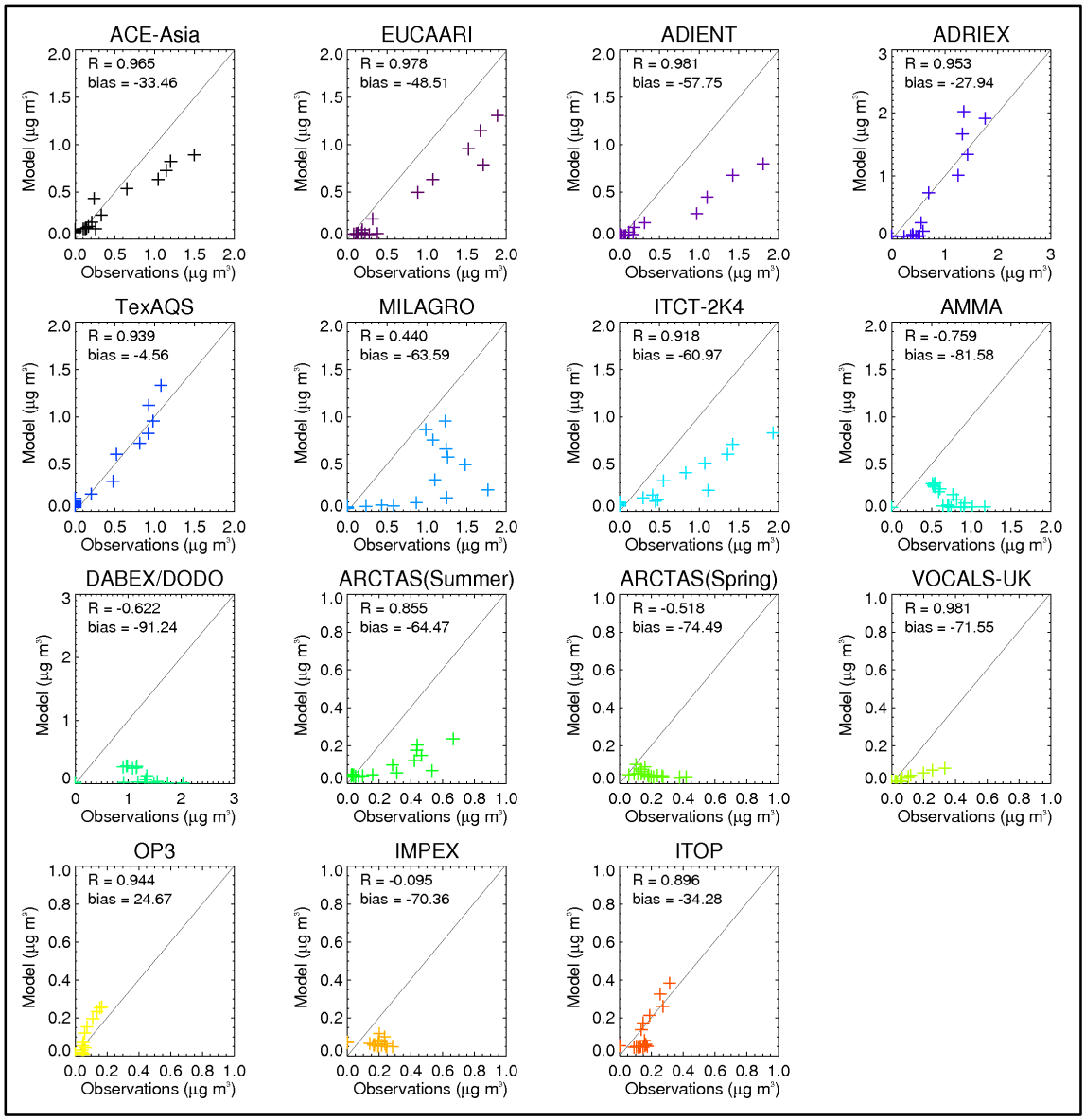

Increases in NH_3 of +1.23% over Canada occurred between 2008 and 2000 (European Environment Agency, January 2014a), but are unlikely to account for ammonium profile underestimations over the ARCTAS summer field campaign. Contradicting ECCAD-GEIA ACCMIP data U.S. specific changes in NH_3 emissions (which report increases in U.S. NH_3 emissions) the U.S. EPA indicate that (in relation to 2000) NH_3 emissions reduced by (–)18.16% in 2004 (corresponding to the ITCT-2K4 field campaign) and by (–)16.92% in 2006 (corresponding to

the TexAQS and IMPEX field campaigns) (U.S. Environmental Protection Agency, 2015). This indicates that GMV4-nitrate should be overestimating ammonium profiles over the United States, but slight over-predictions are seen over the TexAQS campaign region (Figure 3.22). Ultimately changes in ammonium are a product of changes in NH_3, NO_X and SO_2 emissions.

Model-observation NH_3 profile comparisons for the VOCAL-UK show that the GMV4-nitrate simulated NH_3 profile underestimates observed profile for 2008 (Figure 3.22). This can be partly explained through increases in ECCAD-GEIA ACCMIP compiled NH_3 emissions over Peru and Chile; when comparing the differences between 2008 and 2000 emissions (Lamarque et al., 2010a; Heald et al., 2011).

Annual increases in NH_3 emissions over West Africa from 2006–2000 ($+1x10^5$ kg(NH_3) m^{-2}) (Lamarque et al., 2010a) help explain why over West Africa the DABEX/DODO and AMMA campaigns greatly underestimate ammonium profiles (Figure 3.22). Additionally both the AMMA and DABEX/DODO aircraft field campaigns were conducted over regions of biomass burning, where aged biomass aerosols would be observed (Heald et al., 2011), which is found to emit large amounts of reactive nitrogen compounds (such as NH_3); this is estimated as the second most important source of NH_3 after agriculture, with estimations subject to large uncertainties (Whitburn et al., 2015).

Whitburn et al. (2015) found that over the region relating to the AMMA and DABEX/DODO aircraft field campaigns GFEDv3.1 and GFASv1.0 inventories underestimate NH_3 emissions between 2008–2011 in comparison to IASI (Infrared Atmospheric Sounding Interferometer) measurements, indicating that NH_3 emissions considered within GMV4-nitrate (GFEDv1.0) could be underestimating biomass burning sources of NH_3. This could explain the differences in ammonium profiles seen in model-observation comparisons over the AMMA and DABEX/DODO aircraft field campaign sites.

Additionally, differences between simulated and field campaign ammonium concentration profiles could be attributed to the time of year at which field campaigns were conducted and the length of time of the campaigns (Figure 3.16); with AMMA being conducted for two months over summer and DABEX/DODO being conducted for two months over winter, but also both being campaigns which observed biomass burning events which would have not been accounted for in SO_2 and ammonia emissions used in GMV4-nitrate. Additionally the conditions campaigns were investigating can partly explain differences seen between simulated and observed ammonium profiles over the MILAGRO campaign.

Figure 3.23: Comparison of regionally partitioned annual mean model simulated ammonium profile concentrations against aircraft field campaign profile concentrations for the aircraft field campaigns collated by Heald et al. (2011): for Europe, North America, South America, West Africa and Asia. Pearson regression (R) and normalised mean biases (bias) are presented to highlight disparity between model and observational data.

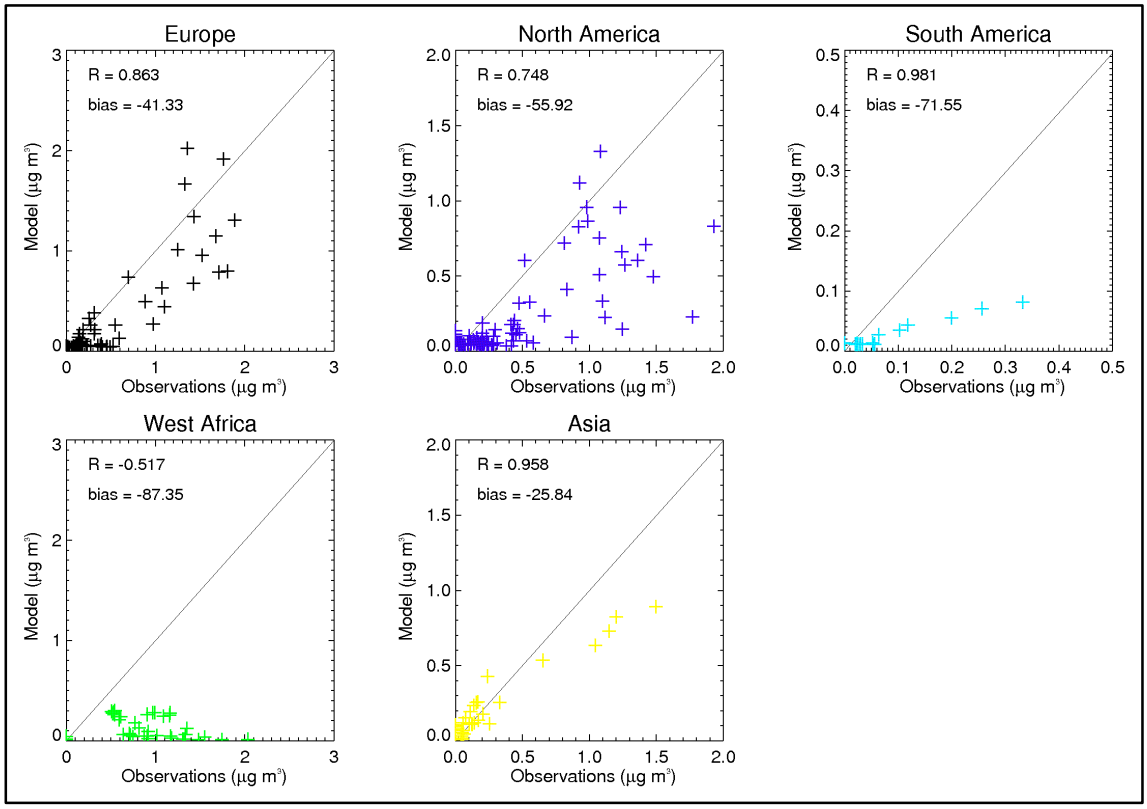

Figure 3.24: Difference between annual mean model simulated ammonium profiles and aircraft field campaign observations collated by Heald et al. (2011) over field campaigns.

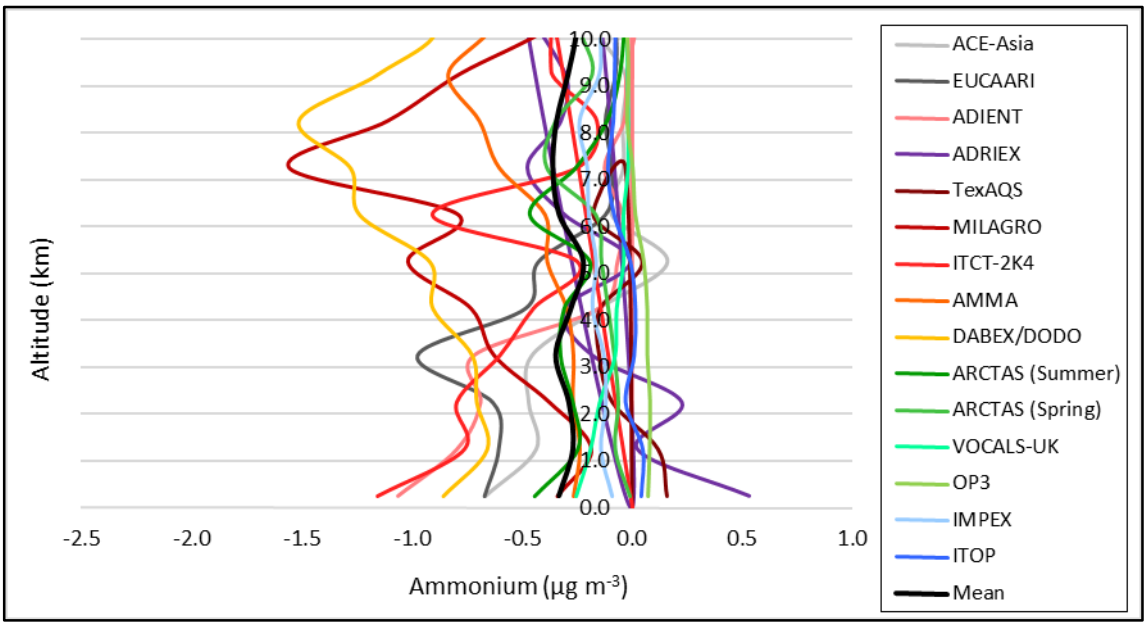

Overall GMV4-nitrate's simulation is seen to underestimate ammonium profiles over most field campaign sites (Figure 3.22), with these underestimations being partly driven by underestimations in the GFEDv3.1 NH_3 emissions (Whitburn et al., 2015). Analyses of ammonium model-observation comparisons for all field campaigns indicate that biases range between –91.24% to –24.67%, with the model returning a global model bias of –59.05%.

When investigating the relationship be model and observational ammonium concentrations on a continental scale (Figure 3.23), the model is seen to underestimate ammonium over each region (Europe [bias = –41.33%; R = 0.863], North America [bias = –55.92%; R = 0.748], South America [bias = –71.55%; R = 0.981], West Africa [bias = –87.35%; R = –0.517] and Asia [bias = –25.84%; R = 0.958]), thus identifying the model's tendency to globally underestimate ammonium profiles.

Figure 3.24 shows that accumulated site mean differences between the model and field campaign observations indicate that GMV4-nitrate underestimates ammonium profiles globally, with underestimations generally greater above 6 km.

3.3.2.4 Evaluation against organic aerosol observations

Figure 3.25 compares GMV4-nitrate simulated organic aerosol vertical concentration profiles against observational organic aerosol concentrations obtained and collated from aircraft field campaigns as compiled by Heald et al. (2011). In order to conduct this comparison an organic aerosol mass (OA) to organic carbon (OC) ratio of 1.4 is used (Russell, 2003). Russell (2003) found that the ratio of OA:OC is dependent on the number of functional groups to the number of carbons in the chain. This results in 90% of the measurements collected returning ratios between 1.2–1.6, with mean values just below 1.4. This is in agreement with the range of 1.3–1.5 from Canagaratna et al. (2015), but lower than their 'Improved-Ambient' OM:OC ratio of total OA of 1.84; based on ambient Aitken mode measurements.

GMV4-nitrate underestimates OA over the majority of field campaigns, with the exceptions being comparisons against the VOCALS-UK and OP3 campaigns (Heald et al., 2011). Despite underestimating OA aircraft campaign profiles, 9 out of the 15 site's GMV4-nitrate simulated profiles lie within the standard deviation of observations (ADRIEX, TexAQS, MILAGRO, ITCT-2K4, AMMA, DABEX/DODO, ARCTAS summer, ARCTAS spring, IMPEX and ITOP); but this does not necessitate good agreement between GMV4-nitrate and field campaign data. The model over the EUCAARI, ADIENT, TexAQS and ITCT-2K4 field campaigns shows agreement with the

standard deviation of observations above ~2 km. Additionally 9 out of the 15 model follow the shape of observational profiles.

Figure 3.25: Annual mean model simulated organic aerosol profiles compared against mean aircraft field campaign data collated by Heald et al. (2011): GMV4-nitrate vertical profiles in dashed red; mean, median and standard deviation of aircraft field campaigns in black solid, dashed and solid horizontal lines respectively.

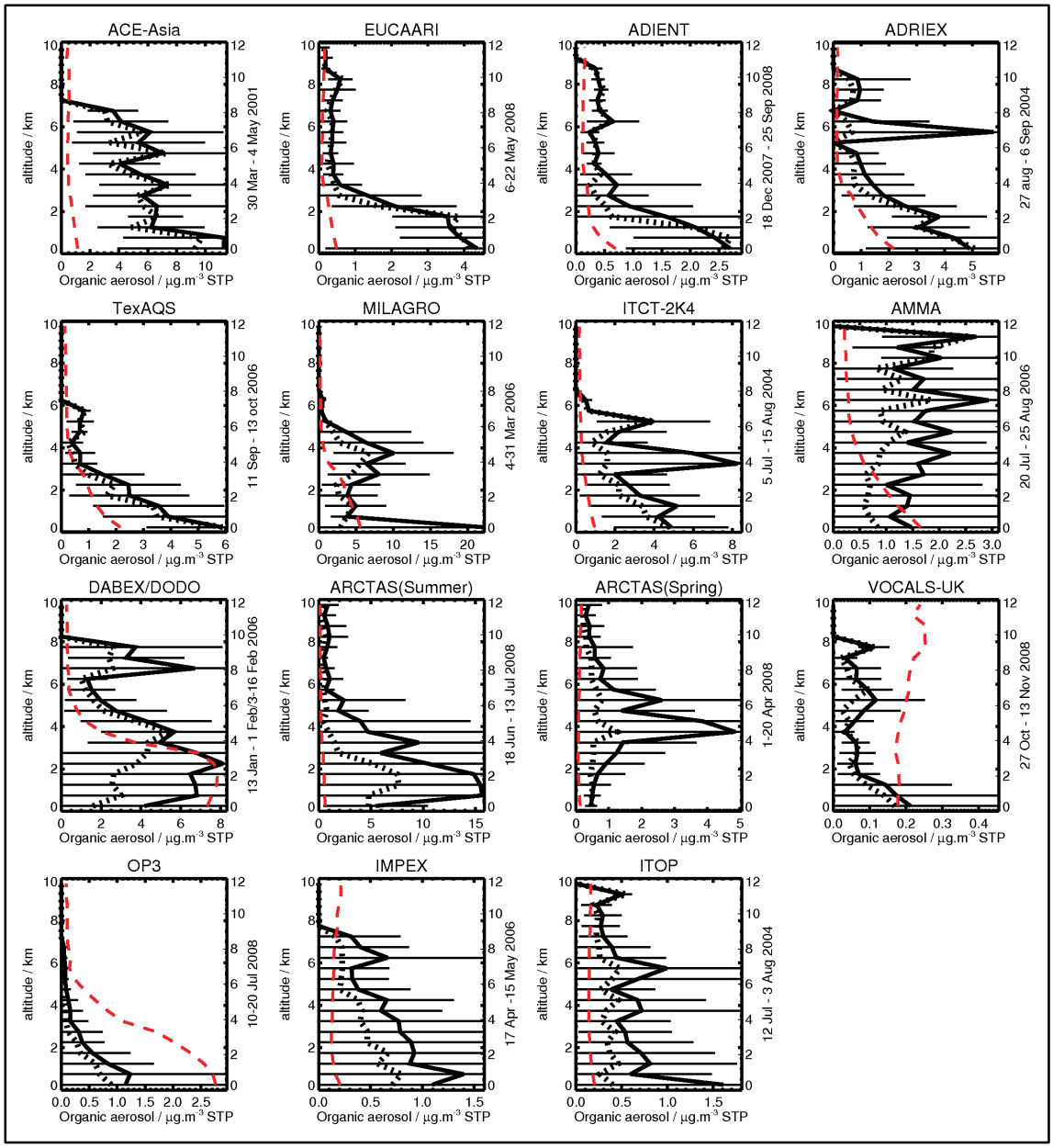

Over Europe OC emissions are found to increase by up to 15–20 % (ECCAD GEIA-ACCMIP emissions inventory data) in 2004, and by up to ~40% over 2008 (Lamarque et al., 2010a) relative to 2000; emissions increases which contribute to model underestimations of OA profiles over Europe. Model profiles over Europe tend to replicate the shape of observational

profiles, but underestimate OA concentrations below ~4 km and in most cases simulate concentrations outside the standard deviation of observational data (Heald et al., 2011).

Over North and Central America increases and decreases in OC emissions are observed in 2006 and 2004 in relation to 2000. Relating to the ITCT-2K4 campaign (which underestimates OA profile) in 2004 the field campaign crosses regions which see increases of ~10% and reductions of up to ~35% (Lamarque et al., 2010a). While in relation to the MILAGRO field campaign (2006) increases in OC emissions of up to ~40% are seen. In relation to the TexAQS and IMPEX campaigns increases in OC emissions of ~10% are seen (Lamarque et al., 2010a). These increases help contribute to explaining why the model underestimates over these field campaign routes.

Over Asia small reductions in OC emissions are seen in 2001 (ACE-Asia) and 2008 (OP3). Despite these reductions the model underestimates the OA profile over the ACE-Asia field campaign, but greatly overestimates the OA profile over the OP3 field campaign; with comparisons for both campaigns showing very little agreement with the standard deviation of observational data (Heald et al., 2011; Lamarque et al., 2010a).

In relation to ARCTAS spring small increases (Northern Canada) and small reductions (Alaska) are seen over the field campaign, while in relation to ARCTAS summer small increases in OC emissions are primarily seen over the field campaign path. Despite this the model underestimates OA in relation to the associated field campaigns (Lamarque et al., 2010a).

In 2000 over West Africa (relating to the AMMA and DABEX/DODO campaigns) increase in OC emissions of between ~10 to ~20% are observed (Lamarque et al., 2010a). Despite these increases the model demonstrates varying levels of skill in this region; skilfully replicating the DABEX/DODO field campaign while underestimating the AMMA profile above ~1 km (Heald et al., 2011).

Differences between model-observation comparisons over the ITCT-2K4 (Warneke et al., 2006), TexAQS, MILAGRO (Karl et al., 2009), ARCTAS summer, ARCTAS spring (de Gouw et al., 2006), IMPEX, AMMA (Murphy et al., 2010; Capes et al., 2009) can be attributed to local or transported biomass burning emissions which through the release of VOCs (volatile organic compounds) result in the formation of organic aerosols (Murphy et al., 2010).

ITCT-2K4 campaign observations conducted in 2004 are influenced by wide-spread fires over Northern Canada and Alaska (Heald et al., 2006; Heald et al., 2011). ARCTAS summer and ARCTAS spring field campaign observations (conducted in 2008) were influenced by boreal

fires, including Siberia and North America with most of the pollution plumes being transported in from Europe and Asia (Singh et al., 2010; Wang et al., 2011). In 2006 the AMMA campaign coincided with a peak in SH agriculture burning (Reeves et al., 2010), resulting in contributions from aged and elevated fire plumes (Murphy et al., 2010), which could explain the peaks in high altitude OA concentrations in the AMMA and ARCTAS (spring) field campaign concentration profile. In 2006 the DABEX/DODO field campaign observations were dominated by Western Africa fire activity (Heald et al., 2011).

Figure 3.26: Comparison of annual mean model simulated organic aerosol profile concentrations against mean aircraft field campaign profile concentrations for the aircraft field campaigns collated by Heald et al. (2011). Pearson regression (R) and normalised mean biases (bias) are presented to highlight disparity between model and observational data.

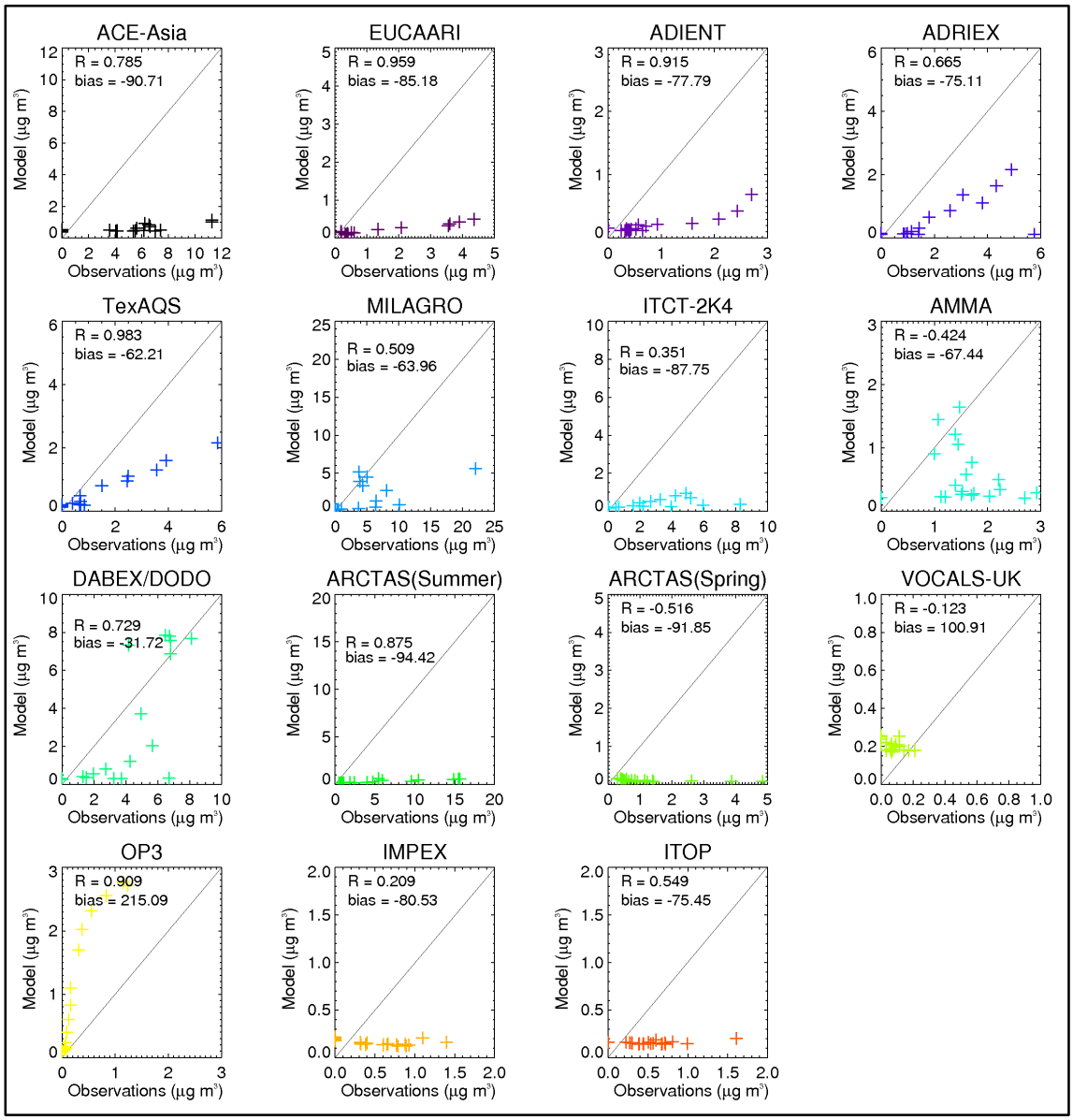

In addition to the influences from fire on field campaign OA concentration profiles, anthropogenic pollution outflow has been shown to affect OA concentrations; as seen with ACE-Asia (2001), MILAGRO (2006), ADIENT (2008), ADRIEX (2004), EUCAARI (2008) and TexAQS (2006) aircraft fields campaign observations (Heald et al., 2011).

The degree to which the model underestimates OA concentration profiles collated by Heald et al., (2011) is highlighted in Figure 3.26. Over all but two sites (VOCALS-UK and OP3) the model underestimates OA concentration profiles (indicated by the negative biases returned): with campaign biases ranging between –94.42% to +215.09%, and a global model bias of –71.91%.

Figure 3.27: Comparison of regionally partitioned annual mean model simulated organic aerosol profile concentrations against aircraft field campaign profile concentrations for the aircraft field campaigns collated by Heald et al. (2011): for Europe, North America, South America, West Africa and Asia. Pearson regression (R) and normalised mean biases (bias) are presented to highlight disparity between model and observational data.

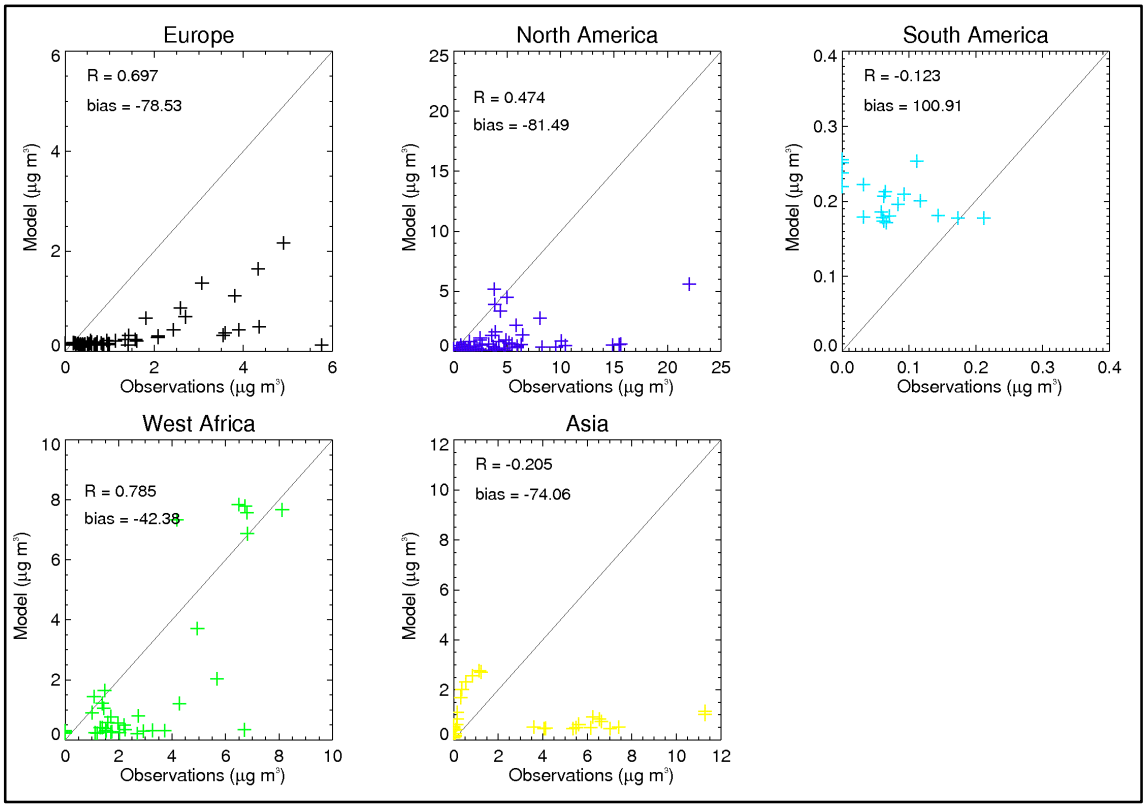

When resolving individual model-observation site comparisons in to continental regions (Europe, North America, South America, West Africa and Asia) the South American region is the only one to present a positive bias, i.e. indicating that the model overestimates in this region, but also returns a negative correlation. Figure 3.27 shows that negative biases are returned over Europe [bias = –78.53%; R = 0.697], North America [bias = –81.49%; R = 0.474],

West Africa [bias = –42.38%; R = 0.785] and Asia [bias = –74.06%; R = 0.205], while a positive bias is returned over South America [bias = +180.80%; R = –0.500].

Mann et al. (2010) evaluated the annual mean organic carbon concentrations for the lowest model level within TOMCAT-GLOMAP-mode version 6 (uncoupled model) over North America using the IMPROVE network. Mann et al. (2010) evaluated a bias of –0.72% [R = 0.40] over December 2000 and a bias of –0.42% [R = 0.83] over June 2000. In comparison to Mann et al. (2010) and using data from Heald et al. (2011) over North America (corresponding with the Tex-AQS, MILAGRO, ITCT-2K4, ARCTAS summer, ARCTAS spring and IMPEX campaigns) and for the lowest observations (at ~250 m) an annual mean bias of –77.35% [R = 0.950] was calculated. Even though GMV4-nitrate returns a far greater negative bias (i.e. underestimations in organic aerosols), the values derived here are in relative agreement with the analysis of the full profiles over the North America region (in Figure 3.27).

Figure 3.28: Difference between annual mean model simulated organic aerosol profiles and aircraft field campaign observations collated by Heald et al. (2011) over field campaigns.

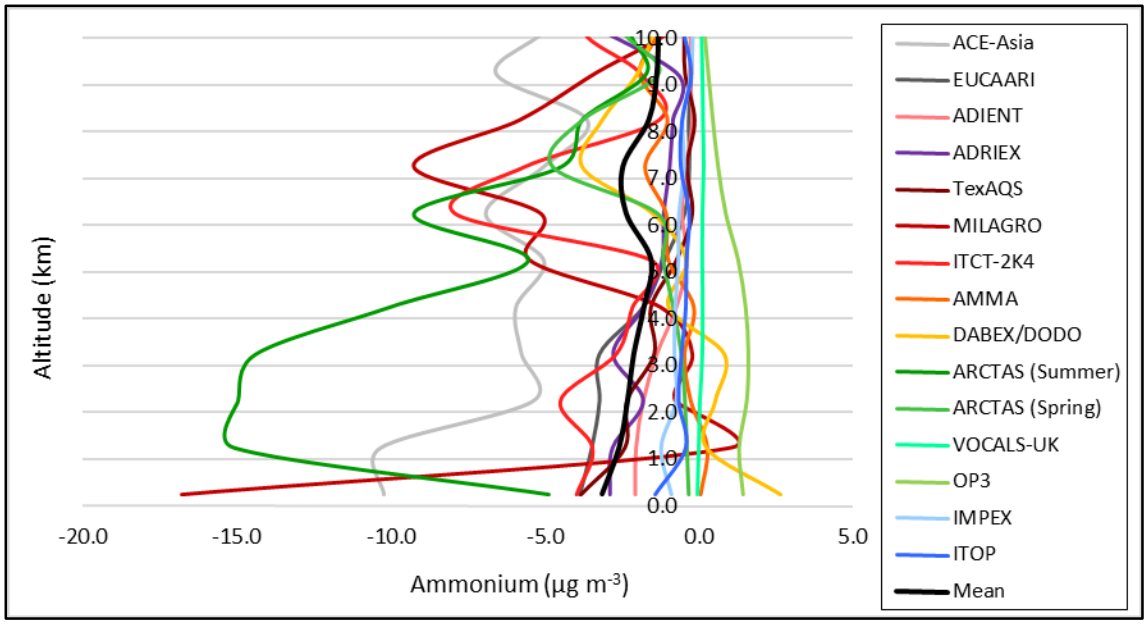

Figure 3.28 shows the accumulated site mean differences between the model and field campaign observations. This indicates that GMV4-nitrate underestimates organic aerosol profiles globally; with the greatest underestimations observed at ground level, and an additional peak at ~3.5 km.

Even though there have been increases in global OC emissions, model underestimations of OA are primarily due to underestimations in global OA sources (Heald et al., 2011; Spracklen et al., 2011b), and the lack of anthropogenic SOA within GMV4-nitrate. Spracklen et al. (2011b) suggest that the use of a 100 Tg yr^{-1} source of anthropogenically-controlled SOA (secondary

organic aerosol) would result in better agreement with IMPROVE observations. The result of increasing anthropogenic SOA emissions to ~100 Tg yr^{-1} on model-observation comparisons has been investigated by Heald et al. (2011), showing improved model simulation correlation with aircraft field campaigns.

Additionally, due to the model underestimations of OA being primarily due to underestimations in global OA sources and the lack of anthropogenic SOA within GMV4-nitrate is difficult to identify the extent to which comparison annual mean OA concentration profiles against campaign data acquired over varying periods of time (as illustrated in Figure 3.16) can have. Though based on sulfate, nitrate and ammonium model-observations it would be likely to result in an impact model evaluation, with campaigns conducted over greater time frames returning mean concentrations more representative of the annual mean concentrations simulated by GMV4-nitrate.

3.4 Summary and Conclusions

The main way the nitrated-extended version of the TOMCAT-GLOMAP-mode coupled model (GMV4-nitrate) (Benduhn et al., 2016) differs from the TOMCAT-GLOMAP-mode couple model version 6 (GMV6) (Mann et al., 2010) is through the inclusion of the inorganic dissolution module discussed by Benduhn et al. (2016). A dissolution module is a thermodynamic module required for the partitioning of semi-volatile inorganic aerosols (Benduhn et al., 2016).

Dissolution is the combination of condensation and partial dissociation. GMV6 considers the condensation of sulfuric acid, which condenses irreversibly under tropospheric conditions. While GMV4-nitrate considers semi-volatile species (such as water, HNO_3, HCl and NH_3) in addition, which may re-evaporate from the aerosol phase as a function of temperature and chemical composition in the atmosphere (Benduhn et al., 2016).

GMV4-nitrate follows the same gas-phase advected tracer setup as GMV6 (Mann et al., 2010), but with the addition of an NH_3 tracer. In GMV4-nitrate a hybrid solver is utilised to tackle numerical instability and computational expense in order to allow the simulation of semi-volatile inorganic gases in to the aerosol liquid phase (Benduhn et al., 2016).

To calculate the aerosol cloud albedo effect (aCAE), aerosol direct radiative effect (aDRE) and ozone direct radiative effect (O3DRE) methodologies used in previously published literature by Spracklen et al. (2011a), Rap et al. (2013) and Richards et al. (2013) (respectively) are applied.

Evaluation of the gas-phase chemistry within GMV4-nitrate is conducted through the comparison of model simulations without aviation emissions against ozonesonde data compiled by Tilmes et al. (2012). The 41 ozonesonde launch sites considered by Tilmes et al. (2012) span the global domain with ozonesonde profiles obtained between 1987–2011. Evaluation of GMV4-nitrate simulated profiles (using CMIP5 recommended emissions) against those compiled by Tilmes et al., (2012) show that the model can skilfully replicate ozone profiles, while replicating regional and altitudinal variations in ozone concentrations.

The model is able to replicate ozone profiles, demonstrate seasonal variability, with the level of agreement between model and ozonesonde profiles being dependant on location and altitude. Analysis of seasonal profiles across each site yields a global mean bias (NMB) of +4.36%, while analysis of global annual mean profiles returns a mean bias of +5.31% (with a bias of +6.98% when the model-observations comparison from Praha is considered).

Grouping model-observation scatters plots in to latitudinal bands regional trends are seen. Partitioned in to latitudinal bands seasonal profiles indicate that GMV4-nitrate overestimates over the 90°N–60°N and 30°S–60°S bands, underestimates over the 30°N–30°S band and returns both negative and positive biases over the 60°N–30°N and 60°S–90°S bands. Considering annual mean concentrations positive biases are found for the 90°N–60°N, 60°N–30°N and 30°S–60°S latitudinal bands, with negative biases between 30°N–30°s and 60°S–90°S.

Evaluation of model performance over latitudinal and altitudinally resolved regions, shows that the GMV4-nitrate shows greatest global model skill between 400<hPa<700 (representing the lower troposphere) with an annual mean bias of 3.75%. The next best performing level is representative of the upper troposphere (100<hPa<400) with a mean bias of 5.14%, while the surface layer (700<hPa<1000) returns an annual mean bias of 6.11%. Ultimately greatest model skill is seen in the NH and SH mid-latitude regions (60°N–30°N and 30°S–60°S bands) within the lower troposphere and surface layer (400<hPa<700 and 700<hPa<1000 levels).

Evaluation of the aerosol-phase chemistry within GMV4-nitrate was conducted through comparison of sulfate, nitrate, ammonium and organic carbon simulated concentration profiles against the aircraft field campaigns conducted between 2001 to 2008 collated by Heald et al., (2011). GMV4-nitrate is able to replicate observational sulfate profiles while overestimating observational concentrations, but is in fair agreement with GEOS-Chem simulations from Heald et al. (2011). The model is seen to generally underestimate nitrate profiles over the majority of the global domain, but demonstrates skill in replicating European nitrate profiles. The model is capable of replicating observed ammonium profiles over the

majority of field campaigns investigated. Additionally, the model underestimates observed organic aerosol profiles over the majority of the global domain, but is capable of replicating the shape of profiles returned by field campaigns.

Model analysis over each site indicate that GMV4-nitrate returns biases ranging between –71.72% to +190.26% for sulfates, –99.31% to –47.62% for nitrates, –91.24% to +24.67% for ammonium and –94.42% to +215.09% for organic aerosols. Taking all campaigns in to account global mean biases of +8.90% were found for sulfates, –93.89% for nitrates, –59.05% for ammonium and –71.91% for organic aerosols; indicating that globally in comparison to observations used the model overestimates sulfates, while underestimates nitrates, ammonium and organic aerosols.

Discrepancies between simulated aerosol profiles with field campaign observations taken from literature can be partly attributed to differences between the year simulations were conducted for (2000) and the year field campaigns were conducted (2008–2001), changes in global SO_2, NO_X and NH_3 emissions, along with previously assessed disparities in global emissions datasets (Whitburn et al.; Spracklen et al., 2011b). Additionally, discrepancies in model evaluation will arise from the varying timeframes each field campaign was conducted over, the time of year each campaign was conducted over along with the conditions each field campaign was investigating.

Overall GMV4-nitrate is able to skilfully replicate ozone and sulfate profiles with global annual mean biases of +5.31% [seasonal mean = +4.368%] and 38.92% respectively. Global annual mean biases for nitrates, ammonium and organic aerosols indicate model underestimations (–93.89%, –59.05% and –71.91% respectively), while model mean biases for sulfates indicate model overestimations (+8.90%). Nitrate and ammonium underestimations will be due to higher model SO_2 sources, while underestimations in organic aerosol are due to global underestimations anthropogenic SOA emission of ~100 Tg yr^{-1} (Spracklen et al., 2011b).

4 Development of an extended aviation emissions inventory, inclusive of speciated hydrocarbons

4.1 Introduction

Aviation emits a large range of gas-phase and aerosol-phase species, such as: nitrogen oxides (NO_X), carbon monoxide (CO), speciated hydrocarbons (HCs), sulfur dioxide (SO_2), black carbon (BC) and organic carbon (OC).

CMIP5 (5^{th} Climate Model Intercomparison Project) recommended historical aviation emissions currently consist of NO_X and BC mass emissions alone (Lamarque et al., 2009). Recently there have been efforts to include CO, HCs and SO_2 emissions within aviation emissions inventories (Wilkerson et al., 2010; Eyers et al., 2004; Quantify Integrated Project, 2005-2012; Skowron et al., 2013), due to their impact on air quality and climate (Woody et al., 2011; Hoor et al., 2009; Myhre et al., 2011; Olsen et al., 2013b; Barrett et al., 2010; Barrett et al., 2012).

This section extends the CMIP5 recommended aviation emissions inventory (Lamarque et al., 2009) to include additional species. The dataset that will be developed here includes NO_X and BC emissions taken directly from Lamarque et al. (2009), with the extension provided through the creation of emission datasets for aviation-borne CO, speciated HCs, SO_2 and OC. In contrast to existing datasets aviation HC datasets will be speciated out in to formaldehyde (HCHO), ethane (C_2H_6), propane (C_3H_8), methanol (CH_3OH), acetaldehyde (CH_3CHO), and acetone ($(CH_3)_2CO$).

The extended aviation emissions inventory created here (Section 4.3) allows for the impact of aviation emissions on atmospheric concentrations and climate to be assessed in Section 5.4.1. In Section 6.4.2 the impact of standard aviation on premature mortalities due to changes in aviation-induced surface layer $PM_{2.5}$ are assessed, using this extended aviation emissions inventory as a baseline. In Section 5.4 the standard aviation emissions inventory is used as a baseline when investigating the impact of the use of alternative fuels in global commercial aviation. A description of the creation of the alternative fuel based datasets is given in Section 7.3.1.

4.2 Background

4.2.1 5th Coupled Model Intercomparison Project (CMIP5) historical aviation emissions

CMIP5 (5th Coupled Model Intercomparison Project) historical aviation emissions are used as the base for the creation of the new emissions inventory. By using CMIP5 recommended historical aviation emissions for year 2000 as a common base (i.e. NO_X and BC mass emissions), this allows for the atmospheric and climate impacts from the extended inventory developed here to be compared against those resulting from the use of CMIP5 recommended aviation emissions alone. CMIP5 recommended aviation emissions (Lamarque et al., 2010b) are based on the methodology used by Eyers et al. (2004), which allows for the inclusion of a wide-range of phases of flight (inclusive of taxi, take-off and landing) as well as scaling to International Energy Agency (IEA) fuel sales to account for underestimations which can arise from "bottom up" inventories.

CMIP5 aviation emissions of NO_X and BC for the year 2000 are reported at a resolution of 0.5° longitude x 0.5° latitude x 610 m altitude for each month (Lamarque et al., 2010b).

4.2.2 Aviation emission species included in the extended aviation emissions inventory

As previously discussed in Section 2.2 the complete combustion of kerosene should only yield the following products: carbon dioxide (CO_2); water vapour (H_2O_V); nitrogen (N_2); oxygen (O_2); and sulfur dioxide (SO_2) (Lee et al., 2009). In reality incomplete combustion occurs, resulting in the emission of the following chemical species: CO_2; H_2O_V; N_2; O_2; NO_X (nitrogen oxides); CO (carbon monoxide); HCs (hydrocarbons); SO_2; BC (black carbon) (Lee et al., 2009; Lee et al., 2010); and OC (organic carbon) (Bond et al., 2004).

Expansion of CMIP5 recommended aviation emissions will result in the inclusion of aviation-borne CO, HCs, SO_2 and OC. HCs are speciated out in to HCHO (formaldehyde), C_2H_6 (ethane), C_3H_8 (propane), CH_3OH (methanol), CH_3CHO (acetaldehyde), and $(CH_3)_2CO$ (acetone). The overarching aim is to represent aviation emitted species resulting from real-world combustion (as discussed above and in Section 2.2), while following recent efforts to represent the spectrum of aviation-borne emissions released in to the atmosphere (Wilkerson et al., 2010; Eyers et al., 2004; Olsen et al., 2013b; Skowron et al., 2013; Quantify Integrated Project, 2005-2012; Lee et al., 2009).

4.2.3 Understanding the creation of previous kerosene based aviation emissions dataset

Aviation emissions are a product of fuelburn and the emissions indices of each species specific emissions index (EI_x). Emissions indices (EI_x) represent the amount of a species of interest (x) emitted per kg of aviation fuel combusted; represented as EI_x g kg(fuel)$^{-1}$ (Eyers et al., 2004; Olsen et al., 2013b). As the CMIP5 emissions inventory does not provide aviation fuelburn this needs to be calculated first in order to derive the emissions datasets for each of the additional emission species required to extend the aviation CMIP5 emissions inventory. In order to calculate fuelburn an understanding of the relationship between aviation fuelburn and emissions indices for aviation-borne species is required.

Past studies have shown that emissions of CO_2 (Lee et al., 2009; Eyers et al., 2004; Kim et al., 2007; Wilkerson et al., 2010; Owen et al., 2010), water vapour (H_2O) (Eyers et al., 2004; Kim et al., 2007; Wilkerson et al., 2010) and SO_2 (Kim et al., 2007; Wilkerson et al., 2010) can be linearly scaled from fuelburn since they are based on total fuel composition (Wilkerson et al., 2010; Hadaller and Momenthy, 1993; Lee et al., 2010). Whereas emissions of NO_X, CO and HCs are not typically linearly scalable, as these emissions are a function of a multitude of variables: fuelburn, referenced emissions indices at sea level conditions, ambient pressure and temperature, and additionally for NO_X specific humidity (Wilkerson et al., 2010; Lee et al., 2010; DuBois and Paynter, 2006; Baughcum et al., 1996). This relationship is given by the Boeing Fuel Flow Method 2 (BFFM2) which considers variations in combustor efficiency with flight conditions (DuBois and Paynter, 2006; Baughcum et al., 1996; Owen et al., 2010); as represented below (DuBois and Paynter, 2006; Baughcum et al., 1996) (Equation 4.1 – Equation 4.3):

$$EI_{NO_X\_ALT} = EI_{NO_X\_SL}\left(\frac{\delta_{amb}^{1.02}}{\theta_{amb}^{3.3}}\right)^{y} e^{H}$$

Equation 4.1

$$EI_{CO\_ALT} = EI_{CO\_SL}\left(\frac{\theta_{amb}^{3.3}}{\delta_{amb}^{1.02}}\right)^{x}$$

Equation 4.2

$$EI_{HC\_ALT} = EI_{HC\_SL}\left(\frac{\theta_{amb}^{3.3}}{\delta_{amb}^{1.02}}\right)^{x}$$

Equation 4.3

Where θ_{amb} is a function of ambient temperature in degrees Rankine (R) (Equation 4.4), and δ_{amb} a function of ambient pressure in pressure per square inch absolute (Equation 4.5). Rankine (or degrees Rankine) is a linear thermodynamic scale where 0 °R is the same as 0 K, and where 459.67 °R is exactly equal to 0 °F (equivalent to 255.37 K and −17.78 °C).

$$\theta_{amb} = T_{amb}/518.67\ R$$

Equation 4.4

$$\delta_{amb} = P_{amb}/14.696\ psia$$

Equation 4.5

The factor H used in order to calculate the idealised emissions index for NO_X as a function of the specific humidity (SH) of air at altitude; given by Equation 4.6 (DuBois and Paynter, 2006; Baughcum et al., 1996).

$$H = \left(-19 \times (SH-0.00634)\right)$$

Equation 4.6

In past studies both linear (Wilkerson et al., 2010; Lamarque et al., 2010b) and non-linear (Wayson et al., 2009; Eyers et al., 2004) dependencies have been used when investigating the relationship between fuelburn and BC emissions.

Wayson et al. (2009) discuss that BC mass emissions are related to smoke number as per first order approximate (FOA) 3.0; where smoke number acts as a surrogate for plume opacity, which defined by FOA 1.0 acts as a mechanism to estimate non-volatile PM (particulate matter) emissions from aircraft (ICAO, Undated-b; Wayson et al., 2009). This relationship is shown to be non-linear (Wayson et al., 2009), and variable due to variations in engine behaviour with variations in power setting and engine type (Eyers et al., 2004).

NO_X and BC emission datasets within the CMIP5, QUANTIFY Integrated Project and AERO2k emissions inventories were created by Eyers et al. (2004) using the FAST (Future Aviation Scenario Toolkit) model in conjunction with the PIANO (Project Interactive Analysis and Optimisation) aircraft performance model (Eyers et al., 2004; Olsen et al., 2013b; Lamarque et al., 2010b).

The FAST model employs a two-step process to calculate aviation-emitted soot concentrations. The first step assesses emitted soot concentrations at sea level static conditions (SLS) (Eyers et al., 2004), by considering the turbine inlet temperature (T_3) based on the Brayton/Joule cycle (Eyers et al., 2004; Eastop and McConkey, 1993). The Brayton/Joule cycle is thermodynamic cycle that ideally considers a constant pressure open loop system, e.g. that within a jet engine or gas turbine (Eastop and McConkey, 1993). The next step uses the BC emissions index for SLS conditions as a base to evaluate BC emissions indices for other conditions (as shown in Equation 4.7).

$$C_{soot} = C_{soot_{SLS}} \cdot \left(\frac{\Phi}{\Phi_{SLS}}\right)^{2.5} \cdot \left(\frac{P_3}{P_{3_{SLS}}}\right)^{1.35} \cdot \left(\frac{e^{(-20000/T_3)}}{e^{(-20000/T_{3_{SLS}})}}\right)$$

Equation 4.7

Where P_3 = Combustor inlet pressure

T_3 = Flame temperature

Φ = Equivalence ratio.

Due to the complicated relationship between combustion, ambient pressures and temperatures in relation to the BC production at sea level static conditions some recent aviation emissions inventories have produced BC emissions dataset assuming a linear relationship between aviation fuelburn and BC emissions indices (Wilkerson et al., 2010; Lamarque et al., 2010b).

In the 2004 version of the Aviation Environmental Design Tool (AEDT) developed by the Federal Aviation Administration (FAA) with the support of the Volpe National Transportation System Centre used a BC emissions index of 0.2 g kg(fuel)$^{-1}$, representing the take-off and climb phases of the flight cycle. This was updated to an emissions index of 0.035 g kg(fuel)$^{-1}$ for their 2006 version of the AEDT emissions inventory in order to better represent the cruise phase of flight, and associated emissions (Wilkerson et al., 2010).

Lamarque et al. (2010b) discuss the production of CMIP5's aviation BC emissions datasets from fuelburn estimated from FAST and PIANO; where fuelburn is assigned to routes using great circle assumptions and a BC emissions index of 0.025 g kg(fuel)$^{-1}$ from Eyers et al. (2004).

Akin to BC mass emissions (and associated emissions indices), BC particle number emissions are dependent on engine power settings in addition to sampling location (Wey et al., 2007). Despite this AERO2k have assessed an aviation-borne particle number emissions index of

2.58×10^{14} particles kg(fuel)$^{-1}$ (Eyers et al., 2004). In tandem with BC particle number emission indices, assessment of the associated geometric mean diameter (GMD) and geometric standard deviation (σ) particle size distributions can be evaluated for BC and OC. This methodology allows for a range of particle sizes to be considered. This is of great importance when aiming to understand aviation-induced impacts on climate as well as human health (Eyers et al., 2004).

Aviation-borne OC emissions are found to be related to the emission of aviation-borne BC emissions, and dependant on the combustion process (Bond et al., 2004). Aviation-borne carbonaceous particulate emissions are found to be largely consisting of black carbon, with a ratio between BC and OC emissions of 4:1 (Bond et al., 2004). As such the OC emissions index to be used in this study will be a quarter of the BC emissions index used by Eyers et al. (2004), i.e. 0.00625 g kg(fuel)$^{-1}$.

4.3 Methodology for extending the CMIP5 aviation emissions inventory for year 2000 to include additional species

As discussed in Section 4.2.1 the aviation-emission datasets created here are based on the CMIP5 historical aviation emissions inventory for 2000 (Lamarque et al., 2010b). Here the creation of emissions datasets for CO, speciated HCs, SO_2, OC and BC number is discussed.

This section is split up to discuss the derivation of aviation fuelburn, aviation emissions indices used and how they are obtained or derived, presentation of the new aviation emissions inventory and, calculation of the geometric mean diameter (GMD) which is used to enable GMV4-nitrate to enter aviation BC and OC emissions in to the relevant size mode.

4.3.1 Calculation of aviation fuelburn

Aviation fuelburn (fuelburn) is calculated using the CMIP5 BC emissions dataset provided by IIASA (International Institute for Applied Systems Analysis), compiled by Lamarque et al. (2009) using the emissions index for BC (EI_{BC}) derived by Eyers et al. (2004). This is achieved using Equation 4.8:

$$\text{fuelburn}_{i,j,k} = \frac{\text{BC}_{i,j,k}}{\text{EI}_{\text{BC}}} \cdot 1000$$

Equation 4.8

Where i,j,k = denote grid position in the lon, lat and vertical position of array

EI_{BC} = Black carbon emissions index (0.025 g kg(fuel)$^{-1}$)

1000 = factor to convert EI from g kg(fuel)$^{-1}$ to kg kg(fuel)$^{-1}$

An annual aviation fuelburn of 200.97 Tg(fuel) is calculated for year 2000, which is within the mid-range of estimates from existing emissions inventories [176–214.1 Tg(fuel)] (Eyers et al., 2004; Lamarque et al., 2010b; Quantify Integrated Project, 2005-2012; Wilkerson et al., 2010; Lee et al., 2005).

Figure 4.1: Aviation annual fuelburn distributions: (a) total collapsed horizontal spatial, and (b) zonal distribution.

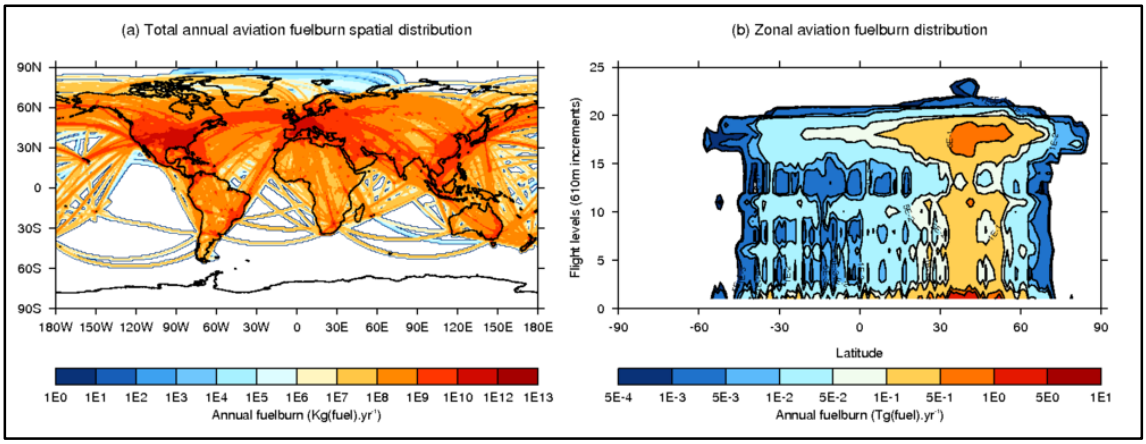

Figure 4.1(a) shows the spatial distribution of aviation fuelburn. The majority of fuelburn occurs in the Northern Hemisphere (NH). In 2000 92.5% [185.86 Tg(fuel)] of aviation fuelburn occurs in the NH, while 7.5% [15.12 Tg(fuel)] occurs in the SH. Fuelburn is greatest in the main flight corridors, i.e. over the Atlantic Ocean connecting Europe to the U.S. Eastern seaboard and over the Pacific Ocean between Asia and the U.S. Western seaboard. From Figure 4.1(b) it is seen that attitudinally the majority of aviation emissions are released between the cruise region of flight (~8–12 km) and near ground level over the NH, primarily between 15°N–70°N. Peaks in fuelburn at the surface will be due to the inclusion of phases of the aircraft flight cycle where engine power settings will be lower (e.g. taxi, idle and ground idle), resulting in reduced combustor efficiencies (Knighton et al., 2007; Airbus, 2008), along with associated ground operations which consume fuel and the occurrence of delays which require aircraft re-routing the stacking of aircraft (Lamarque et al., 2010b).

Figure 4.2(a) compares fuelburn calculated from CMIP5 against that reported by the Quantify Integrated Project (2005-2012). Differences between the emissions inventory fuelburns range between 0.70 Tg(fuel) [4.03%] in March to 2.14 Tg(fuel) [13.25%] February; when comparing the QUANTIFY Integrated Project to CMIP5 derived fuelburn [QUANTIFY–CMIP5]. Both the

QUANTIFY Integrated Project and CMIP5 historical aviation emissions datasets were created using the FAST model in conjunction with the PIANO performance model (Olsen et al., 2013b). These differences in levels of fuelburn between the CMIP5 and QUANTIFY Integrated Project inventories can be attributed to fuelburn within the QUANTIFY Integrated Project inventory being scaled up to IEA (International Energy Agency) aviation fuel bunker sales (Owen et al., 2010). Scaling to fuel bunker sales allows for delays, holding patterns and the re-routing of aircraft to be considered as the methodologies used to compile aircraft routes used to derived aviation inventories consider idealised aircraft operations, and risk underestimating aviation fuelburn and associated emissions resulting from real world aircraft operations (Owen et al., 2010). Additionally monthly aviation fuelburn correlates with monthly flight traffic for year 2000 (Eyers et al., 2004). As such monthly fuelburn follows the same trends in flight demand, i.e. increases in flight demand over the Summer months and Christmas, and decreases over the Winter and Spring.

Figure 4.2: Monthly aviation fuelburn for the year 2000: (a) monthly aviation fuelburn derived from CMIP5 data and the QUANTIFY Integrated Project, and (b) monthly Northern and Southern Hemisphere fractional contributions to fuelburn.

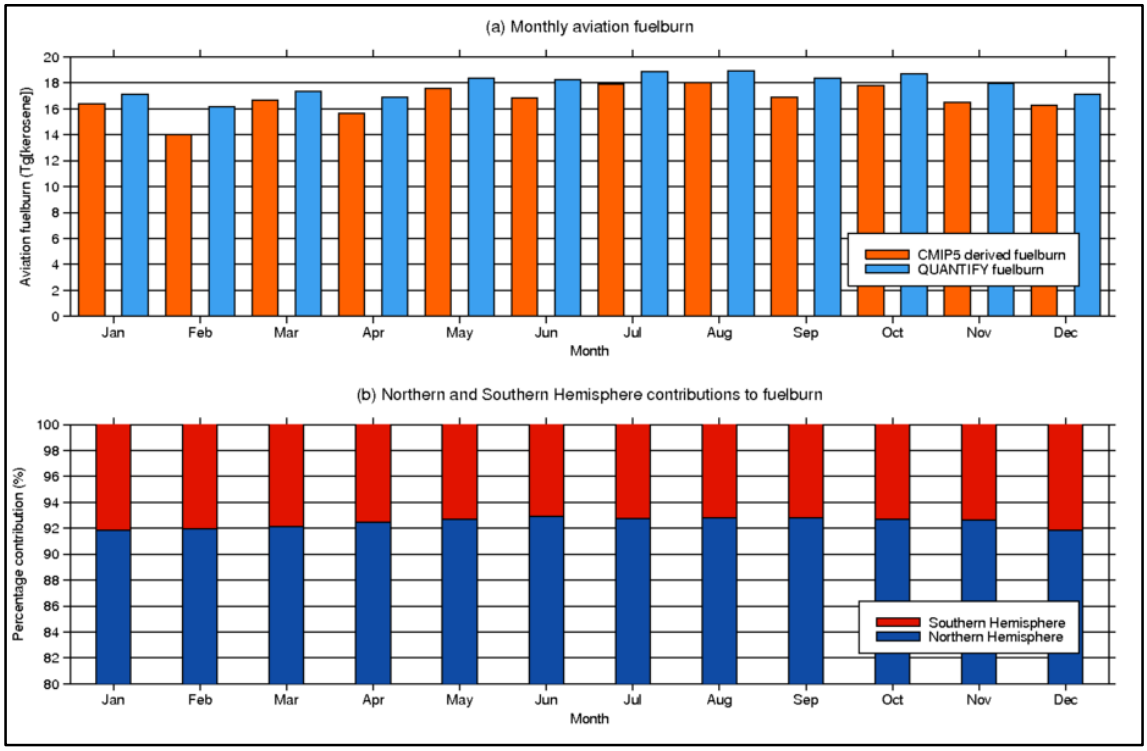

Figure 4.2 (b) shows that over the course of the year the majority of aviation fuelburn occurs over the NH, with monthly NH contributions to fuelburn ranging between 91.8–92.9% accompanied by Southern Hemisphere (SH) contributions ranging between 7.1–8.2%. This indicates that the majority of the atmospheric, climatic, air quality and human impacts of aviation are expected to occur in the NH.

4.3.2 Aviation emission indices and calculation of emission species specific datasets

Monthly resolved aviation emissions datasets are created using monthly resolved aviation fuelburn data ($fuelburn_{i,j,k}$) in conjunction with emissions indices for the aviation-borne species of interest (Equation 4.9). Emissions indexes (EI_x) represent the amount of specie of interest (x) emitted per kg of aviation fuel combusted.

$$emissions_{x\,i,j,k} = \frac{fuelburn_{i,j,k} \cdot EI_x}{1000}$$

Equation 4.9

Where i,j,k = denote grid position in the lon, lat and vertical position of array

EI_x = emissions index for species of interest (x) in g kg(fuel)$^{-1}$

fuelburn = grid resolved fuelburn

For species which are typically not linearly-scalable with fuelburn such as CO, HCs, BC particle number, and OC mass without additional information on ambient conditions, sea-level static conditions, and flame temperature (i.e. temperature of the flame within the combustor) in tandem with assumptions on the make-up of the global aviation fleet these species are treated as linearly scalable (Wilkerson et al., 2010; Eyers et al., 2004; Bond et al., 2004; Hopke, 1985).

For speciated hydrocarbons emissions indices a combination of published emissions indices (in the cases of formaldehyde, methanol, acetone and acetaldehyde) (Knighton et al., 2007; Spicer et al., 1994) and published experimental data (in the cases of ethane and propane) (Anderson et al., 2006) were used. These were used in conjunction with parameters for engine power settings (percentage) obtained from the Airbus Flight Crew Training Manual (Airbus FCTM) for the A318/A319/A320/A321 (Airbus, 2008). The Airbus FCTM for the Airbus A318/A319/A320/A321 range helps highlight a minimum engine power settings for phases of flight above idle of 40%. This assumption is consistent with engine power requirements for the cruise phase of flight (Airbus, 2008) and assumes that majority of emissions occur during cruise.

Anderson et al. (2006)'s experimental work on the EXCAVATE study reported measurements for 33 HCs, taken at four differing power settings (4-7%, 26%, 47% and 61%) relating to four phases of engine operation and flight (idle, approach, low cruise and high cruise), along with three background samples taken throughout the course of the experiment. As such when

deriving emissions indices using experimental data from Anderson et al. (2006) emissions data for power settings above 40% are used.

For a normal global aviation fleet operating on 100% kerosene an emissions index for carbon monoxide (EI_{CO}) of 3.61 g kg(fuel)$^{-1}$ is employed (Table 4.1), as used by the FAA's AEDT 2006 (Wilkerson et al., 2010).

An EI_{CO} of 3.61 g kg(fuel)$^{-1}$ is substituted in to Equation 4.9 for EI_x in order to calculate the CO emissions dataset. The EI_{CO} used here is at the higher end of emissions indices from current literature [2–3.61 g kg(fuel)$^{-1}$], but from one for the more recent sources (Lee et al., 2010; Eyers et al., 2004; Wilkerson et al., 2010).

Emissions indices for speciated hydrocarbons were taken from a range of sources. An emissions index for formaldehyde (EI_{HCHO}) of 1.24 g kg(fuel)$^{-1}$ was taken (Table 4.1) from work by Spicer et al. (1994). This value falls in agreement with emissions indices derived by Knighton et al. (2007) during work on the NASA sponsored APEX project (Aircraft Particle Emission Experiment) conducted at NASA's Dryden Flight Research Centre over April 2004. This project was conducted using NASA's DC-8 with CFM56-2-C1 engines. This emissions index was obtained at a power setting of 4%, relating to "ground idle" conditions (Knighton et al., 2007).

Using Equation 4.9, substituting EI_{HCHO} (where EI_{HCHO} = 1.24 g kg(fuel)$^{-1}$) for EI_x, the emissions dataset for HCHO is calculated.

Emissions indices for methanol (EI_{CH_3OH} = 0.22 g kg(fuel)$^{-1}$), acetone ($EI_{(CH_3)_2CO}$ = 0.18 g kg(fuel)$^{-1}$) and acetaldehyde (EI_{CH_3CHO} = 0.33 g kg(fuel)$^{-1}$) are taken from the NASA APEX study based on the relationship between formaldehyde and these species for engine power settings of 4% and 7% (Knighton et al., 2007) (Table 4.1). These emissions indices fed in to Equation 4.9 in order to create aviation emissions datasets for methanol, acetone and acetaldehyde; through substitution of for EI_{CH_3OH}, $EI_{(CH_3)_2CO}$ and EI_{CH_3CHO} (in turn) for EI_x.

Emissions indices for ethane ($EI_{C_2H_6}$) and propane ($EI_{C_3H_8}$) were calculated using experimental data from the NASA EXCAVATE study (EXperiment to Characterize Aircraft Volatile Aerosol and Trace-species Emissions), conducted at NASA's Langley Research Centre over January 2002 using a B757 with Rolls-Royce RB211-535E4 engines (Anderson et al., 2006).

Emission indices for ethane ($EI_{C_2H_6}$) and propane ($EI_{C_3H_8}$) are calculated using published experimental data from Anderson et al., (2006) in conjunction with a general HC emissions index from the AEDT emissions inventory (EI_{HC} = 0.52 g kg(fuel)$^{-1}$) (Wilkerson et al., 2010),

assuming engine power settings above 40% in line with FCTM for the Airbus A318/A319/A320/A321 range (Airbus, 2008). These emissions indices are calculated using the following process: conversion of experimental data (from literature) from ppbv to mg m^{-3}; conversion of background concentrations from ppbv to mg m^{-3}; calculation of concentration changes due to aviation; calculation of mass fraction of each aviation-borne NMHC specie, and finally; derivation of ethane and propane emissions indices.

Firstly, measurements $[X_{xpt}]$ in ppbv for each NMHC of the aviation emitted species measureable via the EXCAVATE project are converted to $mg.m^{-3}$ as per Equation 4.10:

$$[X_{xpt}]_{mg\ m^{-3}} = \left(\sum_{n=1}^{expts} [X_{xpt}]_{ppbv} \Big/ expts \right) \cdot \frac{MW_X}{24.45 \cdot 1000}$$

Equation 4.10

Where $[X_{xpt}]_{mg\ m^{-3}}$ = measured species concentration in mg m^{-3}

$[X_{xpt}]_{ppbv}$ = measured species concentration in ppbv

expts = number of experiments providing measurements

MW_X = molecular weight of species X (g mol^{-1})

24.45 = volume of air at standard atmospheric pressure (m^3)

1000 = factor to convert from micrograms to milligrams

Next the same process is used for the background readings (Equation 4.11). Background readings are taken to account for ambient concentrations of measured species, thus allowing for the calculation of increases in species concentrations only attributable to aircraft engine operations.

$$[X_{bk}]_{mg\ m^{-3}} = \left(\sum_{n=1}^{samples} [X_{bk}]_{ppbv} \Big/ samp\,les \right) \cdot \frac{MW_X}{24.45 \cdot 1000}$$

Equation 4.11

Where $[X_{bk}]_{mg\ m^{-3}}$ = background species concentration in mg m^{-3}

$[X_{bk}]_{ppbv}$ = background species concentration in ppbv

samples = number of background samples

Once both the mass based concentrations for engine measurements and background measurements are calculated the change in concentration due to engine operation are ($[X_{avi}]_{mg\ m^{-3}}$) estimated. This is calculated as follows (Equation 4.12):

$$[X_{avi}]_{mg\ m^{-3}} = [X_{xpt}]_{mg\ m^{-3}} - [X_{bk}]_{mg\ m^{-3}}$$

Equation 4.12

This then allows for the mass fraction of each aviation-borne NHMC (X_{mass_frac}) to be calculated from the mass concentration of the emitted HC species of interest and the total mass concentration of all emitted NMHC species (Equation 4.13):

$$X_{mass\_frac} = \left([X_{avi}]_{mg\ m^{-3}} \Big/ \sum_{n=1}^{NMHC\_species} [X_{avi}]_{mg\ m^{-3}} \right)$$

Equation 4.13

Finally emissions indices for ethane ($EI_{C_2H_6}$) and propane ($EI_{C_3H_8}$) are derived using their mass fractions and general emissions index for HCs from the FAA's AEDT emissions inventory of 0.52 g kg^{-1} (EI_{HC_AEDT}) as per Equation 4.14 and Equation 4.15 (presented in Table 4.1):

$$EI_{C_2H_6} = C_2H_{6_{mass\_frac}} \cdot EI_{HC\_AEDT}$$

Equation 4.14

$$EI_{C_3H_8} = C_3H_{8_{mass\_frac}} \cdot EI_{HC\_AEDT}$$

Equation 4.15

Following the process outlined above the emissions indices for ethane ($EI_{C_2H_6}$) and propane ($EI_{C_3H_8}$) were calculated as 0.0394 g $kg(fuel)^{-1}$ and 0.03 g $kg(fuel)^{-1}$, respectively. Using the ethane and propane emissions indices derived here aviation emissions datasets for ethane and propane are calculated using Equation 4.9, substituting EI_x for $EI_{C_2H_6}$ (ethane) and $EI_{C_3H_8}$ (propane) respectively. For sulfur dioxide an emission index (EI_{SO_2}) of 1.176 g $kg(fuel)^{-1}$ is used (Wilkerson et al., 2010) (Table 4.1), which makes the assumption that global civil aviation jet fuel has an average sulfur content of 600 ppm (Barrett et al., 2012). Again, as with the case of carbon monoxide this emissions index is at the higher end of emissions indices from previous

studies (Lee et al., 2010). The sulfur dioxide emissions dataset is calculated using Equation 4.9, while substituting EI_{SO_2} for EI_x.

As with the BC mass emissions index (EI_{BC_mass}), the emissions index for BC particle number ($EI_{BC\_particle}$) of $2.58x10^{14}$ particles kg(fuel)$^{-1}$ is taken from Eyers et al. (2004). Feeding $EI_{BC\_particle}$ in to Equation 4.9 allows for calculation of an emissions dataset for aviation-borne particle emissions. For OC a relationship between BC and OC of 4:1 is taken from Bond et al. (2004) and Hopke (1985), an emissions index (EI_{OC}) of 0.00625 g kg(fuel)$^{-1}$ is derived (Table 4.1). As with all previous aviation-borne emissions species EI_{OC} is used within Equation 4.9 to calculate the aviation emissions dataset for OC.

From the emissions indices derived or obtained from literature (Table 4.1) a monthly resolved emissions inventory covering a 3-D domain is created. Table 4.1 refers to the studies which have directly provided emissions indices or published experimental work which provided the data processed to calculate emissions indices.

Table 4.1: Emissions indices used to derive aviation emissions inventory for year 2000.

Emissions species		Power setting / flight cycle	Emissions index EI_x (g kg^{-1})	Reference/Study
Nitrogen oxides	NO_X	Cycle average	13.2	Eyers et al. (2004)
Carbon monoxide	CO	Cycle Average	3.61	Wilkerson et al. (2010)
Formaldehyde	HCHO	LTO cycle	1.24	Knighton et al. (2007); Spicer et al. (1994)
Ethane	C_2H_6	47 and 61%	0.0394	Anderson et al. (2006)
Propane	C_3H_8	47 and 61%	0.03	Anderson et al. (2006)
Methanol	CH_3OH	LTO cycle	0.22	Knighton et al. (2007)
Acetone	$(CH_3)_2CO$	LTO cycle	0.18	Knighton et al. (2007)
Acetaldehyde	CH_3CHO	LTO cycle	0.33	Knighton et al. (2007)
Sulfur dioxide	SO_2	n/a	1.176	Wilkerson et al. (2010)
Black carbon mass	C	Cycle average	0.025	Eyers et al. (2004)
Black carbon part	n/a	Cycle average	$2.58x10^{14}$	Eyers et al. (2004)
Organic carbon	C	Cycle average	0.00625	Bond et al. (2004); Hopke (1985)

4.3.3 New aviation emissions inventory: CMIP5-extended

Using the emissions indices presented in Table 4.1 in conjunction with Equation 4.9 a new aviation emissions inventory (CMIP5-extended) was created for year 2000; an emissions inventory which considers aviation-borne NO_X, CO, speciated HCs, SO_2, BC, OC and particle number emissions.

Figure 4.3 presents the magnitude of the monthly totals in aviation emitted species, reflecting the monthly trend in fuelburn (Figure 4.2) which is a product of monthly flight demand. Monthly resolved aviation emissions allow for model simulations to have the capability to investigate seasonal variations in simulated atmospheric changes.

Figure 4.3 when considered alongside Figure 4.2, further highlights the relationship between monthly resolved fuelburn and emissions release, i.e. magnitude of aviation emissions released are a product of aviation fuelburn and emissions, as per Equation 4.9.

Table 4.2: Total annual aviation emissions for year 2000, emissions indices and global species emissions range from literature.

Species	Global emissions for year 2000 – this study (Tg of species)	Emissions index (g kg^{-1} of fuel)	Range of annual global emissions from previous studies (Tg of species)
NO_X	2.786	13.89[a]	1.61–3.286[a,h,i,j,k,l,m]
CO	0.724	3.61[b]	0.33–1.15[a,h,i,j]
HCHO	0.249	1.24[c,d]	n/a
C_2H_6	0.007899	0.0394[e]	n/a
C_3H_8	0.006014	0.03[e]	n/a
CH_3OH	0.044	0.22[d]	n/a
$(CH_3)_2CO$	0.036	0.18[d]	n/a
CH_3CHO	0.066	0.33[d]	n/a
SO_2	0.236	1.1760[b]	0.182–0.222[a,h,i,j]
BC	0.005012	0.0250[a]	0.0039–0.0068[a,b,h,i,j,k]
OC	0.001253	0.00625[f,g]	0.003[i]

[a]Eyers et al. (2004), [b]Wilkerson et al. (2010), [c]Spicer et al. (1994), [d]Knighton et al. (2007),[e]Anderson et al. (2006), [f]Bond et al. (2004), [g]Hopke (1985), [h]Olsen et al. (2013b), [i]Unger (2011), [j]Lee et al. (2010), [k]Lamarque et al. (2010b), [l]Quantify Integrated Project (2005-2012), [m]Skowron et al. (2013).

Figure 4.3: Monthly mean aviation emissions for year 2000 for (a) nitrogen oxides (NO_X), (b) carbon monoxide (CO), (c) formaldehyde (HCHO), (d) ethane (C_2H_6), (e) propane (C_3H_8), (f) acetone ($(CH_3)_2CO$), (g) acetaldehyde (CH_3CHO), (h) methanol (C CH_3OH), (i) sulfur dioxide (SO_2), (j) black carbon mass (BC), (k) BC particle number, and (l) organic carbon (OC).

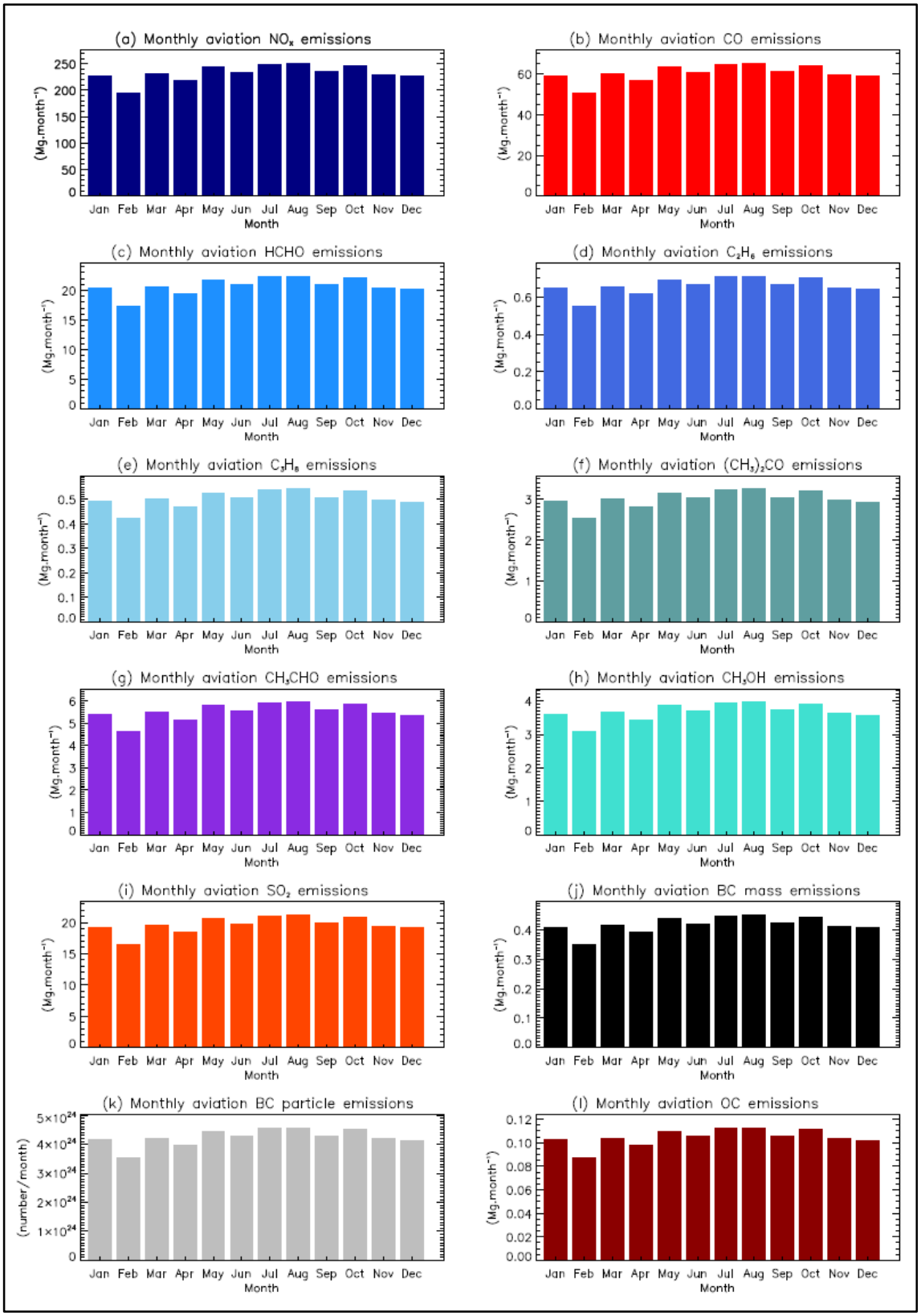

Table 4.2 compares aviation emissions calculated in this work against emissions calculated by previous studies. The emissions of NO_X and BC calculated here fall within the range of previous studies (Eyers et al., 2004; Olsen et al., 2013b; Unger, 2011; Lee et al., 2010; Quantify Integrated Project, 2005-2012; Lamarque et al., 2010b; Skowron et al., 2013). In contrast, CO, SO_2 and OC emissions are above current the range of previous estimates (Eyers et al., 2004; Wilkerson et al., 2010; Olsen et al., 2013b; Unger, 2011; Lee et al., 2010; Lamarque et al., 2010b).

Figure 4.4 provides a comparison between the emissions inventory created here (CMIP5-extended) and the AERO2k, the QUANTIFY Integrated Project and FAA's AEDT inventories, i.e. through presenting current emission inventory values relative to the new emissions inventory created here (CMIP5-extended).

From this it is seen that despite quite similar levels of fuelburn (87.6–107% of fuelburn from inventory represented in Figure 4.4 and Table 4.2 relative to CMIP5-extended) (Eyers et al., 2004; Lamarque et al., 2010b; Quantify Integrated Project, 2005-2012; Wilkerson et al., 2010; Lee et al., 2005), there can be quite a difference in annual emissions of CO [93.8%–159% for CO] (Eyers et al., 2004; Wilkerson et al., 2010), BC mass [77.8–136% for BC] (Eyers et al., 2004; Wilkerson et al., 2010; Quantify Integrated Project, 2005-2012) and OC [239% for OC] (Wilkerson et al., 2010); due to the range of emissions indices used in the different aviation emissions inventories (Eyers et al., 2004; Wilkerson et al., 2010; Olsen et al., 2013b; Lee et al., 2010; Unger, 2011; Lamarque et al., 2010b; Skowron et al., 2013).

Figure 4.4: Comparison of the extended CMIP5 emissions inventory with the AERO2k, QUANTIFY and FAA's AEDT emissions inventories. The CMIP5-extended data is used as a benchmark for comparison.

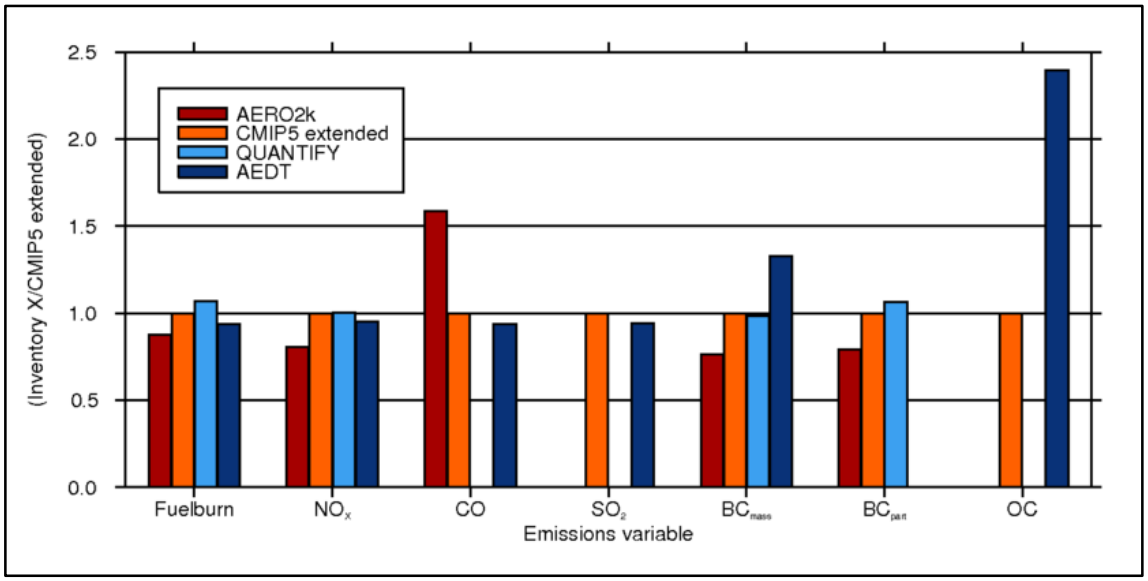

4.3.4 Calculation of geometric mean diameter (GMD) for carbonaceous emissions

Finally the geometric mean diameter (GMD) for BC and OC particles is calculated. The GMD is required in order to enter BC and OC emissions in to the relevant size-resolved mode in the global aerosol model (depicted Table 3.1 in Section 3.2.3.1).

As the emissions indices for BC mass (EI_{BC_mass}), OC mass (EI_{OC_mass}) and particle number ($EI_{BC\_particle}$) are treated as linearly scalable with fuelburn, a relationship between carbonaceous aerosol mass emitted (BC and OC) and particle number of 8.26×10^{18} particles kg^{-1} emitted is obtained. This allows the GMD (D_g) to be calculated from the relationship of volume of carbonaceous aerosols released and total number of particles emitted, as per Equation 4.16.

$$D_g = \sqrt[3]{\frac{BCOC_{volume}}{\left(\frac{\pi}{6}\right) \cdot BCOC_{part} \cdot e^{\left(4.5 \times \left(\log(\sigma)\right)^2\right)}}}$$

Equation 4.16

Where D_g = geometric mean diameter (nm)

$BCOC_{volume}$ = total volume of BC and OC particle (nm^3)

$BCOC_{part}$ = total number of BCOC particles (number)

σ = standard deviation

A standard deviation of 1.59 is used (Stier et al., 2005). $BCOC_{part}$ is directly calculated through annual fuelburn and the emission index for total carbonaceous particles emitted ($EI_{BC\_particle}$), while the total volume of BC and OC particles is calculated using Equation 4.17:

$$BCOC_{volume} = 1 \times 10^{27} \cdot \left(\left(\frac{BC_{mass}}{\rho_{BC}}\right) + \left(\frac{OC_{mass}}{\rho_{OC}}\right)\right)$$

Equation 4.17

Where BC_{mass} = total mass of aviation BC emitted (kg)

OC_{mass} = total mass of aviation OC emitted (kg)

ρ_{BC} = density of BC ($kg\ m^{-3}$)

ρ_{OC} = density of OC ($kg\ m^{-3}$)

Together Equation 3.1 and Equation 4.17 allowed for the derivation of the GMD using Equation 4.18:

$$D_g = \sqrt[3]{\frac{1\times10^{27} \cdot \left(\left(\frac{BC_{mass}}{\rho_{BC}}\right) + \left(\frac{OC_{mass}}{\rho_{OC}}\right)\right)}{\left(\frac{\pi}{6}\right) \cdot BCOC_{part} \cdot e^{\left(4.5 \times \left(\log(\sigma)\right)^2\right)}}}$$

Equation 4.18

Equation 4.18 in conjunction with a total annual BC and OC mass [6.26 Mg a^{-1}], the total number of carbonaceous particles emitted [$5.17x10^{25}$] and σ [1.59], a GMD (D_g) of 50.46 nm for standard kerosene based aviation emissions was calculated. This diameter matches the Aitken mode within the TOMCAT-GLOMAP-mode model (Mann et al., 2010).

4.4 Summary and Conclusions

The majority of previous aviation emission inventories only include a subset of the species emitted by aviation (Eyers et al., 2004; Quantify Integrated Project, 2005-2012; Skowron et al., 2013; Lamarque et al., 2010a; Wilkerson et al., 2010). The CMIP5 recommended historical aviation emissions inventory only include aviation NO_X and BC mass emissions (Lamarque et al., 2010a), providing the potential impacts on aviation-induced ozone and aerosols to be omitted and their associated impacts on climate, air quality and human health (Lee et al., 2010; Unger et al., 2013; Barrett et al., 2012; Yim et al., 2015). This section outlined the methodology to extend the CMIP5 emissions inventory to include carbon monoxide, speciated hydrocarbons (formaldehyde, propane, ethane, methanol, acetaldehyde and acetone), sulfur dioxide, organic carbon and the number of carbonaceous particles (i.e. particle number). Along with calculating the geometric mean diameter of carbonaceous particles emitted, as required by GMV4-nitrate to enter BC and OC aerosol emissions in to the correct size mode.

Total global fuelburn from aviation for year 2000 was calculated to be 200.97 Tg(fuel). When considering global flight paths it is evaluated that 92.48% of annual fuelburn occurs in the Northern Hemisphere, with the remaining 7.52% occurring in the Southern Hemisphere. Monthly variations in fuelburn are observed in line with previous work (Quantify Integrated Project, 2005-2012), with a minimum of 14.51 Tg fuelburn in February and a maxima of 18.03 Tg fuelburn in August in line with annual variations in global flight demand (Eyers et al., 2004).

Emissions indices were taken directly from literature or produced using published experimental data (Anderson et al., 2006). Emission indices were combined with fuelburn to calculate year 2000 aviation emissions for the following species: 2.786 Tg a^{-1} NO_X; 0.724 Tg a^{-1} CO; speciated HCs totalling 0.409 Tg a^{-1}; 0.236 Tg a^{-1} SO_2; 5.012 Mg a^{-1} BC; and 1.25 Mg a^{-1} OC. Aviation NO_X and BC annual emissions calculated for the new emissions inventory developed here fell within the ranges provided by literature, while CO, SO_2 and OC annual emission rates fell outside the ranges from literature. Additionally the annual emission rates of speciated hydrocarbons could not be compared with existing literature as these specific values are not currently available (Table 4.2 in Section 4.3).

In comparison to other recent aviation emissions inventories (AEDT, QUANTIFY and AERO2k) differences were observed. These differences are attributed to differences in species-specific emissions indices and fuelburn within each emissions inventory.

Through understanding the relationship between emissions of BC and OC mass and the total number of carbonaceous particle emitted by aviation, a mean geometric diameter (D_g) of 50.46 nm was calculated. Using a standard deviation of 1.59 nm (Stier et al., 2005) a log-normal distribution of size distribution of total carbonaceous particles emitted can be derived, with a D_g of 50.46 nm, indicating that particles with the mean geometric diameter derived here would be introduced in to the model within the Aitken mode.

5 Investigating the impact of an extended aviation emissions inventory on the atmosphere and climate

5.1 Introduction

Model simulations conducted for CMIP5 (5th Coupled Model Intercomparison Project) aim to better evaluate the role of atmospheric chemistry in driving climate change as part of the Atmospheric Chemistry and Climate Model Intercomparison Project (ACCMIP), results of which feed in to the Integrated Panel on Climate Change's (IPCC) 5th Assessment Report (AR5) (Lamarque et al., 2013b). Recommended historical emissions for aviation used by the CMIP5 models, consist only of aviation NO_X (nitrogen oxides) and BC (black carbon) mass emissions (Lamarque et al., 2010b). Recent aviation emissions inventories have made efforts to include aviation-borne CO (carbon monoxide), HCs (speciated hydrocarbons), SO_2 (sulfur dioxide) and OC (organic carbon) emissions (Wilkerson et al., 2010; Eyers et al., 2004; Quantify Integrated Project, 2005-2012).

Through use of the CMIP5-extended aviation emissions inventory created in Section 4.3 (which considers NO_X, CO, HCs, SO_2, BC and OC emissions), this Chapter investigates the atmospheric and climatic impacts of aviation as modelled using the nitrate-extended version of the TOMCAT-GLOMAP-mode coupled model (GMV4-nitrate) (Section 5.4.1). As previously discussed in Section 1.1.1 with future projected decreases in global anthropogenic SO_2 emissions in tandem with projected increases in ammonia (NH_3) nitrate aerosols have the potential to become the more dominant forcing aerosol component, as such the use of a chemistry-aerosol model that considers the formation of nitrate aerosols is of importance, hence the use of the nitrate-extended version of the TOMCAT-GLOMAP-mode coupled model.

Simulated climatic impacts using the CMIP5-extended emissions inventory are compared to those simulated using standard CMIP5 recommended emissions in order to investigate the atmospheric and climatic responses that could be missed through the use of an aviation emissions inventory with fewer emitted species (Section 5.4.2). In Section 5.4.3 sensitivity studies consider the impacts of the inclusion of CO, speciated HCs and SO_2 emissions in turn; thus investigating the relative impacts of the inclusion of these additional aviation emissions species in relation to the CMIP5 recommended aviation emissions inventory. Finally, simulated gas- and aerosol-phase simulated atmospheric concentrations driven by the use of the CMIP5-extended emissions inventory are re-evaluated against observational data (Section 5.5).

5.2 Background

5.2.1 Chemical composition of jet fuel

Through understanding the chemical composition of kerosene, it possible to gain an understanding of why comprehensive aviation emission inventories are required when investigating the atmospheric and climatic impact of civil aviation.

Typically aviation kerosene (Jet A-1/Jet A) is a multicomponent fuel with a carbon chain length of C_8–C_{16} Blakey et al. (2011), with the most common type (Jet A-1) having a chemical formula of $C_{12}H_{23}$ (Lee et al., 2010).

The main component make up of Jet A-1 is predominately of paraffin origin (with straight chained, isoparaffins and cycloparaffins or naphthenes being present), accounting for 70–85% of its content. The split between these paraffins is variable based on the different type of raw crude oil used. Aromatics contribute to up to 25% of the fuel blend, containing unsaturated cyclic hydrocarbons (Blakey et al., 2011).The high H:C ratio for n- and iso-paraffin gives a high heat to weight ratio and results in a clean burn. The presence of cycloparaffins reduces the H:C ratio, but their presence helps reduce the fuel freezing point (Blakey et al., 2011).

Additionally, jet fuel also contains trace amounts of sulfur, nitrogen and oxygen containing hydrocarbon species, originating from the raw crude oil feedstock used. Sulfur is present in the form of mercaptans, sulfides, disulfides, thiophenes and other sulfur containing compounds (Blakey et al., 2011). Ultimately the current total sulfur content of Jet A/Jet A-1 fuel is limited to 3000 ppm by ASTM specification ASTM D1655-09a (Blakey et al., 2011; ASTM International, 2012b).

5.2.2 Aviation emitted species

This section summarises aviation emitted species and then briefly discusses the atmospheric and climatic impacts that they have – discussed in greater detail in Section 2.2 and Section 2.4.

Figure 2.6 from Section 2.2 highlights the vast range of aviation emissions species that are release in reality, in relation to the idealised products of combustion. This range in real-world aviation emissions is a product of the different phases of flight aircraft undergo which relates to the engine power settings (Anderson et al., 2006; Knighton et al., 2007; Airbus, 2008; Baughcum et al., 1996; Commercial Aviation Safety Team, October 2012), along with ambient

and combustion conditions which effect combustion efficiency (Eastop and McConkey, 1993; DuBois and Paynter, 2006).

The CMIP5-recommended historical aviation non-CO_2 emissions inventory for year 2000 only report datasets for NO_X and BC mass emissions. In comparison the CMIP5-extended aviation emissions inventory developed in Section 4.3 report non-CO_2 aviation emission datasets for a total of 12 chemical species (inclusive of six speciated hydrocarbons).

The inclusion of CO and speciated HCs have been previously found to show minimal atmospheric impacts in the upper troposphere/lower stratosphere (UTLS), due to the magnitude of HCs released from civil aviation, resulting in negligible changes in aviation-induced O_3 (Hayman and Markiewicz, 1996; Lee et al., 2010).

Recent aviation emissions inventories now include CO and HCs (Eyers et al., 2004; Lee et al., 2009; Wilkerson et al., 2010; Olsen et al., 2013b), and with past and projected rates of growth in aviation (Gudmundsson and Anger, 2012; IATA, 2015; Kreutz et al., 2008; Lee et al., 2009; Penner et al., 1999) the impact of these species (CO and HCs) will increase in magnitude. In this Chapter sensitivity experiments will be conducted to investigate the relative impacts of both aviation-borne CO and speciated HC emission on the aviation-induced radiative effects (O3DRE, aDRE, aCAE and resulting RE_{comb}) (Section 5.4.3).

5.2.3 Ozone radiative impact estimates from aviation NO_X only emission driven studies

Figure 5.1 helps put in to context the range in aviation-induced short-lived ozone radiative effect (RE) estimates from studies that only consider aviation NO_X emissions. Later in this section, the impact of including CO and speciated HC emissions on the RE from aviation-induced SL-O_3 from previous studies that only consider aviation NO_X emissions will be revisited, and compared to estimates obtained in this study (Section 5.4.1.2.1).

To aid with the comparison of SL-O_3 RE impacts from each study, Figure 5.1 weights REs in terms of Tg of nitrogen emitted (Tg(N)) from aviation. The spread in SL-O_3 RE estimates is due to different aviation NO_X inventories and chemical transport models (CTMs) used, whether an ensemble of model predictions were assessed, the ozone production efficiencies within the models utilised, and vertical (and horizontal) distribution of aviation NO_X emissions (Table 5.1) (Köhler et al., 2008; Myhre et al., 2011; Holmes et al., 2011; Hoor et al., 2009; Frömming et al., 2012; Skowron et al., 2013).

Figure 5.1: Range in aviation-induced short-lived ozone (SL-O_3) radiative effect estimates from studies which only consider aviation NO_X emissions (Köhler et al., 2008; Myhre et al., 2011; Holmes et al., 2011; Hoor et al., 2009; Frömming et al., 2012; Skowron et al., 2013).

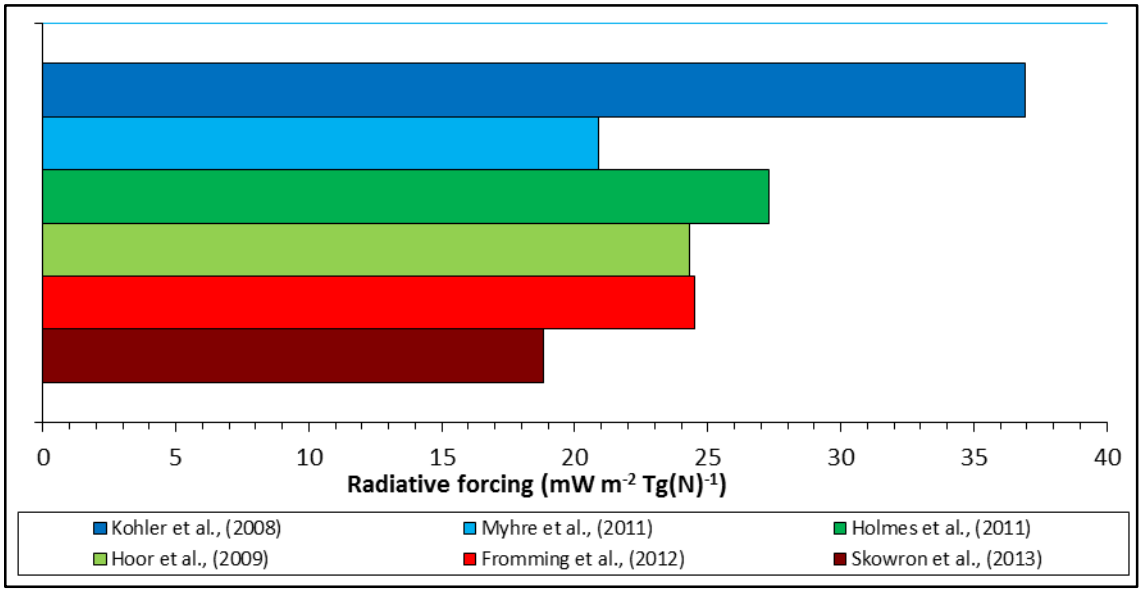

Table 5.1: Studies which consider aviation NO_X emissions only, to quantify the aviation-induced short-lived ozone (SL-O_3) radiative effect (RE), and the models and aviation emissions inventories used (Köhler et al., 2008; Myhre et al., 2011; Holmes et al., 2011; Hoor et al., 2009; Frömming et al., 2012; Skowron et al., 2013).

Study	Ensemble (Y/N – [number of models/datasets])	Model(s)	Inventory used
Köhler et al., (2008)	N[n/a]	p-TOMCAT	AERO2k
Myhre et al., (2011)	Y[5]	Oslo CTM2 TM4 p-TOMCAT LMDz-INCA UCI	QUANTIFY
Holmes et al., (2011)	Y[22]	UCI, LMDz-INCA, p-TOMCAT, TM4, Oslo-CTM2, ULAQ, NASA-2015, NASA-1992, ECHAM4.L39(DLR)/CHEM, HadAM3-STOCHEM, STOCHEM	QUANTIFY AERO2k TRADEOFF NASA 1992 NASA 2015
Hoor et al., (2009)	N[n/a]	ECHAM5/MESSy	QUANTIFY
Fromming et al., (2012)	N[n/a]	ECHAM4.L39(DLR)/CHEM	TRADEOFF 2000
Skowron et al., (2013)	Y[6]	MOZART	FAA's AEDT AEM AERO2k REACT4C TRADEOFF

From the studies considered in Figure 5.1 and Table 5.1 (Köhler et al., 2008; Myhre et al., 2011; Holmes et al., 2011; Hoor et al., 2009; Frömming et al., 2012; Skowron et al., 2013) a mean SL-O_3 RE of 24.47 mW m^{-2} $Tg(N)^{-1}$ is calculated with a standard deviation of 5.81 mW m^{-2} $Tg(N)^{-1}$.

When a full range of aviation emission species are considered (Section 2.2) the impact of aviation on changes in atmospheric O_3 concentrations can be better evaluated. The inclusion of CO emissions will participate in the consumption of OH to form H and CO_2 (Reaction 2.21), which results in the cycling of OH to HO_2 (Reaction 2.22). In the presence of NO_X, the HO_2 formed replenishes NO_2 and OH concentrations (Reaction 2.1) leading to net O_3 formation (Reaction 2.3 – Reaction 2.4) (Fowler et al., 1997; Jenkin and Clemitshaw, 2000).

The inclusion of HCs can lead to reductions in OH (Reaction 2.4), and the formation of NO_2 which can aid in the formation of O_3 (Reaction 2.24 – Reaction 2.25). Aviation-induced HCHO can lead to increases in HO_2 (Reaction 2.26 – Reaction 2.28), which can lead to increases in OH and convert NO to NO_2 (Reaction 2.1) (Fowler et al., 1997; Jenkin and Clemitshaw, 2000).

The through the formation of nitric acid (HNO_3) from NO_2 and OH (Reaction 2.2), aviation-borne emissions can contribute to the formation of nitrates (NO_3^-) in the troposphere (Reaction 2.20). Additionally gas-phase SO_2 reacts with OH in the sulfate formation process (Reaction 2.29 – Reaction 2.31) (Fowler et al., 1997; Jenkin and Clemitshaw, 2000), while SO_2 in the aqueous-phase can form sulfates via Reaction 2.32 (Jacobson, 1997).

5.3 Methodology

5.3.1 CMIP5-extended aviation emissions inventory

The investigations carried out in this section use the extended aviation emissions inventory created in Section 4.3. In comparison to CMIP5 recommended aviation emissions (Lamarque et al., 2009) this extended aviation emissions inventory provides 3-D gridded data for CO, speciated HCs (HCHO, C_2H_6, C_3H_8, CH_3OH, $(CH_3)_2CO$, CH_3CHO), SO_2, OC mass and particle numbers (Table 4.2).

Figure 5.2 and Figure 5.3 show the distribution of species that are not considered in the CMIP5 recommended aviation emissions dataset. Most emissions occur in the Northern Hemisphere (NH) and the cruise region of flight (i.e. between an altitude of ~8–12 km).

Figure 5.2: Zonal distributions of CMIP5-extended aviation emissions: (a) nitrogen oxides, (b) carbon monoxide, (c) total HCs, (d) sulfur dioxide, (e) black and organic carbon, and (f) particle number.

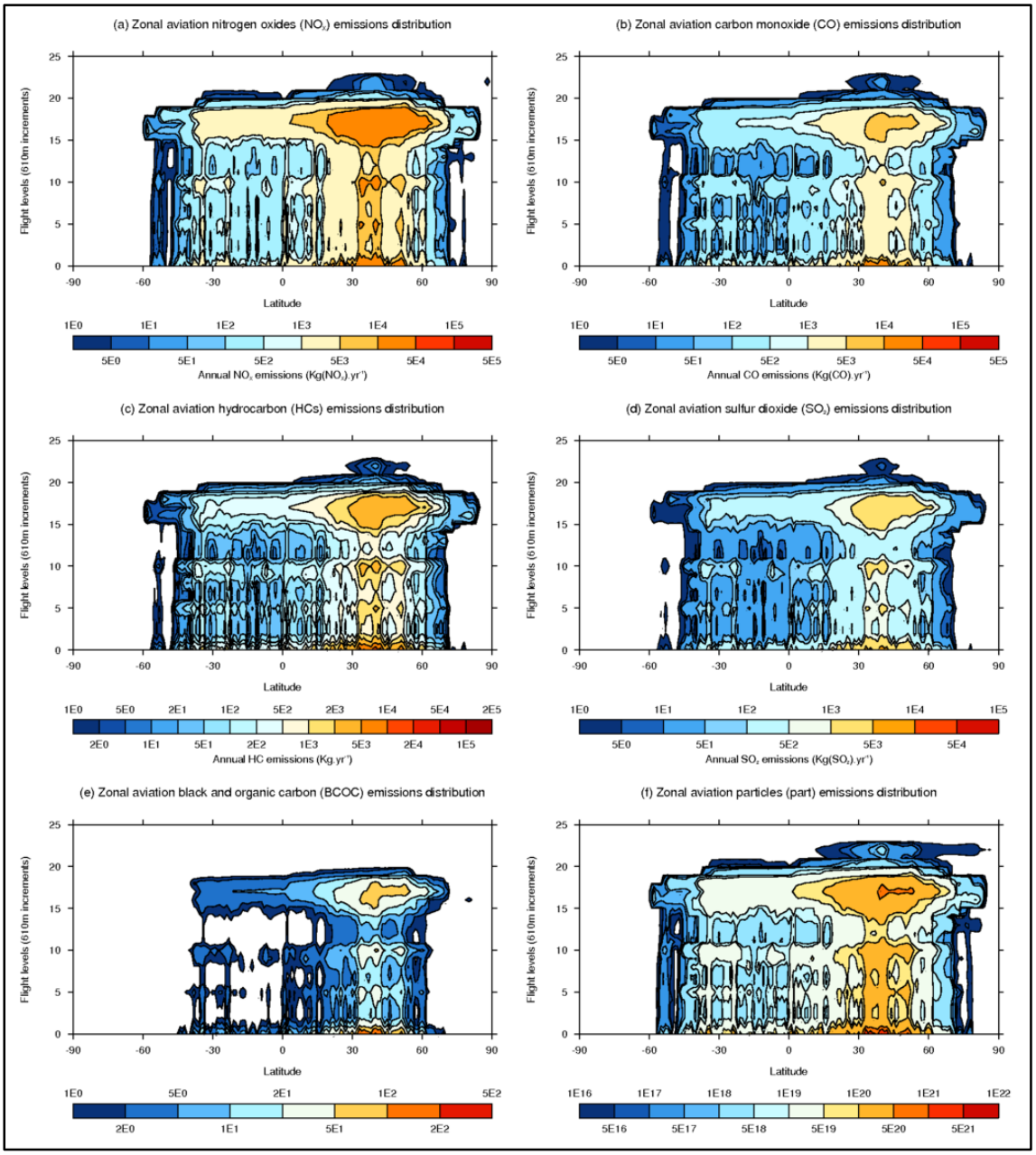

Also due to the methodology used to create the CMIP5-extended aviation emissions inventory (Section 4.3) the zonal distributions of CO and total HC emissions in comparison follow the distributions shown by NO_X and BC. HCs and CO were treated as linearly scalable with fuelburn when in reality these emissions are dependent on ambient and combustor conditions (DuBois and Paynter, 2006; Baughcum et al., 1996; Owen et al., 2010).

Figure 5.3: Spatial total column distribution of CMIP5-extended aviation emissions: (a) nitrogen oxides, (b) carbon monoxide, (c) total HCs, (d) sulfur dioxide, (e) black and organic carbon, and (f) particle number.

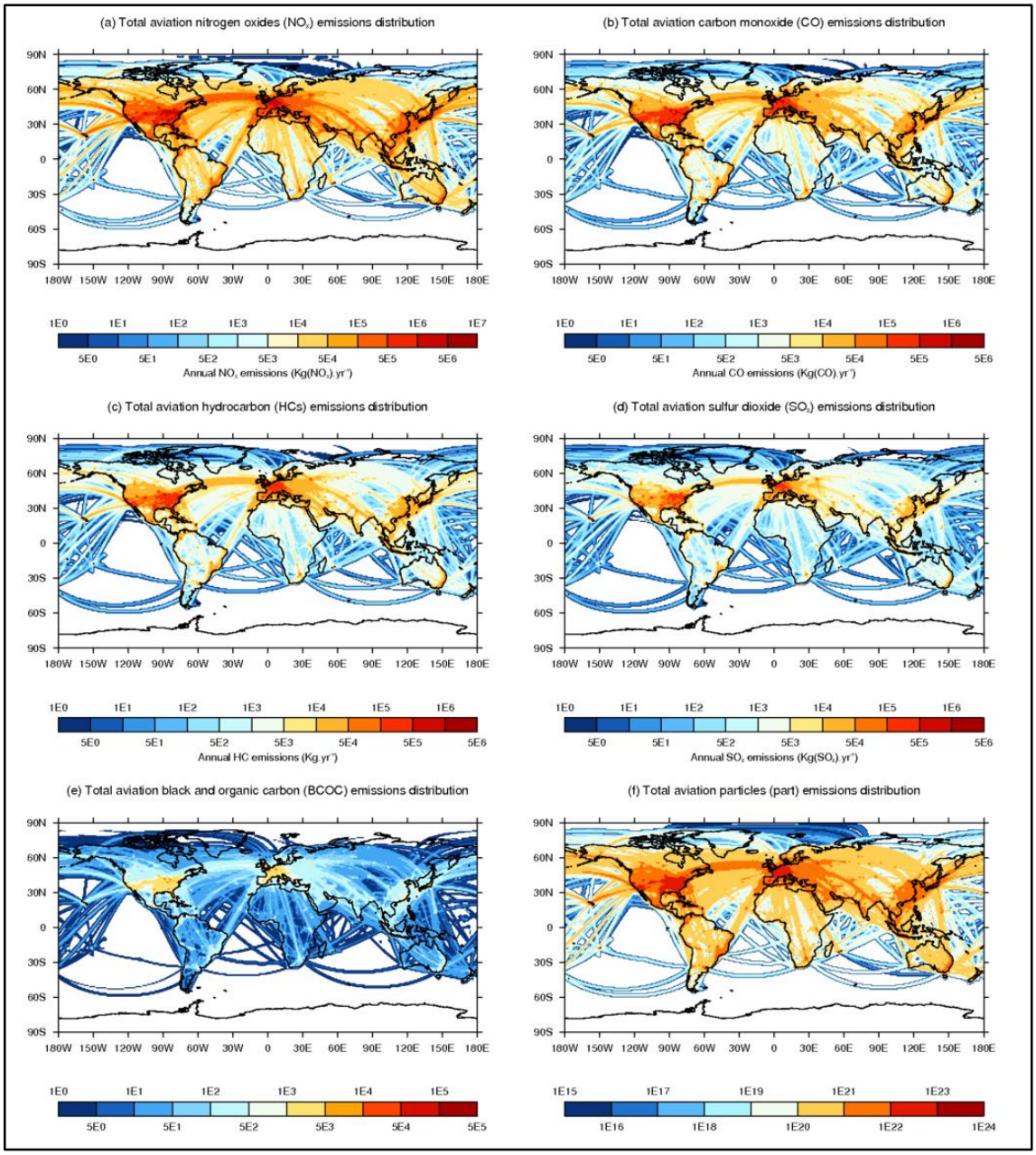

5.3.2 Simulations conducted

In order to investigate the atmospheric and climatic impact of an extended aviation-emissions inventory in comparison to the recommended historical aviation emissions from CMIP5, the first three scenarios outlined from Table 5.2 are simulated. CMIP5 recommended historical aviation emissions are taken from Lamarque et al. (2009), while the CMIP5-extended aviation emissions (relating to the NORM scenario) are developed in Section 4.3.

These simulations are conducted for year 2000, thus considering year 2000 meteorology from the ECMWF (European Centre for Medium-Range Weather Forecasts), in conjunction with anthropogenic and natural emissions for the associated year.

Table 5.2: Simulations conducted to investigate the impact of aviation based on the use of an extended-emissions inventory in comparison to the CMIP5 recommended emissions in conjunction with seven sensitivity studies.

Scenarios	Aviation species considered	
NOAVI	No aviation emissions	
NORM (CMIP5-extended)	All aviation emissions (NO_X, CO, HCs, SO_2, BC and OC)	
CMIP5	NO_X and BC emissions only	
NoCO	No CO	(Simulation NORM as base)
NoHCs	No HCs	(Simulation NORM as base)
$NoSO_2$	No SO_2	(Simulation NORM as base)

In order to quantify the importance of each of the aviation-emitted species (or species group in the case of HCs) three sensitivity experiments are conducted to investigate each non-CO_2 specie in turn (NoCO, NoHCs and $NoSO_2$ simulations).

All simulations were conducted for 16 months from September 1999 to December 2000 inclusive, with the first four months discarded as spin-up time, with results from all simulations being compared against a simulation with aviation emissions excluded (NOAVI).

5.4 Results and Discussion

This section is split in to three parts aiming to investigate: the impact of an extended aviation emission inventory; a comparison between the atmospheric and climatic impact of the use of the CMIP5-extended aviation emissions inventory in relation to the CMIP5 recommended historical aviation emissions inventory for 2000, and; sensitivity studies aiming to assess the contribution of each aviation-borne emission species in turn (with speciated HCs treated as one set).

5.4.1 Impact of an extended aviation emissions inventory

Here aviation-induced atmospheric and climate perturbations driven by the use of the CMIP5-extended aviation emissions inventory developed in Section 4.3 (represented by the simulation NORM in Table 5.2) are discussed. Initially atmospheric perturbations from aviation-borne

non-CO_2 emissions are investigated and discussed, followed by investigating the climatic impact via evaluation of the ozone direct radiative (O3DRE), aerosol direct radiative (aDRE) and aerosol cloud albedo (aCAE) effects.

5.4.1.1 Aviation-induced atmospheric perturbations

Here the absolute and percentage changes in gas- and aerosol-phase emissions induced by aviation non-CO_2 emissions are discussed in turn, comparing the outcomes from this study with existing work where possible.

5.4.1.1.1 Gas-phase perturbations

Figure 5.4 to Figure 5.9 present the absolute and percentage changes (NORM in relation to NOAVI) in nitrogen oxides (NO_X), ozone (O_3), hydroxyl radical (OH), hydroperoxyl (HO_2), nitric acid (HNO_3), nitrous acid (HONO), peroxyl acetyl nitrate (PAN) and sulfur dioxide (SO_2).

From these figures it is seen that the majority of aviation-induced NO_X perturbations from the NORM simulation occur in the NH about cruise level (~8–12 km), in line with the release of aviation emissions (Figure 5.2) and zonal distributions seen in previous work (Lee et al., 2010; Stevenson et al., 2004).

The use of the CMIP5-extended aviation emissions inventory is found to result in an increase in mean zonal NO_X concentrations of 7.16 pptv [mean ΔNO_X = +4.91%] relative to NOAVI, with a maximum zonal concentration of 143.23 pptv in the NH in the cruise region of flight, and minimum zonal concentration of –1.86 pptv at the surface (Figure 5.4(a)). Maximum zonal percentage increases of +72.67% are found to occur about the cruise region of flight (in line with the release of aviation emissions), with minimum percentage changes [min ΔNO_X = –0.88%] again occurring at the surface (Figure 5.4(b)).

Lee et al., (2010)'s found maximum percentage increases in aviation-induced NO_X concentrations of ~40% in the cruise region of flight for 1990. Differences between these two studies can be explained by the year of simulation and aviation emission NO_X emissions considered; where Lee et al., (2010) consider NO_X emissions of 0.56 Tg(N) based on the NASA 1991/1992 emissions inventory while this study considers annual NO_X emissions of 0.85 Tg(N) for year 2000 (Lee et al., 2010).

When considering aviation-induced NO_X (NORM–NOAVI) about the cruise level of flight maximum absolute concentration increases of 0.21 ppbv are seen to occur over Western

Europe (Figure 5.4(c)), along with maximum percentage increases (Figure 5.4(d)). Horizontal distributions of NO_X are similar to Kentarchos and Roelofs (2002) with maximum perturbations occurring over the NH in the cruise region of flight.

Figure 5.4: Aviation-induced annual mean concentration changes (a,c) and percentage changes (b,d) in NO_X concentrations resulting from the use of the CMIP5-extended aviation emissions inventory: Top panels present zonal means, while bottom panels present perturbations at 10.71 km.

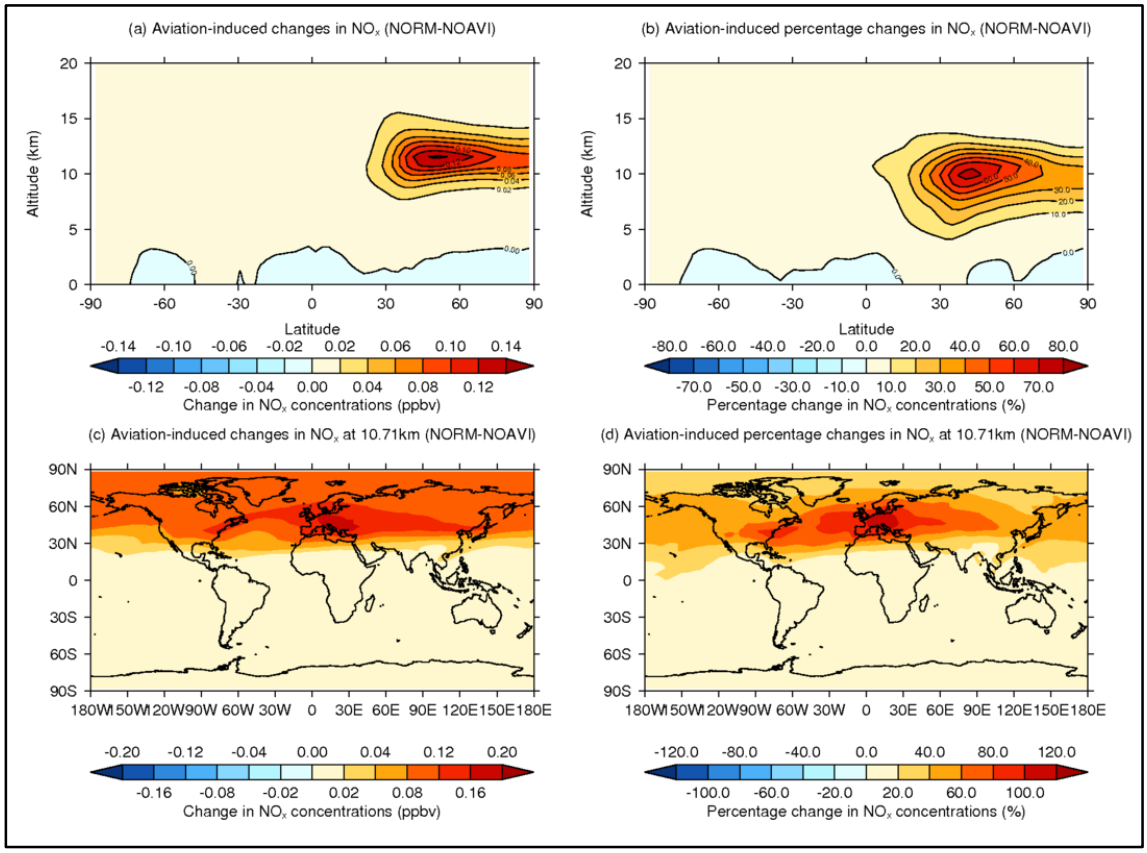

Aviation increases simulated global NO_X burdens by 40.65 Gg, and by 28.51 Gg [+70.13%] within the cruise region of flight (7.6–12.4 km) – Table 5.3. Khodayari et al. (2014b) estimate aviation increases the global NO_X burden by 16.43 Gg and 13.14 Gg for CAM4 and CAM5 respectively. The lower estimated increases in the global NO_X burden could be attributed to the differences in the chemistry with the models used Khodayari et al. (2014b) (CAM4 and CAM5).

Inter-seasonal variations (not presented here) in NO_X concentrations highlight that maximum zonal mean perturbations in aviation-induced NO_X concentrations occur during the MAM season (March, April and May) [max ΔNO_X = 269.09 pptv], while higher global monthly mean perturbations in NO_X concentrations occur over the MAM [mean ΔNO_X = 6.75 pptv] and SON (September, October and November) [mean ΔNO_X = 7.49 pptv] seasons. Peaks in aviation-

induced O_3 concentrations over MAM could be attributed to increases in solar insolation in the Spring months contributing to the ozone formation process. Greater aviation-induced monthly mean NO_X concentrations seen in the SON season could be attributed to the lower levels of solar insolation received during the NH winter, reducing OH formation from the photo-dissociation of HONO (Reaction 2.7), which in turn slowing down the conversion rate of NO_2 + OH to HNO_3, and O_3 formation through the photodissociation of NO_2 to NO (Jenkin and Clemitshaw, 2000; Fowler et al., 1997).

Table 5.3: Aviation-induced gas-phase species burdens within the full and cruise-level domains resulting from the use of the CMIP5-extended aviation emissions inventory for year 2000, in comparison to current literature. Percentage contribution for cruise-level (7.6<km<12.4) in relation to the full domain presented shown in brackets (Khodayari et al., 2014b; Gauss et al., 2006; Wild et al., 2001).

Study and domain		NO_X (Gg)	O_3 (Tg)	OH (Mg)	PAN (Gg)	HONO (Mg)	HNO_3 (Gg)	SO_2 (Gg)
This study	Full domain	40.65	3.90	4.98	12.99	77.50	85.43	1.06
	Cruise level	28.51 (70.13%)	1.38 (35.36%)	2.37 (47.61%)	3.78 (29.13%)	53.78 (69.39%)	46.19 (54.07%)	2.13 (200.8%)
Gauss et al., (2006)			4.24					
Wild et al., (2001)			3.79					
Khodayari et al., (2014)	CAM4	16.43	8.00	6.00				
	CAM5	13.14	9.00	7.00				

Aviation-induced O_3 is found to primarily occur in the NH mid-latitude region along the cruise region of flight (Figure 5.5), in line with the emission of aviation NO_X (Figure 5.2) and aviation-induced perturbations in atmospheric NO_X concentrations (Figure 5.4). The zonal and spatial absolute and percentage concentration changes simulated here (NORM–NOAVI) replicate the aviation-induced O_3 distribution patterns presented in previous work (Koffi et al., 2010; Köhler et al., 2008; Unger, 2011; Stevenson et al., 2004; Søvde et al., 2014; Kentarchos and Roelofs, 2002; Khodayari et al., 2014b; Hoor et al., 2009; Grooß et al., 1998).

The use of the CMIP5-extended aviation emissions inventory (NORM) in relation a scenario with no aviation emission (NOAVI) results in an increase annual mean zonal O_3 concentrations of +0.40 ppbv [mean ΔO_3 = 0.73%], with maximum zonal mean concentrations of 2.11 ppbv [max ΔO_3 = +2.87%] again in the NH mid-latitude cruise region (Figure 5.5(a,b)). The maximum annual zonal mean peaks seen from this work are in line with the range of 1–6 ppbv seen in recent literature (Grooß et al., 1998; Unger, 2011; Köhler et al., 2008). Globally mean increases in O_3 of 0.22 ppbv [mean ΔO_3 = 0.48%] are simulated. Increases in O_3 concentrations are seen at the surface despite the reductions in surface NO_X concentrations shown in Figure 5.4. This increases in surface O_3 concentrations is due to the higher lifetime of O_3 in upper troposphere (Kentarchos and Roelofs, 2002), which enables O_3 production to be decoupled from the release of aviation emissions (i.e. have transboundary effects) (Fowler et al., 1997; Jenkin and Clemitshaw, 2000; Lee et al., 2010), resulting in changes in O_3 concentrations at the surface.

Figure 5.5: Aviation-induced annual mean concentration changes (a,c) and percentage changes (b,d) in O_3 concentrations resulting from the use of the CMIP5-extended aviation emissions inventory: Top panels present zonal means, while bottom panels present perturbations at 10.71 km.

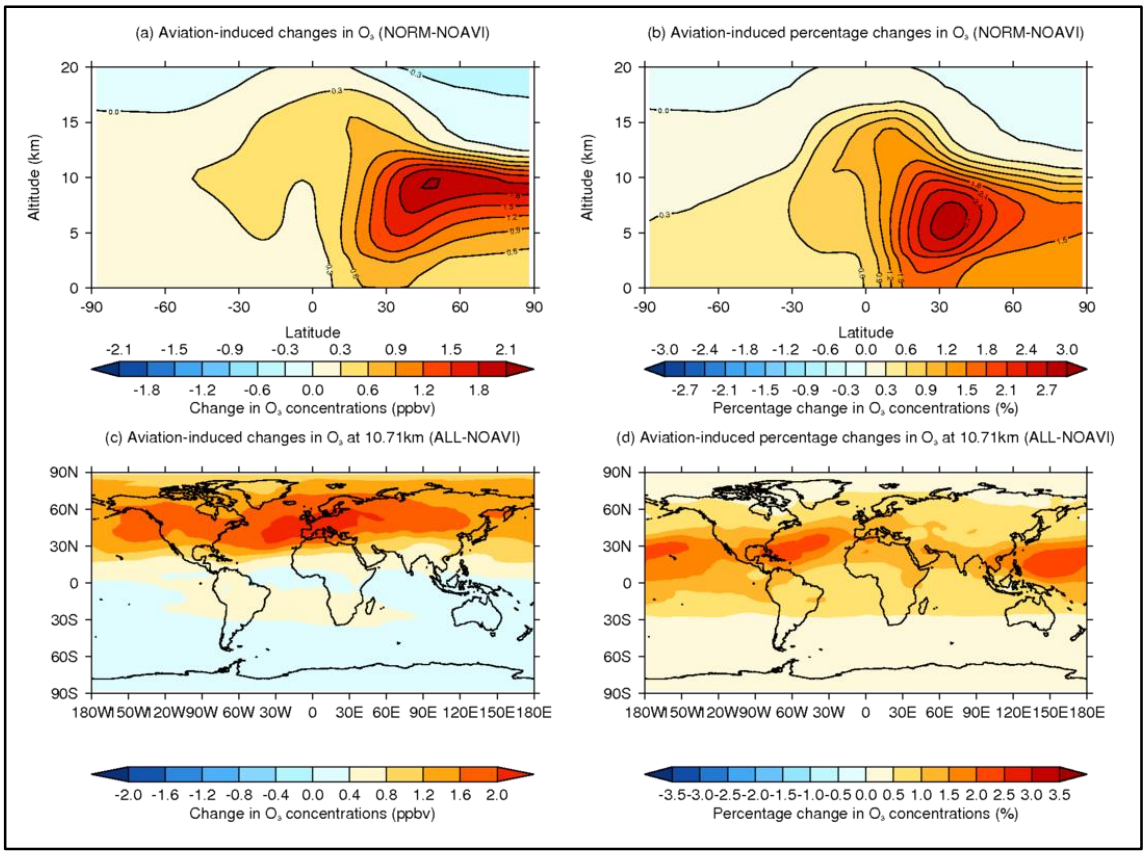

Over the JJA season (June, July and August) increases in zonal mean concentration of up to 2.71 ppbv [max_{JJA} ΔO_3 = +2.76%] is simulated (NORM–NOAVI), zonal mean concentration increases of up to 1.60 ppbv [max_{DJF} ΔO_3 = +2.99%] over the DJF season (December, January

and February) – not shown here. Søvde et al. (2014) find a that over JJA max zonal means range between 4.8–8.8 ppbv, and peak ranging between 3.4–4.4 ppbv between DJF. GMV4-nitrate correlates with this seasonal trend, but returns lower values.

Khodayari et al. (2014b) using CAM4 and CAM5 estimate maximum zonal concentrations of 5–6 ppbv over January and 11–12 ppbv over July. Again GMV4-nitrate follows this pattern, but gives a lower peak zonal O_3 concentration of 1.57 ppbv for January and 2.87 ppbv for July.

The higher zonal max ΔO_3 found by Khodayari et al. (2014b) correlates with the changes in global ozone burdens simulated by CAM4 and CAM5 [CAM4 O_3 burden = 8.00 Tg; CAM5 O_3 burden = 9.00 Tg], in comparison to GMV4-nitrate [GMV4-nitrate ΔO_3 burden = 3.90 Tg]. GMV4-nitrate also finds that 35.36% [1.40 Tg] of aviation-induced O_3 occurs within the cruise-level (Table 5.3).

The lower aviation-induced O_3 concentrations simulated here can be attributed to the lower net O_3 chemical production efficiency (OPE) within GMV4-nitrate [$OPE_{GMV4\text{-}nitrate}$ = 1.33], in comparison to OPEs for CAM4 and CAM5 [OPE_{CAM4} = 2.89; OPE_{CAM5} = 3.25] (Khodayari et al., 2014b; Wilkerson et al., 2010).

Figure 5.5(c,d) shows that around the cruise range of flight, the main increases in O_3 concentrations occur in the NH between 30°N–70°N, with relative increases in O_3 being located between 0°N–30°N, correlating with previous work (Kentarchos and Roelofs, 2002).

Zonal and spatial absolute and percentage O_3 concentration changes simulated by GMV4-nitrate relative to NOAVI (NORM–NOAVI) are in line with NO_X perturbations (Figure 5.4), the NH dominated nature of aviation emissions and the location of global flight paths (Figure 5.2 and Figure 5.3), and the NH summer (i.e. higher levels of solar insolation).

Akin to O_3, aviation-induced OH returns the largest perturbations in the NH upper tropospheric region, between 20°N–40°N, i.e. the extra-tropic region, returning maximum zonal increases in OH concentrations of 0.014 pptv [max ΔOH = 15.03%] (Figure 5.6).

In addition to upper tropospheric increases in OH concentrations small decreases in OH are seen in the NH at ~11 km [min ΔOH = –0.003 pptv; min ΔOH = –11.56%] in the lower stratosphere, resulting in small reductions but which have a high relative impact due to the lower back background concentrations in this region. Globally aviation increases annual mean OH concentrations by 1.02×10^{-3} pptv [mean ΔOH = 1.16%], with annual mean zonal concentrations changes of 1.12×10^{-3} pptv [mean ΔOH = 1.29%].

Figure 5.6: Aviation-induced annual mean zonal absolute (a) and percentage (b) changes in OH concentrations resulting from the use of the CMIP5-extended aviation emissions inventory.

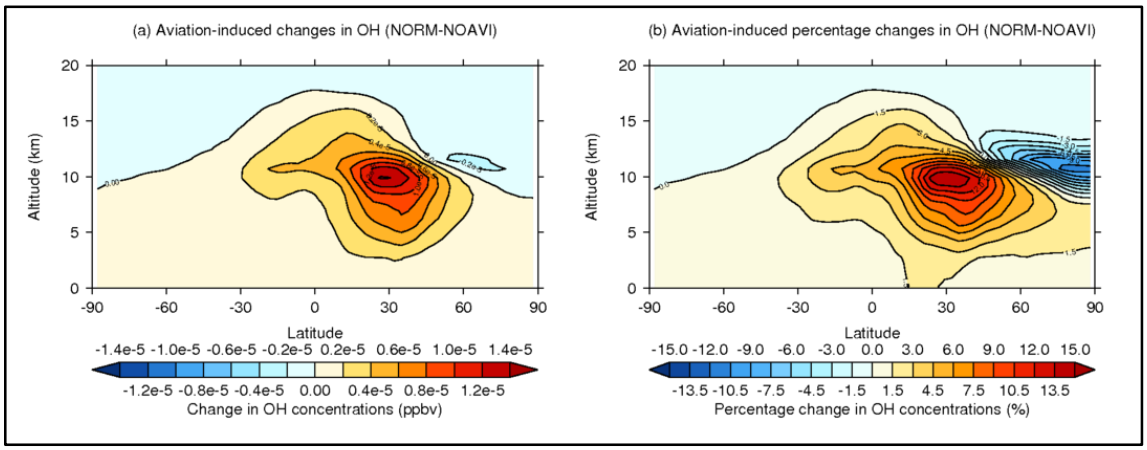

Hoor et al. (2009) in their work investigating the impact of emissions from transportation (road, shipping and aviation) on O_3 and OH, find that aviation emissions (from the QUANTIFY Integrated Project) return reductions in OH in the upper troposphere/lower stratosphere about the tropopause as well as maxima in aviation-induced OH concentrations at ~30°N, along the cruise region of flight (8–12 km). GMV4-nitrate returns reductions in OH concentrations about the Northern Hemisphere tropopause, with a pocket maximum in OH reductions at 60°N at 11.6 km, while also returning maxima in aviation-induced OH concentrations at ~30°N about the cruise region of flight. Aviation-induced OH concentrations can be attributed to the reaction of HO_2 with NO (Reaction 2.1), the photolysis of HONO (Reaction 2.8), production of OH via reaction of HO_2 and NO_3 (Reaction 2.9), and the reaction of HO_2 with O_3 (Reaction 2.10) (Fowler et al., 1997; Jenkin and Clemitshaw, 2000).

GMV4-nitrate simulates that aviation emissions result in an increase in the global OH burden of 4.98 Mg within the full model domain, with 47.61% of this increase [2.37 Mg] occurring within the cruise region of flight (Table 5.3).

Aviation NO_X emissions additionally result in the formation of nitric acid (HNO_3), required as an intermediary step in the formation of ammonium nitrate. Depending on conditions, i.e. time of day and local O_3 concentrations, HNO_3 can be primarily produced via Reaction 2.2 which consumes OH and Reaction 2.19 which consumes the N_2O_5 formed through the reaction of NO_2 with NO_3 via Reaction 2.18 (Section 2.3.1) (Fowler et al., 1997; Jenkin and Clemitshaw, 2000). The formation of HNO_3 from N_2O_5 (Reaction 2.19) in the troposphere occurs extremely slowly in the gas-phase, so occurs predominantly on cloud water and aerosol surfaces and in the dark (i.e. night-time, or during winter), as it is unstable in sunlight (Fowler et al., 1997; Jenkin and Clemitshaw, 2000). As such GMV4-nitrate NORM simulations highlight that aviation increases

both O_3 and OH concentrations (Figure 5.5 and Figure 5.6 respectively), returning increases in atmospheric HNO_3 concentrations (Figure 5.7).

Figure 5.7 shows that aviation-induced HNO_3 occurs in the region that aviation emissions dominate, the NH about the cruise region of flight. Aviation-induced HNO_3 annual zonal concentrations peak at 0.13 ppbv [max ΔHNO_3 = +32.72%], with an annual zonal mean increase of 0.009 ppbv [mean ΔHNO_3 = +4.29%] and global mean increase of 0.006 ppbv [mean ΔHNO_3 = +3.53%].

GMV4-nitrate simulations show that aviation emissions result in an increase in the global HNO_3 burden of 85.43 Gg within the full model domain, with 54.06% of this increase [46.19 Gg] occurring within the cruise region of flight (Table 5.3).

Figure 5.7: Aviation-induced annual mean zonal absolute (a) and percentage (b) changes in HNO_3 concentrations resulting from the use of the CMIP5-extended aviation emissions inventory.

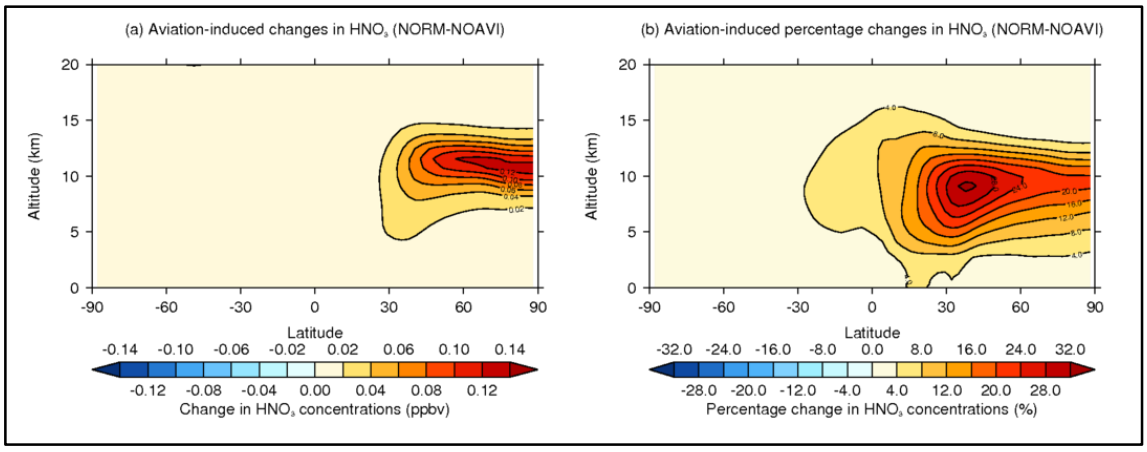

Figure 5.8 show the impact on aviation emissions on HONO and PAN concentrations. Aviation-induced HONO and PAN are of importance as they can act as a reservoir for NO_X, thus resulting in aviation-induced O_3 having transboundary effects, i.e. uncoupling aviation O_3 impacts from their point of release (Fowler et al., 1997; Jenkin and Clemitshaw, 2000; Lee et al., 2010). Additionally PAN formation can result in aviation-induced O_3 formation occurring downwind of where aviation NO_X is released (Lee et al., 2010).

The NORM simulations conducted using GMV4-nitrate give a peak in the annual mean zonal HONO concentrations of 0.17 pptv [max ΔHONO = +76.20%] and peak in annual PAN concentrations of 3.08 pptv [max ΔPAN = +2.16%] (Figure 5.8). Annual zonal mean concentrations for HONO were simulated as 7.88×10^{-3} pptv [mean ΔHONO = +5.12%], and 6.34 pptv [mean ΔPAN = +0.49%] for PAN. Globally mean increases in HONO of 7.93×10^{-3} pptv

[mean ΔHONO = +4.75%] were simulated along with global mean increased in PAN of 0.35 pptv [mean ΔPAN = 0.08%].

Figure 5.8(a,b) shows that aviation-induced HONO dominates in the NH about the cruise region of flight, between 20°N–60°N. HONO is an important by-product of aviation as it acts as night-time reservoir for NO_X, being broken down in to OH and NO via photolysis (Reaction 2.8 in Section 2.3.1.4). The formation of this NO_X reservoir can be enhanced by the formation of HO_2 through the release of aviation-borne HCs; if there is enough NO_X present (Reaction 2.23 to Reaction 2.28 in Section 2.3.3) (Fowler et al., 1997; Jenkin and Clemitshaw, 2000).

Figure 5.8: Aviation-induced annual mean zonal absolute (left panes) and percentage (right panes) changes in HONO (top panes) and PAN (bottom panes) concentrations resulting from the use of the CMIP5-extended aviation emissions inventory.

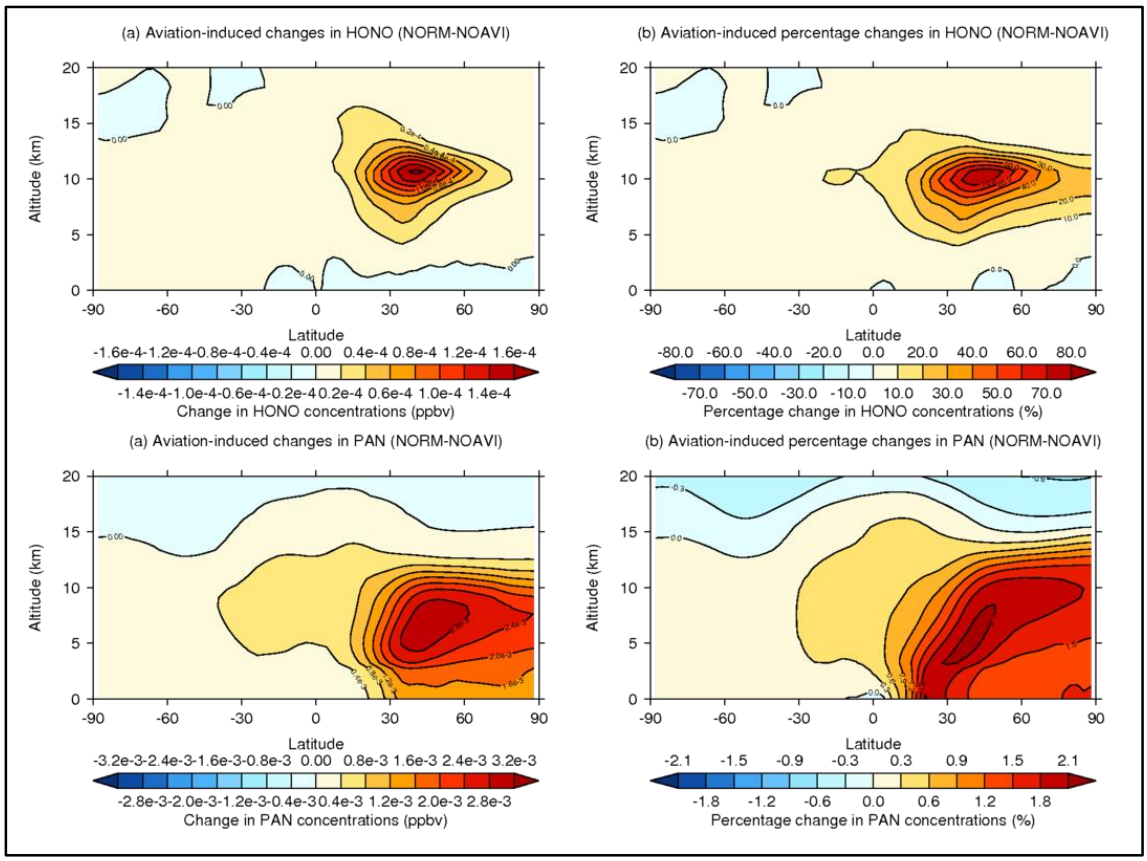

From Figure 5.8(c,d) it is seen that the aviation-induced PAN mainly occurs over the NH, with increases in PAN extending from above the cruise region of flight to near surface level, demonstrating PAN's capacity to have transboundary effects. This is linked to how the thermal degradation of PAN decreases with increases in altitude, i.e. shifting the equilibrium of Reaction 2.13 to the right-hand-side (Section 2.3.1.4) (Lee et al., 2010; Fowler et al., 1997; Jenkin and Clemitshaw, 2000). Figure 5.8(c,d) also shows that aviation-induced PAN extend down to the surface despite Figure 5.4(a,b) showing that aviation-induced NO_X increases don't

extend down to the surface. These increases in near surface PAN concentrations can be attributed to the degradation of HCs (with ≥ C_2) from aviation and other (surface) anthropogenic sources due aviation-induced OH increases which do extend down to the surface (Figure 5.6). Additionally in this study through the inclusion of aviation-borne HCs the impact of aviation-induced PAN is more accurately represented, as PAN is a product of the degradation of a large range of organic compounds (with ≥ C_2) (Fowler et al., 1997; Jenkin and Clemitshaw, 2000).

Through the inclusion of the CMIP5-extended aviation emissions inventory with speciated HCs GMV4-nitrate simulates increases in the global HONO burden of 77.50 Mg and PAN burden of 12.99 Gg, with 69.39% [53.78 Mg] of the HONO and 29.13% [3.78 Gg] of the PAN burden increases occurring in the cruise region of flight. The relative contributions of these increases in global burdens within the cruise region of flight further highlight the potential widespread impact (transboundary effect) of aviation-induced PAN.

Figure 5.9: Aviation-induced annual mean zonal absolute (left panes) and percentage (right panes) changes in SO_2 (top panes) and H_2SO_4 (bottom panes) concentrations resulting from the use of the CMIP5-extended aviation emissions inventory.

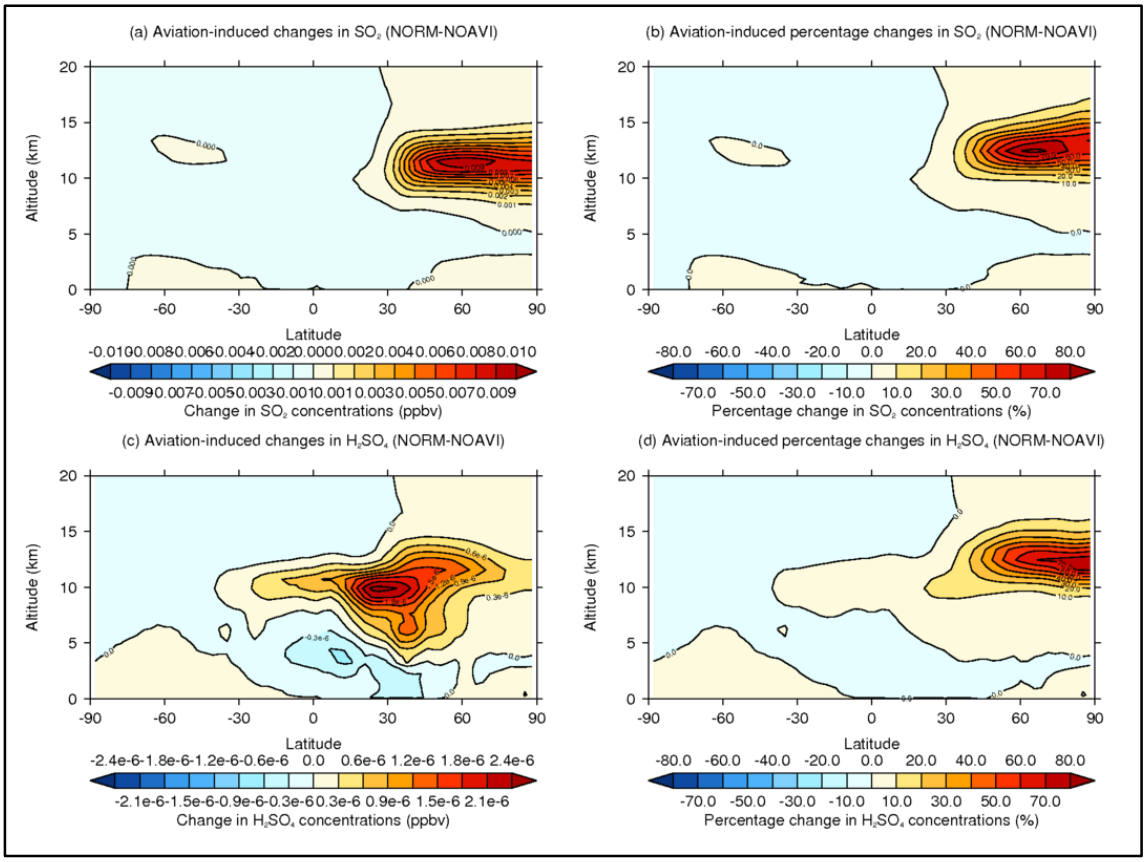

The inclusion of aviation SO_2 emissions is found to increase the annual mean atmospheric zonal SO_2 concentrations by up to 9.90 pptv [max ΔSO_2 = +82.48%] in the NH mid-latitude

region within the cruise region of flight (Figure 5.9). Zonal mean SO_2 concentrations are simulated to increase by 0.29 pptv [mean ΔSO_2 = +2.29%], with annual mean global SO_2 concentrations increasing by 0.14 pptv [mean ΔSO_2 = +0.88%].

From Figure 5.9(a,b) it is seen that the majority of the impact of SO_2 emissions are seen at cruise level, with smaller impacts at the surface-layer. Aviation returns a net increase the global SO_2 burden of 1.06 Gg, despite increasing atmospheric SO_2 burden by 2.13 Gg within the cruise-level (Table 5.3). This is a result of aviation-induced reductions in SO_2 seen over the majority of the Southern Hemisphere (SH), and lower tropospheric regions of the NH (Figure 5.9).

Aviation SO_2 emissions are of importance due to the formation of sulfates and the H_2SO_4 products ability to form new particles, to condense upon existing particles, allow some non-soluble particles to move in to the soluble phase enhancing their ability to act as cloud condensation nuclei (CCN) (Mann et al., 2010; Verheggen, 2009).

Figure 5.9(c,d) highlights the greater zonal spread of aviation-induced H_2SO_4, demonstrating the potential of aviation-induced H_2SO_4 to impact aerosol at low-cloud level. Zonal annual mean concentrations of H_2SO_4 are estimated to increase by up to 2.56×10^{-3} pptv [max ΔH_2SO_4 = +77.24%], with increases in mean global H_2SO_4 concentrations of 7.44×10^{-5} pptv [mean ΔH_2SO_4 = 0.92%].

5.4.1.1.2 Aerosol-phase perturbations

Figure 5.10 and Figure 5.11 present the absolute and percentage changes (NORM in relation to NOAVI) in sulfates, nitrates, ammonium, BC, OC and BCOC (the sum of BC and OC). Akin to aviation-induced changes in gas-phase species the majority of aerosol-phase perturbations primarily occur over the NH and along cruise-level of flight.

Figure 5.10(a) shows that the highest annual mean zonal concentration increases aviation-induced sulfates occur at the surface [8.00 ng m^{-3}], with aviation-induced zonal concentrations decreasing with increases in altitude. This pattern reflects the distribution in aviation-induced sulfates simulated by Righi et al., (2013) who simulate aviation-induced increases in sulfates of up to 10.0 ng m^{-3} at the surface, and increases of between 2–5 ng m^{-3} at cruise level (Righi et al., 2013). Additionally in the NH high-latitude regions decreases in sulfates arise. Figure 5.10(b) shows that despite the greatest absolute changes in aviation-induced sulfate concentrations occurring close to the surface, the greatest zonal percentage increases occur

closer to the cruise level of flight [max Δsulfates = +4.07%]. This behaviour in annual mean zonal aviation-induced absolute and relative sulfate concentrations is seen in existing literature (Righi et al., 2013). Zonal mean increases in aviation-induced sulfate of 1.04 ng m^{-3} are simulated [mean Δsulfates = +0.63%] for year 2000.

Figure 5.10: Aviation-induced annual mean zonal absolute (left panes) and percentage (right panes) changes in sulfate (top panes), nitrate (middle panes) and ammonium (bottom panes) concentrations resulting from the use of the CMIP5-extended aviation emissions inventory.

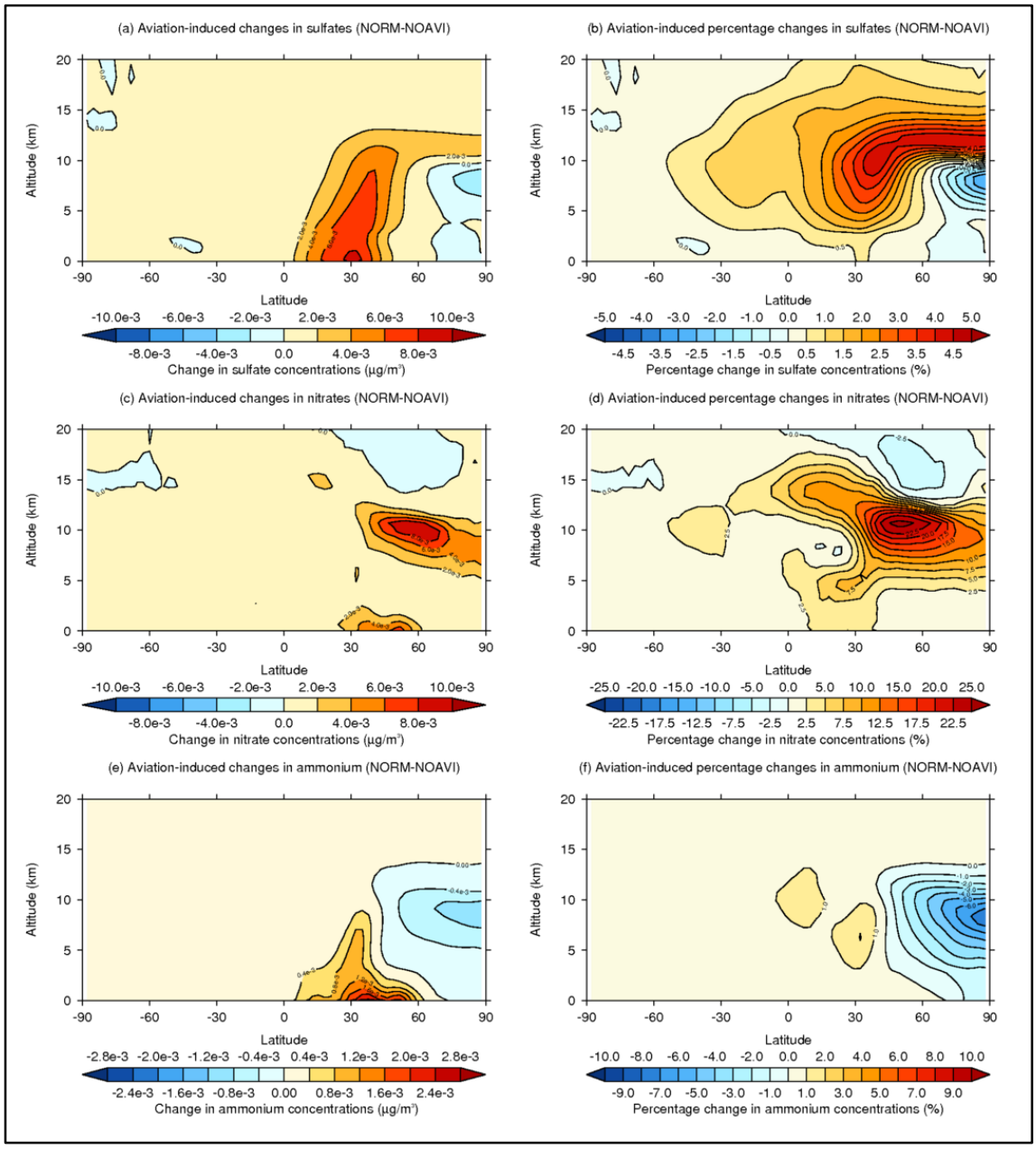

In both cases (absolute and relative changes) greatest reduction in sulfates [min Δsulfates = –3.72 ng m^{-3}; min Δsulfates = –3.05%] is simulated between 70°N–90°N at ~8 km.

The reductions in annual mean zonal sulfate concentrations and higher sulfate concentration increase closer to surface level are a product of aviation emitted NO_X, SO_2 emissions and other natural and anthropogenic ground sources of SO_2 emissions. This is due to the oxidation of non-aviation SO_2 by aviation-induced OH produced from aviation NO_X emissions, and not directly from aviation-emitted SO_2 (Barrett et al., 2010). In addition, the formation of ammonium sulfate is dependent on available atmospheric ammonia (Bauer et al., 2007; Unger, 2011). As ammonia is predominantly from surface sources, peaks in concentrations of aviation-induced sulfates occur near the surface (Figure 5.10(a)).

Globally, aviation is simulated to increase annual mean sulfate concentrations by 0.83 ng m^{-3} [mean Δsulfates = 0.71%], resulting in an aviation-induced sulfate burden of 12.95 Gg, with 32.25% [4.18 Gg] of this burden increase occurring in the cruise phase of flight (Table 5.4). Righi et al., (2013) estimated that aviation emissions increase the global sulfate burden by 3.2 Gg. In their work they utilise the QUANTIFY Integrated Project, which reports aviation NO_X and BC mass emissions, while deriving SO_2 and direct sulfate emissions using emissions indices from Lee et al., (2010) in conjunction with BC emissions (Lee et al., 2010; Righi et al., 2013).

Table 5.4: Aviation-induced aerosol-phase species burdens within the full and cruise-level domains resulting from the use of the CMIP5-extended aviation emissions inventory for year 2000, in comparison to current literature. Percentage contribution for cruise-level (7.6<km<12.4) in relation to the full domain presented shown in brackets (Righi et al., 2013).

Study and domain		Sulfates (Gg)	Nitrates (Gg)	Ammonium (Gg)	BC (Gg)	OC (Gg)
This study	Full domain	12.95	5.58	0.86	0.49	0.21
	Cruise level	4.18 (32.25%)	2.92 (52.38%)	-0.005 (-0.55%)	0.14 (28.70%)	-0.18 (-86.10%)
Righi et al., (2013) – Cruise		3.2	-1.1	-0.2	0.1	

From Figure 5.10(c,d) the greatest aviation-induced absolute and relative increases in aviation-induced nitrates are simulated to dominate in the NH between 30°N–70°N within the cruise region of flight, with maximum annual mean zonal concentration increases of 9.06 ng m^{-3} [max Δnitrates = +24.70%]. Akin to aviation-induced changes in sulfate concentration (Figure 5.10(a)) increases in nitrates are also simulated close to the surface (Figure 5.10(c)). This increase in surface nitrate is due to the availability of atmospheric ammonia and the chemical

mechanism governing the formation of ammonium nitrate (Bauer et al., 2007; Unger, 2011). Zonal mean increases in nitrate concentrations of 0.60 ng m^{-3} are simulated [mean Δnitrates = +2.39%], with global mean increases of 0.36 ng m^{-3} [mean Δnitrates = 1.93%].

This investigation finds that aviation increases the global nitrate burden by 5.58 Gg, with 52.38% [2.92 Gg] of this increase occurring at cruise level. In comparison to Righi et al., (2013) who simulate decreases in the global aviation-induced nitrate burden of –1.1 Gg, this investigation sees an increase (Table 5.4). This is as the simulations conducted here estimate greater increases in aviation-induced nitrates at cruise level, and lower reductions in higher altitude aviation-induced perturbations in nitrates in comparison to Righi et al. (2013).

Figure 5.10(e,f) show that in in line with aviation-induced reductions in sulfates in the NH, reductions in ammonium arise; with zonal mean reductions peaking at –1.00 ng m^{-3} [min Δammonium = –7.43%]. Reductions in the formation of ammonium sulfate ($(NH_4)_2.SO_4$) mean that for each molecule of the sulfate ion (SO_4^{2-}) not consumed in the formation of $(NH_4)_2.SO_4$ two molecules of the ammonium cation will not be used in this process. Considering this is tandem with the formation of ammonium nitrate ($NH_4.NO_3$) in this region, the reductions in ammonium will be a function of $(NH_4)_2.SO_4$ not formed and $NH_4.NO_3$ formed.

Peaks in ammonium formed are simulated close to the surface level in line with the main source of ammonia, and where the formation of sulfates are formed – relating to the chemistry of the formation process of ammonium sulfate (Bauer et al., 2007; Unger, 2011). Here peaks in ammonium zonal concentrations of +0.073 ng m^{-3} are simulated Figure 5.10(e). These aviation-induced changes in global ammonium concentrations result in an increase in the global mean ammonium concentration of +0.055 ng m^{-3} [mean Δammonium = +0.42%], resulting in an increase in the global ammonium burden of 0.86 Gg; with a reduction in the cruise-level burden of –4.71 Mg in relation to the NOAVI simulation.

The perturbations in BC simulated here compare well with current literature. Wei et al., (2001) simulate maximum zonal increases in aviation-induced BC concentrations of 0.33 ng m^{-3} at ~12.5 km, in comparison to the maximum zonal increase of increase of 0.33 ng m^{-3} [max ΔBC = 14.55%] simulated here seen in the NH between 30°N–90°N (Figure 5.11(a,b)). Additionally this study simulates decreases in BC zonal concentrations of up –0.28 ng m^{-3} [min ΔBC = –4.88%] at ~8 km between 70°N–90°N (Figure 5.11(a,b)).

The key difference between the study by Wei et al., (2001) and this study are the aviation emissions inventories used. They use the NASA-1992 emissions inventory, which considers

annual aviation-borne BC emissions of 4.4 Mg yr^{-1} (Wei et al., 2001; Penner et al., 1999; Olsen et al., 2013b), in comparison to the annual BC emissions of 5.012 Mg yr^{-1} considered here. Globally aviation increases global mean BC concentrations by 0.032 ng m^{-3} [mean ΔBC = 3.11%], resulting in an increase in the global BC burden by 0.49 Gg, with 28.70% (0.14 Gg) of this increase occuring in the cruise region of flight (Table 5.4).

Figure 5.11(c,d) shows that aviation induces a general global increase in OC, but with aviation-induced reductions in OC dominating in the NH about the cruise region of flight. Zonal decreases of up to –2.31 ng m^{-3} [min ΔOC = –7.75%] are simulated, while globally aviation is simulated to increase the mean global OC concentration by 0.013 ng m^{-3} [mean ΔOC = +1.10%]. This results in an aviation-induced increase in the global OC burden of 0.21 Gg, in tandem with a decrease in the cruise-level OC burden of –0.18 Gg (in relation to NOAVI) (Table 5.4).

Figure 5.11: Aviation-induced annual mean zonal absolute (left panes) and percentage (right panes) changes in black carbon (top panes) and organic carbon (bottom panes) concentrations resulting from the use of the CMIP5-extended aviation emissions inventory.

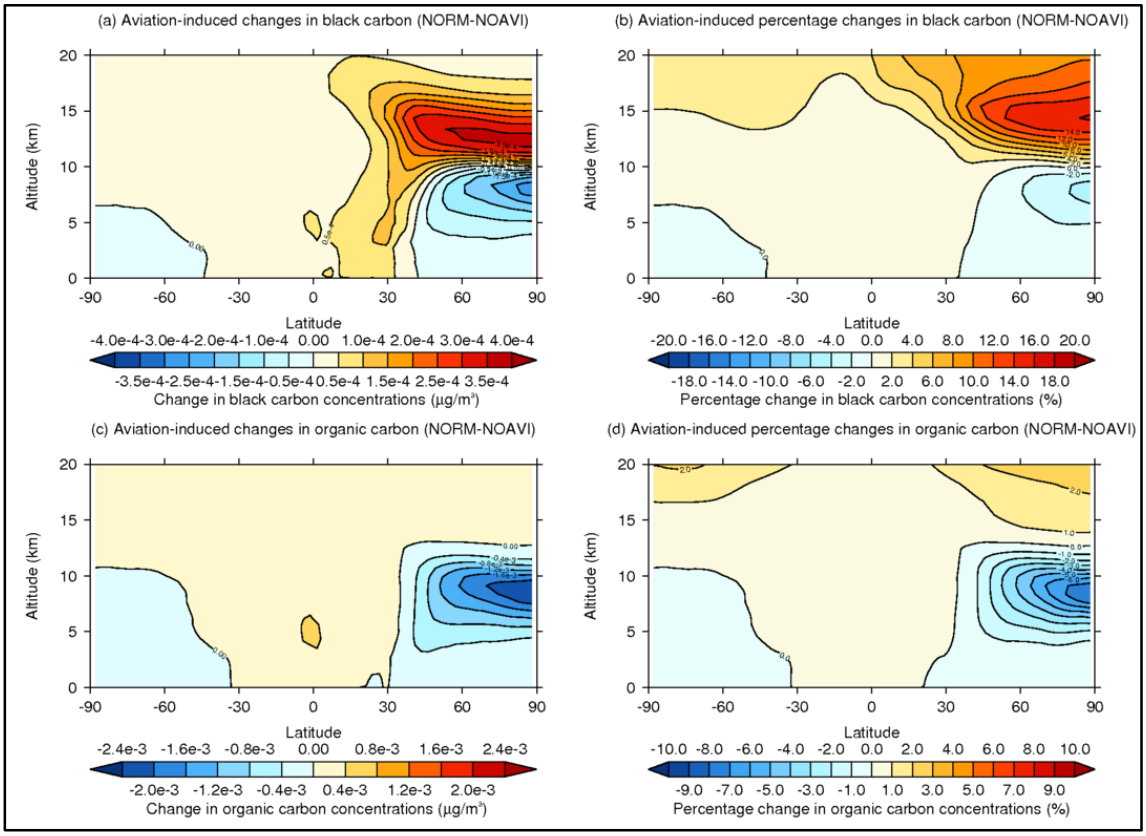

Decreases in BC and OC simulated in the NH between ~40°N–90°N (Figure 5.11) could be attributed to SO_2 emissions forming H_2SO_4 condensing on to BC and OC aerosols or through the process of aging, allowing these otherwise insoluble aerosol particles to move in to the soluble mode (Mann et al., 2010). When moved in to the soluble mode they can participate in CCN

formation, allowing these aerosol particles to participate in cloud formation, and the subsequent wet deposition of these particles.

Aviation emissions are also estimated to increase global surface $PM_{2.5}$ (particulate matter within the 2.5 μm size range) concentrations by 3.93 ng m^{-3}, resulting in a relative increase in global mean surface $PM_{2.5}$ concentrations of 0.10%. Though these global mean increases may seem small in comparison to the EU (European Union) $PM_{2.5}$ guidance limit of 10 μg m^{-3} as stipulated by the World Health Organisation (WHO, 2013) and the theoretical minimum-risk exposure distribution range of 5.8–8.8 μg m^{-3} (Lim et al., 2012), when regional surface mean values are considered the impact of aviation on surface $PM_{2.5}$ concentrations in made clearer. Over Europe aviation increases $PM_{2.5}$ concentrations by 20.34 ng m-3 [+0.26%], equating to 0.35% of the WHO EU guidance value. The impact of aviation on surface layer $PM_{2.5}$ concentrations and its resulting impact on human health via increases in premature mortality is discussed in far greater detail in Chapter 6.

5.4.1.1.3 Cloud condensation nuclei perturbations

Investigating the impact of aviation on the concentrations of cloud condensation nuclei (CCN) is of importance as these perturbations can cause aerosol cloud albedo effect (investigated later in Section 5.4.1.2.3). We estimate the concentration of CCN using the number concentration of soluble particles with a dry diameter of greater than 50 nm (Dp > 50 nm).

From the use of the CMIP5-extended aviation emissions inventory CCN concentrations are found to increase by up to 45.27 cm^{-3} [max ΔCCN = +8.35%] over the Himalayas at this model level, with considerable relative increases of between 1–3% over the Atlantic and Pacific oceans, and mean low-cloud level increase of 2.30 cm^{-3} (Figure 5.12). These increases over the Pacific and Atlantic oceans have the potential to induce cloud brightening, resulting in an increased albedo over that region (i.e. over the ocean body), resulting in a cooling effect, with the potential to induce a negative aerosol cloud albedo effect (aCAE). It has to be acknowledged that this primarily due assuming a low-cloud level of 0.96km and the model evaluates height using a hybrid sigma-pressure (σ-p) methodology (i.e. terrain tracking at the surface resolving to a pressure levels at the top of the model domain), which through the assumption of a set height/pressure level will most likely plot a region over the Himalayas which is not representative of where low-level clouds would reside. Thus a large amount of uncertainty will reside over this region.

Figure 5.12: Aviation-induced annual mean low-cloud level (left panes) zonal (right panes) absolute (top panes) and percentage (bottom panes) changes in CCN (Dp>50 nm) resulting from the use of the CMIP5-extended aviation emissions inventory: low-cloud level taken as 0.96 km.

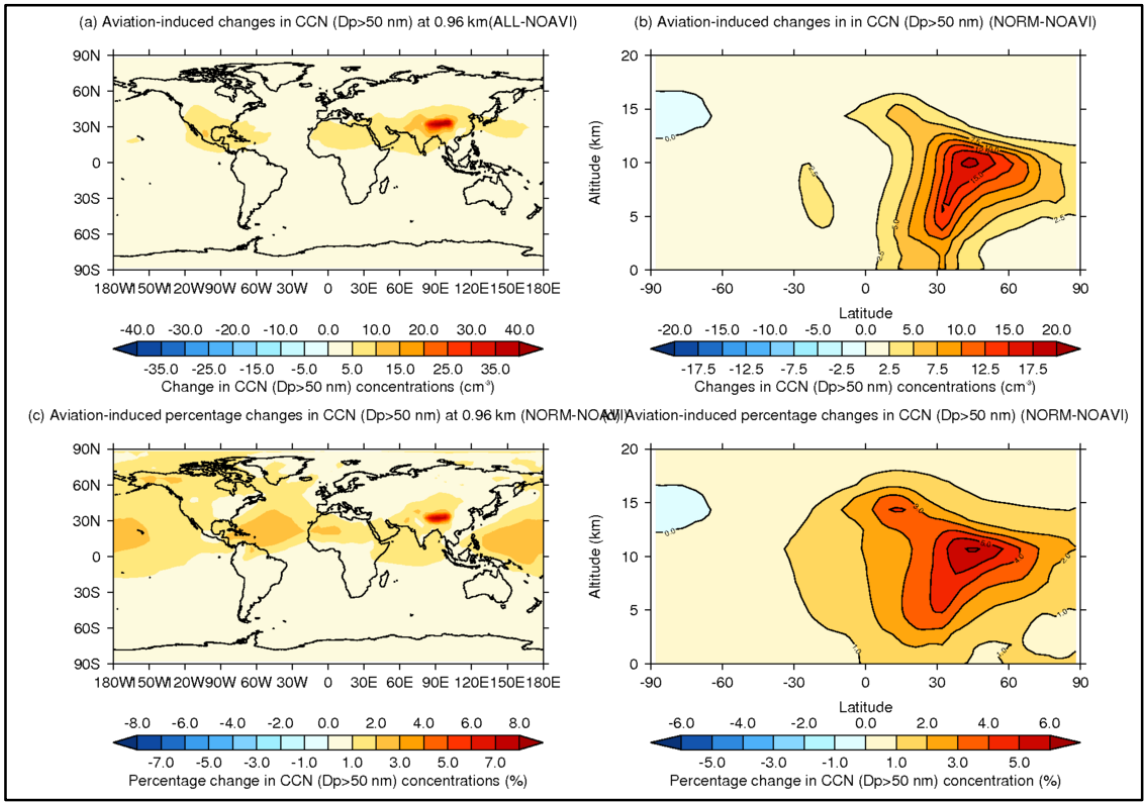

The greatest zonal impacts occur in line with the release of aviation-borne emissions, i.e. in the NH and at cruise-level, with zonal increases of up to 17.95 cm^{-3} [max ΔCCN =6.16%]; a region above low-cloud level.

5.4.1.2 Aviation-induced radiative effects (RE)

This section investigates aviation-induced radiative effects resulting from use of the CMIP5-extended aviation emissions inventory derived in Section 4.3 and investigated in the sections prior. Here the ozone direct radiative (O3DRE), aerosol direct radiative (aDRE) and aerosol cloud albedo (aCAE) effects are investigated, along with the combined radiative effect (RE_{comb}).

5.4.1.2.1 Ozone direct radiative effect (O3DRE)

Figure 5.13 presents the aviation-induced short-term O3DRE for year 2000, resulting from the use of the CMIP5-extended aviation emissions inventory within GMV4-nitrate. Here it is estimated that aviation emissions result in a global annual mean O3DRE of +8.86 mW m^{-2}. In line with the spatial pattern of the release of aviation emissions (Figure 5.3) the majority of the O_3 induced warming occurs over the NH; primarily between the latitudinal region between

20°N–50°N, over Europe, North America, Northern Africa and the Middle East. Overall aviation-induced O_3 is simulated to result in a warming effect over the entire globe. Globally the O3DRE ranges between 0.57–31.23 mW m^{-2}.

Figure 5.13: Aviation-induced ozone direct radiative effect (O3DRE) for year 2000.

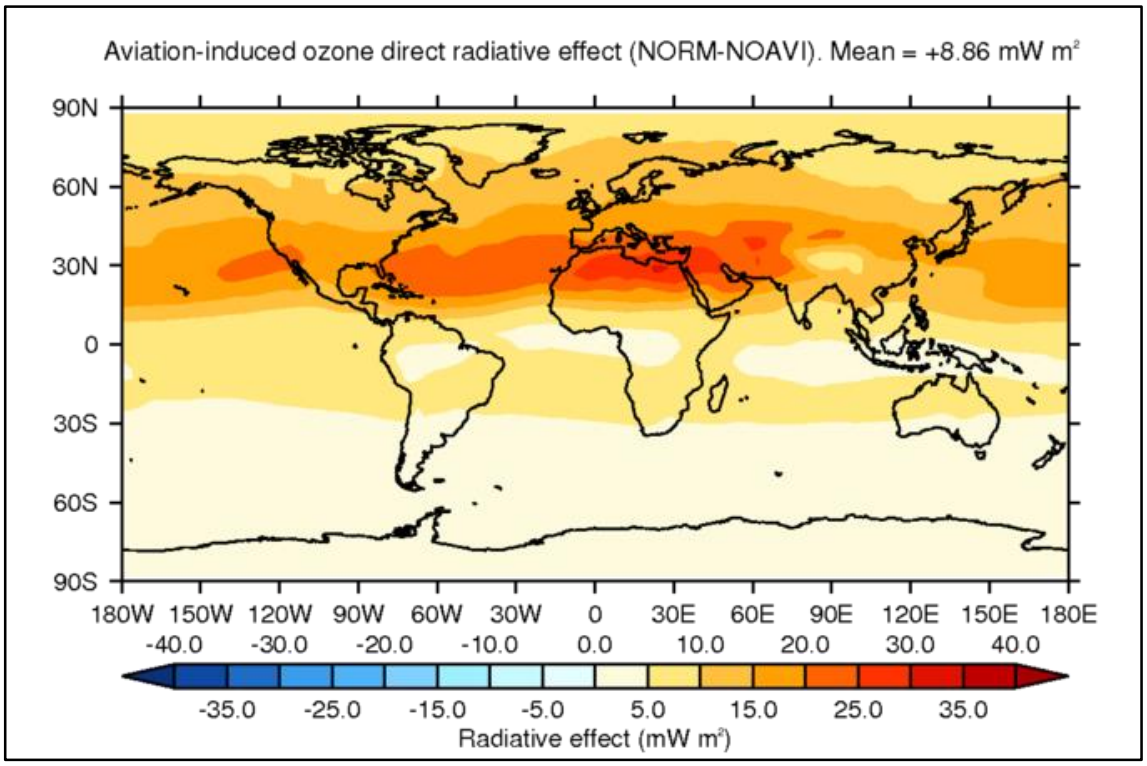

In order to compare the short-term O3DRE found from this study investigating the impact of using an extended aviation emissions inventory with previous work O3DREs are considered in terms of mW m^{-2} $Tg(N)^{-1}$. By normalising aviation-induced O3DREs in terms of aviation N emissions, differences between the total amounts of aviation NO_X/N emitted within each aviation emissions inventory can be accounted for. This study returns a O3DRE of 10.45 mW m^{-2} $Tg(N)^{-1}$; one of the lower values in the range [7.39–44.2 mW m^{-2} $Tg(N)^{-1}$] (Myhre et al., 2011; Holmes et al., 2011; Lee et al., 2009; Sausen et al., 2005; Frömming et al., 2012; Hoor et al., 2009; Unger, 2011; Unger et al., 2013; Khodayari et al., 2014a) presented in Figure 5.14.

The low O3DRE estimated by this study can be partially attributed to the higher OPEs (ozone production efficiencies) within the models/model ensembles considered to compile the comparison in O3DREs presented in Figure 5.14. GMV4-nitrate's OPE is evaluated as 1.34, in comparison to the range of 1–2.9 from recent work (Myhre et al., 2011; Unger, 2011; Wilkerson et al., 2010; Khodayari et al., 2014b).

Figure 5.14: Ozone direct radiative effect (O3DRE) from this study in comparison to estimates from literature: Short-term ozone (ST-O_3) RE considered alone (Unger et al., 2013; Khodayari et al., 2014a; Köhler et al., 2008; Myhre et al., 2011; Holmes et al., 2011; Hoor et al., 2009; Lee et al., 2009; Sausen et al., 2005; Frömming et al., 2012; Skowron et al., 2013).

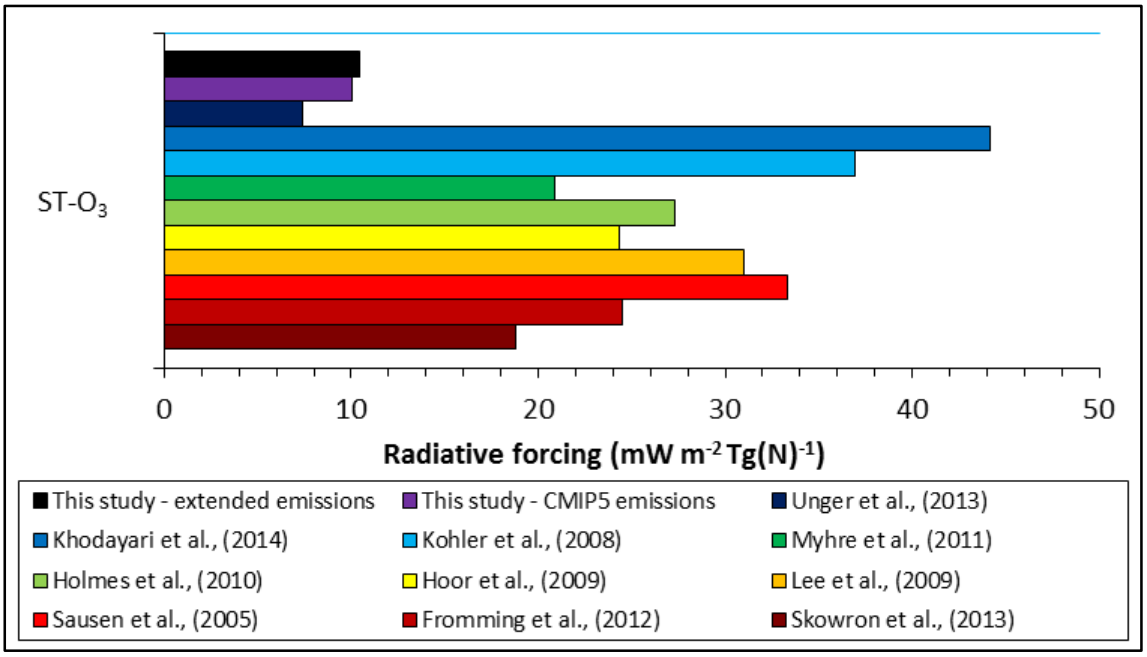

Taking in to account the O3DRE derived using the CMIP5-extended aviation emissions inventory an ensemble mean short-term O3DRE of 23.88 m^{-2} $Tg(N)^{-1}$ and σ=11.66 mW m^{-2} $Tg(N)^{-1}$ is calculated, in comparison to the ensemble mean short-term O3DRE of 25.10 m^{-2} $Tg(N)^{-1}$ and σ=11.39 mW m^{-2} $Tg(N)^{-1}$ calculated using the studies referred to in Figure 5.14.

5.4.1.2.2 Aerosol direct radiative effect (aDRE)

The resulting aviation-induced warming and cooling resulting from aviation emissions for year 2000 are presented in Figure 5.15. This study estimates that aviation emissions cause a global annual mean aDRE of +1.40 mW m^{-2}, i.e. induce a warming effect. As with the O3DRE, warming primarily occurs over the NH in line with the release of aviation emissions (Figure 5.3(d,e)). From Figure 5.15 the majority of warming occurs over North America, Europe and East Asia. In addition to the warming impact aDRE noticeable cooling effects are simulated over between 70°N–90°N, Eastern China, the Mediterranean Sea and the Western United States. Globally the aDRE ranges between –7.91 to 7.39 mW m^{-2}.

Comparing the aDRE estimated by this study with previous literature can be difficult as not all the same aerosol components are considered by each model, e.g. Gettelman and Chen (2013) only focus on sulfates and BC, while Unger (2011) considers the formation of sulfates, nitrates, BC and OC. In additional some models consider the aerosol components as internal mixtures

(Gettelman and Chen, 2013), while others consider them to be externally mixed (Unger, 2011). Differences in the modelled mixing state (i.e. whether aerosols are considered as externally or internally mixed) can affect the effective refractive index, water activity, and size distribution of aerosols calculated, which in turn impacts calculated aerosol optical properties and estimates in the aerosol direct radiative effect. In reality the real mixed state is expected to lie somewhere in between these two extremes (Lesins et al., 2002).

Figure 5.15: Aviation-induced aerosol direct radiative effect (aDRE) for year 2000.

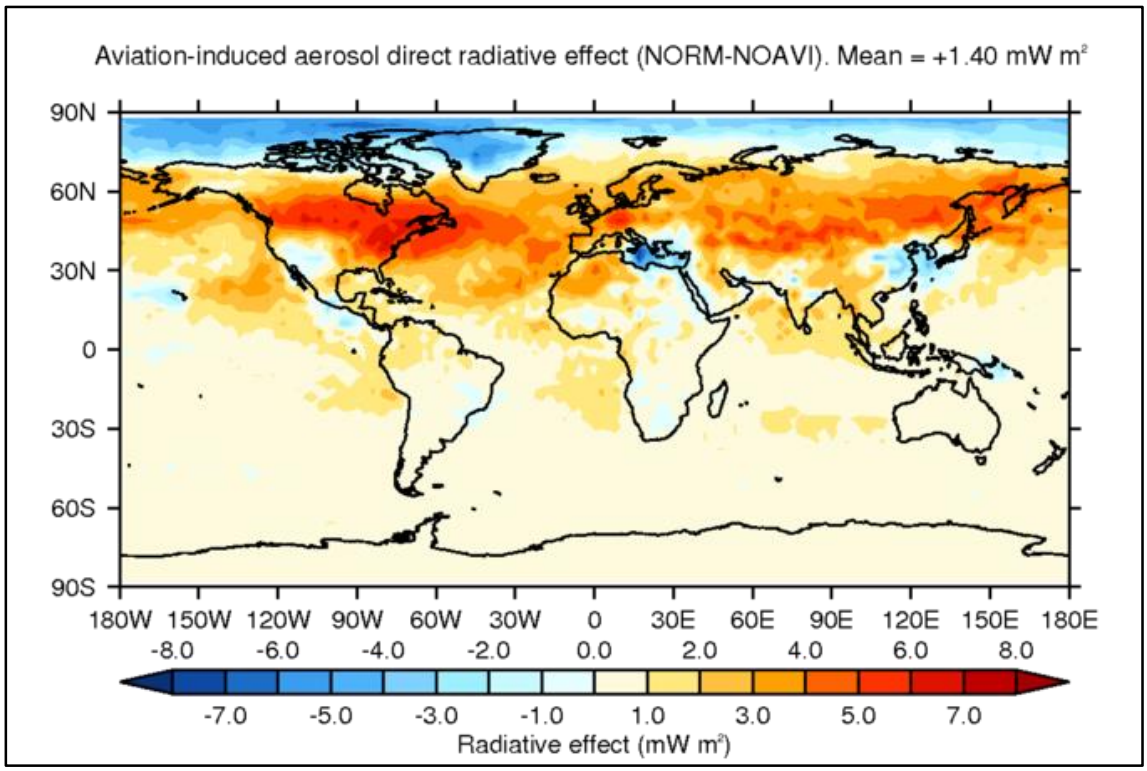

This study simulates a global annual mean aDRE of +1.4 mW m^{-2} in comparison to the range of +20 to –28 mW m^{-2} from previous literature (Sausen et al., 2005; Lee et al., 2009; Gettelman and Chen, 2013; Fuglestvedt et al., 2008; Balkanski et al., 2010; Unger, 2011; Unger et al., 2013; Righi et al., 2013) (Figure 5.16). When considering recent work referred to in Figure 5.16 (except for the range given by Righi et al. (2013)) in addition to the aDRE calculated here an ensemble mean aDRE of –2.26 mW m^{-2} and σ=3.62 mW m^{-2} is calculated (Sausen et al., 2005; Lee et al., 2009; Gettelman and Chen, 2013; Fuglestvedt et al., 2008; Balkanski et al., 2010; Unger, 2011; Unger et al., 2013).

The positive forcing estimated by this study in relation to the previous studies referred to in Figure 5.16 is likely due to the differences in aviation induced aerosol-phase specie burdens. Righi et al., (2013) found that aviation provided the following burden increases for year 2000 from the inclusion of aviation emitted NO_X, SO_2, sulfates and BC: Δsulfates = 3.2 Gg; ΔBC = 0.1 Gg; Δnitrates = –1.1 Gg; and ΔNH_4 = –0.2 Gg (Righi et al., 2013). Whereas this study finds the

following changes in the same aerosol-phase species: Δsulfates = 12.92 Gg; ΔBC = 0.51 Gg; Δnitrates = 5.66 Gg; and ΔNH_4 = 0.86 Gg. Along with burdens changes in sodium (ΔNa^+ = 1.45 Gg), dust (Δdust = –6.67 Gg) and chloride (ΔCl^- = –1.94 Gg).

Figure 5.16: Aerosol direct radiative effect (aDRE) from this study in comparison to estimates from literature (Sausen et al., 2005; Lee et al., 2009; Gettelman and Chen, 2013; Fuglestvedt et al., 2008; Balkanski et al., 2010; Unger, 2011; Unger et al., 2013).

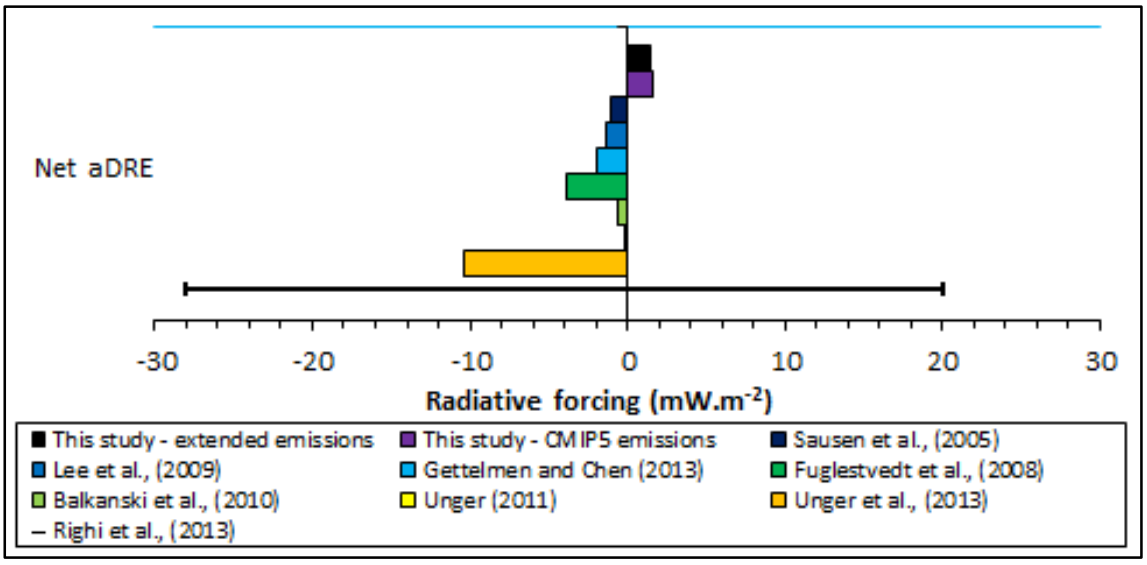

Based on the changes in burdens resulting from the year 2000 simulation conducted here in line with previous work it would be assumed that a negative aDRE would arise, but this study actually returns a positive aDRE. This is explained through treatment of aerosol species as internally mixed (Mann et al., 2010), which results in a greater BC warming effect through enhanced BC absorption (Balkanski et al., 2010).

5.4.1.2.3 Aerosol cloud albedo effect (aCAE)

The aCAE induced by aviation is presented in Figure 5.17. GMV4-nitrate simulates that through the use of the CMIP5-extended aviation emissions inventory developed here an annual global mean aCAE of –23.55 mW m^{-2} is simulated. Globally it is simulated that the aCAE ranges between –162.34 to 15.94 mW m^{-2}.

Akin to O3DRE and aDRE the main impacts of aviation emissions are seen in the NH, but unlike the O3DRE and aDRE the aCAE is shifted south, demonstrating a cooling aCAE between 30°S–60°N. The main cooling aCAE occurs over the Atlantic and Pacific oceans in line with aviation-induced perturbations in line with increases in CCN (Dp>50 nm) perturbations seen in Figure 5.12.

Figure 5.17: Aviation-induced aerosol cloud albedo effect (aCAE) for year 2000.

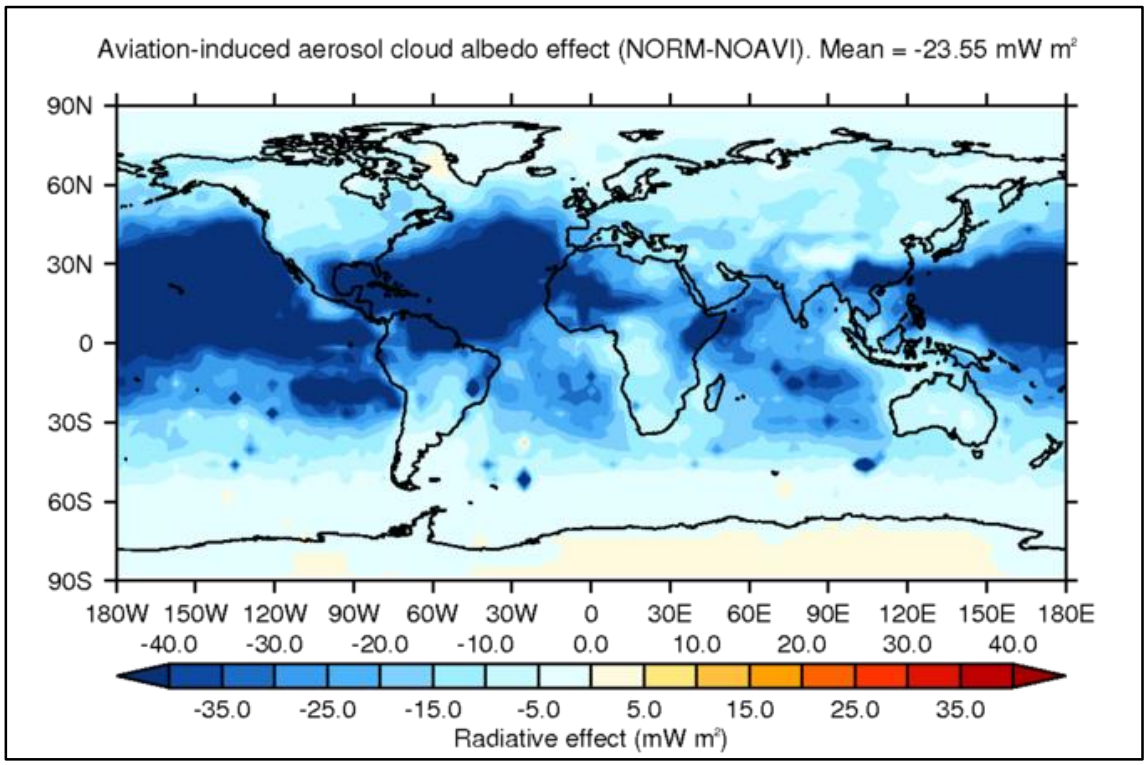

The aCAE derived in this study [–23.55 mW m^{-2}] is found to provide a greater cooling effect in comparison to the range provided by Righi et al. (2013) and Gettelman and Chen (2013) of –15.4 to –18 mW m^{-2}, but with the aCAE from this study lying within the range of uncertainty given by the aforementioned studies [–4.8 to –29 mW m^{-2}] – (Figure 5.18).

Figure 5.18: Aerosol cloud albedo effect (aCAE) from this study in comparison to estimates from literature (Gettelman and Chen, 2013; Righi et al., 2013).

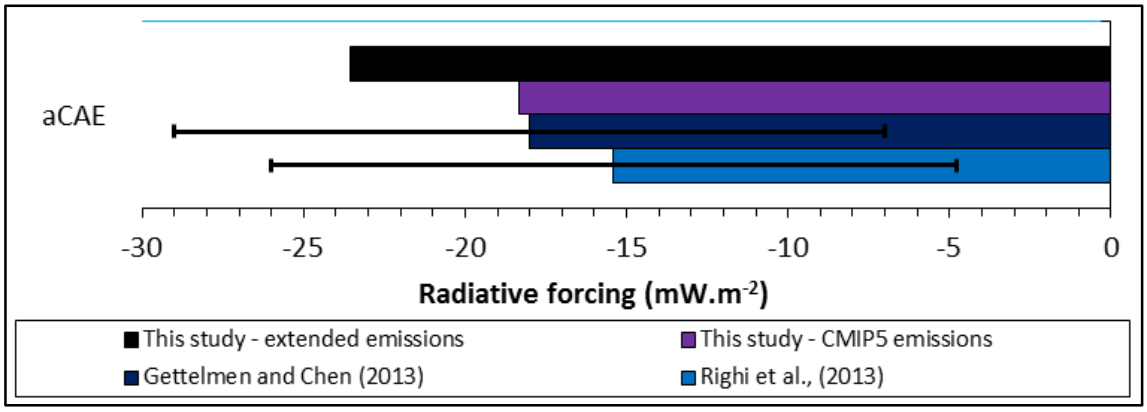

The level of variations between the aCAE found in this study and previous studies referred to in Figure 5.18 is explained by the different aerosol-phase species considered in each of the studies and the effects they have on cloud cover. Gettelman and Chen (2013) consider the effects of sulfates (cooling) and BC (warming) again treated as internally mixed, along with water vapour (warming). While here this study considers sulfates, nitrates, ammonium, organic carbon, black carbon, sodium and chloride from sea salt and dust.

5.4.1.2.4 Combined radiative effect (RE_{comb})

The annual global mean combined radiative effect (RE_{comb}) from O3DRE, aDRE and aCAE from the release of aviation non-CO_2 emissions is estimated at –13.29 mW m^{-2}, with warming effects dominating the NH and cooling effects dominating the equatorial and southern mid-latitude regions (Figure 5.19). The combination of the O3DRE, aDRE and aCAE effects result in RE_{comb} ranging between –159.87 and 24.20 mW m^{-2}. Figure 5.19 shows that the component radiative effects which contribute most to the overall combined radiative effect (RE_{comb}) are the O3DRE and aCAE; where their respectively influences are clearly seen in the NH between 60°N–30°S.

Figure 5.19: Aviation-induced combined radiative effect (RE_{comb}) for year 2000.

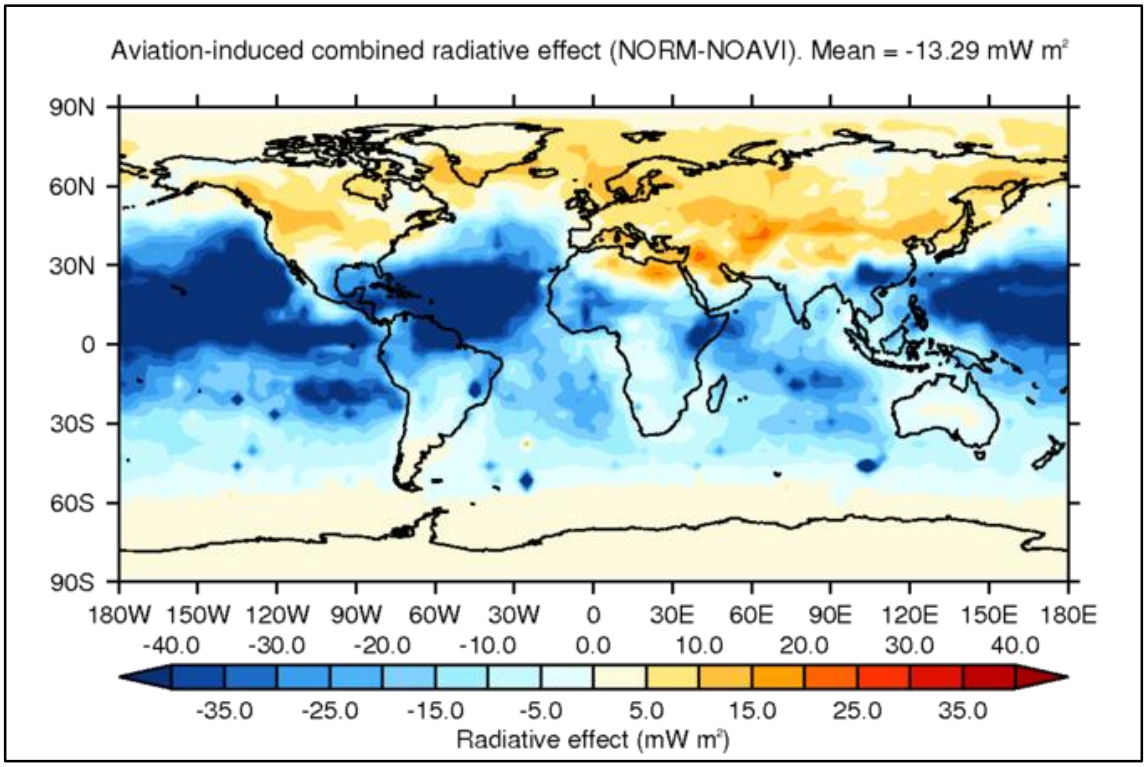

Figure 5.20 summarises how the O3DRE, aDRE and aCAE and RE_{comb} found in this investigation compare to previous estimates. Using ranges in estimates from current literature for the O3DRE [6–36.24 mW m^{-2}], aDRE [–28 to +20 mW m^{-2}], aCAE [–29 to +4.8 mW m^{-2}] current literature provides a broad range for the RE_{comb} of –51 to 51.44 mW m^{-2} (when low and high end estimates are considered) (Unger et al., 2013; Khodayari et al., 2014a; Köhler et al., 2008; Myhre et al., 2011; Holmes et al., 2011; Hoor et al., 2009; Lee et al., 2009; Sausen et al., 2005; Frömming et al., 2012; Skowron et al., 2013; Gettelman and Chen, 2013; Fuglestvedt et al., 2008; Balkanski et al., 2010; Unger, 2011; Righi et al., 2013); a range in which estimates in O3DRE, aDRE, aCAE and REcomb made here fit in to.

Figure 5.20: Combined (RE_{comb}) and component (O3DRE, aDRE and aCAE) component radiative effects from this study: Black bars highlight range of estimates from existing published literature.

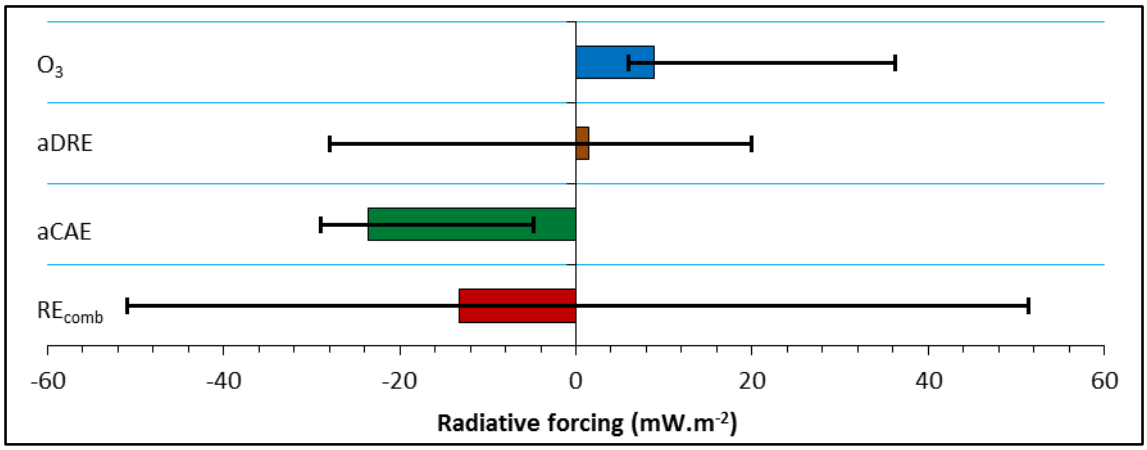

5.4.2 Comparison of aviation-induced impacts from an CMIP-extended aviation emissions inventory with CMIP5-recommended aviation emissions

This section investigates and quantifies the impact of the use of an extended aviation emissions inventory (as derived in Section 4.3) represented by the NORM simulation (Table 5.2) in relation to CMIP5 recommended aviation emissions (CMIP5 simulation) for the year 2000 (Lamarque et al., 2010b). This investigation is carried out in two parts: investigation of atmospheric perturbations in gas- and aerosol-phase species; and investigation of the impacts these perturbations have on the resulting radiative impacts (O3DRE, aDRE, aCAE and RE_{comb}).

5.4.2.1 Aviation-induced atmospheric perturbations: comparison of CMIP5-extended and CMIP5-recommnded aviation emissions

Through investigating concentration differences in atmospheric gas- and aerosol-phase species between the NORM and CMIP5 simulations, indications on how the inclusion of additional emission species can effect aviation REs can be gained.

5.4.2.1.1 Gas-phase perturbations

When investigating the impact of the inclusion of CO, speciated HCs, SO_2 and OC emissions on the atmospheric concentrations of gas-phase species (i.e. the use of CMIP5-extended in relation to CMIP5), the following differences are seen (Figure 5.21). Annual zonal mean NO_X concentrations are reduced by –0.07% [mean ΔNO_X = –0.19 pptv], ozone is increased by +0.02% [mean ΔO_3 = +20.61 pptv], OH increased by +0.02 % [mean $\Delta OH = +1.42 \times 10^{-5}$ pptv], and HNO_3 concentrations increase by +0.08% [mean ΔHNO_3 = +0.36 pptv].

Figure 5.21: Aviation-induced annual mean zonal percentage changes in (a) NO_X, (b) O_3, (c) OH, (d) HNO_3, (e) HONO, (f) PAN, (g) SO_2 and (h) H_2SO_4 representing the difference between the use of the CMIP5-extended and CMIP5 aviation emissions inventories.

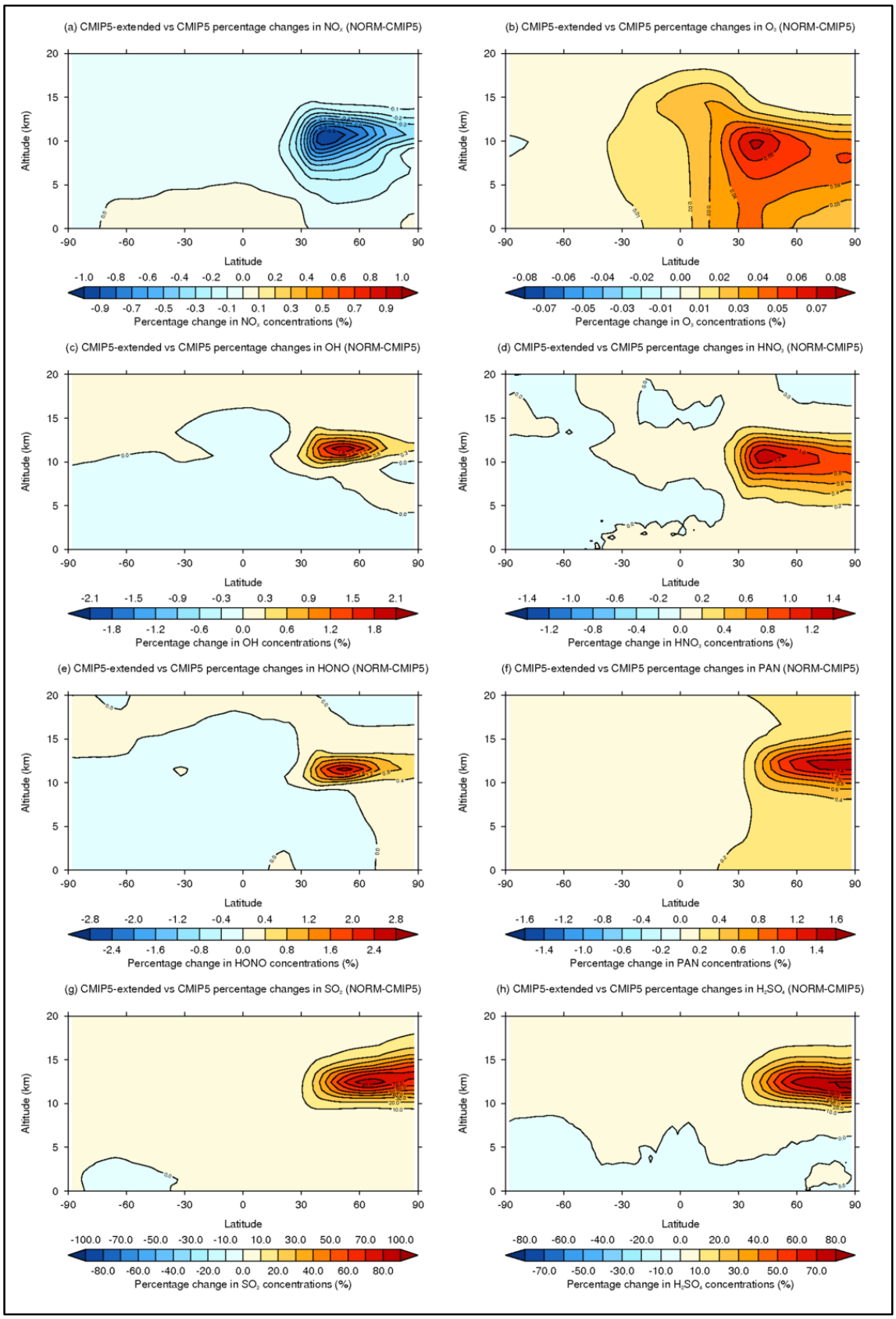

Potential NO_X reservoir species HONO and PAN annual zonal mean concentrations are increased by +0.03% [mean ΔHONO = $+7.03x10^{-5}$ pptv] and +0.15% [mean ΔPAN = +0.12 pptv] respectively. While SO_2 and H_2SO_4 (species which are important for the formation of new particles and the aging of particles) see increases in their annual zonal concentrations of +3.58% [mean ΔSO_2 = +0.62 pptv] and +3.25% [mean ΔH_2SO_4 = $+8.23x10^{-5}$ pptv].

Increases in O_3, OH, HNO_3, HONO, PAN, SO_2, H_2SO_4 and decreases in NO_X are simulated when using CMIP-extended in comparison to CMIP5 recommended emissions, with peaks occurring in the NH cruise-level region of flight – in agreement with the release of aviation emissions (Figure 5.2). Decreases in NO_X can be partially attributed to introduction of HCs aiding in increased PAN formation and through increased O_3 formation via HC initiated HO_2 production (Section 2.3.3). The impact of the inclusion of aviation-borne CO, speciated HCs, SO_2 and OC on global and cruise-level gas-phase species burdens is presented in Figure 5.4.

In line with the changes in annual zonal mean distributions shown in Figure 5.21, decreases in the global NO_X burden is simulated across the complete global domain [–0.98 Gg] and along the altitudinal band relating to the cruise-level of flight [–0.58 Gg] (Table 5.5).

Table 5.5: Differences in aviation-induced gas-phase species burdens resulting from the use of an extended emissions inventory (CMIP5-extended in relation to CMIP5 recommended) within the full and cruise-level domains for year 2000.

Study and domain	NO_X (Gg)	O_3 (Tg)	OH (Mg)	PAN (Gg)	HONO (Mg)	HNO_3 (Gg)	SO_2 (Gg)
Full domain	-0.98	0.14	0.02	1.86	0.27	2.65	5.65
Cruise level	-0.58	0.05	0.04	0.65	0.57	2.09	3.64

As previously discussed OH and O_3 formation is dependent on NO_X emissions (Fowler et al., 1997; Jenkin and Clemitshaw, 2000; Hoor et al., 2009; Myhre et al., 2011; Lee et al., 2010) along with emissions of CO and HCs (Lee et al., 2010; Fowler et al., 1997; Jenkin and Clemitshaw, 2000) (Section 2.3.1, Section 2.3.2 and 2.3.3). Thus from the emission of CO and speciated HCs, a reduction in NO_X is seen, along with increases in the global burdens of O_3 [+0.14 Tg] and OH [+0.02 Mg] (Table 5.5). As the production of HNO_3, PAN and HONO are functions of NO_X concentrations (Section 2.3.1.4) (Fowler et al., 1997; Jenkin and Clemitshaw, 2000), decreases in aviation-induced NO_X burdens are accompanied by increases in aviation-induced burdens of HNO_3, PAN and HONO [ΔHNO_3 burden = +2.65 Gg; ΔPAN burden = +1.86 Gg; ΔHONO burden = +0.27 Gg]. Additionally increased PAN formation and reductions in NO_X

will also be a result of the introduction of aviation emitted HCs (Fowler et al., 1997; Jenkin and Clemitshaw, 2000).

A difference in global SO_2 burdens of 5.65 Gg is simulated between the NORM and CMIP5 simulations (Table 5.5). For the NORM case (which uses the CMIP5-extended aviation emissions inventory) a global burden of 1.06 Gg is simulated, while for the CMIP5 case (which uses CMIP5 recommended aviation emissions) a change in the global SO_2 burden in relation to the NOAVI case of –4.59 Gg is simulated; due to the effect of aviation NO_X reacting with SO_2 from other anthropogenic (and natural) sources (Barrett et al., 2010).

5.4.2.1.2 Aerosol-phase perturbations

The inclusion of CO, speciated HCs, SO_2 and OC emissions results in the changes in atmospheric concentrations of the aerosol-phase species seen in Figure 5.22, i.e. representing the impact of the use of the CMIP5-extended emissions inventory (NORM simulation) in relation to the use of the CMIP5 recommended emissions inventory (CMIP5 simulation).

Annual zonal mean sulfate concentrations are increased by +0.73% [mean Δsulfate = +1.04 ng m^{-3}], accompanied by decreases in nitrate concentrations of –0.12% [mean Δnitrate = –0.07 ng m^{-3}]. This trade-off between increases in sulfate concentrations and the reduction in nitrate concentrations can be explained by the relationship between the formation mechanisms governing the two aerosol species along with the low ammonia concentrations in this region (Bauer et al., 2007). In line with the magnitude in increases in aviation-induced sulfates between the NORM and CMIP5 simulations in relation to the decreases in aviation-induced nitrates, comparison of the NORM and CMIP5 simulations result in an increase in ammonium concentrations of +0.21 [mean Δammonium = +0.08 ng m^{-3}].

When considering the differences between the NORM and CMIP5 simulations on BC and OC perturbations the main increases in concentrations are simulated over the NH at the cruise-level of flight, while over the rest of the zonal domain reductions are seen. Regional reductions in BC and OC can partly explained through effect of the inclusion of SO_2 emissions. SO_2 emissions will form H_2SO_4, which can condense on to the BC and OC particles enabling BC and OC aerosol particles to move from the insoluble mode to soluble, allowing them to participate in CCN formation, and BC and OC aerosol particles being subsequently rained-out, hence the decreases seen. In the regions where BC decreases and H_2SO_4 increases, the reductions in BC are small ~0.5% in comparison to increases in H_2SO_4 (~10%). Overall this results in an increase

in annual zonal mean BC concentrations of +0.18% [mean ΔBC = +0.005 ng m^{-3}] and increase in annual mean OC concentrations of +0.08% mean [ΔOC = +0.015 ng m^{-3}].

Figure 5.22: Aviation-induced annual mean zonal percentage changes in (a) sulfates, (b) nitrates, (c) ammonium, (d) black carbon, and (e) organic carbon, representing the difference between the use of the CMIP5-extended and CMIP5 aviation emissions inventories.

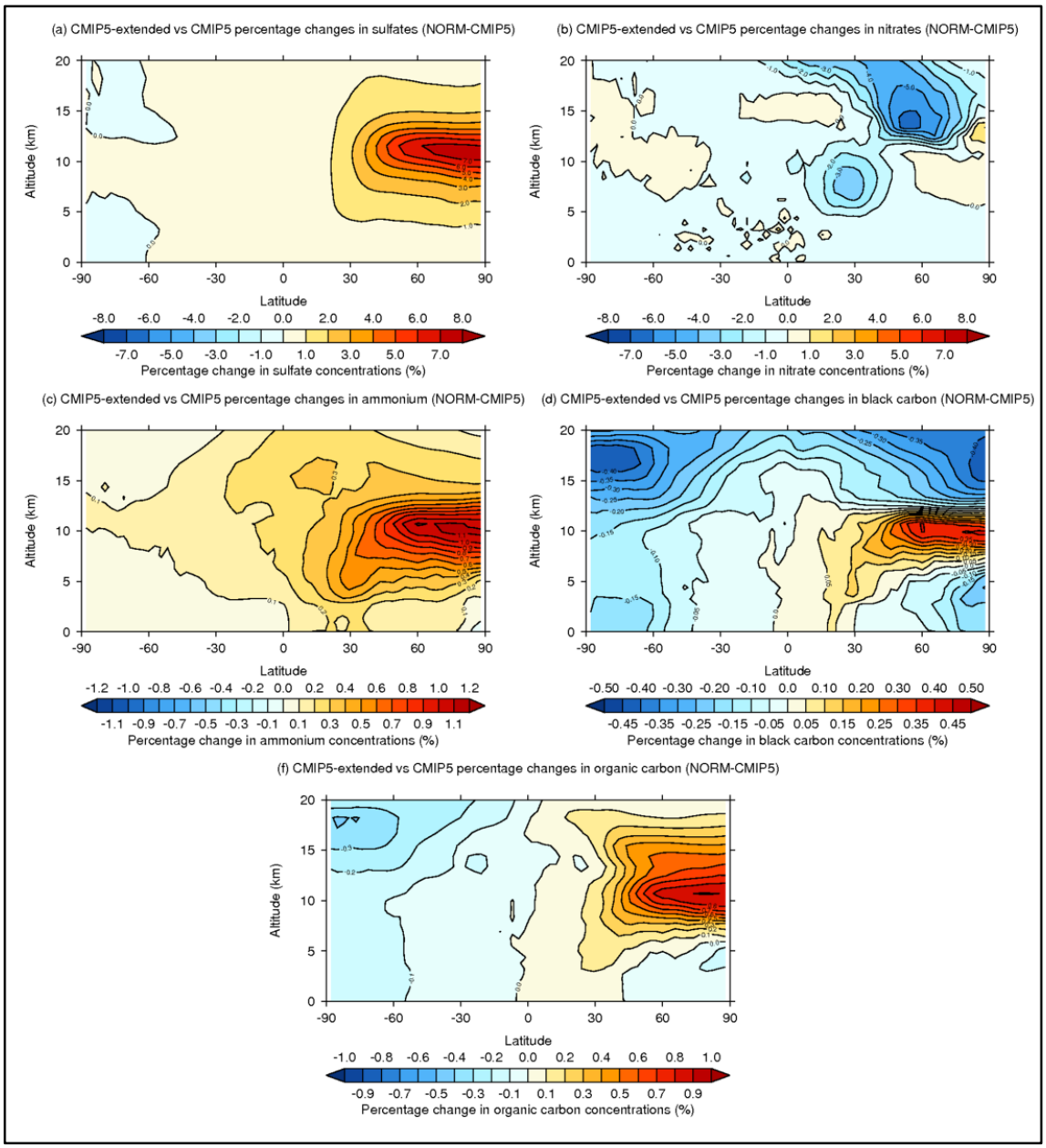

In line with the annual zonal means presented in Figure 5.22 increases in the global burdens in sulfate [+9.22 Gg], ammonium [+0.55 Gg], BC [+0.004 Gg] and OC [+0.15 Gg] and decreases in the global burden of nitrates [–0.21 Gg] are found when the CMIP5-extended emissions inventory is used in comparison to the CMIP5 recommended emissions inventory (Table 5.6).

Table 5.6: Differences in aviation-induced aerosol-phase species burdens resulting from the use of an extended emissions inventory (CMIP5-extended in relation to CMIP5 recommended) within the full and cruise-level domains for year 2000.

Domain	Sulfates (Gg)	Nitrates (Gg)	Ammonium (Gg)	BC (Gg)	OC (Gg)
Full domain	9.22	-0.21	0.55	0.004	0.15
Cruise level	3.68	-0.09	0.12	0.007	0.09

When focusing on the cruise-level of flight a similar trend is seen with increases in sulfates [+3.68 Gg], ammonium [+0.12 Gg], BC [+0.007 Gg] and OC [+0.09 Gg], while decreases in nitrates [–0.09 Gg] are returned (Table 5.6).

5.4.2.1.3 Cloud condensation nuclei perturbations

Figure 5.23(a) shows how the inclusion of additional aviation-borne emission species increases in CCN (Dp>50 nm) concentrations are seen at low-cloud level, with greatest increases seen over the Pacific and Atlantic oceans. At low-cloud level mean increases in CCN (Dp>50 nm) of 0.17 cm^{-3} [0.44%] result – when comparing the use of the CMIP5-extended aviation emissions inventory to the CMIP5 recommended aviation emissions inventory (Figure 5.23(a)).

In line with the release of the majority of aviation emissions between 8–12 km in the NH, annual zonal mean CCN (Dp>50 nm) peak within that region. An annual zonal mean increase in CCN (Dp>50 nm) of 0.78 cm^{-3} [0.41%] results from the inclusion of these additional aviation emitted species (Figure 5.23(b)).

Figure 5.23: Aviation-induced annual mean (a) low-cloud level and (b) zonal percentage difference in CCN (Dp>50 nm) representing the difference between the use of the CMIP5-extended and CMIP5 aviation emissions inventories: low-cloud level taken as 0.96 km.

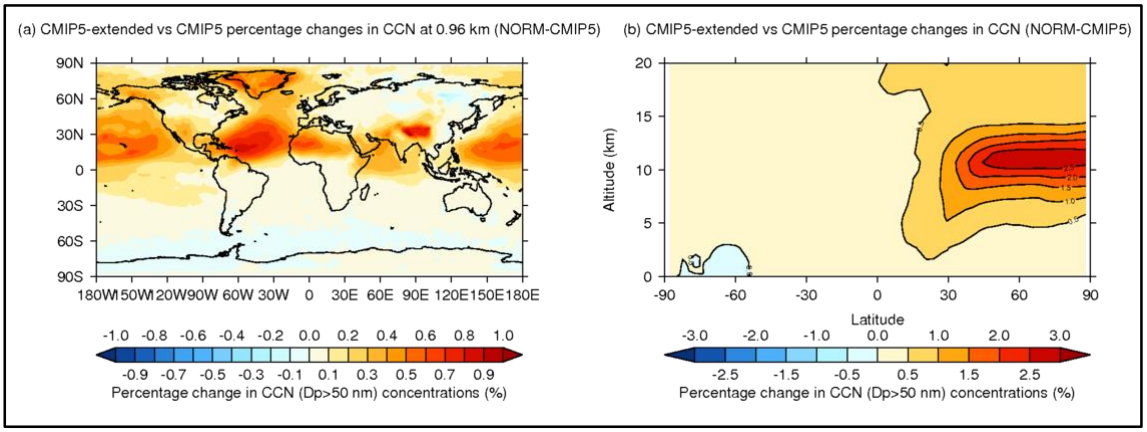

Differences in aviation-induced CCN (Dp>50 nm) perturbations between the NORM and CMIP5 simulations indicate that through the inclusion of additional aviation-emitted species (such as SO_2), aviation has the potential to increase the aviation-induced cooling effect; resulting from sulfates enhancing the cooling effect of the aerosol cloud albedo effect (aCAE) – which further investigated in Section 5.4.2.2.

5.4.2.2 Aviation-induced radiative effects (RE): comparison of CMIP5-extended and CMIP5-recommended aviation emissions

In line with the increases in atmospheric O_3 resulting from the use of the CMIP5-extended emission inventory in comparison to CMIP5 recommended aviation emissions (NORM–CMIP5) an increase in the O3DRE is seen [mean ΔO3DRE = +0.35 mW m^{-2}] (Figure 5.24(a)). This increase in the O3DRE is a result of the inclusion of CO and speciated hydrocarbons (Fowler et al., 1997; Jenkin and Clemitshaw, 2000). This effect on the O3DRE indicates through the use of the CMIP5 emissions inventory alone aviation results in a mean O3DRE of +8.51 mW m^{-2} (Figure 5.25(a)).

Figure 5.24: Difference in aviation-induced radiative effects simulated when considering the use of the CMIP5-extended aviation emissions inventory in relation to CMIP5 recommended aviation emissions inventory: (a) O3DRE, (b) aDRE, (c) aCAE, and (d) RE_{comb}.

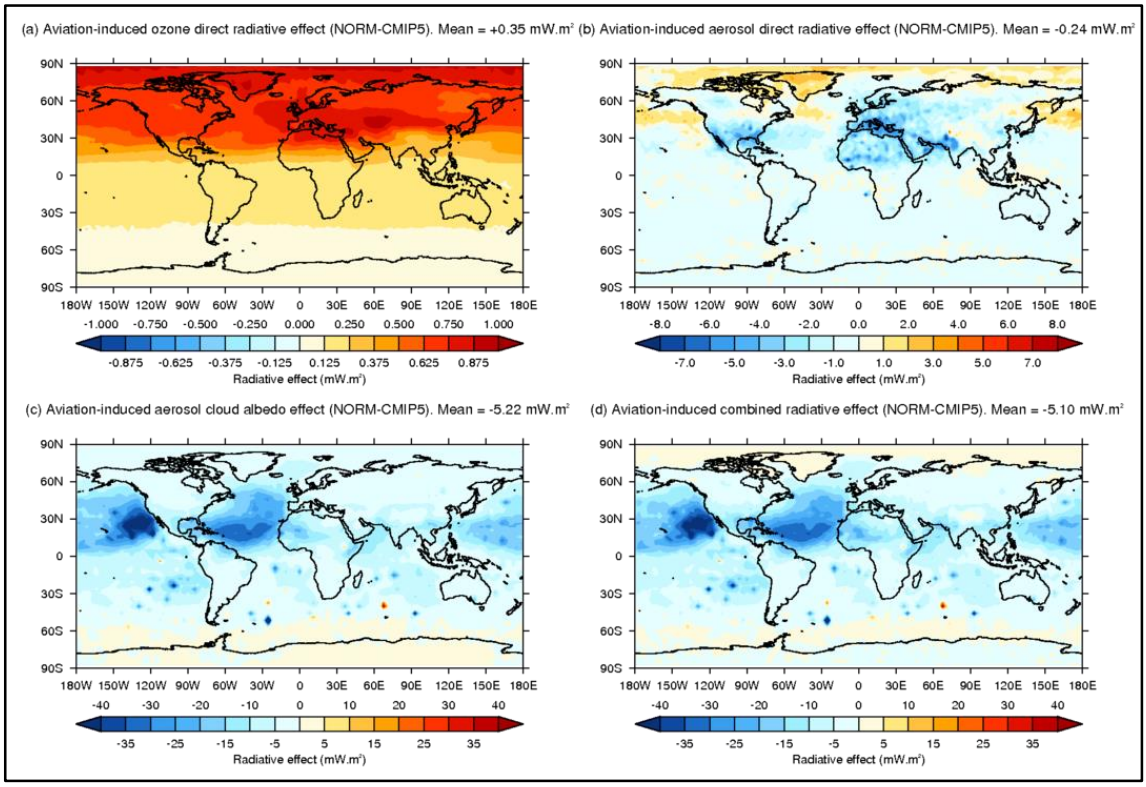

This comparison (NORM–CMIP5) finds that through the inclusion of additional aviation emitted species (such as SO_2) the mean aDRE from aviation is reduced by –0.24 mW m^{-2} (Figure 5.24(b))

in comparison to the aDRE from CMIP5 emissions alone [mean aDRE = +1.64 mW m^{-2}] (Figure 5.25 (b)). This reduction is primarily driven by the inclusion of SO_2 emissions which through the formation of sulfates impart a cooling effect through the scattering of incoming solar radiation (Boucher et al., 2013). This difference in aDRE is in line with the differences in aviation-induced sulfates, nitrates, ammonium, BC and OC seen between the use of CMIP5-extended and CMIP5 aviation emissions (Figure 5.22).

Figure 5.24 (c) shows that the use of CMIP5-extended emissions inventory provides an additional –5.22 mW m^{-2} of cooling through the aCAE (NORM–CMIP5), in comparison to CMIP5 emissions driven case (CMIP5) which simulates a global annual mean aCAE of –18.33 mW m^{-2} (Figure 5.25(c)). When considering the increases in CCN (Dp>50 nm) concentrations seen at low-cloud level in Figure 5.23(a) due to the inclusion of additional aviation emission species (NORM–CMIP5) this enhanced cooling from the aCAE would be expected.

Figure 5.25: Aviation-induced radiative effects simulated when considering the use of CMIP5 recommended aviation emissions inventory: (a) O3DRE, (b) aDRE, (c) aCAE, and (d) RE_{comb}.

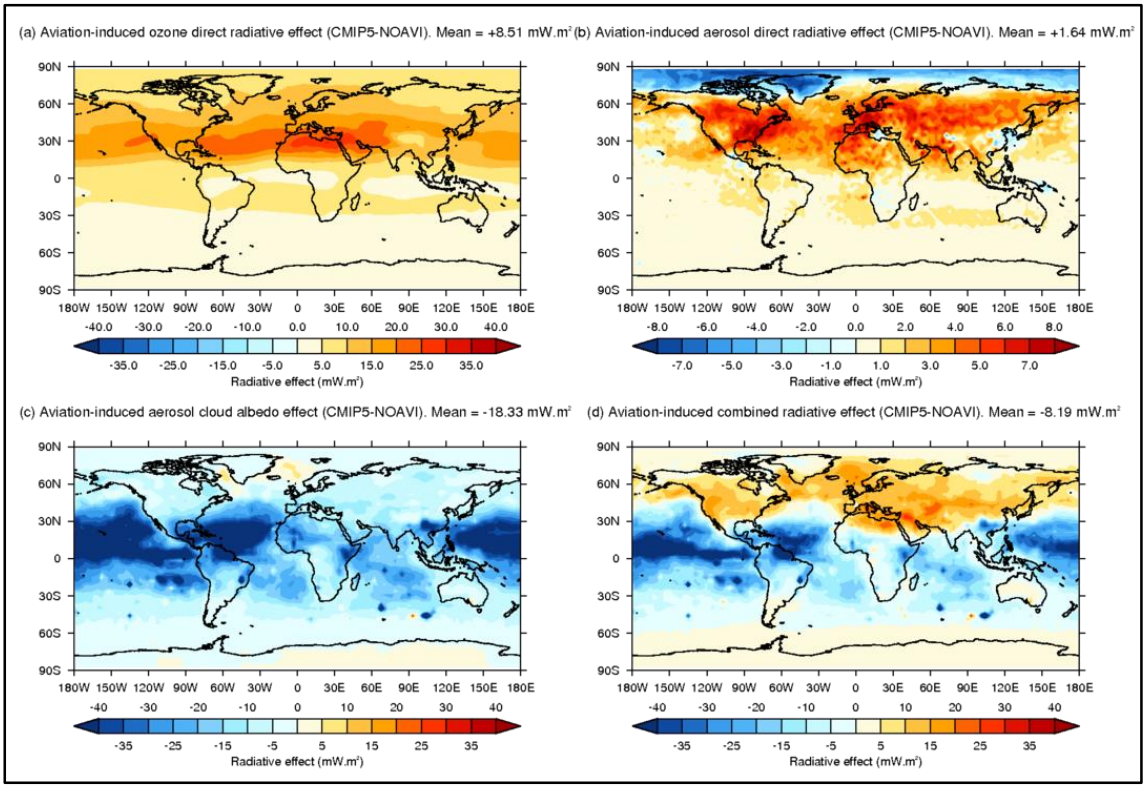

Overall the use of the CMIP5-extended aviation emissions inventory developed in Section 4.3 changes the annual global mean RE_{comb} by –5.10 mW m^{-2} (Figure 5.24(d)) in comparison to when CMIP5 emissions are used (i.e. CMIP5 simulation), which returns a RE_{comb} of –8.19 mW m^{-2} (Figure 5.25 (d)). It should be noted that the large overall RE_{comb} signal is due to the cancellation effects of large positive and negative signals, thus demonstrating that small changes in concentrations have large radiative effects.

5.4.3 Sensitivity studies: evaluating the impact of carbon monoxide, speciated hydrocarbons and sulfur dioxide emissions

This section investigates the impact of including aviation CO, speciated HCs and SO_2 emissions to the atmospheric and climatic impacts of aviation emissions; thus aiming to identify and demonstrate the importance of including different aviation emissions species within an aviation emissions inventory.

5.4.3.1 The impact of aviation-borne carbon monoxide (CO) emissions

Here the impact of a sensitivity experiment considering the omission of aviation CO emissions from the CMIP5-extended emissions inventory is investigated (NoCO). Figure 5.26(a) indicates that if aviation CO emissions are excluded a RE_{comb} of –13.76 mW m^{-2} results, dominated by reductions in the O3DRE of (–)0.13 mW m^{-2} and enhanced cooling from the aCAE of (-)0.32 mW m^{-2}, accompanied by a small change in the aDRE of –0.02 mW m^{-2}. Surmised, exclusion of aviation CO emissions can result in an enhanced estimation in the net cooling effect resulting from the aviation RE_{comb} (ΔRE_{comb} = –0.47 mW m^{-2}).

Reductions in the O3DRE are due global mean reductions in aviation-induced O_3 concentrations of (–)0.003%. This small reduction in O_3 concentrations is due to the near null ozone production cycle driven by CO emissions (Wayne, 2000) (i.e. CO emissions have little effect), but most importantly indicating that O_3 production is NO_X limited in the region aviation emissions are introduced. The small decreases in the aDRE and aCAE simulated can be explained by the small increases in scattering aerosols such as sulfates [Δsulfates = +0.17%; +0.018 ng m^{-3}], nitrates [Δnitrates = +0.21%; 0.008 ng m^{-3}], ammonium [Δammonium = +0.18%; +0.001 ng m^{-3}] and, organic carbon [ΔOC = +0.44%; 0.002 ng m^{-3}]. In addition to increases in scattering aerosol concentrations, increases in the absorbing aerosol BC are simulated [ΔBC = +0.48%; +0.001 ng m^{-3}]. These increases in aerosol burdens can be attributed to increases in the global aviation-induced OH burden of $6.7x10^{-2}$ Mg(OH).

Aviation-borne CO emissions effect sulfate and nitrate concentrations (i.e. increase their concentrations) through increases in HO_2 (Reaction 2.21 and Reaction 2.22), which can result in increases concentrations of NO_2 and OH (Reaction 2.1). These resulting increases in NO2 and OH concentration can contribute to increases in HNO_3 (Reaction 2.2), required for the formation of ammonium nitrate (Reaction 2.20). While CO induced increases in OH can aid in the production of H_2SO_4 (Reaction 2.29 to Reaction 2.31) which can go on to produce ammonium sulfate (Reaction 2.23 and Reaction 2.24). Additionally, CO-induced H_2SO_4 can aid

in reduction of atmospheric concentrations of BC and OC, via the condensation of H_2SO_4 on to BC and OC aerosol particles enabling them to be treated as soluble aerosol particles.

Figure 5.26: Differences in aviation-induced radiative effects [O3DRE, aDRE, aCAE and REcomb] when considering the omission of aviation-borne (a) carbon monoxide (NoCO), (b) speciated hydrocarbons (NoHCs), and (c) sulfur dioxide ($NoSO_2$) emissions in relation to the CMIP5-extended aviation emissions inventory.

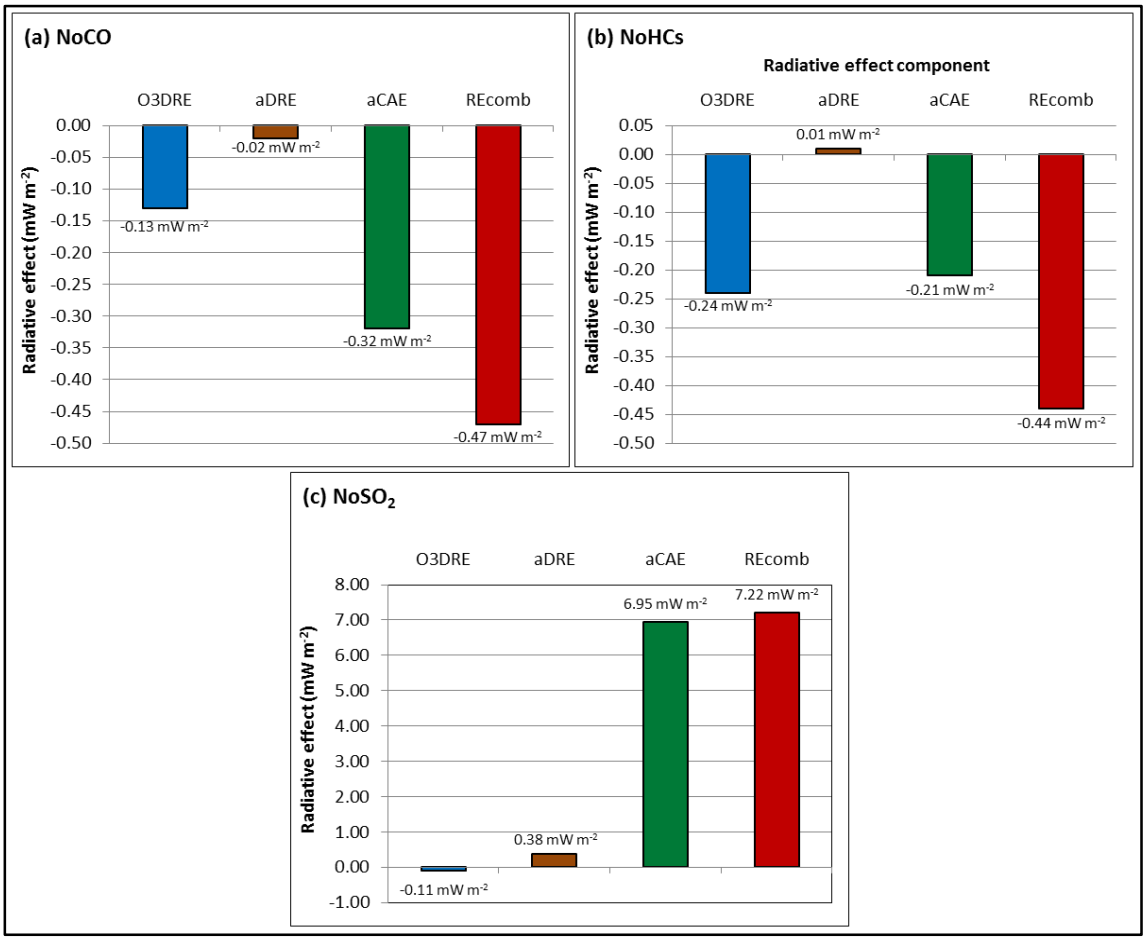

From these sensitivity study aviation CO emissions are estimated to contribute towards to 1.47% of the aviation-induced O3DRE, while decreasing the aviation aDRE by 1.43% and increasing the aviation-induced aCAE by 1.36%. Changes driven by the NoCO sensitivity run within all aviation RE components together results in a net increase in aviation non-CO_2 emission induced cooling RE_{comb} of 3.54%.

5.4.3.2 The impact of aviation-borne speciated hydrocarbon (HCs) emission

Figure 5.26(b) presents the impact on aviation-induced RE effect components (O3DRE, aDRE, aCAE and RE_{comb}) when aviation-borne speciated HC emissions are not included within an aviation emissions inventory. Here is seen that the exclusion of aviation HC emissions reduce the estimates in O3DRE by (–)0.24 mW m^{-2}, increases aDRE estimates by (+)0.01 mW m^{-2} and

reduces the aCAE by (–)0.21 mW m^{-2}. Akin to the NoCO simulations, the exclusion of speciated HCs (NoHCs), results in a possible overestimation in the net cooling effect resulting from aviation [RE_{comb} = –13.73 mW m^{-2}; ΔRE_{comb} = –0.44 mW m^{-2}].

The greater reductions in the O3DRE resulting from the NoHCs sensitivity run in comparison to the NoCO sensitivity run is a result of the greater reductions in aviation-induced O_3 concentrations of (–)0.005% [–15.17 pptv]. The NoHCs sensitivity simulation estimates that aviation-borne HC emissions contribute to 2.71% of the aviation O3DRE impact. This higher impact on aviation-induced O_3 is due to the considerable impact the inclusion of HC chemistry has on evaluating O_3 estimates despite the lower relative emissions of aviation-HCs in comparison to other aviation emitted species (Lee et al., 2010; Kentarchos and Roelofs, 2002).

Here small increases in the aDRE are seen [+0.71%] due to smaller increases (in relation to the NoCO sensitivity run) in scattering aerosols such as sulfates [Δsulfates = +0.11%; +0.004 ng m^{-3}], nitrates [Δnitrates = +0.19%; +0.005 ng m^{-3}] and ammonium [Δammonium = +0.18%; +3.23x10^{-5} ng m^{-3}]. In addition larger increases in the absorbing aviation-induced BC [ΔBC = +0.48%; +8.35x10^{-4}] are simulated along with increases in the scattering refractory aerosol OC [ΔOC = +0.44%; +0.003 ng m^{-3}]. Additionally the NoHCs simulation is estimated to increase the cooling effect from the aviation-induced aCAE by 0.89%.

5.4.3.3 The impact of aviation-borne sulfur dioxide (SO_2) emission

The climatic impacts of the exclusion of aviation-borne SO_2 emissions from an aviation emissions inventory are seen in Figure 5.26(c). Here it is seen that through the exclusion of aviation SO_2 emissions ($NoSO_2$) the O3DRE is decreased by (–)0.11 mW m^{-2}, the aDRE is increased by (+)0.38 mW m^{-2}, in addition to a large decrease in the aviation-induced aCAE of (+)6.95 mW m^{-2}. Due to dominating effect of SO_2 emissions on aviation's aCAE the combined radiative effect (RE_{comb}) is increased by (+)7.22 mW m^{-2}, resulting in a RE_{comb} of –6.07 mW m^{-2}.

This sensitivity study returns the lowest impact on the aviation-induced O3DRE, with reductions of (–)0.002%, reductions lower than those induced by the NoCO and NoHCs sensitivity runs which result in a 1.24% reduction in the aviation-induced O3DRE. Additionally, the omission of aviation SO_2 emissions increases aviation-induced aDRE warming by 27.14%. This increase is primarily influenced by reductions in aviation-induced sulfates [Δsulfates = –0.43%; –0.391 ng m^{-3}] and ammonium [Δammonium = –0.031%; –0.022 ng m^{-3}], despite small increases in nitrates [Δnitrates = +0.93%; +0.012 ng m^{-3}] and OC [ΔOC = +0.49%; +0.003 ng m^{-3}], along with small increases in BC [ΔBC = +0.51%; 2.42x10^{-4} ng m^{-3}].

The large reductions in sulfates result in global mean reductions in CCN (Dp>50 nm) concentrations of (–)0.41%, explaining the 54.33% reduction in aviation non-CO_2 emission driven aCAE cooling effect. Ultimately this NoSO_2 sensitivity run highlights the importance of considering aviation SO_2 emissions due to its climatic impacts; demonstrating that a considerable cooling impact could be omitted if aviation SO_2 emissions were not included.

5.5 Evaluating model responses with the inclusion of CMIP5-extended aviation emissions

In order to evaluate CMIP5-extended aviation emissions driven model simulations against the observations, the same processes and observational datasets used in Section 3.3 to evaluate GMV4-nitrate with CMIP5 recommended aviation emissions was used to re-evaluate the model and the impact of the use of the CMIP5-extended aviation emissions inventory. Again for O_3 observational data collated by Tilmes et al. (2012) is used (repeating the process used in Section 3.3.1), with the re-evaluation of aerosol fields (sulfates, nitrates, ammonium and organic carbon) again evaluated against aircraft field campaigns collated by Heald et al. (2011) are used (repeating the evaluation process used in Section 3.3.2).

5.5.1 Evaluation of aviation emission driven gas-phase responses

Here Ozone (O_3) profiles simulated using GMV4-nitrate and the extended aviation emissions inventory developed in Section 4.3 are evaluated against observational data in order to investigate the effect the inclusion of aviation emissions; akin to those conducted in Section 3.3.1. As in Section 3.3.1 this re-evaluation is conducted in two parts: an initial comparison of annual mean model-observations comparisons for the 41 ozonesonde launch sites compiled by Tilmes et al. (2012) resolved in to latitudinal bands (Figure 5.27); and model-observation comparisons after resolving launch sites by latitude and altitude (Figure 5.28).

Comparisons of simulated seasonal O_3 profiles using CMIP5-extended against observations are not provided here as the resulting comparison plots return very similar profiles as those seen in Figure 3.5 and Figure 3.6, returning the same seasonal and regional trends. The same is also true for the seasonal model-observation comparison plots presented in Figure 3.7 and the seasonally resolved model-observation comparison plots resolved in to latitudinal bands as previously presented in Figure 3.8.

In Section 5.4.1 it was seen that through the inclusion of aviation-borne emissions (NORM simulation) increases in atmospheric ozone concentrations arise. As such Figure 5.27 (in

comparison to Figure 3.9 from Section 3.3.1) shows that through the inclusion of aviation emissions increases in model biases occur over each latitudinal band. These increases in model bias result lower levels of model underestimation over the 30°N–30°S and 60°S–90°S latitudinal bands, but greater levels of model overestimation over other regions (90°N–60°N, 60°N–30°N and 30°S–60°S). Due to the small increases in O_3 concentrations very small changes in the Pearson regression (R) are seen; with changes in regression each latitudinal band are seen when it is examined beyond three decimal places.

Figure 5.27: Annual mean model-observation comparisons (inclusive of CMIP5-extended aviation emissions – NORM) for all 41 ozonesonde launch sites compiled by Tilmes et al. (2012), grouped in to latitudinal bands (90°N–60°N; 60°N–30°N; 30°N–30°S; 30°S–60°S; and 60°S–90°S). Regression and bias from non-aviation driven simulations (NOAVI) presented in bottom right corners.

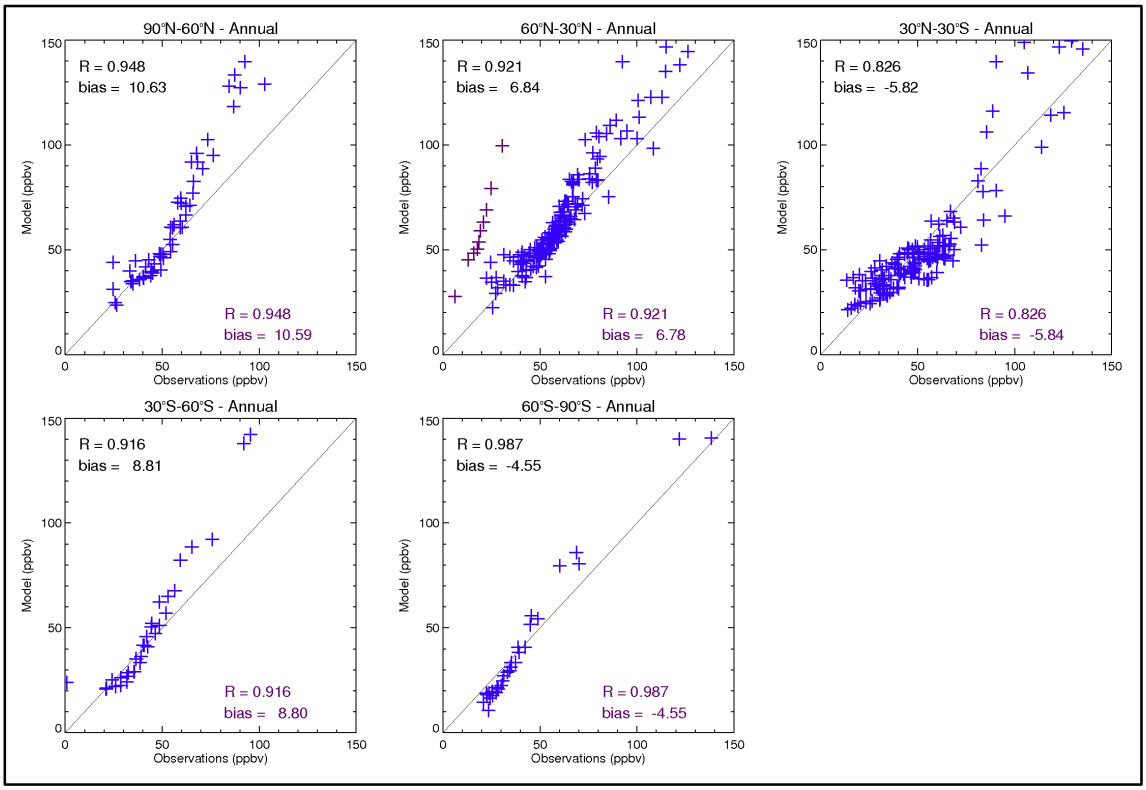

Changes in model bias are also assessed when partitioning model-observation comparisons by latitudinal and altitudinal bands, again resulting in greater levels in overestimations in regions which previously overestimated ozone and reducing levels of underestimations in regions which previously underestimated ozone. Akin to the levels of model skill demonstrated in Section 3.3.1 from Figure 3.10, Figure 5.28 returns the same levels of model skill over each associated region, along with the same levels of model skill over each latitudinal region (Figure 5.27), and each latitudinally and altitudinally partitioned region (Figure 5.28).

Figure 5.28: Annual mean model-observation comparisons (inclusive of CMIP5-extended aviation emissions – NORM) for all 41 ozonesonde launch sites compiled by Tilmes et al. (2012), grouped in to latitudinal bands (90°N–60°N; 60°N–30°N; 30°N–30°S; 30°S–60°S; 60°S–90°S) and altitudinal bands (100<hPa<400; 400<hPa<700; and 700<hPa<1000). Regression and bias from non-aviation driven simulations (NOAVI) presented in bottom right corners.

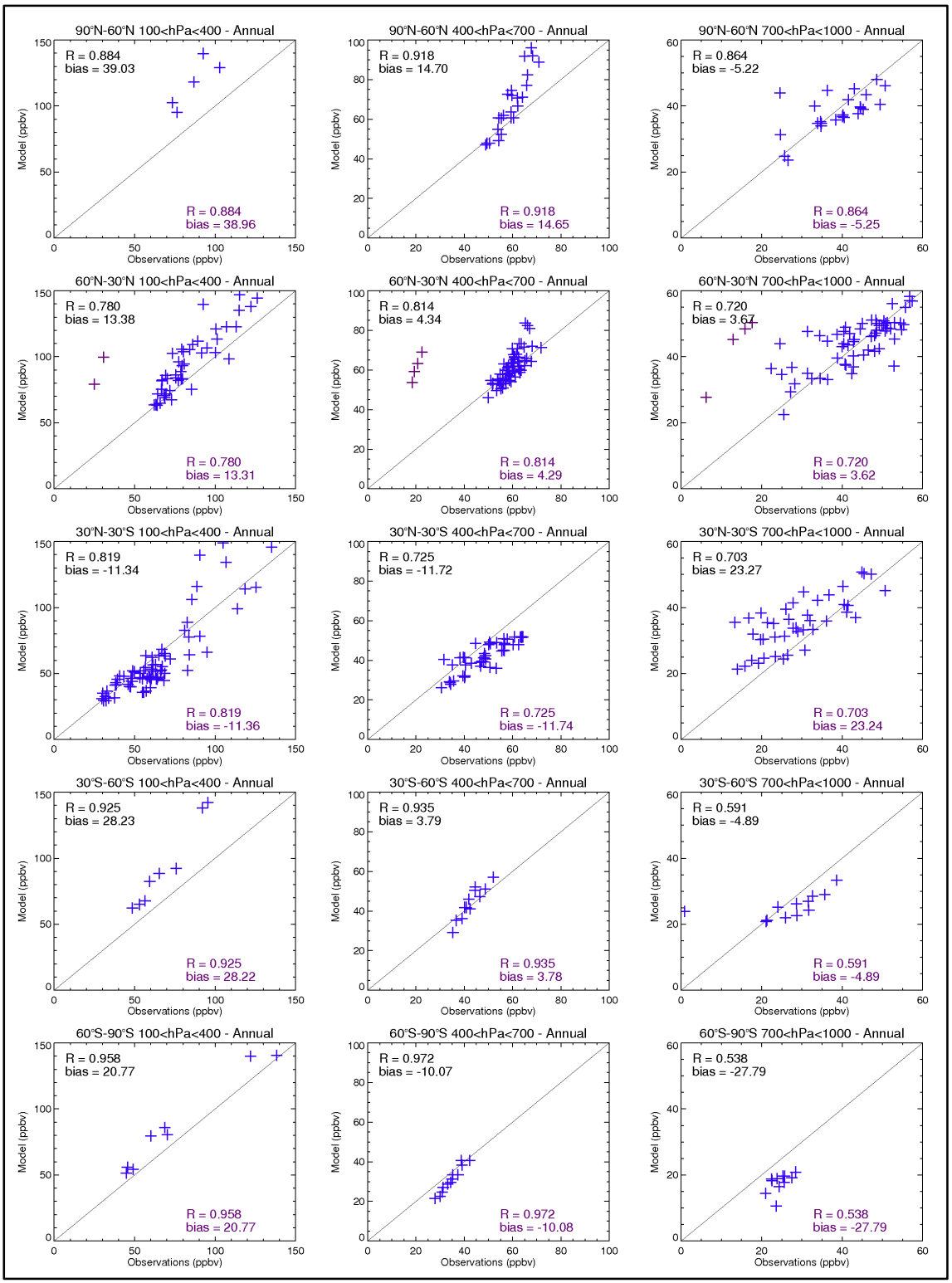

Through re-evaluation of GMV4-nitrate (inclusive of aviation emissions) it is shown that aviation-induced ozone generally increase model biases, resulting in an annual mean model bias of 5.36% (excluding Praha), in comparison to the annual mean model bias of 5.31% (excluding Praha) returned when only considering CMIP5 recommended aviation emissions.

5.5.2 Evaluation of aviation emission driven aerosol-phase responses

The following figures show how GMV4-nitrate model simulations for the year 2000 inclusive of CMIP5-extended aviation emissions inventory compare to vertical aerosol profiles for sulfates (Figure 5.29), nitrates (Figure 5.30), ammonium (Figure 5.31), and organic carbon (Figure 5.32) with observations from Heald et al. (2011). These aviation emissions driven simulations are also compared to GMV4-nitrate simulations driven by CMIP5 historical aviation emissions (as previously discussed in Section 3.3.2).

Comparisons of simulated annual mean model simulated aerosol profiles (sulfates, nitrates, ammonium and organic aerosols) against observations from Heald et al. (2011) are not provided here as individual aerosol component profiles and trends simulated using CMIP-extended show very similar profiles and trends to those simulated using CMIP5 (Figure 3.12, Figure 3.17, Figure 3.21 and Figure 3.25). The same similarities are seen for site specific model-observation comparison scatter plots (Figure 3.13, Figure 3.18, Figure 3.22 and Figure 3.26).

When aviation emissions are included in GMV4-nitrate simulations used for comparison with aircraft field campaign observations collated by Heald et al. (2011) very little differences are seen between the Pearson regressions (R) between the simulations with the CMIP5-extended aviation emissions inventory (NORM) and simulations with CMIP aviation emissions (CMIP5) (Figure 5.29, Figure 5.30, Figure 5.31 and Figure 5.32). For each of the aerosol species case's (sulfates, nitrates, ammonium and organic aerosols both sets of simulations provide near overlapping datapoints (as seen in Figure 5.29, Figure 5.30, Figure 5.31 and Figure 5.32). Though this near overlapping of datapoints could be due to noise within the model, though due changes in vertical aerosol profile concentrations (Figure 5.33) it is likely due to the small increases in aerosol concentrations induced through the use of CMIP5-extended.

The main differences which arise are within the variations in the biases returned between each set of simulations. Over four of the regions biases in sulfate model-observation comparisons are seen to increase (Europe, North America, West Africa and Asia) while improve over South America (Figure 5.29), indicating that through the use of CMIP-extended the further overestimates sulfates. When model-observation comparisons for nitrates (Figure 5.30),

ammonium (Figure 5.31) and organic aerosols (Figure 5.32) there are overall improvements in model skills when CMIP5-extended is used as opposed through the use of CMIP5, shown through improvements in model bias showing lower levels of model underestimation – expect in the case of organic aerosols over South America. Overall model skill is improved when CMIP5-extended aviation emissions are used as opposed to CMIP5 aviation emissions.

Figure 5.29: Regionally resolved model-observation sulfate comparisons for simulations driven by CMIP-extended (cross-hairs) and CMIP5 (diamonds) aviation emissions compared against field campaigns collated by Heald et al. (2011). Regression (R) and normalised mean biases (bias) for aviation emissions case in black, and in red without.

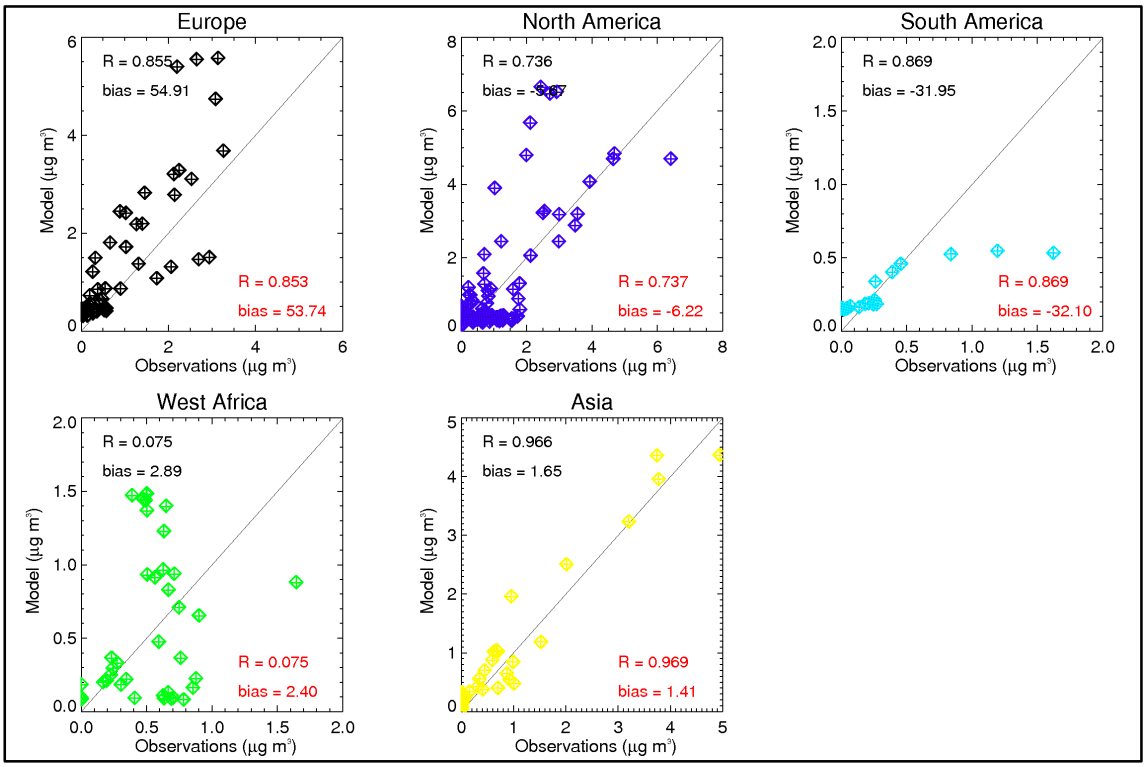

The main differences which arise are within the variations in the biases returned between each set of simulations. Over four of the regions biases in sulfate model-observation comparisons are seen to increase (Europe, North America, West Africa and Asia) while improve over South America (Figure 5.29), indicating that through the use of CMIP-extended the further overestimates sulfates. When model-observation comparisons for nitrates (Figure 5.30), ammonium (Figure 5.31) and organic aerosols (Figure 5.32) there are overall improvements in model skills when CMIP5-extended is used as opposed through the use of CMIP5, shown through improvements in model bias showing lower levels of model underestimation – expect in the case of organic aerosols over South America. Overall model skill is improved when CMIP5-extended aviation emissions are used as opposed to CMIP5 aviation emissions.

Figure 5.30: Regionally resolved model-observation nitrate comparisons for simulations driven by CMIP-extended (cross-hairs) and CMIP5 (diamonds) aviation emissions compared against field campaigns collated by Heald et al. (2011). Regression (R) and normalised mean biases (bias) for aviation emissions case in black, and in red without.

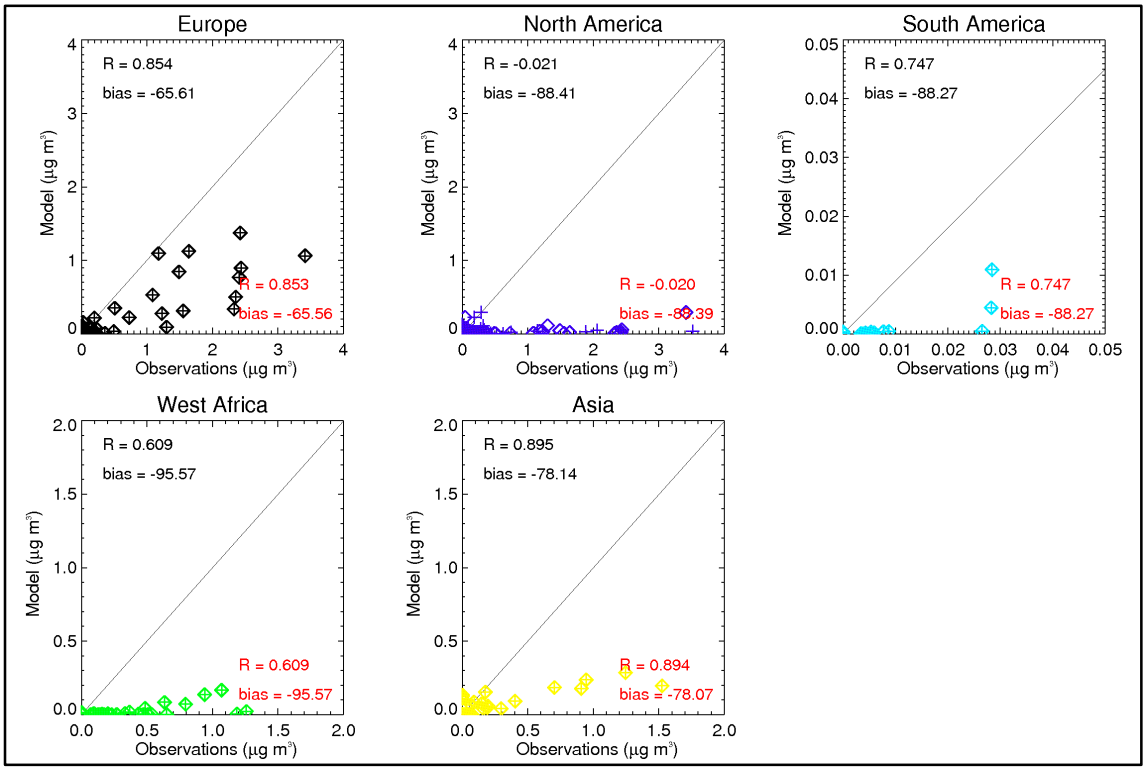

Figure 5.31: Regionally resolved model-observation ammonium comparisons for simulations driven by CMIP-extended (cross-hairs) and CMIP5 (diamonds) aviation emissions compared against field campaigns collated by Heald et al. (2011). Regression (R) and normalised mean biases (bias) for aviation emissions case in black, and in red without.

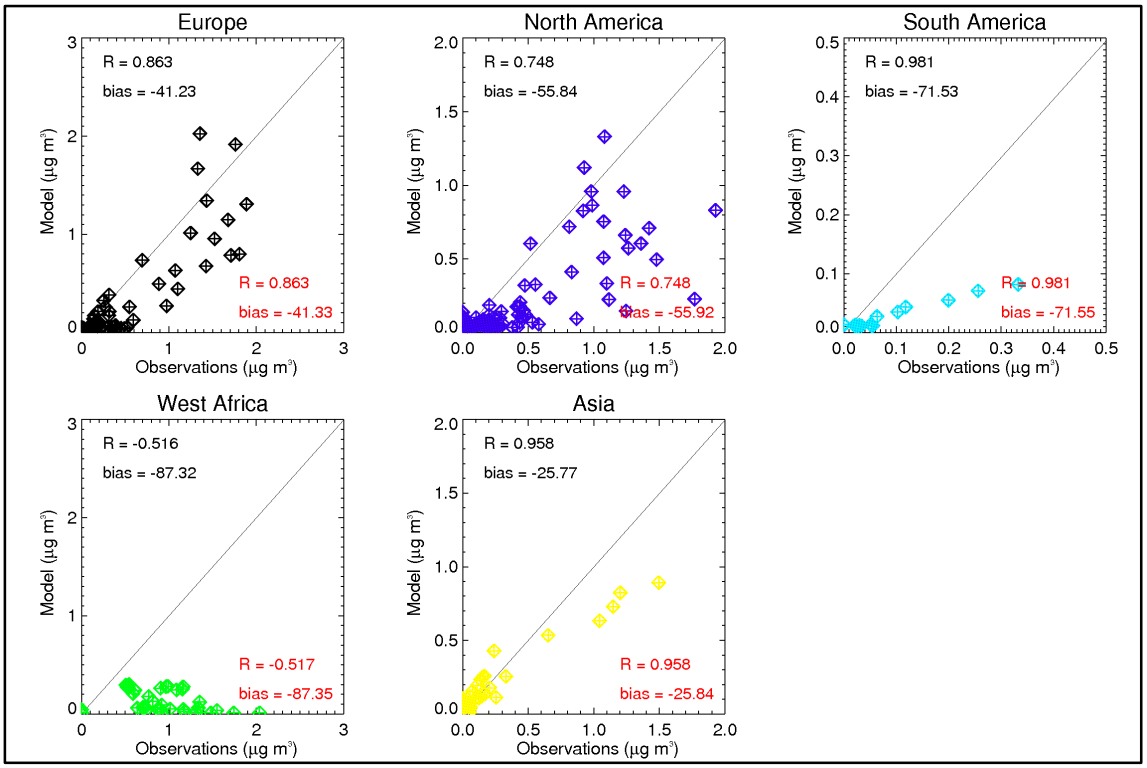

Figure 5.32: Regionally resolved model-observation organic aerosol comparisons for simulations driven by CMIP-extended (cross-hairs) and CMIP5 (diamonds) aviation emissions compared against field campaigns collated by Heald et al. (2011). Regression (R) and normalised mean biases (bias) for aviation emissions case in black, and in red without.

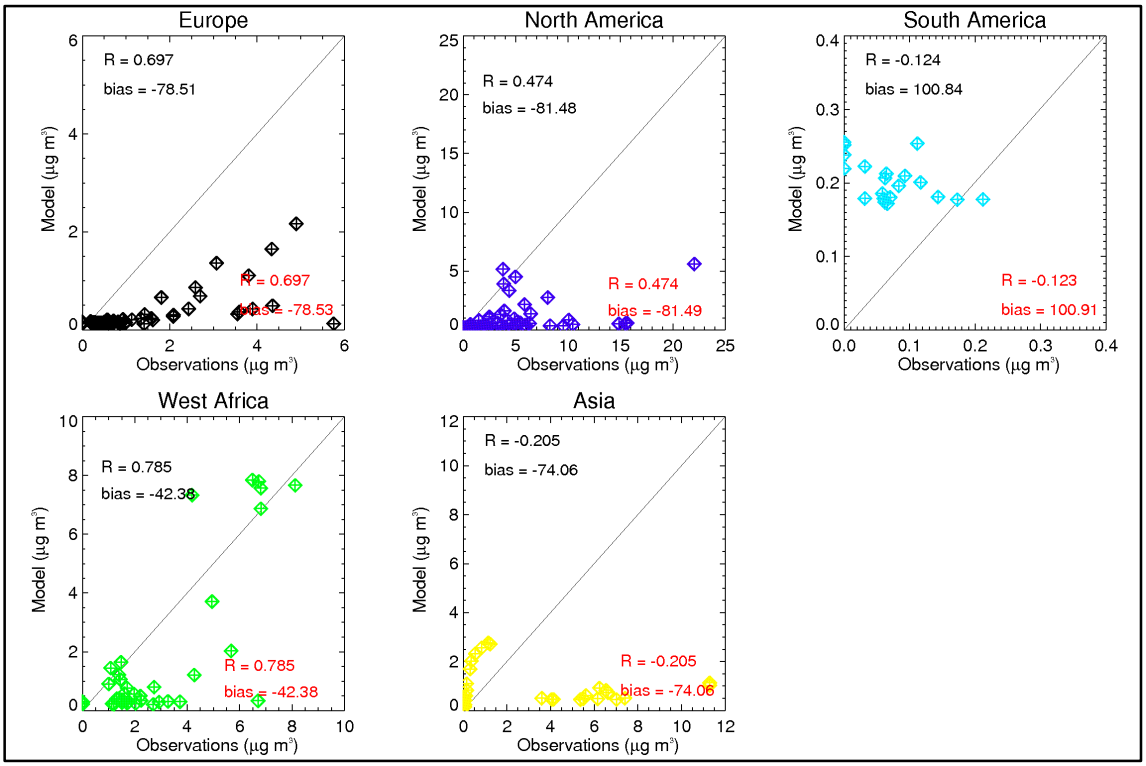

Figure 5.33: Differences in simulated vertical sulfate (a), nitrate (b), ammonium (c) and organic aerosol (d) profiles between simulations using the CMIP5-extended and CMIP5 recommended aviation emissions inventories for aircraft field campaign flightpaths used by Heald et al. (2011). Mean vertically-resolved changes are represented by the solid black line.

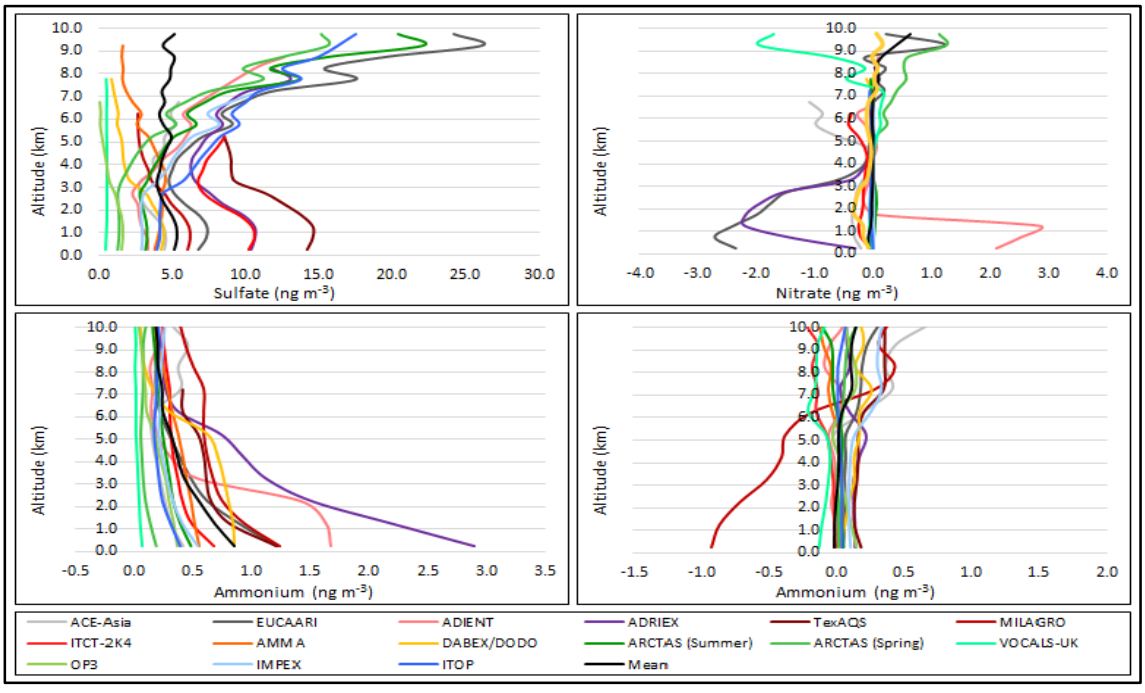

When the spread in differences in simulated aerosol concentrations between simulations (NORM–CMIP5) over each of the campaigns was evaluated a clearer picture of global the effects of the inclusion of a full array of aviation emissions within GMV4-simulations can be seen; with mean simulated changes between the use of the two aviation emissions inventories (CMIP5-extended and CMIP5) represented by solid black lines. Overall from the differences in sulfate, nitrate, ammonium and organic aerosol vertical profiles presented in Figure 5.33 vertically-resolved mean increases in sulfates, ammonium and organic aerosols are observed, while mean reductions in nitrates are observed; when comparing the impact of CMIP5-extended in relation to CMIP5. Overall CMIP5-extended (in relation to CMIP5) is seen to provide the following mean vertically-resolved increase in concentrations: sulfates = 4.65 ng m^{-3}; nitrates = –0.07 ng m^{-3}; ammonium = 0.35 ng m^{-3}; and organic aerosol = –0.24 ng m^{-3}. Over the cruise region of flight (100<hPa<400) the model underestimates all model species considered. The use of CMIP5-extended is estimated to reduce model underestimations in sulfates, ammonium and organic aerosols, and increase model underestimations in nitrates; thus improving model skill in region of the atmosphere most relevant to this study.

5.6 Summary and Conclusions

Using the nitrate-extended version of the TOMCAT-GLOMAP-mode coupled model (GMV4-nitrate) the impact of aviation emissions on atmospheric concentrations of gas- and aerosol-phase species, and their resulting climatic impacts were investigated. This initial investigation utilised the aviation emissions inventory developed in Section 4.3 (CMIP5-extended), which considers NO_X, CO, speciated HCs, SO_2, BC and OC emissions (Section 5.4.1). The impact of the use of this extended emissions inventory is then compared to the atmospheric and climatic impacts from aviation when considering CMIP5 recommended aviation emissions alone (NO_X and BC) (Section 5.4.2). Contributions from the additional emission species are then investigated in Section 5.4.3. Finally gas- and aerosol-phase concentrations simulated inclusive of CMIP5-extended emissions are re-evaluated against observational data (Section 5.5).

In line with the distribution of aviation emissions the majority of aviation-induced perturbations in gas- and aerosol-phase species occur in the Northern Hemisphere, with most cases returning the greatest changes in the cruise region of flight. Use of the CMIP5-extended aviation emissions inventory simulates that year 2000 aviation increases global annual mean concentrations of NO_X [ΔNO_X mean = 6.56 pptv; ΔNO_X burden = 40.65 Gg]. As a result of aviation-induced increases in atmospheric global mean concentrations and burdens of O_3 [ΔO_3 mean = 0.22 ppbv; ΔO_3 burden = 3.90 Tg] and OH [ΔOH mean = 1.02×10^{-3} pptv; ΔOH burden =

2.37 Mg]. In addition to the impact on O_3 and OH, aviation NO_X emissions are simulated to result in increases in the NO_X temporary reservoirs HONO [ΔHONO mean = $7.93x10^{-3}$ pptv; ΔHONO burden = 53.78 Mg] and PAN [ΔPAN mean = 0.35 pptv; ΔPAN burden = 3.78 Gg], as well the nitrate aerosol precursor HNO_3 [ΔHNO_3 mean = 6.14 pptv; ΔHNO_3 burden = 46.19 Gg].

In line with the release SO_2 emissions atmospheric concentrations and burdens of SO_2 increase [ΔSO_2 mean = 0.14 pptv; ΔSO_2 burden = 1.06 Gg], resulting in increases in H_2SO_4 [ΔH_2SO_4 mean = $7.44x10^{-3}$ pptv; ΔH_2SO_4 burden = 1.61 Mg]. Increases in H_2SO_4, allow an increase in sulfate formation (Fowler et al., 1997; Jenkin and Clemitshaw, 2000), which in turn can act as CCN (Dp>50 nm) (Mann et al., 2010; Verheggen, 2009). Additionally H_2SO_4 can allow insoluble aerosols modes to be moved to the soluble mode (Mann et al., 2010).

Aviation increases global concentrations and burdens of sulfates [Δsulfates mean = 0.83 ng m^{-3}; Δsulfates burden = 12.95 Gg], nitrates [Δnitrates mean = 0.36 ng m^{-3}; Δnitrates burden = 5.58 Gg] and ammonium [Δammonium mean = 0.06 ng m^{-3}; Δammonium burden = 0.86 Gg]; but with reductions in ammonium in the NH cruise region of flight. Aviation is also increases global annual mean concentrations and burdens of BC [ΔBC mean = 0.032 ng m^{-3}; ΔBC burden = 0.49 Gg] and OC [ΔOC mean = 0.0.13 ng m^{-3}; ΔOC burden = 0.21 Gg]. Through the increase in atmospheric aerosol concentrations aviation mean increases in low-cloud level (~0.96 km) mean CCN (Dp>50 nm) concentrations of 2.30 cm^{-3} are estimated, with the greatest relative increases occurring over the Pacific and Atlantic oceans.

Increases in O_3 simulated this results in an O3DRE of +8.86 mW m^{-2}, which when considered in terms of mW m^{-2} $Tg(N)^{-1}$ equates to an O3DRE of 10.45 mW m^{-2} $Tg(N)^{-1}$; a value that fits within the range of current estimates from literature of 7.39–44.2 mW m^{-2} $Tg(N)^{-1}$. In comparison to current literature the lower O3DRE estimated here for shirt-lived O_3 is due to the lower OPE within GMV4-nitrate [$OPE_{GMV4\text{-}nitrate}$ = 1.33]; where current literature shows a range OPE of 1–3.25, with an associated range in O3DRE estimates of 7.39–36.95 mW m^{-2} $Tg(N)^{-1}$].

Due to the combined increases in scattering and absorbing aerosols, aviation is estimated to return a warming aDRE of +1.40 mW m^{-2}, which lies within the range of estimates from literature of +20 to –28 mW m^{-2}. Additionally due to aviation-induced aerosol perturbations and resulting increases in CCN (Dp>50 nm) concentrations a cooling aCAE of –23.55 mW m^{-2} is simulated, an estimate that lies within the range of –4.8 to –29 mW m^{-2} from literature. These estimates results in a mean combined radiative effect (RE_{comb}) from O3DRE, aDRE and aCAE from the release of aviation non-CO_2 emissions of –13.29 mW m^{-2}.

Comparing atmospheric perturbations driven by the use of the CMIP5-extended emissions inventory in comparison to CMIP5 recommended aviation emission, reductions in aviation-induced NO_X [ΔNO_X burden = –0.98 Gg] are estimated, along with increases in O_3 [+0.14 Tg(O_3)], OH [+0.02 Mg(OH)], PAN [+1.86 Gg(PAN)], HONO [+0.27 Mg(HONO)], HNO_3 [+2.65 Gg(HNO_3)], SO_2 [+5.65 Gg(SO_2)] and H_2SO_4 [ΔH_2SO_4 burden = +1.28 Mg(H_2SO_4)]. Also comparison of CMIP5-extended driven aerosols perturbations with CMIP5 driven aerosol perturbations shows increases in sulfates [Δsulfates = +9.22 Gg], ammonium [Δammonium = +0.55 Gg], BC [ΔBC = +0.004 Gg] and OC [ΔOC = +0.15 Gg] are evaluated, as well as reductions in nitrates [Δnitrates = –0.21 Gg]. These increases in the global aerosol burden, primarily driven increases in aviation-induced sulfates, result in increases in low-cloud level mean CCN (Dp>50 nm) of +0.44% with the greatest relative increases over the Atlantic and Pacific oceans. As a result these differences in gas- and aerosol-phase species between CMIP5-extended and CMIP5 driven simulations returns in the O3DRE estimate [mean ΔO3DRE = +0.35 mW m^{-2}], a decrease in the aDRE [mean ΔaDRE = +1.64 mW m^{-2}], and an increase in the aviation-induced cooling aCAE [mean ΔaCAE = –5.22 mW m^{-2}] arise.

The NoCO sensitivity run shows that aviation CO emissions contribute to 1.47% of the O3DRE and 1.43% of the aDRE, while further enhancing the aCAE by 1.36%, resulting in an increase in the aviation non-CO_2 cooling effect of 3.54%. The NoHC sensitivity run shows that speciated HC emissions are responsible for 2.71% of the O3DRE, 0.71% of the aDRE, while increasing the aCAE by 0.89% resulting in an increases in the cooling aviation RE_{comb} of 3.17%. Through the NoSO2 sensitivity run SO_2 emissions are estimated to be responsible for 1.24% of the O3DRE, increase the aDRE by 27.14% due to the exclusion of aviation SO_2 emissions, a reduction in the cooling aCAE of 29.51%, resulting in a decreases in the cooling RE_{comb} of 54.33%. Overall these sensitivity runs show that CO, speciated HCs and SO_2 emissions all have impacts of the aviation O3DRE, SO_2 emissions having considerable impacts on the aDRE and the aCAE; responses which would not be captured if the emission of these species were not considered.

Re-evaluation of GMV4-nitrate simulated ozone profiles with observational profiles from Tilmes et al. (2012) shows that over all latitudinal bands the model bias increases, i.e. returning greater overestimations over regions where the model previously overestimated O_3, and lower levels of underestimations over regions which previously underestimated ozone. This effect is also seen over the regions presented in Figure 5.28 when model-observational profiles were partitioned by latitude and altitude. Despite the majority of aviation emissions being released in the cruise region of flight (represented by the 100<hPa<400 region in Figure 5.28) in the Northern Hemisphere the greatest relative changes in bias are seen between 400<hPa<700

globally, and between 400<hPa<1000 in the Northern Hemisphere. When considering aerosol concentrations (sulfates, nitrates, ammonium and organic aerosol) over the regions considered (Europe, North America, South America, West Africa and Asia) overall model overestimations in sulfates increase, while model underestimations in nitrates, ammonium and organic aerosols decrease. When concentrating on a higher altitude range to consider the cruise region of flight (100<hPa<400) the model is seen to underestimate sulfates, nitrates, ammonium and organic aerosol; with CMIP5-extended improving model biases when evaluating simulated sulfate, ammonium and organic aerosols in comparison to CMIP5.

6 Impacts of aviation fuel sulfur content on climate and human health

6.1 Introduction

Civil aviation has an average fuel sulfur content (FSC) ranging between 550–700 ppm; typically assumed as 600 ppm (Barrett et al., 2012). Aviation-induced aerosols formed at the surface have been shown to adversely affect air quality and human health (Barrett et al., 2010; Barrett et al., 2012; Levy et al., 2012; Woody et al., 2011). This is through the direct release and formation of aerosols from aviation emissions.

Due to the nature of aviation the release of aviation emissions can occur throughout all phases of flight, inclusive of take off and landing and cruise (Commercial Aviation Safety Team, October 2012). The vertical distribution of aviation emissions as seen in Figure 4.1(a) and Figure 5.3 highlight the main regions in which emissions are released, the cruise region of flight (between 8–12 km) and take off and landing region (altitude > 1 km). Within that aviation emissions inventories taxi and ground operation emissions will be included within the lowest flight level; pertaining to the ground level. In order to reduce these adverse air quality and human impacts of aviation the use of ultra-low sulfur jet (ULSJ) fuel has been proposed. The use of ULSJ fuel in civil aviation has been shown to reduce the air quality and human impact of aviation-induced aerosols (Barrett et al., 2012).

This Chapter investigates the impact of varying FSC between 0–6000 ppm on aviation-induced $PM_{2.5}$ in the surface atmosphere, while estimating associated aviation-induced premature mortality through the use of concentration response functions (CRFs) for cardiopulmonary disease and lung cancer. In addition, resultant changes in planetary boundary layer CCN (cloud condensation nuclei) with a dry diameter of less than 50 nm (Dp > 50 nm), along with the resulting impact on climate via changes in radiative effect (RE) are investigated. The REs due to changes in tropospheric ozone and aerosols are calculated using a radiative transfer model.

The nitrate-extended version of TOMCAT-GLOMAP-mode coupled model (described in Section 3.2 and referred to as GMV4-nitrate) is used in conjunction with the CMIP5 extended aviation emissions inventory developed in Section 4.3 to quantify global atmospheric responses in aerosol and ozone (O_3), from the FSC scenarios investigated in this section. The radiative effects from aviation-induced tropospheric O_3 (O3DRE), aerosol direct radiative effect (aDRE) and aerosol cloud albedo effect (aCAE) are estimated using a radiative transfer model. These component REs are used to estimate the combined radiative effect (RE_{comb}) resulting from civil aviation, and how variations in aviation FSC effect the RE_{comb}.

6.2 Background

Aviation emissions, as well as their perturbations to atmospheric chemical composition, have the ability to degrade surface air quality, resulting in negative impacts on human health. Surface layer particulate matter (PM) concentrations are affected by the dry deposition of aviation-induced particulate matter (i.e. through processes such as gravitational settling), i.e. in the absence of precipitation (Mann et al., 2010). Short-term exposure to fine PM can result in respiratory and cardiovascular ailments. Long-term exposure to fine PM can result in chronic respiratory and cardiovascular diseases, lung cancer, chronic changes in physiological functions and mortality (World Health Organisation, 2003; Ostro, 2004; Pope et al., 2002). The mechanisms through which aviation-induced $PM_{2.5}$ affect human health and the risks associated with the distribution and size of particulates are discussed in Section 2.6.2.

Lim et al. (2012) estimated in 2010 pollution from particulate matter (from ambient particulate matter pollution and household air pollution from solid fuels) was responsible for 6,702,313 [6,467,402–8,005,738] mortalities. When exposure to ambient ozone pollution was included estimates in mortality from air pollution rises to 6,854,747 [5,519,674–8,273,169] mortalities. In this study a theoretical-minimum-risk exposure distribution of 5.8–8.8 μg m^{-3} was considered.

In the US, aviation emissions are estimated to lead to adverse health effects in ~11,000 people (ranging from mortality, respiratory ailments and hospital admissions due to exacerbated respiratory conditions) and ~23,000 work loss days per annum (Ratliff et al., 2009). LTO (landing and take-off) aviation emissions over the US increase $PM_{2.5}$ concentrations, particularly around airports (Woody et al., 2011), increasing US mortality rates by ~160 per annum. Barrett et al. (2012) and Barrett et al. (2010) estimate that global aviation emissions, inclusive of LTO and cruise emissions, are annually responsible for ~10,000 premature mortalities.

Yim et al. (2015), expanding on the work of Barrett et al. (2012) assessed that aviation-induced $PM_{2.5}$ and O_3 are responsible for 16,000 mortalities a^{-1} [90% CI: 8,300–24,000]; with 87% and 13% of these mortalities being due to $PM_{2.5}$ and O_3 respectively (13,920 [95% CI: 7,220–20,880] mortalities a^{-1}). Differences in aviation-induced premature mortalities due to increases in cases of cardiopulmonary disease and lung cancer between Yim et al. (2015) and Barrett et al. (2012), 13,920 and 10,000, are due to the methodology used by Yim et al. (2015) to assess mortality. Where Yim et al. (2015) consider dispersion on a local (~1 km), near-airport (~10 km), regional (~1,000 km) and global scale (~10,000 km). With additional differences between

these two studies arising from Yim et al. (2015) estimating local airport to estimate local concentrations of secondary sulfate $PM_{2.5}$ due to aircraft ground emissions along with using a plume correction factor.

Recently Morita et al. (2014) using the methodology to derive the relative risk (RR) from exposure to surface $PM_{2.5}$ from Burnett et al. (2014) assessed that aviation results in 405 (95% CI: 182–648) mortalities a^{-1} due to increases in cases of lung cancer, stroke, ischemic heart disease, trachea, bronchus, and chronic obstructive pulmonary disease. While Jacobson et al. (2013) using the methodology from Jacobson (2010) estimate 310 (95% CI: –400 to 4,300) mortalities a^{-1} due to cardiovascular effects.

Taking these studies in account, and the different methodologies applied and modes or mortality investigated aviation is estimated to be responsible for between 310–13,920 mortalities a^{-1} due to aviation-induced increases in surface $PM_{2.5}$ concentrations. In addition to variations in global estimates of aviation-induced premature mortality studies have also demonstrated differences in regional estimates of premature mortality. Barrett et al. (2012) estimated aviation to be re

The introduction of cleaner fuels and pollution control technologies have been shown to improve ambient air quality and reduce adverse health effects of fossil fuel combustion (World Health Organisation, 2005). One proposed solution to reduce the adverse health effects of aviation $PM_{2.5}$ is the use of ultra-low sulfur jet fuel (ULSJ), reducing the formation of sulfate PM (Hileman and Stratton, 2014; Barrett et al., 2012; Barrett et al., 2010; Ratliff et al., 2009). ULSJ fuels typically have a fuel sulfur content (FSC) of 15 ppm, compared with a FSC of between 550–750 ppm as seen in standard aviation fuels (Jet A-1/Jet A) (Barrett et al., 2012). Current global regulatory standards for aviation fuel (ASTM D1655 and MOD STAN DEF 91-91) specify a maximum FSC of 3000 ppm (ASTM International, 2012b; Ministry of Defence, 2011). Barrett et al. (2012) estimate that the use of ULSJ fuel (where FSC = 15 ppm) reduces ground level $PM_{2.5}$, annually avoiding ~2300 (95% CI: 890–4200) mortalities globally.

Altering the sulfur content of aviation fuel also modifies the net climate impact of aviation emissions. A reduction in fuel sulfur content reduces the formation of cooling sulfate aerosols, increasing the net warming effect of aviation emissions (Barrett et al., 2012; Unger, 2011). The roles of sulfate both in climate cooling and in increasing surface PM concentrations mean that policy makers must consider both health and climate when considering effects from potential reductions in sulfur emissions from a given emissions sector, including aviation (Fiore et al., 2012).

6.3 Methodology

6.3.1 Simulations conducted

To explore the impact of aviation FSC on air quality, premature mortality, low-cloud level CCN and climate, jet fuel FSC was varied globally from 0–6000 ppm across 11 model experiments. These spanned a range of scenarios from a desulfurised aviation fleet scenario (FSC = 0 ppm) to twice the FSC specified by the standards ASTM D1655 and Ministry of Defence's Defence Standard 91-91 (FSC = 6000 ppm) (ASTM International, 2012b; Ministry of Defence, 2011). This includes scenarios representing standard aviation and one representing the use of ULSJ fuel. These scenarios are summarised in Table 6.1.

Three simulations vary the vertical distribution of aviation emissions (GROUND, SWITCH1 and SWITCH2). GROUND collapses aviation emissions to ground level to investigate the impact of removing the vertical distribution aspect of aviation emissions. In the next two, a low FSC (15 ppm) is applied below cruise-level flight (<8.54 km) (Köhler et al., 2013; Lee et al., 2009) combined with increased FSCs at altitudes above (SWITCH1 and SWITCH2). These two scenarios investigate whether changes in the vertical distribution of aviation SO_2 emissions could increase climate cooling, whilst minimising aviation-induced premature mortality resulting from changes in surface-layer $PM_{2.5}$. The SWITCH1 scenario increases FSC in line with the HIGH scenario above 8.54 km, while SWITCH2 is designed to emit the same total global SO_2 emissions as standard aviation (NORM).

Table 6.1: Fuel sulfur content and global SO_2 emissions applied in each experiment.

Scenario name	Description	FSC (ppm)	Total SO_2 emitted (Tg)
NOAVI	No aviation emissions	n/a	0.0
NORM	Standard aviation emissions scenario	600	0.236
DESUL	Desulfurised case	0	0.0
ULSJ	Ultra low sulfur jet fuel	15	0.00589
HALF	Half FSC of normal case	300	0.118
TWICE	Twice FSC of normal case	1200	0.472
HIGH	FSC at international specification limit	3000	1.179
OVER	Twice FSC specification limit	6000	2.358
GROUND	All emissions emitted at surface level (FSC as NORM)	600	0.236
SWITCH1	ULSJ FSC to 8.54 km, HIGH FSC content above	15/3000	0.491
SWITCH2	ULSJ FSC to 8.54 km, FSC = 1420 ppm above	15/1420	0.236

All simulations are conducted for 16 months from September 1999 to December 2000 inclusive, with the first four months discarded as spin-up time. The results from all simulations are compared against a simulation exclusive of aviation emissions (NOAVI).

6.3.2 Evaluating aviation-induced mortality

Excess premature mortality from cardiopulmonary diseases and increases in cases of lung cancer due to long-term exposure to aviation-induced $PM_{2.5}$ were calculated using increases in annual mean surface $PM_{2.5}$ concentrations for all aerosol species as used by Ostro (2004). $PM_{2.5}$ was used as a measure of likely health impacts because chronic exposure is associated with adverse human health impacts including morbidity and mortality (Dockery et al., 1993; Pope and Dockery, 2006). $PM_{2.5}$ is particulate matter within a size diameter of 2.5 µm, which has the capacity to adversely affect air quality and human health. Aerosols with the $PM_{2.5}$ size category are derived within the model by calculating the mass of total aerosols and individual aerosol components with the size range of interest.

Annual excess mortality is related to changes in $PM_{2.5}$ via a concentration response-function (CRF) (Ostro, 2004; Pope et al., 2004). This response-function considers concentrations of $PM_{2.5}$ for a perturbed case (defined by scenario specific simulations as per Table 6.1) in relation to a baseline case with no aviation emissions (NOAVI). Through comparison against the NOAVI scenario this study is able to estimate aviation-induced premature mortalities.

To calculate aviation-induced excess mortality, the relative risk function (RR) for both cardiopulmonary disease and lung cancer needed to be determined. The relative risk (RR) is the multiple of risk of the outcome in one scenario compared to another scenario (Zhang and Yu, 1998). This is a function of both baseline and perturbed $PM_{2.5}$ concentrations, and the disease specific cause-specific coefficient (β) – Equation 6.1 (Ostro, 2004; Schmidt et al., 2011).

$$RR = \left[\frac{(X+1)}{(X_0+1)}\right]^{\beta}$$

Equation 6.1

Where RR = Relative risk function

X = Scenario perturbed case surface $PM_{2.5}$ concentrations

X_0 = No aviation baseline case surface $PM_{2.5}$ concentrations

β = β coefficient, specific to disease.

β coefficients for cardiopulmonary disease mortality of 0.15515 [95% CI = 0.05624–0.2541] and lung cancer of 0.232 [95% CI = 0.086–0.379] are used, based on the recommended health outcomes and risk outcomes to calculate the environmental burden of disease (EBD) (Pope et al., 2002; Ostro, 2004). Use of the β coefficients limits as stipulated by the 95% confidence interval (CI) allow for the low-, mid- and high-range mortality values to be calculated. Use of this confidence interval assumes relatively small errors within the surface-layer concentrations used to derive the RR.

After determining the relative risk functions, the attribution factor (AF) of health effects from air pollution from the exposure to air pollution, i.e. surface layer $PM_{2.5}$ concentrations, are calculated using Equation 6.2:

$$AF = \frac{RR-1}{RR}$$

Equation 6.2

The population under 30 is considered (P_{30}), on a country specific basis is then calculated using Equation 6.3 as per the methodology outlined by Ostro (2004) and the recommended health outcomes and risk functions used to calculate the EBD. This uses the country specific population (P) from the Gridded World Population (GWP; version3) project (Center for International Earth Science Information Network, 2012), in tandem with country specific data on the fraction of the population under 30 (F_{30}) (Ostro, 2004):

$$P_{30} = P \times F_{30}$$

Equation 6.3

Finally increases in mortality due to aviation-induced surface-layer $PM_{2.5}$ concentrations are calculated (E) for both cardiopulmonary disease and lung cancer. This uses baseline mortality rates (i.e. deaths per 1000 people) represented by the population incidence for a given health effect (B) (Mathers et al., 2008), and the population under 30 in each country (Equation 6.4) (Ostro, 2004; Schmidt et al., 2011).

$$E = AF \times B \times P_{30}$$

Equation 6.4

Combining equations Equation 6.1, Equation 6.2, Equation 6.3 and Equation 6.4, the resulting equation is then used to evaluate aviation-induced mortality for each mechanism (i.e. cardiopulmonary disease and lung cancer) (Equation 6.5).

$$E = \left(\frac{\left[\frac{(X+1)}{(X_0+1)}\right]^{\beta} - 1}{\left[\frac{(X+1)}{(X_0+1)}\right]^{\beta}} \right) \times B \times P \times F_{30}$$

Equation 6.5

It is acknowledged that the CRF outlined by Ostro (2004) is not the most recent CRF available to evaluate mortality from long term exposure to $PM_{2.5}$ (Burnett et al., 2014). Though through the use of Ostro (2004)'s log-linear function this study is able to compare estimates in aviation-induced mortality evaluated in this Chapter to be compared against previous estimates from Barrett et al. (2012).

6.4 Results and Discussion

Here the results and discussion are split up in to the following subsections in order to concentrate separately on each of the main aspects investigated:

- Surface $PM_{2.5}$ perturbations,
- Aviation-induced mortality,
- Sensitivity of cloud condensation nuclei formation to aviation FSC,
- Sensitivity of radiative effects with variation in FSC, and,
- Relationship between aviation-induced radiative effects and mortality due to aviation non-CO_2 emissions.

6.4.1 Surface $PM_{2.5}$ perturbations

Figure 6.1 shows the impact of aviation with standard FSC (FSC = 600 ppm; NORM) on global atmospheric surface $PM_{2.5}$ concentrations. The greatest absolute increases in annual mean $PM_{2.5}$ concentrations were simulated over Central Europe and Eastern China, with increases of up to 78.4 ng m^{-3} over Europe (Figure 6.1(a)). Aviation emissions result in larger fractional changes in annual mean $PM_{2.5}$ concentrations (of up to 0.8%) over North America and Europe in comparison to global annual mean $PM_{2.5}$ fractions increases [0.1%] (Figure 6.1(b)).

Figure 6.1: Aviation-induced (FSC = 600 ppm: NORM) $PM_{2.5}$ concentrations: (a) absolute (NORM–NOAVI) and (b) percentage changes ((NORM–NOAVI)/NOAVI). Boxes show the European (20°W–40°E, 35°N–66°N), North American (169°W–51°W, 21°N–80°N) and Asian (65°E–124°E, 4°N–46°N) regions.

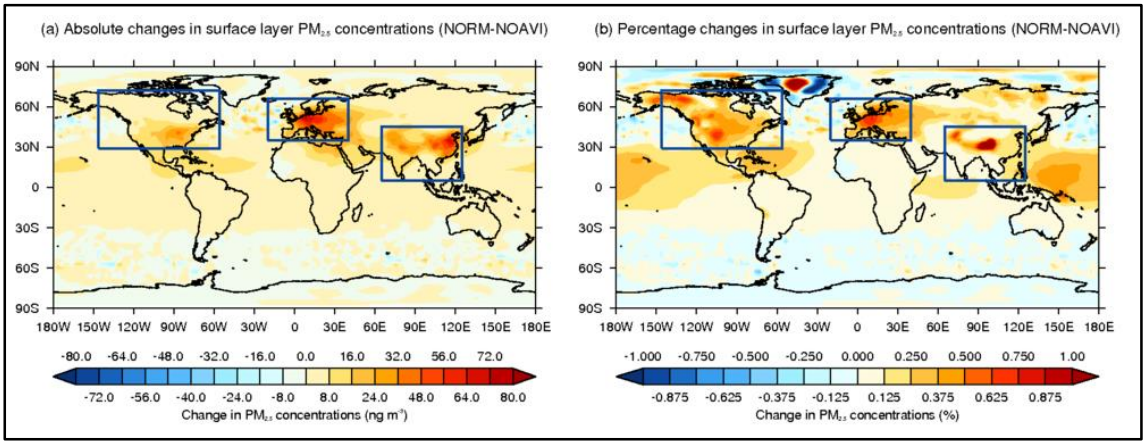

From Figure 6.1 it is seen that aviation-induced contributions to surface $PM_{2.5}$ concentrations at the surface are small, at the most providing increases of 1%. As such, associated estimates in premature mortality will also be relatively small – as estimated is Section 6.4.2.

Figure 6.2: Impact of aviation FSC on (a) global, (b) European (20°W–40°E, 35°N–66°N), (c) North American (169°W–51°W, 21°N–80°N), and (d) Asian (65°E–124°E, 4°N–46°N) surface annual mean PM2.5 mass concentrations. Dashed trendlines demonstrate are linear fits for the relationship between PM2.5 perturbations and FSC.

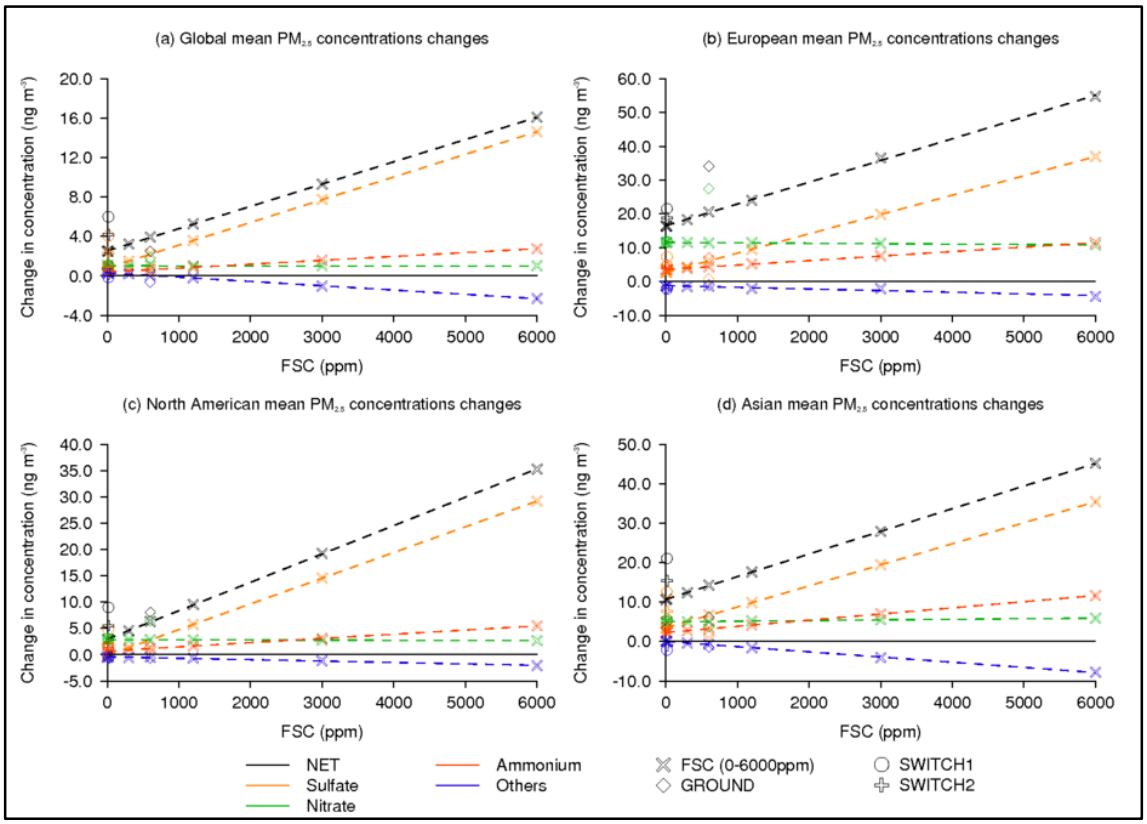

Figure 6.2 and Table 6.2 show the impact of aviation emissions on global and regional mean $PM_{2.5}$ concentrations, as a function of FSC. With standard FSC (NORM; FSC = 600 ppm), aviation increases global mean surface $PM_{2.5}$ concentrations by 3.93 ng m^{-3}; with increases in $PM_{2.5}$ dominated by sulfates [56.2%], nitrates [26.0%] and ammonium [16.0%] (Figure 6.3).From Figure 6.1 it is seen that aviation-induced contributions to surface PM2.5 concentrations at the surface are small, at the most providing increases of 1%. As such, associated estimates in premature mortality will also be relatively small – as estimated is Section 6.4.2.

Figure 6.2 and Table 6.2 also shows the impact of changes in FSC on global and regional $PM_{2.5}$ concentrations. Aviation emissions are simulated to increase European mean $PM_{2.5}$ concentrations by 20.6 ng m^{-3} and Asian $PM_{2.5}$ concentrations by 14.3 ng m^{-3} (***Figure*** 6.2 (b,d) and Table 6.2), substantially more than over North America where an increase of 6.3 ng m^{-3} is estimated (***Figure*** 6.2(c) and Table 6.2). Increases in $PM_{2.5}$ are dominated by nitrates over Europe [55.5%]. Over North America increases in aviation-induced nitrates contribute an equivalent amount to aviation-induced sulfate [44.4%], while over Asia their contribution to increases in aviation-induced $PM_{2.5}$ are noticeably lower than sulfates [35.6%]. Regionally, sulfates contribute to increases in $PM_{2.5}$ of 46.9% over Asia, 44.6% over North America and 30.0% over Europe (Figure 6.3).

Increases in FSC result in increases in $PM_{2.5}$ concentrations, due to increases in sulfate $PM_{2.5}$ combined with small reductions in nitrate $PM_{2.5}$. Simulated changes to sulfate, nitrate, ammonium and total $PM_{2.5}$ are found to be linear with respect to FSC (***Figure*** 6.2). The linearity of the dependence of aviation-induced $PM_{2.5}$ on FSC was statically analysed via significance tests (R^2 and *p*-values). Globally, the relationship gives $R^2 > 0.99$ and *p*-value = 2.52×10^{-12}; over Europe $R^2 > 0.99$ and *p*-value = 4.48×10^{-9}, over North America $R^2 > 0.99$ and *p*-value = 1.76×10^{-11} and; over Asia $R^2 > 0.99$ and *p*-value = 1.83×10^{-12}. The near-linear response is likely due to the small emission perturbations that have been applied relative to global aerosol emissions. It is likely that larger emission perturbations would lead to a non-linear response in atmospheric aerosol.

The impacts of variations in FSC on surface $PM_{2.5}$ concentration are found to be regionally variable. This is illustrated through investigating the rate of change in mean surface $PM_{2.5}$ concentrations with aviation FSC (as per the metric $d(PM_{2.5}/FSC)$). Using this metric it is found that aviation emissions produce the greatest sensitivity in $PM_{2.5}$ concentrations over Europe [6.44×10^{-3} ng m^{-3} ppm^{-1}], followed by Asia [5.74×10^{-3} ng m^{-3} ppm^{-1}] and North America [5.40×10^{-3} ng m^{-3} ppm^{-1}], with global $PM_{2.5}$ being the least sensitive to aviation FSC [2.26×10^{-3} ng m^{-3} ppm^{-1}].

Table 6.2: Mean $PM_{2.5}$ concentration changes in aviation-induced Net, sulfate, nitrate, ammonium and other aerosols components relative to no aviation (NOAVI) due to variations in aviation FSC: For the Global, European and North American regions

Region	Scenario	Species (ng m^{-3})				
		Net	Sulfates	Nitrates	Ammonium	Others
Global	DESUL	2.50	0.81	1.02	0.38	0.28
	ULSJ	2.53	0.84	1.02	0.39	0.27
	HALF	3.21	1.50	1.02	0.50	0.19
	NORM	3.93	2.21	1.02	0.63	0.07
	TWICE	5.26	3.57	1.03	0.87	-0.21
	HIGH	9.29	7.73	1.03	1.58	-1.05
	OVER	16.08	14.62	1.01	2.75	-2.30
	GROUND	2.49	0.82	1.80	0.51	-0.65
	SWITCH1	5.99	4.05	1.08	0.99	-0.14
	SWITCH2	4.19	2.34	1.03	0.67	0.15
Europe	DESUL	16.40	2.65	11.55	3.53	-1.33
	ULSJ	16.37	2.73	11.53	3.54	-1.44
	HALF	18.27	4.34	11.51	3.92	-1.50
	NORM	20.59	6.17	11.43	4.34	-1.35
	TWICE	24.03	9.51	11.44	5.14	-2.05
	HIGH	36.55	19.85	11.21	7.54	-2.06
	OVER	54.75	36.95	10.79	11.48	-4.46
	GROUND	34.10	0.78	27.45	6.93	-1.06
	SWITCH1	21.51	7.27	11.79	4.67	-2.21
	SWITCH2	18.80	4.84	11.56	4.04	-1.64
North America	DESUL	2.86	-0.14	2.83	0.67	-0.51
	ULSJ	2.94	-0.08	2.83	0.68	-0.48
	HALF	4.52	1.32	2.83	0.92	-0.55
	NORM	6.32	2.82	2.81	1.17	-0.47
	TWICE	9.53	5.73	2.81	1.66	-0.67
	HIGH	19.26	14.56	2.77	3.11	-1.18
	OVER	35.26	29.20	2.67	5.47	-2.08
	GROUND	8.03	0.81	6.40	1.45	-0.64
	SWITCH1	8.99	4.81	2.95	1.64	-0.41
	SWITCH2	5.51	2.18	2.85	1.12	-0.63
Asia	DESUL	10.59	3.38	4.96	2.26	0.00
	ULSJ	10.79	3.47	5.00	2.29	0.02
	HALF	12.40	5.00	5.04	2.74	-0.38
	NORM	14.27	6.69	5.08	3.24	-0.74
	TWICE	17.63	9.85	5.20	4.18	-1.61
	HIGH	27.88	19.47	5.51	7.00	-4.10
	OVER	45.17	35.43	5.91	11.64	-7.81
	GROUND	6.14	2.28	3.80	1.53	-1.48
	SWITCH1	21.06	12.51	5.56	5.14	-2.14
	SWITCH2	15.39	7.69	5.16	3.60	-1.06

Figure 6.3: Relative percentage changes in aviation-induced surface sulfates, nitrates, ammonium and other modelled aerosol component species concentrations ([NORM–NOAVI]/NOAVI): for the (a) global, (b) European, (c) North American and (d) Asian regions.

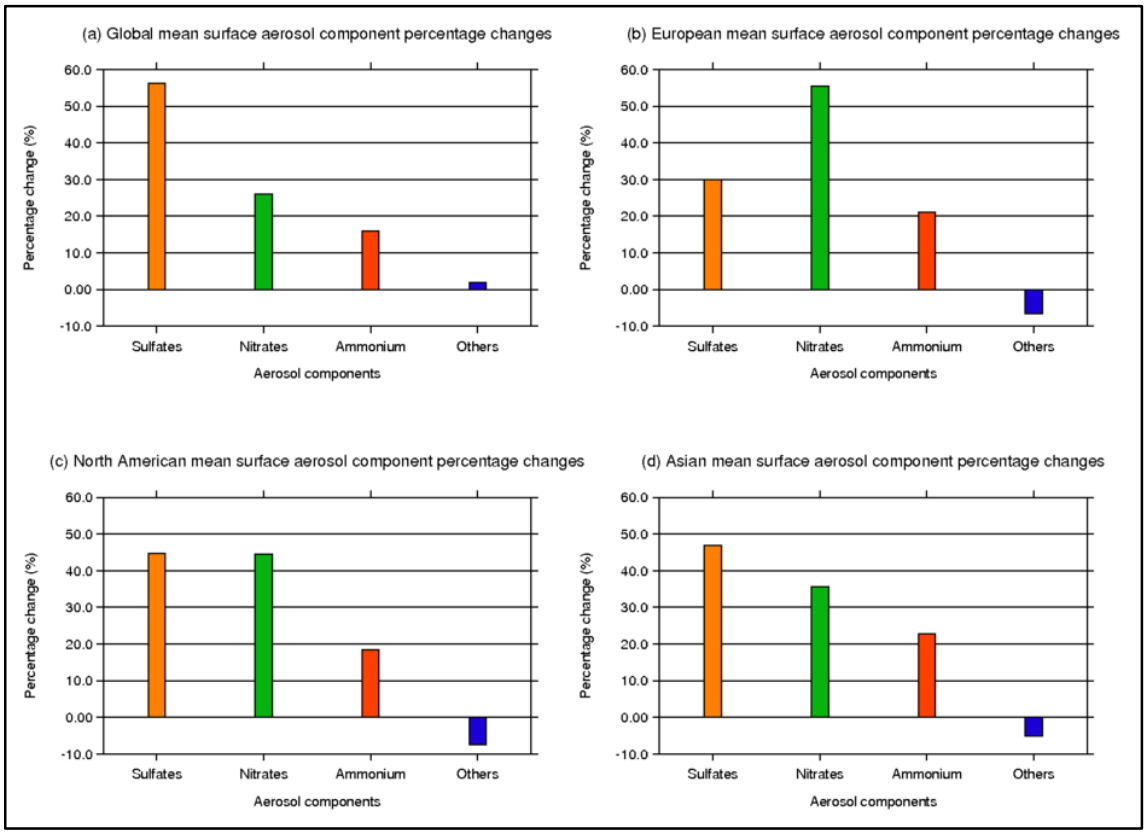

It is expected that regional domains extending over populated regions will show a greater tendency to $PM_{2.5}$ formation in comparison to the global domain, due to the interaction of other anthropogenic emission sources. This is as these regions generally include industrial and agricultural regions, from where non-aviation-borne anthropogenic emissions can be released (Lamarque et al., 2010a). *Exempli gratiā* non-aviation-borne emissions (e.g. SO_2) can interact with aviation-borne NO_X emissions resulting in the formation of ammonium sulfate (Barrett et al., 2010), demonstrating additional routes through which aviation emissions can impact on regional and global aerosol burden for individual species (Table 6.2).

Figure 6.4 shows that the majority of surface sulfate $PM_{2.5}$ perturbations occur within the 0°N–45°N latitude band. This could be explained by the formation of HONO from NO emissions directly emitted or formed from NO_2 (Fowler et al., 1997; Breider et al., 2010). HONO acts a temporary reservoir for both NO_X and OH, with both of these species being released via photolysis (Fowler et al., 1997). The latitudinal band at which the majority of these perturbations occur is in line with peaks in incoming solar radiation over the Northern Hemisphere summer and the emissions of aviation-borne NO_X. The resulting increase in OH

concentrations from the photolysis of HONO then promotes the formation of sulphuric acid from aviation-borne SO_2 emissions (Laaksonen et al., 2008; Finlayson-Pitts and Pitts Jr, 2000).

Figure 6.4: Aviation-induced (FSC = 600 ppm; NORM) aerosol component $PM_{2.5}$ absolute changes in concentration (NORM–NOAVI): (a) sulfate, (b) nitrate, (c) ammonium, and (d) other species. Boxes show the European (20°W–40°E, 35°N–66°N), North American (169°W–51°W, 21°N–80°N), and Asian (65°E–124°E, 4°N–46°N) regions.

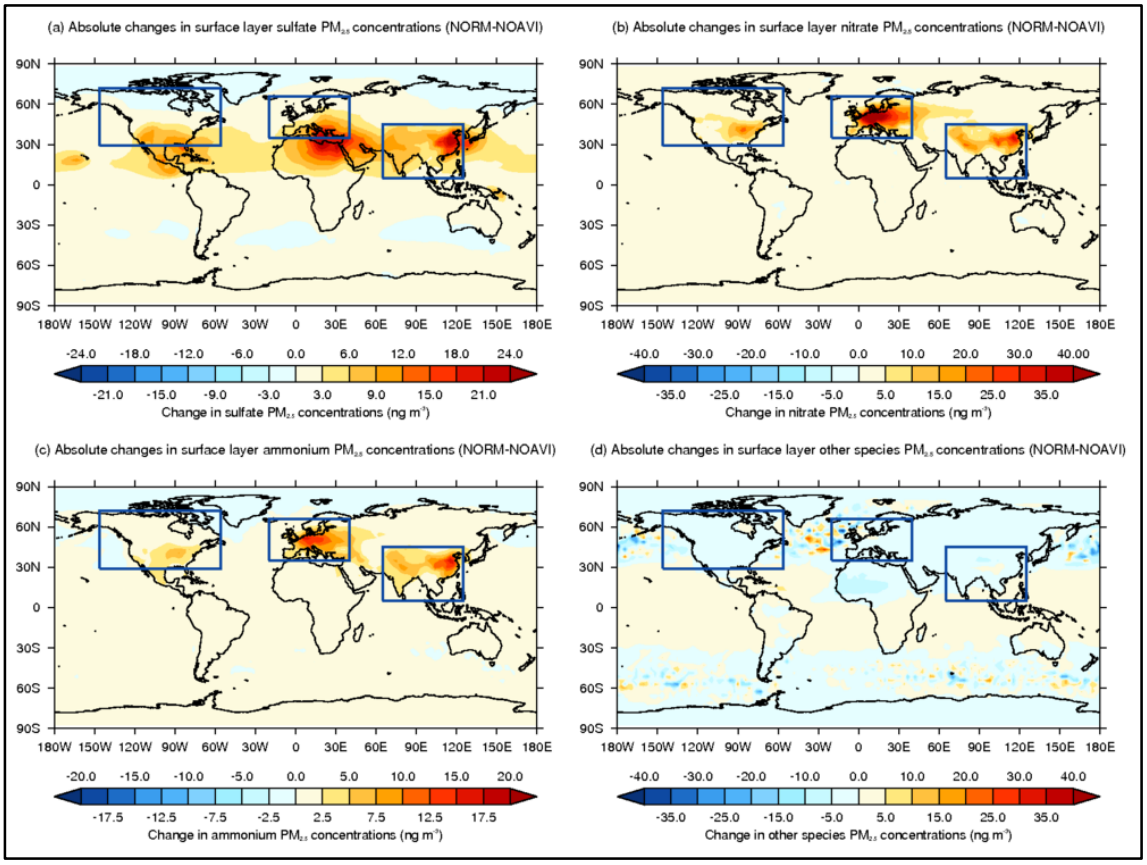

Figure 6.5(a) shows that the largest relative changes in the sulfate component of aviation-induced $PM_{2.5}$ occur over the Northern Hemisphere, with a mean change in sulfate $PM_{2.5}$ of 0.20% [2.21 ng m^{-3}]. Regionally aviation-borne emissions increase sulfate $PM_{2.5}$ concentrations by 0.48% [6.69 ng m^{-3}] over Asia, by 0.23% [6.13 ng m^{-3}] over Europe, and increases of 0.18% [2.82 ng m^{-3}] over North America. Additionally, Figure 6.5 shows absolute and percentage differences in global and regional aviation-induced aerosol components (NORM–NOAVI): sulfates, nitrates, and ammonium. Along with relative percentage differences in BC, OC, Na^+, dust and Cl (referred to as 'others').

As in Chapter 5, it has to be noted that the model evaluates height using a hybrid sigma-pressure (σ-p) methodology (i.e. terrain tracking at the surface resolving to a pressure levels at the top of the model domain), which through the assumption of a set height/pressure level will

most likely plot a region over the Himalayas which is not necessarily that representative of the level being plotted. Thus a large amount of uncertainty will reside over this region.

Figure 6.5: Aviation-induced (FSC = 600 ppm; NORM) aerosol component $PM_{2.5}$ percentage changes in concentration (NORM–NOAVI): (a) sulfate, (b) nitrate, (c) ammonium, and (d) other species. Boxes show the European (20°W–40°E, 35°N–66°N), North American (169°W–51°W, 21°N–80°N), and Asian (65°E–124°E, 4°N–46°N) regions.

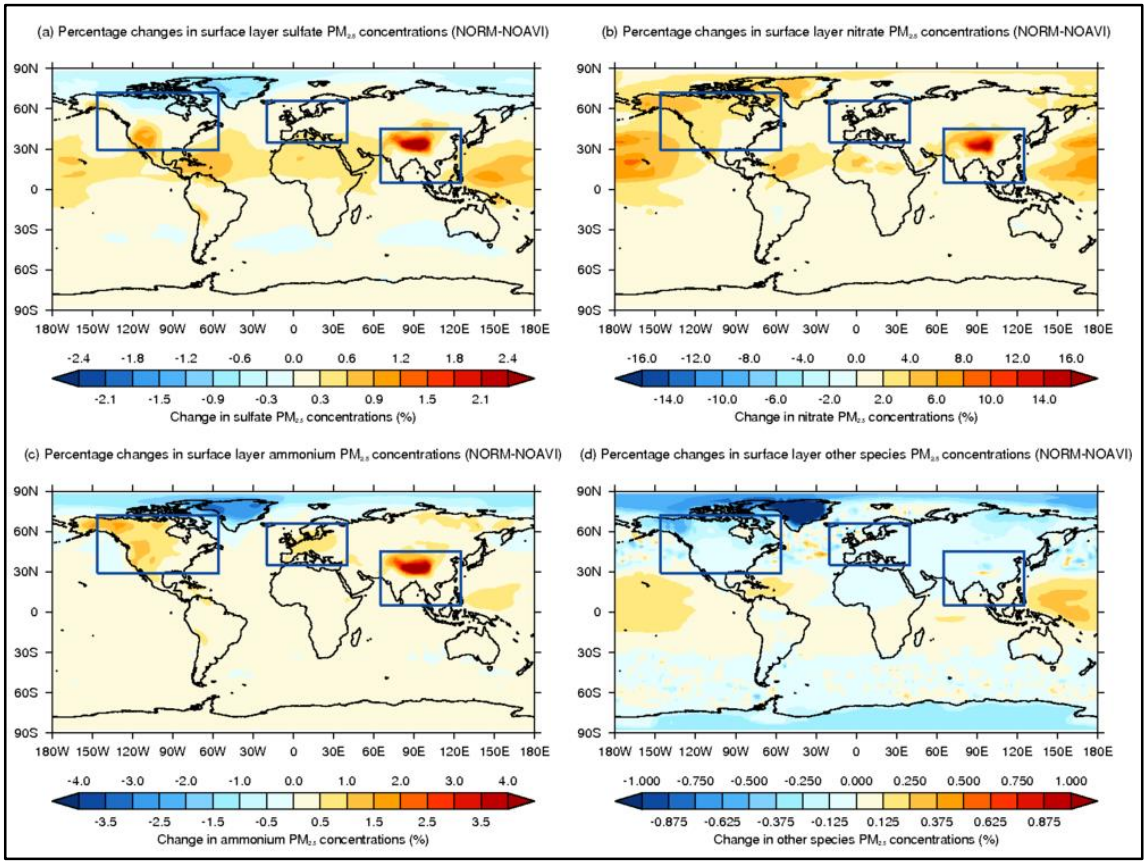

Perturbations in absolute surface nitrate $PM_{2.5}$ concentrations (Figure 6.4(b)) display a strong relationship with the distribution of aviation NO_X emissions (seen in Figure 5.3(a)). Aviation NO_X emissions participate in the formation of HNO_3 (Reaction 2.2) and then the subsequent formation of $NH_4.NO_3$ (Fowler et al., 1997) from anthropogenic and natural sources of ammonia (NH_3) (Reaction 2.20); a process dependent on the thermodynamic state and gas-phase concentrations of H_2SO_4, HNO_3 and NH_3 (Unger, 2011; Bauer et al., 2007).Figure 6.5(b) shows that the global mean relative change in nitrates is 1.56% [1.02 ng m^{-3}]. When considering changes over the regions of interest, the North American region demonstrates a greater relative change in aviation-induced nitrate $PM_{2.5}$ perturbations [2.63%; 2.81 ng m^{-3}], in comparison to Asia [2.48%; 5.08 ng m^{-3}] and Europe [1.03%; 11.30 ng m^{-3}].

Figure 6.4(c) shows a strong relationship between the formation of aviation-induced surface ammonium $PM_{2.5}$ concentrations with aviation-borne NO_X emissions and the global distribution

ammonia sources (Dentener and Crutzen, 1994; Janssens-Maenhout et al., 2012) (which can increase the partial pressure of NH_3 (Unger, 2011)). Regions with higher NH_3 partial pressures will allow for increases in the formation of ammonium nitrate ($NH_4.NO_3$), in addition to the formation of ammonium sulfate ($(NH_4)_2.SO_4$) (Bauer et al., 2007). Akin to nitrate perturbations (Figure 6.4(b) and Figure 6.5(b)), Figure 6.5(c) highlight that Asia witnesses a greater relative increase in aviation-induced surface layer ammonium $PM_{2.5}$ [0.72%; 3.24 ng m^{-3}], in comparison to North America [0.40%; 1.17 ng m^{-3}] and Europe [0.39%; 4.29 ng m^{-3}]; in comparison to the global mean of 0.19% [0.63 ng m^{-3}].

The importance of aviation-induced sulfates, nitrates and ammonium in comparison to other aerosol components considered in GMV4-nitrate (BC, OC, Na^+, dust and CL^-) is highlighted in Figure 6.5(d). Where global and regional decreases are seen; with mean absolute changes being up to an order of magnitude lower and relative changes being up to a factor of 10^3 lower than for sulfates, nitrates and ammonium.

When considering potential improvements to surface air quality ***Figure*** 6.2, Figure 6.8 and Table 6.2 show how the use of ULSJ (FSC = 15 ppm) affect global mean and regional aviation-induced $PM_{2.5}$ concentrations and aviation-induced sulfate and nitrate zonal distributions. The use of ULSJ fuel (FSC = 15 ppm) reduces global annual mean surface $PM_{2.5}$ concentrations (in relation to the NORM case) by 35.7% [1.41 ng m^{-3}]; predominantly through reductions in sulfates [–1.37 ng m^{-3}; –62.1%] and ammonium [–0.24 ng m^{-3}; –37.9%], which are marginally offset by increases in nitrates [+3.17x10^{-3} ng m^{-3}; +0.3%].

Barrett et al., (2012) estimate that swapping to ULSJ fuel reduces global mean sulfate concentrations by 0.96 ng m^{-3}, ammonium by 0.25 ng m^{-3}, with increases in nitrate concentrations of 0.27 ng m^{-3}; resulting in a net reduction in these three aerosol components of 0.89 ng m^{-3}. When comparing changes to these three aerosol species alone, this study simulated a net reduction of 1.61 ng m^{-3}. When all aerosol components modelled by GMV4-nitrate are considered a net reduction in surface $PM_{2.5}$ of 1.41 ng m^{-3} is estimated. This is due to an increase in the other aerosol species modelled (BC, OC, Na^+, dust and Cl^-) of +0.20 ng m^{-3} [+282%]; consisting of a reduction in BCOC of 3.44x10^{-3} ng m^{-3} [–11.76%] at the surface. This increase in the other aerosol species is primarily driven by increases in dust aerosols. This increase in dust could be attributed to a reduction in H_2SO_4 due the implementation of the ULSJ fuel case resulting in a reduction in the condensation of H_2SO_4 on dust aerosols, thus resulting in a reduction amount of dust transferred in soluble aerosol modes. When in the soluble mode these dust aerosols could act at CCN if with the correct size range, participating

in cloud droplet, thus providing an additional mode through which dust aerosols can be removed from the atmosphere.

Simulated aviation-induced surface-layer $PM_{2.5}$ concentrations from this study for both the standard aviation (NORM; FSC = 600 ppm) and the ULSJ fuel case (ULSJ; FSC = 15 ppm) (Figure 6.6(a,b,)) are compared to fields simulated by Barrett et al., (2012) (Figure 6.6(c,d)) (Barrett et al., 2012). This study simulates increases in $PM_{2.5}$ from standard aviation of up to 0.08 µg m^{-3} over Europe while Barrett et al. (2012) simulate increases in $PM_{2.5}$ concentrations over Europe of up to 0.4 µg m^{-3}; i.e. giving maximum sulfate $PM_{2.5}$ concentrations a factor of 5 greater than those simulated using GMV4-nitrate.

Figure 6.6: Aviation-induced surface $PM_{2.5}$ concentrations for (a,c) NORM (FSC = 600 ppm) and (b,d) ULSJ (FSC = 15 ppm), a comparison of simulated changes from TOMCAT-GLOMAP-mode (a,b) with GEOS-Chem (c,d): GEOS-Chem simulations from Barrett et al. (2012).

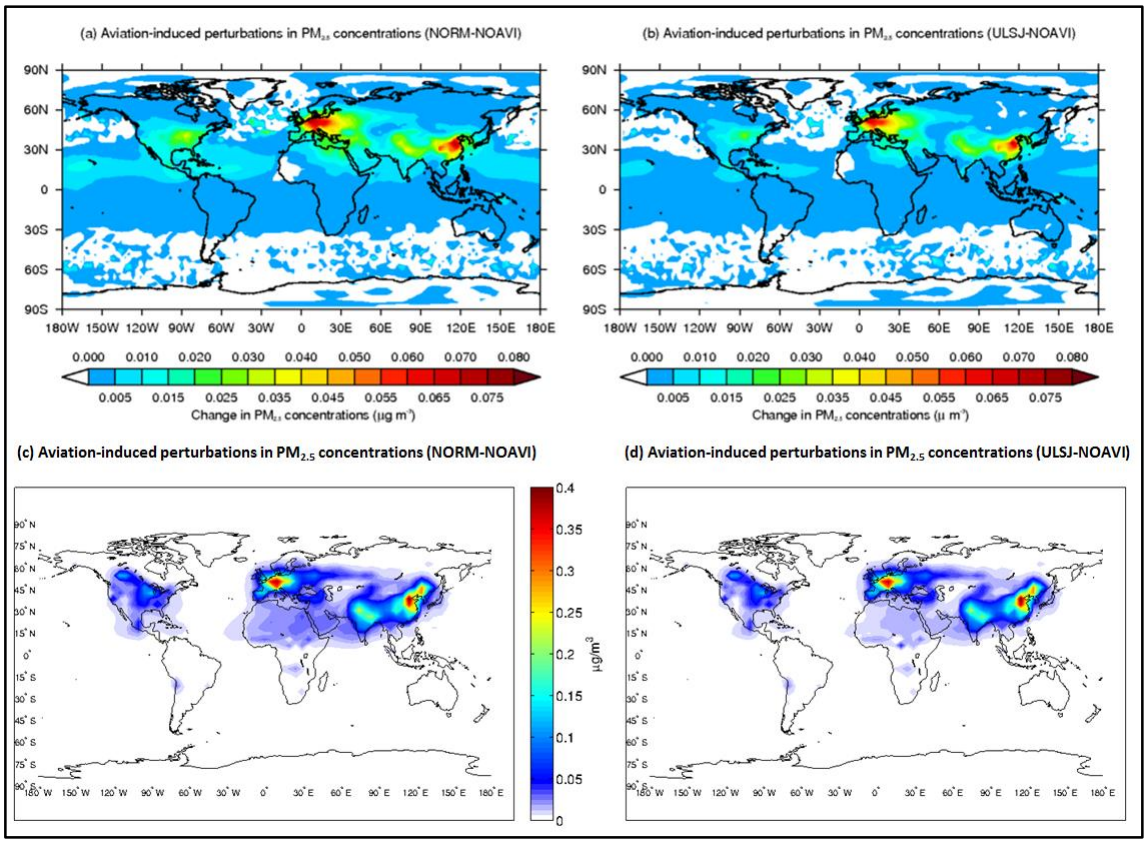

The differences in simulated surface-layer $PM_{2.5}$ perturbations help explain the differences in aviation-induced mortality described in Section 6.4.2 due to increases in cases of cardiopulmonary disease and lung cancer. Additionally Barrett et al. (2012) only considered BC, OC, sulfate, nitrate and ammonium aerosols, while GMV4-nitrate simulates sodium, dust, chloride in addition to these other aerosol. This study estimates that reductions in aviation-induced sodium from sea salt (Na^+) is responsible for ~3% of reductions in aviation-induced

$PM_{2.5}$ at the surface (when comparing the NORM and ULSJ case simulations), but acknowledge that is considered to be natural/intert. It is also estimated that aviation-induced dust increased by (+)61.82% when (relative to the NORM simulation), demonstrating the importance of considering all aerosol components due to their varied impacts.

Figure 6.7(a,b) shows that GMV4-nitrate simulations for aviation-induced perturbations in surface-layer sulfate concentrations for standard aviation (NORM; FSC = 600 ppm) and an ULSJ fuel case (ULSJ; FSC = 15 ppm) compare well against simulations conducted by Barrett et al. (2012) (Figure 6.7(c,d)). Reductions in surface sulfate concentrations over the United States, the Mediterranean/North Africa, East Asia and over the Pacific due to the implementation of ULSJ fuel show similar reductions to those seen by Barrett et al. (2012).

Figure 6.7: Aviation-induced surface sulfate concentrations for (a,c) NORM (FSC = 600 ppm) and (b,d) ULSJ (FSC = 15 ppm), a comparison of simulated changes from the nitrate-extended TOMCAT-GLOMAP-mode coupled model (a,b) with GEOS-Chem (c,d): GEOS-Chem simulations from Barrett et al. (2012).

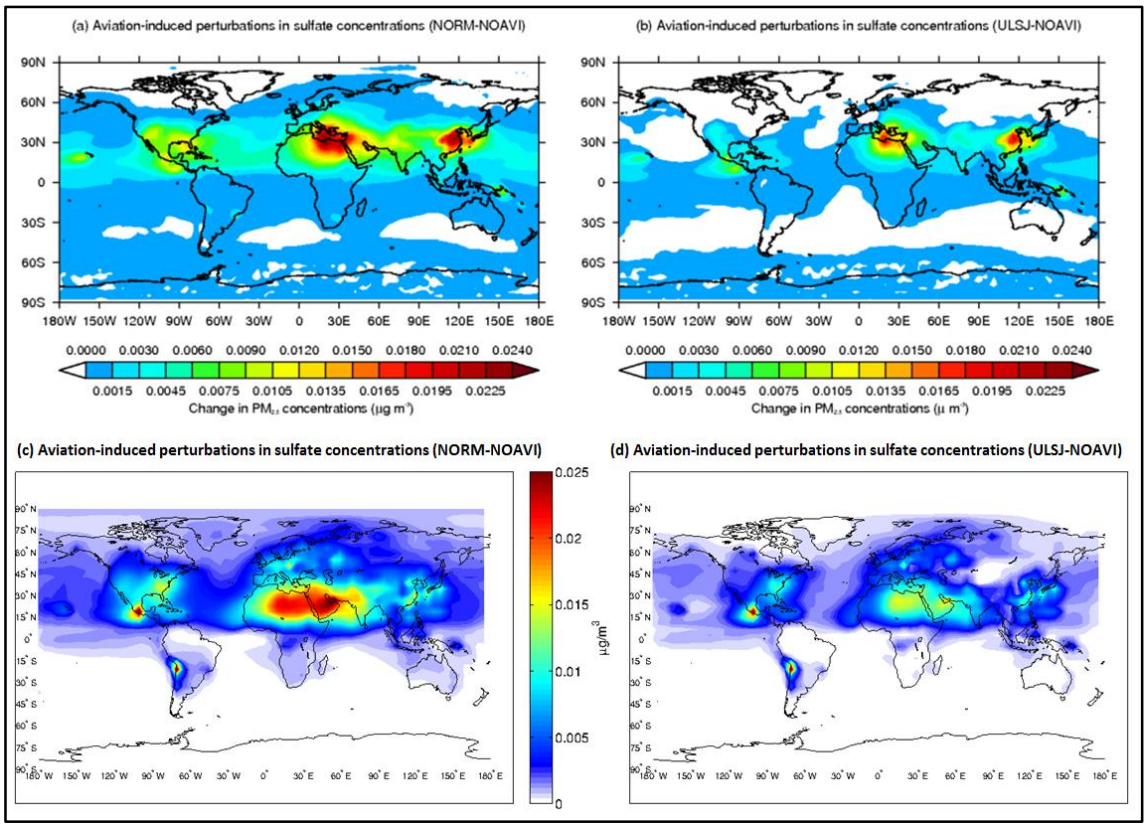

Maxima in surface layer concentrations due to standard aviation (NORM) from this study of ~0.025 µg m^{-3} over the Mediterranean/North Africa agree with previous work using GEOS-Chem (Barrett et al., 2012). The simulations conducted here using GMV4-nitrate show stronger influences in sulfate concentrations over East Asia, and lower changes over Mexico in comparison to Barrett et al., (2012)'s simulation using GEOS-Chem; which in part can be

explained by the differences in aviation emissions inventories used by Barrett et al., (2012) and here, i.e. fuelburn and distribution (Barrett et al., 2012).

Regional and global analysis of mean reductions in $PM_{2.5}$ due to the implementation of a ULSJ fuel strategy shows that larger mean reductions in $PM_{2.5}$ are simulated regionally in comparison to global mean reductions: Europe [**–**4.21 ng m^{-3}]; Asia [–3.48 ng m^{-3}]; North America [**–**3.38 ng m^{-3}]; and globally [–1.43 ng m^{-3}] (***Figure*** 6**.**2(b,c) and Table 6.2). When considering fractional changes over the global and regional domains swapping to ULSJ fuel reduces aviation-induced $PM_{2.5}$ by 53.4% over North America, by 35.7% over the global domain, by 24.4% over Asia, and by 20.5% over Europe.

The smaller fractional change in $PM_{2.5}$ over Europe is caused by smaller fractional reductions in aviation sulfate [**–**55.7%] and ammonium [–18.4%] compared to over North America, which sees a reduction in ammonium of 41.6% and reduction in sulfates of 103%. Indicating that over the US the ULSJ fuel scenario sees a reduction in sulfates in relation to the NOAVI scenario. This reduction in the fractional changes in sulfates formed over the US could be attributable to the ratio of other anthropogenic sources of SO_2 to NO_X (SO_2:NO_X), where over the US this ratio is <1.0, while over Europe and Asia a ratios of >1.0 exists (Lamarque et al., 2010a). Global variations in the SO_2:NO_X ratio arise due to the different regional anthropogenic NO_X and SO_2 emissions (Lamarque et al., 2010a).

GMV4-nitrate simulates reductions in aviation-induced sulfates of 48.1% [–3.22 ng m^{-3}] over Asia, comparable to reductions in sulfate $PM_{2.5}$ simulated over Europe [–55.93%; 3.43 ng m^{-3}]. Along with a reduction in Asian nitrates [–1.6%; 0.08 ng m^{-3}], which helps explain why Asia witnesses a greater fraction change in aviation-induced $PM_{2.5}$ in comparison to Europe. GMV4-nitrate simulates increases in nitrates when an ULSJ fuel strategy (ULSJ; FSC = 15 ppm) is implemented over Europe and North America of +0.94% and 0.85% respectively (Table 6.2).

Figure 6.8 shows the impact of changing to ULSJ fuel on zonal mean sulfate and nitrate concentrations relative to standard fuel (ULSJ–NORM). Table 6.3 reports the global aerosol burden from aviation under different emission scenarios in relation to a NOAVI scenario. Figure 6.8 shows the main reductions in aviation-induced sulfates and increases in aviation-induced nitrates from use of ULSJ fuel (FSC = 15 ppm) in relation to standard aviation (NORM; FSC = 600 ppm) occur around the cruise altitude of flight. In line with where the majority of emissions are released (Figure 4.1 in Section 4.3), resulting in smaller absolute and fractional changes at the surface-layer.

Taking this strategy further the complete desulfurisation of jet fuel (FSC = 0 ppm; DESUL) GMV4-nitrate simulates reductions in global mean aviation-induced surface-layer $PM_{2.5}$ concentrations of 36.5% [–1.43 ng m^{-3}]; with changes in sulfates [–1.40 ng m^{-3}; –63.5%] and ammonium [–0.24 ng m^{-3}; –38.8%] dominating.

Under this scenario (DESUL) reductions in surface-layer sulfate $PM_{2.5}$ from aviation are 105% [–2.96 ng m^{-3}] over North America, 63.5% [–1.40 ng m^{-3}] globally, 57.1% [–3.52 ng m^{-3}] over Europe, and 48.1% [–3.31 ng m^{-3}] over Asia. Under the complete desulfurisation of aviation decreases in nitrates are simulated over Europe [0.13 ng m^{-3}; 1.12%], North America [2.40x10^{-2} ng m^{-3}; 0.85%], and the global domain [1.45x10^{-3} ng m^{-3}; 1.12%], while over Asia an increase of 2.49% [0.13 ng m^{-3}] is simulated.

Figure 6.8: Simulated zonal differences in sulfate (a) and nitrate (b) concentrations produced from the use of ULSJ fuel relative to standard aviation fuel (ULSJ–NORM).

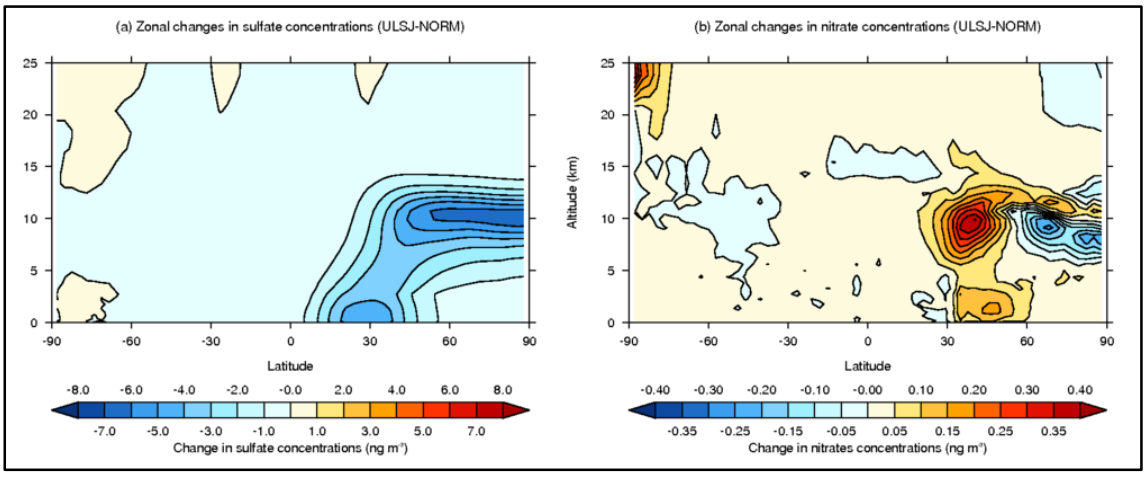

When the FSC of aviation fuel is varied between 0–6000 ppm increases in global mean surface $PM_{2.5}$ concentrations of up to 16.08 ng m^{-3} [+309%] are simulated, but as with the other cases discussed regional variations occur (***Figure*** 6.2 and Table 6.2). When aviation FSC is increased to 6000 ppm (OVER; FSC = 6000 ppm) $PM_{2.5}$ concentrations are increased over the European domain by 54.75 ng m^{-3} [+166%], by 45.17 ng m^{-3} [+217%] over the Asian domain, and by 35.26 ng m^{-3} [458%] over the North American domain. These larger increases in global and regional $PM_{2.5}$ concentrations are driven by large increases in aviation FSC; where FSC is increased by a factor of 10 in relation to standard aviation (NORM; FSC = 600 ppm).

In relation to standard aviation (NORM; FSC = 600 ppm), the ground release of aviation emissions (GROUND; FSC = 600 ppm) there is a decrease in aviation-induced surface-layer $PM_{2.5}$ concentrations of –1.44 ng m^{-3} [–36.7%] globally. Regionally surface-layer concentrations

are decrease by –8.12 ng m^{-3} [–57.0%] over the Asian domain, but increase by +13.52 ng m^{-3} [+65.7%] over the European and by +1.71 ng m^{-3} [+27.1%] over North America.

Reductions in global mean $PM_{2.5}$ concentrations from the ground release of aviation-emissions can be explained by changes in the timeframes that certain microphysical processes such as dry deposition and sedimentation, scavenging and coagulation can occur. Through a reduction in the altitude at which these emissions are released the timeframe during which coagulation can occur will be reduced, increasing dry deposition; decreasing aviation-induced aerosols lifetime per unit height (Mann et al., 2010; Spracklen et al., 2005a). In addition through the release of emissions and subsequent formation of aerosols below low-level clouds rates of scavenging (washout) can be increased, further reducing their atmospheric lifetime. This impact is highlighted when comparing the global burden of all aviation-induced aerosols for the GROUND case [1.87 Gg] in comparison to the NORM case [16.94 Gg]; resulting in a reduction in aerosols within the $PM_{2.5}$ size range of 15.07 Gg annually.

To investigate variations in FSC between the take-off / landing and the cruise phases of flight, two scenarios (SWITCH1 and SWITCH2) are simulated (***Figure*** 6.2 and Table 6.2). The SWITCH1 scenario produces increases in global mean aviation-induced surface-layer $PM_{2.5}$ concentrations of +2.05 ng m^{-3} [52.2%]. Regionally Asian concentrations are increased by +6.79 ng m^{-3} [47.6%], North American concentrations increase by +2.67 ng m^{-3} [+42.2%], while European mean concentrations increase by +0.93 ng m^{-3} [+4.5%]; all in comparison to the NORM case.

The SWITCH2 scenario is designed to emit the same global total sulfur emission as standard aviation (0.236 Tg(SO_2)), but again with altitudinal variations in FSC. The SWITCH2 simulation is seen to increase global mean surface aviation-induced $PM_{2.5}$ concentrations by +0.26 ng m^{-3} [+6.6%]. Regionally increases in $PM_{2.5}$ concentrations over Asia are seen +1.12 ng m^{-3} [7.6%], but with reductions over Europe [–1.8 ng m^{-3}; –8.7%] and North American [–0.8 ng m^{-3}; –12.8%] in comparison to the NORM case due to the change in the vertical distribution of aviation SO_2 emissions.

Under the NORM case (FSC = 600 ppm), a global aviation-induced aerosol burden of 16.94 Gg is simulated, dominated by sulfates (76.3%) and nitrates (33.4%). The use of ULSJ fuel (FSC = 15 ppm) reduces the global aerosol burden by 26.8%; with an associated reduction in aviation-induced sulfates of 69.1%, and increase in nitrates of 4.5%. Complete desulfurisation of aviation fuel reduces the global aerosol burden by 28.4%; reducing the aviation-induced global sulfate burden by 71.6%, and increasing the nitrate burden by 5.1% (Table 6.3). When aviation

emissions contain no sulfur (DESUL; FSC = 0 ppm), aviation-induced sulfates are formed a result of aviation NO_X induced OH perturbations, which participate in the formation of H_2SO_4 from other anthropogenic and natural sources of SO_2 (Finlayson-Pitts and Pitts Jr, 2000; Laaksonen et al., 2008; Barrett et al., 2010).

For the standard FSC scenario (NORM; FSC = 600 ppm), 36.2% of aviation-attributable sulfates formed at the surface-layer are associated with aircraft NO_X emissions and not directly with aviation sulfur emissions. This is less than Barrett et al. (2010)'s estimate of more than half. The use of ULSJ fuel and the complete desulfurisation of jet fuel are estimated to increase aviation-induced nitrate burdens by 4.5% and 5.1% respectively (Table 6.3). Although much of this increase occurs at altitudes above the surface (Figure 6.8), thus reducing aviation's impact on surface $PM_{2.5}$ concentrations.

Table 6.3: Global aviation-induced aerosol mass burdens for different emissions scenarios. Values in parentheses show percentage changes relative to NORM case.

Scenario	All components (Gg)	Sulfates (Gg)	Nitrates (Gg)
NORM	16.94	12.92	5.66
ULSJ	12.40 (–26.8%)	3.99 (–69.1%)	5.91 (+4.5%)
DESUL	12.13 (–28.4%)	3.67 (–71.6%)	5.95 (+5.1%)
No$NO_X$$SO_2$	1.00 (–88.3%)	0.33 (–97.5%)	0.12 (–97.9%)

Exploring the combined impact of both aviation NO_X emission reductions and fuel desulfurisation (No$NO_X$$SO_2$), GMV4-nitrate estimates a reduction in the global aviation-induced aerosol burden of (–)88.3% (Table 6.3), with an associated reduction in aviation-induced surface $PM_{2.5}$ concentrations of –95.0%. This implies that limited sulfate reductions are achieved through reducing FSC alone, with further reductions in aviation-induced $PM_{2.5}$ sulfates requiring additional controls on aviation NO_X emissions.

6.4.2 Aviation-induced premature mortality

Figure 6.9 presents annual aviation-induced premature mortalities, due to cardiopulmonary disease and lung cancer, for the year 2000. Premature excess mortalities presented are due to variations in FSC (FSC = 0–6000 ppm), and variations in the vertical distribution of aviation emissions (GROUND, SWITCH1 and SWITCH2) – Table 6.1.

GMV4-nitrate simulates that standard aviation (NORM; FSC = 600 ppm) is responsible for 3,597 [95% CI: 1,307–5,888] premature mortalities a^{-1} due to associated aviation-induced surface

perturbations in $PM_{2.5}$. This estimate (and associated range) is a result of the functions used to calculate aviation-induced mortality (discussed in Section 6.3.2). Low-, mid- and high-range are used to account for uncertainty within the cause-specific coefficient β. Mid-range estimates for aviation-induced premature mortalities, represent 36% of Barrett et al., (2012)'s estimate of ~10,000 mortalities a^{-1} (Barrett et al., 2012).

Figure 6.9: Estimates in (a) global, (b) European, (c) North American, and (d) Asian aviation-induced mortality as function of FSC and changes in vertical emissions distribution: FSC = 0–6000 ppm; GROUND; SWITCH1 and; SWITCH2 scenarios.

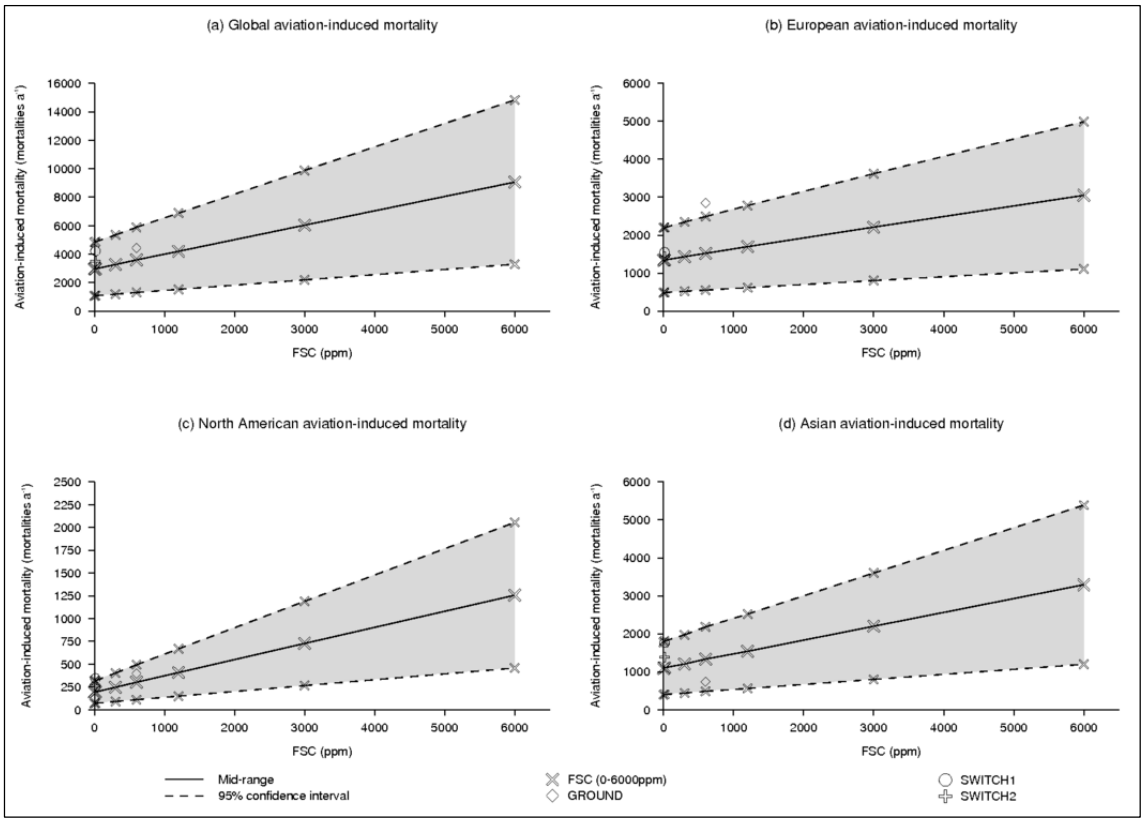

Estimates in global aviation-induced premature mortality are greatest over the Northern Hemisphere, accounting for 98.7% of global aviation-induced premature mortalities. Over Europe, Asia and North America 42.3%, 37.0 and 8.4% of aviation-induced premature mortality are estimated to occur, respectively (Table 6.4 and Figure 6.9(a)).

Greater levels of aviation-induced premature mortality are simulated by Barrett et al. (2012). This could be attributed to the greater concentrations of aviation-induced surface-layer $PM_{2.5}$ simulated in their study; particulary over highly populated areas. Their study simulated maxmium aviation-induced $PM_{2.5}$ concentrations over Europe, eastern China and eastern North America; greater than those simulated in this study by up to a factor of 5 over Europe and eastern China, and up toa factor of 2.5 over eastern North America. Aviation-induced sulfate concentrations simulated here compare well those simulated by Barrett et al. (2012),

indicating that differences in aviation-induced surface $PM_{2.5}$ concentrations are a result of other aerosol components.

Table 6.4: Aviation-induced mortality based on variations in FSC and vertical distributions of aviation-emissions (Low–, Mid– and High–range estimates): Estimates for the Global, European, North American and Asian spatial domains.

Scenario	Aviation-induced mortality (mortalities a^{-1})			
	Global Mid-range (low – high)	**European Mid-range (low – high)**	**North American Mid-range (low – high)**	**Asian Mid-range (low – high)**
DESUL	2950 (1072 – 4830)	1344 (489 – 2201)	192 (70 – 315)	1084 (394 – 1774)
ULSJ	2973 (1080 – 4868)	1343 (488 – 2199)	194 (71 – 318)	1105 (401 – 1809)
HALF	3266 (1187 – 5348)	1434 (521 – 2348)	246 (89 – 402)	1203 (437 – 1971)
NORM	3597 (1307 – 5888)	1521 (553 – 2490)	301 (110 – 493)	1332 (484 – 2182)
TWICE	4201 (1526 – 4201)	1698 (617 – 2780)	408 (148 – 668)	1538 (558 – 2518)
HIGH	6034 (2193 – 9879)	2212 (804 – 3620)	727 (265 – 1189)	2198 (798 – 3599)
OVER	9057 (3292 – 14826)	3049 (1108 – 4990)	1256 (457 – 2055)	3290 (1195 – 5388)
GROUND	4421 (1607 – 7237)	2847 (1035 – 4659)	397 (145 – 651)	738 (268 – 1208)
SWITCH1	4221 (1534 – 6911)	1551 (564 – 2539)	343 (125 – 561)	1766 (641 – 2892)
SWITCH2	3510 (1275 – 5746)	1435 (522 – 2349)	261 (95 – 427)	1385 (503 – 2267)

The use of ULSJ fuel results in 2,973 [95% CI: 1,080–4,867] global premature mortalities per annum. Therefore swapping from standard FSC to ULSJ has the potential to prevent 624 [95% CI: 227–1,021] aviation-induced global premature mortalities a^{-1} (Table 6.4 and Table 6.5); a 17.4% reduction. Regionally, the implementation of an ULSJ fuel strategy reduces annual premature mortality by 228 mortalities a^{-1} [–17.1%] over Asia, by 178 mortalities a^{-1} [–35.1%] over Europe, and by 107 mortalities a^{-1} [–11.7%] over North America.

Table 6.5: Changes in aviation-induced mortality due to variations in FSC, ground level emissions release (GROUND) and variations in vertical emissions release (SWITCH).

Scenario	Change in aviation-induced mortality (mortalities a^{-1}) [95% CI]	(%)
DESUL	–647 [–235 to –1059]	–18.0
ULSJ	–624 [–227 to –1021]	–17.3
HALF	–331 [–120 to –541]	–9.2
NORM	– –	–
TWICE	+604 [+220 to +989]	+16.8
HIGH	+2,438 [+886 to +3,990]	+67.8
OVER	+5,461 [+1,985 to 8,938]	+151.8
GROUND	+825 [+300 to +1,349]	+22.9
SWITCH1	+625 [+227 to +1,023]	+17.4
SWITCH2	–87 [–32 to –142]	–2.4

Figure 6.10 further illustrates that the ULSJ strategy has the potential to produce noticeable reductions in aviation-induced mortality over North America [–35.5%; 107 mortalities a^{-1}], Asia [–17.1%; 228 mortalities a^{-1}] and Europe [–11.7%; 178 mortalities a^{-1}]. Barrett et al. (2012) estimate that swapping to ULSJ fuel results in ~2,300 [95% CI: 890–4,200] fewer premature global mortalities a^{-1}; a reduction of 23%. In their work, the use of ULSJ reduced global mean sulfate concentrations by 0.96 ng m^{-3}, ammonium by 0.25 ng m^{-3} with increases in nitrate concentrations of 0.27 ng m^{-3}; resulting in a net reduction in these three aerosol components of 0.89 ng m^{-3}.

Figure 6.10: Aviation-induced mortality for (a) standard aviation (NORM) and (b) mortalities avoided through the implementation of an ULSJ fuel strategy.

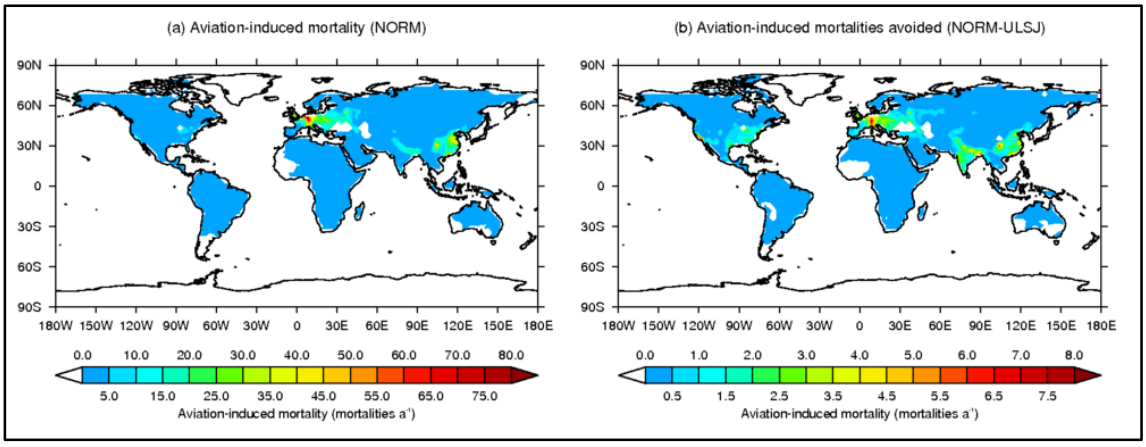

In comparison, this study estimates larger reductions in sulfates of 1.37 ng m^{-3}, lower reductions in ammonium of 0.24 ng m^{-3}, and much lower increases in nitrates of 3.17×10^{-3} ng m^{-3}; resulting in a net reduction of 1.61 ng m^{-3} (when considering these three components

alone). When considering all aerosol components, GMV4-nitrate simulates a net reduction in surface-layer $PM_{2.5}$ of 1.41 ng m^{-3}. This is due to increases in other aerosol species (BC, OC, Na^+, dust and Cl^-) of +0.20 ng m^{-3}, inclusive of a reduction in BCOC of $3.4x10^{-3}$ ng m^{-3}.

Investigating mortalities avoided on a country-specific basis, GMV4-nitrate simulates a reduction in aviation-induced premature mortalities over the United States of 108 [95% CI: 29–176], in line with Barrett et al. (2012)'s estimate of 120 [95% CI: 46–260]. Over China the use of ULSJ fuel reduces premature mortalities by 111 [95% CI: 40–181], whereas Barrett et al. (2012) estimate a reduction of 220 [95% CI: 85–390] (Barrett et al., 2012). In this study over India a reduction in aviation-induced premature mortality of 72 [95% CI: 26–119] would arise from the use of ULSJ fuel, in comparison to Barrett et al. (2012)'s estimation of 870 [95% CI: 340–1600]. While over Germany this study simulates a reduction in aviation-induced premature mortality of 22 [95% CI: 8–36], compared to previous estimates of 83 [95% CI: 32–150].

Differences between the two studies in estimates of mortalities avoided from the implementation of a ULSJ fuel strategy can in part be explained by the models used by Barrett et al., (2012) and here (GMV4-nitrate). Barrett et al. (2012) use GEOS-Chem with a model resolution of 4° x 5° over 47 levels which is constrained to consider sulfates, nitrates, ammonium, BC and OC. While utilising aviation emissions from the FAA's aviation environmental design tool (AEDT) for 2006 (Wilkerson et al., 2010). In addition their simulations are conducted for 2006 (Barrett et al., 2012), while in study considers the impacts for year 2000. Additionally, despite greater reductions in global mean surface layer $PM_{2.5}$ concentrations simulated here for the ULSJ fuel case, Barrett et al. (2012) simulate greater reductions in $PM_{2.5}$ over populated regions, which will likely result in greater reductions in aviation-induced premature mortality.

Differences in estimates of aviation-induced premature mortality and associated estimates in reductions in premature mortality reductions from the use of ULSJ fuel can be explained by the differences in aviation-induced surface $PM_{2.5}$ perturbations between the two studies. Differences in aviation-induced surface $PM_{2.5}$ concentrations drive the log-linear response of the mortality function. This study simulated maximum perturbations in aviation-induced $PM_{2.5}$ concentrations of up to 80 ng m^{-3} over Europe and China, while Barrett et al. (2012) simulated increases of up to 400 ng m^{-3} over these regions.

Figure 6.11: Aviation-induced mortality due to variations in FSC and changes in vertical aviation-emissions distributions (GROUND, SWITCH1 and SWITCH2 scenarios). Boxes show the European (20°W–40°E, 35°N–66°N), North American (169°W–51°W, 21°N–80°N), and Asian (65°E–124°E, 4°N–46°N) regions

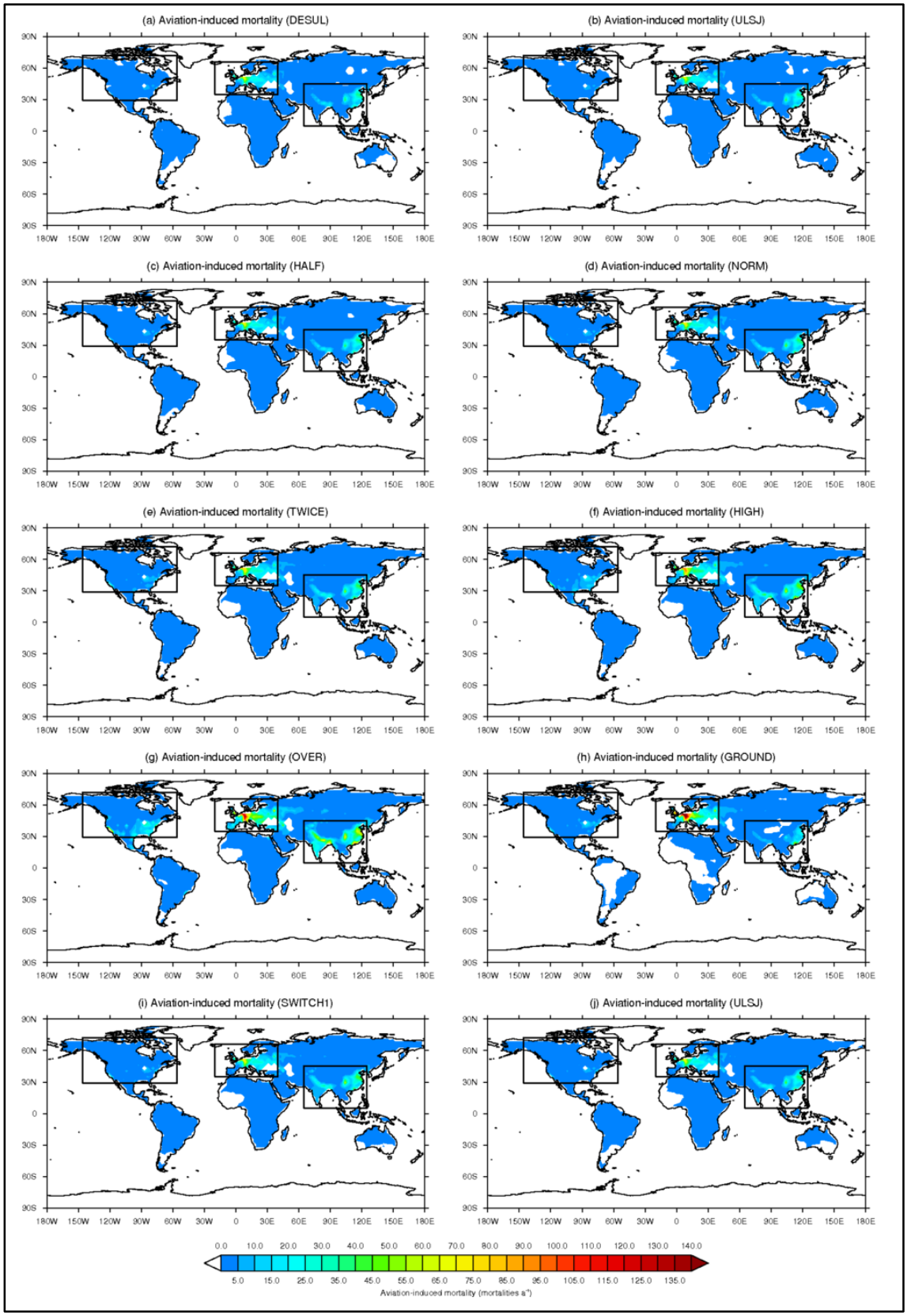

Taking investigations in to the effects of variations in FSC further, as seen in Table 6.1, it is found that decreases in FSC result in lower rates of annual mortality and increases in FSC result in increase annual mortality (Table 6.4). Table 6.5 presents estimates in changes in aviation-induced mortality in relation to standard aviation (NORM; FSC = 600 ppm). Table 6.5 and Figure 6.11 show how decreases in FSC can decrease aviation-induced premature mortality by up to 647 [95% CI: 235–1,059]; for a desulphurised fuel case (DESUL). And how simulated increased in FSC of up to 6000 ppm (OVER) estimate increases aviation-induced premature mortality of up to 5,461 [95% CI: 1,985–8,938].

Figure 6.11 illustrates how the density of aviation-induced premature moralities increases with increases in FSC, in line with aviation flight paths (Figure 4.1 in Section 4.3) and population density, reflecting the influence of aviation on surface $PM_{2.5}$ concentrations, its distribution and populated regions most sensitive to aviation-borne emissions. Simulated increases in mortality with FSC follow a log-linear relationship determined by relative increase in aviation-induced $PM_{2.5}$ (%) and the β function used to determine mortality. This study finds that globally variations in FSC increase surface $PM_{2.5}$ between 0.06–0.42%; a range that elicits a near linear response in aviation-induced mortality, as seen in Figure 6.9.

Collapsing the release of aviation-borne emissions to ground-level (GROUND) simulates an increase in aviation-induced mortality of 22.9% [+825 mortalities a^{-1}], correlating with increases in surface level $PM_{2.5}$ concentrations relative to standard aviation (NORM) – ***Figure*** 6.2 and Table 6.2. The SWITCH1 case produces increases in aviation-induced mortality of +17.4% [+625 mortalities a^{-1}]. The SWITCH2 case, which emits the same amount of SO_2 as standard aviation, results in an estimated decrease in mortality of 2.4% [–87 mortalities a^{-1}] in comparison to the NORM case.

6.4.3 Sensitivity of cloud condensation nuclei (CCN) to aviation FSC

Aviation emissions with a standard FSC (NORM; FSC = 600 ppm) increase global mean CCN (Dp > 50 nm) at low-cloud level (879 hPa; 0.96 km) by 1.0% (Figure 6.12 and Figure 6.13). Simulated increases in CCN concentrations are greater in the Northern Hemisphere [+4.21 cm^{-3}; +1.7%] compared to the Southern Hemisphere [+0.44 cm^{-3}; +0.4%]. Maximum increases in low-level CCN are simulated over the Pacific, central Atlantic and Arctic Oceans. CCN at low-level clouds (~879 hPa) are concentrated on, as this relates to liquid clouds. Regionally, increases in CCN at 879 hPa of 8.21 cm^{-3} [1.4%] are simulated over Asia, 3.26 cm^{-3} [1.3%] over North America, 3.01 cm^{-3} [0.7%] over Europe, 2.93 cm^{-3} [1.6%] over the Atlantic and 2.54cm^{-3} [1.6%] over the Pacific Ocean.

Figure 6.12: Aviation-induced changes in low-level (879 hPa) CCN (DP > 50 nm) for FSC variations, GROUND, SWITCH1 and SWITCH2 scenarios: Blue boxes define North American and European regions, while black boxes define Atlantic (60°W–14°W, 1.4°S–60°N) and Pacific (135°–121°W,15°S–60°N).

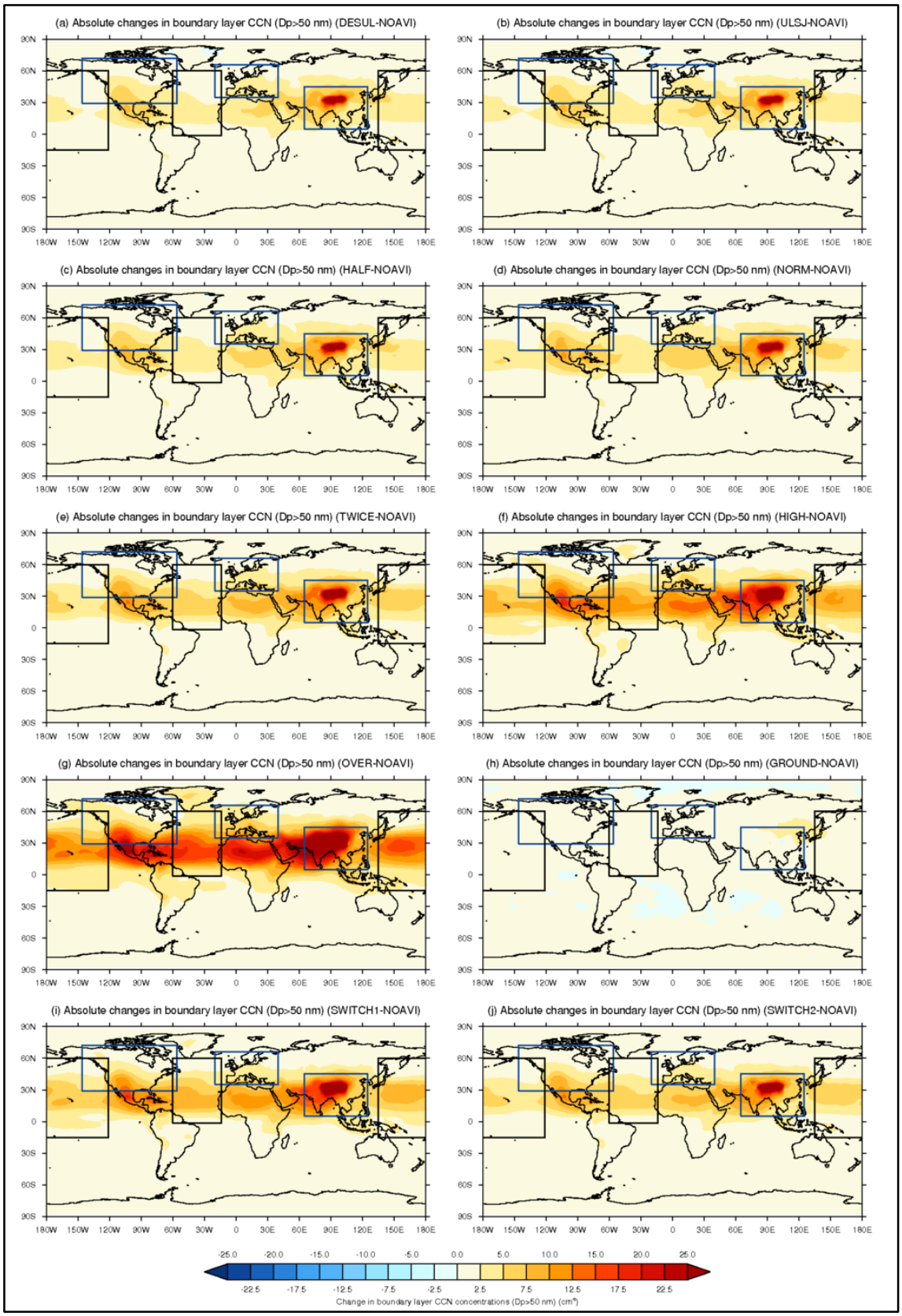

Figure 6.13: Aviation-induced percentage changes in low-level (879 hPa) CCN (DP > 50 nm) for FSC variations, GROUND, SWITCH1 and SWITCH2 scenarios: Blue boxes define North American and European regions, while black boxes define Atlantic (60°W–14°W, 1.4°S–60°N) and Pacific (135°E–121°W, 15°S–60°N).

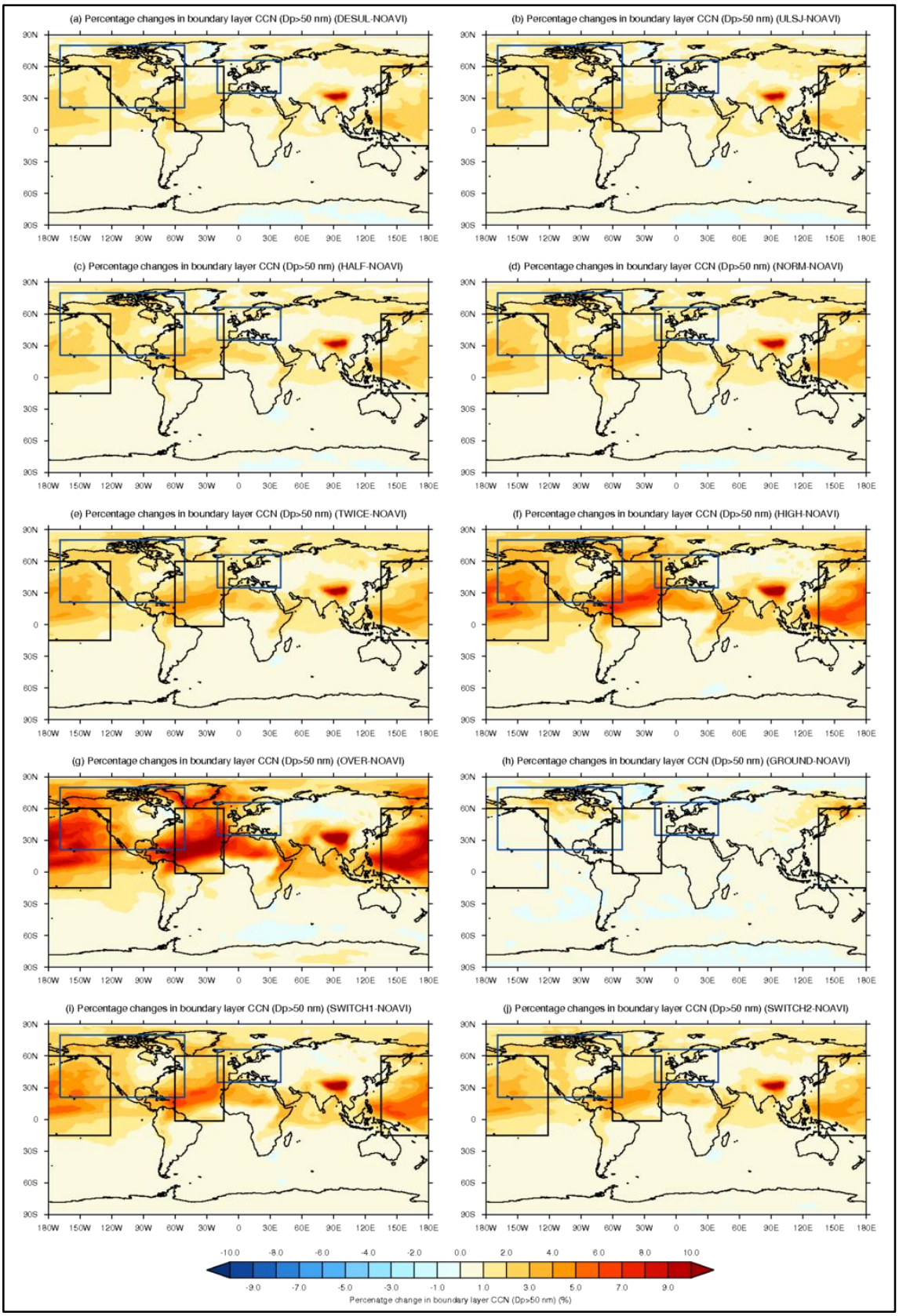

The use of ULSJ fuel (ULSJ; FSC = 15 ppm) produces reductions in global mean low-level CCN concentrations of 0.42 cm^{-3} [–18.2%], relative to the NORM case (Figure 6.12(b) and Figure 6.13(b)). The ULSJ fuel scenario reduces Northern Hemisphere mean CCN concentrations by 0.76 cm^{-3} [–19.4%], and Southern Hemisphere concentrations by 0.08 cm^{-3} [–11.5%] (Figure 6.12 and Figure 6.13). Figure 6.14 which follows shows the sensitivity of low-level CCN concentrations as a function of FSC. As with $PM_{2.5}$, simulated changes in CCN are found to be linear with respect to FSC (Figure 6.14), with regional variations in the magnitude of response.

Figure 6.14: Global and regional variations in CCN (Dp > 50 nm): (a) changes in mean concentrations and (b) percentage changes.

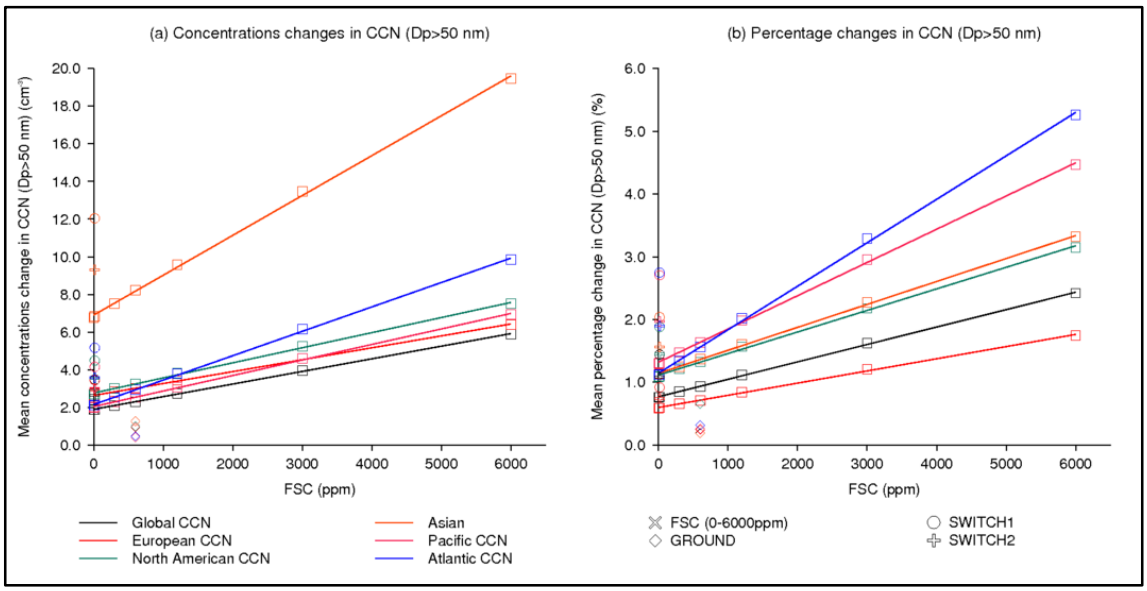

As with analysis of the relationship between aviation-induced surface-layer $PM_{2.5}$ concentrations and FSC, the linearity of aviation-induced low-level (879 hPa) CCN (Dp > 50nm) with FSC was statically analysed via significance tests; obtaining R^2 and *p*-values. This yields the following: Globally $R^2 > 0.99$ and *p*-value = 2.3×10^{-9}; over Europe $R^2 > 0.99$ and *p*-value = 1.4×10^{-8}; over North America $R^2 > 0.99$ and *p*-value = 3.0×10^{-8}; Pacific $R^2 > 0.99$ and *p*-value = 4.2×10^{-9} and; Atlantic $R^2 > 0.99$ and *p*-value = 3.8×10^{-9}.

In line with $PM_{2.5}$ and aviation-induced premature mortality there are regional variations in CCN perturbations. Regional CCN sensitivities due to variation in FSC rank in the following order: Asia [$+2.12 \times 10^{-3}$ cm^{-3} ppm^{-1}] > Atlantic [$+13.0 \times 10^{-4}$ cm^{-3} ppm^{-1}] > Pacific [$+8.2 \times 10^{-4}$ cm^{-3} ppm^{-1}] > North America [$+8.0 \times 10^{-3}$ cm^{-3} ppm^{-1}] > global [$+6.7 \times 10^{-4}$ cm^{-3} ppm^{-1}] > Europe [$+6.3 \times 10^{-4}$ cm^{-3} ppm^{-1}] – showing that over the Asian region perturbations in CCN are most sensitive to aviation-borne emissions Figure 6.14. The high sensitivity to CCN formation over aviation over Asia and low sensitivity to CCN formation over Europe could be attributed to the distribution of aviation emissions in tandem with the distribution of monthly-mean low-cloud

occurtenc; as seen by the cloud fraction observations from MODIS for 2001 (Chang and Li, 2005).

The implementation of an ULSJ fuel strategy (ULSJ; FSC = 15 ppm) produces reductions in both aviation-induced CCN global and regional mean concentrations. Reductions are simulated to be largest over Asia [–1.39 cm^{-3}; –16.87%], followed by over Atlantic region [–0.81 cm^{-3}; –27.76%], North America [–0.55 cm^{-3}; –16.89%], the Pacific region [–0.51 cm^{-3}; –20.22%], the global domain [–0.42 cm^{-3}; –18.21%] and finally over Europe [–0.4 0 cm^{-3}; –13.41%] (Table 6.6 and Table 6.7). Like the implementation of the ULSJ fuel strategy when aviation fuel is completely desulfurised further reductions were simulated; following the same reduction trends as seen in with ULSJ (Table 6.6 and Table 6.7).

Table 6.6: Changes in global and regional mean concentrations of low-level CCN (Dp > 50nm) due to variations in FSC, ground level emissions release (GROUND) and variations in vertical emissions release (SWITCH).

	Change in low-level CCN concentrations					
Scenario	**Global**	**Europe**	**North America**	**Asia**	**Atlantic ocean**	**Pacific ocean**
	(cm^{-3})	**(cm^{-3})**	**(cm^{-3})**	**(cm^{-3})**	**(cm^{-3})**	**(cm^{-3})**
DESUL	–0.43	–0.41	–0.57	–1.44	–0.54	–0.82
ULSJ	–0.42	–0.40	–0.55	–1.39	–0.51	–0.81
HALF	–0.20	–0.17	–0.27	–0.69	–0.26	–0.41
NORM	–	–	–	–	–	–
TWICE	0.44	0.42	0.56	1.37	0.54	0.85
HIGH	1.66	1.60	1.97	5.25	2.06	3.24
OVER	3.58	3.38	4.25	11.26	4.40	6.92
GROUND	–1.89	–2.06	–2.26	–6.95	–2.12	–2.46
SWITCH1	1.18	0.44	1.22	3.83	1.61	2.24
SWITCH2	0.34	-0.04	0.28	1.10	0.49	0.65

Figure 6.14(a) shows that absolute changes in Asian CCN are most sensitive to increases in FSC, whereas changes in European CCN due to FSC are least sensitive. Figure 6.14(b) shows that when fractional changes are considered Atlantic responses to FSC induced CCN are greatest; while over European responses are again shown to be the least sensitive. Indicating that fuel strategies involving variations in FSC could yield regional effects on CCN, and affect climate via changes to the aCAE (aerosol cloud albedo effect).

Regional effects of variations in aviation FSC on CCN formation are further highlighted in Figure 6.13, where relative increases in low-level CCN are seen to be greater over the Atlantic and

Pacific Oceans, a change which could result in increases in cloud droplet number concentrations (CDNC) over these regions. The resulting increase in CDNC has the potential to have a brightening effect on clouds, reducing the amount of solar insolence that reaches the ocean bodies below and reducing the heat absorbed by the Earth's climate system; thus returning a cooling effect via perturbations in the aCAE.

Table 6.7: Percentage changes in global mean concentrations of low-level CCN (Dp > 50nm) due to variations in FSC, ground level emissions release (GROUND) and variations in vertical emissions release (SWITCH).

Scenario	Change in low-level CCN concentrations					
	Global (%)	Europe (%)	North America (%)	Asia (%)	Atlantic ocean (%)	Pacific ocean (%)
DESUL	–18.59	–13.62	–17.60	–17.51	–21.20	–27.91
ULSJ	–18.21	–13.41	–16.89	–16.87	–20.22	–27.76
HALF	–8.75	–5.63	–8.17	–8.44	–10.05	–13.85
NORM	–	–	–	–	–	–
TWICE	19.04	14.09	17.27	16.69	21.35	29.11
HIGH	72.28	53.30	60.44	63.89	81.00	110.66
OVER	155.65	112.26	130.21	137.05	173.39	236.54
GROUND	–82.13	–68.68	–69.26	–84.64	–83.62	–84.00
SWITCH1	51.22	14.61	37.48	46.65	63.58	76.51
SWITCH2	14.60	–1.37	8.48	13.44	19.14	22.19

Releasing aviation emissions at the surface increases global mean low-level CCN by 0.4 cm^{-3} relative to NOAVI, with a reduction of (–)82.1% [–1.89 cm^{-3}] relative to the NORM case (i.e. GROUND–NORM). That is, injecting aviation emissions into the free troposphere in the standard scenario (NORM; FSC = 600 ppm) is more than 5 times more efficient at creating CCN compared to when the same emissions are released at the surface [GROUND CCN = 0.41 cm^{-3}; NORM CCN = 2.30 cm^{-3}]; both in relation to the NOAVI scenario (Table 6.6 and Table 6.7).

Similar behaviour has been demonstrated previously for volcanic SO_2 emissions (Schmidt et al., 2012). Demonstrating that volcanic SO_2 emissions injected into the free troposphere (FT) are more than twice as effective at producing new CCN compared to boundary layer emissions of DMS. The injection of aviation SO_2 emissions at the surface will increase both deposition rates and aqueous phase oxidation of SO_2 resulting in the growth of existing CCN, but not the formation of new CCN. In contrast, when SO_2 is emitted into the FT the dominant oxidation mechanism is to H_2SO_4, leading to the formation of new CCN through particle formation and the condensational growth of particles to larger sizes. Subsequent entrainment of these new

particles into the lower atmosphere results in enhanced CCN concentrations in low-level clouds.

This reduced CCN formation from the ground release of aviation emissions goes on to have implications on the resulting aviation-induced aCAE (Section 6.4.4). Regionally the greatest reductions in low-level CCN are simulated over Asia [–6.95 cm^{-3}; –84.6%], with the lowest absolute reductions simulated over Europe [–2.06 cm^{-3}; –68.7%]. Over North America, the Atlantic and Pacific oceans reductions in CCN of –2.26 cm^{-3} [–69.3%], –2.12 cm^{-3} [–83.6%] and –2.46 cm^{-3} [–84.0%] are simulated respectively; resulting in noticeable reductions in low-level CCN over the Pacific and Atlantic oceans (Figure 6.12(h) and Figure 6.13(h)) in relation to the standard case (Figure 6.12(d) and Figure 6.13(d)).

The SWITCH1 scenario results in increases in global mean low-level CCN (in relation to the NORM case) of +1.18 cm^{-3} [+51.2%], an increase attributed to increases in aviation-emitted SO_2 within this scenario of a factor of 2.08 in relation to the standard (NORM) case (which emits 0.236 Tg(SO_2) in total per annum). Regionally this scenario results in increases in low-level CCN across each region investigated. With Asian CCN increased by 3.83 cm^{-3} [+46.7%], North America CCN increased by 1.22 cm^{-3} [+37.5%], European CCN increased by 0.44 cm^{-3} [14.6%], CCN over the Pacific ocean increased by 2.24 cm^{-3} [76.51%], and CCN over the Atlantic ocean increased by 1.61 cm^{-3} [63.6%]. These increases in CCN concentrations result in large increases in the aCAE induced cooling effect (Section 6.4.4).

The SWITCH2 scenario emits the same mass of SO_2 as in the NORM case (0.236 Tg(SO_2)). SWITCH2 results in increases in global mean low-level CCN concentrations of 0.34 cm^{-3} [14.6%]. Regionally this scenario simulates increases in low-level CCN over Asia [+1.10 cm^{-3}; 13.4%], the Pacific Ocean [+0.65 cm^{-3}; 22.2%], the Atlantic Ocean [+0.49 cm^{-3}; 19.1%], North America [+0.28 cm^{-3}; 8.5%], but reductions over Europe [–0.04 cm^{-3}; –1.4%].

6.4.4 Sensitivity of aerosol and ozone radiative effect to FSC

Here, the climatic effect of standard aviation and variations in FSC are discussed. As the FSC is varied aviation-induced sulfates will vary, thus impacting the aerosol direct radiative effect (aDRE) and aerosol cloud albedo effect (aCAE). GMV4-nitrate simulations for standard aviation (NORM; FSC = 600 ppm) in conjunction with the Edwards-Slingo radiative transfer model estimate the global mean combined radiative effect (RE_{comb}) from aviation to be –13.29 mW m^{-2} (Table 6.8). The combined climate effect is a result of warming from the aerosol direct

radiative effect (aDRE) of +1.4 mW m^{-2} and O_3 direct RE (O3DRE) of +8.9 mW m^{-2}, and a cooling effect from the aerosol cloud albedo effect (aCAE) of –23.6 mW m^{-2} (Figure 6.15).

Table 6.8: Aviation-induced radiative effect due to variations in FSC: Ozone direct effect (O3DRE), Aerosol direct radiative effect (aDRE), aerosol cloud albedo effect (aCAE) and combined radiative effect (RE_{comb}).

Scenario	Radiative effect (mW m^{-2})			
	O3DRE	aDRE	aCAE	RE_{comb}
DESUL	8.74	1.78	–16.60	–6.08
ULSJ	8.74	1.76	–16.82	–6.32
HALF	8.75	1.54	–20.13	–9.84
NORM	8.86	1.40	–23.55	–13.29
TWICE	8.80	1.07	–30.51	–20.64
HIGH	8.88	–0.08	–50.19	–41.39
OVER	9.02	–2.41	–82.09	–75.48
GROUND	1.48	5.85	–2.31	5.02
SWITCH1	8.89	2.07	–42.37	–31.41
SWITCH2	8.80	1.93	–28.89	–18.16

Figure 6.15 shows the O3DRE, aDRE, aCAE and RE_{comb} for standard aviation emissions. Increases in O3DRE are simulated to primarily occur in the Northern Hemisphere between 15°–60°N (Figure 6.15(a)), in line with the location of the majority of aviation NO_X emissions; resulting in an aviation-induced ozone radiative effect of +8.86 mW m^{-2}.

Normalising O3DRE for standard aviation (NORM; FSC = 600 ppm) to aviation NO_X emissions (represented in Tg of N), returns a normalised O3DRE of +10.5 mW m^{-2} $Tg(N)^{-1}$, which is at the lower end of current estimates [7.4–37.0 mW m^{-2} $Tg(N)^{-1}$] (Myhre et al., 2011; Holmes et al., 2011; Lee et al., 2009; Sausen et al., 2005; Frömming et al., 2012; Hoor et al., 2009; Unger, 2011; Unger et al., 2013; Köhler et al., 2008; Khodayari et al., 2014a; Skowron et al., 2013). This is attributed to the lower net O_3 chemical production efficiency within GMV4-nitrate (1.33). Unger (2011) estimate an O3DRE of 7.4 mW m^{-2} $Tg(N)^{-1}$ with a model OPE of ~1, while the ensemble of models considered by Myhre et al. (2011) have an OPE range of 1.5–2.4, resulting in an O3DRE range of 16.2–25.4 mW m^{-2} $Tg(N)^{-1}$.

The aDRE [+1.4 mW m^{-2}] estimate from this study for standard aviation (NORM; FSC = 600 ppm) lies in the middle of the range from previous studies. Aviation aerosol DRE has been previously assessed as highly uncertain, ranging between –28 to +20 mW m^{-2} (Righi et al., 2013). When sum of aDRE due to aviation-induced sulfates, nitrates, BC and OC are considered alone (where available), previous studies estimate a range between –0.6 and –10.4 mW m^{-2}

(Balkanski et al., 2010; Fuglestvedt et al., 2008; Unger et al., 2013; Gettelman and Chen, 2013; Lee et al., 2009; Sausen et al., 2005) (as seen in Section 2.4.3.3 and Section 5.4.1.2.2).

Figure 6.15: Aviation-induced radiative effect for standard aviation (NORM: FSC = 600ppm): (a) O_3 DRE, (b) aerosol DRE and, (c) aerosol CAE and, (d) combined radiative effect (O3DRE + aDRE + aCAE).

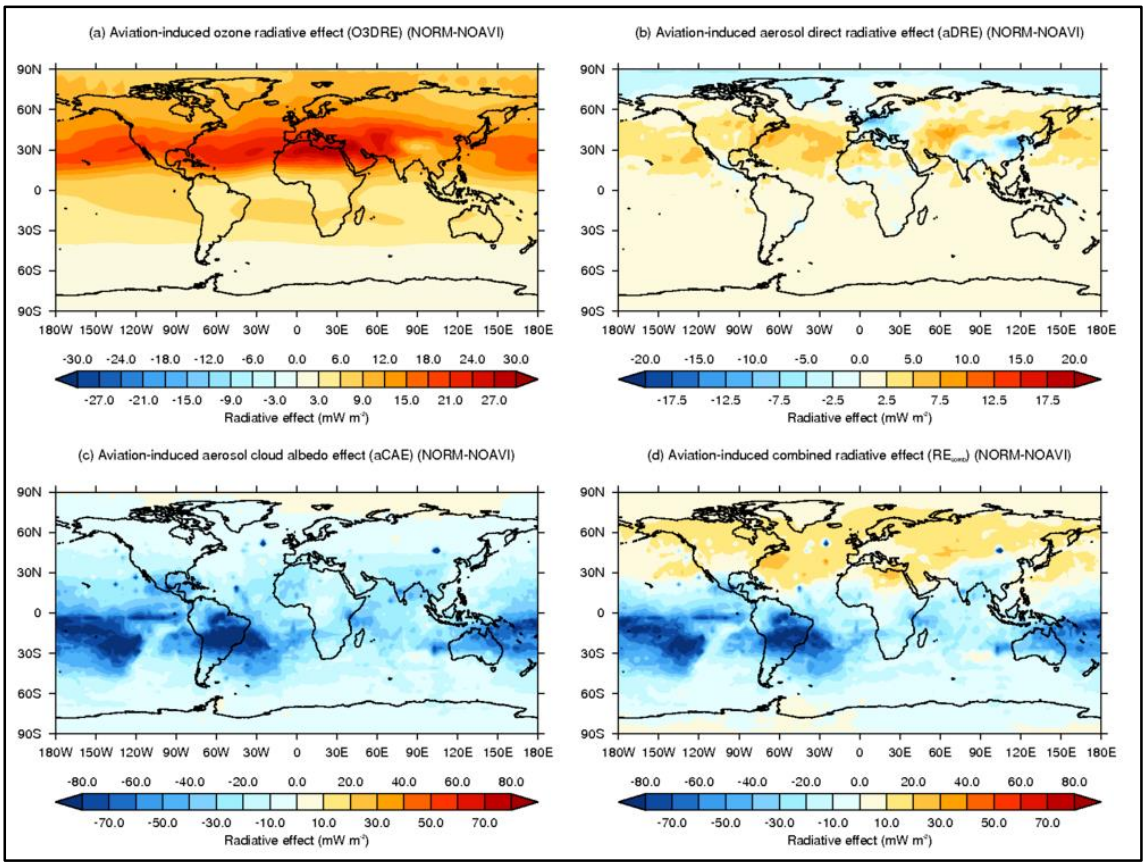

Regionally, standard aviation emissions (NORM: FSC = 600 ppm) produce negative aDRE over Europe [up to –12.5 mW m^{-2}] and Asia [up to –17.5 mW m^{-2}], and warming influences over south-west Asia and the western Atlantic ocean [up to +10 mW m^{-2}] (Figure 6.15(b)). The cooling influence of the aDRE over these regions are attributed to high increases in total column concentrations of aviation-induced sulfates and nitrates, while the regions of higher positive aDRE show a correlation with higher total column BC:SO_4 + NO_3 ratio values.

The positive aviation-induced aDRE estimated here is a result of the higher levels of aviation-induced BC concentrations simulated over the Northern Hemisphere at ~250 hPa. In comparison to previous work aviation-induced BC mass concentrations simulated by GMV4-nitratre are a factor of 8 greater during the DJF season, and a factor of 5 greater during the JJA season (Hendricks et al., 2004) (Figure 6.16). Additionally, in comparison to previous work, GMV4-nitrate simulates a greater level of aviation-induced BC perturbations above the cruise region of flight (Hendricks et al., 2004; Righi et al., 2013) (Figure 6.16 and Figure 6.17).

Figure 6.16: Comparison of aviation-induced black carbon concentrations in the free troposphere for the DJF (a, c) and (b, d) seasonal means: (a) and (b) are from Hendricks et al., (2004) for 250 hPa, (c) and (d) are from work done for this study for 236 hPa (Hendricks et al., 2004).

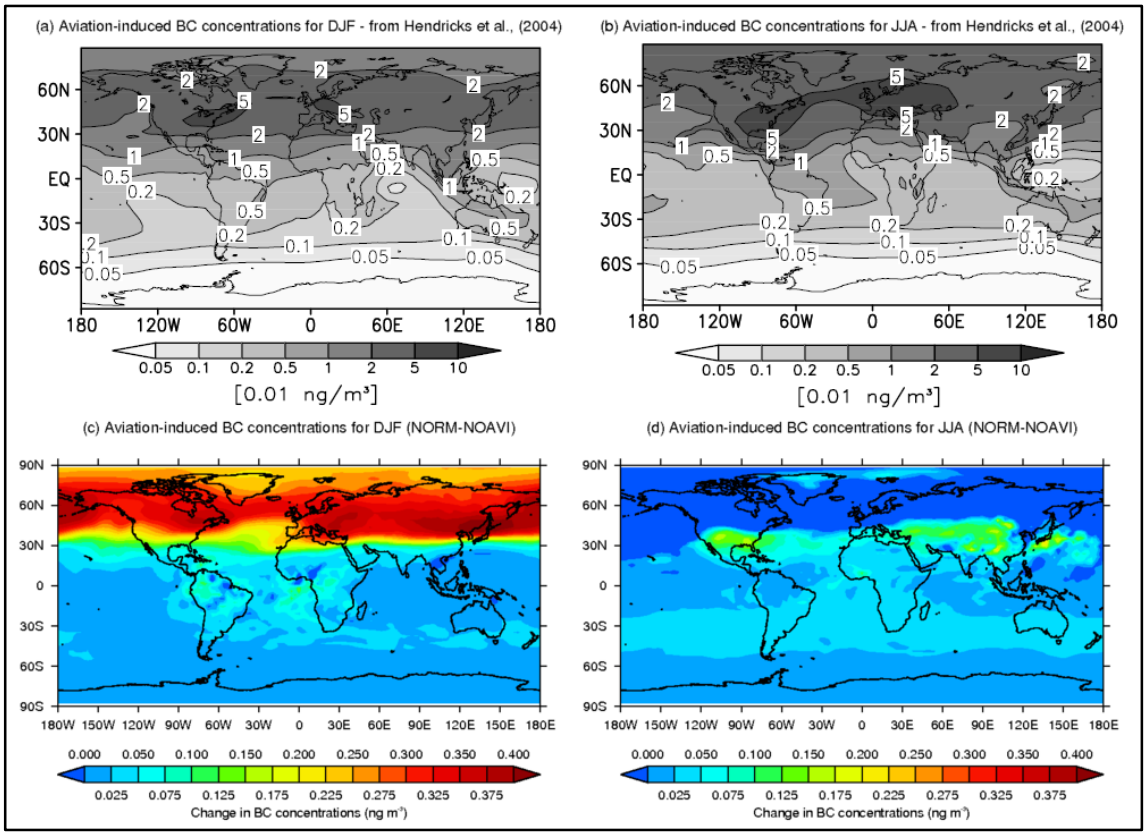

Figure 6.17: Comparison of aviation-induced zonal black carbon concentrations: from (a) Righi et al., (2013), and (b) work done for this study (Righi et al., 2013).

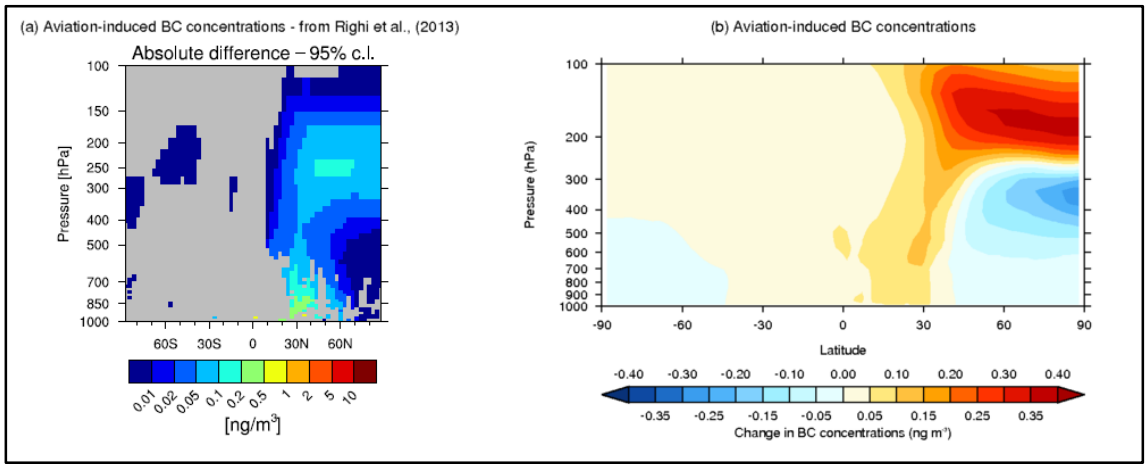

Standard aviation emissions (NORM: FSC = 600 ppm) produce a global mean aerosol cloud albedo effect (aCAE) of –23.55 mW m^{-2} with larger localised aCAE cooling effects over the Atlantic and Pacific oceans [aCAE > 100 mW m^{-2}] (Figure 6.15(c)). These localised regions of elevated cooling over the Pacific and Atlantic oceans correlate with high levels of aviation-induced CCN (Dp > 50 nm) over these regions (Figure 6.13(d)).

The aviation-induced aCAE estimates from this study lie within the range of uncertainty from previous literature: Righi et al. (2013) estimate an aviation aCAE range of –15.4±10.6 mW m^{-2}, while Gettelman and Chen (2013) estimate an aviation aCAE range of –18±11 mW m^{-2}.

The resulting aviation-induced combined radiative effect (RE_{comb}) is the combined effect of O3DRE, aDRE and aCAE (Figure 6.15(d)). Figure 6.15(d) shows that over the Northern Hemisphere an overall warming effect is simulated, while over the Southern Hemisphere there is a larger cooling effect, particularly over the Southern Pacific and Atlantic oceans. Northern Hemisphere warming influences are a result of the aviation-induced aDRE and O3DRE, while Southern Hemisphere cooling occurs due to the influence of aviation aCAE concentrated about the equator. Southern Hemisphere cooling due to enhanced aviation-induced aCAE (Figure 6.15(c)) can be explained by the global percentage increases in CCN (Dp > 50nm) (Figure 6.13); indicating how sensitive the Southern Hemisphere is to changes in CCN. Additionally, from Figure 6.15(b) it is seen that aviation-induced negative aDREs in south-east Brazil and east South Africa, further contributing to this effect.

This study estimates that the implementation of ULSJ fuel within global aviation produces a global mean RE_{comb} of –6.32 mW m^{-2}. Thus, swapping from standard aviation fuel to ULSJ fuel reduces the net cooling effect from aviation non-CO_2 emissions by 6.97 mW m^{-2}. This compares to a reduction of 3.3 mW m^{-2} estimated by Barrett et al. (2012). The difference between reductions in the net cooling effect from aviation non-CO_2 emissions between Barrett et al. (2012) and values estimated here are primarily a result of reductions in the aCAE cooling effect in relation to standard aviation (NORM; FSC = 600 ppm) of +6.73 mW m^{-2}, along with smaller contributions from increases in aDRE of 0.36 mW m^{-2} and small reductions in the warming from the O3DRE of 0.12 mW m^{-2} (Figure 6.18 and Figure 6.19).

Increases in the aDRE and reductions in the aCAE are due to reductions in sulfate formation; a result of reductions in aviation FSC. Changes in aCAE result from reductions in low-level CCN, influenced by decreases in FSC (Figure 6.12(b) in comparison to Figure 6.12(d)). This reduction in CCN will result in a reduction in cloud droplet number concentrations (CDNC), which in turn reduces the brightness and lifetime of low-level cloud. Figure 6.19(c) highlights this effect on the RE_{comb}, with increases in RE in relation to standard aviation (NORM) predominately occurring over the Southern Pacific and Atlantic oceans.

When aviation is fully desulfurised (DESUL; FSC = 0 ppm), the RE_{comb} induced by aviation non-CO_2 emissions are very similar to that simulated for ULSJ fuel with a RE_{comb} of –6.1 mW m^{-2} [aDRE = +1.8 mW m^{-2}; aCAE = –16.6 mW m^{-2}; and O3DRE = +8.7 mW m^{-2}]. These further

reductions in aviation FSC for the DESUL case, further reduce the O3DRE, increase the aDRE and reduce the cooling aCAE effect; resulting in an increase in RE_{comb} of +7.21 mW m^{-2} in relation to the NORM case (Figure 6.19(b)).

Figure 6.18 shows the sensitivity of aviation non-CO_2 emissions induced RE in relation to FSC. Increases in FSC result in reductions in the aDRE, changing from a positive aDRE for low FSC scenarios to a negative aDRE for high FSC (FSC > 1200 ppm). As the FSC is increased, the resulting aCAE exhibits a larger cooling effect, i.e. becoming more negative with increases in FSC, increasing by a factor ~5 as FSC is increased from 0 to 6000 ppm [–16.6 mW m^{-2} for FSC = 0 ppm to –82.1 mW m^{-2} for FSC = 6000 ppm] (Figure 6.18 and Figure 6.19). As a result the RE_{comb} is dominated by FSC influenced changes in the aCAE. Therefore it is found that increases in FSC provide a cooling effect due to the dominating effect from the aviation-induced aCAE.

As with the relationships between surface level $PM_{2.5}$ concentrations, low-level aviation-induced (879 hPa) and FSC, a linear relationship between changes in aviation-induced radiative effects and FSC are seen. Statistical testing yielded the following values: for the O3DRE R^2 > 0.88 and *p*-value = 1.48×10^{-3}; for the aDRE R^2 > 0.99 and *p*-value = 2.97×10^{-7}; for the aCAE R^2 > 0.99 and *p*-value = 2.71×10^{-11}; and for the RE_{comb} R^2 > 0.99 and *p*-value = 5.40×10^{-11}.

Figure 6.18: Aviation-induced radiative effects due to variations in fuel sulfur content (FSC), the ground release of aviation emissions (GROUND), and variations in the vertical distribution of aviation SO_2 emissions (SWITCH1 and SWITCH2 simulations).

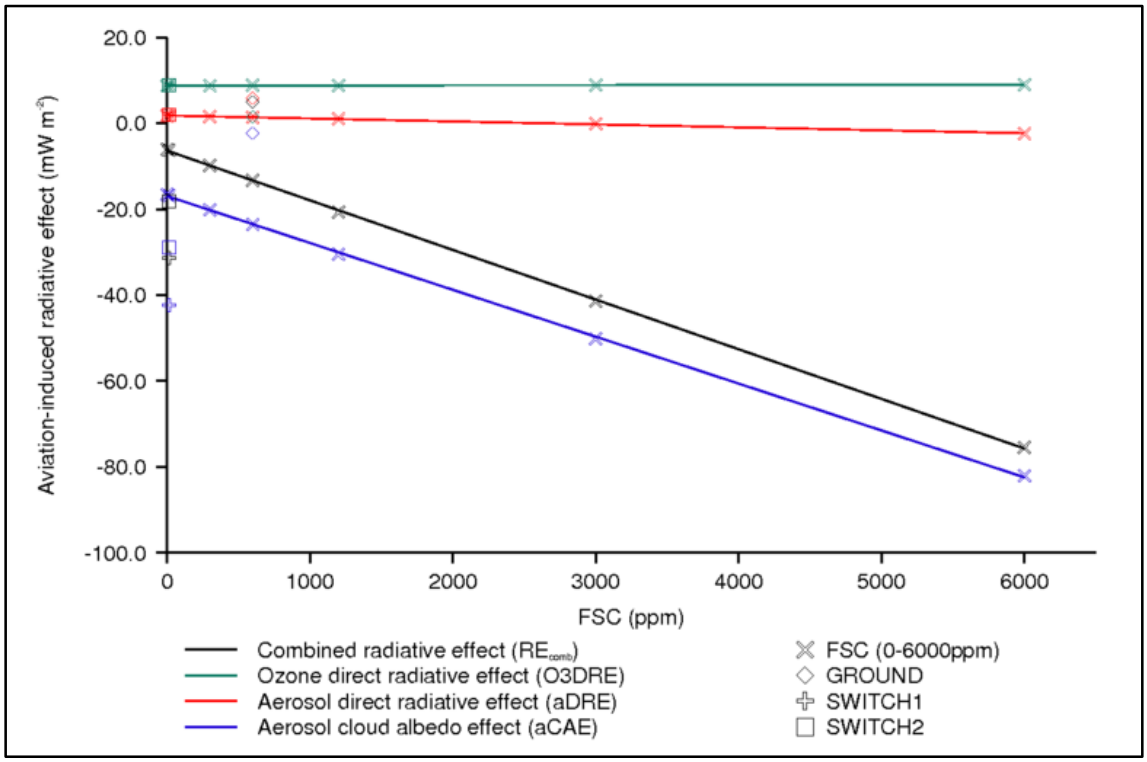

Figure 6.19: Differences in simulated combined radiative effects (RE_{comb}) in relation to standard (NORM) aviation-induced net radiative effect (experiment–NORM).

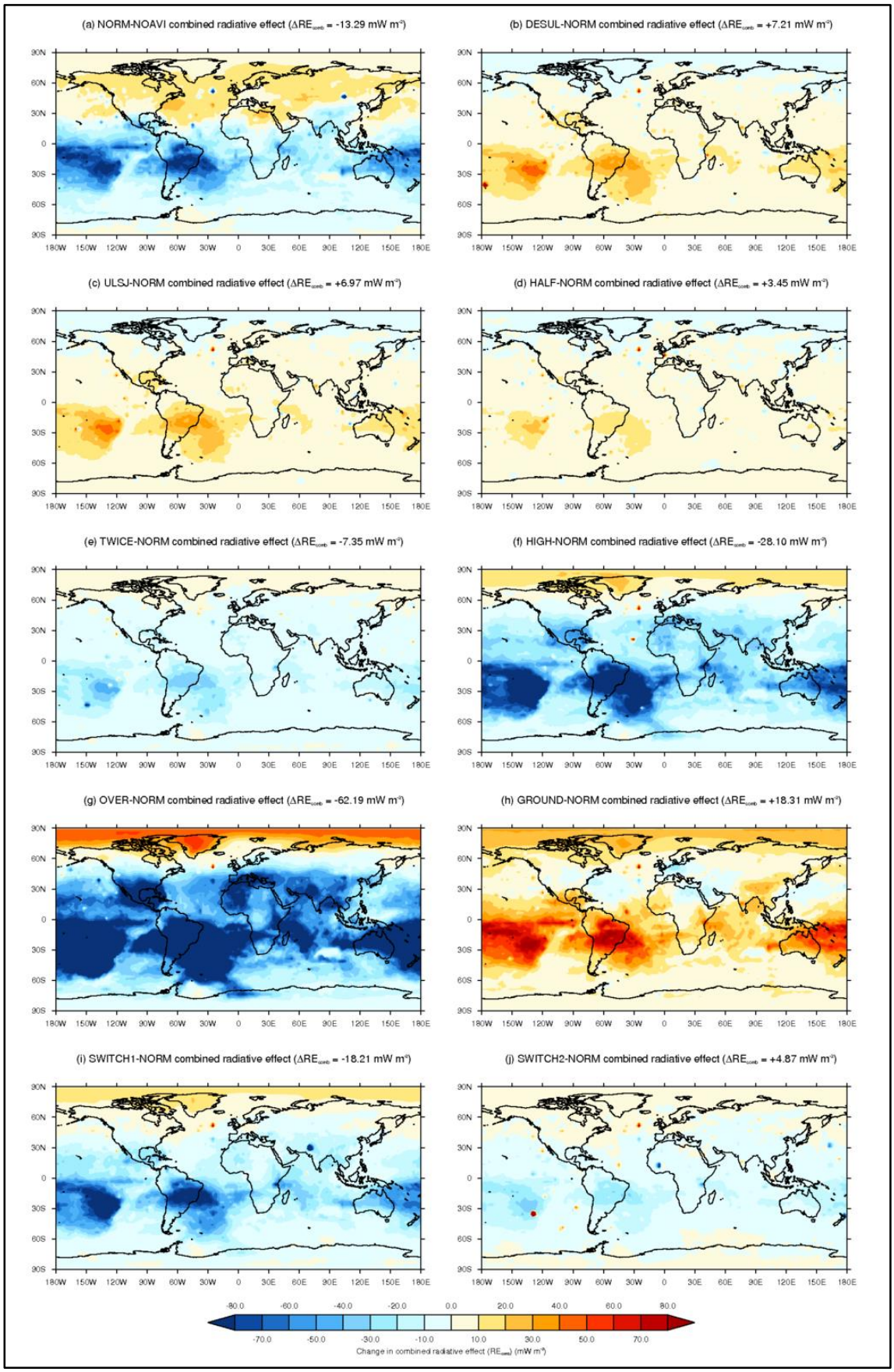

The injection of all aviation emissions at the surface level (GROUND) results in a RE_{comb} of 5.02 mW m^{-2}; consisting of an O3DRE of 1.48 mW m^{-2}, an aDRE of 5.85 mW m^{-2} and an aCAE of –2.31 mW m^{-2}. This reduction in the O3DRE of –7.38 mW m^{-2} (Table 6.8 and Figure 6.18) is due to reduced global aviation-induced concentrations and associated global burdens. Global mean aviation-induced surface ozone concentrations are reduced from 0.15 ppbv (NORM) to 0.03 ppbv when all aviation emission species are released at the surface layer. Releasing aviation emissions at the surface also reduces the global ozone burden by 3.1 Tg. This is a reflection of increases in the sensitivity of the ozone production efficiency (OPE) of NO_X with increases in altitude, and sensitivity of the atmosphere to ozone formation due to lower background NO_X and NMHC (non-methane hydrocarbon) concentrations (Johnson et al., 1992; Hauglustaine et al., 1994; Hauglustaine and Koffi, 2012; Köhler et al., 2008; Skowron et al., 2013; Stevenson and Derwent, 2009; Snijders and Melkers, 2011), and ozone's ability to act as a stronger greenhouse gas in the upper troposphere as identified by Rap et al. (2015).

The change in aCAE of +21.24 mW m^{-2} is a result of simulated reductions in low-level CCN production (Figure 6.12(h) and Figure 6.13(h)), resulting from increasing sulfates deposition rates and increases in the aqueous phase oxidation of SO_2 resulting in the growth of existing CCN, but not new CCN formation (Schmidt et al., 2012).

The increases in the aDRE of 4.45 mW m^{-2} (GROUND–NORM) is partially a result of reductions in the amount of BC particles that are aged, i.e. moving from the insoluble mode to the soluble mode, due to a reduction in sulfates that can age BC (Schmidt et al., 2012; Mann et al., 2010). Literature shows that with increases in altitude of release BC can exert a stronger radiative forcing per unit mass (Samset and Myhre, 2011; Lund et al., 2014; Zarzycki and Bond, 2010), but the level of increases in aDRE seen here can be attributed to increases in rates of deposition and washout of sulfate aerosol (Mann et al., 2010), reducing the cooling effect aviation-induced sulfates would induce (Balkanski et al., 2010; Fuglestvedt et al., 2008; Lee et al., 2009; Sausen et al., 2005; Unger, 2011; Unger et al., 2013; Gettelman and Chen, 2013).

SWITCH1 results in a larger cooling aCAE [–42.37 mW m^{-2}], a larger warming aDRE [+2.07 mW m^{-2}], and a larger O3DRE [+8.89 mW m^{-2}], resulting in increased aviation-induced cooling [RE_{comb} = –31.41 mW m^{-2}]. Which in relation to standard aviation (NORM) provides an additional –18.1 mW m^{-2} [136%] of aviation-induced cooling (Table 6.8 and Figure 6.18).

The SWITCH2 scenario results in a larger cooling aCAE [–28.89 mW m^{-2}], a larger warming aDRE [+1.93 mW m^{-2}], but smaller O3DRE [+8.80 mW m^{-2}]. This scenario again results in additional

aviation-induced cooling [RE_{comb} = –18.16 mW m^{-2}], but to a smaller extent than the SWITCH1 case providing an additional –4.87 mW m^{-2} [36.6%] (Table 6.8 and Figure 6.18).

6.4.5 Relationship between aviation-induced radiative effects and mortality due to non-CO_2 aviation emissions

Figure 6.20 shows the RE_{comb} and mortality estimates for different aviation emission scenarios. Increases in FSC lead to approximately linear increases in both mortality and the negative RE_{comb}. The impact of FSC on mortality and RE is quantified here in terms of d(mortalities)/d(FSC) [mortalities ppm^{-1}] and d(RE)/d(FSC) [mW m^{-2} ppm^{-1}]. To quantify mortality using this metric it is assumed that the mortality function described in Section 6.3.2 is eliciting a near-linear response when considering the relative increases in aviation-induced surface $PM_{2.5}$ despite the essentially log-linear nature of the function used to calculate mortality (Equation 6.5).

Figure 6.20: Relationship between net radiative effect [sum of O_3, aerosol direct and aerosol indirect effects] and annual mortality rates: for low-, mid- and high-range mortality sensitivities. Shaded boxes identify regions where combinations of 'increased warming', 'increased cooling', 'higher mortality' and 'lower mortality' occur – with intersection located where the impact of mid-range NORM case estimates lie.

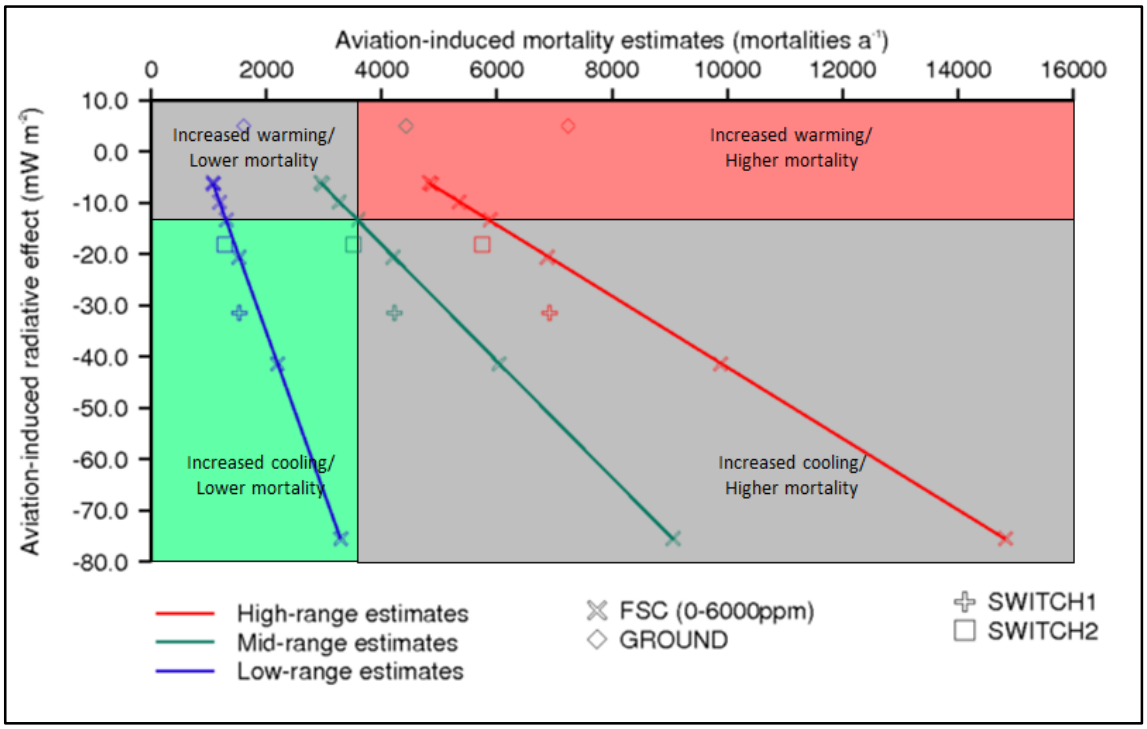

When considering variations in FSC (between 0–6000 ppm) while maintaining the distribution of aviation emissions, the sensitivity of global premature mortality with FSC is estimated as

1.02 mortalities ppm^{-1} [95% CI = 0.37 to 1.64 mortalities ppm^{-1}]. The different slopes presented in Figure 6.20, which are resultant of the levels of uncertainty in the disease specific cause-specific coefficient β help identify the uncertainties present when aiming to evaluate aviation-induced premature mortalities from long-term exposure to $PM_{2.5}$ resulting from the factors discussed in Ostro (2004), demonstrating the sensitivity of coupled climate-and-health impacts induced by variations in aviation FSC

In this study mortality relationships can be approximated as linear, as emissions perturbations simulated in this study resulting in a RR which lies within the linear portion of the CRF from Ostro (2004) to derive a RR lies within the linear range of this relationship. The global mean RE_{comb} is assessed to have a sensitivity of $–1.16x10^{-2}$ mW m^{-2} ppm^{-1}, consisting of large changes to the aCAE [$–1.09x10^{-2}$ mW m^{-2} ppm^{-1}], combined to much smaller changes in aDRE [$–6.88x10^{-4}$ mW m^{-2} ppm^{-1}] and O3DRE [$+4.37x10^{-5}$ mW m^{-2} ppm^{-1}].

Figure 6.20 shows that a GROUND release sensitivity case results in an increase of 825 [95% CI: 300–1349] mortalities a^{-1} along with changes in RE_{comb} of +18.31 mW m^{-2}, resulting in a warming in relation to the standard (NORM) case; taking aviation's impact in to the 'increased warming/higher mortality' zone. In relation to standard aviation (NORM case; FSC = 600 ppm) the ground release of aviation emissions reduces aviation-induced cooling and increases aviation-induced premature mortalities.

The SWITCH1 case takes aviation-induced climatic impacts in to the 'increased cooling' zone, but moves the impact further along in to the 'higher mortality' zone. This is due to increases in aviation-induced premature mortalities of +625 [95% CI: 227–1023] mortalities a^{-1} and additional cooling through a change in aviation-induced RE_{comb} of –18.12 mW m^{-2}.

An ideal scenario would allow aviation to achieve both increased cooling while providing optimal reductions in aviation-induced mortality. The SWITCH2 scenario considered here moves towards this but does avoid as many aviation-induced premature mortalities as achieved by the desulfurised case (DESUL; FSC = 0 ppm). The SWITCH2 case returns reductions in aviation-induced premature mortalities of –87 [95% CI: –32 to –142] mortalities a^{-1}, with an additional cooling of –4.87 mW m^{-2} dominated by contributions from the aCAE.

Essentially intersect in Figure 6.20 helps identify the point at which the implelemtation of FSC stratigies could adversely impact human mortality, the combined cooling effect from aviation (RE_{comb}) from aviation non-CO_2 emissions, or both. Through the implementation of a FSC strategy like the use of ULSJ fuels aviation-induced premature mortality is reduced, but the

cooling effect from aviation non-CO_2 emissions is reduced. While through increases in FSC the cooling effect from aviation non-CO_2 emissions can be increased, but to the detriment of human health. Importantly Figure 6.20 also shows that through variations in the vertical distribution of aviation FSC it is possible to both reduce aviation-induced premature mortality while increasing the aviation-induced cooling effect (from non-CO_2 emissions). This figure highlights that there is the risk that a strategy to alleviate one issue (aviation-induced premature mortality), can risk causing adverse impacts in another aspect; increasing the warming impact of aviation in this case. As discussed before Figure 6.20 the dilemmas that policy and strategy makers may face going forwarding to the future (Fiore et al., 2012).

6.5 Summary and Conclusions

Using the nitrate-extended version of the TOMCAT-GLOMAP-mode coupled model (GMV4-nitrate) the impact of variations in aviation FSC on aerosol and ozone concentrations, premature mortality and radiative effect on climate have been estimated. It is estimated that standard aviation (NORM; FSC = 600 ppm) is responsible for 3,597 premature mortalities a^{-1} due to increased surface layer $PM_{2.5}$ concentrations, in line with previous work (Barrett et al., 2012). Aviation-induced mortalities are found to be highest over Europe, eastern North America and eastern China; reflecting larger regional perturbations in surface layer $PM_{2.5}$ concentrations. Comparing these estimates with total global premature mortalities from ambient air pollution from all anthropogenic sources, aviation is estimated to be responsible for 0.1% [95% CI: 0.04–0.18%] of annual premature mortalities (Lim et al., 2012).

Calculating the top-of-atmosphere (TOA) ozone, aerosol direct radiative (aDRE), aerosol cloud albedo (aCAE) and combined radiative effects (RE_{comb}) aviation non-CO_2 emissions result in a net cooling effect, as found in previous work. For year 2000 aviation emissions with a standard fuel sulfur content (NORM: FSC = 600 ppm), a global annual mean TOA RE_{comb} of **–**13.29 mW m^{-2} is estimated; due to a combination of O3DRE [+8.86 mW m^{-2}], aDRE [+1.40 mW m^{-2}] and aCAE [**–**23.55 mW m^{-2}].

Variations in aviation FSC between 0–6000 ppm identify that increases in FSC lead to increases in surface $PM_{2.5}$ concentrations, and increased aviation-induced mortality. Increases in FSC also leads to increased aviation-induced cooling through a more negative RE_{comb} due to a stronger cooling aCAE influence, while also resulting in increases in mortality. The use of ultra-low sulfur jet fuel (ULSJ; FSC = 15 ppm), is estimated to prevent 624 [95% CI: 227–1,021] mortalities a^{-1} compared to standard aviation. Swapping to ULSJ fuel is estimated to increase the global mean

RE_{comb} by +6.97 mW m^{-2}, in comparison to standard aviation emissions, largely due to a reduced aCAE. Here a larger warming effect is estimated from the use of ULSJ fuel than previously assessed by Barrett et al. (2012), as they do not evaluate changes in the aCAE.

Absolute reductions in FSC result in limited reductions in aviation-induced surface layer $PM_{2.5}$. Aviation-NO_X emissions are estimated to be responsible for 36.2% of aviation-induced sulfate perturbations. Thus further reductions in aviation-induced $PM_{2.5}$ can potentially be achieved if NO_X emission reductions are implemented in tandem with reductions to fuel sulfur content.

In line with previous work, decreasing the altitude at which ozone forming species are emitted result in a reduction in aviation-induced ozone, and associated O3DRE. Explained by the relationship between altitude and OPE, and the inverse relationship between altitude and background pollutant concentrations; as seen in our ground-release scenario (GROUND case).

Additionally the sensitivity of emission injection altitude on aerosol, mortality and aerosol RE was explored. Injecting aviation emissions at the surface results in a reduction in global mean concentrations of $PM_{2.5}$ (relative to NORM), but with higher regional concentrations over central Europe and eastern America; resulting in higher annual aviation premature mortality. It is found that aviation emissions are a factor 5 less efficient at creating CCN when released at the surface, resulting in an aCAE of –2.31 mW m^{-2}, a reduction of 90.1% in relation to the standard aviation scenario. When aviation SO_2 emissions are injected into the free-troposphere, the dominant oxidation pathway is to H_2SO_4 followed by particle formation and condensational growth of new particles to larger sizes. Subsequent entrainment of these new particles into the lower atmosphere leads to increased CCN concentrations and impacts on cloud albedo. Aviation SO_2 emissions are therefore particularly efficient at forming CCN with resulting impacts on cloud albedo.

The impact of applying altitude dependent variations in aviation FSC was also explored, testing a scenario with a high FSC in the free troposphere and low FSC near the surface, resulting in the same global aviation sulfur emission as in the standard aviation case (SWITCH2). In this scenario, aviation-induced premature mortalities were reduced by 2.4% [–87 mortalities a^{-1}] and the magnitude of the negative RE_{comb} was increased by 36.6%, providing an additional cooling impact of climate of –4.88mW m^{-2}.

The simulations conducted for the investigations in this section suggest that the climate and air quality impacts induced by aviation are sensitive to aviation fuel FSC, and the altitude of emissions. These simulations explored a range of scenarios to maximise climate cooling and

reduce air quality impacts. The use of ULSJ fuel (FSC = 15 ppm) at low altitude combined with high FSC in the free troposphere results in increased climate cooling whilst reducing aviation mortality. Though it is believed that more complicated emission patterns, for example, the use of high FSC only whilst over oceans might further enhance this effect. However it is noted that the greatest reductions in aviation-induced mortality are simulated for a scenario that considers the complete desulfurisation of aviation fuel.

7 Investigating the atmospheric and climatic impacts of the use of alternative fuels in aviation

7.1 Overview

The aviation sector aims to reduce its CO_2 and non-CO_2 emissions through the use of ACARE (Advisory Council for Aeronautics Research in Europe) and industry agreed commitments (ATAG, 2011; ACARE, 2011). One of the methodologies proposed to reduce emissions from the sector in the short- to mid-term future is the use of alternative fuels (ATAG, 2011).

ASTM standard D7566-11a discusses the alternative fuels that are approved for use within aviation. As per ASTM standard D7566-11a the use of Fischer-Tropsch (FT) fuels in blends of 50:50 (i.e. a blend of 50% alternative fuel with 50% Jet A-1/Jet A on a volume basis), along with the use of HEFA (hydroprocessed esters and fatty acids) synthetic fuels have been approved for use in commercial aviation (Airlines for America, 2011; ASTM International, 2011a).

The use of alternative fuels in aviation is seen as a way for the sector to reduce its CO_2 emissions, however little attention has been given to the impacts of their non-CO_2 emissions. Here the impact of non-CO_2 emissions from the use of alternative fuels in aviation on the ozone direct radiative effect, aerosol direct radiative effect and aerosol cloud albedo effect are investigated for the first time.

This Chapter investigates the use of four alternative fuel blend scenarios: two based on the use of FT fuels and the remaining two based on the use of Fatty Acid Methyl Ester (FAME) fuels. This Chapter will discuss the creation of the FT and FAME fuel blend scenario emissions inventories used in the following investigations (Section 7.3.1), the resulting atmospheric perturbations in gas- and aerosol-phase species produced in the model (Section 7.4.1.1 and Section 7.4.1.2), the impacts on surface-layer air quality and how this affects human health (Section 7.4.1.3), along with the resulting climatic impact from the use of FT and FAME fuel blends (Section 7.4.2).

7.2 Background

Alternative aviation fuels have been identified as a mechanism to allow the aviation sector to reduce its CO_2 emissions in line with industry targets (Figure 1.7 in Section 1.6). In addition to reducing net CO_2 emissions from the sector (Timko et al., 2011; Lobo et al., 2011), the use of alternative aviation fuels has the potential to reduce emissions of aviation non-CO_2 species, dependent on alternative fuel and fuel blend used. Additionally, the use of alternative fuels can result in changes in the geometric mean diameter (GMD) of black and organic carbon (BCOC), compared with those for Jet A-1 fuel (shown in Table 7.6 in Section 7.3.1).

Fischer-Tropsch (FT), FAME (fatty acid methyl esters) and alternative fuels derived from a range of biological feedstocks (including camelina, jatropha and algae) demonstrate properties comparable to that of Jet A-1 (ICAO, 2010; Timko et al., 2011; Lobo et al., 2011). These fuels have a net heat of combustion (ΔH_{comb}) ranging between 36.9–44.3 MJ kg^{-1}, compared to 43.5 MJ kg^{-1} for Jet A-1, while having a fuel sulfur content (FSC) of 0 < FSC < 15 ppm (ICAO, 2010; Timko et al., 2011; Lobo et al., 2011). In addition to these desired similarities, there are undesired properties, such as in the case of FAME fuels (100%) which have a viscosity (ν) greater than that stipulated by the ASTM specification on jet fuel, i.e. where ν = 10.7 mm^2 s^{-1} for FAME fuels (100% blend), where standards stipulate a maximum viscosity (ν_{max}) of 8.0 mm^2 s^{-1} (Timko et al., 2011; ASTM International, 2012b).

Numerous tests and demonstrations have been carried out on a range of alternative fuels, investigating alternative fuel to Jet A-1 blends ranging from 20:80 to 50:50. These tests investigated and demonstrated the feasibility of their use in existing aircraft in the short- to mid-term future (ICAO, 2010).

Additionally in 2008 the body formerly known as the Air Transport Association (ATA) and now known as Airlines for America (A4A) announced rigorous safety, environmental, supply reliability and economic feasibility requirements for alternative fuels to potential suppliers. With these requirements upheld via the 'Commercial Aviation Alternative Fuels: The A4A Commitment'. Additionally A4A supports and promotes the development of viable alternatives derived from biomass and other sources materials, under the proviso that they do not compete with food supplies (Airlines for America, 2011).

Highlighting industry commitments to utilise alternative jet in commercial aviation, British Airways plan to convert domestic waste to produce over 50,000 tonnes of biojet fuel for use in their fleet flying out from London City Airport. This biojet fuel is to be produced by Solena via

the process of plasma gasification using waste from the surrounding area (SOLENA Fuels, 2015; European Biofuels Technology Platform, 2015).

Fischer-Tropsch (FT) fuels are an attractive alternative for jet fuels as they are nearly free of heteroatoms (i.e. free from hydrogen or carbon atoms) and aromatics as they affect jet fuel thermal stability (Kirklin and David, 1992), have a high thermal stability and very low sulfur levels (Roets et al., 1997) and a comparable energy content to Jet A-1/Jet A (Timko et al., 2011).

7.2.1 Standards and specifications for the use of alternative fuels in aviation

The Federal Aviation Administration (FAA) certifies aircraft and engines. They do not certify jet fuel, but provide information on the type of fuels approved for the use by these aircraft and engines. US airlines comply with the FAA's 'Airline Fuelling Manuals,' based on jet fuels recognised by the FAA, i.e. jet fuels that have been determined to meet all necessary requirements (Airlines for America, 2011). In the US, jet fuel specifications are provided by ASTM International via standard ASTM D1655 (for aviation turbine fuels) and ASTM D7566 (for aviation turbine containing synthesised hydrocarbons) (Airlines for America, 2011). In the UK standards for civil and military aviation turbine fuels are controlled via the Ministry of Defence Standard 91-91 (Ministry of Defence, 2011).

It is required that alternative jet fuels not only meet the specifications provide by ASTM D1655, ASTM D7566 and MOD Def Stan 91-91, but that these fuels ensure that their performance and characteristics match those of conventional fuels (Jet A-1/Jet A) at each stage of distribution, delivery, storage and utilisation in the aircraft and its engines (Airlines for America, 2011). Thus allowing for their use as 'drop-in' fuels (i.e. capable of integrating in to existing fuel infrastructure), in the short- to mid-term future.

Currently specifications are in place for the use of bioderived synthetic fuels produced via the Fischer-Tropsch process and Hydroprocessed Esters and Fatty Acid (HEFA) derived fuels (ASTM International, 2011c; ASTM International, 2014).

In light of ASTM's decision to remove specification barriers to alternative aviation fuels talks are underway regarding possible contracts between fuel producers and buyers. If successful and in tandem with expansion to existing Fischer-Tropsch facilities it may be possible for IATA to reach their goal of a 10% use within commercial aviation by 2017 (CAAFI, 2015).

7.2.1.1 Specification ASTM D7566-11a: Aviation Turbine Fuel Containing Synthesized Hydrocarbons

ASTM International approved and introduced specification D7566 for 'Aviation Turbine Fuel Containing Synthesized Hydrocarbons' in August 2009. ASTM D7566 allows for the use of alternative fuels in commercial and military jet aircraft, in blends containing up to 50% bioderived synthetic components alongside conventional jet fuel (Airlines for America, 2011; ASTM International, 2011a; ICAO, Undated-a; ASTM International, 2011c). Under the caveat that these fuels are certified for use by the equipment certifying authorities (ASTM International, 2011c). This resulted in the introduction of the first new jet fuel in 20 years (ICAO, Undated-a; ICAO, 2010). Fuels must demonstrate they are safe (ICAO, 2010; Airlines for America, 2011), effective and otherwise meet the specification and the requirements to be deployed as jet fuels, i.e. being of similar ilk to fuels under ASTM D1655 (Airlines for America, 2011). While adhering to specific requirements for the bioderived synthetic fuel component; such as thermal stability, distillation control and limitations on the amount of trace material allowed (ASTM International, 2011a).

ASTM specification D7566 approves the use of synthetic fuels in blends of 50:50 produced via the Fischer-Tropsch process, along with HEFA (hydroprocessed esters and fatty acids) synthetic fuels (Airlines for America, 2011; ASTM International, 2011a). Aiming to implement mechanisms to promote the seamless integration of bioderived fuels in to the current distribution infrastructure used by D1655 governed fuels, i.e. standard jet fuel (Jet A1/Jet A) (ASTM International, 2011a). In addition, this specification governed by ASTM International is hoping to lay the foundations for other bioderived renewable blending components (ASTM International, 2011a).

Specification D7566-11a only applies to specified alternative fuels at the point of manufacture. Once the fuel has been produced it can be regarded as fuel having been produced under specification D1655. Though this specification applies to synthetic aviation fuels for use in civil commercial and military aircraft, it can be also be used to evaluate the quality of the resultant fuel along the distribution system (ASTM International, 2011c).

By introducing a standard that requires alternative fuels to fulfil almost the same criteria as conventional kerosene based aviation fuels, this integration and transition should be made simpler. Specification ASTM D7566 also places stipulations on additives that can be used in conjunction with these alternative fuels (ASTM International, 2011c) in order to ensure the

resulting fuel blends have similarities to Jet A-1 (ASTM International, 2012b; ASTM International, 2011c).

In addition to requirements surrounding the physical and chemical properties of alternative aviation fuels, safety requirements also need to be met. ASTM D7566-10a requires fuel to be clean and free of any contamination (including microbial) prior to use, as contamination can accelerate corrosion of structural components (ASTM International, 2011c). Additionally the use of surfactants is discussed within the specification to reduce the particle size of solid or liquid contaminants and increase the time period required for these contaminants to settle out of the fuel (ASTM International, 2011c).

As with specifications on the physical and chemical properties for alternative aviation fuels, the same applies to the additives used. During operation a minimum level of aromatic compounds are specified in order to prevent the shrinkage of aged elastomer seals within the aircraft in order to prevent fuel leakage. There are also restrictions on the concentrations of other species, such as mercaptan sulfur (R–S–H) which has been shown to deteriorate elastomer seals (ASTM International, 2011c; ASTM International, 2012b). An elastomer is a natural or synthetic polymeric material which may experience large and reversible elastic deformations (Callister Jr, 1997).

Later amendments to ASTM D7566 (v11a and ASTM WK36267) discuss the list of alternative aviation fuels specified for use branching out to include hydrotreated depolymerised cellulosic jet (HDCJ) fuel and other possible fuels. This is on the proviso that they can be safely used as blending components for conventional fossil fuel derived aviation fuels (ASTM International, 2012a; ASTM International, 2014). Forward movements like this have the potential to allow the expedient growth of alternative fuels in aviation as blending components; but only once the FAA deem their inclusion in aviation equipment appropriate and safe.

ASTM working document WK34934 (Revision of D7566 - 11a Standard Specification for Aviation Turbine Fuel Containing Synthesized Hydrocarbons) aims to follow suit with its equivalent UK standard (the Ministry of Defence Standard 91-91). To do so ASTM International invited the Energy Institute to prepare a revised version of D7566, inclusive of the appropriate references for IP (Institute of Petroleum) methods (ASTM International, 2011b).

7.2.1.2 UK Ministry of Defence Standard 91-91: Issue 7, Amendment 1 – reference to alternative fuels

The inclusion of aviation fuels from unconventional sources is acknowledged in the UK Ministry of Defence Standard 91-91 (MOD STAN DEF 91-91). This standard outlines that both semi-synthetic and synthetic fuels must adhere to additional requirements and that these are stipulated on a case by case basis. There is recognition that there is a need for a framework that can be used to assess both conventional and alternative fuels (Ministry of Defence, 2011).

MOD DEF STAN 91-91 also highlights the cross-over between UK and US specifications for alternative aviation jet fuels (ASTM International, 2011a; ASTM International, 2011c), discussing the use of synthetic jet fuels as a blending component within 50:50 fuel blends (on a volume basis). This further compounds the industry's long-term aim to integrate and use alternative fuels as a 'drop-in' fuel in existing distribution and infrastructure (Ministry of Defence, 2011).

7.2.2 Types of alternative fuels for use in civil and military aviation

The main alternative fuels included within ASTM D7566-11a and UK DEF STAN 91-91, along with fuels being considered by the ASTM working paper WK36267 are (ASTM International, 2011c; Ministry of Defence, 2011; ASTM International, 2011a):

- Fischer-Tropsch (FT) fuels – such as those developed by SASOL Limited,
  - Semi-synthetic aviation turbine fuel,
  - Synthetic Iso-Paraffinic Kerosene,
  - Fully synthetic jet fuel,
- Hydroprocessed Esters and Fatty Acids (HEFA),
- Hydrotreated Depolymerised Cellulosic Jet (HDCJ) fuel.
- Fatty Acid Methyl Esters (FAME).

7.2.2.1 Fischer-Tropsch fuels

Fuels produced via the Fischer-Tropsch (FT) process/synthesis are made by initially gasifying biomass or solid fossil fuel feedstocks, or through the steam reformation of methane to produce a synthesis gas stream (syngas). This syngas is predominately made up of carbon monoxide (CO) and hydrogen (H_2) (Dry, 2002; Renewable Jet Fuels, Undated). After being scrubbed of impurities and species that could cause poisoning and deactivation of the catalyst

used (Kreutz et al., 2008), the syngas is converted using iron-based catalysts at temperatures of between 300–350˚C into gasoline and linear low molecular mass olefins. When lower temperatures are used 200–240˚C and iron or cobalt catalysts, high molecular mass linear waxes (paraffinic wax) are produced (Dry, 2002).

Reaction 7.1 describes the general reaction that occurs when the syngas containing CO and H_2 is converted using FT synthesis (Prins et al., 2005):

$$n\ CO + 2n\ H_2 \rightarrow [-CH_2-]_n + n\ H_2O \qquad \Delta H = -159.2\ Kj.mol^{-1}$$

Reaction 7.1

The resultant paraffinic wax is then selectively cracked (hydrocracked) and isomerised to produce fuels that can be dropped-in to existing fossil fuel based transportation fuel infrastructure.

7.2.2.2 Hydroprocessed Esters and Fatty Acids

Hydroprocessed Esters and Fatty Acids (HEFA) fuels are also known as Hydroprocessed Renewable Jet (HRJ) fuels. HEFAs are produced by initially reacting natural oils, lipids, from derived from plant oils or animal fats with hydrogen in order to produce saturated hydrocarbons (Guzman et al., 2010; Renewable Jet Fuels, Undated). During this initial stage oxygen bonds and double-carbon bonds are saturated with hydrogen to produce synthetic paraffin's (C15 to n-C18). This process is typically conducted under high hydrogen pressure with the lipids being at relatively high temperatures (Guzman et al., 2010).

The next stage of the process is to selectively crack and isomerise these long chain hydrocarbons to produce the desired primary diesel fuel, jet fuel and propane (Renewable Jet Fuels, Undated).

7.2.2.3 Hydrotreated Depolymerised Cellulosic Jet (HDCJ) fuel

Hydrotreated depolymerised cellulosic jet (HDCJ) fuel is produced from lignocellulosic feedstocks, via conversion routes based on pyrolysis, hydrothermal liquefaction, or a hybrid process (Mawhood et al., 2014; Melero et al., 2012). These feedstocks are depolymerised in to simple sugars, which are then subsequently transformed in to valuable molecules, which are refined to produce an energy-dense biomass-derived refinery-processable feedstock (Melero et al., 2012).

The lignocellulosic materials fed in to this process are separated in to their constituent parts, lignin, cellulose and hemicellulose, and then depolymerised in to their associated building blocks. Lignin is depolymerised in to aromatic alcohols, cellulose is depolymerised in to glucose and hemicellulose is depolymerised in to a mixture of sugars; mainly pentose (Melero et al., 2012).

Cellulose is the favoured building blocks of HDCJ fuel as the building blocks of lignin are aromatic compounds (Melero et al., 2012). Lignin and its associated aromatic constituent parts if still present in the end product causes smokiness and higher levels of soot within associated emissions (Ministry of Defence, 2011).

These depolymerised products are then hydrotreated using a heterogeneous catalyst and hydrogen as a reactant, a process which promotes the removal of oxygen (hydrodeoxygenation) in the form of water and further depolymerisation. This process is conducted at high pressures and temperatures (de Wild et al., 2009).

7.2.2.4 Fatty Acid Methyl Esters (FAME)

Fatty acid methyl esters (FAME) are fatty acid esters, closer to fossil fuel derived diesel fuel than kerosene: as such classified as a biodiesel. FAMEs can be produced from vegetable oils, animal fats or waste cooking oils via the process of transesterification; where the fats and oils are reacted with methanol in the presence of an acid or base catalyst (European Biofuels Technology Platform, Undated; Uryga-Bugajska et al., 2011; Gryglewicz, 1999) (Figure 7.1). This results in an end product with similar physical and chemical properties to conventional diesel (Uryga-Bugajska et al., 2011), such as a high cetane number (Gryglewicz, 1999).

Figure 7.1: Transesterification process for the production of Fatty Acid Methyl Esters (European Biofuels Technology Platform, Undated).

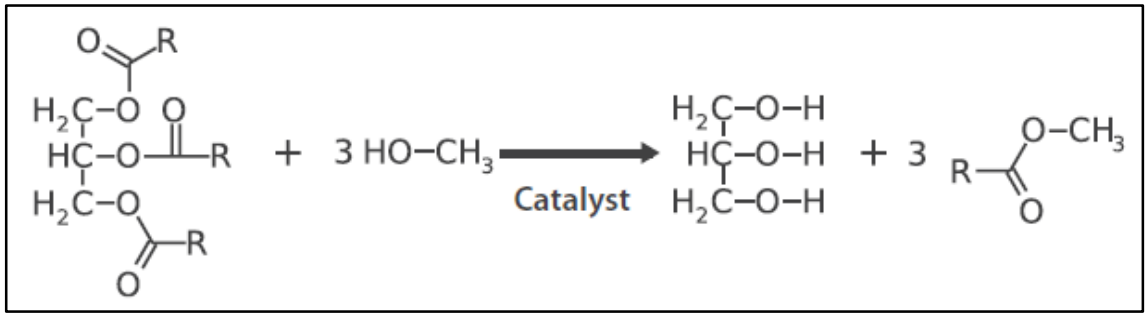

Some of the most common feedstocks used to produce FAMEs are rapeseed, sunflower, soybean, palm oil and waste or spent oils (European Biofuels Technology Platform, Undated).

Despite FAMEs having similar desirable properties to diesel and the wide range of feedstock they can be produced from, they have certain properties which are undesirable. These range from a lower freezing point, poor thermal stability, and most importantly a higher oxygen content which impacts on the overall heating value of the fuel, which will require the combustion of a greater amount of fuel to obtain the equivalent energy to standard fuel (Daggett et al., 2007; Uryga-Bugajska et al., 2011).

7.2.3 Tests conducted on alternative fuels for commercial use

The use of alternative fuels in aviation is seen as a CO_2 emissions reduction strategy which can be implemented in the short- to mid-term future, with growth in the use of alternative fuels in aviation projected to increase steadily from the 2020s (Figure 1.7 in Section 1.6) (ATAG, 2011).

Since 2008 there have been numerous tests conducted in commercial and civil aviation using a variety of different alternative fuels ranging from the algae derived to the Fischer-Tropsch GTL (gas to liquid) (ICAO, 2011). Some of these test flights have been utilising a 50:50 Jet A (or Jet A-1) to alternative fuel mix, demonstrating the real world application of the fuel mix specification stipulated by ASTM D7566 and UK Defence Standard 91-91 (ASTM International, 2011c; Ministry of Defence, 2011).

Current flight tests and industry commitment to alternative fuel production help demonstrate the types of blends and types considered by the industry, which help feed in to the alternative fuel scenarios investigated in Section 7.4.

7.3 Methodology

7.3.1 Creation of a dataset for emissions from alternative aviation fuels

Here, emissions indexes for nitrogen oxides (NO_X), carbon monoxide (CO), speciated hydrocarbons (HCs), sulfur dioxide (SO_2), black carbon (BC) and organic carbon (OC) are derived, followed by the creation of emissions inventories for four alternative fuel scenarios.

Two scenarios are based on the use of Fischer-Tropsch (FT) fuels, while the remaining two are based on the use of fatty acid methyl esters (FAME). FT fuels have been approved for use in aviation in blends of up to 50% (ASTM International, 2011c; Airlines for America, 2011; ASTM International, 2011a; ICAO, Undated-a); while FAMEs have been approved for use in concentrations of up to 5 mg kg^{-1}, industry working towards a limit of 100 mg kg^{-1} (Ministry of Defence, 2011).

The alternative fuels scenario emissions inventories created here consider the following scenarios:

1. Fischer-Tropsch (FT) scenarios
    a. 50% blend of Fischer-Tropsch fuel with kerosene,
    b. 100% Fischer-Tropsch fuel mix,
2. Fatty acid methyl ester (FAME) scenarios
    c. 20% blend of FAME with kerosene, and,
    d. 40% blend of FAME with kerosene.

Both sets of emissions indices, for FT and FAME combustion, are derived using experimental data obtained by Lobo et al. (2011) and Timko et al. (2011), from work conducted on a CFM International CFM56-7B turbo-fan jet engine in conjunction with the extended aviation emissions inventory for standard aviation derived and described in Section 4.3 (CMIP5-extended)

Timko et al., (2011) present emissions indexes for CO and HCHO for power settings relating to ground idle (4%) and idle (7%), relative to Jet A. In this study the emission indices based on idle are used to create the CO and HCHO datasets (i.e. engine power rating of 7%).

As the emission indices for CO and HCHO developed in Section 4.3 are for Jet A-1 ($EI_{CO_{Jet\ A\text{-}1}}$ and $EI_{HCHO_{Jet\ A\text{-}1}}$ respectively), to use the factors presented by Timko et al. (2011), these first need to be converted to relate to Jet A fuel, producing $EI_{CO_{Jet\ A}}$ and $EI_{HCHO_{Jet\ A}}$ respectively. This conversion is achieved using the factors ($factor_{CO_{Jet\ A1\ to\ Jet\ A}}$ and $factor_{HCHO_{Jet\ A1\ to\ Jet\ A}}$) given in Table 7.1, in conjunctions with Equation 7.1 and Equation 7.2, for CO and HCHO respectively.

$$EI_{CO_{Jet\ A}} = \frac{EI_{CO_{Jet\ A1}}}{factor_{CO_{Jet\ A1\ to\ Jet\ A}}}$$

Equation 7.1

$$EI_{HCHO_{Jet\ A}} = \frac{EI_{HCHO_{Jet\ A1}}}{factor_{HCHO_{Jet\ A1\ to\ Jet\ A}}}$$

Equation 7.2

Using this process the Jet A emission indices for CO and HCHO are calculated as: $EI_{CO_{Jet\ A}}$ = 4.46 g kg^{-1} fuel and $EI_{HCHO_{Jet\ A}}$ = 2.03 g kg^{-1} fuel (Table 7.4). These Jet A emissions indices are then used in tandem with Equation 7.3 and Equation 7.4, and the relative emission indices from

Table 7.1 ($factor_{CO_{Jet\ A\ to\ Fuel\ X}}$ and $factor_{HCHO_{Jet\ A\ to\ Fuel\ X}}$) to calculate the EIs for CO and HCHO for each of the alternative fuel scenario.

$$EI_{CO_{Fuel\ X}} = EI_{CO_{Jet\ A}} \cdot factor_{CO_{Jet\ A\ to\ Fuel\ X}}$$

Equation 7.3

$$EI_{HCHO_{Fuel\ X}} = EI_{HCHO_{Jet\ A}} \cdot factor_{HCHO_{Jet\ A\ to\ Fuel\ X}}$$

Equation 7.4

Table 7.1: Carbon monoxide (CO) and formaldehyde (HCHO) emission indices relative to Jet A – taken from Timko et al. (2011).

Fuel / Fuel blend	Carbon monoxide (CO) ($g\ kg^{-1}$)	Formaldehyde (HCHO) ($g\ kg^{-1}$)
Jet A	1.0	1.0
Jet A-1	0.81	0.61
50% FT	0.82	0.79
100% FT	0.69	0.57
20% FAME	0.76	0.68
40% FAME	0.74	0.68

The emissions indices for CO and HCHO for each of the alternative fuel scenarios discussed in Section 5.4 calculated using the process outlined above are presented in Table 7.4.

NO_X emissions indices ($EI_{NO_{X_{Fuel\ X}}}$) for the alternative fuel scenarios (50% FT, 100% FT, 20% FAME and 40% FAME) are calculated using the NO_X emissions index correction factors derived by Timko et al. (2011) (Table 7.2).

Table 7.2: Emissions index adjustment factors used to derive emissions indices for Fischer-Tropsch (FT) and fatty acid methyl ester (FAME) alternative fuel scenarios: 50% FT, 100% FT, 20% FAME, and 40% FAME blends (Timko et al., 2011; Lobo et al., 2011).

Species	**Emissions index adjustment factors**				**References**
	FT		**FAME**		
	50%	**100%**	**20%**	**40%**	
Nitrogen oxides	0.95	0.90	0.77	0.71	Timko et al., (2011)
Sulfur dioxide	0.50	0.00	0.80	0.60	Related to kerosene
Black carbon mass	0.385	0.16	0.6625	0.4625	Lobo et al., (2011)
Carbonaceous particles	0.495	0.275	0.605	0.49	Lobo et al., (2011)

The NO_X emissions indices ($EI_{NO_{X_{Fuel\ X}}}$) are calculated using Equation 7.5 in conjunction with the NO_X emissions index for Jet A-1 ($EI_{NO_{X_{Jet\ A\text{-}1}}}$) taken from Section 4.3:

$$EI_{NO_{X_{Fuel\ X}}} = EI_{NO_{X_{Jet\ A\text{-}1}}} \cdot factor_{NO_{X_{Jet\ A\text{-}1\ to\ Fuel\ X}}}$$

Equation 7.5

For the other speciated hydrocarbons (HCs) factors relating to the emissions indices for HCs of interest and HCHO for both alternative fuels and Jet A-1 were used (Timko et al., 2011) – Equation 7.6. Timko et al. (2011) present normalised emissions indices for the following speciated HCs: methanol, acetone and acetaldehyde, ethylene and propene. The emissions indices for ethylene and propene were assumed as proxies for ethane and propane respectively (as they were the closest reported HCs normalised by formaldehyde) (Table 7.3).

Table 7.3: Speciated hydrocarbon (HC) emissions normalised by alternative fuel blend specific formaldehyde (HCHO) emissions (Timko et al., 2011).

Species	VOC emissions normalised by HCHO				References
	FT		FAME		
	50%	100%	20%	40%	
Ethane	1.15	1.28	1.14	1.16	Timko et al., (2011)
Propane	1.50	1.80	1.01	1.07	Timko et al., (2011)
Methanol	0.99	1.30	0.94	0.93	Timko et al., (2011)
Acetone	1.32	1.80	1.04	1.07	Timko et al., (2011)
Acetaldehyde	1.51	1.89	1.07	1.03	Timko et al., (2011)

These factors are derived using Equation 7.6 (Timko et al., 2011):

$$factor_{HC_{Fuel\ X}} = \left(\frac{EI_{HC_{Fuel\ X}}}{EI_{HCHO_{Fuel\ X}}}\right) \Big/ \left(\frac{EI_{HC_{Jet\ A\text{-}1}}}{EI_{HCHO_{Jet\ A\text{-}1}}}\right)$$

Equation 7.6

Where $EI_{HC_{Fuel\ X}}$ = emissions index for HC of interest for alternative fuel X

$EI_{HCHO_{Fuel\ X}}$ = emissions index for HCHO for alternative fuel X

$EI_{HC_{Jet\ A\text{-}1}}$ = emissions index for HC of interest for Jet A1

$EI_{HCHO_{Jet\ A\text{-}1}}$ = emissions index for HCHO for Jet A1

Which when rearranged allows the emissions index for individual HCs for each of the alternative fuels in question ($EI_{HC_{Fuel\ X}}$) to be calculated via Equation 7.7:

$$EI_{HC_{Fuel\ X}} = factor_{HC_{Fuel\ X}} \cdot \left(\frac{EI_{HC_{Jet\ A\text{-}1}}}{EI_{HCHO_{Jet\ A\text{-}1}}} \right) \cdot EI_{HCHO_{Fuel\ X}}$$

Equation 7.7

Where $factor_{HC_{Fuel\ X}}$ = factor specific to speciated HC of interest for alternative fuel

SO_2 emissions are assumed to be directly proportional to the ratio of kerosene in the fuel blend (Lee et al., 2010), thus adjustment factors used are related to the fraction of Jet A or Jet A-1 remaining in the fuel blend; as seen in Table 7.2.

BC mass and particle emissions indexes were derived through considering the percentage reductions given by the use of FT and FAME fuels (Lobo et al., 2011), with the ratio of BC:OC emissions as prescribed by Bond et al. (2004) citing Hopke (1985) applied to calculate OC emissions; i.e. using a BC:OC ratio of 4:1.

Table 7.4: Emissions indices derived for Fischer-Tropsch (FT) and fatty acid methyl ester (FAME) alternative fuel scenarios: 50% FT, 100% FT, 20% FAME, and 40% FAME blends.

Species	Emissions index (g/kg of fuel blend)				References
	FT		FAME		
	50%	100%	20%	40%	
Nitrogen oxides	12.54	11.88	10.16	9.37	Timko et al., (2011)
Carbon Monoxide	3.65	3.08	3.39	3.30	Timko et al., (2011)
Formaldehyde	1.606	1.159	1.382	1.382	Timko et al., (2011)
Ethane	0.0587	0.0471	0.0501	0.0509	Timko et al., (2011)
Propane	0.0583	0.0505	0.0338	0.0358	Timko et al., (2011)
Methanol	0.282	0.267	0.231	0.228	Timko et al., (2011)
Acetone	0.308	0.303	0.209	0.215	Timko et al., (2011)
Acetaldehyde	0.645	0.583	0.394	0.379	Timko et al., (2011)
Sulfur dioxide	0.588	0.000	0.941	0.706	Related to kerosene
Black carbon mass	0.0096	0.0040	0.0166	0.0116	Lobo et al., (2011)
Organic carbon mass	0.0024	0.0010	0.0041	0.0029	Lobo et al., (2011)
Carbonaceous part*	$1.277e^{14}$	$6.985e^{13}$	$1.561e^{14}$	$1.264e^{14}$	Lobo et al., (2011)

*emissions indices for carbonaceous particles are presented in particles $kg(fuel)^{-1}$ combusted

Staying in line with the power setting range used when deriving the speciated HC emissions indices for Jet A-1 fuel of 47–61% (Section 4.3); consistent with parameters taken from the Airbus FCTM for the A318/A319/A320/A321 aircraft range (Airbus, 2008). BC mass and number

reductions are calculated using emissions reduction data for an engine power setting range of 45–65% (Lobo et al., 2011) (Table 7.2).

Through the use of the emissions index adjustment factors for NO_X, CO, HCHO, SO_2, BC_{mass} and carbonaceous particle number from Table 7.2 and normalised factors (in relation to HCHO) for C_2H_6, C_3H_8, CH_3OH, $(CH_3)_2CO$ and CH_3CHO from Table 7.3, in conjunction with emissions indices for Jet A and Jet A-1 from Table 4.2 in Section 4.3 the emissions indices for the FT and FAME scenarios are calculated (Table 7.4).

Finally, when deriving emissions datasets for each of the alternative fuel scenarios, the energy content of FT and FAME fuel blends need to be taken in to account. The higher heating values of combustion (ΔH_{comb}) of the FT and FAME blends considered are presented in Table 7.5, along with the ΔH_{comb} of Jet A-1 and fuel adjustment factors (FAF).

Table 7.5: Density, higher heating values of combustion (ΔH_{comb}) and resulting fuel adjustment factors for each of the alternative fuel scenario blends considered.

Fuel and fuel blends	Density (kg. m^{-3})	ΔH_{comb} (MJ.kg^{-1}))	Fuel adjustment factor
50% FT/50% Jet A-1 blend	776	43.7	0.9954
100% FT fuel	755	44.1	0.9864
20% FAME/80% Jet A-1 blend	808	41.6	1.0457
40% FAME/60% Jet A-1 blend	825	39.6	1.0985
Jet A-1	797	43.5	n/a

Fuel adjustment factors (FAF) are implemented to normalise fuel usage based on fuel energy content (i.e. larger quantities of fuel required for a given journey when it has a lower heating value). Undertaking this methodology it is assumed that when increases in fuel are implemented (as per the FAME scenarios), there would be no effect on capacity and RPK (revenue passenger kilometres).

Taking fuel adjustment factors (FAF) and emissions index adjustment factors (EI_{AF}) into account, the emissions datasets for NO_X and BC_{mass} are calculated using Equation 7.8 and Equation 7.9. The FAF factor is applied in order to conserve distances covered by civil aviation, when the use of alternative fuels is investigated.

$$emissions_{alt\_NO_{X}i,j,k} = CMIP5_{NO_{X}i,j,k} \cdot EI_{AF\_NO_X\_alt} \cdot FAF_{alt}$$

Equation 7.8

$$emissions_{alt\_BC_{i,j,k}} = CMIP5_{BC_{i,j,k}} \cdot EI_{AF\_BC\_alt} \cdot FAF_{alt}$$

Equation 7.9

Where $CMIP5_{NO_X{}_{i,j,k}}$ = original CMIP5 NO_X emissions 3D array

$CMIP5_{BC_{i,j,k}}$ = original CMIP5 BC emissions 3D array

$EI_{AF\_NO_X\_alt}$ = NO_X emissions index adjustment factor

$EI_{AF\_BC\_alt}$ = BC emissions index adjustment factor

FAF_{alt} = fuel adjustment factor

For other aviation emission species, the following methodology is used to calculate their emissions datasets. This uses the emissions indexes presented in Table 7.4 and fuel adjustment factors from Table 7.5:

$$emissions_{alt\_X_{i,j,k}} = \frac{fuelburn_{i,j,k} \cdot EI_{alt_X} \cdot FAF_{alt}}{1000}$$

Equation 7.10

Where $fuelburn_{i,j,k}$ = grid resolved fuelburn (kg a^{-1})

EI_{alt_X} = emissions index for species of interest in g.kg^{-1} fuel

Through use of Equation 7.8, Equation 7.9 and Equation 7.10 along with the emissions indexes (EI_{alt_X}) (Table 7.4) and fuel adjustment factors (FAF) (Table 7.5), the annual emissions for each of the alternative fuel scenarios are calculated; as presented in Table 7.6.

From Table 7.6 it is seen that the implementation of alternative fuels can result in a reduction in annual global emissions of aviation-borne species, with the level of reductions achieved being dependent on the fuel and fuel blend used. Additionally it is noted that for FT fuel blends, increases in global HC emissions can arise.

Figure 7.2 presents annual emissions resulting from the alternative fuel scenarios. This shows that the use of Fischer-Tropsch fuels shows a general decline in NO_X, CO, SO_2, BC and OC emissions (relative to Jet A1) with increases in FT in the fuel blend. When FAMEs are added to the fuel mix there is a general reduction in NO_X, CO, SO_2, BC and OC emissions. Although it is observed that when the percentage of FAMEs in the mix is increased there is an increase in speciated hydrocarbons emissions, in relation to a scenario with a lower FAME blend.

Figure 7.2: Alternative fuel scenarios annual aviation-borne emissions for year 2000 for (a) nitrogen oxides (NO_X), (b) carbon monoxide (CO), (c) formaldehyde (HCHO), (d) ethane (C_2H_6), (e) propane (C_3H_8), (f) methanol (CH_3OH), (g) acetone ($(CH_3)_2CO$), (h) acetaldehyde (CH_3CHO), (i) sulfur dioxide (SO_2), (j) black carbon mass (BC), (k) BC particle number, and (l) organic carbon (OC).

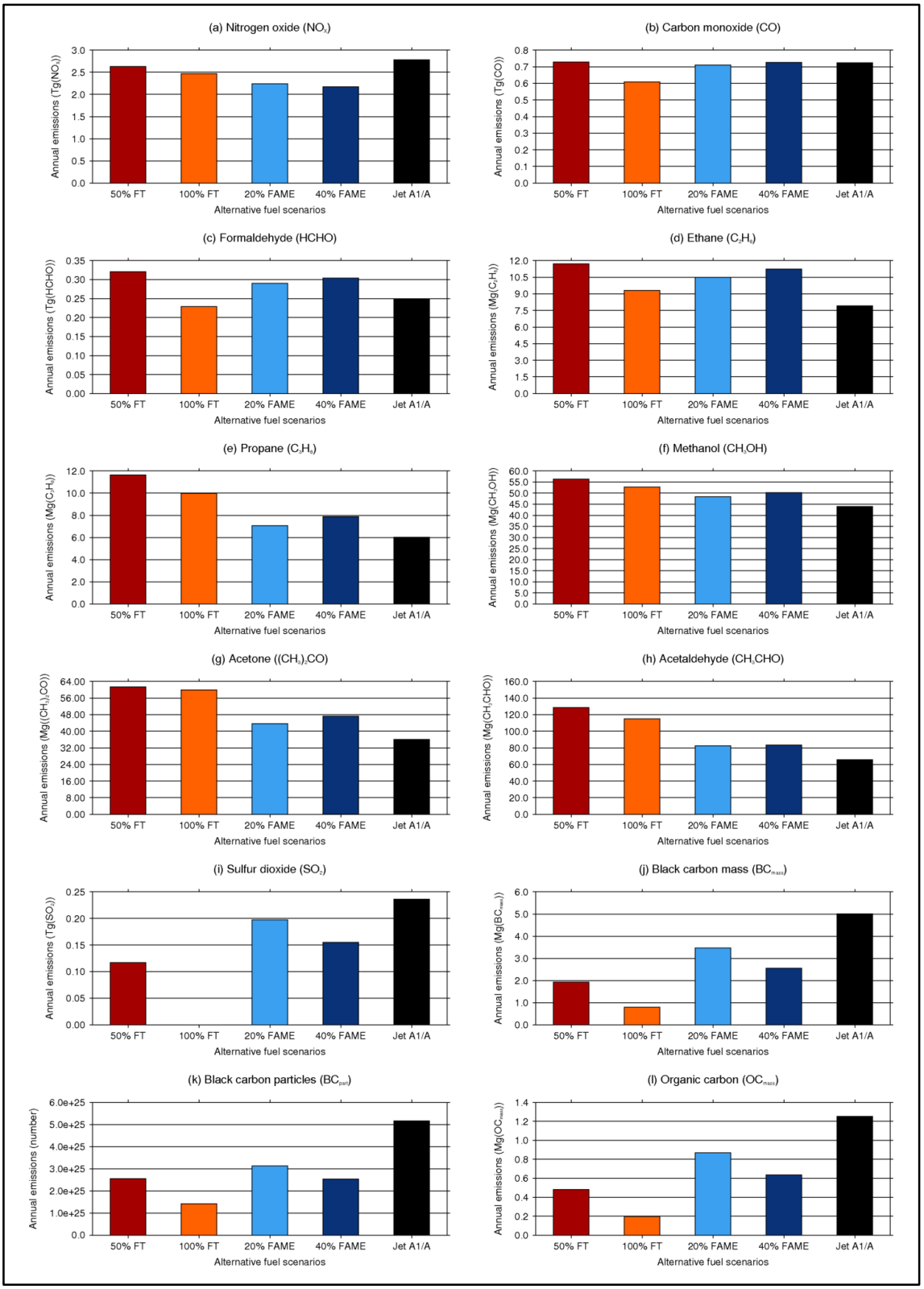

Table 7.6: Total annual aviation emissions for Fischer-Tropsch (FT) and fatty acid methyl ester (FAME) alternative fuel scenarios in comparison to annual emissions from Jet A-1.

Species	Annual global emissions (Tg)*				
	50% FT	100% FT	20% FAME	40% FAME	Jet A-1
NO_X	2.634	2.473	2.243	2.173	2.786
CO	0.591	0.493	0.575	0.604	0.724
HCHO	0.320	0.229	0.290	0.304	0.249
C_2H_6	0.011710	0.009319	0.010496	0.011220	0.007899
C_3H_8	0.011630	0.009978	0.007081	0.007880	0.006014
CH_3OH	0.056	0.053	0.048	0.050	0.044
$(CH_3)_2CO$	0.061	0.060	0.044	0.047	0.036
CH_3CHO	0.129	0.115	0.083	0.083	0.066
SO_2	0.117	0.000	0.197	0.155	0.236
BC_{mass}	0.001921	0.000791	0.003472	0.002546	0.005012
OC_{mass}	0.00048	0.00020	0.00087	0.00064	0.001253
$Carbonaceous_{part}$	$2.56x10^{25}$	$1.42x10^{25}$	$3.13x10^{25}$	$2.53x10^{25}$	$5.17x10^{25}$

*Annual global emissions of carbonaceous particles are presented in particles a^{-1}

Akin to aviation emissions derived from the use of Jet A-1, the GMD (D_g) for each of alternative fuel scenarios is required to adjust the BCOC size distributions fed in to the model to enable these scenarios to be modelled as realistically as possible. This is achieved through the use of Equation 4.16 (Section 4.3) and the use of annual total BC and OC masses, and BC particle numbers for each scenario, resulting in the GMDs presented in Table 7.7.

Table 7.7 shows that with both FT and FAME fuel blends, as the percentage contribution of the alternative fuel component to the fuel blend is increased, an associated reduction to the geometric mean diameter (D_g) arises.

Table 7.7: Geometric mean diameter of black carbon and organic carbon (BCOC) aviation emissions for Fischer-Tropsch and fatty acid methyl ester (FAME) scenarios, along with total $BCOC_{mass}$ and $BCOC_{number}$ emitted.

Scenario		Total $BCOC_{mass}$ ($Tg.yr^{-1}$)	Total $BCOC_{number}$ ($number.yr^{-1}$)	GMD (D_g) (nm)
FT	50%	0.00239	$2.548x10^{25}$	46.41
	100%	0.00099	$1.403x10^{25}$	42.13
FAME	20%	0.00434	$3.272x10^{25}$	52.01
	40%	0.00319	$2.784x10^{25}$	49.50
Jet A-1		0.00626	$5.172x10^{25}$	50.46

In the case of FT fuel blends there is an overall decrease in D_g (in relation to Jet A-1 fuel) as the percentage contribution of FT fuel to the net fuel blend is increased, with relative decreases in BCOC mass being greater than decreases in particle number.

With the FAME fuel blends there is an initial increase in D_g in relation to Jet A-1 fuel for the 20% FAME fuel blend due to a greater reduction particle number compared to BCOC mass. But as the FAME fuel blend is increased to 40% there is a reduction in D_g in relation to Jet A-1 due to the near equal relative decreases in BCOC mass and particle number emitted.

7.3.2 Simulations

To investigate the atmospheric and climate impacts of the use of alternative fuels in the aviation sector, the scenarios outlined in Table 6.1 are simulated. Simulations are conducted for year 2000, using meteorology from the ECMWF (European Centre for Medium-Range Weather Forecasts), in conjunction with anthropogenic and natural emissions for 2000.

Table 7.8: Simulations conducted to investigate the atmospheric impacts of the use of Fischer-Tropsch (FT) and fatty acid methyl ester (FAME) alternative fuels.

Scenario name	Description
NOAVI	No aviation emissions
NORM	100% Jet A-1 fuel
FT50	50% FT/50% Jet A-1 blend
FT100	100% FT fuel
FAME20	20% FAME/80% Jet A-1 blend
FAME40	40% FAME/60% Jet A-1 blend

All simulations were conducted for 16 months from September 1999 to December 2000 inclusive, with the first four months discarded as spin-up time, with results from all simulations being compared against a simulation with aviation emissions excluded (NOAVI). As per previous chapters the only variations applied are those applied to aviation emissions inventories as per the simulations outlined in Table 7.8.

7.4 Results and Discussion

Here the atmospheric perturbations and then the climatic impacts of the use of alternative fuels in aviation based on the four scenarios considered in Table 7.8 are discussed in turn.

7.4.1 Aviation alternative fuel scenario induced atmospheric perturbations

First changes in gas-phase atmospheric composition resulting from alternative aviation fuels are presented, followed by changes in aerosol.

7.4.1.1 Gas-phase changes due to alternative fuels

Figure 7.3–Figure 7.8 show the percentage changes in nitrogen oxides (NO_X), ozone (O_3), hydroxyl radical (OH), nitric acid (HNO_3), peroxyl acetyl nitrate (PAN) and sulfur dioxide (SO_2) in relation to standard aviation (NORM) for the four alternative fuel scenarios investigated: FT50, FT100, FAME20, and FAME40.

Figure 7.3: Percentage change in zonal aviation-induced NO_X in relation to standard aviation for the following alternative fuel scenarios: (a) 50% Fischer-Tropsch; (b) 100% Fischer-Tropsch; (c) 20% Fatty Acid Methyl Esters; and (d) 40% Fatty Acid Methyl Esters.

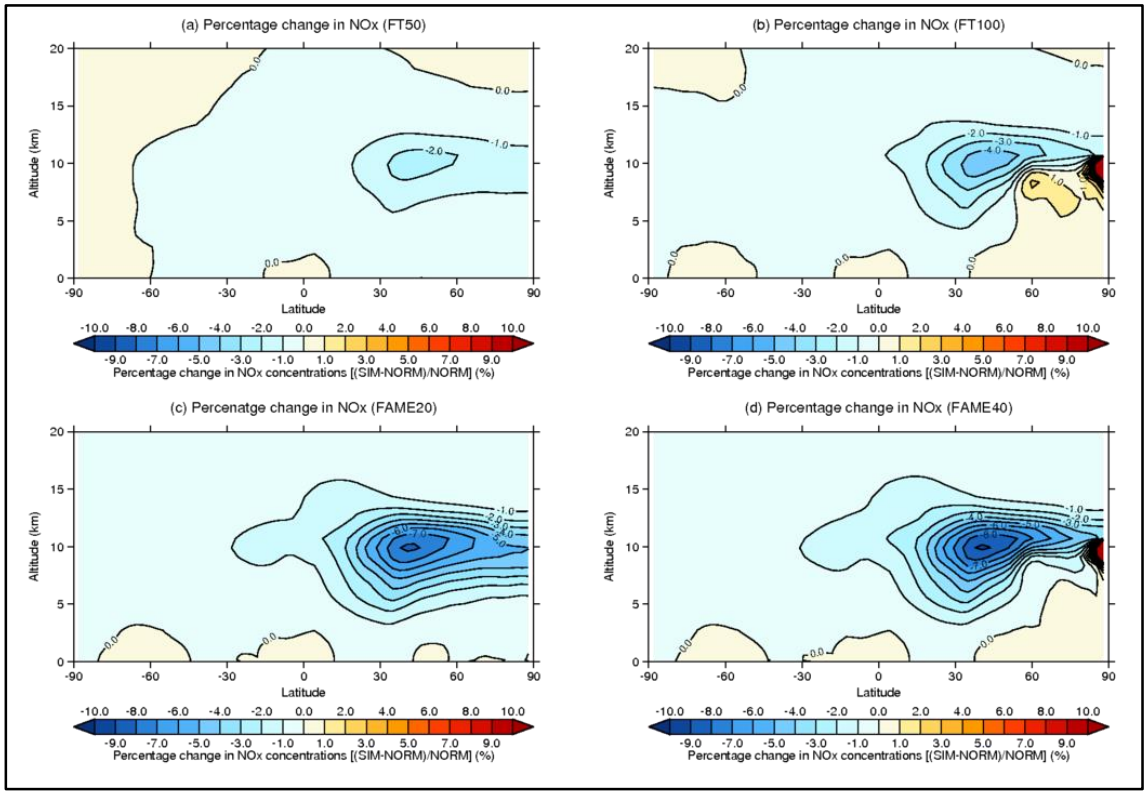

Figure 7.3 shows that FT and FAME alternative fuel scenarios reduce aviation-induced NO_X concentrations. This is due to their lower NO_X emissions indices for each fuel type (FT or FAME) and fuel blend (Table 7.4 and Table 7.8). FAME fuel blends result in mean reductions in aviation-induced NO_X in relation to standard aviation (NORM) [FAME20 ΔNO_X = –0.78 pptv; FAME40 ΔNO_X = –0.89 pptv], in comparison to FT fuel blends [FT50 ΔNO_X = –0.17 pptv; FT100 ΔNO_X = –0.42 pptv]. Greater zonal mean reductions are seen along the cruise region of flight for FAME blends [FAME20 ΔNO_X = –2.78 pptv (–8.21%); FAME40 ΔNO_X = –3.32 pptv (–9.61%)]

in comparison to FT fuel blends [FT50 ΔNO_X = –0.82 pptv (–2.37%); FT100 ΔNO_X = –1.82 pptv (–5.11%)] (Figure 7.3).

Following the reductions in NO_X resulting from the use of alternative fuels (Figure 7.3), reductions in aviation-induced O_3 arise; with FAME fuel blends giving greater reductions [FAME20 ΔO_3 = –0.033 ppbv (–0.058%); FAME40 ΔO_3 = –0.032 ppbv (–0.061%)] in comparison to FT fuel blends [FT50 ΔO_3 = –0.016 ppbv (–0.017%); FT100 ΔO_3 = –0.019 ppbv (–0.031%)].

Zonal mean reductions in O_3 (Figure 7.4) follow the same pattern in O_3 reductions with the greatest reductions seen between 2–10 km, a region that includes the cruise region of flight and the majority of aviation emissions release (Figure 4.1). Greatest zonal mean reductions in O_3 for FAME fuel blends are simulated as: FAME20 ΔO_3 = –0.33 ppbv (–0.48%); FAME40 ΔO_3 = –0.34 ppbv (–0.52%). And greatest zonal mean reductions for FT fuels simulated as: FT50 ΔO_3 = –0.09 ppbv (–0.14%); FT100 ΔO_3 = –0.17 ppbv (–0.26%).

Additionally, changes in surface O_3 concentrations are see not only due to reductions in NO_X emissions from the use of FT and FAME fuels (Timko et al., 2011), but also due to the higher lifetime of O_3 in the upper troposphere (Kentarchos and Roelofs, 2002). This lifetime effect allows aviation-induced impacts on O_3 to be decoupled from the point of release of aviation emissions (Fowler et al., 1997; Jenkin and Clemitshaw, 2000; Lee et al., 2010), hence resulting in changes in O_3 concentrations at the surface.

Due to the relationship between NO_X emissions and the resulting production of OH (Holmes et al., 2011; Myhre et al., 2011), reductions in aviation NO_X emissions not only result in reductions in aviation-induced O_3, but reductions in OH in regions where reductions in O_3 occur, while OH is seen to increase in regions where increases in O_3 are observed (Figure 7.4 and Figure 7.5). Increases in OH concentrations seen in the NH cruise region of flight can also in part be explained through a reduction in aviation-induced sulfates formed (via Reaction 2.29 to Reaction 2.31), as a result of reductions in aviation-emitted SO_2 through the use of the FT and FAME fuels investigated here. As such reductions in aviation-emitted SO_2 result in a reduction in amount of OH consumed (via Reaction 2.29).

The aforementioned decreases in aviation-emitted NO_X result in the following decreases in OH at cruise level: FAME20 ΔOH = –3.80%; FAME40 ΔOH = –4.23%; FT50 ΔOH = –1.07%; FT100 ΔOH = –2.19%. Alongside the following increases in the Northern Hemisphere stratosphere due to increases in aviation-induced NO_X represented in (Figure 7.3): FAME20 ΔOH = +2.68%; FAME40 ΔOH = +4.56%; FT50 ΔOH = +0.86%; FT100 ΔOH =+2.54% (Figure 7.5).

Figure 7.4: Percentage changes in zonal aviation-induced O_3 in relation to standard aviation for the following alternative fuel scenarios: (a) 50% Fischer-Tropsch; (b) 100% Fischer-Tropsch; (c) 20% Fatty Acid Methyl Ester; and (d) 40% Fatty Acid Methyl Ester.

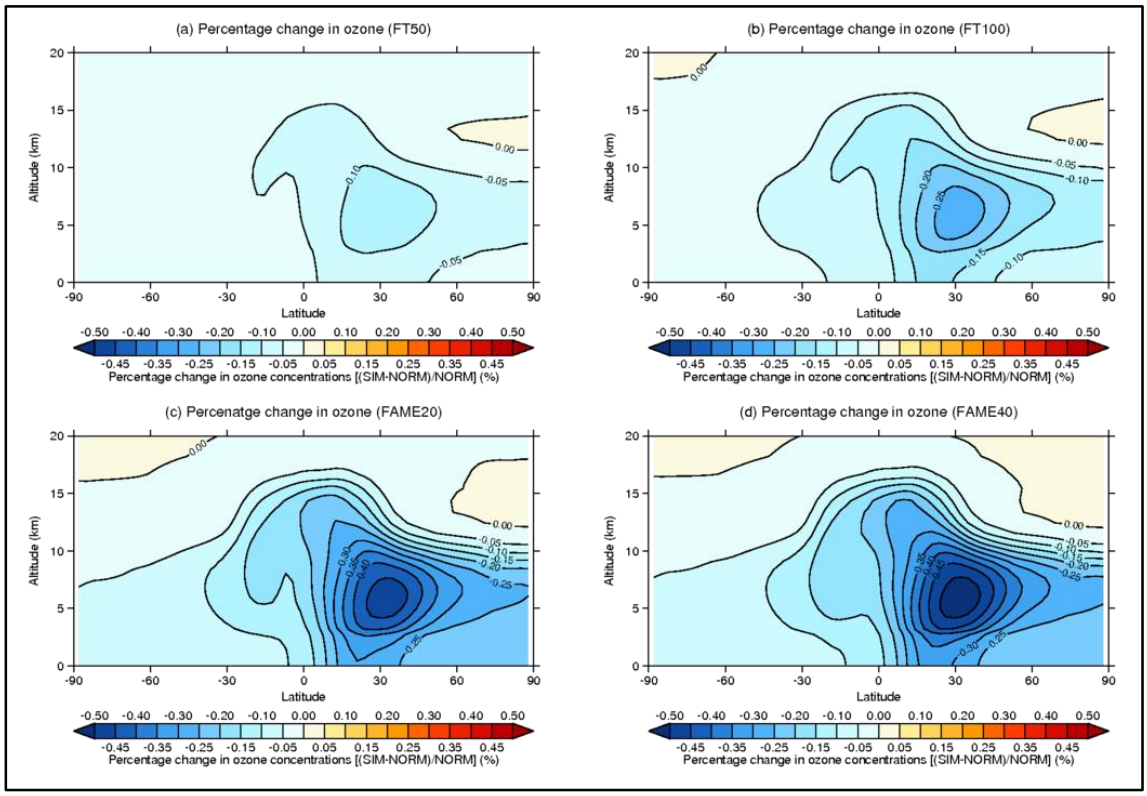

Figure 7.5: Percentage changes in zonal aviation-induced OH in relation to standard aviation for the following alternative fuel scenarios: (a) 50% Fischer-Tropsch; (b) 100% Fischer-Tropsch; (c) 20% Fatty Acid Methyl Ester; and (d) 40% Fatty Acid Methyl Ester.

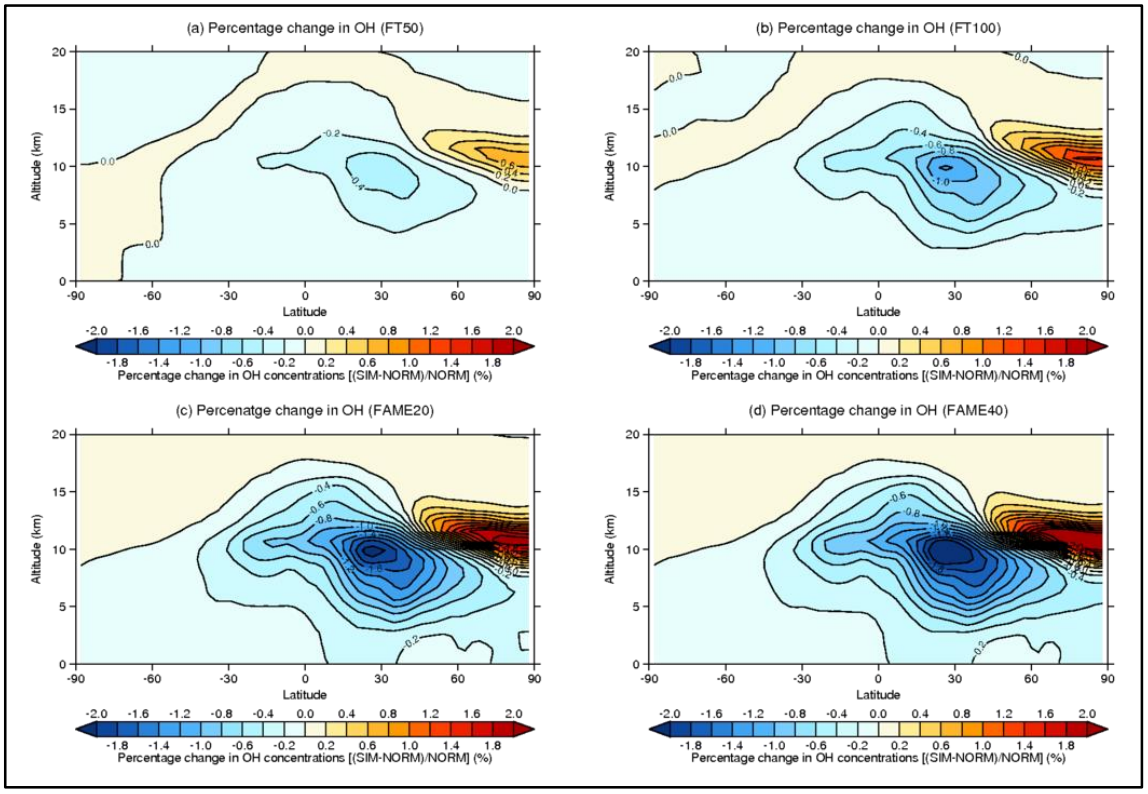

Similar to OH, aviation-induced HNO_3 and PAN perturbations are dependent on the aviation NO_X emissions (Fowler et al., 1997; Jenkin and Clemitshaw, 2000). From reductions in aviation-emitted NO_X seen from the FT and FAME fuel scenarios investigated here, reductions in both aviation-induced HNO_3 and PAN arise. HNO_3 reductions arise due to decreases in NO_X emissions and OH concentrations. While reductions in aviation-induced PAN are due to reductions in NO_X available to react with organic peroxy radicals (such as $CH_3C(O)O_2$); where PAN can act as a reservoir for NO_X (Fowler et al., 1997; Jenkin and Clemitshaw, 2000).

From Figure 7.6 the following maximum zonal mean reductions in HNO_3 (in relation to standard aviation) can be seen, primarily occurring in the Northern Hemisphere in line with the release of aviation NO_X emissions: FAME20 ΔHNO_3 = –5.62%; FAME40 ΔHNO_3 = –6.31%; FT50 ΔHNO_3 = –2.11%; FT100 ΔHNO_3 = –3.47%.

Figure 7.7 shows that primarily reductions in PAN occur with the use of FAME fuels [FAME20 ΔPAN = –0.38%; FAME40 ΔPAN = –0.31%; FT50 = ΔPAN = –0.15%; FT100 = ΔPAN = –0.10%]. The FT50 blend results in a small increase around the NH tropopause of +0.19%. Reductions in PAN arise due to decreases in aviation-induced NO_X. As PAN is formed from the oxidation of HCs in the presence of NO_2, reductions in aviation-induced NO_X (Figure 7.3) and OH (Figure 7.5) from the use of the FT and FAME fuel blends (despite associated increases in aviation emitted HCs) result in global reductions in PAN (Fowler et al., 1997; Jenkin and Clemitshaw, 2000).

It is also seen that reduced increases in cruise level PAN occur when the fraction of FT fuel within the fuel blend is increased, and reduced decreases in PAN occur when the fraction of FAME fuel within the fuel blend is increased. As the fraction of FT fuel within the FT fuel blend is increased a decrease in HC emissions are seen, while as the fraction of FAME fuel within the FAME fuel blends is increased an increase in HC emissions are seen. Thus the changes in PAN simulated here (Figure 7.7) indicate that changes in HCs emitted by aviation have an effect on aviation-induced PAN; with increases in aviation-emitted HCs resulting in increases in aviation-induced PAN. These increases in aviation-induced PAN may not be that clear in Figure 7.7 as PAN formation is also a function of NO_2 (Reaction 2.13), and because the FAME fuel blends release lower levels of NO_X (Figure 7.2 and Table 7.6).

Consistent with changes in the sulfur dioxide emissions indices for the FT and FAME fuel blends (Table 7.4), the FT scenarios give greater reductions in aviation-induced zonal mean concentrations (Figure 7.8) [FT50 ΔSO_2 = –24.58%; FT100 ΔSO_2 = –48.77%], in comparison to the FAME fuel blends investigated [FAME20 ΔSO_2 = –7.93%; FAME40 ΔSO_2 = –16.93%].

Figure 7.6: Percentage changes in zonal aviation-induced HNO_3 in relation to standard aviation for the following alternative fuel scenarios: (a) 50% Fischer-Tropsch; (b) 100% Fischer-Tropsch; (c) 20% Fatty Acid Methyl Ester; and (d) 40% Fatty Acid Methyl Ester.

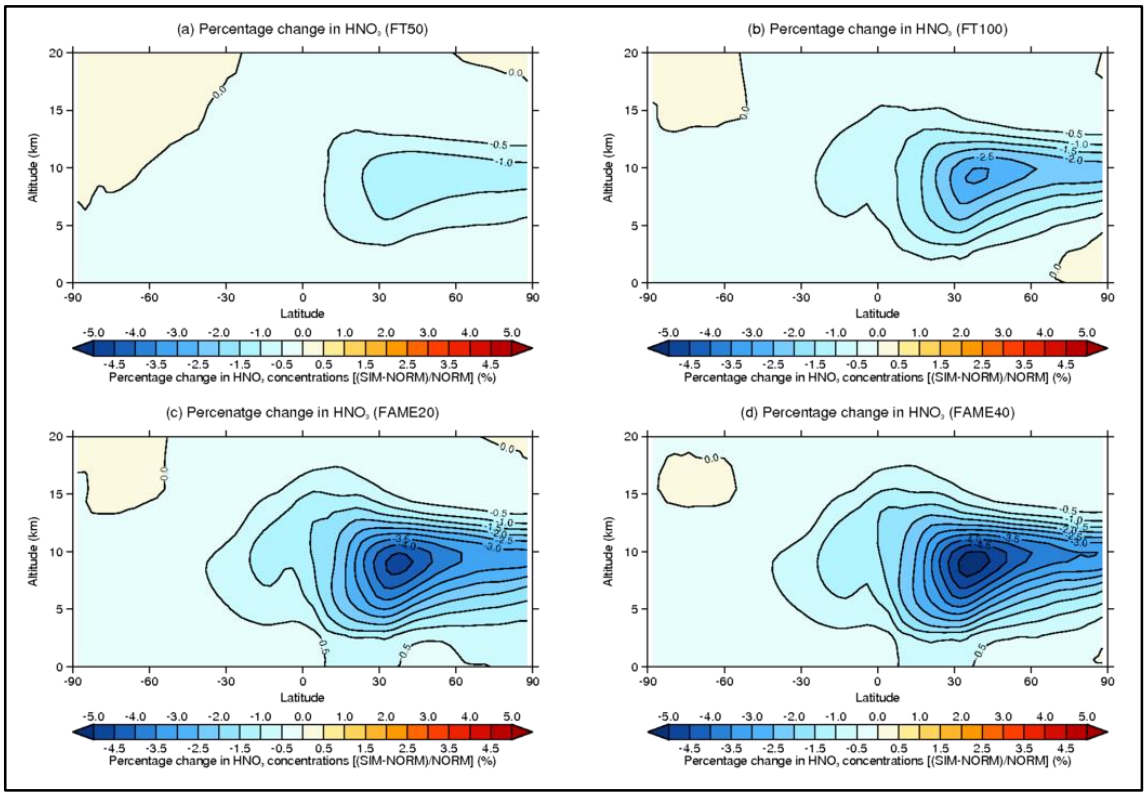

Figure 7.7: Percentage changes in zonal aviation-induced PAN in relation to standard aviation for the following alternative fuel scenarios: (a) 50% Fischer-Tropsch; (b) 100% Fischer-Tropsch; (c) 20% Fatty Acid Methyl Ester; and (d) 40% Fatty Acid Methyl Ester.

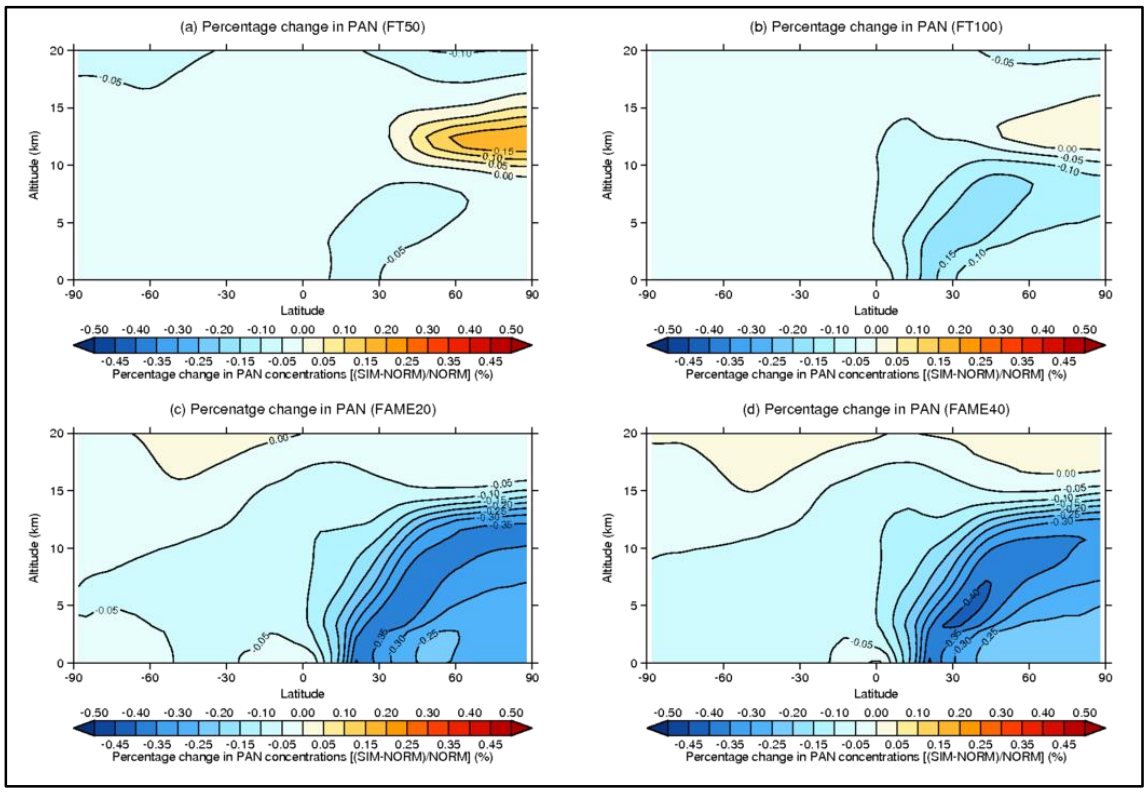

Figure 7.8: Percentage changes in zonal aviation-induced SO_2 in relation to standard aviation for the following alternative fuel scenarios: (a) 50% Fischer-Tropsch; (b) 100% Fischer-Tropsch; (c) 20% Fatty Acid Methyl Ester; and (d) 40% Fatty Acid Methyl Ester.

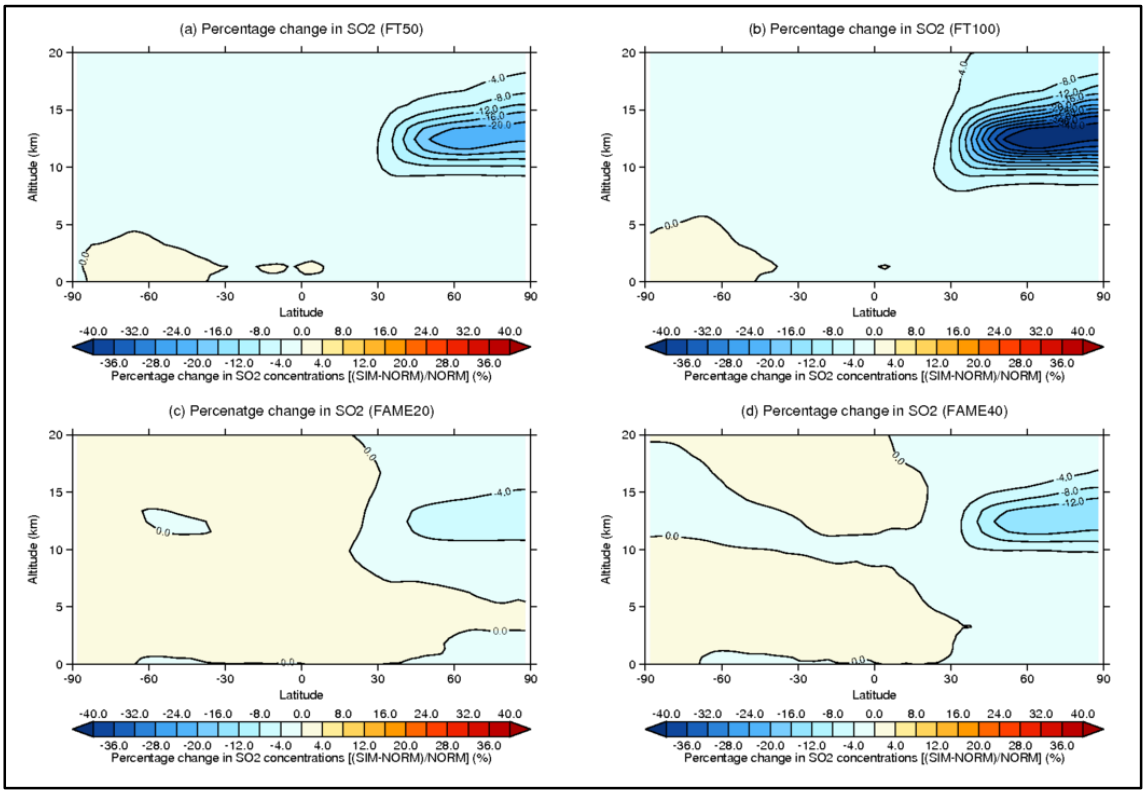

Table 7.9: Changes in aviation-induced gas-phase species burdens due to the use of alternative fuels in aviation: absolute and relative differences in relation to standard aviation-induced perturbations (NORM).

Scenarios	Change in burden				
	NO_X ($Gg\ yr^{-1}$)	O_3 ($Tg\ yr^{-1}$)	OH ($Mg\ yr^{-1}$)	HNO_3 ($Gg\ yr^{-1}$)	SO_2 ($Gg\ yr_{-1}$)
FT50	-2.09 [-5.14%]	-0.22 [-5.70%]	-0.21 [-4217%]	-4.84 [-5.67%]	-2.72 [-256.5%]
FT100	-4.17 [-10.25%]	-0.37 [-9.51%]	-0.45 [-9036%]	-9.30 [-10.88%]	-5.49 [-516.9%]
FAME20	-7.68 [-18.90%]	-0.71 [-18.11%]	-0.86 [-17269%]	-16.00 [-18.73%]	-0.13 [-11.89%]
FAME40	-8.44 [-20.76%]	-0.73 [-18.67%]	-0.94 [-18876%]	-17.09 [-20.00%]	-1.20 [-113.17%]

Table 7.9 shows that, in the two cases of FAME fuel blends investigated, there is the potential to reduce NO_X, O_3, OH and HNO_3 burdens to a greater extent than FT fuel blends. It is also simulated that as the ratio of alternative fuel to Jet A-1 is increased reductions in gas-phase

species burdens are increased, i.e. FAME40 result in greater reductions in burden than FAME20, and FT100 decrease burdens to a greater extent than FT50.

The FT fuel blends, due to their greater ratios of alternative fuel to Jet A-1, have a far greater capacity to reduce aviation-induced SO_2 (due to the linear relationship between fuel sulfur content and Jet A-1 fuel content (Hadaller and Momenthy, 1993)) resulting in a reduction in global burdens of up to 5.49 Gg(SO_2) [–516%] when used as a pure fuel, i.e. scenario FT100.

Despite greater reductions in aviation-induced O_3 by the FAME fuel blend scenarios, in reality these will not be achieved by civil aviation as FAME fuels for use in blending do not meet specification ASTM D1655 for Jet A-1/Jet A fuel, nor do they meet specification ASTM D7566-10 for alternative fuels to be blended in for commercial civil aviation and have been determined as an undesirable contaminant (Timko et al., 2011). FAME fuels are considered contaminants as they are surface active, providing risks for cross contamination in supply chains which handle both jet fuel and biodiesel (JIG, November 2008) and microbial contamination, potentially rendering fuel unusable (Crown Oil Environmental Ltd, 2014).

7.4.1.2 Aerosol-phase changes

This section initially considers aviation-induced perturbations in sulfates, nitrates, ammonium and BCOC (Figure 7.9–Figure 7.12) from the use of the alternative fuel blends investigated in this chapter (Table 7.8). Then this section investigates aviation-induced cloud condensation nuclei (CCN) concentrations, focusing on perturbations at low-level cloud height (Figure 7.13).

Figure 7.9 shows that the use of FT fuels result in greater maximum reductions in aviation-induced zonal mean sulfate concentrations around the cruise region of flight [FT50 ΔSO_4^{2-} = –2.92% (–2.79 ng m^{-3}); FT100 ΔSO_4^{2-} = –6.04% (–5.77 ng m^{-3})] in comparison to the use of FAME fuel blends [FAME20 ΔSO_4^{2-} = –0.60% (–1.08 ng m^{-3}); FAME40 ΔSO_4^{2-} = –1.32% (–1.53 ng m^{-3})]. In line with zonal mean reductions in sulfates (Figure 7.9), FT fuel blends return greater global mean reductions in sulfate concentrations [FT50 ΔSO_4^{2-} = –0.19 ng m^{-3} (–0.14%); FT100 ΔSO_4^{2-} = –0.39 ng m^{-3} (–0.37%)], in comparison to the FAME fuel blends investigated [FAME20 ΔSO_4^{2-} = –0.08 ng m^{-3} (–0.004%); FAME40 ΔSO_4^{2-} = –0.14 ng m^{-3} (–0.06%)].

Annual mean zonal sulfate reductions presented in Figure 7.9 reflect reductions in aviation-induced SO_2 (Figure 7.8) and NO_X (Figure 7.3), further highlighting the relationship between aviation-induced sulfates, aviation SO_2 and NO_X emissions (Barrett et al., 2010; Fowler et al., 1997; Jenkin and Clemitshaw, 2000).

Figure 7.9: Percentage changes in zonal aviation-induced sulfates in relation to standard aviation for the following alternative fuel scenarios: (a) 50% Fischer-Tropsch; (b) 100% Fischer-Tropsch; (c) 20% Fatty Acid Methyl Ester; and (d) 40% Fatty Acid Methyl Ester.

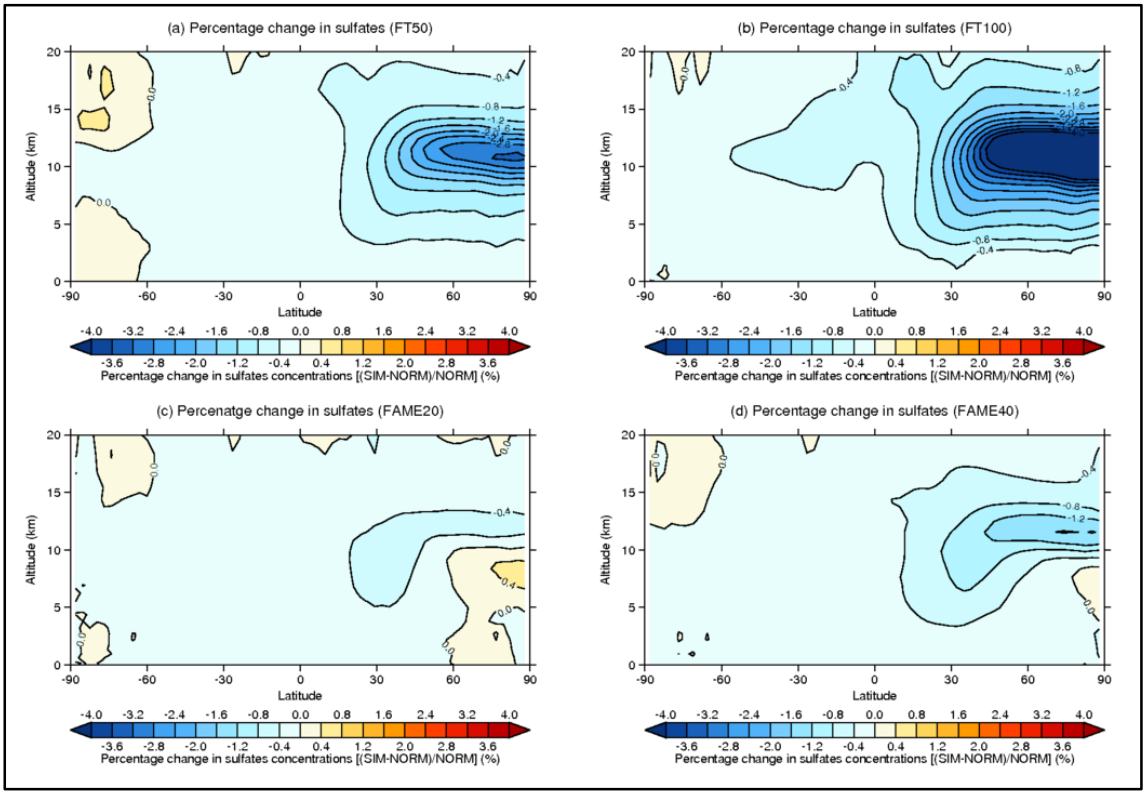

Figure 7.10: Percentage changes in zonal aviation-induced nitrates in relation to standard aviation for the following alternative fuel scenarios: (a) 50% Fischer-Tropsch; (b) 100% Fischer-Tropsch; (c) 20% Fatty Acid Methyl Ester; and (d) 40% Fatty Acid Methyl Ester.

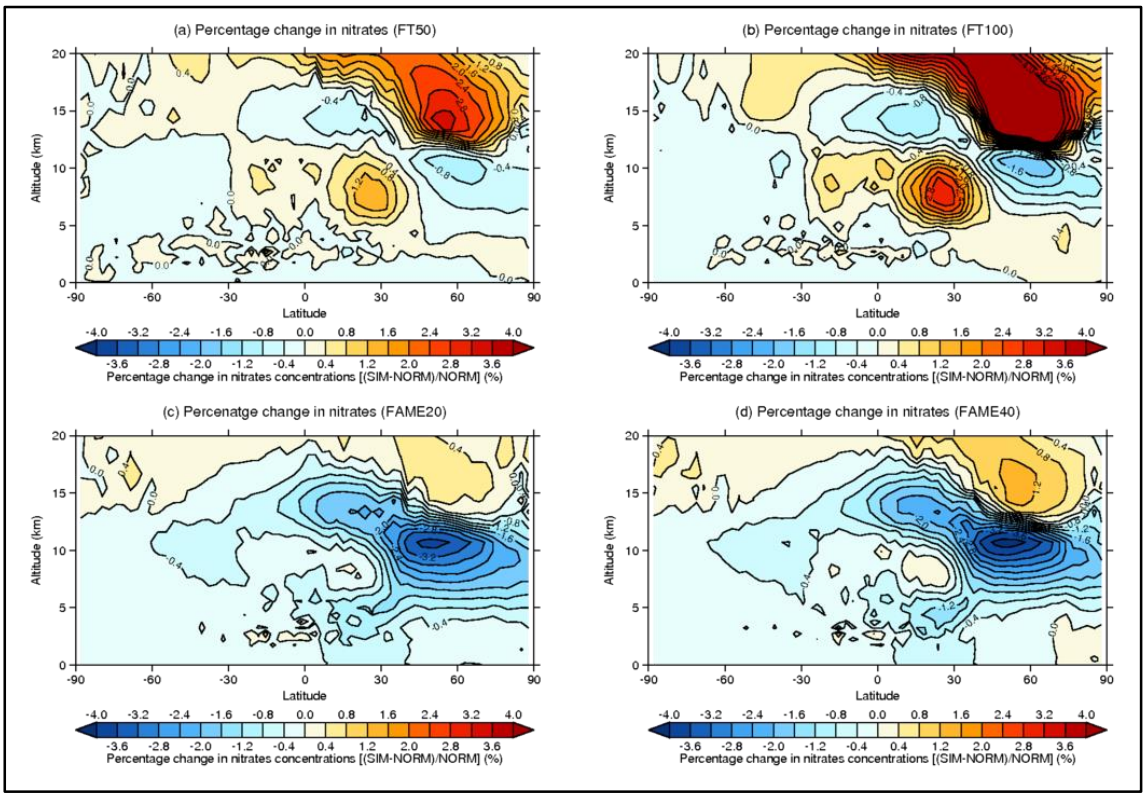

The impact of the use of FT and FAME fuel blends on zonal mean percentage increases in aviation-induced nitrates are presented in Figure 7.10. The use of FAME fuel blends are found to result in greater maximum reductions in aviation-induced zonal mean nitrate concentrations [FAME20 ΔNO_3^- = –2.89% (–1.27 ng m^{-3}); FAME40 ΔNO_3^- = –3.40% (–1.51 ng m^{-3})], in comparison to FT fuel blends [FT50 ΔNO_3^- = –2.78% (–0.19 ng m^{-3}); FT100 ΔNO_3^- = –3.58% (–0.58 ng m^{-3})]. This results in global mean concentration changes in relation to standard aviation (NORM) of: FT50 ΔNO_3^- = –0.003 ng m^{-3}; FT100 ΔNO_3^- =–0.012 ng m^{-3}; FAME20 ΔNO_3^- =–0.042 ng m^{-3}; and FAME40 ΔNO_3^- =–0.042 ng m^{-3}.

Through reductions in aviation emitted SO_2, resulting from the use of FT and FAME fuel blends (Table 7.6), reductions in aviation-induced sulfates arise This increases the availability of atmospheric ammonia to form ammonium nitrate, which primarily increases nitrate concentrations in the upper troposphere/lower stratosphere for the FT fuel blend scenarios, and in the upper stratosphere when FAME fuel blends are considered (Figure 7.10).

As the version of TOMCAT within GMV4-nitrate doesn't simulate stratospheric chemistry but represents stratospheric chemistry using simple tracers to model stratospheric chemistry, using upper boundary conditions for stratospheric ozone and NO_Y species (Chipperfield, 2006; Arnold et al., 2005), changes observed in this region are not as reliable as simulated tropospheric changes.

From Figure 7.10 the following maximum zonal percentage increases in stratospheric nitrate concentrations in relation to standard aviation are simulated: FT50 ΔNO_3^- = +1.07 ng m^{-3} (2.69%); FT100 ΔNO_3^- = +1.02 ng m^{-3} (5.84%); FAME20 ΔNO_3^- = +0.33 ng m^{-3} (1.30%); and FAME40 ΔNO_3^- = +0.39 ng m^{-3} (+1.15%).

Figure 7.11 presents the zonal mean changes in aviation-induced ammonium in relation to standard aviation emissions (NORM). Here it is seen that FT fuel blends provide greater reductions in ammonium [FT50 ΔNH_4^+ = –0.16 ng m^{-3} (–0.46%); FT100 ΔNH_4^+ = –0.47 ng m^{-3} (–0.68%)] in comparison to FAME fuel blends [FAME20 ΔNH_4^+ = –0.10 ng m^{-3} (–0.19%); FAME40 ΔNH_4^+ = –0.14 ng m^{-3} (–0.25%)]. In addition, the FAME fuel blends provide increases in Northern Hemisphere of up +1.10% for FAME20 and up to +1.20% for FAME40.

These increases in NH [between 60°N–90°N] ammonium concentrations simulated from the use of FAME fuels (ΔNH_{NH4_FAME20} of up to +1.10% and ΔNH_{NH4_FAME40} of up to +1.20%) (Figure 7.11), occur in regions where small increases in aviation-induced sulfates occur (between 60°N–90°N, from ground level to the cruise region of flight) (Figure 7.9) and large decreases in

nitrates occur (Figure 7.10). These relative increases in sulfates and nitrates which drive these changes in ammonium will be a result of the relative changes in aviation-emitted SO_2 and NO_X from the FT and FAME fuel blends being investigated here (Figure 7.2 and Table 7.6). Though it has to acknowledged that in both cases there are net global reduction in both aviation-induced sulfates and ammonium.

As the formation of ammonium sulfate takes precedence over the formation of ammonium nitrate in regions with lower partial pressures of ammonia (Bauer et al., 2007) these NH increases in sulfates and large NH decreases in nitrates result in small fractional increases in ammonium (up to ~1.5%) (Figure 7.11). On a molecule to molecule basis the production of ammonium sulfate ($(NH_4)_2.SO_4$) results in more ammonium molecules in relation to the production of ammonium nitrate ($NH_4.NO_3$); hence for each molecule of ammonium sulfate two molecules of ammonium will be produced in relation to the one for ammonium nitrate.

Figure 7.11: Percentage changes in zonal aviation-induced ammonium in relation to standard aviation for the following alternative fuel scenarios: (a) 50% Fischer-Tropsch; (b) 100% Fischer-Tropsch; (c) 20% Fatty Acid Methyl Ester; and (d) 40% Fatty Acid Methyl Ester.

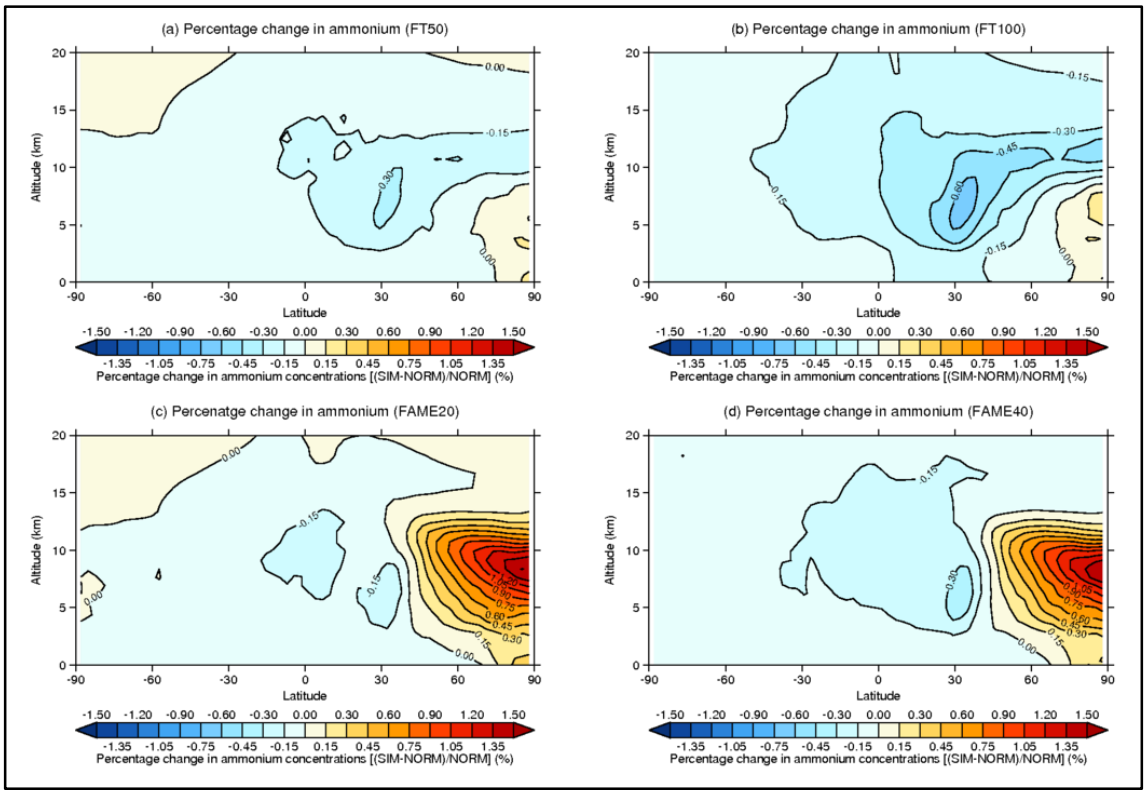

Reflecting reductions in BC and OC emitted from the FT and FAME fuel blends (Table 7.6), the FT fuel scenarios produce much greater zonal mean percentage reductions in BCOC in relation to standard aviation [FT50 ΔBCOC = –0.30 ng m^{-3} (–1.30%); FT100 ΔBCOC = –0.47 ng m^{-3} (–2.25%)], in comparison to the FAME fuel blends [FAME20 ΔBCOC = –0.096 ng m^{-3} (–0.70%); FAME40 ΔBCOC = –0.103 ng m^{-3} (–0.47%)] (Figure 7.12).

Figure 7.12: Percentage changes in zonal aviation-induced BCOC in relation to standard aviation for the following alternative fuel scenarios: (a) 50% Fischer-Tropsch; (b) 100% Fischer-Tropsch; (c) 20% Fatty Acid Methyl Ester; and (d) 40% Fatty Acid Methyl Ester.

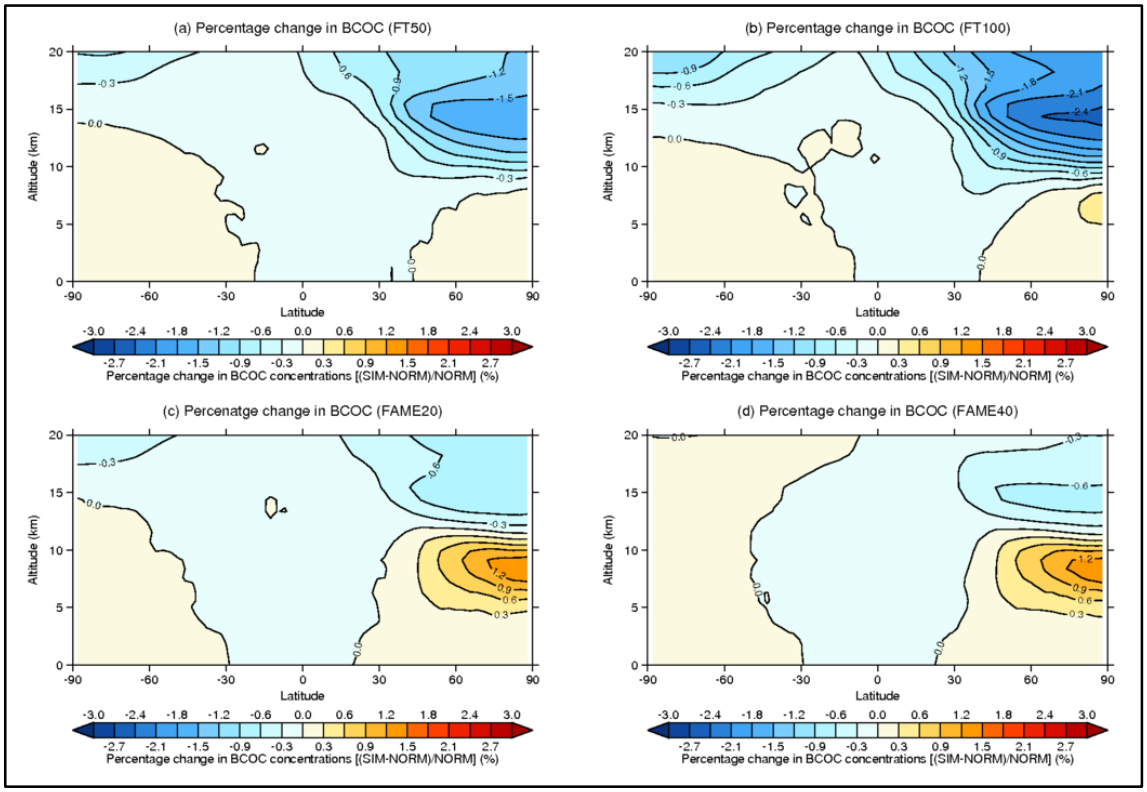

The FT and FAME fuel blends investigated here result in the following global mean changes in black and organic carbon in relation to standard aviation (NORM): FT50 ΔBCOC = –0.02 ng m^{-3} (–0.77%); FT100 ΔBCOC = –0.03 ng m^{-3} (–1.41%); FAME20 ΔBCOC = –0.0059 ng m^{-3} (–0.61%); FAME40 ΔBCOC = –0.0057 ng m^{-3} (–0.22%).

The decreases in combined BC and OC (BCOC) concentrations in the UT seen in Figure 7.12 are primarily driven by decreases in aviation-induced BC concentrations in the UT (not presented), with the FT fuel scenarios returning greater levels of reductions in BC due to the greater reductions in BC emissions from the FT fuel blends (Table 7.6). Despite the same relative decreases in aviation OC emissions (as BC emissions) increases in OC are simulated from the use of FT and FAME fuel blends in relation to standard aviation (NORM) (not shown here). The greatest increases in OC are seen in the NH between about 40°N–90°N from the cruise level of flight to the surface level; thus the combination of the decreases in BC and Increases in OC result in the zonal mean changes in BCOC presented in Figure 7.12.

The atmospheric lifetime of BC is dependent on its atmospheric interactions with other aerosol components, with its lifetime ranging between a few days to weeks (Bond et al., 2013). Typically the tropospheric lifetime of BC is ~1 week to 10 days, while that of OC is ~1 week (Boucher et al., 2013). The increases in OC simulated (Figure 7.12 and Table 7.10), could be a

result of changes in atmospheric composition, arising from alternative fuels notably returning large reductions in SO_2 emissions, which could affect the atmospheric lifetime of OC aerosols.

Table 7.10 presents the reductions in aviation-induced aerosols (sulfates, nitrates, ammonium, black carbon and organic carbon) from alternative fuel scenarios investigated here (Table 7.8). From Table 7.10 it is seen that the FT fuel blends are simulated to return greater reductions in sulfates, BC, OC, and ammonium in relation to FAME fuel blends, while the FAME fuel blends give greater reductions in aviation-induced nitrates compared to the FT fuel blends. As with the gas-phase species, discussed in (Section 7.4.1.1), as the proportion of alternative fuel to the fuel blend is increased, the reductions achieved are increased.

Table 7.10: Changes in aviation-induced aerosol-phase species burdens due to the use of alternative fuels in aviation: absolute and relative differences in relation to standard aviation-induced perturbations (NORM).

Scenarios	Change in burden				
	Sulfates ($Gg\ yr^{-1}$)	**Nitrates ($Gg\ yr^{-1}$)**	**Ammonium ($Gg\ yr^{-1}$)**	**BC ($Gg\ yr^{-1}$)**	**OC ($Gg\ yr_{-1}$)**
FT50	-4.51 [-34.90%]	-0.07 [-1.22%]	-0.26 [-30.56%]	-0.376 [-74.15%]	-0.091 [-33.84%]
FT100	-9.24 [-71.54%]	-0.28 [-5.02%]	-0.52 [-60.98%]	-0.526 [-103.79%]	-0.204 [-75.36%]
FAME20	-1.85 [-14.30%]	-0.98 [17.35%]	-0.11 [-12.70%]	-0.147 [-29.04%]	0.007 [2.61%]
FAME40	-3.42 [-26.44%]	-0.99 [17.53%]	-0.20 [-23.36%]	-0.147 [-29.03%]	0.013 [17.53%]

Ultimately net reductions in aerosol-phase species burdens simulated (for sulfates, nitrates, ammonium, black carbon and organic carbon) are much greater for the FT fuel blends. The FT fuel blend reduces the aviation-induced aerosol burden by 5.31 Gg for the FT50 blend and by 10.78 Gg for the FT100 scenario, while the FAME20 blend reduced the net aviation-induced aerosol burden by 3.08 Gg and the FAME40 blended reduced the burden by 4.74 Gg.

The greater reductions in aviation-induced aerosol burdens produced by the FT scenarios are primarily due to the effects of reductions in the fuel sulfur content of the resulting fuel blend, with 84.96% of the reduction seen by the FT50 blend being attributed to reductions in sulfates formed, with this figure increasing to 85.74% for the FT100 blend. While for the FAME fuel blends, greater reductions in aviation-induced nitrates are seen [FAME20 ΔNO_3^- = –0.98 Gg;

FAME40 ΔNO_3^- = –0.99 Gg], but with lower levels of reductions in aviation-induced sulfates [FAME20 ΔSO_4^{2-} = –1.85 Gg; FAME40 ΔSO_4^{2-} = –3.42 Gg].

These aerosol burden reductions essentially have the potential to result in a smaller reduction in the cooling aerosol cloud albedo effect (aCAE) for the FAME fuel blends in comparison to the FT fuel blends, while the FT fuels blends will have the potential to provide a greater reduction in the warming aerosol direct radiative effect (aDRE) in comparison to the FAME fuel blends.

Figure 7.13: Percentage changes in low-cloud level (0.96 km) aviation-induced CCN (Dp > 50 nm) in relation to standard aviation for the following alternative fuel scenarios: (a) 50% Fischer-Tropsch; (b) 100% Fischer-Tropsch; (c) 20% Fatty Acid Methyl Ester; and (d) 40% Fatty Acid Methyl Ester.

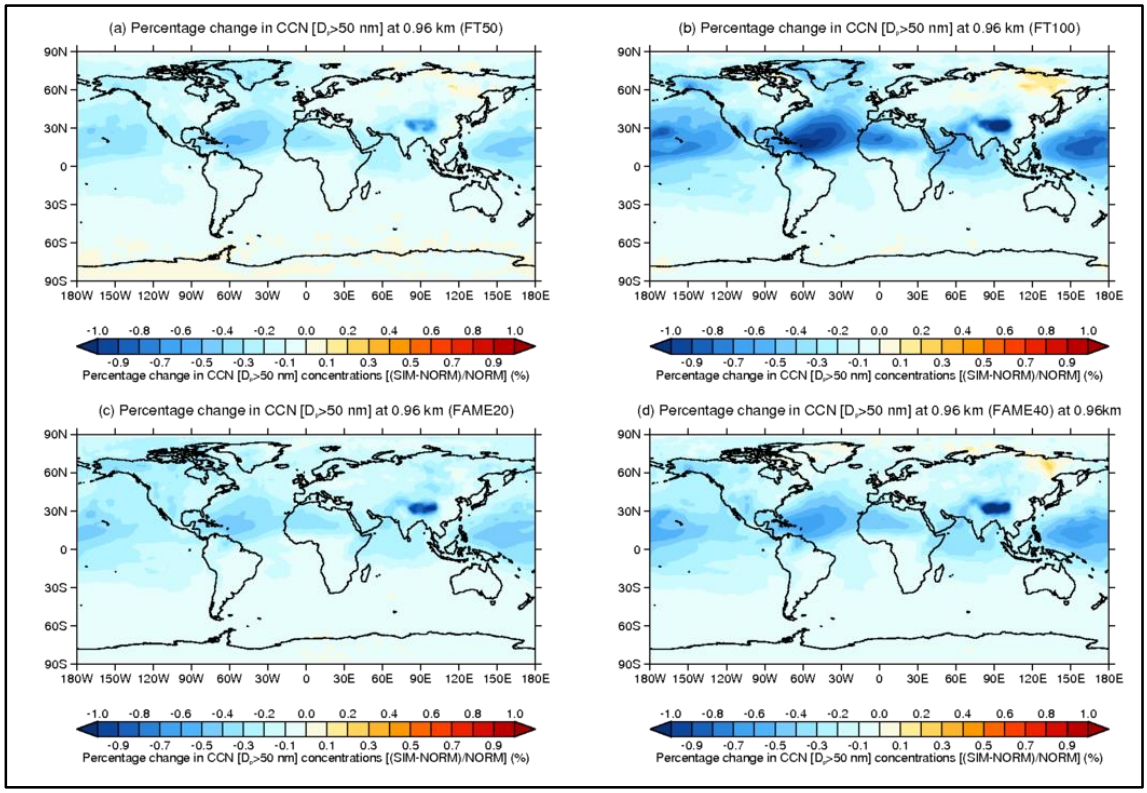

From Figure 7.13, in line with changes in aerosol burdens presented in Table 7.10, FT fuel blends have the potential to return mean greater reductions in aviation-induced CCN [FT50 ΔCCN = –0.46 cm^{-3} (–0.24%); FT100 ΔCCN = –0.90 cm^{-3} (–0.47%)] in relation to FAME fuel blends [FAME20 ΔCCN = –0.43 cm^{-3} (–0.20%); FAME40 ΔCCN = –0.55 cm^{-3} (–0.27%)] at low-cloud level (~0.96 km). These reductions in low-cloud level CCN also show how alternative fuels have the potential to reduce the aviation-induced cooling aCAE.

Reductions in CCN and the greater reductions in CCN at low-cloud level for the FT fuel blends are driven by reductions in aviation-induced sulfates (Figure 7.9 and Table 7.10) and SO_2 emissions (Table 7.6). Figure 7.13 shows that peaks in CCN reductions are simulated to occur

over the mid-Atlantic and the Pacific oceans; which has the potential to decrease the aCAE and reduce aviation-induced cooling over these regions.

7.4.1.3 Impact of alternative fuels on surface-layer air quality

As well as impacting atmospheric gas- and aerosol-phase concentrations and low-cloud level CCN concentrations, FT and FAME fuel blends have the potential to reduce surface-layer $PM_{2.5}$ concentrations – as seen in Figure 7.14.

Figure 7.14: Percentage changes in surface aviation-induced $PM_{2.5}$ in relation to standard aviation for the following alternative fuel scenarios: (a) 50% Fischer-Tropsch; (b) 100% Fischer-Tropsch; (c) 20% Fatty Acid Methyl Ester; and (d) 40% Fatty Acid Methyl Ester.

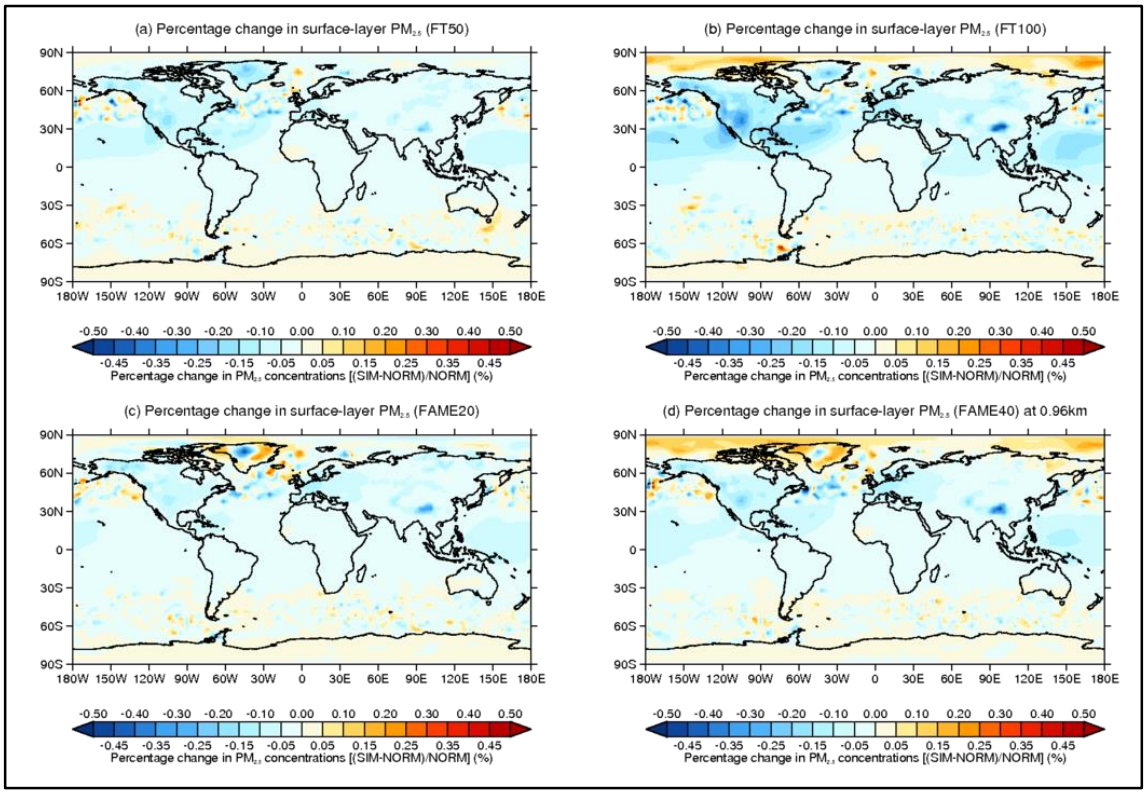

In line with reductions in global aerosol burdens, the FT fuel blends produce greater reductions in mean surface-layer $PM_{2.5}$ concentrations in relation to standard aviation (NORM) [FT50 $\Delta PM_{2.5}$ = –0.80 ng m^{-3} (–0.021%); FT100 $\Delta PM_{2.5}$ = –1.55 ng m^{-3} (–0.038%)], in comparison to FAME fuel blends [FAME20 $\Delta PM_{2.5}$ = –0.71 cm^{-3} (–0.017%); FAME40 $\Delta PM_{2.5}$ = –0.82 cm^{-3} (–0.019%)]. Even though the use of alternative fuels has been simulated to have the potential to improve surface air quality, it has to be acknowledged that the relative improvements estimated are very small.

From Figure 7.14 it is seen that the greatest reductions in aviation-induced surface-layer $PM_{2.5}$ concentrations from the use of alternative fuel blends occur over North America and Europe;

which is in line with spatial distribution of aviation emissions release. Reductions in surface-layer $PM_{2.5}$ concentrations from the use of FT and FAME fuel blends has the capacity to reduce aviation-induced mortalities due to aviation-induced exceedances in cases of cardiopulmonary disease and lung cancer. The methodology used to estimate mortalities from aviation-induced perturbations in surface-layer $PM_{2.5}$ concentrations was previously described in Section 6.3.2.

Table 7.11 demonstrates that in line with reductions in surface-layer $PM_{2.5}$ concentrations presented in Figure 7.14, the use of FT fuel blends result in a greater reduction in aviation-induced mortalities [FT50 Δmort = –460 mortalities a^{-1} [95% CI: –167 to –752]; FT100 Δmort = –799 mortalities a^{-1} [95% CI: –290 to –1,309]], in comparison the FAME fuel blends [FAME20 Δmort = –647 mortalities a^{-1} [95% CI: –235 to –1,059]; FAME40 Δmort = –627 mortalities a^{-1} [95% CI: –228 to –1,027]].

Table 7.11: Aviation-induced mortalities avoided in relation to standard aviation (NORM) through the use of Fischer-Tropsch (FT) and Fatty Acid Methyl Ester (FAME).

Scenario	Aviation-induced mortalities avoided (mortalities a^{-1})		
	Cardiopulmonary disease	Lung cancer	Total mortalities avoided
FT50	409 (148 – 670)	51 (19 – 83)	460 (167 – 752)
FT100	713 (258 – 1167)	87 (32 – 141)	799 (290 – 1309)
FAME20	576 (209 – 944)	71 (26 – 116)	647 (235 – 1059)
FAME40	561 (203 – 919)	67 (25 – 109)	627 (228 – 1027)

Despite the greater mean surface-layer reductions in $PM_{2.5}$ returned by the FAME40 scenario in relation to the FAME20 scenario, simulations of the FAME20 fuel blend scenario yield greater avoidances in aviation-induced mortalities. This difference is explained when considering the differences in surface-layer mean $PM_{2.5}$ concentrations between the FAME40 and FAME20 scenarios ($FAME40_{PM2.5}$–$FAME20_{PM2.5}$), which identifies greater simulated surface-layer $PM_{2.5}$ concentrations for the FAME20 scenario over regions with high population densities: Western Africa, Eastern China, Southern Africa, the UK, Northern China and Southern South America.

Overall it is seen that dependant on the fuel scenario employed, aviation-induced mortalities can be reduced by between 12.8–22.2%; based on estimates for avoidances in mortalities

calculated here for alternative fuels and estimated aviation-induced mortality for standard aviation [3597 mortalities a^{-1}] calculated in Section 6.4.2.

7.4.2 Aviation alternative fuel scenario induced radiative effects (RE)

Here the radiative effects of the FT and FAME fuel blend scenarios investigated in this section are investigated through estimating the ozone direct radiative (O3DRE), aerosol direct radiative (aDRE) and aerosol cloud albedo (aCAE) effects. This is initially done through investigating the differences between the alternative fuel scenarios and standard aviation (EXPT–NORM), and then through investigating the difference between the alternative fuel scenarios and no aviation emissions scenario (EXPT–NOAVI). Finally the combined radiative effect (RE_{comb}) of the O3DRE, aDRE and aCAE is estimated to assess the climatic impact of non-CO_2 emissions from the use of alternative fuels in aviation.

7.4.2.1 Ozone direct radiative effect (O3DRE)

Reductions in the aviation-induced O3DRE (in relation to the NORM simulation, i.e. EXPT–NORM) rank in the order of FAME40 [ΔO3DRE = –1.59 mW m^{-2}] > FAME20 [ΔO3DRE = –1.51 mW m^{-2}] > FT100 [ΔO3DRE = –0.83 mW m^{-2}] > FT50 [ΔO3DRE = –0.49 mW m^{-2}], and reflect the reductions in aviation-induced O_3 seen from implementing the alternative fuel scenarios outlined in Table 7.8 – as seen in Figure 7.15. This results in the following O3DREs (in relation to the NOAVI, i.e. EXPT–NOAVI): $O3DRE_{FT50}$ = +8.37 mW m^{-2}, $O3DRE_{FT100}$ = +8.03 mW m^{-2}, $O3DRE_{FAME20}$ = +7.35 mW m^{-2}, and $O3DRE_{FAME40}$ = +7.27 mW m^{-2}.

As per the reductions in aviation NO_X emitted from the use of the four alternative fuel scenarios investigated here (Table 7.6), reductions in O3DRE of around 5.5% (for FT50), 11.2% (for FT100), 19.5% (for FAME20) and 22.0% (for FAME40) could be expected, due to the relationship between NO_X emissions and O_3 production. In practice this is not seen due to the non-linearity in O_3 chemistry (Myhre et al., 2011) and reductions in CO and speciated HC emissions not following a similar reduction trend (Table 7.4 and Figure 7.2), resulting in O3DRE reductions in order of 5.53% (FT50), 9.57% (FT100), 17.04% (FAME20) and 17.95% (FAME40). Though these reductions are not in line with aviation NO_X emissions reductions (Table 7.4 and Figure 7.2) they are in line with the reductions in global O_3 burdens presented in Table 7.9, where reductions in the global O_3 burden rank in the order of: FT50 $\Delta O3_{burden}$ = –5.70%; FT100 $\Delta O3_{burden}$ = –9.51%; FAME20 $\Delta O3_{burden}$ = –18.11%; and FAME40 $\Delta O3_{burden}$ = –18.67%.

Figure 7.15: Changes in aviation-induced ozone direct radiative effects (O3DREs) resulting from the use of alternative fuels investigated (EXPT–NORM): (a) FT50; (b) FT100; (c) FAME20, and; (d) FAME40.

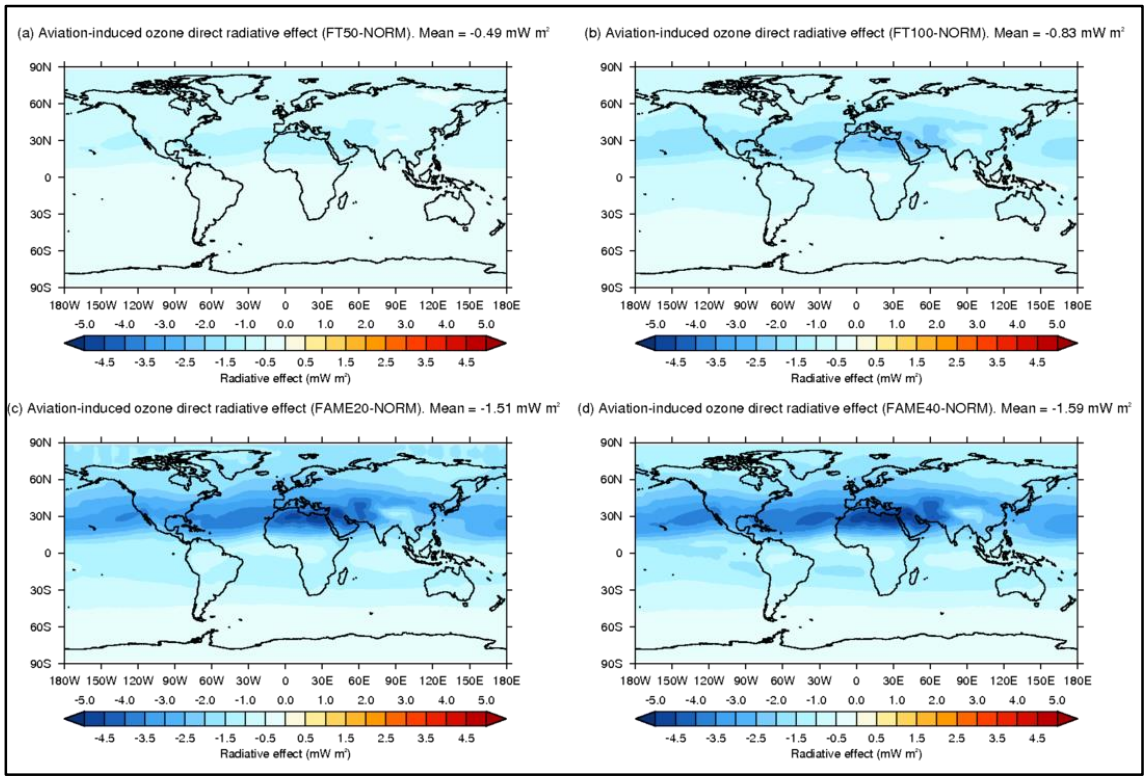

7.4.2.2 Aerosol direct radiative effect (aDRE)

The alternative fuel scenarios investigated here show that in relation to standard aviation (EXPT–NORM) the following changes in aDRE are simulated: $\Delta aDRE_{FT50}$ = –1.41 mW m^{-2}, $\Delta aDRE_{FT100}$ = –1.86 mW m^{-2}, $\Delta aDRE_{FAME20}$ = –0.56 mW m^{-2}, and $\Delta aDRE_{FAME40}$ = –0.53 mW m^{-2} (Figure 7.16). This indicates that through the use of FT fuels, and fuel blends a cooling aDRE is induced, while through the use of FAME fuel blends a warming aDRE results. These simulations estimate that these alternative fuel scenarios return the following aDREs (in relation to NOAVI, i.e. EXPT–NOAVI): $aDRE_{FT50}$ = –0.01 mW m^{-2}, $aDRE_{FT100}$ = –0.46 mW m^{-2}, $aDRE_{FAME20}$ = +0.84 mW m^{-2}, and $aDRE_{FAME40}$ = +0.87 mW m^{-2}.

Negative aDREs (negative effect) result from the use of FT fuels and fuel blends, while for the FAME fuel blends positive aDREs arise (warming effect). The negative aDREs estimated from the use of FT fuels are due to the far greater reductions in aviation-induced BC which imparts a warming effect (Sausen et al., 2005; Lee et al., 2009; Gettelman and Chen, 2013; Fuglestvedt et al., 2008; Balkanski et al., 2010; Unger, 2011; Unger et al., 2013), in comparison to reductions in sulfates, nitrates, ammonium and organic carbon where these species impart a cooling

effect (Sausen et al., 2005; Lee et al., 2009; Gettelman and Chen, 2013; Fuglestvedt et al., 2008; Balkanski et al., 2010; Unger, 2011; Unger et al., 2013) – as seen in Table 7.10.

Figure 7.16: Changes in aviation-induced aerosol direct radiative effects (aDRE) resulting from the use of alternative fuels investigated (EXPT–NORM): (a) FT50; (b) FT100; (c) FAME20, and; (d) FAME40.

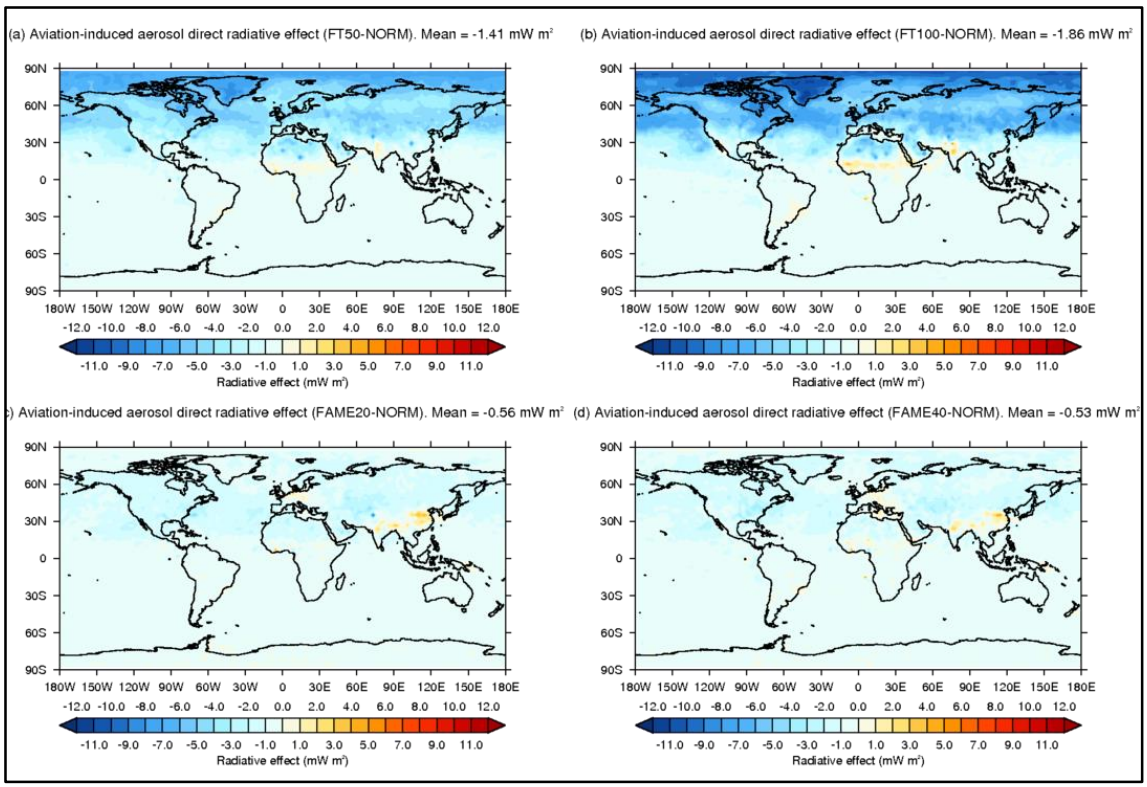

These resulting aDREs are a result of BC induced warming and sulfates, nitrates, ammonium and organic carbon induced cooling. For both the FT and FAME fuels similar relative reductions in sulfates and ammonium in comparison to BC are seen. Though when considering other aviation-induced aerosol species FT fuels and fuel blends see much lower relative reductions in aviation-induced nitrates (an order of magnitude lower) in comparison to FAME fuel blends, while FAME fuel blends result in an increase in aviation-induced organic carbon.

7.4.2.3 Aerosol cloud albedo effect (aCAE)

Figure 7.17 shows that in relation to standard aviation (NORM case) the following changes in aCAE are simulated (EXPT–NORM): $\Delta aCAE_{FT50}$ = +4.30 mW m^{-2}, $\Delta aCAE_{FT100}$ = +8.76 mW m^{-2}, $\Delta aCAE_{FAME20}$ = +3.91 mW m^{-2}, and $\Delta aCAE_{FAME40}$ = +5.49 mW m^{-2}. Indicating that the scenarios investigated here (Table 7.8) would return the following aCAEs (EXPT–NOAVI): $aCAE_{FT50}$ = –19.25 mW m^{-2}; $aCAE_{FT100}$ = –14.79 mW m^{-2}; $aCAE_{FAME20}$ = –19.64 mW m^{-2} and; $aCAE_{FAME40}$ = –18.06 mW m^{-2}.

Figure 7.17: Changes in aviation-induced aerosol cloud albedo effects (aCAE) resulting from the use of alternative fuels investigated (EXPT–NORM): (a) FT50; (b) FT100; (c) FAME20, and; (d) FAME40.

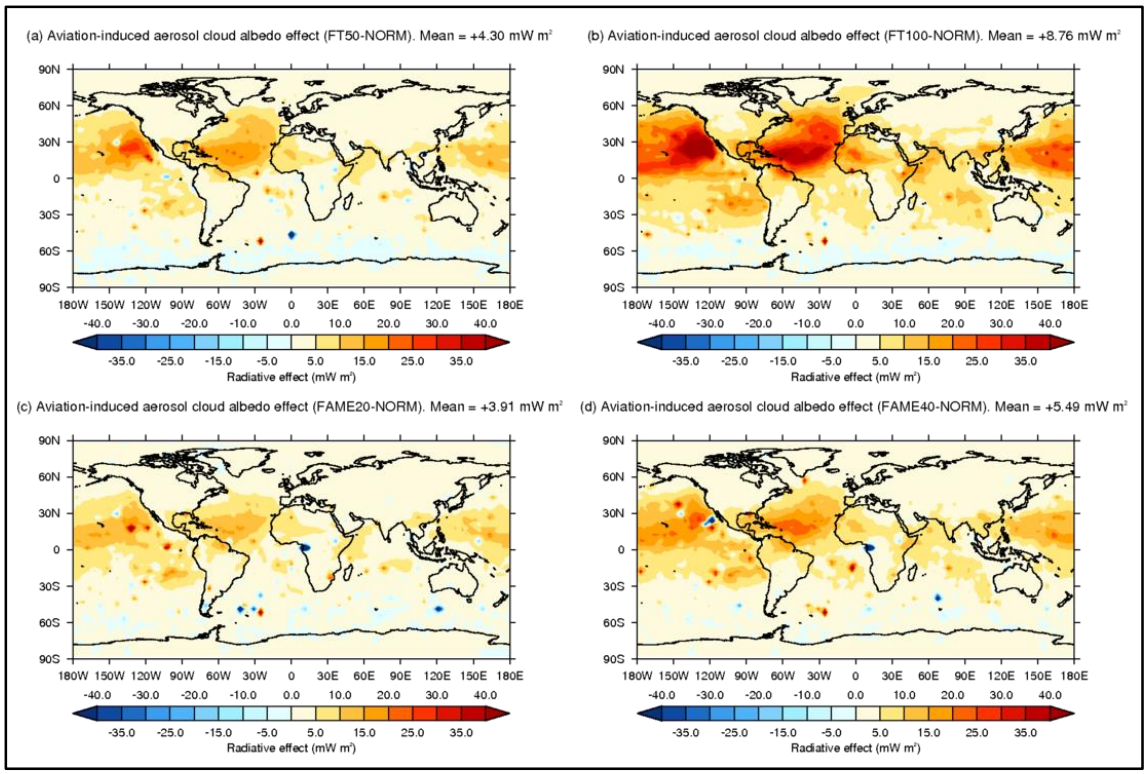

This shows that the use of FT fuels and fuel blends provide greater reductions in the aviation-induced aCAE cooling effect in relation to standard aviation (NORM); in relation to the use of FAME fuel blends. Showing that the use of FT fuel blends return greater reductions in the aviation-induced aCAE, over the use of FAME fuel blends. These changes in the aCAE are driven by changes in aviation-induced CCN (Dp>50 nm), with CCN being influenced by aerosol concentrations within the soluble mode with a dry diameter greater than 50 nm (Dp>50 nm).

Investigating atmospheric aerosol perturbations at low-cloud level (~0.96 km) from the use of FT and FAME fuel blends, reductions in sulfates are seen; with higher reductions from the FT fuels and fuel blends in comparison to the FAME scenarios, in line with SO_2 emissions reductions (Figure 7.2 and Table 7.6). While in terms of nitrate and ammonium perturbations the FAME fuel blend scenarios return greater reductions in comparison to the FT fuel blends due to zonal increases in nitrates between 60°N–90°N; reductions which follow reductions in aviation NO_X emissions (Figure 7.2 and Table 7.6).

Again following reductions in aviation-borne BC and SO_2 emissions, the FT fuel blends see greater mean reductions at low-cloud level in relation to the FAME fuel blends. While for aviation-induced OC perturbations from the use of alternative fuels the lower fuel blends

(FT50 and FAME20) return increases in OC concentrations, while the higher fuel blends (FT100 and FAME40) return reductions in low-cloud level OC concentrations.

Through the combination of all these changes greater reductions in the aCAE are seen for the FAME fuel blends in comparison to the FT fuel blends.

7.4.2.4 Combined radiative effect (RE_{comb})

The combined radiative effect (RE_{comb}) for the FT and FAME fuel blend scenarios investigated here return the following combined radiative effects (EXPT–NOAVI), where: $RE_{combFT50}$ = –10.89 mW m^{-2}, $RE_{comb\ FT100}$ = –7.22 mW m^{-2}, $RE_{comb\ FAME20}$ = –11.45 mW m^{-2}, and $RE_{comb\ FAME40}$ = –9.92 mW m^{-2}. Indicating that in relation to standard aviation (NORM case) the following changes in RE_{comb} are simulated (EXPT–NORM): $\Delta RE_{combFT50}$ = +2.40 mW m^{-2}, $\Delta RE_{combFT100}$ = +6.07 mW m^{-2}, $\Delta RE_{combFAME20}$ = +1.84 mW m^{-2}, and $\Delta RE_{combFAME40}$ = +3.37 mW m^{-2} (Figure 7.18).

Figure 7.18: Changes in aviation-induced combined radiative effects (RE_{comb}) resulting from the use of alternative fuels investigated (EXPT–NORM): (a) FT50; (b) FT100; (c) FAME20, and; (d) FAME40.

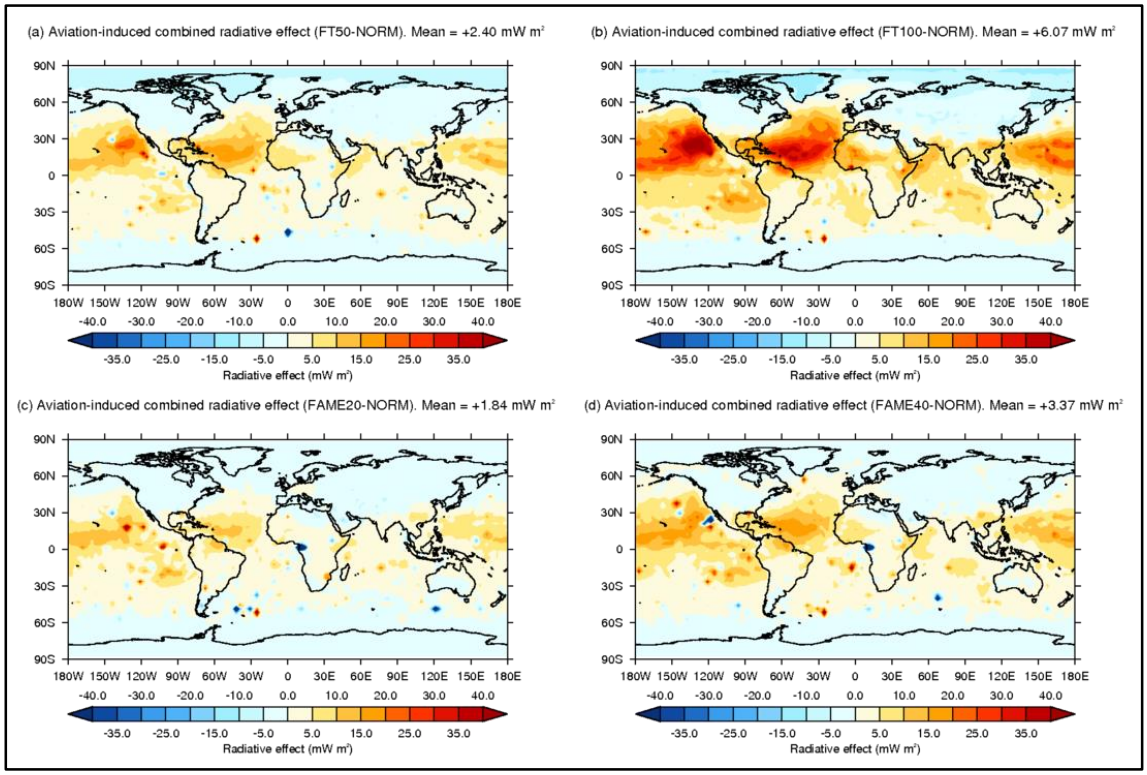

The resulting RE_{comb} show that through the use of FT fuel blends, as the amount of FT introduced in to the fuel blend is increased, greater net reductions in the cooling effect induced by aviation non-CO_2 emissions arise in comparison to the use of FAME fuel blends.

This can be primarily attributed to the higher relative reductions in aviation-induced sulfates resulting from the use of FT fuel blends (Table 7.11).

In comparison to the RE_{comb} resulting from standard aviation (Figure 5.19 in Section 5.4.1.2.4) the Northern Hemisphere is primarily dominated by a warming effect influenced by the combination of the aviation-induced O3DRE and aDRE, while majority of aviation-induced cooling occurs between ~40°N–60°S due to the effect of aviation-induced CCN (Dp>50 nm) on the aCAE dominating over the Atlantic and Pacific oceans.

7.5 Summary and Conclusions

Here the use of FT and FAME fuel blends (FT50, FT100, FAME20 and FAME40) within year 2000 aviation are estimated to reduce annual mean concentrations of gas-phase (NO_X, O_3, OH, HNO_3 and SO_2) and aerosol-phase (sulfates, nitrates, ammonium, BC and OC) in relation to standard aviation (NORM) in the majority of cases. The only exception from this trend is seen for the use of FAME fuel blends and the resulting increases in OC.

When considering gas-phase perturbations alone, despite increases in CO and speciated HC emissions from the use of FT and FAME fuel blends in relation to standard aviation, gas-phase perturbations are seen to be primarily driven by aviation NO_X emissions. Resulting in reductions in the annual aviation-induced global mean concentrations and burdens of NO_X, O_3, OH, HNO_3 and SO_2 (Table 7.9).For aerosol-phase species, reductions in sulfates are far greater for the FT fuel blends due to the lower sulfur content of the fuel in conjunctions with reductions in aviation-induced ammonium, while reductions in aviation-induced nitrates are greater for the FAME fuel blends in line with levels of NO_X emission reductions. Again in line with reductions in aviation-borne BC and OC FT fuel blend provide greater reductions in annual global BC and OC burdens and annual mean concentrations (Table 7.10).In line with the balance between reductions in aviation-induced sulfates, nitrates and ammonium the FT fuel blends result in greater reductions in CCN (Dp>50 nm) in comparison to FAME fuel blends [FT50 ΔCCN = –0.24%; FT100 ΔCCN = –0.47%; FAME20 ΔCCN = –0.20% and; FAME40 ΔCCN = –0.27%]. Reductions which go on to impact the aCAE from FT fuel blends to a greater extent than FAME fuel blends.

The use of the FT and FAME fuel blends investigated here are estimated to reduce mean surface-layer $PM_{2.5}$ concentrations in relation to standard aviation (NORM). Greater reductions in surface-layer $PM_{2.5}$ concentrations are simulated when the use of FT fuels is considered (Figure 7.14); due to the greater sulfate reductions resulting from the use of FT fuels.

As a result of these reductions in surface-layer $PM_{2.5}$ concentrations aviation-induced mortalities from exceedances in cases of cardiopulmonary disease and lung cancer are reduced in turn. This results in greater reductions in aviation-induced annual mortalities from the use of FT fuel blends [FT50 Δmort = –460 mortalities a^{-1}; FT100 Δmort = –799 mortalities a^{-1}], in comparison the use of FAME fuel blends [FAME20 Δmort = –647 mortalities a^{-1}; FAME40 Δmort = –627 mortalities a^{-1}].

When evaluating the top-of-atmosphere (TOA) combined radiative effects (RE_{comb} = O3DRE + aDRE + aCAE) the use of FT and FAME fuel blends (and their associated non-CO_2 emissions) result in a cooling effect as found previous Chapters (Chapter 5 and Chapter 6) and in previous work (Unger et al., 2013; Lee et al., 2009; Sausen et al., 2005; Gettelman and Chen, 2013; Righi et al., 2013).

In relation to standard aviation reductions in the O3DRE occur for all fuel blends in relation to standard aviation were simulated [$\Delta O3DRE_{FT100}$ = –0.83 mW m^{-2}; $\Delta O3DRE_{FT50}$ = –0.49 mW m^{-2}; $\Delta O3DRE_{FAE20}$ = –1.51 mW m^{-2} and; $\Delta O3DRE_{FAME40}$ = –1.59 mW m^{-2}] (Figure 7.15). Reductions in the aDRE were also simulated [$\Delta aDRE_{FT50}$ = –1.41 mW m^{-2}, $\Delta aDRE_{FT100}$ = –1.86 mW m^{-2}, $\Delta aDRE_{FAME20}$ = –0.56 mW m^{-2}, and $\Delta aDRE_{FAME40}$ = –0.53 mW m^{-2}]; with the FT fuel blends resulting in a cooling (negative) aDRE, and the FAME fuel blends resulting in a warming (positive) aDRE (Figure 7.16). For all fuel blends reductions in the cooling effect imparted by the aviation-induced aCAE occur [$\Delta aCAE_{FT50}$ = +4.30 mW m^{-2}, $\Delta aCAE_{FT100}$ = +8.76 mW m^{-2}, $\Delta aCAE_{FAME20}$ = +3.91 mW m^{-2}, and $\Delta aCAE_{FAME40}$ = +5.49 mW m^{-2}] (Figure 7.17).

This indicated that the use of alternative fuel blends decreases the net cooling effect from aviation, as estimated by the combined radiative effect (RE_{comb}) [$\Delta RE_{combFT50}$ = +2.40 mW m^{-2}, $\Delta RE_{combFT100}$ = +6.07 mW m^{-2}, $\Delta RE_{combFAME20}$ = +1.84 mW m^{-2}, and $\Delta RE_{combFAME40}$ = +3.37 mW m^{-2}] (Figure 7.18).

Based on current specification the only scenario investigated here which has real world implications is the FT50 scenario (ASTM International, 2011c; ASTM International, 2012a), demonstrating its suitability for today's civil aviation fleet (Timko et al., 2011). The FT50 scenario is simulated to reduce aviation-induced O_3, as well as reducing aviation's impact on the global aerosol burden.

The FT50 fuel blend scenario results in a reduced aviation-induced O3DRE, aDRE and reduction in the cooling effect from aviation-induced aCAE primarily due to reductions in aviation SO_2 emissions. This returns a reduction in the cooling effect the RE_{comb} from aviation in relation to

standard aviation (NORM). In terms of human health the implementation of the FT50 fuel scenario civil aviation has the potential to reduce aviation-induced mortality (due to exceedances in cardiopulmonary disease and lung cancer) by 460 mortalities a^{-1} [95% CI: –167 to –752].

Though the reductions in global aerosol burden which arises from the use of alternative fuels can reduce aviation's impact on air quality, this reduction in aerosol burden also results in a reduced cooling effect from aviation non-CO_2 emissions, i.e. greater radiative warming, which is not good for climate policies. Although this effect is small, it is an effect that would have to be considered when evaluating and deriving climate policies, as well when the industry evaluates feedstock and processes used to produce these alternative fuels.

8 Conclusions and future work

8.1 Conclusions

This thesis has explored the impacts on climate and air quality from aviation for year 2000, variations in aviation fuel sulfur content (FSC) and the use of alternative fuels within civil aviation through the use of a size-resolved coupled tropospheric chemistry-aerosol microphysics model (the nitrate-extended version of the TOMCAT-GLOMAP-mode coupled model).

Chapter 3 provided a description of the nitrate-extended version of the TOMCAT-GLOMAP-mode coupled model (GMV4-nitrate), along with an evaluation of simulated gas- and aerosol-phase species from GMV4-nitrate without the inclusion of aviation emissions. Evaluation of the gas-phase chemistry within GMV4-nitrate is conducted through comparison against ozonesonde profiles from Tilmes et al. (2012). GMV4-nitrate replicates seasonal and annual mean ozone profiles. Model-observation comparisons of seasonal profiles across each site yielded a global normalised mean ozone bias (NMB) of +3.88, while annual mean profiles (excluding model-observations at Praha due the high biases returned) yield a bias of +5.31%.

Splitting model-observation comparisons in to latitudinal bands, along with partitioning model-observation comparisons in to latitudinal and altitudinal bands demonstrated regional differences in model skill. When annual mean concentrations are considered, positive biases between model and observational ozone concentrations were found (i.e. an indicator of model overestimation) over the NH Polar and mid-latitude regions, as well as over the equatorial region. Splitting model-observation comparisons in to latitudinal bands returned biases in annual mean model-observation comparisons ranging from –6.09% to 10.25%. Resolving model-observation comparisons by latitude and altitude return normalised mean biases ranging from –28.04% to 33.65%, with the lowest normalised mean biases returned near the surface layer (700<hPa<1000) and in the lower troposphere (400<hPa<700).

Evaluation of the aerosol-phase chemistry within GMV4-nitrate was conducted through comparing simulated sulfate, nitrate, ammonium and organic aerosol profiles with profiles compiled by Heald et al. (2011). GMV4-nitrate was assessed to overestimate observational sulfate profiles, but in fair agreement with GEOS-Chem from a previous study, with simulated profiles following the shape of observational profiles (Heald et al., 2011), returning a mean bias of +38.92%. Furthermore model-observation comparisons showed that GMV4-nitrate

underestimates nitrate [–76.79%], ammonium [–42.92%] and organic aerosol [–33.20%] profiles.

Differences between model simulated aerosol profiles and aerosol observations are explained by differences between year of simulation (2000) and year observational profiles were acquired, changes in global SO_2, NO_X and NH_3 emissions as well previously identified underestimations in global organic aerosol sources of ~100 Tg yr^{-1}. In addition to differences between the time periods over which aircraft field campaigns were conducted. Evaluation of GMV4-nitrate demonstrated that the model skilfully replicates ozone profiles with a global annual model mean bias of +6.98%, and 5.31% when observations from Praha are excluded. Though the model overestimations in sulfates and underestimations in nitrates, ammonium and organic aerosol, the model broadly replicated aerosol profiles.

In Chapter 4 an extended aviation emissions inventory was developed (CMIP5-extended); extending on CMIP5 recommended aviation emissions for year 2000 (Lamarque et al., 2009). The CMIP5 recommended aviation emissions inventory only reports NO_X and BC mass emissions, while in reality aviation emits a spectrum of different species (Lee et al., 2009) including a broad range of hydrocarbons (HCs) (Yelvington et al., 2007; Anderson et al., 2006; Knighton et al., 2007). CMIP5-extended was developed to include carbon monoxide (CO), speciated HCs, sulfur dioxide (SO_2) and organic carbon (OC) emissions while also considering the geometric mean diameter (D_g) of aviation's carbonaceous emissions, which is not specified in the standard CMIP5 dataset.

Using published experimental data from ground-based experiments (Anderson et al., 2006; Knighton et al., 2007) emissions datasets for speciated HCs emissions (formaldehyde, propane, ethane, methanol, acetaldehyde and acetone) were derived. Emissions indices from literature were used to create datasets for CO, SO_2 (Wilkerson et al., 2010), and OC emissions (Bond et al., 2004; Hopke, 1985), as well as a dataset for carbonaceous particle numbers released (Eyers et al., 2004). Emissions datasets were compiled using global aviation fuelburn derived using the BC mass dataset from CMIP5 recommended (Lamarque et al., 2009) and the emissions index for BC mass (Eyers et al., 2004). The resulting CMIP5-extended aviation emissions inventory returned the following annual aviation emissions for year 2000: 2.786 Tg a^{-1} NO_X; 0.724 Tg a^{-1} CO; total speciated HCs of 0.409 Tg a^{-1}; 0.236 Tg a^{-1} SO_2; 5.012 Mg a^{-1} BC; and 1.25 Mg a^{-1} OC. A geometric mean diameter of 50.46 nm for carbonaceous particles was calculated, indicating that BC and OC emissions are primarily introduced in to the Aitken mode.

In Chapter 5 GMV4-nitrate was used to evaluate the impact of aviation on atmospheric chemistry and climate, using the CMIP5-extended aviation emissions inventory developed in Chapter 4. Consistent with previous work, increases in aviation emissions result in global mean increases in nitrogen oxides (NO_X) [+4.18%], ozone (O_3) [+0.48%], hydroxyl radical (OH) [+1.16%], NO_X reservoir species nitrous acid (HONO) [+4.75%] and peroxyacyl nitrates (PAN) [+0.08%], nitric acid (HNO_3) [+3.53%] and sulfur dioxide (SO_2) [+0.88%]. In addition to increases in gas-phase species, aerosol species were also simulated, resulting in global mean increases in: sulfates [+0.71%], nitrates [+1.93%], ammonium [+0.42%], black carbon (BC) [+3.11%] and organic carbon (OC) [+1.10%]. Increases in aerosol concentrations drive increase in low-cloud level (~0.96 km) cloud condensation nuclei (CCN; Dp>50 nm) concentrations of 2.30 cm^{-3}. Resulting in the following burden increases: ΔNO_X = 40.65 Gg; ΔO_3 = 3.90 Tg; ΔOH = 4.98 Mg; ΔPAN = 12.99 Gg; ΔHONO = 77.50 Mg; ΔHNO_3 = 85.43 Gg; ΔSO_2 = 1.06 Gg; Δsulfates = 12.95 Gg; Δnitrates = 5.58 Gg; Δammonium = 0.86 Gg; ΔBC = 0.49 Gg, and; ΔOC = 0.21 Gg.

In line with aviation-induced increases in O_3, aviation resulted in a short-term O_3 direct radiative effect (O3DRE) of +8.86 mW m^{-2}. Which when weighted in terms of aviation NO_X emission (nitrogen basis (N)) equates to +10.45 mW m^{-2}, which fits within the range given by current literature of +7.39–44.2 mW m^{-2} $Tg(N)^{-1}$. The lower O3DRE returned in this thesis can be attributed to the lower ozone production efficiency (OPE) of 1.33 within GMV4-nitrate in comparison to the range of 1–2.9 from recent studies. An aerosol direct radiative effect (aDRE) of +1.40 mW m^{-2} is estimated, agreeing with the range +20 to –28 mW m^{-2} from literature. An aerosol cloud albedo effect (aCAE) of –23.55 mW m^{-2} was assessed, which is greater than estimates from literature of –15.4 to –18 mW m^{-2}; fitting within the range of uncertainties reported [–4.8 to –29 mW m^{-2}]. This resulted in a combined radiative effect (RE_{comb}) of –13.29 mW m^{-2}, which sits within the uncertainty range of –51 to 51.44 mW m^{-2} (which considers low and high end estimates) from literature.

Demonstrating the need to include an extensive array of aviation emissions species the differences in atmospheric and climatic impacts between the use of the CMIP5-extended and CMIP5 recommended was investigated. This demonstrated that the use of the CMIP5-extended over the CMIP5 recommended (NORM–CMIP5) yielded reductions in global mean concentrations of NO_X [–0.05%], nitrates [–1.01%], BC [–0.12%], and OC [–0.01%], in conjunction with increases in O_3 [+0.13%], OH [+0.03%], PAN [+0.15%], HONO [+0.02%], SO_2 [+2.94%], sulfates [+0.55%], and ammonium [+0.16%]. The use of CMIP-extended over CMIP recommended also increases low-cloud level CCN (Dp>50 nm) by 0.44%. It is acknowledged

that through the inclusion of additional aviation emission species there are changes in the concentration of species in the atmosphere, but the relative changes are small as seen above.

The differences between these two simulations show that through the use of CMIP5-extended estimates in O3DRE were increased by +0.35 mW m^{-2}, aDRE was reduced by (–)0.24 mW m^{-2}, and increasing the cooling aCAE by (–)5.22 mW m^{-2}. This indicates that from the inclusion of additional aviation emitted species, estimates in the climatic impact can be improved, through the inclusion of interacts that may otherwise be omitted. Sensitivity runs (NoCO, NoHCs and $NoSO_2$) indicated aviation CO emissions account for +0.47 mW m^{-2} of the combined radiative effect (RE_{comb}), that aviation HC emissions account for +0.44 mW m^{-2} and that aviation SO_2 emissions account for –7.22 of the aviation-induced RE_{comb}.

Re-evaluation of GMV4-nitrate's gas- and aerosol-phase responses with CMIP-extended emissions returned increases in the model biases when evaluated simulated ozone concentrations profiles with observational profiles. These increases in model bias are a result of aviation-induced ozone. The introduction of aviation emissions returns improvements in model-observation comparisons over most regions for sulfates, nitrates, ammonium and organic aerosols.

Chapter 6 investigated the impact of variations in aviation fuel sulfur content (FSC) on surface-layer air quality, aviation-induced mortality, low-cloud level CCN (Dp>50 nm) and radiative effect. Variations in FSC ranged from 0–6000 ppm in order to investigate the use of desulfurised jet fuel, ultra-low sulfur jet (ULSJ) fuel and extreme FSC above ASTM D1655-11b specified levels, along with variations in the vertical distribution of aviation SO_2 emissions.

Variations in FSC from 0–6000 ppm were estimated to produce global mean surface-layer $PM_{2.5}$ concentrations ranging from 2.50–16.08 ng m^{-3} (for FSC 0–6000 ppm). Regional increases in surface-layer $PM_{2.5}$ were simulated. Using the d($PM_{2.5}$/FSC) metric aviation was found to return the greatest sensitivity to $PM_{2.5}$ formation over Europe [6.44×10^{-3} ng m^{-3} ppm^{-1}], followed by Asia [5.74×10^{-3} ng m^{-3} ppm^{-1}] and North America [5.40×10^{-3} ng m^{-3} ppm^{-1}], with global $PM_{2.5}$ formation the least sensitive to aviation FSC [2.26×10^{-3} ng m^{-3} ppm^{-1}]. The ground release of aviation emissions was found to reduce the global mean surface-layer $PM_{2.5}$ concentrations by –36.7%. In relation to standard aviation the SWITCH1 scenario simulated increases in surface-layer $PM_{2.5}$ concentrations of +52.2%, while SWITCH2 concentrations by +6.6%; though it should be noted that these large relative changes are based on very small absolute changes to small values.

Standard aviation is assessed to be responsible for 3,597 premature mortalities a^{-1} due to increased surface layer $PM_{2.5}$ concentrations, estimates which lie with range of 310–16,000 mortalities a^{-1} from literature (Jacobson, 2010; Barrett et al., 2012; Burnett et al., 2014; Yim et al., 2015); estimates in aviation-induced mortalities due to various modes of aviation-induced premature mortality. Though it has to be acknowledged that the estimate derived in aviation-induced premature mortality derived in Chapter 6 only consider premature mortalities from increases in cases in lung cancer and cardiopulmonary disease, which when considering this this study provides estimates below the range of 10,000–13,920 provided by Barrett et al. (2012) and Yim et al. (2015) who use the same concentration-response function as this study, evaluating aviation-induced premature mortality from lung-cancer and cardiopulmonary disease alone.

in line with previous work (Barrett et al., 2012). Investigations simulated that through the application of a ULSJ fuel strategy aviation-induced mortalities can be reduced by 625 mortalities a^{-1}, while the use of a desulfurised fuel case estimated reductions in aviation-induced mortality of 647 mortalities a^{-1}. Ultimately variations in FSC from 0–6000 ppm result in 2950–9058 mortalities a^{-1} from aviation. While depending on the strategy used to vary the vertical distribution in aviation-SO_2 emissions, either reductions (SWITCH2) or increases (SWITCH1) in aviation-induced mortality were simulated.

Through variations in FSC from 0–6000 ppm aviation-induced RE_{comb} was found to vary between –6.08 to –75.48 mW m^{-2}, the ground release of aviation emissions resulted in an RE_{comb} of +5.02 mW m^{-2}, varying aviation FSC from 15ppm below cruise-level and 3000 ppm above resulted in a RE_{comb} of –31.41 mW m^{-2} (SWITCH1), and varying FSC from 15ppm below cruise-level to 1420 ppm above resulted in a RE_{comb} of –18.16 mW m^{-2} (SWITCH2). Thus simulations conducted in this chapter suggest that the aviation-induced climate and air quality impacts are sensitive to aviation fuel FSC, and the altitude of emissions release.

Investigating the relationship between aviation-induced mortality and radiative effect, the impact of FSC (ppm) on mortality and RE were quantified in terms of d(mortalities)/d(FSC) [mortalities ppm^{-1}] and d(RE)/d(FSC) [mW m^{-2} ppm^{-1}]. Considering variations in FSC (between 0–6000 ppm), the sensitivity of global premature mortality with FSC was estimated as 1.02 mortalities ppm^{-1}, with the global mean RE_{comb} assessed to have a sensitivity of $–1.16x10^{-2}$ mW m^{-2} ppm^{-1}.

Chapter 7 investigated the impact of the use of Fischer-Tropsch (FT) and fatty acid methyl esters (FAMEs) in aviation on the atmosphere, climate, air quality and mortality. From this

investigation of the use of FT and FAME fuel blends in year 2000 civil aviation was estimated to reduce annual mean concentrations of gas-phase (NO_X, O_3, OH, HNO_3 and SO_2) and aerosol-phase (sulfates, nitrates, ammonium, BC and OC) in relation to standard aviation in the majority of cases. The only exception from this trend is seen for the use of FAME fuel blends and the resulting increases in OC.

FT and FAME fuel blends were estimated to reduce mean surface-layer $PM_{2.5}$ concentrations (in relation to standard aviation): FT50 $\Delta PM_{2.5}$ = –0.61 ng m^{-3} (–0.017%); FT100 $\Delta PM_{2.5}$ = –1.16 ng m^{-3} (–0.022%); FAME20 $\Delta PM_{2.5}$ = –0.55 ng m^{-3} (–0.013%) and; FAME40 $\Delta PM_{2.5}$ = –0.59 ng m^{-3} (–0.006%). The FT fuel blends were found to surface-layer $PM_{2.5}$ concentrations to a greater extent due to larger reductions in sulfates. Due to these reductions in surface-layer $PM_{2.5}$ concentrations reductions in aviation-induced annual mortalities were estimated: FT50 Δmort = –460 mortalities a^{-1}; FT100 Δmort = –799 mortalities a^{-1}; FAME20 Δmort = –647 mortalities a^{-1}; and FAME40 Δmort = –627 mortalities a^{-1}. Additionally, the use of FT and FAME fuel blends was found to decrease the net cooling effect from aviation: $\Delta RE_{combFT50}$ = +2.40 mW m^{-2}, $\Delta RE_{combFT100}$ = +6.07 mW m^{-2}, $\Delta RE_{combFAME20}$ = +1.84 mW m^{-2}, and $\Delta RE_{combFAME40}$ = +3.37 mW m^{-2}].

The FT50 fuel blend is the only scenario currently specified for use in civil aviation (ASTM International, 2011c; ASTM International, 2012a). This scenario demonstrates that aviation-induced O_3 and its associated O3DRE can be reduced, along with the aDRE and cooling effect from the aCAE; resulting in a lower cooling effect from aviation-borne non-CO_2 emissions. Due to reductions in surface-layer $PM_{2.5}$ concentrations associated with this scenario aviation has the potential to reduced aviation-induced mortality by 460 mortalities a^{-1}.

8.2 Future work

This section aims to discuss how the work contained within this thesis could be improved, thus yielding results which would closer represent the real-world impact of aviation on atmospheric concentrations, the climate, air quality and the ultimately human health. To do so this section suggests how the development of an extended aviation emission inventory could be improved (Section 8.2.1), and how the model could be improved to allow it to better simulate nitrogen oxides, ozone and nitric acid concentrations (Section 8.2.2); and ultimately atmospheric species concentrations of the aforementioned will rely on. Improvements aviation emissions inventories would allow for the better representation of civil aviation, aiding the global modelling community, and through updating chemical schemes within the model the aim would be to better simulate atmospheric concentrations and reproduce observations.

8.2.1 Improvements in aviation emissions developed for the CMIP5-extended emissions inventory

In order to accurately describe the differences between CMIP5 recommended emissions and create an expansion of this emissions inventory (CMIP5-extended), a more complicated procedure than implemented in Section 4.3 could be applied when derived datasets for additional aviation emission species which do not scale linearly with fuelburn. In Section 5.4.2 it was highlighted how the inclusion of additional aviation emissions species (CO, speciated HCs, SO_2 and OC) can capture atmospheric and climatic responses which otherwise would be missed, thus providing further rationale for using a methodology that more accurately calculates aviation emissions; thus allowing the global modelling community to better estimate the impact of aviation.

Aviation CO, speciated HC emissions, BC and OC are ideally calculated while taking variations in combustor efficiency and flight conditions in to account (DuBois and Paynter, 2006; Baughcum et al., 1996; Owen et al., 2010):

$$EI_{CO\_ALT} = EI_{CO\_SL}\left(\frac{\theta_{amb}^{3.3}}{\delta_{amb}^{1.02}}\right)^{x}$$

Equation 4.2

$$EI_{HC\_ALT} = EI_{HC\_SL}\left(\frac{\theta_{amb}^{3.3}}{\delta_{amb}^{1.02}}\right)^{x}$$

Equation 4.3

$$C_{soot} = C_{soot_{SLS}} \cdot \left(\frac{\Phi}{\Phi_{SLS}}\right)^{2.5} \cdot \left(\frac{P_3}{P_{3_{SLS}}}\right)^{1.35} \cdot \left(\frac{e^{(-20000/T_3)}}{e^{(-20000/T_{3_{SLS}})}}\right)$$

Equation 4.7

Taking into account pressure, temperature, altitude and ambient conditions a more accurate 3-D emissions datasets can be derived. Combining this adaptation with consideration of aircraft types and emissions indices associated with each type of aircraft type global civil aviation emissions can be improved; thus moving towards the methodology used by Eyers et al. (2004) and Kim et al. (2007).

In doing so aviation-induced gas- and aerosol-phase perturbations and resulting climatic impacts (O3DRE, aDRE and aCAE) can be better assessed, in conjunction with assessments on surface-layer $PM_{2.5}$ concentrations.

8.2.2 Nitric acid branching mechanism

Gottschaldt et al. (2013), Søvde et al. (2011) and Butkovskaya et al. (2007) describe a minor nitric acid (HNO_3) forming branch of the (hydroperoxyl radical) HO_2 and (nitrogen oxide) NO reaction (Reaction 8.1):

$$HO_2 + NO\ (+M) \rightarrow HNO_3\ (+M)$$

Reaction 8.1

This HNO_3-forming branching mechanism provides an alternative reaction pathway for the HO_2 and NO reaction mechanism which is well known to produce OH and NO_2 (Reaction 2.1).

$$HO_2 + NO \rightarrow NO_2 + OH$$

Reaction 2.1

As well as providing an additional route to the formation of HNO_3 (Reaction 2.2):

$OH + NO_2 (+M) \rightarrow HNO_3 (+M)$

Reaction 2.2

Butkovskaya et al. (2005) find that this HNO_3-forming branching mechanism accounts for 0.18–0.87% of HNO_3 formed (at 298K and 223 K, respectively), which in conjunction with the recycling of NO_X this branching mechanism can account for a significant loss in NO (Butkovskaya et al., 2005; Søvde et al., 2011). As such the implications of this HNO_3-forming branching mechanism are reductions in NO_2 concentrations, the resulting formation of ozone (O_3) and OH (Søvde et al., 2011), the oxidative capacity of the atmosphere and as such its ability to oxidise atmospheric methane (CH_4) (Gottschaldt et al., 2013), as well as having the potential to increase the formation of nitrates.

A key nuance of this mechanism (Reaction 8.1) is its dependence on humidity, over the 133–933 hPa pressure range, while its dependence on temperature is yet unknown (Gottschaldt et al., 2013). Gottschaldt et al. (2013) investigated the use of this branching mechanism on aviation-induced O_3 and their resulting climatic impacts. In their study they found that the inclusion of this branching mechanism increased HNO_3 mixing ratios and reduced O_3 burdens, with this impact being enhanced through the inclusion of humidity dependence. To put the potential effect of this mechanism on estimating aviation-induced O_3 in to context Gottschaldt et al. (2013) estimated that through considering a 'dry' mechanism (i.e. no humidity modification) estimates in aviation-induced total column O_3 in DU (Dobson units) could potentially be lowered by (–)0.5%, while a 'wet' mechanism (i.e. with a humidity modification) estimates in aviation-induced O_3 could be reduced by (–)1.8%.

Through the inclusion of the HNO_3-forming branching mechanism within the nitrate-extended TOMCAT-GLOMAP-mode coupled model (GMV4-nitrate) estimations on the impact of aviation (and other transport sectors) can be enhanced. By understanding this mechanism's dependence on humidity, temperature and pressure GMV4-nitrate can be modified to include to Reaction 8.1 switching between rate coefficients dependant on ambient conditions. As with previous work by Gottschaldt et al. (2013) the implementation of this HNO_3-forming branching mechanism would likely result in a reduction in estimations of baseline NO_X concentrations and an associated increase in the relative effect of aviation, i.e. greater concentrations in aviation-induced NO_X and O_3.

Bibliography

ACARE (2011). Flightpath 2050: Europe's Vision for Aviation - Report of the High Level Group on Aviation Research. *In:* Advisory Council for Aeronautics Research in Europe (ed.).

ACARE (June 2010). Aeronautics and Air Transport: Beyond Vision 2020 (Towards 2050) - Background document. *In:* Advisory Council for Aeronautics Research in Europe (ed.).

Adedoyin, A. J., Boer, G., Bojariu, R., Camilloni, I., Doblas-Reyes, F., Fiore, A., Kimoto, M., Meehl, G., Prather, M., Sarr, A., Schär, C., Sutton, R., Oldenborgh, G. J. v., Vecchi, G. & Wang, H.-J. (2013). Near-term Climate Change: Projections and Predictability (Chapter 11). *In:* Stocker, T. F., Qin, D., Plattner, G.-K., Tignor, M., Allen, S. K., Boschung, J., Nauels, A., Xia, Y., Bex, V. & Midgley, P. M. (eds.) *Climate Change 2013: The Physical Science Basis. Contribution of Working Group I to the Fifth Assessment Report of the Intergovernmental Panel on Climate Change (IPCC).* Cambridge, United Kingdom and New York, NY, USA.

Airbus (2008). *A318/A319/A320/A321 FCTM (Flight Crew Training Manual).*

Airlines for America. (2011). *Alternative Aviation Fuels Q&A*. URL: http://www.airlines.org/Pages/Alternative-Aviation-Fuels-QA.aspx.

Alexander, L., Broennimann, S., Charabi, Y. A.-R., Dentener, F., Dlugokencky, E., Easterling, D., Kaplan, A., Soden, B., Thorne, P., Wild, M. & Zhai, P. (2013). Observations: Atmosphere and Surface (Chapter 2). *In:* Stocker, T. F., Qin, D., Plattner, G.-K., Tignor, M., Allen, S. K., Boschung, J., Nauels, A., Xia, Y., Bex, V. & Midgley, P. M. (eds.) *Climate Change 2013: The Physical Science Basis. Contribution of Working Group I to the Fifth Assessment Report of the Intergovernmental Panel on Climate Change (IPCC).* Cambridge, United Kingdom and New York, NY, USA.

Anderson, B. E., Chen, G. & Blake, D. R. (2006). Hydrocarbon emissions from a modern commercial airliner. *Atmospheric Environment,* **40**, 3601-3612.

Andres, R. J. & Kasgnoc, A. D. (1998). A time-averaged inventory of subaerial volcanic sulfur emissions. *Journal of Geophysical Research: Atmospheres,* **103**, 25251-25261.

Arblaster, J. M., Dufresne, J.-L., Fichefet, T., Friedlingstein, P., Gao, X., Jr, W. J. G., Johns, T., Krinner, G., Shongwe, M., Tebaldi, C., Weaver, A. J. & Wehner, M. (2013). Long-term Climate Change: Projections, Commitments and Irreversibility (Chapter 12). *In:* Stocker, T. F., Qin, D., Plattner, G.-K., Tignor, M., Allen, S. K., Boschung, J., Nauels, A., Xia, Y., Bex, V. & Midgley, P. M. (eds.) *Climate Change 2013: The Physical Science Basis. Contribution of Working Group I to the Fifth Assessment Report of the Intergovernmental Panel on Climate Change (IPCC).* Cambridge, United Kingdom and New York, NY, USA.

Arneth, A., Unger, N., Kulmala, M. & Andreae, M. O. (2009). Clean the Air, Heat the Planet? *Science,* **326**, 672-673.

Arnold, S. R., Chipperfield, M. P. & Blitz, M. A. (2005). A three-dimensional model study of the effect of new temperature-dependent quantum yields for acetone photolysis. *Journal of Geophysical Research: Atmospheres,* **110**, D22305.

Arrowsmith, A. & Hedley, A. B. (1975). The Formation Of Ammonium Sulphate Particles By Atmospheric Reactions. *Revista Portuguesa de Quimica,* **17**, 26.

ASTM International (2010). D1655-09a: Standard Specification for Aviation Turbine Fuels. *In:* Section 5: Petroluem Products, L. a. F. F. (ed.) *2010 Annual Book of ASTM Standards.* ASTM International.

ASTM International. (2011a). *ASTM Aviation Fuel Standard Now Specifies Bioderived Components*. URL: http://www.astmnewsroom.org/default.aspx?pageid=2524.

ASTM International. (2011b). *ASTM WK34934 - Revision of D7566-11a Standard Specification for Aviation Turbine Fuel Containing Synthesized Hydrocarbons*. URL: http://www.astm.org/DATABASE.CART/WORKITEMS/WK34934.htm.

ASTM International (2011c). D7566-10a: Standard Specification for Aviation Turbine Fuel Containing Sythesized Hydrocarbons. *In:* Section 5: Petroluem Products, L. a. F. F. (ed.) *2011 Annual Book of ASTM Standards.* ASTM International.

ASTM International. (2012a). *ASTM WK36267 - Revision of D7566-11a Standard Specification for Aviation Turbine Fuel Containing Synthesized Hydrocarbons*. URL: http://www.astm.org/DATABASE.CART/WORKITEMS/WK36267.htm.

ASTM International (2012b). D1655-11b: Standard Specification for Aviation Turbine Fuels. *2011 Annual Book of ASTM Standards.* West Conshohocken, PA, United States: ASTM International.

ASTM International. (2014). *D7655-14c: Standard Specification for Aviation Turbine Fuel Containing Synthesized Hydrocarbons*. URL: http://www.astm.org/Standards/D7566.htm.

ATAG (2011). The right flightpath to reduce aviation emissions. *In:* Air Transport Action Group (ed.).

ATAG. (2012). *ATAG: Facts and Figures*. URL: http://www.atag.org/facts-and-figures.html.

ATAG (2014). Aviation Benefits Beyond Borders: Powering global economic growth, employment, trade links, tourism and support for sustainable development through air transport. *In:* Air Transport Action Group (ed.).

ATAG (May 2013). Revolutionising Air Traffic Management: Practical steps to accelerating airspace efficiency in your region. *In:* Air Transport Action Group (ed.).

Atkinson, J. D., Murray, B. J., Woodhouse, M. T., Whale, T. F., Baustian, K. J., Carslaw, K. S., Dobbie, S., O/'Sullivan, D. & Malkin, T. L. (2013). The importance of feldspar for ice nucleation by mineral dust in mixed-phase clouds. *Nature,* **498**, 355-358.

Bala, G., Bopp, L., Brovkin, V., Canadell, J., Chhabra, A., DeFries, R., Galloway, J., Heimann, M., Jones, C., Quéré, C. L., Myneni, R., Piao, S. & Thornton, P. (2013). Carbon and Other Biogeochemical cycles (Chapter 6). *In:* Stocker, T. F., Qin, D., Plattner, G.-K., Tignor, M., Allen, S. K., Boschung, J., Nauels, A., Xia, Y., Bex, V. & Midgley, P. M. (eds.) *Climate Change 2013: The Physical Science Basis. Contribution of Working Group I to the Fifth Assessment Report of the Intergovernmental Panel on Climate Change (IPCC).* Cambridge, United Kingdom and New York, NY, USA.

Balkanski, Y., Myhre, G., Gauss, M., Rädel, G., Highwood, E. J. & Shine, K. P. (2010). Direct radiative effect of aerosols emitted by transport: from road, shipping and aviation. *Atmos. Chem. Phys.,* **10**, 4477-4489.

Barahona, D., West, R. E. L., Stier, P., Romakkaniemi, S., Kokkola, H. & Nenes, A. (2010). Comprehensively accounting for the effect of giant CCN in cloud activation parameterizations. *Atmos. Chem. Phys.,* **10**, 2467-2473.

Barrett, S. R. H., Britter, R. E. & Waitz, I. A. (2010). Global Mortality Attributable to Aircraft Cruise Emissions. *Environmental Science & Technology,* **44**, 7736-7742.

Barrett, S. R. H., Yim, S. H. L., Gilmore, C. K., Murray, L. T., Kuhn, S. R., Tai, A. P. K., Yantosca, R. M., Byun, D. W., Ngan, F., Li, X., Levy, J. I., Ashok, A., Koo, J., Wong, H. M., Dessens, O., Balasubramanian, S., Fleming, G. G., Pearlson, M. N., Wollersheim, C., Malina, R., Arunachalam, S., Binkowski, F. S., Leibensperger, E. M., Jacob, D. J., Hileman, J. I. & Waitz, I. A. (2012). Public Health, Climate, and Economic Impacts of Desulfurizing Jet Fuel. *Environmental Science & Technology,* **46**, 4275-4282.

Bassett, M. & Seinfeld, J. H. (1983). Atmospheric equilibrium model of sulfate and nitrate aerosols. *Atmospheric Environment (1967),* **17**, 2237-2252.

Bauer, S. E., Koch, D., Unger, N., Metzger, S. M., Shindell, D. T. & Streets, D. G. (2007). Nitrate aerosols today and in 2030: a global simulation including aerosols and tropospheric ozone. *Atmos. Chem. Phys.,* **7**, 5043-5059.

Bauer, S. E. & Menon, S. (2012). Aerosol direct, indirect, semidirect, and surface albedo effects from sector contributions based on the IPCC AR5 emissions for preindustrial and present-day conditions. *J. Geophys. Res.,* **117**, D01206.

Baughcum, S. L., Tritz, T. G., Henderson, S. C. & Pickett, D. C. (1996). Scheduled Civil Aircraft Emission Inventories for 1992: Database Development and Analysis. *NASA CR 4700, Prepared for Langley Research Center*.

Bellouin, N., Rae, J., Jones, A., Johnson, C., Haywood, J. & Boucher, O. (2011). Aerosol forcing in the Climate Model Intercomparison Project (CMIP5) simulations by HadGEM2-ES and the role of ammonium nitrate. *J. Geophys. Res.,* **116**, D20206.

Benduhn, F., Mann, G. W., Pringle, K. J., Topping, D. O., McFiggans, G. & Carslaw, K. S. (2016). Size-resolved simulations of the aerosol inorganic composition with the new hybrid dissolution solver HyDiS-1.0 – Description, evaluation and first global modelling results. *Geosci. Model Dev. Discuss.,* **2016**, 1-54.

Bergamaschi, E., De Palma, G., Mozzoni, P., Vanni, S., Vettori, M. V., Broeckaert, F., Bernard, A. & Mutti, A. (2001). Polymorphism of Quinone-metabolizing Enzymes and Susceptibility to Ozone-induced Acute Effects. *American Journal of Respiratory and Critical Care Medicine,* **163**, 1426-1431.

Berger, A. (2012). The Greenhouse Effect and its intensification. *In:* European Reseach Cource on Atmospheres (ed.). Institut d'Astronomie et de Géophysique Georges Lemaître, Université Catholique de Louvain.

Bernabei, M., Bocchinfuso, G., Carrozzo, P. & De Angelis, C. (2000). Determination of phenolic antioxidants in aviation jet fuel. *Journal of Chromatography A,* **871**, 235-241.

Beusen, A. H. W., Bouwman, A. F., Heuberger, P. S. C., Van Drecht, G. & Van Der Hoek, K. W. (2008). Bottom-up uncertainty estimates of global ammonia emissions from global agricultural production systems. *Atmospheric Environment,* **42**, 6067-6077.

Beyersdorf, A. J., Timko, M. T., Ziemba, L. D., Bulzan, D., Corporan, E., Herndon, S. C., Howard, R., Miake-Lye, R., Thornhill, K. L., Winstead, E., Wey, C., Yu, Z. & Anderson, B. E. (2013). Reductions in aircraft particulate emissions due to the use of Fischer–Tropsch fuels. *Atmos. Chem. Phys. Discuss.,* **13**, 15105-15139.

Blakey, S., Rye, L. & Wilson, C. W. (2011). Aviation gas turbine alternative fuels: A review. *Proceedings of the Combustion Institute,* **33**, 2863-2885.

Boeing (2008). Current Market Outlook 2014–2033. Seattle, WA.

Bond, T. C., Doherty, S. J., Fahey, D. W., Forster, P. M., Berntsen, T., DeAngelo, B. J., Flanner, M. G., Ghan, S., Kärcher, B., Koch, D., Kinne, S., Kondo, Y., Quinn, P. K., Sarofim, M. C., Schultz, M. G., Schulz, M., Venkataraman, C., Zhang, H., Zhang, S., Bellouin, N., Guttikunda, S. K., Hopke, P. K., Jacobson, M. Z., Kaiser, J. W., Klimont, Z., Lohmann, U., Schwarz, J. P., Shindell, D., Storelvmo, T., Warren, S. G. & Zender, C. S. (2013). Bounding the role of black carbon in the climate system: A scientific assessment. *Journal of Geophysical Research: Atmospheres,* **118**, 5380-5552.

Bond, T. C., Streets, D. G., Yarber, K. F., Nelson, S. M., Woo, J.-H. & Klimont, Z. (2004). A technology-based global inventory of black and organic carbon emissions from combustion. *Journal of Geophysical Research: Atmospheres,* **109**, D14203.

Boucher, O. (2015). *Atmospheric Aerosols: Properties and Climate Impacts.* Springer Netherlands.

Boucher, O., Randall, D., Artaxo, P., Bretherton, C., Feingold, G., Forster, P., Kerminen, V.-M., Kondo, Y., Liao, H., Lohmann, U., Rasch, P., Satheesh, S. K., Sherwood, S., Stevens, B. & Zhang, X.-Y. (2013). Clouds and Aerosols (Chapter 7). *In:* Stocker, T. F., Qin, D., Plattner, G.-K., Tignor, M., Allen, S. K., Boschung, J., Nauels, A., Xia, Y., Bex, V. & Midgley, P. M. (eds.) *Climate Change 2013: The Physical Science Basis. Contribution of Working Group I to the Fifth Assessment Report of the Intergovernmental Panel on Climate Change (IPCC).* Cambridge, United Kingdom and New York, NY, USA.

Bouwman, A. F., Lee, D. S., Asman, W. A. H., Dentener, F. J., Van Der Hoek, K. W. & Olivier, J. G. J. (1997). A global high-resolution emission inventory for ammonia. *Global Biogeochemical Cycles,* **11**, 561-587.

Breider, T. J., Chipperfield, M. P., Richards, N. A. D., Carslaw, K. S., Mann, G. W. & Spracklen, D. V. (2010). Impact of BrO on dimethylsulfide in the remote marine boundary layer. *Geophysical Research Letters,* **37**, L02807.

Brühl, C., Pöschl, U., Crutzen, P. J. & Steil, B. (2000). Acetone and PAN in the upper troposphere: impact on ozone production from aircraft emissions. *Atmospheric Environment,* **34**, 3931-3938.

Brunekreef, B. & Holgate, S. T. (2002). Air pollution and health. *The Lancet,* **360**, 1233-1242.

Burnett, R. T., Pope, C. A., Ezzati, M., Olives, C., Lim, S. S., Mehta, S., Shin, H. H., Singh, G., Hubbell, B. & Brauer, M. (2014). An integrated risk function for estimating the global burden of disease attributable to ambient fine particulate matter exposure.

Burroughs, W. J. (2007). *Climate Change: A Multidisciplinary Approach.* Cambridge University Press.

Butkovskaya, N., Kukui, A. & Le Bras, G. (2007). HNO3 Forming Channel of the HO2 + NO Reaction as a Function of Pressure and Temperature in the Ranges of 72−600 Torr and 223−323 K. *The Journal of Physical Chemistry A,* **111**, 9047-9053.

Butkovskaya, N. I., Kukui, A., Pouvesle, N. & Le Bras, G. (2005). Formation of Nitric Acid in the Gas-Phase HO2 + NO Reaction: Effects of Temperature and Water Vapor. *The Journal of Physical Chemistry A,* **109**, 6509-6520.

CAAFI. (2015). *FAQs: What has CAAFI accomplished to date? Fuel Specification Approvals.* URL: http://www.caafi.org/about/faq.html [07/10/2015].

Callister Jr, W. D. (1997). *Materials Science and Engineering: An Introduction.* 4th ed. United States of America: Wiley & Sons, Inc.

Canagaratna, M. R., Jayne, J. T., Jimenez, J. L., Allan, J. D., Alfarra, M. R., Zhang, Q., Onasch, T. B., Drewnick, F., Coe, H., Middlebrook, A., Delia, A., Williams, L. R., Trimborn, A. M., Northway, M. J., DeCarlo, P. F., Kolb, C. E., Davidovits, P. & Worsnop, D. R. (2007). Chemical and microphysical characterization of ambient aerosols with the aerodyne aerosol mass spectrometer. *Mass Spectrometry Reviews,* **26**, 185-222.

Canagaratna, M. R., Jimenez, J. L., Kroll, J. H., Chen, Q., Kessler, S. H., Massoli, P., Hildebrandt Ruiz, L., Fortner, E., Williams, L. R., Wilson, K. R., Surratt, J. D., Donahue, N. M., Jayne, J. T. & Worsnop, D. R. (2015). Elemental ratio measurements of organic compounds using aerosol mass spectrometry: characterization, improved calibration, and implications. *Atmos. Chem. Phys.,* **15**, 253-272.

Capes, G., Murphy, J. G., Reeves, C. E., McQuaid, J. B., Hamilton, J. F., Hopkins, J. R., Crosier, J., Williams, P. I. & Coe, H. (2009). Secondary organic aerosol from biogenic VOCs over West Africa during AMMA. *Atmos. Chem. Phys.,* **9**, 3841-3850.

CENEX. (Undated). *The Low Carbon Vehicle Procurement Programme*. URL: http://www.lcvpp.org.uk/.

Center for International Earth Science Information Network, C. C. U. (2012). National Aggregates of Geospatial Data Collection: Population, Landscape, And Climate Estimates, Version 3 (PLACE III). Palisades, NY: NASA Socioeconomic Data and Applications Center (SEDAC).

Challinor, A. (2011). Unpublished lecture notes: Causation of Climate Change Impacts *SOEE 5550M: Climate Change - Impacts and Adaptations* Univeristy of Leeds.

Chang, F. & Li, Z. (Year). A comparison of the global surveys of high, mid and low clouds from satellite and general circulation models. *In:* Proceedings of the Fifteenth Atmospheric Radiation Measurement (ARM) Science Team Meeting, Daytona Beach, Florida, 14–18 March 2005, 2005.

Chipperfield, M. P. (2006). New version of the TOMCAT/SLIMCAT off-line chemical transport model: Intercomparison of stratospheric tracer experiments. *Quarterly Journal of the Royal Meteorological Society,* **132**, 1179-1203.

Clarke, A. D., Davis, D., Kapustin, V. N., Eisele, F., Chen, G., Paluch, I., Lenschow, D., Bandy, A. R., Thornton, D., Moore, K., Mauldin, L., Tanner, D., Litchy, M., Carroll, M. A., Collins, J.

& Albercook, G. (1998). Particle Nucleation in the Tropical Boundary Layer and Its Coupling to Marine Sulfur Sources. *Science,* **282**, 89-92.

Clarke, A. D., Eisele, F., Kapustin, V. N., Moore, K., Tanner, D., Mauldin, L., Litchy, M., Lienert, B., Carroll, M. A. & Albercook, G. (1999). Nucleation in the equatorial free troposphere: Favorable environments during PEM-Tropics. *Journal of Geophysical Research: Atmospheres,* **104**, 5735-5744.

Clarke, J.-P. (2003). The role of advanced air traffic management in reducing the impact of aircraft noise and enabling aviation growth. *Journal of Air Transport Management,* **9**, 161-165.

Cofala, J., Amann, M., Klimont, Z. & Schopp, W. (2005). Scenarios of World Anthropogenic Emissions of SO2, NOx and CO up to 2030. *Internal report of the Transboundary Air Pollution Programme, .* Laxenburg, Austria: International Institute for Applied Systems Analysis.

Coffin, D. L., Blommer, E., Gardner, D. & Holzman, R. (1969). Effect of air pollution on alteration of susceptibility to pulmonary infection. *Journal of Occupational and Environmental Medicine,* **11**, 556.

Commercial Aviation Safety Team (October 2012). Phases of Flight: Definition and usage notes. Common Taxonomy team, International Civil Aviation Organisation (ICAO).

Commission of the European Communitites. (2009). *Adapting to climate change: Towards a European framework for action - White Paper*. URL: http://eur-lex.europa.eu/LexUriServ/LexUriServ.do?uri=COM:2009:0147:FIN:EN:PDF.

Committee on Climate Change (December 2009). Meeting the UK aviation target - options for reducing emissions to 2050.

Committee on the Environment and Natural Resources (June 2000). Atmospheric Ammonia: Sources and Fate. A Review of Ongoing Federal Research and Future Needs. *In:* Committee on the Environment and Natural Resources: Air Quality Research subcommittee (ed.).

Connolly, K. (2015). G7 leaders agree to phase out fossil fuel use by end of century. *The Guardian,* , 08/06/2015, URL: http://www.theguardian.com/world/2015/jun/08/g7-leaders-agree-phase-out-fossil-fuel-use-end-of-century.

Cook, J., Nuccitelli, D., Green, S. A., Richardson, M., Winkler, B., Painting, R., Way, R., Jacobs, P. & Skuce, A. (2013). Quantifying the consensus on anthropogenic global warming in the scientific literature. *Environmental Research Letters,* **8**, 024024.

Crown Oil Environmental Ltd. (2014). *Fuel contamination*. URL: http://www.crownoilenvironmental.co.uk/fuel-contamination/ [23/10/2015].

Cuijpers, C. E. J., Swaen, G. M. H., Wesseling, G. & Wouters, E. F. M. (1994). Acute respiratory effects of summer smog in primary school children. *Toxicology Letters,* **72**, 227-235.

Daggett, D. L., Hendricks, R. C., Walther, R. & Corporan, E. (2007). Alternate Fuels for use in Commercial Aircraft. *In:* Boeing (ed.).

de Gouw, J. A., Warneke, C., Stohl, A., Wollny, A. G., Brock, C. A., Cooper, O. R., Holloway, J. S., Trainer, M., Fehsenfeld, F. C., Atlas, E. L., Donnelly, S. G., Stroud, V. & Lueb, A. (2006). Volatile organic compounds composition of merged and aged forest fire plumes from Alaska and western Canada. *Journal of Geophysical Research: Atmospheres,* **111**, D10303.

De Nevers, Noel (2000). *Air Pollution Control Engineering.* Second Edition ed. Singapore: McGraw-Hill International.

de Wild, P., Van der Laan, R., Kloekhorst, A. & Heeres, E. (2009). Lignin valorisation for chemicals and (transportation) fuels via (catalytic) pyrolysis and hydrodeoxygenation. *Environmental Progress & Sustainable Energy,* **28**, 461-469.

DeMott, P. J., Chen, Y., Kreidenweis, S. M., Rogers, D. C. & Sherman, D. E. (1999). Ice formation by black carbon particles. *Geophysical Research Letters,* **26**, 2429-2432.

Dentener, F. & Crutzen, P. (1994). A three-dimensional model of the global ammonia cycle. *Journal of Atmospheric Chemistry,* **19**, 331-369.

Dentener, F., Kinne, S., Bond, T., Boucher, O., Cofala, J., Generoso, S., Ginoux, P., Gong, S., Hoelzemann, J. J., Ito, A., Marelli, L., Penner, J. E., Putaud, J. P., Textor, C., Schulz, M., van der Werf, G. R. & Wilson, J. (2006). Emissions of primary aerosol and precursor gases in the years 2000 and 1750 prescribed data-sets for AeroCom. *Atmos. Chem. Phys.,* **6**, 4321-4344.

Dentener, F. J. & Crutzen, P. J. (1993). Reaction of N2O5 on tropospheric aerosols: Impact on the global distributions of NO x , O3, and OH. *Journal of Geophysical Research: Atmospheres,* **98**, 7149-7163.

Department for Transport. (July 2009). *Low Carbon Transport: A Greener Future. A Carbon Reduction Strategy for Transport.* URL: http://www.official-documents.gov.uk/document/cm76/7682/7682.pdf.

Department of Energy and Climate Change. (2008). *Climate Change Act 2008*. URL: http://www.decc.gov.uk/en/content/cms/legislation/cc_act_08/cc_act_08.aspx.

Department of Trade and Industry. (May 2007). *Meeting the Energy Challenge: A White Paper on Energy*. URL: http://www.berr.gov.uk/files/file39387.pdf.

Dockery, D. W., Pope, C. A., Xu, X., Spengler, J. D., Ware, J. H., Fay, M. E., Ferris, B. G. & Speizer, F. E. (1993). An Association between Air Pollution and Mortality in Six U.S. Cities. *New England Journal of Medicine,* **329**, 1753-1759.

Dray, L. (2014). Time constants in aviation infrastructure. *Transport Policy,* **34**, 29-35.

Dry, M. E. (2002). The Fischer–Tropsch process: 1950–2000. *Catalysis Today,* **71**, 227-241.

DuBois, D. & Paynter, G. C. (2006). "Fuel Flow Method2" for Estimating Aircraft Emissions. *SAE Technical Paper Series,* **01**.

Easter, R. C. & Hales, J. M. (1983). *Interpretation of the OSCAR data for reactive gas scavenging.* New York: Elsevier.

Eastop, T. D. & McConkey, A. (1993). *Applied Thermodynamics for Engineering Technologists.* Singapore: Prentics Hall.

Edwards, H. A., Dixon, D. & Wadud, Z. (2015). Optimisation of Aircraft Cost Indices to Reduce Fuel Use. *Transportation Research Board 94th Annual Meeting.* Washington, United States of America.

Edwards, J. M. & Slingo, A. (1996). Studies with a flexible new radiation code. I: Choosing a configuration for a large-scale model. *Quarterly Journal of the Royal Meteorological Society,* **122**, 689-719.

Environment Canada. (2014). *Air Pollutant Emissions Data*. URL: https://www.ec.gc.ca/indicateurs-indicators/default.asp?lang=en&n=58DE4720-1#nox_1.

Eurocontrol (March 2009). European Joint Industry - CDA Action Plan. *In:* Eurocontrol, IATA, CANSO & ACI (eds.).

European Biofuels Technology Platform. (2015). *Biofuels for Air Transport*. URL: http://www.biofuelstp.eu/factsheets/fame-fact-sheet.pdf [26/03/2015].

European Biofuels Technology Platform (Undated). Biofuels Fact Sheet: Fatty Acid Methyl Esters FAME.

European Commission (2009a). Directive 2008/50/EC of the European Parliament and of the Council of 21 May 2008 on ambient air quality and cleaner air for Europe. *Official Journal of the European Union,*.

European Commission. (2009b). *Directive 2009/30/EC of the European Parliament and the Council of 23 April 2009: Amending Directive 98/70/EC as regards the specification of petrol, diesel and gas-oil and introducing a mechanism to monitor and reduce greenhouse gas emissions and amending Council Directive 1999/32/EC as regards the specification of fuel used by inland waterway vessels and repealing Directive 93/12/EEC.* URL: http://eur-lex.europa.eu/LexUriServ/LexUriServ.do?uri=OJ:L:2009:140:0088:0113:EN:PDF.

European Commission (2009c). A Sustainable Future: For Transport.

European Commission. (2011). *Climate Action: Emissions Trading System - Cap*. URL: http://ec.europa.eu/clima/policies/ets/cap_en.htm.

European Commission. (2015). *Reducing emissions from avaition*. URL: http://ec.europa.eu/clima/policies/transport/aviation/index_en.htm [30/09/2015].

European Commission (January 2001). European Aeronautics: A vision for 2020 - Meeting society's needs and winning global leadership.

European Environment Agency. (February 2015). *Emission trends for the main air pollutants, PM, HMs and POPs*. URL: http://www.eea.europa.eu/data-and-maps/daviz/emission-trends-for-the-main#tab-chart_2 [29/04/2015].

European Environment Agency. (January 2014a). *Ammonia (NH3) emissions (APE 003)*. URL: http://www.eea.europa.eu/data-and-maps/indicators/eea-32-ammonia-nh3-emissions-1/assessment-4 [29/04/2015].

European Environment Agency. (January 2014b). *Nitrogen oxides (NOx) emissions (APE 002)*. URL: http://www.eea.europa.eu/data-and-maps/indicators/eea-32-nitrogen-oxides-nox-emissions-1/assessment.2010-08-19.0140149032-3 [29/04/2015].

European Environment Agency. (January 2014c). *Sulphur dioxide (SO_2) emissions (APE 001)*. URL: http://www.eea.europa.eu/data-and-maps/indicators/eea-32-sulphur-dioxide-so2-emissions-1/assessment-3.

Evans, A. (2014). Mitgatng the Climate Impact of Aviaton – Is Technology Enough? : UCL Energy Institute, Unversity College London.

Evans, A. & Schäfer, A. (2013). The rebound effect in the aviation sector. *Energy Economics,* **36**, 158-165.

Eyers, C. J., Addleton, D., Atkinson, K., Broomhead, M. J., Christou, R., Elliff, T., Falk, R., Gee, I., Lee, D. S., Marizy, C., S Michot, Middel, J., Newton, P., Norman, P., Plohr, M., Raper, D. & Stanciou, N. (2004). AERO2K Global Aviation Emissions Inventories for 2002 and 2025. *In:* QinetiQ Ltd (ed.). QINETIQ/04/01113.

Fang, Y., Naik, V., Horowitz, L. W. & Mauzerall, D. L. (2013). Air pollution and associated human mortality: the role of air pollutant emissions, climate change and methane concentration increases from the preindustrial period to present. *Atmos. Chem. Phys.,* **13**, 1377-1394.

Finlayson-Pitts, B. J. & Pitts Jr, J. N. (2000). Chapter 8 - Acid Deposition: Formation and Fates of Inorganic and Organic Acids in the Troposphere. *In:* Pitts, B. J. F.-P. N. (ed.) *Chemistry of the Upper and Lower Atmosphere.* San Diego: Academic Press.

Fiore, A. M., Naik, V., Spracklen, D. V., Steiner, A., Unger, N., Prather, M., Bergmann, D., Cameron-Smith, P. J., Cionni, I., Collins, W. J., Dalsoren, S., Eyring, V., Folberth, G. A., Ginoux, P., Horowitz, L. W., Josse, B., Lamarque, J.-F., MacKenzie, I. A., Nagashima, T., O'Connor, F. M., Righi, M., Rumbold, S. T., Shindell, D. T., Skeie, R. B., Sudo, K., Szopa, S., Takemura, T. & Zeng, G. (2012). Global air quality and climate. *Chemical Society Reviews,* **41**, 6663-6683.

Forster, P., Ramaswamy, V., Artaxo, P., Berntsen, T., Betts, R., Fahey, D. W., Haywood, J., Lean, J., Lowe, D. C., Myhre, G., Nganga, J., Prinn, R., Raga, G., Schulz, M. & Dorland, R. V. (2007). Changes in Atmospheric Constituents and in Radiative Forcing (Chapter 2). *In:* Intergovernmental Panel on Climate Change (ed.) *Climate Change 2007: The Physical Science Basis. Contribution of Working Group I to the Fourth Assessment Report of the Intergovernmental Panel on Climate Change.*

Forster, P. M. d. F., Shine, K. P. & Stuber, N. (2006). It is premature to include non-CO2 effects of aviation in emission trading schemes. *Atmospheric Environment,* **40**, 1117-1121.

Forsyth, P. (2007). The impacts of emerging aviation trends on airport infrastructure. *Journal of Air Transport Management,* **13**, 45-52.

Fountoukis, C. & Nenes, A. (2005). Continued development of a cloud droplet formation parameterization for global climate models. *Journal of Geophysical Research: Atmospheres,* **110**, D11212.

Fowler, D., Coyle, M., Anderson, R., Ashmore, M. R., Bower, J. S., Burgess, R. A., Cape, J. N., Cox, R. A., Derwent, R. G., Dollard, G. J., Grennfelt, P., Harrison, P. M., Hewitt, C. N., Hov, Ø., Jenkin, M. E., Lee, D. S., Maynard, R. L., Penkett, S. A., Smith, R. I., Stedman, J. R., Weston, K. J., Williams, M. L. & Woods, P. J. (1997). *Ozone in the United Kingdom: Fourth Report of the Photochemical Oxidants Review Group, 1997.* United Kingdom Photochemical Oxidants Review Group.

Frömming, C., Ponater, M., Burkhardt, U., Stenke, A., Pechtl, S. & Sausen, R. (2011). Sensitivity of contrail coverage and contrail radiative forcing to selected key parameters. *Atmospheric Environment,* **45**, 1483-1490.

Frömming, C., Ponater, M., Dahlmann, K., Grewe, V., Lee, D. S. & Sausen, R. (2012). Aviation-induced radiative forcing and surface temperature change in dependency of the emission altitude. *J. Geophys. Res.,* **117**, D19104.

Fuglestvedt, J., Berntsen, T., Myhre, G., Rypdal, K. & Skeie, R. B. (2008). Climate forcing from the transport sectors. *Proceedings of the National Academy of Sciences,* **105**, 454-458.

Fuglestvedt, J. S., Shine, K. P., Berntsen, T., Cook, J., Lee, D. S., Stenke, A., Skeie, R. B., Velders, G. J. M. & Waitz, I. A. (2010). Transport impacts on atmosphere and climate: Metrics. *Atmospheric Environment,* **44**, 4648-4677.

G.A. Meehl, T.F. Stocker, W.D. Collins, P. Friedlingstein, A.T. Gaye, J.M. Gregory, A. Kitoh, R. Knutti, J.M. Murphy, A. Noda, S.C.B. Raper, I.G. Watterson, A.J. Weaver & Zhao, Z.-C. (2007). Global Climate Projections (Chapter 10). *In:* Change, I. P. o. C. (ed.) *Climate Change 2007: The Physical Science Basis. Contribution of Working Group I to the Fourth Assessment Report of the Intergovernmental Panel on Climate Change.*

Gauss, M., Isaksen, I. S. A., Lee, D. S. & Søvde, O. A. (2006). Impact of aircraft NOx emissions on the atmosphere – tradeoffs to reduce the impact. *Atmos. Chem. Phys.,* **6**, 1529-1548.

Gettelman, A. & Chen, C. (2013). The climate impact of aviation aerosols. *Geophysical Research Letters,* **40**, 2785-2789.

Gilmore, C. K., Barrett, S. R. H., Koo, J. & Wang, Q. (2013). Temporal and spatial variability in the aviation NOx -related O3 impact. *Environmental Research Letters,* **8**, 034027.

Gottschaldt, K., Voigt, C., Jöckel, P., Righi, M., Deckert, R. & Dietmüller, S. (2013). Global sensitivity of aviation NOx effects to the HNO3-forming channel of the HO2 + NO reaction. *Atmos. Chem. Phys.,* **13**, 3003-3025.

Graf, H.-F., Feichter, J. & Langmann, B. (1997). Volcanic sulfur emissions: Estimates of source strength and its contribution to the global sulfate distribution. *Journal of Geophysical Research: Atmospheres,* **102**, 10727-10738.

Graf, H.-F., Langmann, B. & Feichter, J. (1998). The contribution of Earth degassing to the atmospheric sulfur budget. *Chemical Geology,* **147**, 131-145.

Grooß, J.-u., Brühl, C. & Peter, T. (1998). Impact of aircraft emissions on tropospheric and stratospheric ozone. Part I: chemistry and 2-D model results. *Atmospheric Environment,* **32**, 3173-3184.

Gryglewicz, S. (1999). Rapeseed oil methyl esters preparation using heterogeneous catalysts. *Bioresource Technology,* **70**, 249-253.

Gudmundsson, S. V. & Anger, A. (2012). Global carbon dioxide emissions scenarios for aviation derived from IPCC storylines: A meta-analysis. *Transportation Research Part D: Transport and Environment,* **17**, 61-65.

Guenther, A., Hewitt, C. N., Erickson, D., Fall, R., Geron, C., Graedel, T., Harley, P., Klinger, L., Lerdau, M., McKay, W. A., Pierce, T., Scholes, B., Steinbrecher, R., Tallamraju, R., Taylor, J. & Zimmerman, P. (1995). A global model of natural volatile organic compound emissions. *Journal of Geophysical Research: Atmospheres,* **100**, 8873-8892.

Guibert, S., Snider, J. R. & Brenguier, J.-L. (2003). Aerosol activation in marine stratocumulus clouds: 1. Measurement validation for a closure study. *Journal of Geophysical Research: Atmospheres,* **108**, 8628.

Guzman, A., Torres, J. E., Prada, L. P. & Nuñez, M. L. (2010). Hydroprocessing of crude palm oil at pilot plant scale. *Catalysis Today,* **156**, 38-43.

Hadaller, O. J. & Momenthy, A. M. (1993). Characteristics of Future Aviation Fuels. *Transportation and Global Climate Change, Amercian Council for an Energy-Efficient Economy*.

Hall, J. W., Evans, E. P., Penning-Rowsell, E. C., Sayers, P. B., Thorne, C. R. & Saul, A. J. (2003). Quantified scenarios analysis of drivers and impacts of changing flood risk in England and Wales: 2030-2100. *Global Environmental Change Part B: Environmental Hazards,* **5**, 51-65.

Halmer, M. M., Schmincke, H. U. & Graf, H. F. (2002). The annual volcanic gas input into the atmosphere, in particular into the stratosphere: a global data set for the past 100 years. *Journal of Volcanology and Geothermal Research,* **115**, 511-528.

Hauglustaine, D. & Koffi, B. (2012). Boundary layer ozone pollution caused by future aircraft emissions. *Geophysical Research Letters*.

Hauglustaine, D. A., Balkanski, Y. & Schulz, M. (2014). A global model simulation of present and future nitrate aerosols and their direct radiative forcing of climate. *Atmos. Chem. Phys.,* **14**, 11031-11063.

Hauglustaine, D. A., Granier, C., Brasseur, G. P. & Mégie, G. (1994). Impact of present aircraft emissions of nitrogen oxides on tropospheric ozone and climate forcing. *Geophys. Res. Lett.,* **21**, 2031-2034.

Hayman, G. D. & Markiewicz, M. (1996). Pollution from Aircraft Emissions in the North Atlantic Flight Corridor (POLINAT). European Commission.

Heald, C. L., Coe, H., Jimenez, J. L., Weber, R. J., Bahreini, R., Middlebrook, A. M., Russell, L. M., Jolleys, M., Fu, T. M., Allan, J. D., Bower, K. N., Capes, G., Crosier, J., Morgan, W. T., Robinson, N. H., Williams, P. I., Cubison, M. J., DeCarlo, P. F. & Dunlea, E. J. (2011). Exploring the vertical profile of atmospheric organic aerosol: comparing 17 aircraft field campaigns with a global model. *Atmos. Chem. Phys.,* **11**, 12673-12696.

Heald, C. L., Jacob, D. J., Turquety, S., Hudman, R. C., Weber, R. J., Sullivan, A. P., Peltier, R. E., Atlas, E. L., de Gouw, J. A., Warneke, C., Holloway, J. S., Neuman, J. A., Flocke, F. M. & Seinfeld, J. H. (2006). Concentrations and sources of organic carbon aerosols in the free troposphere over North America. *Journal of Geophysical Research: Atmospheres,* **111**, D23S47.

Hendricks, J., Kärcher, B., Döpelheuer, A., Feichter, J., Lohmann, U. & Baumgardner, D. (2004). Simulating the global atmospheric black carbon cycle: a revisit to the contribution of aircraft emissions. *Atmos. Chem. Phys.,* **4**, 2521-2541.

Hidalgo, H. & Crutzen, P. J. (1977). The tropospheric and stratospheric composition perturbed by NO x emissions of high-altitude aircraft. *Journal of Geophysical Research,* **82**, 5833-5866.

Hileman, J. I. & Stratton, R. W. (2014). Alternative jet fuel feasibility. *Transport Policy*.

Hodnebrog, Ø., Berntsen, T. K., Dessens, O., Gauss, M., Grewe, V., Isaksen, I. S. A., Koffi, B., Myhre, G., Olivié, D., Prather, M. J., Pyle, J. A., Stordal, F., Szopa, S., Tang, Q., van Velthoven, P., Williams, J. E. & Ødemark, K. (2011). Future impact of non-land based traffic emissions on atmospheric ozone and OH – an optimistic scenario and a possible mitigation strategy. *Atmos. Chem. Phys.,* **11**, 11293-11317.

Holmes, C. D., Tang, Q. & Prather, M. J. (2011). Uncertainties in climate assessment for the case of aviation NO. *Proceedings of the National Academy of Sciences,* **108**, 10997-11002.

Holtslag, A. & Boville, B. (1993). Local versus nonlocal boundary-layer diffusion in a global climate model. *Journal of Climate,* **6**, 1825-1842.

Hoor, P., Borken-Kleefeld, J., Caro, D., Dessens, O., Endresen, O., Gauss, M., Grewe, V., Hauglustaine, D., Isaksen, I. S. A., Jöckel, P., Lelieveld, J., Myhre, G., Meijer, E., Olivie, D., Prather, M., Schnadt Poberaj, C., Shine, K. P., Staehelin, J., Tang, Q., van Aardenne, J., van Velthoven, P. & Sausen, R. (2009). The impact of traffic emissions on

atmospheric ozone and OH: results from QUANTIFY. *Atmos. Chem. Phys.,* **9**, 3113-3136.

Hoose, C. & Möhler, O. (2012). Heterogeneous ice nucleation on atmospheric aerosols: a review of results from laboratory experiments. *Atmos. Chem. Phys.,* **12**, 9817-9854.

Hopke, P. K. (1985). *Receptor modeling in environmental chemistry.* Hoboken, N. J: Wiley.

Hoppel, W. A., Frick, G. M., Fitzgerald, J. W. & Larson, R. E. (1994). Marine boundary layer measurements of new particle formation and the effects nonprecipitating clouds have on aerosol size distribution. *Journal of Geophysical Research: Atmospheres,* **99**, 14443-14459.

Houghton, J. (2009). *Global Warming: The Complete Briefing.* Cambridge, UK: Cambridge University Press.

IATA. (2015). *Annual Review 2015*. URL: http://www.iata.org/about/Documents/iata-annual-review-2015.pdf.

IATA. (August 2009). *A global approach to reducing aviation emissions. First stop: carbon-neutral growth by 2020*. URL: http://corporate.airfrance.com/fileadmin/dossiers/img_rte_fr/IATA.pdf.

ICAO (2007). Assessing Current Scientific Knowledge, Uncertainties and Gaps in Quantifying Climate Change, Noise and Air Quality Aviation Impacts. *In:* International Civil Aviation Organisation (ICAO) (ed.). Manchester Metropolitan University, Federal Aviation Authority.

ICAO (2010). Environmental Report 2010: Aviation and Climate Change. *In:* International Civil Aviation Organisation (ICAO) (ed.).

ICAO. (2011). *Main Summary of accomplishments and projected activities on sustainable alternative fuels for aviation*. URL: http://legacy.icao.int/icao/en/Env2010/ClimateChange/GFAAF/Summary.htm.

ICAO. (Undated-a). *Environmental Branch: Alternative Fuels*. URL: http://www.icao.int/icao/en/Env2010/ClimateChange/AlternativeFuels.htm.

ICAO (Undated-b). Guidelines on the use of procedures in the emissions certification of aircraft engines. *In:* International Civil Aviation Organisation (ICAO) (ed.).

IEA (2014). Energy Efficiency Indicators: Fundamentals on Statistics. *In:* International Energy Agency (IEA) (ed.).

IPCC (2007a). Climate Change 2007. Chapter 1: Assessment of observed changes and responses in natural and managed systems. *In:* Intergovernmental Panel on Climate Change (IPCC) (ed.) *Working Group II: Impacts, Adaptation and Vulnerability.*

IPCC (2007b). Summary for Policymakers. *In:* Intergovernmental Panel on Climate Change (IPCC) (ed.) *Climate Change 2007: The Physical Science Basis. Contribution of Working Group I to the Fourth Assessment Report of the Intergovernmental Panel on Climate Change (IPCC).*

IPCC (2013a). Annex III: Glossary [Planton, S. (ed.)]. *In:* Stocker, T. F., Qin, D., Plattner, G.-K., Tignor, M. M. B., Allen, S. K., Boschung, J., Nauels, A., Xia, Y., Bex, V. & Midgley, P. M. (eds.) *Climate Change 2013: The Physical Science Basis. Contribution of Working Group I to the Fifth Assessment Report of the Intergovernmental Panel on Climate Change (IPCC).* Cambridge, United Kingdom and New York, NY, USA: Cambridge University Press.

IPCC (2013b). Summary for Policymakers. *In:* Stocker, T. F., Qin, D., Plattner, G.-K., Tignor, M. M. B., Allen, S. K., Boschung, J., Nauels, A., Xia, Y., Bex, V. & Midgley, P. M. (eds.) *Climate Change 2013: The Physical Science Basis. Contribution of Working Group I to the Fifth Assessment Report of the Intergovernmental Panel on Climate Change (IPCC).* Cambridge, United Kingdom and New York, NY, USA: Cambridge University Press.

IPCC (2014a). Summary for Policymakers. *In:* Field, C. B., Barros, V. R., Dokken, D. J., Mach, K. J., Mastrandrea, M. D., Bilir, T. E., Chatterjee, M., Ebi, K. L., Estrada, Y. O., Genova, R. C., Girma, B., Kissel, E. S., Levy, A. N., MacCracken, S., Mastrandrea, P. R. & White, L. L. (eds.) *Climate Change 2014: Impacts, Adaptation, and Vulnerability. Part A: Global and*

Sectoral Aspects. Contribution of Working Group II to the Fifth Assessment Report of the Intergovernmental Panel on Climate Change (IPCC). Cambridge, United Kingdom and New York, NY, USA: Cambridge University Press.

IPCC (2014b). Synthesis Report. *In:* Intergovernmental Panel on Climate Change (ed.) *Climate Change 2014: The Physical Science Basis. Contribution of Working Group I, II and III to the Fifth Assessment Report of the Intergovernmental Panel on Climate Change (IPCC) [Core Writing Team, R. K. Pachauri and L. A. Meyers (eds.)].*

ITF (2011). Transport Outlook: Meeting the Needs of 9 Billion People. *In:* International Transport Forum (ITF) (ed.).

Jacob, D. J. (2000). Heterogeneous chemistry and tropospheric ozone. *Atmospheric Environment,* **34**, 2131-2159.

Jacobson, M. Z. (1997). Development and application of a new air pollution modeling system—II. Aerosol module structure and design. *Atmospheric Environment,* **31**, 131-144.

Jacobson, M. Z. (2002). *Athmospheric Pollution: History, Science and Regulation.* Cambridge Universitty Press.

Jacobson, M. Z. (2005). *Fundamentals of Atmospheric Modeling.* Cambridge University Press.

Jacobson, M. Z. (2010). Enhancement of Local Air Pollution by Urban CO2 Domes. *Environmental Science & Technology,* **44**, 2497-2502.

Jacobson, M. Z., Wilkerson, J., Balasubramanian, S., Cooper, W., Jr. & Mohleji, N. (2012). The effects of rerouting aircraft around the arctic circle on arctic and global climate. *Climatic Change,* **115**, 709-724.

Jacobson, M. Z., Wilkerson, J. T., Naiman, A. D. & Lele, S. K. (2013). The effects of aircraft on climate and pollution. Part II: 20-year impacts of exhaust from all commercial aircraft worldwide treated individually at the subgrid scale. *Faraday Discussions,* **165**, 369-382.

Janssens-Maenhout, G., Pagliari, V., Guizzardi, D. & Muntean, M. (2012). I. Gridding: EDGAR emissions distribution on global gridmaps. *In:* European Commision Joint Research Centre (ed.) *Global emission inventories in the Emission Database for Global Atmospheric Research (EDGAR) – Manual (I).*

Jayne, J. T., Leard, D. C., Zhang, X., Davidovits, P., Smith, K. A., Kolb, C. E. & Worsnop, D. R. (2000). Development of an Aerosol Mass Spectrometer for Size and Composition Analysis of Submicron Particles. *Aerosol Science and Technology,* **33**, 49-70.

Jenkin, M. E. & Clemitshaw, K. C. (2000). Ozone and other secondary photochemical pollutants: chemical processes governing their formation in the planetary boundary layer. *Atmospheric Environment,* **34**, 2499-2527.

JIG (November 2008). Product Quality, Bulletin No. 21: Risk of contamination of aviation kerosene (jet fuel) with biodisel.

Johnson, C., Henshaw, J. & McLnnes, G. (1992). Impact of aircraft and surface emissions of nitrogen oxides on tropospheric ozone and global warming. *Nature,* **355**, 69-71.

Johnson, I. (2015). Climate change: Six major energy companies write to United Nations to request help in setting up carbon pricing scheme. *The Independant,* , 31/05/2015, URL: http://www.independent.co.uk/environment/climate-change/climate-change-major-energy-companies-write-to-un-to-request-help-in-setting-up-carbon-pricing-scheme-10288009.html.

Jowit, J. & Wintour, P. (2008). *Cost of tackling global climate change has doubled, warns Stern*. URL: http://www.guardian.co.uk/environment/2008/jun/26/climatechange.scienceofclimatechange.

Kampa, M. & Castanas, E. (2008). Human health effects of air pollution. *Environmental Pollution,* **151**, 362-367.

Karl, T., Apel, E., Hodzic, A., Riemer, D. D., Blake, D. R. & Wiedinmyer, C. (2009). Emissions of volatile organic compounds inferred from airborne flux measurements over a megacity. *Atmos. Chem. Phys.,* **9**, 271-285.

Kentarchos, A. S. & Roelofs, G. J. (2002). Impact of aircraft NOx emissions on tropospheric ozone calculated with a chemistry-general circulation model: Sensitivity to higher hydrocarbon chemistry. *Journal of Geophysical Research: Atmospheres,* **107**, ACH 8-1-ACH 8-12.

Kettle, A. J. & Andreae, M. O. (2000). Flux of dimethylsulfide from the oceans: A comparison of updated data sets and flux models. *Journal of Geophysical Research: Atmospheres,* **105**, 26793-26808.

Khodayari, A., Olsen, S. C. & Wuebbles, D. J. (2014a). Evaluation of aviation NOx-induced radiative forcings for 2005 and 2050. *Atmospheric Environment,* **91**, 95-103.

Khodayari, A., Tilmes, S., Olsen, S. C., Phoenix, D. B., Wuebbles, D. J., Lamarque, J. F. & Chen, C. C. (2014b). Aviation 2006 NOx-induced effects on atmospheric ozone and HOx in Community Earth System Model (CESM). *Atmos. Chem. Phys.,* **14**, 9925-9939.

Kim, B. Y., Fleming, G. G., Lee, J. J., Waitz, I. A., Clarke, J.-P., Balasubramanian, S., Malwitz, A., Klima, K., Locke, M., Holsclaw, C. A., Maurice, L. Q. & Gupta, M. L. (2007). System for assessing Aviation's Global Emissions (SAGE), Part 1: Model description and inventory results. *Transportation Research Part D: Transport and Environment,* **12**, 325-346.

Kim, D.-G. & Kirschbaum, M. U. F. (2015). The effect of land-use change on the net exchange rates of greenhouse gases: A compilation of estimates. *Agriculture, Ecosystems & Environment,* **208**, 114-126.

Kim, K.-H., Kabir, E. & Kabir, S. (2015). A review on the human health impact of airborne particulate matter. *Environment International,* **74**, 136-143.

Kim, M. Y., Lee, S.-B., Bae, G.-N., Park, S. S., Han, K. M., Park, R. S., Song, C. H. & Park, S. H. (2012). Distribution and direct radiative forcing of black carbon aerosols over Korean Peninsula. *Atmospheric Environment*.

Kirklin, P. W. & David, P. (1992). *Aviation Fuel: Thermal Stability Requirements.* ASTM.

Kiselev, A. A. & Karol, I. L. (2000). Model study of tropospheric composition response to NOx and CO pollution. *Environmental Modelling & Software,* **15**, 583-588.

Knighton, W. B., Rogers, T. M., Anderson, B. E., Herndon, S. C., Yelvington, P. E. & Miake-Lye, R. C. (2007). Quantification of Aircraft Engine Hydrocarbon Emissions Using Proton Transfer Reaction Mass Spectrometry. *Journal of Propulsion and Power,* **23**, 949-958.

Koch, D. & Del Genio, A. D. (2010). Black carbon semi-direct effects on cloud cover: review and synthesis. *Atmos. Chem. Phys.,* **10**, 7685-7696.

Koffi, B., Szopa, S., Cozic, A., Hauglustaine, D. & van Velthoven, P. (2010). Present and future impact of aircraft, road traffic and shipping emissions on global tropospheric ozone. *Atmos. Chem. Phys.,* **10**, 11681-11705.

Köhler, M. O. (2010). Chemistry of the Atmosphere and Impacts from Global Aviation. *Encyclopedia of Aerospace Engineering.* John Wiley & Sons, Ltd.

Köhler, M. O., Rädel, G., Dessens, O., Shine, K. P., Rogers, H. L., Wild, O. & Pyle, J. A. (2008). Impact of perturbations to nitrogen oxide emissions from global aviation. *Journal of Geophysical Research: Atmospheres,* **113**, D11305.

Köhler, M. O., Rädel, G., Shine, K. P., Rogers, H. L. & Pyle, J. A. (2013). Latitudinal variation of the effect of aviation NOx emissions on atmospheric ozone and methane and related climate metrics. *Atmospheric Environment,* **64**, 1-9.

Koster, J., Velazco, A., Kosyan, M., Balaban, S. & McDowell, L. (2012). The Hyperion 2 Green Aircraft Project. *50th AIAA Aerospace Sciences Meeting including the New Horizons Forum and Aerospace Exposition.* American Institute of Aeronautics and Astronautics.

Kreutz, T. G., Larson, E. D., Liu, G. & Williams, R. H. (2008). Fischer-Tropsch Fuels from Coal and Biomass. *25th Annual International Pittsburgh Coal Conference,*. Princeton University.

Kulmala, M., Laaksonen, A. & Pirjola, L. (1998). Parameterizations for sulfuric acid/water nucleation rates. *Journal of Geophysical Research: Atmospheres,* **103**, 8301-8307.

Kulmala, M., Riipinen, I., Sipilä, M., Manninen, H. E., Petäjä, T., Junninen, H., Maso, M. D., Mordas, G., Mirme, A., Vana, M., Hirsikko, A., Laakso, L., Harrison, R. M., Hanson, I.,

Leung, C., Lehtinen, K. E. J. & Kerminen, V.-M. (2007). Toward Direct Measurement of Atmospheric Nucleation. *Science,* **318**, 89-92.

Kulmala, M., Vehkamäki, H., Petäjä, T., Dal Maso, M., Lauri, A., Kerminen, V. M., Birmili, W. & McMurry, P. H. (2004). Formation and growth rates of ultrafine atmospheric particles: a review of observations. *Journal of Aerosol Science,* **35**, 143-176.

Laaksonen, A., Kulmala, M., Berndt, T., Stratmann, F., Mikkonen, S., Ruuskanen, A., Lehtinen, K. E. J., Dal Maso, M., Aalto, P., Petäjä, T., Riipinen, I., Sihto, S. L., Janson, R., Arnold, F., Hanke, M., Ücker, J., Umann, B., Sellegri, K., O'Dowd, C. D. & Viisanen, Y. (2008). SO2 oxidation products other than H2SO4 as a trigger of new particle formation. Part 2: Comparison of ambient and laboratory measurements, and atmospheric implications. *Atmos. Chem. Phys.,* **8**, 7255-7264.

Lamarque, J.-F., Kyle, G. P., Meinshausen, M., Riahi, K., Smith, S., Vuuren, D., Conley, A. & Vitt, F. (2011). Global and regional evolution of short-lived radiatively-active gases and aerosols in the Representative Concentration Pathways. *Climatic Change,* **109**, 191-212.

Lamarque, J.-F., Smith, S. J., Bond, T., Cofala, J., Eyring, V., Granier, C., Heil, A., Kainuma, M., Klimont, Z., Lee, D., Liousse, C., Mieville, A., Riahi, K., Schultz, M., Stevenson, D., Van Aardenne, J. & van Vuuren, D. (2009). RCP Database (Version 2.0.5): Historical emissions data (1850 - 2000), International Institute for Applied Systems Analysis,. *In:* International Institute for Applied Systems Analysis (ed.) *RCP Database.*

Lamarque, J. F., Bond, T. C., Eyring, V., Granier, C., Heil, A., Klimont, Z., Lee, D., Liousse, C., Mieville, A., Owen, B., Schultz, M. G., Shindell, D., Smith, S. J., Stehfest, E., Van Aardenne, J., Cooper, O. R., Kainuma, M., Mahowald, N., McConnell, J. R., Naik, V., Riahi, K. & van Vuuren, D. P. (2010a). ACCMIP Emissions for Atmospheric Chemistry and Climate Model Intercomparison Project dataset: Data between year 1850 and 2000. *In:* National Center for Atmospheric Research (NCAR) (ed.). ECCAD-GEIA.

Lamarque, J. F., Bond, T. C., Eyring, V., Granier, C., Heil, A., Klimont, Z., Lee, D., Liousse, C., Mieville, A., Owen, B., Schultz, M. G., Shindell, D., Smith, S. J., Stehfest, E., Van Aardenne, J., Cooper, O. R., Kainuma, M., Mahowald, N., McConnell, J. R., Naik, V., Riahi, K. & van Vuuren, D. P. (2010b). Historical (1850–2000) gridded anthropogenic and biomass burning emissions of reactive gases and aerosols: methodology and application. *Atmos. Chem. Phys.,* **10**, 7017-7039.

Lamarque, J. F., Dentener, F., McConnell, J., Ro, C. U., Shaw, M., Vet, R., Bergmann, D., Cameron-Smith, P., Dalsoren, S., Doherty, R., Faluvegi, G., Ghan, S. J., Josse, B., Lee, Y. H., MacKenzie, I. A., Plummer, D., Shindell, D. T., Skeie, R. B., Stevenson, D. S., Strode, S., Zeng, G., Curran, M., Dahl-Jensen, D., Das, S., Fritzsche, D. & Nolan, M. (2013a). Multi-model mean nitrogen and sulfur deposition from the Atmospheric Chemistry and Climate Model Intercomparison Project (ACCMIP): evaluation of historical and projected future changes. *Atmos. Chem. Phys.,* **13**, 7997-8018.

Lamarque, J. F., Hess, P., Emmons, L., Buja, L., Washington, W. & Granier, C. (2005). Tropospheric ozone evolution between 1890 and 1990. *Journal of Geophysical Research: Atmospheres,* **110**, n/a-n/a.

Lamarque, J. F., Shindell, D. T., Josse, B., Young, P. J., Cionni, I., Eyring, V., Bergmann, D., Cameron-Smith, P., Collins, W. J., Doherty, R., Dalsoren, S., Faluvegi, G., Folberth, G., Ghan, S. J., Horowitz, L. W., Lee, Y. H., MacKenzie, I. A., Nagashima, T., Naik, V., Plummer, D., Righi, M., Rumbold, S. T., Schulz, M., Skeie, R. B., Stevenson, D. S., Strode, S., Sudo, K., Szopa, S., Voulgarakis, A. & Zeng, G. (2013b). The Atmospheric Chemistry and Climate Model Intercomparison Project (ACCMIP): overview and description of models, simulations and climate diagnostics. *Geosci. Model Dev.,* **6**, 179-206.

Lamb, D. & Verlinde, J. (2011). *Physics and Chemistry of Clouds.* Cambridge, United Kingdom and New York, NY, USA: Cambridge University Press.

Lee, D. S., B, B. O., Graham, A., Fichter, C., Lim, L. L. & Dimitriu, D. (2005). Allocation of International Aviation Emissions from Scheduled Air Traffic – Present day and Historical (Report 2 of 3). Manchester Metropolitan University.

Lee, D. S., Fahey, D. W., Forster, P. M., Newton, P. J., Wit, R. C. N., Lim, L. L., Owen, B. & Sausen, R. (2009). Aviation and global climate change in the 21st century. *Atmospheric Environment,* **43**, 3520-3537.

Lee, D. S., Pitari, G., Grewe, V., Gierens, K., Penner, J. E., Petzold, A., Prather, M. J., Schumann, U., Bais, A., Berntsen, T., Iachetti, D., Lim, L. L. & Sausen, R. (2010). Transport impacts on atmosphere and climate: Aviation. *Atmospheric Environment,* **44**, 4678-4734.

Lee, H., Olsen, S. C., Wuebbles, D. J. & Youn, D. (2013). Impacts of aircraft emissions on the air quality near the ground. *Atmos. Chem. Phys.,* **13**, 5505-5522.

Leifsson, L., Ko, A., Mason, W. H., Schetz, J. A., Grossman, B. & Haftka, R. T. (2013). Multidisciplinary design optimization of blended-wing-body transport aircraft with distributed propulsion. *Aerospace Science and Technology,* **25**, 16-28.

Lesins, G., Chylek, P. & Lohmann, U. (2002). A study of internal and external mixing scenarios and its effect on aerosol optical properties and direct radiative forcing. *Journal of Geophysical Research: Atmospheres,* **107**, AAC 5-1-AAC 5-12.

Levy, J. I., Woody, M., Baek, B. H., Shankar, U. & Arunachalam, S. (2012). Current and Future Particulate-Matter-Related Mortality Risks in the United States from Aviation Emissions During Landing and Takeoff. *Risk Analysis,* **32**, 237-249.

Li, H. (2011). Unpublished lecture notes: Fuel Systems and Fuels. *PEME 2140: Aircraft Engines.* University of Leeds.

Lightfoot, P. D., Cox, R. A., Crowley, J. N., Destriau, M., Hayman, G. D., Jenkin, M. E., Moortgat, G. K. & Zabel, F. (1992). Organic peroxy radicals: Kinetics, spectroscopy and tropospheric chemistry. *Atmospheric Environment. Part A. General Topics,* **26**, 1805-1961.

Lim, S. S., Vos, T., Flaxman, A. D., Danaei, G., Shibuya, K., Adair-Rohani, H., AlMazroa, M. A., Amann, M., Anderson, H. R., Andrews, K. G., Aryee, M., Atkinson, C., Bacchus, L. J., Bahalim, A. N., Balakrishnan, K., Balmes, J., Barker-Collo, S., Baxter, A., Bell, M. L., Blore, J. D., Blyth, F., Bonner, C., Borges, G., Bourne, R., Boussinesq, M., Brauer, M., Brooks, P., Bruce, N. G., Brunekreef, B., Bryan-Hancock, C., Bucello, C., Buchbinder, R., Bull, F., Burnett, R. T., Byers, T. E., Calabria, B., Carapetis, J., Carnahan, E., Chafe, Z., Charlson, F., Chen, H., Chen, J. S., Cheng, A. T.-A., Child, J. C., Cohen, A., Colson, K. E., Cowie, B. C., Darby, S., Darling, S., Davis, A., Degenhardt, L., Dentener, F., Des Jarlais, D. C., Devries, K., Dherani, M., Ding, E. L., Dorsey, E. R., Driscoll, T., Edmond, K., Ali, S. E., Engell, R. E., Erwin, P. J., Fahimi, S., Falder, G., Farzadfar, F., Ferrari, A., Finucane, M. M., Flaxman, S., Fowkes, F. G. R., Freedman, G., Freeman, M. K., Gakidou, E., Ghosh, S., Giovannucci, E., Gmel, G., Graham, K., Grainger, R., Grant, B., Gunnell, D., Gutierrez, H. R., Hall, W., Hoek, H. W., Hogan, A., Hosgood Iii, H. D., Hoy, D., Hu, H., Hubbell, B. J., Hutchings, S. J., Ibeanusi, S. E., Jacklyn, G. L., Jasrasaria, R., Jonas, J. B., Kan, H., Kanis, J. A., Kassebaum, N., Kawakami, N., Khang, Y.-H., Khatibzadeh, S., Khoo, J.-P., Kok, C., et al. (2012). A comparative risk assessment of burden of disease and injury attributable to 67 risk factors and risk factor clusters in 21 regions, 1990–2010: a systematic analysis for the Global Burden of Disease Study 2010. *The Lancet,* **380**, 2224-2260.

Lobo, P., Hagen, D. E. & Whitefield, P. D. (2011). Comparison of PM Emissions from a Commercial Jet Engine Burning Conventional, Biomass, and Fischer–Tropsch Fuels. *Environmental Science & Technology,* **45**, 10744-10749.

Lomas, D. A., Silverman, E. K., Edwards, L. D., Miller, B. E., Coxson, H. O. & Tal-Singer, R. (2008). Evaluation of serum CC-16 as a biomarker for COPD in the ECLIPSE cohort. *Thorax,* **63**, 1058-1063.

Löndahl, J., Pagels, J., Swietlicki, E., Zhou, J., Ketzel, M., Massling, A. & Bohgard, M. (2006). A set-up for field studies of respiratory tract deposition of fine and ultrafine particles in humans. *Journal of Aerosol Science,* **37**, 1152-1163.

Lund, M. T., Berntsen, T. K., Heyes, C., Klimont, Z. & Samset, B. H. (2014). Global and regional climate impacts of black carbon and co-emitted species from the on-road diesel sector. *Atmospheric Environment,* **98**, 50-58.

Mahadevan, R. & Asafu-Adjaye, J. (2007). Energy consumption, economic growth and prices: A reassessment using panel VECM for developed and developing countries. *Energy Policy,* **35**, 2481-2490.

Mahashabde, A., Wolfe, P., Ashok, A., Dorbian, C., He, Q., Fan, A., Lukachko, S., Mozdzanowska, A., Wollersheim, C., Barrett, S. R. H., Locke, M. & Waitz, I. A. (2011). Assessing the environmental impacts of aircraft noise and emissions. *Progress in Aerospace Sciences,* **47**, 15-52.

Manktelow, P. T., Carslaw, K. S., Mann, G. W. & Spracklen, D. V. (2009). Variable CCN formation potential of regional sulfur emissions. *Atmos. Chem. Phys.,* **9**, 3253-3259.

Mann, G. W. (29/10/2015 2015). *RE: Chemistry in the nitrate version of GLOMAP.* Type to Kapadia, Z. Z.

Mann, G. W., Carslaw, K. S., Ridley, D. A., Spracklen, D. V., Pringle, K. J., Merikanto, J., Korhonen, H., Schwarz, J. P., Lee, L. A., Manktelow, P. T., Woodhouse, M. T., Schmidt, A., Breider, T. J., Emmerson, K. M., Reddington, C. L., Chipperfield, M. P. & Pickering, S. J. (2012). Intercomparison of modal and sectional aerosol microphysics representations within the same 3-D global chemical transport model. *Atmos. Chem. Phys.,* **12**, 4449-4476.

Mann, G. W., Carslaw, K. S., Spracklen, D. V., Ridley, D. A., Manktelow, P. T., Chipperfield, M. P., Pickering, S. J. & Johnson, C. E. (2010). Description and evaluation of GLOMAP-mode: a modal global aerosol microphysics model for the UKCA composition-climate model. *Geoscientific Model Development,* **3**, 519-551.

Maria, S. F., Russell, L. M., Turpin, B. J. & Porcja, R. J. (2002). FTIR measurements of functional groups and organic mass in aerosol samples over the Caribbean. *Atmospheric Environment,* **36**, 5185-5196.

Mathers, C., Boerma, T. & Fat, D. M. (2008). *The Global Burden of Disease: 2004 Update.* Geneva, Switzerland: WHO Press.

Mathews, J. A. (2010). Designing Energy Industries for the Next Industrial Revolution. *Organizational Dynamics,* **39**, 155-164.

Maurice, L. Q., Lander, H., Edwards, T. & Harrison Iii, W. E. (2001). Advanced aviation fuels: a look ahead via a historical perspective. *Fuel,* **80**, 747-756.

Mawhood, R., Cobas, A. R. & Slade, R. (2014). Establishing a European renewable jet fuel supply chain: the technoeconomic potential of biomass conversion technologies. *Biojet fuel supply Chain Development and Flight Operations (Renjet), .* Imperial College London, European Institute of Innovation and Technology (EIT) – Climate-KIC.

Mayewski, P. A., Meredith, M. P., Summerhayes, C. P., Turner, J., Worby, A., Barrett, P. J., Casassa, G., Bertler, N. A. N., Bracegirdle, T., Naveira Garabato, A. C., Bromwich, D., Campbell, H., Hamilton, G. S., Lyons, W. B., Maasch, K. A., Aoki, S., Xiao, C. & van Ommen, T. (2009). State of the Antarctic and Southern Ocean climate system. *Reviews of Geophysics,* **47**, n/a-n/a.

McCulloch, T. B. (1946). *Aviation Fuel*. United States patent application US53978344A.

Meehl, G. A., Stocker, T. F., Collins, W. D., Friedlingstein, P., Gaye, A. T., Gregory, J. M., Kitoh, A., Knutti, R., Murphy, J. M., Noda, A., Raper, S. C. B., Watterson, I. G., Weaver, A. J. & Zhao, Z.-C. (2007). Global Climate Projections (Chapter 10). *In:* Change, I. P. o. C. (ed.) *Climate Change 2007: The Physical Science Basis. Contribution of Working Group I to the Fourth Assessment Report of the Intergovernmental Panel on Climate Change.*

Meilinger, S. K., Kärcher, B., von Kuhlmann, R. & Peter, T. (2001). On the impact of heterogeneous chemistry on ozone in the tropopause region. *Geophys. Res. Lett.,* **28**, 515-518.

Melero, J. A., Iglesias, J. & Garcia, A. (2012). Biomass as renewable feedstock in standard refinery units. Feasibility, opportunities and challenges. *Energy & Environmental Science,* **5**, 7393-7420.

Ministry of Defence (2011). Defence Standard 91-91. Turbine Fuel, Kerosine Type, Jet A-1. NATO Code: F-35. Joint Service Designation: AVTUR. *Defence Standard.* 18/02/2011 ed. Glasgow, United Kingdon.

Molina, M. J. & Molina, L. T. (2004). Megacities and atmospheric pollution. *Journal of the Air & Waste Management Association,* **54**, 644-680.

Morita, H., Yang, S., Unger, N. & Kinney, P. L. (2014). Global Health Impacts of Future Aviation Emissions Under Alternative Control Scenarios. *Environmental Science & Technology,* **48**, 14659-14667.

Murphy, J. G., Oram, D. E. & Reeves, C. E. (2010). Measurements of volatile organic compounds over West Africa. *Atmos. Chem. Phys.,* **10**, 5281-5294.

Myhre, G., Grini, A. & Metzger, S. (2006). Modelling of nitrate and ammonium-containing aerosols in presence of sea salt. *Atmos. Chem. Phys.,* **6**, 4809-4821.

Myhre, G., Shindell, D., Bréon, F.-M., Collins, W., Fuglestvedt, J., Huang, J., Koch, D., Lamarque, J.-F., Lee, D., Mendoza, B., Nakajima, T., Robock, A., Stephens, G., Takemura, T. & Zhang, H. (2013). Anthropogenic and Natural Radiative Foorcing (Chapter 8). *In:* Stocker, T. F., Qin, D., Plattner, G.-K., Tignor, M. M. B., Allen, S. K., Boschung, J., Nauels, A., Xia, Y., Bex, V. & Midgley, P. M. (eds.) *Climate Change 2013: The Physical Science Basis. Contribution of Working Group I to the Fifth Assessment Report of the Intergovernmental Panel on Climate Change (IPCC).*

Myhre, G., Shine, K. P., Rädel, G., Gauss, M., Isaksen, I. S. A., Tang, Q., Prather, M. J., Williams, J. E., van Velthoven, P., Dessens, O., Koffi, B., Szopa, S., Hoor, P., Grewe, V., Borken-Kleefeld, J., Berntsen, T. K. & Fuglestvedt, J. S. (2011). Radiative forcing due to changes in ozone and methane caused by the transport sector. *Atmospheric Environment,* **45**, 387-394.

Nasir, R. E. M., Kuntjoro, W. & Wisnoe, W. (2014). Aerodynamic, Stability and Flying Quality Evaluation on a Small Blended Wing-body Aircraft with Canard Foreplanes. *Procedia Technology,* **15**, 784-792.

Nenes, A. & Seinfeld, J. H. (2003). Parameterization of cloud droplet formation in global climate models. *Journal of Geophysical Research: Atmospheres,* **108**, 4415.

NOAA. (August 2015). *Trends in Atmospheric Carbon Dioxide: Recent Mauna Loa CO_2 - November 2015*. URL: http://www.esrl.noaa.gov/gmd/ccgg/trends/ [03/11/2015].

Olivié, D. J. L., Cariolle, D., Teyssèdre, H., Salas, D., Voldoire, A., Clark, H., Saint-Martin, D., Michou, M., Karcher, F., Balkanski, Y., Gauss, M., Dessens, O., Koffi, B. & Sausen, R. (2012). Modeling the climate impact of road transport, maritime shipping and aviation over the period 1860–2100 with an AOGCM. *Atmos. Chem. Phys.,* **12**, 1449-1480.

Olsen, S. C., Brasseur, G. P., Wuebbles, D. J., Barrett, S. R. H., Dang, H., Eastham, S. D., Jacobson, M. Z., Khodayari, A., Selkirk, H., Sokolov, A. & Unger, N. (2013a). Comparison of model estimates of the effects of aviation emissions on atmospheric ozone and methane. *Geophysical Research Letters,* **40**, 6004-6009.

Olsen, S. C., Wuebbles, D. J. & Owen, B. (2013b). Comparison of global 3-D aviation emissions datasets. *Atmos. Chem. Phys.,* **13**, 429-441.

Ordoukhanian, E. & Madni, A. M. (2014). Blended Wing Body Architecting and Design: Current Status and Future Prospects. *Procedia Computer Science,* **28**, 619-625.

Ostro, B. D. (2004). Outdoor air pollution: Assessing the environmental burden of disease at national and local levels. *In:* Pruss-Üstun, A., Campbell-Lendrum, D., Corvalán, C. & Woodward, A. (eds.) *WHO Environmental Burden of Disease Series.*

Ostro, B. D. & Rothschild, S. (1989). Air pollution and acute respiratory morbidity: An observational study of multiple pollutants. *Environmental Research,* **50**, 238-247.

Owen, B., Lee, D. S. & Lim, L. (2010). Flying into the Future: Aviation Emissions Scenarios to 2050. *Environmental Science & Technology,* **44**, 2255-2260.

P. Lemke, J. Ren, R.B. Alley, I. Allison, J. Carrasco, G. Flato, Y. Fujii, G. Kaser, P. Mote, R.H. Thomas & Zhang, T. (2007). Observations, Changes in Snow, Ice and Frozen Ground (Chapter 4). *In:* Change, I. P. o. C. (ed.) *Climate Change 2007: The Physical Science Basis. Contribution of Working Group I to the Fourth Assessment Report of the Intergovernmental Panel on Climate Change.* Cambridge University Press, Cambridge, United Kingdom and New York, NY, USA.

Patra, P. K., Krol, M. C., Montzka, S. A., Arnold, T., Atlas, E. L., Lintner, B. R., Stephens, B. B., Xiang, B., Elkins, J. W., Fraser, P. J., Ghosh, A., Hintsa, E. J., Hurst, D. F., Ishijima, K., Krummel, P. B., Miller, B. R., Miyazaki, K., Moore, F. L., Muhle, J., O/'Doherty, S., Prinn, R. G., Steele, L. P., Takigawa, M., Wang, H. J., Weiss, R. F., Wofsy, S. C. & Young, D. (2014). Observational evidence for interhemispheric hydroxyl-radical parity. *Nature,* **513**, 219-223.

Peng, Y., Lohmann, U. & Leaitch, R. (2005). Importance of vertical velocity variations in the cloud droplet nucleation process of marine stratus clouds. *Journal of Geophysical Research: Atmospheres,* **110**, D21213.

Penner, J. E., Lister, D. H., Griggs, D. J., Dokken, D. J. & McFarland, M. (1999). IPCC Special Report: Aviation and the Global Atmosphere - Summary for Policymakers. *In:* Intergovernmental Panel on Climate Change (ed.) *IPCC Special Report: Aviation and the Global Atmosphere.*

Petters, M. D. & Kreidenweis, S. M. (2007). A single parameter representation of hygroscopic growth and cloud condensation nucleus activity. *Atmos. Chem. Phys.,* **7**, 1961-1971.

Pincus, R. & Baker, M. B. (1994). Effect of precipitation on the albedo susceptibility of clouds in the marine boundary layer. *Nature,* **372**, 250-252.

Pitari, G., Mancini, E. & Bregman, A. (2002). Climate forcing of subsonic aviation: Indirect role of sulfate particles via heterogeneous chemistry. *Geophys. Res. Lett.,* **29**, 2057.

Poberaj, C. S., Bintania, R., Velthoven, P. v., Dessens, O., Gauss, M., Isaksen, I. S. A., Grewe, V., Jöckel, P., Hoor, P., Koffi, B., Hauglustaine, D. & Olivié, D. (2010). QUANTIFY model evaluation of global chemistry models: carbon monoxide. *DLR Deutsches Zentrum fur Luft- und Raumfahrt e.V. - Forschungsberichte*, 163-168.

Pope, C. A., Burnett, R. T., Thun, M. J., Calle, E. E., Krewski, D., Ito, K. & Thurston, G. D. (2002). Lung Cancer, Cardiopulmonary Mortality, and Long-term Exposure to Fine Particulate Air Pollution. *JAMA,* **287**, 1132-1141.

Pope, C. A., Burnett, R. T., Thurston, G. D., Thun, M. J., Calle, E. E., Krewski, D. & Godleski, J. J. (2004). Cardiovascular Mortality and Long-Term Exposure to Particulate Air Pollution: Epidemiological Evidence of General Pathophysiological Pathways of Disease. *Circulation,* **109**, 71-77.

Pope, C. A. & Dockery, D. W. (2006). Health effects of fine particulate air pollution: lines that connect. *Journal of the Air & Waste Management Association,* **56**, 709-742.

Pope, C. A., Thun, M. J., Namboodiri, M. M., Dockery, D. W., Evans, J. S., Speizer, F. E. & Heath, C. W. (1995). Particulate air pollution as a predictor of mortality in a prospective study of U.S. adults. *American Journal of Respiratory and Critical Care Medicine,* **151**, 669-674.

Prather, M. J. (1986). Numerical advection by conservation of second-order moments. *Journal of Geophysical Research: Atmospheres,* **91**, 6671-6681.

Preston, H., Lee, D. S. & Hooper, P. D. (2012). The inclusion of the aviation sector within the European Union's Emissions Trading Scheme: What are the prospects for a more sustainable aviation industry? *Environmental Development,* **2**, 48-56.

Pringle, K. J. (2006). *Aerosol-cloud interactions in a global model of aerosol microphysics.* PhD, University of Leeds.

Pringle, K. J., Carslaw, K. S., Fan, T., Mann, G. W., Hill, A., Stier, P., Zhang, K. & Tost, H. (2012). A multi-model assessment of the impact of sea spray geoengineering on cloud droplet number. *Atmos. Chem. Phys.,* **12**, 11647-11663.

Prins, M. J., Ptasinski, K. J. & Janssen, F. J. J. G. (2005). Exergetic optimisation of a production process of Fischer–Tropsch fuels from biomass. *Fuel Processing Technology,* **86**, 375-389.

Quantify Integrated Project. (2005-2012). *EU FP6 Integrated Project QUANTIFY. Quantifying the Climate Impact of Global and European Transport Systems: QUANTIFY emission inventories and scenarios*. URL: http://www.pa.op.dlr.de/quantify/ [15/07/2011].

Ramaswamy, V., Boucher, O., Haigh, J., Hauglustaine, D., Haywood, J., Myhre, G., Nakajima, T., Shi, G. Y., Solomon, S., Betts, R., Charlson, R., Chuang, C., Daniel, J. S., Genio, A. D., Dorland, R. v., Feichter, J., J. Fuglestvedt, Forster, P. M. d. F., Ghan, S. J., Jones, A., Kiehl, J. T., Koch, D., Land, C., Lean, J., U. Lohmann, Minschwaner, K., Penner, J. E., Roberts, D. L., Rodhe, H., Roelofs, G. J., Rotstayn, L. D., Schneider, T. L., Schumann, U., Schwartz, S. E., Schwarzkopf, M. D., Shine, K. P., Smith, S., Stevenson, D. S., F. Stordal, Tegen, I. & Zhang, Y. (2007). Radiative Forcing of Climate Change (Chapter 6). *In:* Houghton, J. T., Ding, Y., Griggs, D. J., Noguer, M., Linden, P. J. v. d., Dai, X., Maskell, K. & Johnson, C. A. (eds.) *Climate Change 2001: The Scientific Basis. Contribution of Working Group I to the Third Assessment Report of the Intergovernmental Panel on Climate Change.*

Rap, A., Forster, P. M., Jones, A., Boucher, O., Haywood, J. M., Bellouin, N. & De Leon, R. R. (2010). Parameterization of contrails in the UK Met Office Climate Model. *J. Geophys. Res.,* **115**, D10205.

Rap, A., Richards, N. A. D., Forster, P. M., Monks, S. A., Arnold, S. R. & Chipperfield, M. P. (2015). Satellite constraint on the tropospheric ozone radiative effect. *Geophysical Research Letters,* **42**, 2015GL064037.

Rap, A., Scott, C. E., Spracklen, D. V., Bellouin, N., Forster, P. M., Carslaw, K. S., Schmidt, A. & Mann, G. (2013). Natural aerosol direct and indirect radiative effects. *Geophysical Research Letters,* **40**, 3297-3301.

Ratliff, G., Sequeira, C., Waitz, I., Ohsfeldt, M., Thrasher, T., Graham, M. & Thompson, T. (2009). Aircraft Impacts on Local and Regional Air Quality in the United States. *PARTNER Project 15 final report.* Massachusetts Institute of Technology.

Reeves, C. E., Formenti, P., Afif, C., Ancellet, G., Attié, J. L., Bechara, J., Borbon, A., Cairo, F., Coe, H., Crumeyrolle, S., Fierli, F., Flamant, C., Gomes, L., Hamburger, T., Jambert, C., Law, K. S., Mari, C., Jones, R. L., Matsuki, A., Mead, M. I., Methven, J., Mills, G. P., Minikin, A., Murphy, J. G., Nielsen, J. K., Oram, D. E., Parker, D. J., Richter, A., Schlager, H., Schwarzenboeck, A. & Thouret, V. (2010). Chemical and aerosol characterisation of the troposphere over West Africa during the monsoon period as part of AMMA. *Atmos. Chem. Phys.,* **10**, 7575-7601.

Renewable Jet Fuels. (Undated). *Biofuels 101: Renewable Jet Fuels*. URL: http://renewablejetfuels.org/what-we-do/biofuels-101.

Rhein, M., Rintoul, S. R., Aoki, S., Campos, E., Chambers, D., Feely, R. A., Gulev, S., Johnson, G. C., Josey, S. A., Kostianoy, A., Mauritzen, C., Roemmich, D., Talley, L. D. & Wang, F. (2013). Observations: Oceans (Chapter 3). *In:* Stocker, T. F., Qin, D., Plattner, G.-K., Tignor, M., Allen, S. K., Boschung, J., Nauels, A., Xia, Y., Bex, V. & Midgley, P. M. (eds.) *Climate Change 2013: The Physical Science Basis. Contribution of Working Group I to the Fifth Assessment Report of the Intergovernmental Panel on Climate Change (IPCC).* Cambridge, United Kingdom and New York, NY, USA.

Richards, N. A. D., Arnold, S. R., Chipperfield, M. P., Miles, G., Rap, A., Siddans, R., Monks, S. A. & Hollaway, M. J. (2013). The Mediterranean summertime ozone maximum: global emission sensitivities and radiative impacts. *Atmos. Chem. Phys.,* **13**, 2331-2345.

Righi, M., Hendricks, J. & Sausen, R. (2013). The global impact of the transport sectors on atmospheric aerosol: simulations for year 2000 emissions. *Atmos. Chem. Phys.,* **13**, 9939-9970.

Roets, P., Botha, J. J. J., Moses, C. A. & Stavinoha, L. L. (1997). Stability and handling of SASOL semi-synthetic jet fuel. *6th International Conference on Stability and Handling of Liquid*

Fuels, . Vancouver, B. C., Canada: International Association for Stability, Handling and Use of Liquid Fuels (IASH).

Rogner, H.-H. & Zhou, D. (2007). Climate Change 2007. Chapter 1: Introduction. *In:* Intergovernmental Panel on Climate Change (IPCC) (ed.) *Climate Change 2007: Mitigation of Climate Change. Contribution of Working Group III to the Fourth Assessment Report of the Intergovernmental Panel on Climate Change.*

Rossow, W. B. & Schiffer, R. A. (1999). Advances in Understanding Clouds from ISCCP. *Bulletin of the American Meteorological Society,* **80**, 2261-2287.

Royal Society (2008). *Ground-level Ozone in the 21st Century: Future Trends, Impacts and Policy Implications.* Royal Society.

Russell, L. M. (2003). Aerosol Organic-Mass-to-Organic-Carbon Ratio Measurements. *Environmental Science & Technology,* **37**, 2982-2987.

S. Solomon, D. Qin, M. Manning, R.B. Alley, T. Berntsen, N.L. Bindoff, Z. Chen, A. Chidthaisong, J.M. Gregory, G.C. Hegerl, M. Heimann, B. Hewitson, B.J. Hoskins, F. Joos, J. Jouzel, V. Kattsov, U. Lohmann, T. Matsuno, M. Molina, N. Nicholls, J. Overpeck, G. Raga, V. Ramaswamy, J. Ren, M. Rusticucci, R. Somerville, T.F. Stocker, P. Whetton, Wood, R. A. & D. Wratt (2007). Technical Summary. *In:* Intergovernmental Panel on Climate Change (ed.) *Climate Change 2007: The Physical Science Basis. Contribution of Working Group I to the Fourth Assessment Report of the Intergovernmental Panel on Climate Change.*

Samset, B. H. & Myhre, G. (2011). Vertical dependence of black carbon, sulphate and biomass burning aerosol radiative forcing. *Geophysical Research Letters,* **38**, L24802.

Saunders, S. M., Jenkin, M. E., Derwent, R. G. & Pilling, M. J. (2003). Protocol for the development of the Master Chemical Mechanism, MCM v3 (Part A): tropospheric degradation of non-aromatic volatile organic compounds. *Atmos. Chem. Phys.,* **3**, 161-180.

Sausen, R. (2002). Expression of Interest for an Integrated Project QUANTIFY: Quantifying the Climate Impact Of Global and European Transport Systems. *In:* Deutsches Zentrum für Luft- und Raumfahrt (DLR) (ed.).

Sausen, R., Isaksen, I., Grewe, V., Hauglustaine, D., Lee, D. S., Myhre, G., Köhler, M. O., Pitari, G., Schumann, U., Stordal, F. & Zerefos, C. (2005). Aviation radiative forcing in 2000: An update on IPCC (1999). *Meteorologische Zeitschrift,* **14**, 555-561.

Schmidt, A., Carslaw, K. S., Mann, G. W., Rap, A., Pringle, K. J., Spracklen, D. V., Wilson, M. & Forster, P. M. (2012). Importance of tropospheric volcanic aerosol for indirect radiative forcing of climate. *Atmos. Chem. Phys.,* **12**, 7321-7339.

Schmidt, A., Ostro, B., Carslaw, K. S., Wilson, M., Thordarson, T., Mann, G. W. & Simmons, A. J. (2011). Excess mortality in Europe following a future Laki-style Icelandic eruption. *Proceedings of the National Academy of Sciences,* **108**, 15710-15715.

Schumann, U. (2005). Formation, properties and climatic effects of contrails. *Comptes Rendus Physique,* **6**, 549-565.

Schumann, U., Arnold, F., Busen, R., Curtius, J., Kärcher, B., Kiendler, A., Petzold, A., Schlager, H., Schröder, F. & Wohlfrom, K. H. (2002). Influence of fuel sulfur on the composition of aircraft exhaust plumes: The experiments SULFUR 1–7. *Journal of Geophysical Research: Atmospheres,* **107**, AAC 2-1-AAC 2-27.

Scott, C. E. (2013). *The Biogeochemical Impacts of Forests and the Implications for Climate Change Mitigation.* PhD, University of Leeds.

Scott, C. E., Rap, A., Spracklen, D. V., Forster, P. M., Carslaw, K. S., Mann, G. W., Pringle, K. J., Kivekäs, N., Kulmala, M., Lihavainen, H. & Tunved, P. (2014). The direct and indirect radiative effects of biogenic secondary organic aerosol. *Atmos. Chem. Phys.,* **14**, 447-470.

Seinfeld, J. H. & Pandis, S. N. (2006). *Atmospheric chemistry and physics: from air pollution to climate change.* Wiley.

Sekhon, R. S. & Srivastava, R. C. (1971). Doppler Radar Observations of Drop-Size Distributions in a Thunderstorm. *Journal of the Atmospheric Sciences,* **28**, 983-994.

Shirley, T. R., Brune, W. H., Ren, X., Mao, J., Lesher, R., Cardenas, B., Volkamer, R., Molina, L. T., Molina, M. J., Lamb, B., Velasco, E., Jobson, T. & Alexander, M. (2006). Atmospheric oxidation in the Mexico City Metropolitan Area (MCMA) during April 2003. *Atmos. Chem. Phys.,* **6**, 2753-2765.

Singh, H. B., Anderson, B. E., Brune, W. H., Cai, C., Cohen, R. C., Crawford, J. H., Cubison, M. J., Czech, E. P., Emmons, L., Fuelberg, H. E., Huey, G., Jacob, D. J., Jimenez, J. L., Kaduwela, A., Kondo, Y., Mao, J., Olson, J. R., Sachse, G. W., Vay, S. A., Weinheimer, A., Wennberg, P. O. & Wisthaler, A. (2010). Pollution influences on atmospheric composition and chemistry at high northern latitudes: Boreal and California forest fire emissions. *Atmospheric Environment,* **44**, 4553-4564.

Singh, H. B., O'Hara, D., Herlth, D., Bradshaw, J. D., Sandholm, S. T., Gregory, G. L., Sachse, G. W., Blake, D. R., Crutzen, P. J. & Kanakidou, M. A. (1992). Atmospheric measurements of peroxyacetyl nitrate and other organic nitrates at high latitudes: Possible sources and sinks. *Journal of Geophysical Research: Atmospheres,* **97**, 16511-16522.

Skowron, A., Lee, D. S. & De León, R. R. (2013). The assessment of the impact of aviation NOx on ozone and other radiative forcing responses – The importance of representing cruise altitudes accurately. *Atmospheric Environment,* **74**, 159-168.

Slinn, W. G. N. (1982). Predictions for particle deposition to vegetative canopies. *Atmospheric Environment (1967),* **16**, 1785-1794.

Snijders, T. A. & Melkers, J. A. (2011). Effect of cruise altitude and alternative aviation fuels on radiative forcing. TU Delft.

SOLENA Fuels. (Year). An Introduction to Solena Fuels Corporation. *In:* World Waste to Energy City Summit, May 19-20 2015 2015 London, UK.

Søvde, O. A., Hoyle, C. R., Myhre, G. & Isaksen, I. S. A. (2011). The HNO3 forming branch of the HO2 + NO reaction: pre-industrial-to-present trends in atmospheric species and radiative forcings. *Atmos. Chem. Phys.,* **11**, 8929-8943.

Søvde, O. A., Matthes, S., Skowron, A., Iachetti, D., Lim, L., Owen, B., Hodnebrog, Ø., Di Genova, G., Pitari, G., Lee, D. S., Myhre, G. & Isaksen, I. S. A. (2014). Aircraft emission mitigation by changing route altitude: A multi-model estimate of aircraft NOx emission impact on O3 photochemistry. *Atmospheric Environment,* **95**, 468-479.

Spicer, C. W., Holdren, M. W., Riggin, R. M. & Lyon, T. F. (1994). Chemical composition and photochemical reactivity of exhaust from aircraft turbine engines. *Ann. Geophys.,* **12**, 944-955.

Spracklen, D. V. (2005). *Development and application of a Global Model of Aerosol Processes.* PhD, University of Leeds.

Spracklen, D. V., Bonn, B. & Carslaw, K. S. (2008a). Boreal forests, aerosols and the impacts on clouds and climate. *Philosophical Transactions of the Royal Society A: Mathematical, Physical and Engineering Sciences,* **366**, 4613-4626.

Spracklen, D. V., Carslaw, K. S., Kulmala, M., Kerminen, V.-M., Sihto, S.-L., Riipinen, I., Merikanto, J., Mann, G. W., Chipperfield, M. P., Wiedensohler, A., Birmili, W. & Lihavainen, H. (2008b). Contribution of particle formation to global cloud condensation nuclei concentrations. *Geophysical Research Letters,* **35**, n/a-n/a.

Spracklen, D. V., Carslaw, K. S., Pöschl, U., Rap, A. & Forster, P. M. (2011a). Global cloud condensation nuclei influenced by carbonaceous combustion aerosol. *Atmos. Chem. Phys.,* **11**, 9067-9087.

Spracklen, D. V., Jimenez, J. L., Carslaw, K. S., Worsnop, D. R., Evans, M. J., Mann, G. W., Zhang, Q., Canagaratna, M. R., Allan, J., Coe, H., McFiggans, G., Rap, A. & Forster, P. (2011b). Aerosol mass spectrometer constraint on the global secondary organic aerosol budget. *Atmos. Chem. Phys.,* **11**, 12109-12136.

Spracklen, D. V., Pringle, K. J., Carslaw, K. S., Chipperfield, M. P. & Mann, G. W. (2005a). A global off-line model of size-resolved aerosol microphysics: I. Model development and prediction of aerosol properties. *Atmospheric Chemistry and Physics,* **5**, 2227-2252.

Spracklen, D. V., Pringle, K. J., Carslaw, K. S., Chipperfield, M. P. & Mann, G. W. (2005b). A global off-line model of size-resolved aerosol microphysics: II. Identification of key uncertainties. *Atmos. Chem. Phys.,* **5**, 3233-3250.

Stern, N. (2006). *The Stern Review: The Economics of Climate Change. Executive Summary*. URL: http://webarchive.nationalarchives.gov.uk/+/http://www.hm-treasury.gov.uk/stern_review_report.htm [11/03/2011].

Stern, N. (2015). *Why Are We Waiting? The Logic, Urgency, and Promise of Tackling Climate Change.* United States of America: MIT Press.

Stettler, M. E. J., Boies, A. M., Petzold, A. & Barrett, S. R. H. (2013). Global Civil Aviation Black Carbon Emissions. *Environmental Science & Technology,* **47**, 10397-10404.

Stevenson, D. S. & Derwent, R. G. (2009). Does the location of aircraft nitrogen oxide emissions affect their climate impact? *Geophysical Research Letters,* **36**, L17810.

Stevenson, D. S., Doherty, R. M., Sanderson, M. G., Collins, W. J., Johnson, C. E. & Derwent, R. G. (2004). Radiative forcing from aircraft NOx emissions: Mechanisms and seasonal dependence. *Journal of Geophysical Research: Atmospheres,* **109**, D17307.

Stevenson, D. S., Johnson, C. E., Collins, W. J. & Derwent, R. G. (2003). The tropospheric sulphur cycle and the role of volcanic SO2. *Geological Society, London, Special Publications,* **213**, 295-305.

Stevenson, D. S., Young, P. J., Naik, V., Lamarque, J. F., Shindell, D. T., Voulgarakis, A., Skeie, R. B., Dalsoren, S. B., Myhre, G., Berntsen, T. K., Folberth, G. A., Rumbold, S. T., Collins, W. J., MacKenzie, I. A., Doherty, R. M., Zeng, G., van Noije, T. P. C., Strunk, A., Bergmann, D., Cameron-Smith, P., Plummer, D. A., Strode, S. A., Horowitz, L., Lee, Y. H., Szopa, S., Sudo, K., Nagashima, T., Josse, B., Cionni, I., Righi, M., Eyring, V., Conley, A., Bowman, K. W., Wild, O. & Archibald, A. (2013). Tropospheric ozone changes, radiative forcing and attribution to emissions in the Atmospheric Chemistry and Climate Model Intercomparison Project (ACCMIP). *Atmos. Chem. Phys.,* **13**, 3063-3085.

Stier, P., Feichter, J., Kinne, S., Kloster, S., Vignati, E., Wilson, J., Ganzeveld, L., Tegen, I., Werner, M., Balkanski, Y., Schulz, M., Boucher, O., Minikin, A. & Petzold, A. (2005). The aerosol-climate model ECHAM5-HAM. *Atmos. Chem. Phys.,* **5**, 1125-1156.

Stocker, T. F., Dahe, Q., Plattner, G.-K., Alexander, L. V., Allen, S. K., Bindoff, N. L., Bréon, F.-M., Church, J. A., Cubasch, U., Emori, S., Forster, P., Friedlingstein, P., Gillett, N., Gregory, J. M., Hartmann, D. L., Jansen, E., Kirtman, B., Knutti, R., Kanikicharla, K. K., Lemke, P., Marotzke, J., Masson-Delmotte, V., Meehl, G. A., Mokhov, I. I., Piao, S., Ramaswamy, V., Randall, D., Rhein, M., Rojas, M., Sabine, C., Shindell, D., Talley, L. D., Vaughan, D. G. & Xie, S.-P. (2014). Technical Summary. *In:* Stocker, T. F., Qin, D., Plattner, G.-K., Tignor, M., Allen, S. K., Boschung, J., Nauels, A., Xia, Y., Bex, V. & Midgley, P. M. (eds.) *Climate Change 2013: The Physical Science Basis. Contribution of Working Group I to the Fifth Assessment Report of the Intergovernmental Panel on Climate Change (IPCC).*

Stockwell, W. R. & Calvert, J. G. (1983). The mechanism of the HO-SO2 reaction. *Atmospheric Environment (1967),* **17**, 2231-2235.

Stokes, R. H. & Robinson, R. A. (1966). Interactions in Aqueous Nonelectrolyte Solutions. I. Solute-Solvent Equilibria. *The Journal of Physical Chemistry,* **70**, 2126-2131.

Stratton, R. W., Wong, H. M. & Hileman, J. I. (June 2010). Life cycle greenhouse gas emissions from alternative jet fuel. PARTNER Project 28 report. Version 1.2. Partnership for AiT Transportation Noise and Emissions Reduction. An FAA/NANA/Transport Canada sponsored Centre of Excellence.

Sullivan, A. P., Peltier, R. E., Brock, C. A., de Gouw, J. A., Holloway, J. S., Warneke, C., Wollny, A. G. & Weber, R. J. (2006). Airborne measurements of carbonaceous aerosol soluble in water over northeastern United States: Method development and an investigation into water-soluble organic carbon sources. *Journal of Geophysical Research: Atmospheres,* **111**, D23S46.

Sustainable Aviation (2011). Progress Report 2011.

Sustainable Aviation (July 2013). Sustainable Aviation Fuels Progress Paper.

Sustainable Aviation (September 2010). Inter-dependencies between emissions of CO2, NOx & Noise from aviation. *Policy Discussion Paper.*

Sustainable Aviation (Undated-a). SBAC Aviation and Environment Briefing Paper – ACARE Explained.

Sustainable Aviation (Undated-b). SBAC Aviation and Environment Briefing Paper – Alternative Aviation Fuels.

The Royal Society (September 2009). Geoengineering the climate: Science, governance and uncertainty.

The Shift Project Data Portal. (Undated). *Breakdown of GHG emissions by Sector and gas: World Sectoral breakdown of GHG Emissions in 2010 - World Bank (World Development Indicators) sourced*. URL: http://www.tsp-data-portal.org/Breakdown-of-GHG-Emissions-by-Sector-and-Gas#tspQvChart.

Thompson, A. M., Tao, W.-K., Pickering, K. E., Scala, J. R. & Simpson, J. (1997). Tropical Deep Convection and Ozone Formation. *Bulletin of the American Meteorological Society,* **78**, 1043-1054.

Tiedtke, M. (1989). A Comprehensive Mass Flux Scheme for Cumulus Parameterization in Large-Scale Models. *Monthly Weather Review,* **117**, 1779-1800.

Tilmes, S., Lamarque, J. F., Emmons, L. K., Conley, A., Schultz, M. G., Saunois, M., Thouret, V., Thompson, A. M., Oltmans, S. J., Johnson, B. & Tarasick, D. (2012). Technical Note: Ozonesonde climatology between 1995 and 2011: description, evaluation and applications. *Atmos. Chem. Phys.,* **12**, 7475-7497.

Timko, M. T., Herndon, S. C., de la Rosa Blanco, E., Wood, E. C., Yu, Z., Miake-Lye, R. C., Knighton, W. B., Shafer, L., DeWitt, M. J. & Corporan, E. (2011). Combustion Products of Petroleum Jet Fuel, a Fischer–Tropsch Synthetic Fuel, and a Biomass Fatty Acid Methyl Ester Fuel for a Gas Turbine Engine. *Combustion Science and Technology,* **183**, 1039-1068.

Twomey, S. (1977). The Influence of Pollution on the Shortwave Albedo of Clouds. *Journal of the Atmospheric Sciences,* **34**, 1149-1152.

U.S. Energy Information Administration (2010). International Energy Outlook 2010

U.S. Environmental Protection Agency (2008). National Ambient Air Quality Standards for Ozone: 40 CFR Parts 50 and 58. *Federal Register.*

U.S. Environmental Protection Agency. (2014a). *National Trends in Nitrogen Dioxide Levels*. URL: http://www.epa.gov/airtrends/nitrogen.html [10/06/2015].

U.S. Environmental Protection Agency. (2014b). *National Trends in Ozone Levels*. URL: http://www.epa.gov/airtrends/ozone.html [10/06/2015].

U.S. Environmental Protection Agency. (2014c). *National Trends in Particulate Matter Levels*. URL: http://www.epa.gov/airtrends/pm.html [10/06/2015].

U.S. Environmental Protection Agency. (2014d). *National Trends in Sulfur Dioxide Levels*. URL: http://www.epa.gov/airtrends/sulfur.html [10/06/2015].

U.S. Environmental Protection Agency. (2014e). *Regional Trends in Sulfur Dioxide Levels*. URL: http://www.epa.gov/airtrends/sulfur.html.

U.S. Environmental Protection Agency. (2015). *National Emissions Inventory (NEI) Air Pollutant Emissions Trends Data*. URL: http://www.epa.gov/ttn/chief/trends/index.html [29/04/2015].

Uherek, E., Halenka, T., Borken-Kleefeld, J., Balkanski, Y., Berntsen, T., Borrego, C., Gauss, M., Hoor, P., Juda-Rezler, K., Lelieveld, J., Melas, D., Rypdal, K. & Schmid, S. (2010). Transport impacts on atmosphere and climate: Land transport. *Atmospheric Environment,* **44**, 4772-4816.

Unger, N. (2010). Short-lived non-CO2 pollutants and climate policy: fair trade? *Environmental Science & Technology,* **44**, 5332-5333.

Unger, N. (2011). Global climate impact of civil aviation for standard and desulfurized jet fuel. *Geophys. Res. Lett.,* **38**, L20803.

Unger, N. (2012). Global Climate Forcing by Criteria Air Pollutants. *Annual Review of Environment and Resources,* **37**, 1-24.

Unger, N., Bond, T. C., Wang, J. S., Koch, D. M., Menon, S., Shindell, D. T. & Bauer, S. (2010). Attribution of climate forcing to economic sectors. *Proceedings of the National Academy of Sciences*.

Unger, N., Menon, S., Koch, D. M. & Shindell, D. T. (2009a). Impacts of aerosol-cloud interactions on past and future changes in tropospheric composition. *Atmos. Chem. Phys.,* **9**, 4115-4129.

Unger, N. & Pan, J. L. (2012). New Directions: Enduring ozone. *Atmospheric Environment,* **55**, 456-458.

Unger, N., Shindell, D. T., Koch, D. M., Amann, M., Cofala, J. & Streets, D. G. (2006a). Influences of man-made emissions and climate changes on tropospheric ozone, methane, and sulfate at 2030 from a broad range of possible futures. *J. Geophys. Res.,* **111**, D12313.

Unger, N., Shindell, D. T., Koch, D. M. & Streets, D. G. (2006b). Cross influences of ozone and sulfate precursor emissions changes on air quality and climate. *Proceedings of the National Academy of Sciences of the United States of America,* **103**, 4377-4380.

Unger, N., Shindell, D. T., Koch, D. M. & Streets, D. G. (2008). Air pollution radiative forcing from specific emissions sectors at 2030. *J. Geophys. Res.,* **113**, D02306.

Unger, N., Shindell, D. T. & Wang, J. S. (2009b). Climate forcing by the on-road transportation and power generation sectors. *Atmospheric Environment,* **43**, 3077-3085.

Unger, N., Zhao, Y. & Dang, H. (2013). Mid-21st century chemical forcing of climate by the civil aviation sector. *Geophysical Research Letters,* **40**, 641-645.

United Nations Economic Commission for Europe (1999). Protocol to the 1979 Convention on Long-range Transboundary Air Pollution to Abate Acidification, Eutrophication and Ground-level Ozone. *Protocol to Abate Acidification, Eutrophication and Ground-level Ozone: The 1999 Gothenburg Protocol to Abate Acidification, Eutrophication and Ground-level Ozone. .*

Uryga-Bugajska, I., Pourkashanian, M., Borman, D., Catalanotti, E. & Wilson, C. W. (2011). Theoretical investigation of the performance of alternative aviation fuels in an aero-engine combustion chamber. *Proceedings of the Institution of Mechanical Engineers, Part G: Journal of Aerospace Engineering*.

Van Der Werf, G. R., Randerson, J. T., Collatz, G. J. & Giglio, L. (2003). Carbon emissions from fires in tropical and subtropical ecosystems. *Global Change Biology,* **9**, 547-562.

van der Werf, G. R., Randerson, J. T., Giglio, L., Collatz, G. J., Mu, M., Kasibhatla, P. S., Morton, D. C., DeFries, R. S., Jin, Y. & van Leeuwen, T. T. (2010). Global fire emissions and the contribution of deforestation, savanna, forest, agricultural, and peat fires (1997–2009). *Atmos. Chem. Phys.,* **10**, 11707-11735.

Vaughan, D. G., Comiso, J. C., Allison, I., Carrasco, J., Kaser, G., Kwok, R., Mote, P., Murray, T., Paul, F., Ren, J., Rignot, E., Solomina, O., Steffen, K. & Zhang, T. (2013). Observations: Cryosphere (Chapter 4). *In:* Stocker, T. F., Qin, D., Plattner, G.-K., Tignor, M., Allen, S. K., Boschung, J., Nauels, A., Xia, Y., Bex, V. & Midgley, P. M. (eds.) *Climate Change 2013: The Physical Science Basis. Contribution of Working Group I to the Fifth Assessment Report of the Intergovernmental Panel on Climate Change (IPCC).* Cambridge, United Kingdom and New York, NY, USA.

Vedantham, A. & Oppenheimer, M. (1998). Long-term scenarios for aviation: Demand and emissions of CO2 and NOx. *Energy Policy,* **26**, 625-641.

Verheggen, B. 2009). Aerosol formation and climate: Part I. *RealClimate: Climate science from climate scientists* [Online]. URL: http://www.realclimate.org/index.php/archives/2009/04/aerosol-formation-and-climate-part-i/ Accessed].

Vinnikov, K. Y., Robock, A., Stouffer, R. J., Walsh, J. E., Parkinson, C. L., Cavalieri, D. J., Mitchell, J. F. B., Garrett, D. & Zakharov, V. F. (1999). Global Warming and Northern Hemisphere Sea Ice Extent. *Science,* **286**, 1934-1937.

Wang, Q., Jacob, D. J., Fisher, J. A., Mao, J., Leibensperger, E. M., Carouge, C. C., Le Sager, P., Kondo, Y., Jimenez, J. L., Cubison, M. J. & Doherty, S. J. (2011). Sources of carbonaceous aerosols and deposited black carbon in the Arctic in winter-spring: implications for radiative forcing. *Atmos. Chem. Phys.,* **11**, 12453-12473.

Wang, Y., Jacob, D. J. & Logan, J. A. (1998). Global simulation of tropospheric O3-NO x - hydrocarbon chemistry: 3. Origin of tropospheric ozone and effects of nonmethane hydrocarbons. *Journal of Geophysical Research: Atmospheres,* **103**, 10757-10767.

Warneke, C., de Gouw, J. A., Stohl, A., Cooper, O. R., Goldan, P. D., Kuster, W. C., Holloway, J. S., Williams, E. J., Lerner, B. M., McKeen, S. A., Trainer, M., Fehsenfeld, F. C., Atlas, E. L., Donnelly, S. G., Stroud, V., Lueb, A. & Kato, S. (2006). Biomass burning and anthropogenic sources of CO over New England in the summer 2004. *Journal of Geophysical Research: Atmospheres,* **111**, D23S15.

Watkins, A., Danilewitz, M., Kusha, M., Massé, S., Urch, B., Quadros, K., Spears, D., Farid, T. & Nanthakumar, K. (2013). Air Pollution and Arrhythmic Risk: The Smog Is Yet to Clear. *Canadian Journal of Cardiology,* **29**, 734-741.

Wayne, R. P. (2000). *Chemistry of Atmospheres.* Third ed.: Oxford University Press.

Wayson, R. L., Fleming, G. G. & Iovinelli, R. (2009). Methodology to Estimate Particulate Matter Emissions from Certified Commercial Aircraft Engines. *Journal of the Air & Waste Management Association,* **59**, 91-100.

Wei, C. F., Larson, S. M., Patten, K. O. & Wuebbles, D. J. (2001). Modeling of ozone reactions on aircraft-related soot in the upper troposphere and lower stratosphere. *Atmospheric Environment,* **35**, 6167-6180.

Wey, C. C., Anderson, B. A., Wey, C., Miake-Lye, R. C., Whitefield, P. & Howard, R. (2007). Overview on the Aircraft Particle Emissions Experiment (APEX). *Journal of Propulsion and Power,* **23**, 898-905.

Whitburn, S., Van Damme, M., Kaiser, J. W., van der Werf, G. R., Turquety, S., Hurtmans, D., Clarisse, L., Clerbaux, C. & Coheur, P. F. (2015). Ammonia emissions in tropical biomass burning regions: Comparison between satellite-derived emissions and bottom-up fire inventories. *Atmospheric Environment*.

Whitt, D. B., Jacobson, M. Z., Wilkerson, J. T., Naiman, A. D. & Lele, S. K. (2011). Vertical mixing of commercial aviation emissions from cruise altitude to the surface. *J. Geophys. Res.,* **116**, D14109.

WHO (2013). Review of evidence on health aspects of air pollution: REVIHAAP project: final technical report. WHO Regional Office for Europe.

Wild, O., Prather, M. J. & Akimoto, H. (2001). Indirect long-term global radiative cooling from NOx Emissions. *Geophys. Res. Lett.,* **28**, 1719-1722.

Wilkerson, J. T., Jacobson, M. Z., Malwitz, A., Balasubramanian, S., Wayson, R., Fleming, G., Naiman, A. D. & Lele, S. K. (2010). Analysis of emission data from global commercial aviation: 2004 and 2006. *Atmos. Chem. Phys.,* **10**, 6391-6408.

Williams, V. & Noland, R. B. (2006). Comparing the CO_2 emissions and contrail formation from short and long haul air traffic routes from London Heathrow. *Environmental Science & Policy,* **9**, 487-495.

Winchester, N., McConnachie, D., Wollersheim, C. & Waitz, I. A. (2013). Economic and emissions impacts of renewable fuel goals for aviation in the US. *Transportation Research Part A: Policy and Practice,* **58**, 116-128.

Woody, M., Haeng Baek, B., Adelman, Z., Omary, M., Fat Lam, Y., Jason West, J. & Arunachalam, S. (2011). An assessment of Aviation's contribution to current and future fine particulate matter in the United States. *Atmospheric Environment,* **45**, 3424-3433.

World Health Organisation (2000). Air Quality Guidelines for Europe. *European Series, No. 91.* Copenhagen, Denmark.

World Health Organisation (2003). Health Aspects of Air Pollution with Particulate Matter, Ozone and Nitrogen Dioxide. Bonn, Germany.

World Health Organisation (2005). Air Quality Guidelines a Global Update 2005: Particulate matter, ozone, nitrogen dioxide and sulphur dioxide. Germany.

Wuebbles, D., Gupta, M. & Ko, M. (2007). Evaluating the impacts of aviation on climate change. *Eos Trans. AGU,* **88**.

Yelvington, P. E., Herndon, S. C., Wormhoudt, J. C., Jayne, J. T., Miake-Lye, R. C., Knighton, W. B. & Wey, C. (2007). Chemical Speciation of Hydrocarbon Emissions from a Commercial Aircraft Engine. *Journal of Propulsion and Power,* **23**, 912-918.

Yim, S. H. L., Lee, G. L., Lee, I. H., Allroggen, F., Ashok, A., Caiazzo, F., Eastham, S. D., Malina, R. & Barrett, S. R. H. (2015). Global, regional and local health impacts of civil aviation emissions. *Environmental Research Letters,* **10**, 034001.

Young, P. J., Archibald, A. T., Bowman, K. W., Lamarque, J. F., Naik, V., Stevenson, D. S., Tilmes, S., Voulgarakis, A., Wild, O., Bergmann, D., Cameron-Smith, P., Cionni, I., Collins, W. J., Dalsøren, S. B., Doherty, R. M., Eyring, V., Faluvegi, G., Horowitz, L. W., Josse, B., Lee, Y. H., MacKenzie, I. A., Nagashima, T., Plummer, D. A., Righi, M., Rumbold, S. T., Skeie, R. B., Shindell, D. T., Strode, S. A., Sudo, K., Szopa, S. & Zeng, G. (2013). Pre-industrial to end 21st century projections of tropospheric ozone from the Atmospheric Chemistry and Climate Model Intercomparison Project (ACCMIP). *Atmos. Chem. Phys.,* **13**, 2063-2090.

Zarzycki, C. M. & Bond, T. C. (2010). How much can the vertical distribution of black carbon affect its global direct radiative forcing? *Geophysical Research Letters,* **37**, L20807.

Zdanovskii, A. (1948). New methods for calculating solubilities of electrolytes in multicomponent systems. *Zhur. Fiz. Kim,* **22**, 1475-1485.

Zhang, J. & Yu, K. F. (1998). What's the relative risk?: A method of correcting the odds ratio in cohort studies of common outcomes. *JAMA,* **280**, 1690-1691.

Zhang, L., Gong, S., Padro, J. & Barrie, L. (2001). A size-segregated particle dry deposition scheme for an atmospheric aerosol module. *Atmospheric Environment,* **35**, 549-560.

Zhang, Y., Seigneur, C., Seinfeld, J. H., Jacobson, M., Clegg, S. L. & Binkowski, F. S. (2000). A comparative review of inorganic aerosol thermodynamic equilibrium modules: similarities, differences, and their likely causes. *Atmospheric Environment,* **34**, 117-137.